SEDIMENTOLOGY OF THE STURTIAN ICEHOUSE: PERSPECTIVES FROM NAMIBIA, AUSTRALIA AND WESTERN USA

by

Marie Elen Busfield

A thesis submitted for the degree of

Doctor of Philosophy

at the University of London

Department of Earth Sciences

Royal Holloway, University of London

August 2015

Declaration

I, Marie Elen Busfield, hereby declare that this thesis and the work presented in it is entirely my own, unless otherwise stated. The main body of this thesis, Chapters 3-5, forms a collection of co-authored papers which are either published, in press or accepted for publication. I am responsible for the data collection throughout this thesis, for primary authorship of three of the included papers, and responsible for the content of all co-authored work. Detailed statements of contribution are included on the cover page of each paper, along with a full bibliographic reference.

Signed

Dated

Acknowledgments

First and foremost, my thanks go to Dan Le Heron, who conceptualised the original project, and followed its expansion and evolution with great excitement over the years. For always offering a very long leash, and reining me in when necessary, I'm very grateful. I've been incredibly fortunate to have carried out some pretty amazing field work throughout this project, much of it with Dan's assistance, guidance and unbridled enthusiasm. There are not all that many people you could spend more than 5 months in the field with and still be on great terms at the end of it! Numerous globally distributed academics are thanked for their help with fieldwork logistics, including Tony Prave (St Andrews), Alan Collins (University of Adelaide) and Fred Kamona (University of Namibia), and further thanks go to Benjamin Moorhouse (University of Otago), Erwan Le Ber (RHUL), Paulus Mungandjera and Ralph Muyamba (both UNAM) for assistance in the field. Cynthia Kienitz certainly deserves an honourable mention for making our stays in the Death Valley region beyond compare. Back at RHUL, Neil Holloway is warmly thanked for thin section preparation, especially for putting up with my pedantic requests about orientation! And various reviewers, anonymous and otherwise, are acknowledged for their contribution to improving and fine tuning the body of papers presented in this thesis.

This work would not have been possible without the financial support of numerous funding bodies. Royal Holloway covered my PhD studentship as well as contribution to field work costs through the Helen Shackleton Award, and internally from the departmental research committee. The remaining fieldwork and other costs were funded by the National Geographic Explorers Fund, Fermor Fund, Novus Consulting Research Grant, BSRG, IAS and the University of London Postgraduate Research Grants.

Huge thanks go to my ever supportive family. My parents, sister, brother-in-law and grandparents have done an incredible job of at least pretending to care about rocks over the years, and perhaps more importantly have provided ample non-geological distractions. For that I must also thank numerous PhD students within Earth Sciences and Geography, who achieved the incredible feat of making even the sleepy town of Egham an enjoyable place to live. On that front, thanks especially go to the various members/survivors of Caddy Close and St Judes Rd, for sharing in the good and the bad of Surrey student living.

Last and certainly not least, I'm very grateful to Professor Mike Hambrey (Prifysgol Aberystwyth) and Dr Bethan Davies (RHUL) for an enjoyable and insightful viva, which stimulated a lot of interesting discussion and ample food for thought.

List of Publications

Le Heron, D.P. & Busfield, M.E. *accepted.* Pulsed iceberg delivery driven by Sturtian ice sheet dynamics: an example from Death Valley, California. *Sedimentology* Special Issue (2015-2016).

Busfield, M.E. & Le Heron, D.P. *in press.* A Neoproterozoic ice advance sequence, Sperry Wash, California. *Sedimentology* Special Issue (2015-2016). doi: 10.1111/sed.12210

Le Heron, D.P., Busfield, M.E., Prave, A.R. 2014. Neoproterozoic ice sheets and olistoliths: multiple glacial cycles in the Kingston Peak Formation, California. *Journal of the Geological Society*, **171**, 525-538.

Busfield, M.E. & Le Heron, D.P. 2014. Sequencing the Sturtian icehouse: dynamic ice behaviour in South Australia. *Journal of the Geological Society*, **171**, 443-456.

Le Heron, D.P., Busfield, M.E., Collins, A.S. 2014. Bolla Bollana boulder beds: A Neoproterozoic trough mouth fan in South Australia. *Sedimentology*, **61**, 978-995.

Busfield, M.E. & Le Heron, D.P. 2013. Glacitectonic deformation in the Chuos Formation of northern Namibia: implications for Neoproterozoic ice dynamics. *Proceedings of the Geologists' Association*, **124**, 778-789.

Le Heron, D.P., Busfield, M.E., Kamona, A.F. 2013. An interglacial on snowball Earth? Dynamic ice behaviour revealed in the Chuos Formation, Namibia. *Sedimentology*, **60**, 411-427.

Le Heron, D.P., Busfield, M.E., Le Ber, E., Kamona, A.F. 2013. Neoproterozoic ironstones in northern Namibia: Biogenic precipitation and Cryogenian glaciation. *Palaeogeography, Palaeoclimatology, Palaeoecology*, **369**, 48-57.

"the dry wilting sun, glare and perspiration made the thought of an ice sheet at that very spot most incredible but alluring"

A.P. Coleman 1926
Ice Ages: Recent and Ancient

Abstract

The Cryogenian icehouse has long attracted significant attention because of the exceptionally widespread distribution of glaciogenic sediments, and the paradoxical accumulation of these sediments at tropical to sub-tropical palaeolatitudes. As a result, extreme models of global glaciation have been invoked to freeze the tropical latitudes through runaway climate and ice-albedo feedbacks, the eponymous 'Snowball Earth'. However, these predictions conflict with the evidence from the geological record, and cannot be readily replicated by available palaeoclimatological reconstructions. This thesis examines three exceptionally well-exposed older Cryogenian ('Sturtian') successions in northern Namibia, South Australia and the Death Valley region of western USA to improve understanding of the scale, mobility and thermal regime of Cryogenian ice masses. Detailed sedimentology, palaeocurrent analyses and thin section micromorphology are utilised to unravel sedimentological processes active under the Sturtian icehouse. In northern Namibia, these data reveal the first recorded example of subglacial glaciotectonic deformation in the Otavi Mountainland, pre- to syn-glacial ironstone facies which support photosynthetic microbial communities, and evidence of interglacial conditions interrupting a thick glaciogenic palaeovalley fill. In South Australia, the first known Neoproterozoic trough mouth fan is recorded, alongside evidence of dynamic advance-retreat cyclicity recognised within a glacial sequence stratigraphic framework. Meanwhile, in the Death Valley region, extremely heterolithic, predominantly coarse-grained facies support high debris loads and strong meltwater influence in the glacial depositional environment, clear variation in direct glacial influence across the depositional basin, and a distinct retrogradational retreat and progradational advance sedimentary architecture. Cumulatively, these data support the presence of grounded, marine-terminating temperate to polythermal ice masses subject to multiple episodes of advance and retreat, including periods of ice minima to open water conditions. These characteristics are more akin to Phanerozoic icehouse intervals than models of extreme global glaciation, and thus militate against the 'hard' snowball Earth hypothesis. In the absence of reliable geochronological data, diachronous glaciation cannot be inferred, although strong evidence is presented for disparate, dynamic ice masses operating under an active hydrological regime.

Table of Contents

List of Figures

1. Introduction

1. Introduction

1.1. The Neoproterozoic Icehouse

The Neoproterozoic icehouse is widely recognised as the most extensive glacial interval in Earth's history, and has attracted significant attention over the last few decades on account of its numerous apparent climatic paradoxes. Glacially-influenced successions deposited during this interval have been identified on almost every modern continent (Evans, 2000), with the preserved record dominated by glaciomarine facies. In contrast to Phanerozoic icehouse periods, Neoproterozoic glacial successions appear to accumulate at low palaeolatitudes (Evans, 2000; Hoffman & Li, 2009; Evans & Raub, 2011), are immediately overlain by near-ubiquitous 'cap' carbonate facies (Kennedy, 1996; Hoffman et al., 1998) and are commonly associated with the re-appearance of ironstones, following a billion year hiatus in the stratigraphic record (Hoffman & Schrag, 2002; Eyles & Januszczak, 2004; Klein, 2005). These characteristics have been used to argue in favour of an extreme global glaciation (Kirschvink, 1992; Hoffman et al., 1998), driving both severe equatorial cooling and sub-ice seawater anoxia (and hence stability of ferrous iron), followed by a catastrophic deglaciation and return to tropical carbonate production. The geological record, however, is out of kilter with the predictions of a globally frozen Earth, wherein extremely thick successions of debris-laden, meltwater influenced glaciogenic sediments interrupted by intervals of non-glacial deposition are suggestive of far more dynamic, polythermal and disparate ice masses in operation (Chapters 3-5; Etienne et al., 2007; Arnaud et al., 2011).

In light of the extensive and voluminous sedimentary exposures preserved worldwide (Hambrey & Harland, 1981; Arnaud et al., 2011), the large number of studies which target their broader scale stratigraphy (e.g. Prave, 1999; Macdonald et al., 2013), and the significant advances in our understanding of glacial depositional processes over the past few decades (e.g. Hambrey, 1994; Bennett & Glasser, 2009; Benn & Evans, 2010), the finer scale, process-based sedimentology remains to be carried out on several of these Neoproterozoic successions. These data are integral to our understanding of the scale, mobility and glacier thermal properties of the ice masses, and therefore key to gauging the severity of this purportedly global glaciation. As the most globally widespread record of glaciogenic deposition known in Earth's history, these deposits have the capacity to represent an extreme end member of global environmental change. Their often vast thicknesses also offer an important archive of glacial depositional processes, enabling direct access to exceptionally well preserved glaciomarine sequences which are largely inaccessible beneath today's oceans.

This thesis targets three study areas which allow the breadth and heterogeneity of Neoproterozoic glaciomarine sequences to be explored in detail, encompassing the birthplace of the controversial Snowball Earth hypothesis (northern Namibia), the type area of the older 'Sturtian' glaciation (South Australia), and some of the most lithologically diverse glaciomarine sedimentary sequences in the Neoproterozoic record (Death Valley region). These sites enable glacial environments to be characterised and compared across discrete sedimentary basins and ice catchments, and therefore offer a comprehensive review of an array of glacial depositional processes and ice mass dynamics active under the Neoproterozoic icehouse. Previous studies have a tradition of discussing these glacial intervals in reference to global scale phenomena, see below, whereas this work aims to generate higher resolution sedimentary and stratigraphical frameworks to provide more detailed insight into local and regional scale trends and variations, with the view to facilitating future broader scale correlation as more refined chronostratigraphic techniques become available.

1.2. Global glaciation and the Snowball Earth

1.2.1. Early ideas

The first Neoproterozoic formation recognised to contain glacially transported material, based on the presence of extrabasinal erratic clasts, was the Port Askaig Tillite on the Isle of Islay, western Scotland (Thomson, 1871). Comparable deposits were soon recognised in Australia (Woodward, 1884), Norway (Reusch, 1891) and Svalbard (Garwood & Gregory, 1898), where the occurrence of striated and faceted clasts, glacial pavements, and lithological similarities to Quaternary tills were cited as evidence of their glacial origin. The beginning of the 20th century saw the incidence of reported occurrences multiply rapidly throughout Oceania (Howchin 1901, 1903), Asia (Willis, 1904; Holland, 1908), North America (Hintze, 1913), Africa (Rogers, 1915; Beetz, 1929), Europe (Nikolaev, 1930) and South America (Moraes Rego, 1930), so that by the 1930s Neoproterozoic glacial deposits were recognised on every modern continent except for Antarctica (Hoffman, 2011). It should be noted that several of these earlier studies mistakenly correlated the deposits with the lower Cambrian or 'Eocambrian', and therefore direct references to a Precambrian glaciation slowly and sporadically appear later in the literature (e.g. Coleman, 1916; Yokoyama, 1911; Rogers, 1927; David, 1932). In South Australia, the presence of two distinct Neoproterozoic glacial horizons was interpreted as early as 1913, and the term 'Sturtian', now synonymous with the older interval, introduced at the end of that decade (Jack, 1913; Howchin, 1920).

During the 1920s and 1930s the consensus of collected works began to emerge of an 'extreme' glaciation at the end of the Precambrian, argued to be more severe than glacial conditions during the Pleistocene, and perhaps more comparable to the Late Palaeozoic Ice Age (Coleman, 1926; Kulling, 1934; Davies, 1940; Gevers & Beetz, 1940, Lee & Lee, 1940; Robert, 1940). However, at this time, theories of continental drift were met with some reluctance, and means of establishing the palaeolatitude of ancient deposits were still in their infancy, therefore notions of the scale and global distribution of ice masses remained limited. In fact, some of the early arguments implying 'extreme' glaciation were based on the deposition of the glacial deposits at their current latitude e.g. till in South China at c. 31°N (Willis et al., 1907; Coleman, 1926). Within a few decades, however, the advent and successful application of palaeomagnetism would demonstrate that these early predictions of the equatorward extent of the ice were extremely conservative (Harland & Bidgood, 1959; Bidgood & Harland, 1961; Girdler, 1964). New data which suggested the deposition of Neoproterozoic glacial deposits almost exclusively within 40° of the equator was considered to raise two critical possibilities: 1) the glacial interpretation of these deposits was incorrect, calling for detailed re-examination of their sedimentology, or 2) to glaciate even the tropical and equatorial regions, the whole planet must have been glaciated (Girdler, 1964; Harland, 1964a,b).

1.2.2. The debate over global glaciation

Concomitant with the emergence of new palaeomagnetic data, renewed interest surfaced in the carbonate facies associated with Neoproterozoic glacial deposits. This unusual association was recognised early in the 20th century (e.g. David, 1903; Norin, 1937; Robert, 1940; Mawson, 1949), and the possible implications for the marine deposition of the glacial facies inferred (David, 1903). Throughout the 1950s-70s several studies drew attention to the apparently conformable contacts between glacial deposits and their overlying carbonates (e.g. Harland & Wilson, 1956; Katz, 1961; Martin, 1965), and the similarly distinctive character of these carbonate facies in numerous locations worldwide (Dow, 1965; Biju-Duval & Gariel, 1969; Dunn et al., 1971; Rankama, 1973). Global reviews of the latitudinal distribution of carbonate facies throughout geological time place them consistently within 35° north and south of the equator (Rodgers, 1957; Briden, 1970). Therefore, the significance of these relationships was three-fold: 1) they verified the unusually low palaeolatitudes suggested by palaeomagnetic data, 2) conformable contacts supported glacial deposition at sea-level, and thus high-altitude glaciation could not be used to account for their near equatorial distribution, and 3) the globally widespread precipitation of carbonates with shared unique facies characteristics could be used to argue for a global causal mechanism.

In his review of Late Precambrian glaciation, or the 'great infra-Cambrian ice age', Harland (1964a) argued that these characteristics, in tandem with the remarkably widespread distribution of glacial deposits, were suggestive of 'a very small number of discrete, simultaneous, severe, prolonged ice ages'. It is argued that if low-latitude, low elevation tropical regions are glaciated, it follows that higher latitudes and elevations would have been glaciated also, and therefore glaciation must have been severe and widespread (Harland, 1964a,b). These papers emphasise the probability of at least two, perhaps three, discrete Precambrian glacial intervals, wherein alternating 'warm' carbonate and 'cold' glacial facies attest to rapid switches in global climate (Harland, 1964a, b). These early ideas were quickly replicated by simple radiative energy-balance models which generated, through slightly reducing solar radiation, positive ice-albedo feedbacks towards global freezing; the so-called 'white Earth' (Eriksson, 1968; Budyko, 1969; Sellers, 1969). Although providing an attractive mechanism of driving global glaciation, the models did not offer a means of climatic amelioration, and therefore could not yet explain the return to tropical carbonate precipitation.

Whilst theories began to pick up pace on the causes of global glaciation, sceptics focussed on re-examination of the studied sedimentary sequences, especially in light of advances in the understanding of mass flow depositional processes (e.g. Kuenen & Migliorini; Crowell, 1957; Banerjee, 1966; Hubert, 1966). In a bid to avoid genetic terminology such as 'tillites', the terms 'pebbly mudstone' and 'mixtite', and somewhat confusingly 'tilloid', were introduced for poorly sorted, matrix-rich sediments with a range of clast sizes (e.g. Crowell, 1957; Pettijohn, 1957; Schermerhorn & Stanton, 1963; Schermerhorn, 1974), where the term 'diamictite' is typically favoured today (Chapter 2, Table 2.1). These studies stressed the abundant evidence supporting both laminar and turbiditic mass flow deposition in the late Neoproterozoic sedimentary record, and therefore questioned the glacial origin of these sedimentary rocks, as well as others previously identified as 'tillites'. This widespread re-examination began to draw attention to the perhaps previously under-appreciated role of tectonic basin configuration and mass flow processes, and by extension the over-zealous use of the term 'tillite' in earlier studies (see discussion in Chapter 2), but failed to recognise that these mass flows could be transporting glaciomarine debris (Schermerhorn, 1974). This is somewhat surprising given the wealth of studies which emerged in this period emphasising the broad spectrum of sedimentary deposits associated with glacial intervals, including turbidites and debrites, and that true 'tillites' were not the only testament to glaciomarine depositional processes (e.g. Harland, 1964a; Schwarzbach, 1964; Kilburn et al., 1965; Reading & Walker, 1966; Perry & Roberts, 1968; Spencer, 1971).

1.2.3. Causal mechanisms of global cooling

Since the glaciomarine origin of Neoproterozoic sedimentary sequences adequately stood up to the criticisms from the mass flow proponents, debates continued over the palaeoclimatological enigma of freezing the warm tropical and sub-tropical latitudes. Williams (1972) argued for a planetary causal mechanism, whereby an adjustment in the Earth's obliquity (the angle between the ecliptic and equatorial planes) from relatively low modern values of 22-24° to higher values in the Neoproterozoic (>54°) could drastically alter the palaeoclimate; a theory known as the 'high-tilt Earth'. This was considered to have the combined effect of preferentially warming the poles rather than the equator (see **Fig. 1.1**), and promoting enhanced seasonality i.e. extreme temperature fluctuations (Williams, 1972, 1975, 2000). This would in turn result in less distinct climatic zonation, wherein hot and cold climate indicators could become juxtaposed (Williams & Schmidt, 2004). The theory is hampered by a lack of proof for high obliquity at this time (Vanyo & Awramik, 1982, 1985), or an appropriate mechanism by which to alter it (Néron de Surgy & Laskar, 1997; Pais et al. 1999; Levrard & Laskar, 2003), particularly given the stabilising effect of a coupled Earth-Moon system (Laskar et al., 1993; Fairchild & Kennedy, 2007). Moreover, even with an appropriate mechanism, carbonate belts would likely be situated under the preferentially warmer poles, and therefore would not be closely associated with low latitude glacial deposits, as observed in the geological record.

An alternative theory emerged from the climate science community through renewed discussion of the 'white Earth' scenario (Eriksson, 1968; Budyko, 1969; Sellers, 1969). Walker et al. (1981) advocated the role of carbon cycling in modulating the planet's global temperature change, wherein increased silicate weathering (and CO_2 drawdown) facilitated cooling, whilst reduced silicate weathering favoured CO_2 build up and resultant warming. This offered an important escape mechanism from the runaway glaciation proposed in earlier energy-balance models (e.g. Budyko, 1969). Under this scenario, the proposed global ice cover would greatly inhibit silicate weathering, enabling sufficient increase in atmospheric CO_2 to switch from a severe icehouse to a much warmer greenhouse, and hence from deposition of glaciomarine sequences to overlying cap carbonates.

1.2.4. Stratigraphic significance of glacial horizons

The number of well-documented glacial sedimentary sequences continued to grow throughout the 1980s, aided in particular by an expansive international effort to collate data on the geologic record of ancient (i.e. pre-Pleistocene) glaciations (Hambrey & Harland, 1981). This volume includes 90 papers on the

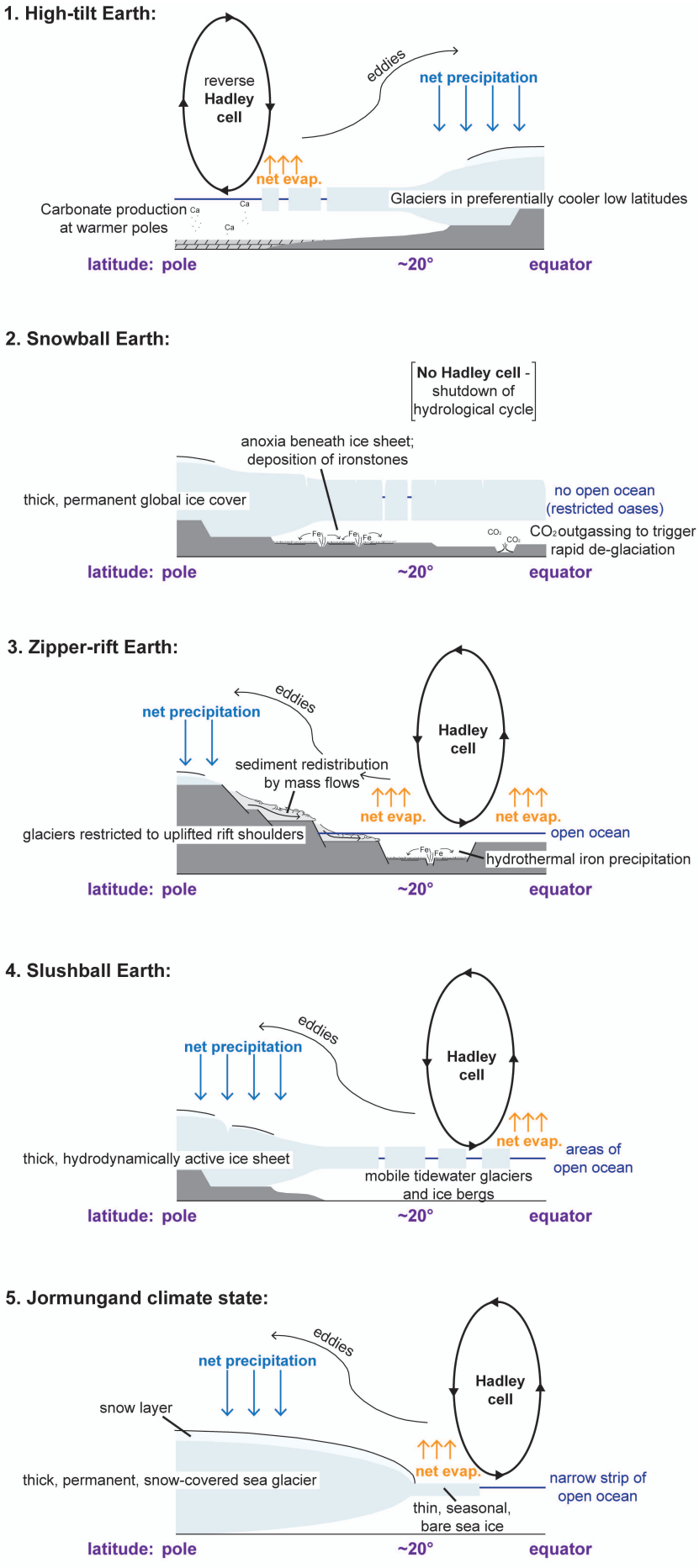

Fig 1.1: Schematic diagrams representing the principal conceptual and climatic models put forward to explain low-latitude glaciation during the Neoproterozoic icehouse. See text for detailed description. Diagram modified after Abbot et al. (2011).

Neoproterozoic glacial record from globally widespread sections, and clearly outlines some common lithological and stratigraphical characteristics worldwide. In their review of the included texts, Hambrey and Harland (1985) align two glacial intervals with periods of global glaciation, the Sturtian (c. 800-790 Ma) and Varangian (c. 720-610 Ma) glacial epochs, so named after their South Australian (Sturt Gorge) and Norwegian (Varangerfjord) type sections (Harland, 1964b; Preiss et al., 1998). They also reference putative evidence for more localised pre-Sturtian and post-Varangian events, termed the Lower Congo (c. 900-770 Ma) and Late Sinian (c. 610-580 Ma), respectively. Since geochronological constraints were still relatively poorly developed at this time (Chumakov, 1981; Hambrey & Harland, 1985), and formal stratigraphic nomenclature differed considerably from today, a critical review of these chronostratigraphic developments is avoided herein. The key outcome was that a global consensus to improve stratigraphic correlation was underway (e.g. Trompette, 1982), and the preservation of at least two glacial horizons appeared to be a characteristic feature within several formations.

Sedimentologically, this period represents a time of clear advances in the understanding of Neoproterozoic glacial depositional environments. Following the earlier criticisms of Schermerhorn (1974) and others, a concerted effort was made to outline the numerous lines of evidence supporting a glacial influence, and critically to distinguish those lines of evidence which indicated direct glaciogenic deposition or re-sedimented glacial material i.e. primary or secondary deposits. Evidence of the former included the presence of glacially-striated pavements and roches moutonnées (e.g. Deynoux & Trompette, 1981), faceted and striated clasts (e.g. Rocha Campos & Hasui, 1981a, b), ice-rafted dropstones and till pellets (e.g. Eisbacher, 1981), and varvites (e.g. Hambrey et al., 1981), whilst several studies also cited evidence of primary periglacial activity, such as polygonal structures and sandstone wedges (e.g. Spencer, 1981). The predominance of re-worked glaciogenic material in the Neoproterozoic glacial record is plainly manifest, with numerous localities preserving a high volume of turbidity current and mass flow deposits (e.g. Aalto, 1981; Visser, 1981), including evidence of soft sediment remobilisation (e.g. Cahen & Lepersonne, 1981). These features, in tandem with other intercalated marine deposits, e.g. pillow lavas, carbonate interbeds, served to highlight the prominence of glaciomarine deposits in the preserved record, with the abrupt transition to overlying 'cap dolostones' interpreted to record a pronounced post-glacial marine transgression (Hambrey & Harland, 1981).

During this period, isotopic analyses also became more widely used as a potential chronostratigraphic tool, with several studies worldwide recognising a distinct positive (or isotopically heavy) $\delta^{13}C$ signature prior to glaciation, followed by a shift to negative (or isotopically light) $\delta^{13}C$ signatures immediately preceding the

glacial horizons as well as in the post-glacial cap carbonates (Knoll et al., 1986; Fairchild & Spiro, 1987). These patterns were attributed to ocean circulation patterns which drove greater burial of light ^{12}C prior to glaciation, and hence enrichment of the surface waters in isotopically heavy ^{13}C, and conversely reduced circulation and burial during and after glaciation, enabling upwelling of the buried carbon, and precipitation of isotopically depleted carbonates (e.g. Knoll et al., 1986, 1996). Curiously, oxygen isotope compositions were found to be less depleted than anticipated, by comparison to modern high-latitude meltwaters (Fairchild et al., 1989) and high-latitude syn-glacial limestones in the Permian record (e.g. Rao & Green, 1982). This was considered to lend support to the evidence favouring glaciation at low palaeolatitudes, where meltwater would be expected to show a much less pronounced depletion in ^{18}O (Fairchild & Spiro, 1987; Fairchild et al., 1989). These data coincided with developments in understanding of remnant magnetization processes (McCabe & Elmore, 1989), and in turn the first robust palaeomagnetic data confirming a low palaeolatitude of <10° for the Marinoan (Varangian) Elatina Formation in South Australia (Embleton & Williams, 1986; Sumner et al., 1987; Schmidt et al., 1991).

At the beginning of the 1990s, the importance of these glacial intervals as a globally significant chronostratigraphic marker was formally recognised (Plumb, 1991), and the subdivision of the 'Cryogenian' proposed to encompass these deposits. The boundaries were provisionally set at 850 – 650 Ma, and therefore subject to further investigation, whilst the post-Cryogenian terminal Neoproterozoic period (now known as the Ediacaran) was yet to be formally named.

1.2.5. Snowball Earth

Since its inception in the early 1990s, the term Snowball Earth has become synonymous with discussions of Cryogenian glaciation. The theory brings together a number of the existing hypotheses outlined above, with a view to developing a unifying whole earth systems approach. It is argued that glaciation, or at least unusually cold climate conditions, would have first been triggered by the accumulation of land masses within middle to low palaeolatitudes, significantly increasing both the albedo and rates of silicate weathering in the tropics (Kirschvink, 1992; Schrag et al., 2002). This would have the combined effect of reflecting warm solar energy and drawing down more CO_2, initially nucleating ice at high elevations before runaway ice-albedo feedbacks took over, driving ice accumulation towards low palaeolatitudes (e.g. Budyko, 1969; Manabe & Broccoli, 1985; Hoffman & Schrag, 2002). This would result in a global ice cover (**Fig. 1.1**), including most of the ocean surface, save for a few laterally restricted oases (Kirschvink, 1992; Hoffman et al., 1998). The proposed ice carapace effectively seals off the world's oceans, considerably impeding both the hydrological cycle and

atmosphere-ocean interaction, and thus promoting widespread seawater anoxia: a condition where ferrous iron (Fe^{2+}) is stable. This is argued to facilitate the gradual build up soluble iron, subject to rapid oxidation once the ice carapace is removed, and hence precipitation of end glacial or 'last-gasp' ferric (Fe^{3+}) ironstones (Kirschvink, 1992). Under this scenario, CO_2 outgassing from volcanic and hydrothermal sources can build up to critical levels in the atmosphere, ultimately triggering a rapid switch from extreme icehouse to extreme greenhouse conditions (Caldeira & Kasting, 1992; Kirschvink, 1992; Hoffman et al., 1998), and an abrupt transition to warm water carbonate production, in a similar mechanism to the self-reversing climate amelioration proposed by Walker et al. (1981).

The Snowball Earth hypothesis offers an attractive mechanism of generating ice masses at low palaeolatitudes, and one which has been successfully replicated in numerous climate simulations. Attempts at modelling a 'Snowball Earth' frequently predict accumulation of thick, floating sea glaciers (thick layers of mobile floating sea ice independent of continental ice masses; Warren et al., 2002) which preferentially flow towards equatorial latitudes (e.g. Donnadieu et al., 2003; Goodman, 2006; Li & Pierrehumbert, 2011; Ashkenazy et al., 2013). Under the crucial *assumption* of a global ice cover, these glaciers would grow to thicknesses of several hundred metres (Goodman & Pierrehumbert, 2003; Abbot et al., 2013), preventing photosynthesis in the marine realm save for restricted oases (e.g. Hoffman & Schrag, 2002; Tziperman et al., 2012) or regions of thin tropical sea ice (e.g. McKay, 2000; Pollard & Kasting, 2005). However, the development of thin ice at the tropics has proven difficult to replicate in simple numerical models (e.g. Warren et al., 2002; Goodman, 2006; Abbot et al., 2013). Whilst the Snowball Earth hypothesis offers stratigraphic explanations for the abrupt upper and lower contacts of glacial deposits, the unusual association of ironstone facies and the switch to cap carbonate deposition, neither the hypothesis nor the modelled simulations make predictions for the behaviour of ice masses during glaciation. Critically, runaway feedbacks into and out of the icehouse world do not offer an internal metronome for controlling glacial maxima or minima during an individual glaciation, and thus no means to generate advance-retreat cyclicity. Moreover, the concept of 'sea glaciers', far removed from our understanding of the modern or palaeo-cryosphere, make predictions of their depositional record difficult to ascertain.

1.2.6. Zipper-rift Earth

Such a controversial model of a globally frozen Earth re-ignited criticism from proponents of the syntectonic mass flow camp, now elegantly re-packaged as the 'Zipper-rift Earth' hypothesis. Drawing on the conclusions of Schermerhorn (1974), Eyles & Januszczak (2004) stress the non-glacial derivation of diamictite assemblages,

arguing instead that the majority of purported glacial sediments are rift-related mass flows, deposited during the fragmentation of Rodinia. Associated ironstones are therefore attributed to isolated rift basins subject to extensional hydrothermal activity. In this model, glaciers, if present, are restricted to elevated rift-shoulders, leading to widespread re-working of glaciogenic sediments (**Fig. 1.1**).

This model is significant in highlighting the important interplay of basin configuration and active tectonics on sediment accumulation and redistribution (Eyles & Januszczak, 2004, 2007); an undoubtedly important control on available accommodation (Fairchild & Kennedy, 2007). However, abundant evidence has continued to emerge over more than 100 years of studies on Neoproterozoic sedimentary sequences which provide ample support for glaciomarine, glaciofluvial, terrestrial and ice-contact glacially influenced deposition, irrespective of tectonic setting (e.g. Hambrey & Harland, 1981; Arnaud et al., 2011). Sediment gravity flow processes, whilst pervasive at this time, are recognised as a significant contributor to both ice-distal and ice-proximal glacial environments (e.g. Laberg & Vorren, 2000; Elverhøi et al., 2002; Ó Cofaigh et al., 2002, 2003; Ravier et al., 2014), and are therefore not indicative of restricted, glaciated hinterlands.

1.2.7. Slushball Earth

Although perhaps disproportionately critical of the evidence for primary glacial depositional processes, Eyles and Januszczak (2004, 2007) did critically outline key sedimentological data which repudiate the Snowball Earth hypothesis, especially the arguments for shutdown of the hydrological cycle. The abundant evidence for extensive subaqueous clastic systems, with large volumes of debris transported by the combined influence of gravity and water cannot comply with an inactive hydrological cycle (Eyles & Januszczak, 2004). Similar arguments emerged from advocates of glaciomarine deposition, where the intercalation of dropstone-bearing and dropstone-free strata (Condon et al., 2002), pulsed glacial advance and retreat sequences (Leather et al., 2002), and evidence of open water conditions (Allen et al., 2004), argued for much more dynamic, hydrologically active ice masses than predicted under a 'Snowball Earth'. This original, more extreme hypothesis was therefore referred to as the 'hard' Snowball (e.g. Runnegar, 2000), and arguments for a 'soft' Snowball or 'Slushball' Earth came to light.

A term originally coined by Schrag and Hoffman (2001) in response to model experiments of Hyde et al. (2000), the 'Slushball Earth' predicts accumulation of ice at low palaeolatitiudes but accompanied by regions of open water near the equator, with obvious benefits for the survival of marine habitats throughout a glaciation. In order to maintain this scenario, open water regions must remain near the equator (**Fig. 1.1**),

with the average ocean-sea ice interface predicted to reach c. 25-40° palaeolatitude (Hyde et al., 2000). This model does not therefore require a complete global ice cover, but still argues for globally synchronous glaciation (Fairchild & Kennedy, 2007).

The attraction of this hypothesis is that it conforms with evidence supporting low latitude glaciation, but under a more typical cryosphere, as compared to what we know of the Ordovician, Late Palaeozoic, and Pleistocene glaciations, and the behaviour of our current ice masses. Alongside significant advances in modern facies analysis (e.g. Middleton, 2003), and especially our understanding of glacial depositional and deformational processes (e.g. McCarroll & Rijsdijk, 2003; van der Meer et al., 2003; Evans et al., 2006; Menzies et al., 2006), the sedimentological similarities between Neoproterozoic glacial sediments and their younger Phanerozoic and modern counterparts become plainly apparent (see Etienne et al., 2007 for review). Comparisons can readily be drawn between the thickness of preserved sequences, nature of the sedimentary facies, sedimentary architecture, and cyclicity of both glacial advance and retreat sequences, and glacial-interglacial transitions (Etienne et al., 2007). The close interbedding of glacial and non-glacial strata, including thick packages of remobilised turbiditic and laminar mass flows, mirror the styles of sedimentation recorded at recently glaciated continental margins (e.g. Dowdeswell et al., 1996; Elverhøi et al., 2002; Ó Cofaigh et al., 2002). In places, these non-glacial packages reach km-scale thicknesses, which in tandem with the evidence for storm-wave agitation of the sediments (Le Heron et al., 2011) is difficult to envisage beneath a sustained, near-global ice sheet.

However, as yet, model experiments have struggled to generate a robust 'Slushball' where equatorial, low-latitude ice caps and open water exist contemporaneously (e.g. Donnadieu et al., 2003; Lewis et al., 2007; Goddéris et al., 2011). Donnadieu et al. (2003) found that the coldest climate simulation which retained open equatorial waters, at 990 ppm CO_2, accumulates only high-elevation ice caps (>1500 m), with low-elevation ice sheets restricted to >20-30° latitude. Meanwhile, dynamic sea-ice behaviour, a condition which open waters should facilitate, appears to prohibit ice growth to sufficient thickness to sustain stable sea glaciers, unless completely ice covered (Lewis et al., 2007). Arguably, though, the greatest drawback of the Slushball model is that it fails to offer hitherto unprecedented or unique Earth process behaviour, as would be anticipated to grow ice at lower palaeolatitudes than any other interval in Earth's history. From an uniformitarian perspective, this may also be regarded as the strength of this model if appropriate climate solutions come to light.

1.2.8. Jormungand climate state

More recently, an interim between the Snowball and Slushball models has been proposed, wherein the majority of the Earth's surface is ice covered, but a thin band of open ocean remains in the equatorial regions (<5-15°; **Fig. 1.1**). The climate state is moderated by the variation between high-albedo snow cover and low-albedo bare sea ice (Abbot et al., 2011). As in the Snowball model, runaway ice-albedo feedbacks drive the ice latitude towards the equator, but progress slows dramatically at c. 20-30° where the subtropical 'desert' belt is met. This cold and dry environment limits precipitation, leading to bare (snow free) sea ice with a much lower ice-albedo feedback, alongside much reduced silicate weathering. This inhibits further reduction of atmospheric CO_2 concentration, and therefore prevents the climate entering a Snowball state (Abbot et al., 2011; Pierrehumbert et al., 2011; Yang et al., 2012). A similar model of CO_2 build-up is envisaged to trigger rapid deglaciation and post-glacial cap carbonate deposition.

Acknowledging the capacity for error in palaeomagentic data, results thus far support deposition of the majority of glacigenic deposits at low to moderate palaeolatitudes, as opposed to exclusively equatorward of the proposed 5-15° ice latitude. Significantly, these deposits are interpreted as the product of mobile, polythermal ice sheets, which may be difficult to replicate under the arid, low net precipitation 'desert' zone of a Jormungand climate state.

1.3. The low-latitude glaciation paradox: a recent perspective

The accumulation of glacigenic deposits at tropical to subtropical palaeolatitudes presents a significant palaeoclimatological obstacle, one which model experiments have thus far struggled to adequately overcome (see Goddéris et al., 2011 for review). The crux of the argument lies in the tipping point of climate stability, and whether it is possible to cool equatorial latitudes sufficiently to develop marine-terminating ice sheets without invoking global glaciation. Based on our current understanding of global climate, and the requisite boundary conditions, ice advance below 30° latitude would trigger runaway feedback loops towards extreme cooling (Budyko, 1969; Sellers, 1969; Caldeira & Kasting, 1992; Goddéris et al., 2011), leading to rapid and near-synchronous glaciation of low palaeolatitudes. However, climatic amelioration following such an extreme icehouse, particularly to deposit syn- to post-glacial warm water carbonates, is difficult to explain (Hoffman & Schrag, 2002).

Several hypotheses exist which have attempted to resolve these issues, but none as yet correspond well with the evidence from the geological record. This discrepancy highlights the need for more detailed

examination of Neoproterozoic glacial deposits, and provides the basis for the sedimentological analyses presented in Chapters 3, 4 and 5 herein. Below, a brief synthesis of the recent developments in understanding of the timing, location and style of Cryogenian glaciation is provided in order to outline the global context of these new data, and their significance relative to the paradox of low-latitude glaciation.

1.3.1. Discrete or diachronous?

Although significant advances have been made in Neoproterozoic geochronology in recent years, the question of how many glaciations are recorded, and their relative synchronicity, remains to be addressed (see Condon & Bowring, 2011 for review). In the majority of regions, two glacially-influenced successions are recognised, wherein their occurrence is used to define the Cryogenian Period from c. 720-635 Ma. These successions are traditionally attributed to an older Sturtian (c. 720-663 Ma) and younger Marinoan (<654-635 Ma) glaciation (Macdonald et al., 2010; Condon & Bowring, 2011), so-named after their type localities in South Australia (e.g. Preiss et al., 1998). The historical nomenclature of 'Varangian' for the younger glaciation was substituted following uncertain age correlation across the North Atlantic (Kennedy et al., 1998; Fairchild & Kennedy, 2007). A third, significantly less widespread glacial interval is also recognised in the Ediacaran Period, and termed the Gaskiers glaciation (c. 584-582 Ma; Bowring et al., 2003) following its Newfoundland type section.

Many early studies consider these as three discrete, globally synchronous glaciations, each demonstrating an abrupt worldwide termination (Kirschvink, 1992; Hoffman et al., 1998; Hoffman & Schrag, 2002). However, as a greater number, especially of more reliable, geochronological data become available the picture becomes less clear. Radioisotopic dates spanning a much wider age range are increasingly used to argue in favour of diachronous glaciations (e.g. Fairchild & Kennedy, 2007; Allen & Etienne, 2008), more akin to the better constrained Phanerozoic icehouse intervals. A persistent problem remains with identifying how much of the stratigraphic record is preserved, particularly in glacially-influenced successions which are subject to widespread erosion and re-working during repeated ice advances. This issue, in tandem with questions on the precision and reliability of dates hinders current inferences on the timing, duration and global correlation of glacial events (Condon & Bowring, 2011).

Despite these issues and the greater discordance in radioisotopic age constraints, three broad glacial intervals remain (Fairchild & Kennedy, 2007; Condon & Bowring, 2011), with current estimates predicting a c. 55 Ma duration for the older Cryogenian glaciation (Rooney et al., 2014), <10 Ma for the younger Cryogenian interval (Condon & Bowring, 2011) and up to 2.6 Ma for the Ediacaran glaciation (Bowring et al., 2003).

Therefore, for ease of comparison and in the absence of a more refined correlation scheme, the traditional 'Sturtian', 'Marinoan' and 'Gaskiers' nomenclature will be adopted herein. All of the studied sections within this thesis have traditionally been correlated with the 'Sturtian' glaciation, and shall be referred to as such throughout, although it should be emphasised this terminology does not implicitly imply a direct age correlation between study sites, but a broad temporal association with the relatively older glacial interval.

1.3.2. Palaeolageographic reconstructions

One of the more puzzling aspects of the Neoproterozoic icehouse is the abundant evidence favouring accumulation of glacially-influenced sediments near the equator (**Fig. 1.2**). Global palaeomagnetic data compilations repeatedly demonstrate low to moderate palaeolatitudes, and an absence of near-polar (>60°) glacial deposits (Evans, 2000; Hoffman & Li, 2009; Evans & Raub, 2011). Whilst it is widely accepted that the reliability of palaeomagnetic data is not beyond repute, the most robust examples, derived from the Upper Tindir, Nantuo and Elatina formations, are all consistent with low-latitude glaciation (Hoffman & Schrag, 2002; Evans & Raub, 2011). Results from the Elatina Formation, in particular, have proven to be reproducible at numerous laboratories, and passed several independent assessments including field stability tests, thus definitively supporting glacial deposition within 10° of the equator (Sumner et al., 1987; Sohl et al., 1999; Evans & Raub 2011).

These data are used in concert with geological control points to inform palaeogeographic reconstructions at the time of glacigenic deposition (broadly 715 Ma, 635 Ma and 580 Ma; **Fig. 1.2**). Prior to the Cryogenian Period, the majority of palaeocontinents were amalgamated as the supercontinent Rodinia (Li et al., 2008 and refs within), the break-up of which is considered to largely coincide with, or immediately precede, the Sturtian glacial interval (Hoffman & Li, 2009; Evans, 2013). Throughout the Cryogenian, the separating palaeocontinents appear to occupy low to moderate palaeolatitudes (<45°), predominantly clustered in equatorial reaches (<15°; Li et al., 2008; Hoffman & Li, 2009). These reconstructions are consistent with the occurrence of both syn- and post-glacial carbonate deposits, recognised to accumulate within 35° of the palaeoequator throughout the Phanerozoic to present day (Hoffman & Li, 2009). By the Ediacaran (Gaskiers) glaciation, the majority of palaeoecontinents have migrated to higher palaeolatitudes (**Fig. 1.1**), more consistent with younger icehouse periods e.g. the Late Palaeozoic and Pleistocene glaciations.

This thesis includes three study regions, northern Namibia, South Australia and the Death Valley region of the western US, which are all considered to occupy low palaeolatitudes during the Sturtian glacial

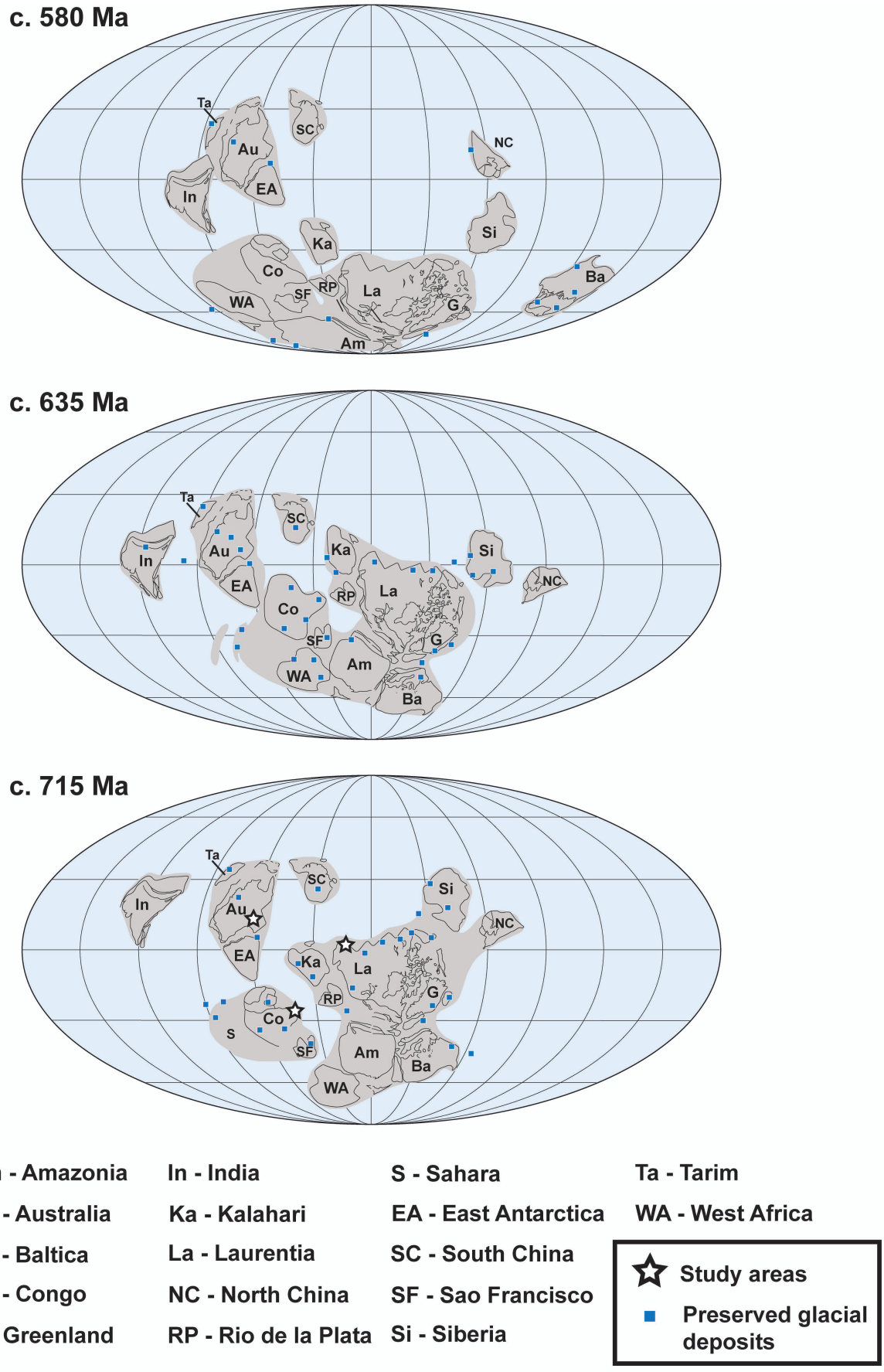

Fig. 1.2: Palaeogeographic reconstructions of the Sturtian (c. 720 Ma), Marinoan (c. 635 Ma) and Gaskiers (c. 580 Ma) glacial intervals. Blue Squares indicate recorded glacial successions, white stars indicate studied successions discussed herein (Chapters 3-5). Modified after Li et al. (2008) and Hoffman & Li (2009).

interval (c. 715 Ma, **Fig. 1.2**). These regions offer extremely well preserved and sedimentologically diverse records of Neoproterozoic glaciation (Chapters 3-5), and crucially occupy geographically discrete sedimentary basins. This enables comparison of local, regional and inter-regional depositional characteristics, sedimentary architectures and glaciological histories within separate basins, which are therefore subject to distinct sedimentary inputs and ice catchments. This enables the scale, behaviour and glacier thermal regime of ice masses feeding each basin to be assessed independently, without making global scale inferences on the cryosphere.

1.3.3. Sedimentology of the Sturtian icehouse

The Snowball Earth hypothesis has done wonders for generating a huge amount of interest in the Cryogenian cryosphere from the geological, geochemical, palaeoclimatological and modelling communities. However, it fails to adequately explain the nature of the preserved sedimentological record, and offers little insight into the behaviour of ice masses during glaciation itself. Under a globally frozen ocean, it is hard to envisage active marine depositional systems since the hydrological system would be significantly impeded, restricting subaqueous sediment transport, whilst subaerial input would be hampered by the widespread ice cover. The arguments for thick, extensive floating 'sea glaciers' disassociated from continental land masses (Warren et al., 2002; Goodman & Pierrehumbert, 2003; Abbot et al., 2013) have no known analogues today, or evidence for comparable conditions during Phanerozoic glaciations (e.g. Hambrey et al., 2007). The argument can be made that the Cryogenian cryosphere was unique (e.g. Hoffman, 2009), a prerequisite for glaciating the lower latitudes, but the studied sedimentological record thus far can be adequately explained with reference to known glacial depositional processes in the modern and Phanerozoic records (Etienne et al., 2007; Allen & Etienne, 2008). Why then invoke unusual glaciological conditions to explain their deposition?

Over the past 20-25 years especially, huge advances have been made in our understanding of glacial depositional and deformational processes, with studies of Quaternary glaciogenic sediments at the forefront of these changes. These include greater understanding of the mass flow processes dominating glaciomarine shelves (e.g. Dowdeswell & Ó Cofaigh, 2002; Ó Cofaigh et al., 2013a, b), the realisation that subglacial depositional systems rest on a deformation continuum, and that this deformation can vary spatially and temporally (e.g. Piotrowski et al., 2004; Evans et al., 2006; Menzies et al., 2006), alongside the wealth of valuable information that can be gleaned from micro-scale analyses, especially on macroscopically massive diamictites (e.g. van der Meer, 1993; Menzies, 2000a; Carr, 2004; Phillips et al., 2011). Following these

advances, and the outlined discrepancies between the conceptual and geological understanding of the Cryogenian cryosphere, a detailed re-examination is timely.

The studies included within this thesis span a much needed resurgence in studies of Neoproterozoic sedimentary sequences. Following Hambrey and Harland's (1981) influential volume, another expansive collection of papers was published by the Geological Society of London in 2011 on the 'Geological Record of Neoproterozoic Glaciations' (Arnaud et al., 2011). This volume includes 10 review papers summarising the state of the science with regards to geological and climatological understanding of the Neoproterozoic glaciations, alongside 60 studies of globally distributed sedimentary successions. These studies emphasise the abundant evidence for a glacial influence on deposition, the resolution of (and gaps in) the geochronologic and chemostratigraphic records, the prevalence of mass flow depositional processes, and begin to outline the important interplay of the tectonic basin configuration (Arnaud et al., 2011). Overall, however, there is scant reference to the nature of the ice masses, and even less to the glacier thermal regime (Arnaud et al., 2011). Several studies note evidence for glacial advance and retreat sequences (e.g. Allen et al., 2011; Shields-Zhou et al., 2011; Prave et al., 2011), although few attempt to sequence these trends in detail (e.g. Link & Christie-Blick, 2011; Stouge et al., 2011). A small number of studies report evidence of glaciotectonic deformation, with a few notable exceptions (e.g. Arnaud & Fairchild, 2011; Hoffman & Halverson, 2011; Rocha-Campos et al., 2011), and micromorphological techniques are applied to <10% of the studied sections (e.g. Guimarães et al., 2011; Lund et al., 2011; Master & Wendorff, 2011). Crucially, within this volume, less than a third of the studies discuss deposits confidently associated with the Sturtian interval (Arnaud et al., 2011), demonstrating their distinct under-representation in the published record.

1.4. Thesis outline

The available conceptual and climatic models fail to provide a comprehensive explanation of phenomena observed in the geological record, whilst key inferences from the geological record on the scale, behaviour and thermal regime of the ice masses remain to be carried out. Evidently, therefore, further examination of the preserved record is required before reliable advances can be made. This thesis focuses on the Sturtian glacial interval due to **A)** the paucity of sedimentological data as compared to the younger Cryogenian glaciation, **B)** the poorly understood preservation of associated ironstones, and **C)** the abundance of rift-related successions which provide a tectonic context for glaciation.

The thesis applies detailed sedimentological analyses to three broadly age-equivalent but geographically distinct Sturtian glaciogenic successions in northern Namibia (Chapter 3), southern Australia (Chapter 4) and western USA (Chapter 5). Macro- and micro-scale sedimentology permits characterisation of the processes and environments of deposition, and hence the changing glacial influence on sedimentation. This enables both the dynamics of glacier advance-retreat cycles to be elucidated, and the relative position of the ice front to be mapped out. Examination of geographically discreet successions therefore provides insight into the styles of glaciation on both a local and regional scale, but in the absence of reliable chronostratigraphic markers does not attempt a temporal correlation. The thesis comprises a series of papers, each written as a stand-alone contribution, which together provide a broad synthesis of Sturtian glaciomarine depositional settings and the glaciology of the Cryogenian icehouse. Chapter 3 (Busfield & Le Heron, 2013; Le Heron et al., 2013a, b), Chapter 4 (Busfield & Le Heron, 2014; Le Heron et al., 2014a) and parts of Chapter 5 (Busfield & Le Heron, in press; Le Heron et al., 2014b) have already been published, whilst the remainder of Chapter 5 is accepted for publication (Le Heron & Busfield, accepted). The results of this research, its implications for the extent and distribution of Sturtian ice masses, and how it addresses the aims and objectives outlined below will be synthesised in Chapter 6.

1.4.1. Aims and objectives

The over-arching aim of this thesis is to improve the resolution of the sedimentary record during the Sturtian glacial interval at geographically discrete and sedimentologically diverse study sites. Within this remit, this work will seek to address a series of constituent aims, outlined below;

1. *Characterise the spectrum of glacial depositional environments preserved in the Sturtian record.*

The nature of the depositional environments and their sedimentary processes, the relative glacial influence on sedimentation (i.e. proximity of the ice margin), and the nature of the preserved record remains to be addressed in several glacially-influenced Neoproterozoic basins.

2. *Assess how ironstones relate to Sturtian glaciation.*

The re-emergence of ironstones in the stratigraphic record after a c. 1 billion year hiatus concomitant with early Cryogenian glaciation has been used to suggest a genetic link. In order to test this hypothesis a detailed understanding of the sedimentology and depositional history of these ironstones, and especially their stratigraphic relationship with glaciogenic deposits, is required.

3. ***Examine the influence of basin configuration on the preserved sedimentary record.***

Arguments favouring a predominantly rift-related origin for Cryogenian sedimentary sequences (e.g. Zipper-Rift hypothesis) demonstrate the need to clearly outline the influence of the syn-sedimentary basin configuration, how this can be differentiated from the influence of glaciation, and most importantly how the two interact.

4. ***Assess the behaviour and thermal regime of Sturtian ice masses.***

The question of how dynamic Sturtian ice masses were, their mobility and their glacial thermal regime are integral to characterising the Sturtian icehouse and model predicitions of Neoproterozoic glaciation.

5. ***Attempt to constrain the location of the ice front, and by extension the scale of Sturtian ice masses.***

The ice margin is an extremely important setting for understanding the nature of the subglacial bed, the dynamics of the overriding ice sheet and for mapping out the changing positions of the terminus, and therefore both the extent and behaviour of Neoproterozoic ice sheets.

1.4.1.1. Objectives

- At each study site, the detailed macro-scale sedimentology of the sections will be recorded in order to characterise the sedimentary facies, sedimentary stacking patterns (i.e. grading pattern), contact relationships and syn-sedimentary deformation structures. Orientated samples will be collected for thin section analyses, and palaeocurrent indicators will be measured where possible. These data will enable an assessment of the array of facies and depositional processes recorded in Neoproterozoic glacial sedimentary environments, the palaeoflow across the glaciated margin and of the ice itself to be examined, and compared, and the criteria for recognising a glacial influence on sedimentary sequences to be critically evaluated. Where present, the contact relationships between ironstone facies and glaciogenic facies will be analysed in detail to inform understanding of any genetic relationship.

- The sedimentology and structural fabrics of thin sections will be analysed using standard micromorphological techniques. This will provide further evaluation of the criteria to distinguish glacial and non-glacial sedimentary rocks, especially in relation to glaciotectonic deformation features, additional palaeocurrent data through measurement of micro-scale kinematic indicators, and a relative chronology

of deformation events through examination of cross-cutting fabrics and structures, often more clearly picked out under cross-polarised light (e.g. plasmic fabrics, see Chapter 2).

- The nature and extent (i.e. proximity) of glacial influence on sedimentary packages will be assessed in the context of glacial advances and retreats in order to characterise both the scale and mobility of ice masses feeding the basin. The sedimentary stacking patterns, key bounding surfaces and advance/retreat signature of these sequences will be used to generate a glacial sequence stratigraphic framework. This will enable the criteria to define an advance or retreat sequence to be critically evaluated, and the nature of these records across different basins and especially different tectonic configurations to be assessed, e.g. under variable accommodation. This will be explored as a potential higher resolution framework on which to pin geochronological, palaoemagnetic and chemostratigraphic data as they become available, and thus facilitate future regional to possibly global correlation.

- The macro- and micro-scale sedimentology, palaeoflow, deformational history and advance-retreat cyclicity of these sequences will be used to inform detailed depositional models and palaeoenvironmental reconstructions of individual basins during the Sturtian glaciation. This will enable the style of deposition, dynamics of the ice masses and nature of the preserved depositional record to be compared between basins in order to assess whether the sedimentary systems and ice masses behaved in a similar manner. This will not be an attempt at chronostratigraphic correlation, but will aim to characterise common (or unique) depositional processes, ice mass mobility and glacier thermal regimes active during the Sturtian icehouse and how they fit into the broader context of the Cryogenian cryosphere.

The methodologies utilised to address these objectives, alongside a critical evaluation of these techniques, is provided in Chapter 2 below. The aims and objectives outlined above provide the basis for the research presented in the main body of the thesis (Chapters 3-5), and will be specifically addressed in the concluding synthesis (Chapter 6.)

2. Methods

2. Methods

This chapter details the sedimentological, stratigraphical and structural techniques used to answer the research aims and objectives outlined in Chapter 1. Although the methods employed are widely recognised as standard techniques, they each have their own limitations, and can be subject to varying approaches depending on disciplinary background (geology, geography, soil science etc.). As such, in each case the rationale behind the approach will be described, the chosen technique explained, and the potential restrictions to each method will be critically evaluated. One of the over-arching problems with cross-disciplinary methods, e.g. sedimentology, is a multitude of competing and oft misconstrued terminology and therefore the definitions and origins of the preferred nomenclature throughout this thesis will be offered herein (**Tables 2.1-2.4**). The research methods employed in this thesis can be broadly categorised under three components: 1) Sedimentary logging, 2) Thin section analysis, and 3) Sequence stratigraphy. These will be described in turn below.

2.1. Sedimentary logging

2.1.1. Rationale of approach

Sedimentary logging offers a systematic and standardised method of recording sedimentary data in the field in a format which is widely recognised and therefore widely accessible. Significantly, it offers a template onto which a growing body of data can be added over time, and therefore with the view to improving the resolution of the Neoproterozoic glacial record (Chapter 1) it is an extremely valuable tool. This approach also readily facilitates correlation between locally and regionally distributed study sites, and offers a strong visual comparison between the globally widespread successions studied within this thesis.

2.1.2. Sedimentary logging technique

Field data collection – Graphic sedimentary logs were typically produced at either a 1:2 or 1:5 (cm:m) scale in order to record the maximum level of detail within the available time, usually equivalent to between 100 and 300 m of logged section per day. Sedimentary sections were logged, described and photographed to record textural characteristics (e.g. grain size, sorting, colour), structural characteristics (e.g. sedimentary structures, bedding, folding), a qualitative assessment of clast lithology and shape, and any lateral and vertical changes (e.g. bed thickness and geometry, stacking patterns) following standard sedimentological techniques (Tucker, 1996, 2011; Hubbard & Glasser, 2005). Where possible, palaeoflow data were collected through measuring

either the azimuth of apparent flow, or the dip and dip direction of ripple foresets or fold limbs. These were later corrected for regional dip using recorded bedding data and Stereonet 7 software (see Allmendinger et al., 2012).

In each study site, vertical continuity of exposure was sought through careful reconnaissance, including tracing beds a short distance (<10 m) along strike to a better preserved exposure, or beginning a new log further along strike where this was not possible. In areas of comparatively poor exposure composite logs were generated (e.g. Le Heron et al., 2013a), although this was avoided as much as possible. Multiple GPS co-ordinates were recorded against the logged sections to ensure upper and lower contacts and key horizons (e.g. particularly thick or distinctive beds) could be accurately located and correlated as necessary.

Illustration and facies description – All logged sections were illustrated using Adobe Illustrator CS5 or CS6, where clast morphologies, sedimentary textures and bed boundaries were drawn to replicate field observations as closely as possible. Standard sedimentological symbols were used to denote grading patterns, sedimentary structures, onlap/offlap relationships and lithology (see Nichols, 2009).

Sedimentary facies were described and grouped into distinct facies associations (see **Table 2.1** for definitions), defined on the basis of common lithological characteristics as opposed to genetic classifications. This descriptive approach was adopted to retain clear distinction between sediment description (the raw data) and depositional history (interpretation of the data), and to avoid blanket interpretations of facies which share many lithological characteristics, but not the same key diagnostic criteria (e.g. dropstones). Facies classifications therefore follow the descriptive approach of Moncrieff (1989), as illustrated in **Table 2.2** (modified after Hambrey & Glasser, 2003).

2.1.3. Limitations

Sedimentary logging is a well recognised, widely used descriptive and illustrative tool for analysing sedimentary sequences. However, there is scope for subjectivity on how the data is recorded, presented and interpreted depending on the disciplinary background and experience of the author and the reader. This in itself was a strong motivator for adopting a descriptive rather than genetic classification approach. In this case, data are recorded in a standardised sedimentological format (after Tucker, 1996, 2011), using quantitative grain size (after Wentworth, 1922) and textural classifications (after Moncrieff, 1989 as modified by Hambrey & Glasser, 2003), designed to ensure objective field data collection. Any subjectivity with regards to genetic

classification is therefore restricted to facies interpretations, and can be clearly differentiated from the core data.

Another key limitation, especially in the case of cross-disciplinary research, is terminology. The use of descriptive or genetic nomenclature has already been discussed as an important consideration, and this is especially true where the genetic connotation of the term can be extremely variable. A classic example in the case of glacial sedimentary systems is the term 'till' (or its lithified equivalent 'tillite'). This term can be used to denote material deposited directly from a glacier or ice mass (sensu Lawson, 1981) or expanded to include all poorly sorted sediment containing glacially transported material (sensu Harland et al., 1966), the latter incorporating both re-worked and directly deposited glacial material. To avoid this possible ambiguity the terms 'primary till' for directly deposited glacial material and 'secondary till' for resedimented glacial material were introduced (Dreimanis, 1989), although these still encompass a broad spectrum of melt-out, lodgement, sublimation, deformation, squeeze flow and flow tills, and offer little clarification for material re-worked within, on top of and below the ice itself. As such, throughout this thesis the applied interpretive nomenclature is process-derived, with the prefix glacio- or glaciogenic as appropriate, e.g. glaciogenic debris flows. This has the benefit of avoiding potentially mis-leading genetic terminology, and retains consistency across all sedimentary facies, with or without a direct glacial influence. Of course some non-genetic terminology is also subject to various definitions, most notably the term 'diamicton' (or its lithified equivalent 'diamictite'), and therefore the definitions favoured throughout this thesis are provided in Table 2.1 for clarification.

Several studies of glaciogenic sediments adopt a system of lithofacies codes to categorise facies and facies associations, where given letters are used to denote specific lithological, textural and structural criteria (e.g. Eyles et al., 1983; Evans & Benn, 2004). This system was designed as a rapid and systematic means of identifying sediments, and retaining consistent nomenclature for different lithofacies across numerous studies. However, several of the designated codes have genetic implications, thereby resulting in interpretive nomenclature before detailed facies interpretations have been made. Additionally, the multitude of codes adopted within this system can prove difficult to follow, especially across a multi-disciplinary audience who may or may not be familiar with the various complex acronyms. The descriptive method adopted herein is considered a more accessible system, not reliant on learning a prescriptive set of codes, and one which is consistent in distinguishing sedimentary observations and interpretations throughout.

	Name	Φ (phi)	Description	Origin
Non-genetic classification				
Mud(stone)			Fine-grained argillaceous sediment/rock containing a mixture of clay (<4 μm) and silt (>4 μm) sized particles	Stow (1981), Allaby & Allaby (2003), Middleton (2003)
Clay(stone)		8	Fine-grained argillaceous sediment/rock containing predominantly (>67%) clay sized particles (<4 μm)	
Silt(stone)		7 6 5	Fine-grained argillaceous sediment/rock containing predominantly (>67%) silt sized particles (>4 μm)	
Sand(stone)	Fine sand	4 3	Siliciclastic sediment/sedimentary rock consisting of grains 63 to 2000 μm in size	
	Medium	2		
	Coarse	1		
	Very coarse	0		
Granule(stone)		-1 -2	Siliciclastic sediment/sedimentary rock consisting of grains 2 to 4 mm in size	Allaby & Allaby (2003), Middleton (2003), Nicholls (2009)
Conglomerate	Pebble	-3 -4	Siliciclastic sediment/sedimentary rock with rounded clasts 4 to 64 mm in size	
	Cobble	-5 -6 -7	Siliciclastic sediment/sedimentary rock with rounded clasts 64 to 256 mm in size	
	Boulder	-8	Siliciclastic sediment/sedimentary rock with rounded clasts >256 mm in size	
Breccia			Siliciclastic sediment/sedimentary with angular clasts >4mm in size (pebble, cobble or boulder)	
Diamict(on/ite)			Non-sorted or poorly sorted terrigenous or marine sediment that contains a wide range of particle sizes and between 1-50% gravel content (particles >2 mm in size)	Modified after Flint (1960), Moncrieff (1989), Hambrey & Glasser (2003)
Ironstone			Sedimentary rock containing >15 wt.% Fe_2O_3	James (1954)
Limestone			Calcareous sedimentary rock composed predominantly of calcium carbonate	Allaby & Allaby (2003), Nicholls (2009)
Dolomite/stone			Calcareous sedimentary rock composed predominantly of calcium magnesium carbonate	
Genetic classification				
Turbidite			Sedimentary deposit of a turbidity current (i.e. a turbulent sediment gravity flow)	Allaby & Allaby (2003), Nicholls (2009)
Debrite			Sedimentary deposit of a debris flow (i.e. a laminar sediment gravity flow)	
Glaciotectonite			Body of sediment deformed by glacial stresses when in an unlithified or semi-lithified state	Modified after van der Wateren (2002) and Benn & Evans (2010)
Till(ite)	Primary		Unsorted deposit with a wide range of grain sizes deposited by direct glacial processes i.e. melt-out, lodgement, sublimation or deformation by the ice	Dreimanis (1989), Hambrey (1994)
	Secondary		Remobilised sediment which was initially deposited by direct glacial processes, and now contains re-worked glacially transported material	

Table 2.1: Non-genetic and genetic terminology for sediments and sedimentary rocks used throughout this thesis

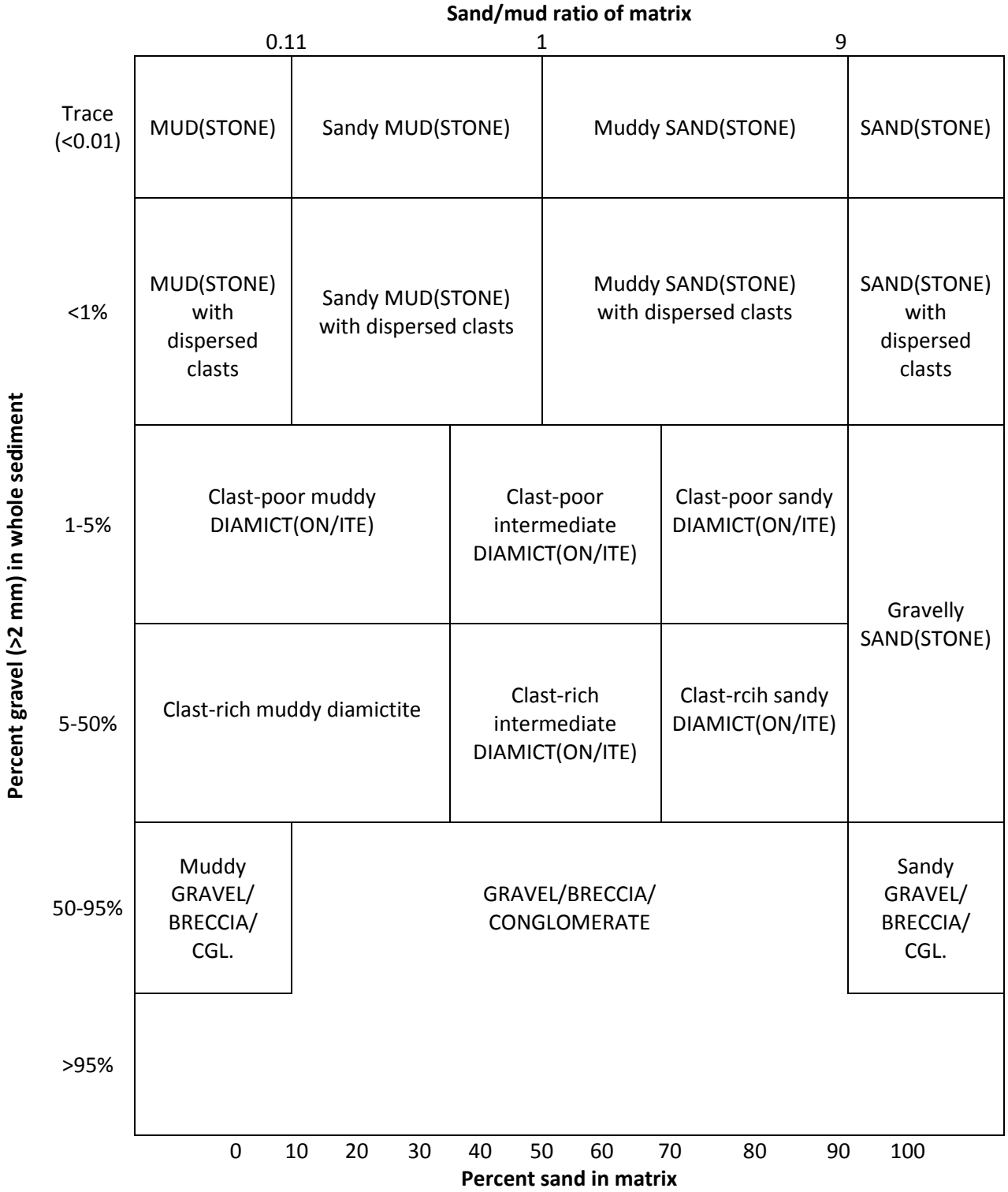

Table 2.2: Textural classification for clastic sediments and sedimentary rocks used to inform descriptive facies approach used in this thesis. Modified after Moncrieff (1989) and Hambrey & Glasser (2003).

2.2. Thin section analysis

2.2.1. Rationale of approach

Analysis of rock and (soft) sediment thin sections enables both qualitative and quantitative examination of sedimentary textures, lithological composition, fabrics and structures on the micro-scale. This has proven to be a particularly useful tool in the analysis of diamicts and diamictites which are typically massive on the macro-scale, but can yield a huge amount of detail on the micro-scale. In the context of glacial sedimentary systems, these techniques play an integral role in differentiating remobilised glacial sediments from those directly deposited by the ice, in distinguishing the products of mass movement or glaciotectonic deformation, and, of particular importance in ancient depositional systems, in identifying syn-sedimentary or post-depositional (tectonogenetic) deformation.

2.2.2. Thin section analysis technique

Sampling strategy – Samples were collected from sedimentary units whose macro-scale sedimentology was unclear (typically massive diamictites) or those which exhibited clear macro-scale deformation structures. Under the latter scenario, the sequence was sampled at intervals where macro-scale changes in deformation style were apparent, with a view to examining a broad spectrum of structures at the micro-scale, alongside any up-section evolution in deformation regime. Since the studied sedimentary rocks were well lithified, sampling was possible using a rock hammer, often exploiting pre-existing weaknesses such as bedding, and thus avoiding significant damage to the outcrop. Care was taken to accurately orientate the samples relative to depositional way up, and the strike of the sample was measured to ensure any kinematic indicators could be correctly orientated.

Thin section production – Thin sections were cut parallel to the recorded strike of the sample as well as perpendicular to this cut, in order to appreciate the 3D orientation of micro-scale structures. Thin sections were cut using standard rock thin sectioning procedures by Neil Holloway in the Department of Earth Sciences at Royal Holloway.

Thin section analysis – Thin sections were analysed using a petrographic microscope at low magnification (1x and 2x), under both plane- and cross-polarised light, alongside examination of high resolution photographs and digital scans of the sections. Micro-scale features were described using standard sedimentological, structural and micromorphological techniques (sensu van der Meer, 1993; Menzies, 2000a; Tucker, 2001).

Micromorphology, although originally developed within the soil science community (Brewer, 1976), has seen a growing application in Quaternary science (Lachniet et al., 2001; Menzies & Zaniewski, 2003; van der Meer & Menzies, 2011) and more recently in studies of ancient sedimentary systems (Benn & Prave, 2006; Arnaud, 2008, 2012; Fleming, 2014) as a descriptive, illustrative and quantitative method of analysing sediments on the micro-scale. This includes widely applicable, non-genetic terminology (see **Table 2.3**), a method of systematically and objectively illustrating sediment thin sections (Phillips et al., 2011), and quantitative counts of the number and frequency of individual features (e.g. Carr et al., 2006).

Analysed thin sections in this thesis were illustrated using Adobe Illustrator CS5 or CS6, wherein an interpretive sketch was drawn to highlight the micro-scale sedimentology (lithology, lamination, grading), clast fabrics (morphology, distribution), and the nature of sedimentary and deformation structures (brittle/ductile, vergence, shape). These interpretive sketches were displayed adjacent to the high resolution photographs of the thin sections in order that the raw data and interpretive data remained distinct, and accompanied by annotated high magnification (4x and 10x) photographs of individual features, as seen in both plane and cross-polarised light.

2.2.3. Limitations

As with the sedimentary logging technique, one of the key considerations in methods of thin section analysis is the choice of terminology. This is partly due to the sometimes disparate communities working on active, Quaternary or ancient (pre-Pleistocene) glacial sedimentary systems. For example, micromorphology is now a widely recognised approach in both soil science and Quaternary sedimentology (e.g. van der Meer & Menzies, 2011), but has demonstrated a comparatively slower uptake in ancient sedimentary systems where 'standard' geological terminology prevails. Over the past 20 years, Quaternary studies have been at the forefront of micro-scale analyses of glacial sediments, and have played a key role in demonstrating the value of the approach for distinguishing different sedimentological and deformational processes, as well as recognising and naming important diagnostic criteria (e.g. Lachniet et al., 2001; Menzies & Zaniewski, 2003; Phillips et al., 2007; van der Meer & Menzies, 2011). Given that these studies adopted the micromorphological approach, this nomenclature has become standard in association with micro-scale glacial sedimentology, and therefore equivalent 'geological' terms are not always available. Studies within this thesis, alongside a growing number of other studies in ancient glacial regimes (Menzies, 2000b; Fleming, 2014; Ravier et al., 2014), have therefore chosen to adopt the micromorphological approach, and recognise the potential for it to become a 'standard'

Name	Description	Origin
Birefringence	The double refraction of light under crossed polarisers where one ray of light is retarded relative to the other. Enables interference colours to be visualised by turning the stage of the microscope	Brewer (1976), Menzies (2000a), Allaby & Allaby (2003)
Cutan	Material, typically clay, accumulated on or against surfaces or structural elements e.g. *skeleton grains*, walls of pores	Allaby & Allaby (2003), Zaniewski & van der Meer (2005)
Dispersion tail	Concentration of smaller grains or *plasma* in the lee of a larger grain	Brewer (1976), Busfield & Le Heron (2013b)
Domain(s)	Small zones where similarly orientated clay particles behave (optically) like a single crystal	Menzies (2000a), van der Meer et al. (2012)
Intraclast(s)	Fragment of sediment re-worked in soft sediment (unlithified) state, typically clay or silt grade	Modified after van der Meer et al. (2012)
Matrix	Interstitial material between larger particles, fragments or crystals. See also *plasma*	Menzies (2000a), Allaby & Allaby (2003)
Necking structure	Variety of *turbate structure*. Alignment of smaller grains occurs between adjacent larger grains	Lachniet et al. (1999)
Plasma	Clay sized (<4 μm) particles occupying interstitial space between larger particles. May exhibit *birefringence*. See also *matrix*	Menzies (2000), Zaniewski & van der Meer (2005)
Plasmic Fabric	Orientation of *plasma domains* based on the optical properties (*birefringence*) of aligned *plasma* particles. Common varieties include:	Brewer (1976), Menzies (2000a), Zaniewski & van der Meer (2005), Busfield & Le Heron (2013)
Asepic	Anisotropic *plasma domains*, little to no preferred orientation. Argillasepic = dominantly clay-sized particles. Silasepic = dominantly silt-sized particles	
Masepic	Short *domains* with a single preferred orientation	
Bimasepic	Two dominant preferred orientations. Termed Lattisepic where these directions are perpendicular	
Insepic	Small clusters of orientated *plasma* particles where clusters show no preferred orientation	
Multisepic	Multiple (>2) preferred orientations	
Skelsepic	Fabric preferentially orientated around *skeleton grains*	
Omnisepic	Random orientation of various *plasma domains*	
Unistrial	Elongate, discrete bands of *birefringent plasma*	
Pressure shadow	Typically massive *domain* of lower strain adjacent to a clast. Synonymous with strain shadow	Phillips et al. (2011)
Turbate structure	Circular arrangement of grains around a core stone or rigid matrix. Long axes of orientated grains exhibit a parallel or radial orientation relative to the margins of the core	Hiemstra & Rijsdijk (2003)
Skeleton grain(s)	Single grains larger than clay particles (>4 μm) which can thus be studied individually. Synonymous with clast(s)	Modified after van der Meer et al. (2012)

Table 2.3: Non-genetic terminology to describe sediments and sedimentary rocks on the micro-scale, as used throughout this thesis.

technique across multiple disciplines. In the meantime, and to avoid possible confusion, a glossary of terms is provided within the relevant results chapters (e.g. Chapter 3.3), and in **Table 2.3** above.

With the view to developing an objective approach to micro-scale analyses, Phillips et al. (2011) devised a 'microstructural mapping' technique which advocates following a systematic step-by-step guide to thin section illustration and interpretation. This methodology involves initially illustrating the scanned or photographed thin section by drawing on clast long axes, then identifying lines of similarly orientated long axes, before grouping these lines into bands or clusters of shared orientation. This in theory enables the deformation fabric of each zone to be identified, and most importantly highlights the cross-cutting nature of different bands of fabric so that a relative chronology of deformation events can be produced. However, this technique is partially dependent on having a suitably clast-rich thin section, and also relies on a high proportion of elongate clasts so that the clast long axes can be readily distinguished. There is also a potential scale limitation in standard rock thin sectioning procedures, where cut sections typically measure 50 x 25 mm, significantly limiting the scale of clasts, fabrics and structures visible compared to the 90 x 65 mm sections standard in Quaternary soft sediment thin sectioning procedures (Palmer et al. 2008; Lea & Palmer, 2014).

Although designed as an objective analysis tool, one of the major limitations of the 'microstructural mapping' technique, as well as thin section micromorphology more generally, is the issue of subjectivity. Attempting to map trains or bands of similarly orientated clasts is in essence a method of pattern spotting, and anyone who has spent enough time staring at sediment thin sections will realise it's easy to spot patterns when looking for them. This technique has been successfully applied to several Quaternary soft sediment thin sections (e.g. Phillips et al., 2011; Narloch et al., 2012; Vaughan-Hirsch et al., 2013), but did not prove effective in its application to the Neoproterozoic thin sections analysed herein. In this case, it was difficult to have confidence in the numerous possible patterns revealed, and therefore a simple illustrative and descriptive technique was adopted in its place. Interpretive sketches were used to highlight key features clearly visible in the raw image (photograph/scan of the thin section), without illustrating subjective patterns or fabrics over the image. It is contended that the availability of larger rock thin sections, or more clast-rich sediment samples may prove more amenable to the mapping technique.

Through statistical and psychological experiments, Leighton et al. (2013) determined that operator bias does exist in micro-scale analyses, which can be a factor of the operator's previous experience, as well as a sub-conscious drive towards success through achieving consistent analyses (e.g. similar numbers of observed features) across different samples or studies. In order to mitigate operator bias, samples were routinely

compared to recorded examples of individual features to ensure consistent identification, and identified features were verified between the authors of the studies to certify their uniform recognition (e.g. Busfield & Le Heron, 2013, 2015). Thin section analysis was conducted in short (< 1 hour) intervals to avoid learned base rates in the number of features anticipated to be identified, in addition to inherited 'pattern spotting' behaviour through over-exposure. Leighton et al. (2013) demonstrate that, despite inherent bias, the observer sensitivity (i.e. ability to recognise micro-scale features) increases with observer experience. These additional considerations are therefore designed to ensure a more neutral response bias, avoiding over-conservative or over-liberal detection of individual features.

2.3. Glacial sequence stratigraphy

2.3.1. Rationale of approach

An important aspect of improving the resolution of the Neoproterozoic glacial sedimentary record is a detailed understanding of ice mass behaviour and mobility, as reflected in the preservation of advance, retreat or stillstand sequences. Therefore a glacial sequence stratigraphic framework was developed in order to identify sets of genetically related strata, and their key bounding surfaces, relative to the first-order control of glacier or ice mass dynamics, as opposed to typical external forces such as eustacy or isostacy. The rationale behind this scheme was to define criteria which could be used to recognise advance or retreat trends in the depositional record, particularly where preserved successions are thin or incomplete. This framework could also facilitate integration of future geochronological data as they become available, with the view to characterising the changing mass balance of these ice masses in both time and space.

2.3.2. Glacial sequence stratigraphic framework

Under the sedimentary logging technique, the nature of bed boundaries (erosional, onlapping, offlapping, conformable, unconformable) was identified, alongside the style of sedimentary stacking patterns (normally graded, reverse graded, ungraded). Key bounding surfaces were identified through the preservation of major disconformities or laterally extensive changes in facies character, and numbered sequentially up-section as individual sequence boundaries. Progradational, retrogradational or aggradational sedimentary architectures could then be determined between each sequence boundary, through careful examination of the sedimentary stacking patterns (see **Table 2.4** for definitions).

Term	Definition	Origin
Sequence stratigraphy	Chronostratigraphic framework for the analysis of genetically related sediment packages, and their relation to sea-level changes.	Modified after Allaby & Allaby (2003), Nichols (2009)
Stacking/ Grading pattern	The overall vertical grading pattern of sedimentary bedsets i.e. normal (retrogradational), reverse (progradational) or ungraded (aggradational).	Le Heron et al. (2013b), Busfield & Le Heron (in press)
Glacial sequence stratigraphy	Sequence stratigraphic model driven by glacier dynamics, and independent of other external forces e.g. eustacy, isostacy.	Powell & Cooper (2002), Busfield & Le Heron (2014)

Individual systems tracts and sequence boundaries are recognised as:

Acronym	*Definition*	*Characteristic features*
GAST	Glacial Advance Systems Tract	- Basal erosion surface(s) - Coarse-grained, coarsening upwards sediment packages - Thin/absent outcrop exposure - Direct glacial influence e.g. rain-out, glaciotectonism
GRST	Glacial Retreat Systems Tract	- Planar/onlapping basal surfaces - Fine-grained, fining upwards sediment packages - Thick, well preserved outcrop exposures - Little direct glacial influence, re-worked or rafted glacial debris
GMaST	Glacial Maximum Systems Tract	- Most ice-proximal sediments within sequence - Aggradational to progradational stacking pattern - Direct glacial influence e.g. rain-out, glaciotectonism, subglacial deposition - Often associated with GES
GMiST	Glacial Minimum Systems Tract	- Least ice-proximal sediments within sequence - Retrogradational or aggradational stacking pattern - Little direct glacial influence and/or evidence of ice-free conditions - Often associated with ITS
GAS	Glacial Advance Surface	- First (re)appearance of IRD (offshore) - Progradational wedge (onshore) - Sharp contact, may show abrupt facies dislocation - Onset of advance systems tracts; overlain by GAST
GES	Glacial Erosion Surface	- Regional scale unconformity - Significant sequence boundary
ITS	Iceberg Rafting Termination Surface	- Last stratigraphic appearance of IRD - Onset of retreat systems tracts; overlain by GRST

Table 2.4: Glacial sequence stratigraphic terminology, and characteristic features of individual systems tracts, modified after the scheme of Powell and Cooper (2002) as applied to the Neoproterozoic successions in Busfield and Le Heron (2014).

The sequence stratigraphic framework was developed following the model of Powell and Cooper (2002), which applied the approach to temperate, glaciated fjord and shelf regions in Alaska. Glacial advance systems tracts (GAST) were recognised through the association of glacial erosion surfaces (GES), an influx of coarser grained deposits, often within coarsening upward packages, and an increase in glaciogenic indicators e.g. striated clasts, ice-rafted debris. Conversely, glacial retreat systems tracts (GRST) were associated with regressive (onlap) surfaces, finer grained sediment typically with normally-graded stacking patterns, and a general paucity of glaciogenic indicators (see Busfield & Le Heron, 2014). The onset of advance, or the glacial advance surface (GAS), was attributed to the first appearance of IRD, and the last appearance attributed to the onset of retreat, termed the iceberg rafting termination surface (ITS, Powell & Cooper, 2002).

2.3.3. Limitations

The glacial sequence stratigraphic method again introduces a new set of nomenclature which may or may not be familiar to a multi-disciplinary audience, and therefore definitions are available in **Table 2.4** above. Within the sedimentological community, sequence stratigraphic terminology is widely recognised (e.g. Catuneanu, 2006; Emery & Myers, 2009), and therefore its modification in the context of glaciated basins should not be particularly mis-leading. It is recognised that the use of associated acronyms could cause confusion, and care has been taken throughout this thesis to avoid the use of erroneous acronyms, but they are retained here for simplicity and concision. Their definitions are provided in the relevant results chapters (see also **Table 2.4**).

The major limitation of the glacial sequence stratigraphic scheme is that it is clearly far from being consistently replicable at present, which is partly dependent on identifying a comprehensive set of 'testable' criteria. For example, the appearance of ice-rafted debris is not in itself a reliable indicator of glacial advance (sensu Powell & Cooper, 2002) since the calving of icebergs is a significant contributor to mass loss (Benn et al., 2007). At the same time, other features which would be robust indicators of advance, e.g. subglacial deformation, were not recorded within the original framework (Powell & Cooper, 2002), although their importance has been recognised within sequence stratigraphic schemes elsewhere (e.g. Pederson, 2012). Nonetheless, the scheme can produce a much higher resolution glacial history than standard sedimentological observations alone, and where correlation between sections is possible, does offer important insight into the differential preservation of advance and retreat sequences across areas of variable accommodation space (see Busfield & Le Heron, 2014).

3. Northern Namibia

3.1. Introduction

Northern Namibia can be thought of as the birthplace of the modern Snowball Earth hypothesis, representing the first sedimentary section where the early ideas of Kirschvink (1992) were applied and expanded in detail (Hoffman et al., 1998). As with many Cryogenian successions, two glacial intervals are commonly recognised throughout Namibia, the older Chuos Formation (Sturtian equivalent) and younger Ghaub Formation (Marinoan equivalent). Evidence for a glacial influence in the Chuos was first recognized in the central Damara Belt (Gevers, 1931), and later correlated with the 'Varianto' Formation in the Otavi Mountainland (Hoffmann & Prave, 1996). In this region, previous studies had variously referred to the younger glacial horizon as the 'Otavi Tillite' (Le Roex, 1941) or the 'Chuos Formation' (Hedberg, 1979), which was later re-named the Ghaub Formation to avoid confusion (Hoffmann & Prave, 1996).

The majority of recent studies have concentrated on the younger Ghaub Formation (e.g. Hoffman, 2005; Bechstädt et al., 2009; Domack & Hoffman, 2011), especially its relation to the Snowball Earth hypothesis (Hoffman et al., 1998; Eyles & Januszczak, 2007), with little examination of the Chuos Formation since the work of Henry et al. (1986) in the central Damara Belt. Several authors have argued in favour of a glacial influence on deposition (e.g. Martin, 1965; Hedberg, 1979; Henry et al., 1986), facing fierce opposition from those preferring a non-glacial sediment gravity flow interpretation (e.g. Miller, 1983; Porada, 1983; Porada & Wittig, 1983a,b; Martin et al., 1985). Within proponents of the glacial hypothesis, the mode of deposition, i.e. whether proglacial or subglacial, remains unclear (Hoffman, 2011). Significantly, the Chuos Formation includes thick, well preserved ironstone facies whose stratigraphic and genetic relationship to the glacial deposits awaits further testing (Martin 1965; Hoffman & Halverson, 2008).

This chapter comprises three studies in the Otavi Mountainland and eastern Kaokoveld which critically examine: 1) the sedimentology of associated ironstone facies (Chapter 3.2); 2) the glaciotectonic origin of macro- and micro-scale deformation structures (Chapter 3.4); and 3) the evidence for a changing glacial influence on the sedimentology of a palaeovalley fill (Chapter 3.3). These studies will therefore shed light on the nature of Sturtian glacial depositional environments in northern Namibia, the genetic link between ironstone deposition and glaciation, and the relative position of the ice front and its implications for the scale and mobility of ice masses at this time.

3.2. Stromatolitic ironstones, Otavi Mountainland

Neoproterozoic ironstones in northern Namibia: Biogenic precipitation and Cryogenian glaciation

Le Heron, D.P., Busfield, M.E., Le Ber, E. and Kamona, A.F.

Palaeogeography, Palaeoclimatology, Palaeoecology 2013a, v. **369**, 48-57.
doi:10.1016/j.palaeo.2012.09.026

Statement of contribution

- ***Data collection***
  - Busfield and Le Heron logged the ironstone and diamictite sections in the Otavi Mountainland (Figs. 1b & 3), and Busfield collected rock samples for later lithological analysis.
  - Busfield and Le Heron developed preliminary interpretations of the facies and depositional processes. Le Heron raised the analogy of iron-reducing microbial communities in acid mine drainage environments, and Busfield developed early ideas of photosynthetic CO_2 drawdown and the requirement for ice minimum conditions to provide sufficient photic energy to sustain microbial communities.
  - Busfield logged and collected samples from comparable microbial-bearing ironstone facies in the Opuwo region, north-western Namibia, where the intercalation of diamictites and ironstones is more pronounced, and where dropstone structures are preserved within ironstone facies (Fig. 7), re-enforcing preliminary ideas of a gradational transition between the ironstone and overlying glaciogenic diamictites.
- ***Manuscript text***
  - Le Heron wrote the first draft of the manuscript whilst in the field on the back of Le Heron and Busfield's preliminary discussions. Le Heron also invited Le Ber to examine the stromatolite structures by comparison to his own work on the overlying Berg Aukas Formation.
  - Busfield co-authored subsequent and final drafts of the manuscript by modifying the text throughout.
  - Le Ber and Kamona reviewed an early draft of the manuscript.
- ***Figures***
  - Figures 1-3 were illustrated by Le Heron, and Figure 5 by Le Ber.
  - Busfield and Le Heron contributed photographs to figures throughout.

Palaeogeography, Palaeoclimatology, Palaeoecology 369 (2013) 48–57

Contents lists available at SciVerse ScienceDirect

Palaeogeography, Palaeoclimatology, Palaeoecology

journal homepage: www.elsevier.com/locate/palaeo

Neoproterozoic ironstones in northern Namibia: Biogenic precipitation and Cryogenian glaciation

D.P. Le Heron [a,*], M.E. Busfield [a], E. Le Ber [a], A.F. Kamona [b]

[a] Department of Earth Sciences, Queen's Building, Royal Holloway University of London, Egham, Surrey, TW20 0BY, UK
[b] Geology Department, University of Namibia, Windhoek, Namibia

ARTICLE INFO

Article history:
Received 24 January 2012
Received in revised form 13 July 2012
Accepted 12 September 2012
Available online 13 October 2012

Keywords:
Ironstone
Snowball Earth
Neoproterozoic
Cryogenian

ABSTRACT

The precipitation of Cryogenian ironstones has been attributed to a spectrum of mechanisms ranging from virtually instantaneous "rusting of the seas" in response to post-snowball Earth ice meltback, to localised hydrothermal activity during fragmentation of Rodinia. The former model presupposes that ironstone deposition took place following peak glaciation. In the Chuos Formation of the Otavi Mountain Land, northern Namibia, ironstone facies precede, and are vertically gradational into, diamictites. Evidence for glaciation in the diamictites includes 1) dropstone textures, 2) subglacially deformed and attenuated, thinly stratified diamictites, supported by 3) the co-occurrence of soft-sediment striations. The underlying ironstones contain evidence for tractional processes (large-scale cross bedding) and biogenic growth (stromatolites) in strata rich in magnetite and hematite. Using the analogy of acidophile biomats in modern acid mine drainage environments, where photosynthetic bacteria construct stromatolites, fixing CO_2 and Fe intracellularly, it is suggested that Cryogenian acidophile biomats did likewise, triggering ironstone precipitation and local CO_2 drawdown, thereby facilitating concomitant glaciation.

1. Introduction

Yeo (1981) first proposed that Neoproterozoic ironstones resulted from hydrothermal activity in small, Red Sea-type rift basins, during the breakup of Rodinia. Conversely, their unusual recurrence in the Cryogenian, following a 1.1 billion year stratigraphic hiatus, led many studies to invoke a direct association with concomitant snowball-type global glaciations (Hoffman and Schrag, 2002). Martin (1965) proposed that Namibian ironstones in the Chuos Formation were deposited due to stagnation under an ice cover. In a global context, this concept was expanded by Kirschvink (1992) who suggested that toward the end of snowball event, where weathering and oxidation of the oceans was inhibited under a carapace of global ice cover, "rusting of the seas" led to deposition of a ferruginous blanket of marine sediment. This hypothesis, however, inadequately accounts for the intra-glacial stratigraphic occurrence of ironstones, particularly in older Cryogenian glacial successions (e.g. Eyles and Januszcak, 2004; Eyles, 2008; Le Heron et al., 2011).

In their recent review of Neoproterozoic chemical sediments, Hoffman et al. (2011) identified three alternative mechanisms of ironstone precipitation under a snowball Earth pretext: 1) ferrous versus euxinic anoxia under a cover of sea ice, 2) subglacial, sulphate-rich ferrous waters, and 3) localization of oxidative titration. This latter mechanism follows from Hoffman and Halverson (2008) who envisaged oxic meltwater plumes, discharged into ferrous basin waters at ice-shelf grounding-lines. These mechanisms require ocean anoxia induced by overlying ice, and do not consider the possibility of non-glacially-induced anoxia, nor fault-related fluids as a source of soluble iron.

Namibia (Fig. 1a) is an excellent natural laboratory in which to test hypotheses of Cryogenian ironstone deposition. The Chuos Formation is a diamictite-rich sedimentary unit of Cryogenian age associated with iron formations whose correlatives are widely distributed across Namibia. The objectives of the present paper are twofold: 1), to present sedimentological evidence for biologically mediated ironstone precipitation in the Chuos Formation and 2) to demonstrate that this ironstone precipitation preceded deposition of observed glaciogenic deposits, based on field observations. Konhauser et al. (2002) argued that chemolithotrophs or photoferrotrophs (bacteria) had the potential to generate most, if not all the ferric iron in Archaean banded iron formations. Those authors did not infer an intracellular iron fixing mechanism, and bacterial precipitation of iron is rarely entertained as a depositional mechanism in younger (Neoproterozoic) strata. Additionally, the implications of this evidence for Cryogenian glacial cycles are discussed, suggesting that in the Chuos, at least, ironstone deposition heralded ice sheet growth.

2. Study area and stratigraphy

The Otavi Mountain Land, in northern Namibia, is an area of extensive outcrop of Neoproterozoic strata at the southern margin of the Owambo Basin (Fig. 1b). The strata comprise two laterally extensive glacial successions, belonging to the Chuos Formation (older Cryogenian) and Ghaub Formation (younger Cryogenian) (Hoffmann

* Corresponding author.
E-mail address: le_herondaniel@hotmail.com (D.P. Le Heron).

0031-0182/$ – see front matter © 2012 Elsevier B.V. All rights reserved.
http://dx.doi.org/10.1016/j.palaeo.2012.09.026

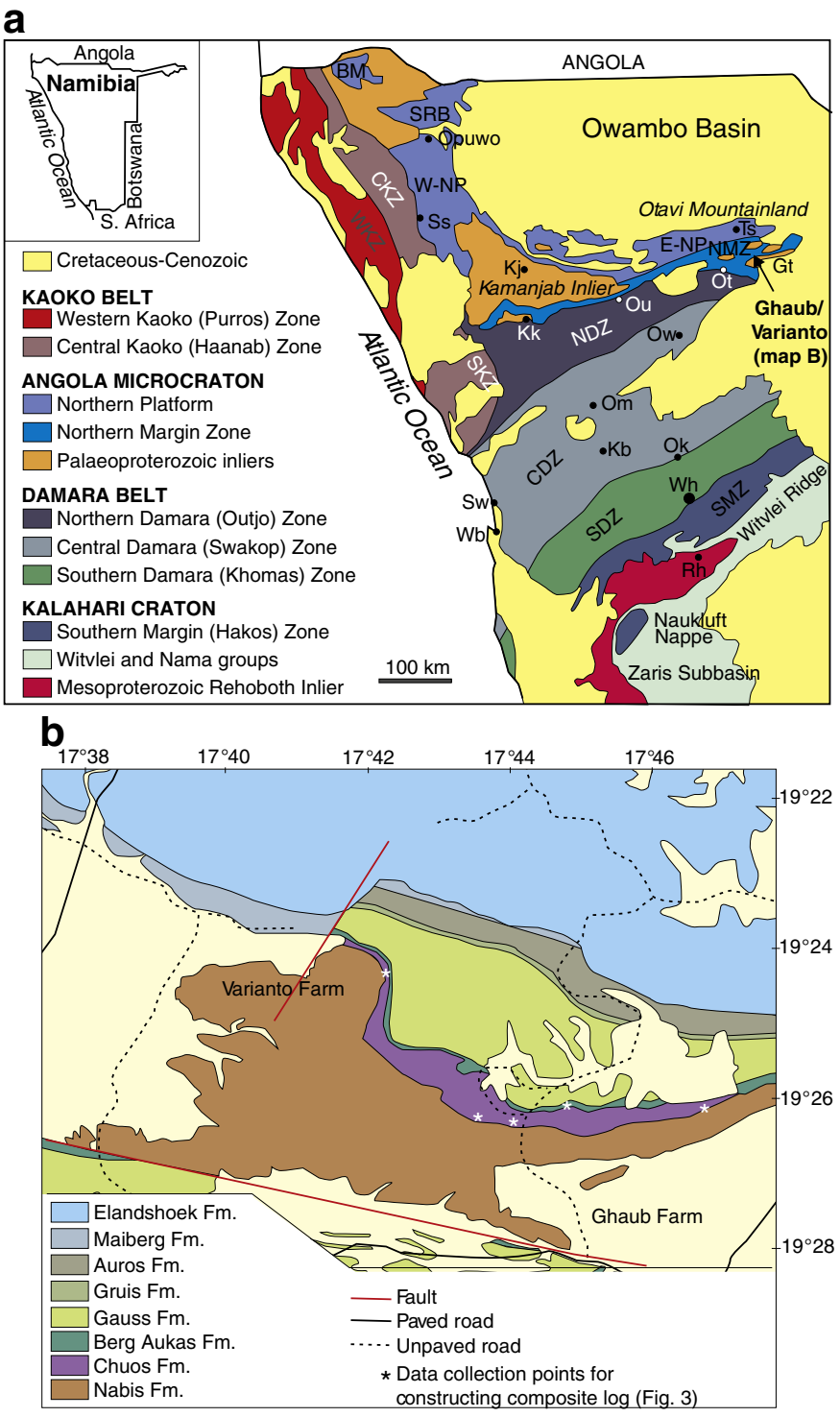

Fig 1. a: Geotectonic map of Namibia showing the location of the Otavi Mountain Land belt at the southern flank of the Owambo Basin (after Hoffman and Halverson, 2008). b: Location of the Ghaub and Varianto farms in the Otavi Mountain Land in northern Namibia. Note the location of observations used to compile the composite section in this small region (Fig. 3). Geological base map after Geological Survey of Namibia (2008).

and Prave, 1996) (Fig. 2). The Ghaub Formation has been subject to extensive scrutiny with a spectrum of arguments as to its genesis through purely gravitational instability (Eyles and Januszczak, 2007), and as to its glaciogenic signature (e.g. Bechstadt et al., 2009; Domack and Hoffman, 2011). The Chuos Formation, meanwhile, has been neglected by comparison to younger mineral rich carbonate strata above (e.g. Kamona and Günzel, 2007). Earlier analyses of the Chuos Formation concentrated on meta-sediments in the vicinity of its type section south of Windhoek and in the Damara Belt (Gevers, 1931; de Kock and Gevers, 1933; Martin et al., 1985; Henry et al., 1986; Badenhorst, 1988). More modern stratigraphic analyses several hundred kilometres to the west of the Otavi Mountain Land demonstrate that the Chuos Formation is cradled in a rift-related, fault bounded palaeotopography (Hoffman and Halverson, 2008), and hence its substrate also changes along strike, across the southern flank of the Owambo Basin. In the area of Ghaub and Varianto farms, the study

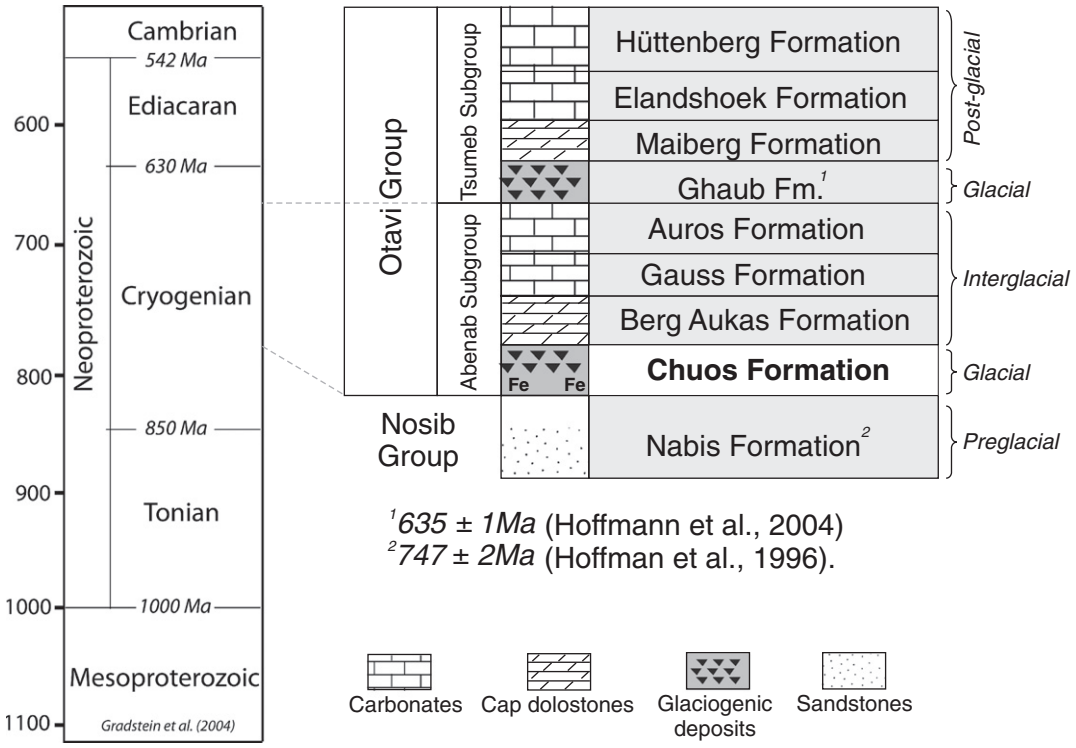

Fig. 2. Stratigraphy on the Cryogenian succession exposed in the Ghaub and Varianto farm areas of the Otavi Mountain Land. Stratigraphic hierarchy and formation names after Hoffmann and Prave (1996). U–Pb ages from the Askevold Formation (Hoffman et al., 1996) are from further west: this formation is not preserved beneath the Chuos Formation in the present study area.

interval comprises the Nabis Sandstone Formation of the Nosib Group, overlain by the Chuos Formation and succeeded by the Berg Aukas Formation (Fig. 2). This particular area has been mapped at the 1:250,000 scale (Geological Survey of Namibia, 2008). Age constraints include 747 ± 2 Ma from the Naauwport volcanics, locally beneath the Chuos Formation (Hoffman et al., 1996) and 635 ± 1 Ma from ash beds in the younger Ghaub Formation (Hoffmann et al., 2004). Owing A composite stratigraphy, assembled from observations from closely spaced localities over 12 field days (Fig. 1B), is included in this paper (Fig. 3) as the basis for our descriptions and interpretations.

3. Description of strata

The Chuos Formation rests on a ~1 km thick succession of conglomerates and sandstones of the Nabis Formation which crops out as part of the E–W striking Nosib Anticline (Fig. 1). Thickly bedded clast- and matrix-supported conglomerates bear rounded clasts of meta-sedimentary quartzite, vein quartz, red-weathering quartz-porphyry, brown-weathering metavolcanics with quartz amygdales, and dark grey-weathering quartz-feldspar agglomerate: these conglomerates fine up to parallel-laminated sandstones.

An angular unconformity can be demonstrated between the Nabis and Chuos formations, expressed as differences in dip of beds above and below the contact (Fig. 3). In the Ghaub and Varianto farm areas, the Chuos Formation is divisible into 1) an ironstone member at the base and 2) a diamictite member above (Fig. 3). Ferruginous phases in the ironstone include (1) isolated magnetite crystals, (2) magnetite crystal clusters, (3) magnetite stringers along cross-bed foresets and (4) botryoidal hematite (Fig. 4).

Ironstone facies include cross-bedded, coarse-grained sandstones, texturally comparable to the uppermost Nabis sandstones, intercalated with bedding-orthogonal dome structures of 5–10 cm amplitude (Fig. 5a–d) spaced up to 1 m apart. The dome structures often contain crinkly laminae which at the flanks dip at 75° with respect to underlying and overlying bed boundaries (Fig. 3: 8 m, 16–18 m, 22–24 m, and 29–31 m). Internally, the dome structures are composed of sand- to granule-grade laminae intercalated with hematite-rich microcrystalline laminae (Fig. 5e–f). Intercalation of these lithologies occurs on a millimetre scale. Thickening of the sand- to granule-grade laminae into interdome areas is demonstrable; these truncate underlying laminations at the dome flanks (Fig. 5f). Between the domes, the intercalation is also preserved in bedding parallel, crinkly centimetric bands (Fig. 3: 4–7 m). These are compositionally identical to the laminations in the domes, and are incorporated as clasts in the overlying diamictite member (Fig. 6a). In our study area, Hedberg (1979) observed “ferruginous concretions and Liesegang rings … in the lower part of the unit” (p. 55). These are restricted to the ironstone member, forming triangular-shaped nodules (Fig. 6b) as well as globule-shaped concretions (Fig. 6c). The Liesegang laminae can be demonstrated to crosscut both the dome structures and the inter-dome crinkly laminae. They can be clearly distinguished from sedimentary laminations as no grain size changes are apparent between the rings.

The contact with the overlying diamictite member is highly gradational and concordant (Fig. 3, 34 m). The diamictites, which retain magnetite content throughout, are often poorly bedded, but locally well stratified (Fig. 3). Clasts are randomly oriented, and occur in several population sets. The first, in the <5 cm diameter range, comprises sub-rounded to angular meta-sandstone clasts. The second, in a 5–25 cm diameter category, comprises very well rounded meta-sandstones and quartzites, identical to those in the Nabis Formation. A third population of clasts is restricted to the topmost beds of the diamictite, where a zone of comparatively more exotic clasts occurs. These include granite gneiss, mica schist, hornblende schist, mudstone and andesite. Finally, scattered clasts of ironstone are scattered throughout (Fig. 6a).

Near the top of the Chuos Formation (Fig. 3), well stratified diamictites are common (Fig. 6d). Clast-rich and clast-poor domains are intercalated on the centimetre-scale (Fig. 3). Clasts show evidence

for attenuation parallel to stratification; some are fractured and intruded by the diamictite matrix (Fig. 6e). Asymmetric folds, and pervasive lineations trending 162°, deform the deposit. These decimetre to metre-thick intensively sheared intervals intercalate with relatively undeformed diamictite (Fig. 3: 46 m, 48 m, and 52 m) that contains large lonestones with unequivocal impact structures beneath them (Fig. 6f). Soft-sediment striated surfaces, implying transmission of shear in unconsolidated sediments akin to a sliding deck of cards (Sutcliffe et al., 2000; Le Heron et al., 2005) also occur at intervals (Fig. 3, 48 m; Fig. 6g).

4. Interpretation of strata

The Nabis Formation is interpreted as an alluvial fanglomerate succession (Miller, 2008). The angular unconformity between the Nabis and Chuos formations can be seen in the wider context of regional-scale studies in northern Namibia thought to reflect progressive downcutting beneath the latter formation in a rift-related scenario (Eyles and Januszczak, 2007). Elsewhere in northern Namibia, in the Khowarib Fold Belt, a stratigraphic unit known as the Ombombo Subgroup is sandwiched between the Nabis and the Chuos formations (Hoffman and Halverson, 2008). This may suggest either non-deposition of the Ombombo Subgroup in the Ghaub/Varianto farm areas, or deeper erosion beneath the Chuos Formation in this area.

In the basal ironstone member, the cross-beds are interpreted to record the migration of clastic bar systems building out both to the north and to the south. Evidence for classic tidal indicators (e.g. de Vries Klein, 1970) are absent, and bidirectionality may point to subtle switching in gradient, e.g. in response to rift-related slope changes. Whilst the occurrence of magnetite crystals along cross-bed foresets might imply that the crystals were reworked before the succession was lithified, a post-diagenetic origin cannot be discounted.

The dome structures with crinkly laminae are interpreted as stromatolites. In this interpretation, stromatolites are considered "macroscopically layered authigenic microbial sediments with or without abiogenic precipitates" (Riding, 2011, p. 31). Whilst a conservative view is that the biogenic role in the development of stromatolites can only be demonstrated with fossil examples of the dome-building microbes (Buick et al., 1981), emphasis is normally placed on interpretation of the overall stromatolite morphology to infer a microbial control on dome construction (e.g. Awramik et al., 2005). The high dip angle at the dome flanks (>75°) with respect to the bed bases is beyond the angle of repose expected in mechanically or chemically deposited sediments (Hofmann et al., 1999). The dome structures bear no resemblance to soft-sediment deformation structures in other iron formations where delicate flame structures are common in underflow deposits (e.g. Le Heron et al., 2011), or convolute beds/liquefaction structures formed in subglacial settings (Le Heron et al., 2005). However, the high dip angle at the flanks of the dome structures can be explained by the deposition of a sticky, microbially-deposited precipitate to bind the intercalated sand- to granule-sized laminae at a steep angle. In this context, the sand to granule-grade laminae at the dome flanks, and bound in crinkly laminae in the inter-dome areas, is interpreted as mechanically deposited, abiotic sediment (Hofmann et al., 1999). This interpretation accounts for both lateral pinch-out of such laminae against dome flanks and thickening into the inter-dome areas (Fig. 5e, f), because abiotic laminae would be expected to accumulate in local depocentres. Local scour by weak currents in the inter-dome areas explains truncation of the hematite laminations (Fig. 5e, f).

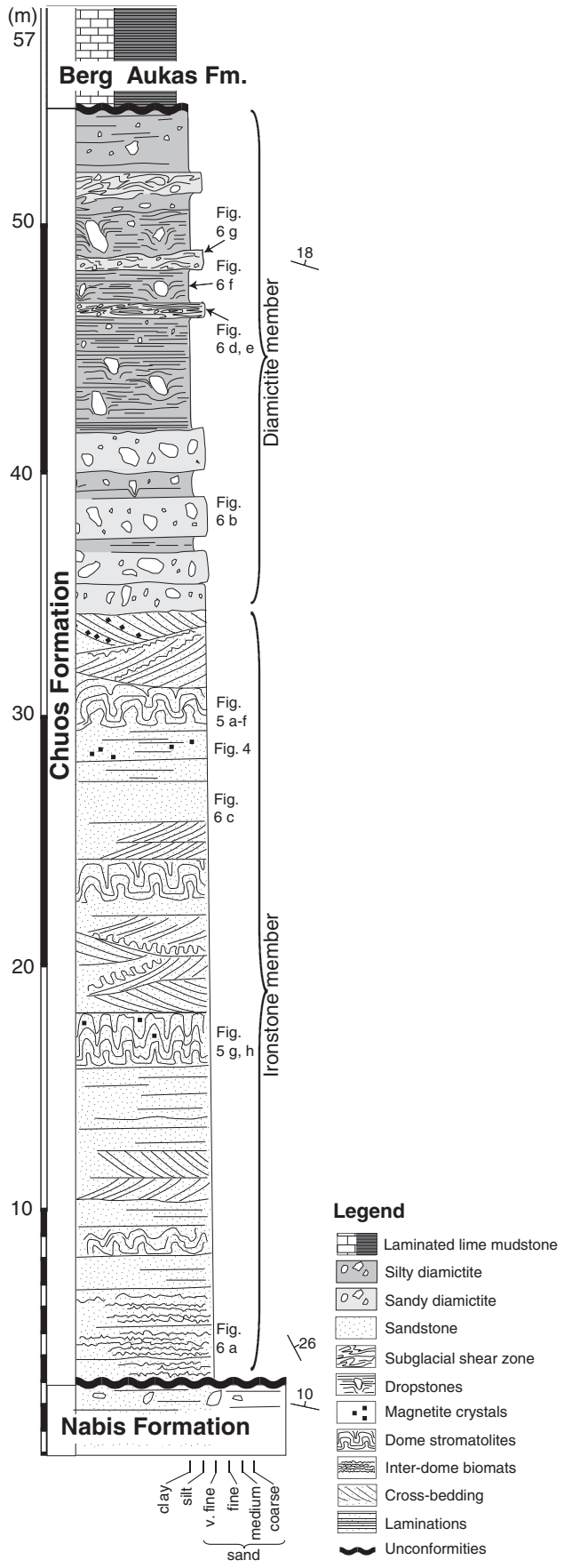

Fig. 3. Composite section of the Chuos Formation cropping out in Ghaub and Varianto farms. Note the angular unconformity with the underlying Nabis Formation and the concordant contact with the Berg Aukas Formation above, together with the informal subdivision of the Chuos Formation into ironstone and diamictite members. The location of photographs and accompanying illustrations in Figs. 4–7 is shown next to the log.

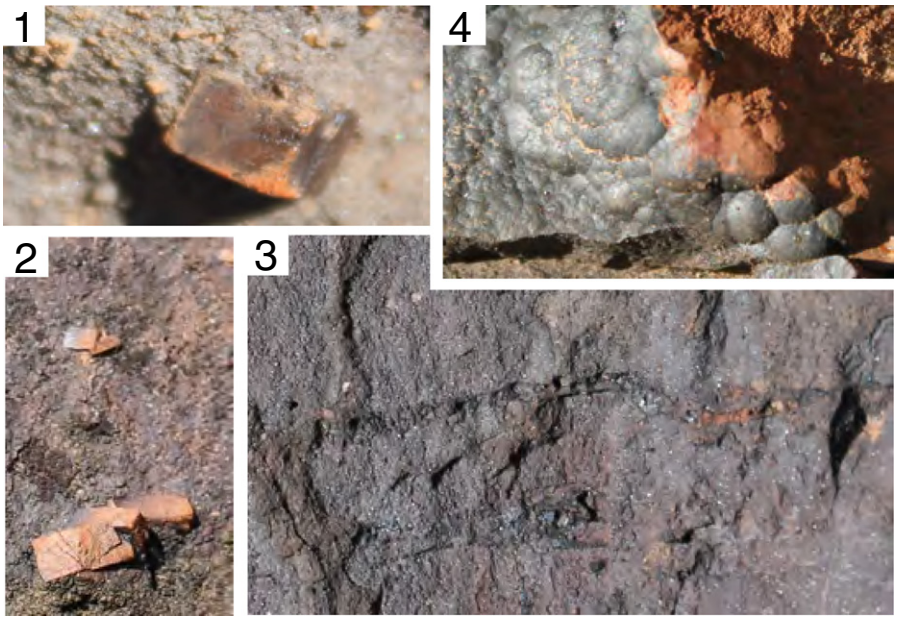

Fig. 4. Ferruginous phases in the lower informal member of the Chuos Formation: 1, isolated magnetite crystals (field of view 1 cm across); 2, magnetite crystal clusters (field of view 0.5 cm across); 3, magnetite stringers along bedding planes (field of view 5 cm across); 4, botryoidal hematite (field of view 2 cm across).

On the basis of the above, given their ferruginous composition, the stromatolites are interpreted as acidophile microbialites, locally reworked by current activity. Acidic conditions play a key role in the activity of iron-fixing bacteria (Brake et al., 2002). These organisms harness energy through oxidation of dissolved Fe (II), which remains stable under low-O_2 and low pH conditions (Konhauser et al., 2005, 2011; Bekker et al., 2010). Bacteria therefore adapt either to water column anoxia (microaerophiles) or more acidic conditions (acidophiles), analogous to the pH values of ~2 surrounding modern acid mine drainage (España et al., 2007). The acidophile tendencies of these framework-building organisms stand in contrast to the cynanobacterial stromatolites' characteristic of many Neoproterozoic strata (Tewari and Seckbach, 2011), yet they fix CO_2 through photosynthesis (Brake et al., 2002). Whilst magnetite can develop during diagenesis or epigenetically (McCabe et al., 1983), it is also possible that this phase may also represent biogenic sedimentation by analogy to magnetotactic stromatolites both modern and ancient elsewhere (Chang et al., 1989; Stolz et al., 1989): this interpretation is tentative because it is noted that crystal forms in those examples are usually microscopic. Regardless, an abiotic diffusional origin of the hematite Liesegang rings must be assumed, thus implying some limited epigenetic dissolution and re-precipitation of iron oxide phases. Based on the above, it is highlighted that stromatolites in the Chuos Formation were probably constructed by a different type of microbial community to the much more common carbonate stromatolites (Tewari and Seckbach, 2011).

The inclusion of meta-sandstone clasts within the diamictite implies extensive reworking of the Nabis Formation at Ghaub and Varianto farms, but the occurrence of schists and meta-granites toward the top of the succession may suggest erosion down to deeper crystalline basement levels; ironstone clasts in the diamictite member reflect cannibalisation of the underlying ironstone member. The stepwise increase in clast size up section in the overlying diamictites, coupled with poorly developed stratification, could be cited as evidence for non-glaciogenic debris flow sedimentation (Eyles and Januszczak, 2007), but evidence for glaciation in the Chuos diamictites is compelling. Attenuated, lozenge-shaped to lenticular clasts in those diamictites are strongly indicative of subglacial shear (van der Wateren et al., 2000). Fractured clasts, injected with diamictite matrix, are interpreted to record reduction of clast strength and brittle failure under high hydrostatic stresses beneath a confining sediment/ice load. The impact structures beneath pebble to boulder-sized lonestones represent ice-rafted debris (IRD). The commonly cited mechanism of rafting by sediment gravity flows (e.g. Eyles and Januszczak, 2007) is rejected due to the absence of imbrication in the outsized fraction, and the lack of correlation between bed thickness and maximum clast size. Finally, the occurrence of soft-sediment striations within sand-prone levels of the stratified diamictite is interpreted as intra-diamictite slip-planes, akin to a sliding deck of cards (Sutcliffe et al., 2000; Le Heron et al., 2005) (Fig. 6h) induced by an overlying ice mass. The co-occurrence of dropstone textures in the diamictites and sub-glacial shear zones allow us to tentatively propose that these strata represent sub-ice sedimentation, in a similar model to that of the younger Ghaub glaciation of northern Namibia (Domack and Hoffman, 2011). In the model, sub-ice marginal wasting (explaining the dropstones) and subglacial shear structures record oscillation of a dynamic grounding line.

5. Discussion: global context of ironstone and diamictites in the Chuos Formation

The concordant and gradational nature of the boundary between the ironstone and diamictite members is important as it allows a temporal connection between them to be inferred, and for a cryptic unconformity or disconformity to be rejected. In the Otavi Mountain Land, the succession initially lacks evidence for glacial processes (ironstone member), with glaciogenic strata becoming more evident upward (the diamictite member). Cannibalisation of shelf successions during subsequent glacial advances commonly destroys the record of

Fig. 5. Examples of dome stromatolites in the ironstone member of the Chuos Formation. a and b: General outcrop photograph and sketch of dome structures growing almost orthogonally to bedding surfaces. Note the steep angle of the flanks of the dome structures, and relatively flat inter-dome area with incipient, small-scale domes in between. c and d: Photograph and sketch of area outlined in b. Note that the interior/core of the dome structure in gently convex with the angle of dip increasing up-structure. e and f: Photograph and sketch of area outlined in d. Note the interlamination of sand- to granule-grade laminae (light coloured) and microcrystalline hematite laminae (dark coloured). Note that the former show thickening into the inter-dome area, pinch out onto the dome flanks, and truncate underlying laminae. These properties indicate a mechanical (i.e. abiotic) origin for the sand- to granule-grade laminae. g and h: Photograph and sketch of further examples of dome stromatolites and associated laminites. Note in these examples the lower profile of the domes and gentler dips at the dome flanks. Stratigraphic position of all photographs shown in Fig. 3.

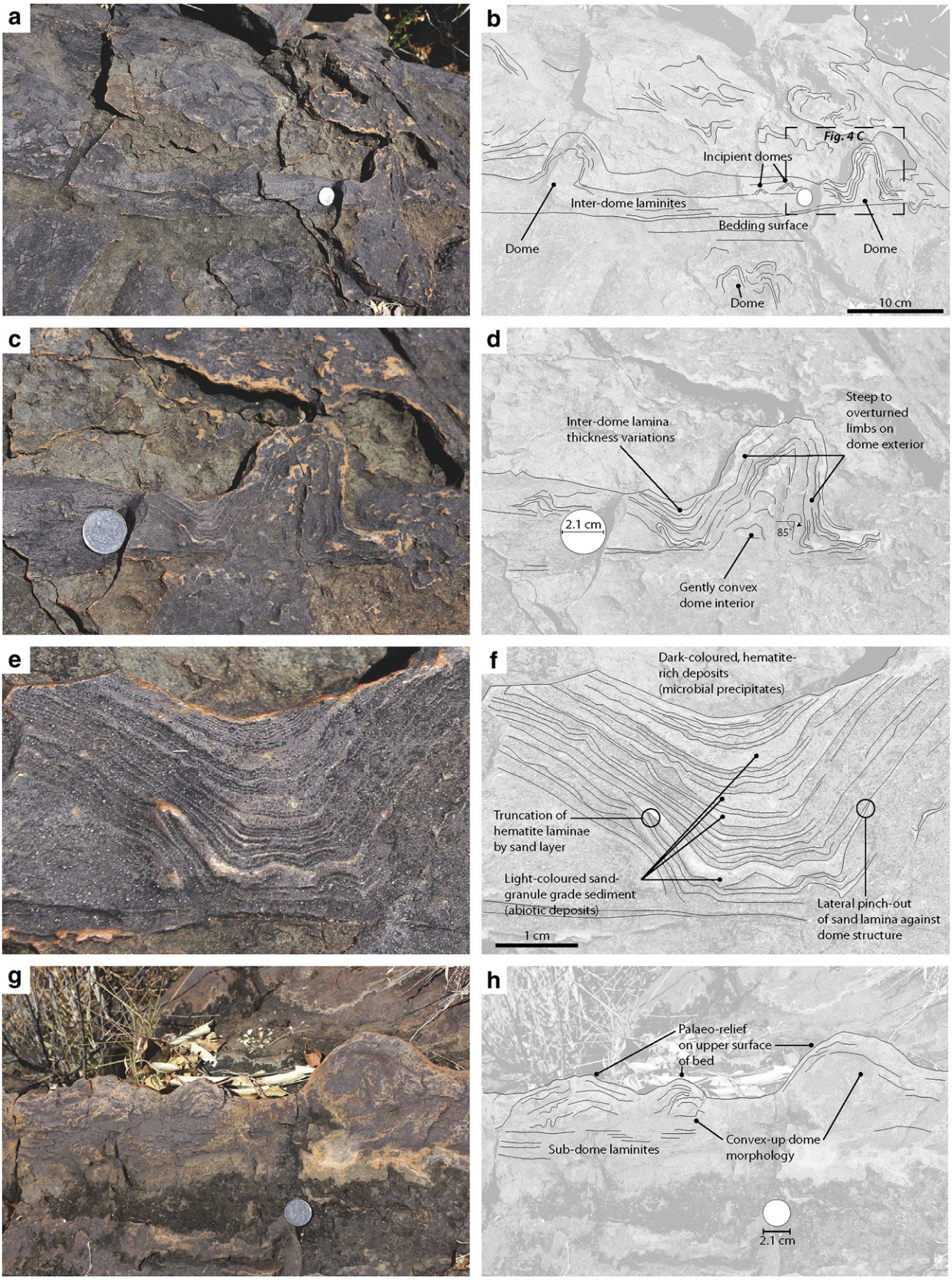
a
b
Fig. 4 C
Incipient domes
Inter-dome laminites
Bedding surface
Dome
Dome
Dome
10 cm
c
d
Inter-dome lamina thickness variations
Steep to overturned limbs on dome exterior
2.1 cm
85°
Gently convex dome interior
e
f
Dark-coloured, hematite-rich deposits (microbial precipitates)
Truncation of hematite laminae by sand layer
Light-coloured sand-granule grade sediment (abiotic deposits)
Lateral pinch-out of sand lamina against dome structure
1 cm
g
h
Palaeo-relief on upper surface of bed
Sub-dome laminites
Convex-up dome morphology
2.1 cm

early glacial advances in a basin. For example, in the Pleistocene record, nine phases of deeply incised, subglacial tunnel valleys have been recognised in the North Sea based on crosscutting relationships (Stewart and Lonergan, 2011). Therefore, in Ghaub/Varianto, the gradational and concordant nature of the contact may indicate that pre-glacial ironstone deposition led directly into the Chuos glaciation. Alternatively, if the diamictite member of the Chuos Formation is assumed to represent a final glacial cycle, the ironstone member represents an interglacial succession.

Beyond our study area, some 500 km to the northwest, domed stromatolite structures have also been observed in the Chuos Formation of the Opuwo region (Figs. 1b; 7). Here, as in the Otavi Mountain Land, stromatolite structures occur beneath diamictites but are also intercalated with them on the metre-scale. The extent of microbialite facies in other Cryogenian ironstones is unclear, and potentially awaits recognition, because ferruginous facies in Neoproterozoic strata are globally extensive (e.g. Kirschvink, 1992; Hoffman and Schrag, 2002). Both Macdonald et al. (2010) and Hoffman et al. (2011) argue that ironstones in Cryogenian strata are uniquely associated with the Sturtian glacial event at about 715 Ma, although evidence is emerging of Ediacaran-aged ironstones from Uruguay (Pecoits et al., in press).

The Rapitan Group (Cryogenian) of western Canada is similar to the Chuos Formation in both lithofacies and basin context, representing deposition in a paraglacial rift basin (Young, 1976; Eisbacher, 1985). An iron-rich, dropstone-bearing unit (the Sayunei Formation) is capped by a diamictite unit (the Shezal Formation) (Hoffman and Halverson, 2011). Measured sections (Fig. 3 of Eisbacher, 1985) illustrate that the most complete successions have a basal ferruginous shale sequence bearing occasional dropstones. These deposits pass gradationally upward, via 5–40 m jaspillite-hematite ironstone at the top of the Sayunei Formation, into diamictites. The ironstone is laterally persistent in depocentres (Eisbacher, 1985). Sea-ice removal may have triggered local grounding line advance, resulting in deposition of the Shezal Formation (Eisbacher, 1985): Hoffman and Halverson (2011) recognised this as a possible catalyst for ironstone precipitation. In addition to an abiotic "rusting of the seas" model, a biologically-mediated mechanism was also considered. Once "the ice cover thinned and finally disappeared, anoxic and oxygenic photosynthesis could have precipitated Fe_2O_3-precursor from anoxic Fe(II)-rich basin waters" (Hoffman et al., 2011). The biogenic mechanism was dismissed by those authors in favour of an abiotic explanation, although the reasons for such preference are unclear. Such a biogenic mechanism for ironstone precipitation, via for example photosynthetic stromatolites, would be in agreement with our observations in Namibia.

In Death Valley (California), a ferruginous rift basin succession (Petterson et al., 2011), again highly comparable to the Chuos Formation, was deposited. The Kingston Peak Formation (Cryogenian) comprises several kilometres of ferruginous glaci-turbidites, diamictites of mass flow affinity and boulder-sized lonestones (Troxel, 1982; Prave, 1999) interpreted as dropstones (Abolins et al., 2000; Corsetti and Kaufman, 2003), deposited beyond the ice grounding line (Mrofka and Kennedy, 2011). Thus, deep-water, iron-rich facies are considered to represent deposition without direct ice sheet influence, in contrast to very similar deposits in the Mackenzie Mountains.

In South America, stratified Fe and Mn ores occur in the Corumbá rift graben of Brazil and in neighbouring Bolivia, are considered to be of hydrothermal origin, and are intercalated with diamictites (Trompette et al., 1998). Urban et al. (1992) attributed the ores to oxidation of Fe and Mn rich rock flour during retreat of mountain glaciers. On the Yangtze Platform (south China), banded ironstones in the Fulu Formation are sandwiched between Cryogenian diamictites of the Chang 'an and Silikou formations (Zhang et al., 2011). Tang et al. (1987) interpreted the ironstones as "interglacial" whereas in a subtly different interpretation Zhang et al. (2011, p. 358) view them as the "waning stage of the Jiangkou glaciation". This latter interpretation stands in contrast to our interpretation of the Chuos succession, where ironstones in Ghaub/Varianto farms were deposited during the waxing stage of glaciation.

In Australia, likely temporal equivalents to the Chuos Formation include the Holowilena and Braemar ironstones of South Australia (Le Heron, 2012). These ironstones occur at slightly different levels along strike, and are fault-bounded, allowing, like their counterparts in the Mackenzie Mountains, in Death Valley, and in Brazil/Bolivia, a connection to fault-transmitted fluids to be inferred (Link and Gostin, 1981). Bekker et al. (2010) envisaged the same mechanism for ironstone precipitation in the Otjosondu region of the central Damara Belt in Namibia, citing associated volcanogenic massive sulphide (VMS) deposits (Buhn et al., 1992) and REE values in support. By direct comparison with the Chuos deposits described herein, the Holowilena ironstone lies beneath a succession of diamictites and ice-rafted debris in the overlying Wilyerpa Formation, interpreted as the deposits of glacial (re)advance (Le Heron et al., 2011). Thus, in a similar way, deposition during glacial waxing is envisaged. Our evidence from Ghaub/Varianto farms does not exclude extensional fault systems during breakup of Rodinia (Eyles and Januszcak, 2004) as providing a source of ferrous iron in solution for acidophile biomats. The stratigraphic context of the ironstones does, however, exclude the model of global ice cover inhibiting iron precipitation (Kirschvink, 1992; Hoffman and Schrag, 2002) during a phase of ice wasting because evidence for glacial waxing, and indeed subglacial processes, is apparent in overlying diamictite deposits.

From the global analogues discussed above, it emerges that diamictites generally occur above iron formations in Canada (Mackenzie Mountains), in the USA (Death Valley), in China (Yangtze Platform) and in South Australia; they are intercalated with them in Brazil and in Bolivia. In our study area, note that there is no direct evidence for glacial processes in the ironstones, thereby challenging the long-held view of anoxia induced by an overlying ice sheet. Furthermore, the need to invoke meltwater plumes to oxidise iron as envisaged by Hoffman and Halverson (2008) and Hoffman et al. (2011) is unnecessary, because stromatolite colonies provide an alternative mechanism of seawater oxidation.

Our field observations of stromatolites in the Chuos Formation and their interpretation should also be seen in the context of recent work by Tziperman et al. (2011). These authors suggest that enhanced flux of organic material from the upper ocean to submarine sediments and porewaters, when subject to remineralization under anoxic conditions by sulphate or iron-reducing bacteria, may have changed the alkalinity of ocean waters sufficiently to precipitate siderite and draw down CO_2 to initiate a snowball Earth. However, this proposed mechanism is distinct from the process highlighted herein, because it is inferred that photosynthetic (and hence sea-floor surface) biomats played a role in drawing down CO_2, at least locally. The occurrence of stromatolites within the ironstones suggests a close analogue to the modern day acidophile biomats that photosynthesise, draw down CO_2, and oxidise ferrous iron (Brake et al., 2002; Brake and Hasiotis, 2008).

The above comparison requires the Chuos biomats to have developed in the photic zone. Therefore, it is suggested that rift-sourced iron fed acidophile biomats which in turn fixed iron in a shallow marine

Fig. 6. a: Clast of the ironstone member incorporated in the diamictite member: microcrystalline hematite laminae are clearly visible. b: Liesegang laminae, recording limited abiotic diffusional re-precipitation of iron oxides. c: Globular concretions of hematite overprinting stromatolitic domes in the ironstone member. d: Well stratified diamictite, showing intercalation of clast-rich and clast-poor zones, with evidence of augen structures and stratification-parallel attenuation of clasts. This is interpreted as a subglacial shear zone. e: Quartzite clast, shattered and intruded by diamictite matrix, in the same subglacial shear zone. f: Large quartzite lonestone with an unequivocal impact structure, enabling it to be interpreted as an ice-rafted dropstone. g: Soft sediment striated surface in the diamictite member. h: Soft-sediment striated surface for comparison in a similar, subglacially deformed sedimentary succession of Late Ordovician age from Libya (Le Heron et al., 2005). The development of soft sediment striated surfaces implies transmission of shear in unconsolidated sediments akin to a sliding deck of cards (Sutcliffe et al., 2000; Le Heron et al., 2005).

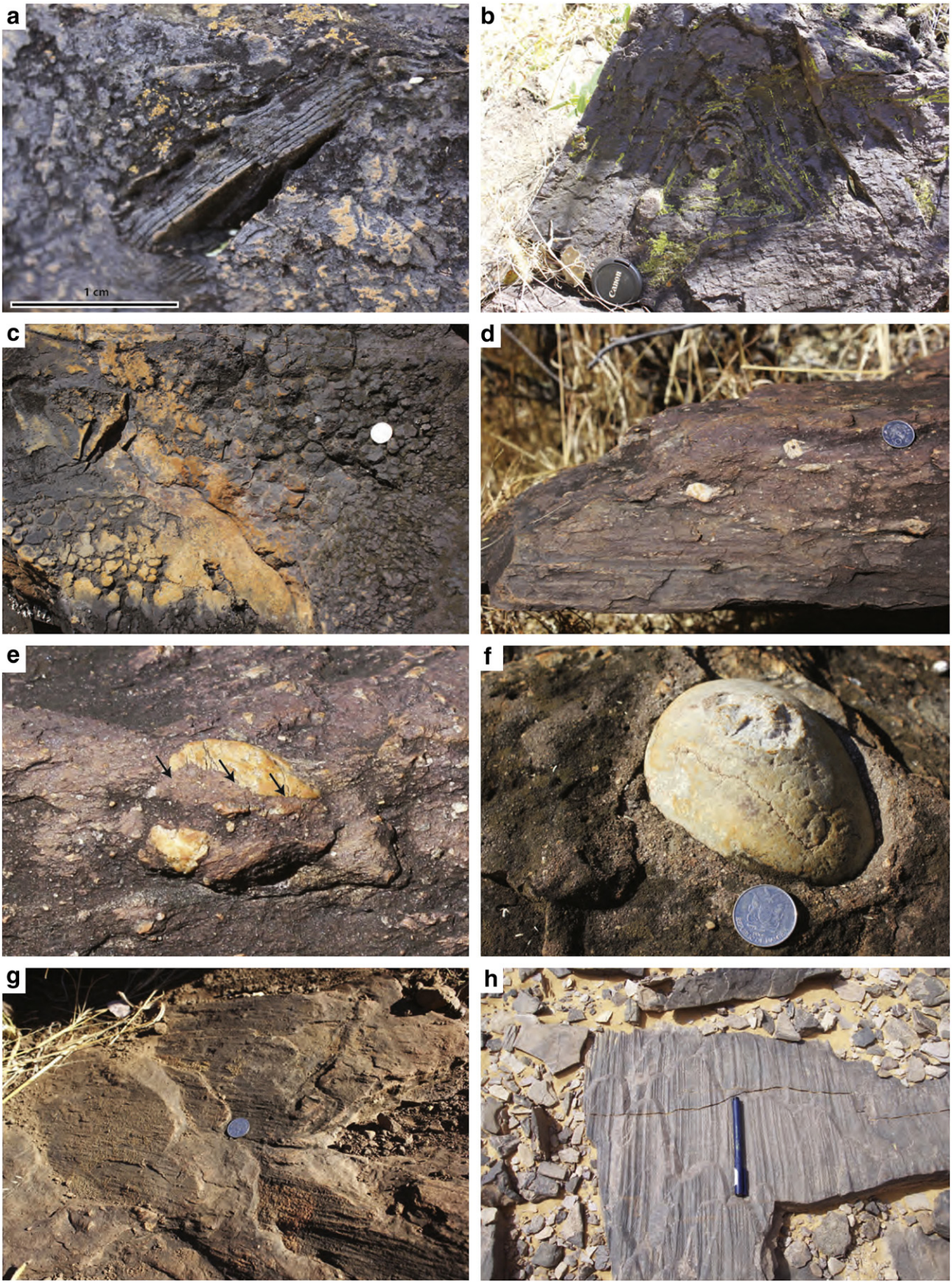
a
1 cm
b
c
d
e
f
g
h

Fig. 7. Domed stromatolites, some 500 km west of Ghaub and Varianto farms, in the Chuos Formation of the remote Opuwo area (see Fig. 1B for location). Identical intercalated microcrystalline hematite and sand- to granule-grade laminations appear to confirm that ironstone microbialites are of significant lateral extent in Namibia. Grid reference: 18°43. 828′S 13°43.749′E.

or possibly lacustrine rift basin. Ferrous iron in solution can stimulate photosynthesis by an estimated 500 to 600% (Pierson et al., 1999), and thus the drawdown of CO_2 during the formation of these structures may also allow us to tentatively postulate that acidophile biomats played a role in cooling. This, however, presents a paradox. Iron formations typically have extremely low organic carbon contents (Hoffman et al., 2011): Fe^{3+} is also an eager electron acceptor supporting microbial respiration on the seafloor or during shallow burial diagenesis (Walker, 1987). Regardless, ironstones in northern Namibia occur concordantly beneath, and are hence temporally transitional into, glacial diamictites. They were deposited either at the onset of the Sturtian glaciation, or during an interglacial within this snowball Earth episode. In either scenario, they record entry into, rather than exit from, extreme glaciation as more commonly suggested (Kirschvink, 1992; Hoffman and Schrag, 2002).

6. Conclusions

- New sedimentological data on the Chuos Formation of northern Namibia reveal that in the Otavi Mountain Land, these Sturtian-age deposits of suspected glaciogenic origin can be divided into two informal members. These are a lower ironstone member, and an upper diamictite member.
- The basal ironstone member, rich in hematite and magnetite, contains 1) evidence for tractional sedimentation (metre-scale cross bedding) and 2) dome structures of 10–15 cm amplitude. These latter structures are characterised by crinkly internal lamination, and at the millimetre scale contain intercalated microcrystalline hematite/magnetite and sand to granule-grade sediment. The dome structures are interpreted as stromatolites probably built from aerotactic and phototactic bacteria. Preliminary mapping suggests that stromatolite intervals extend over at least 500 km of northern Namibia.
- The basal ironstone member shows a gradational contact with the upper diamictite member. This latter unit contains evidence for lonestones with impact structures (interpreted as ice-rafted dropstones), soft-sediment striated surfaces (scratching of an unconsolidated sediment surface beneath a grounded ice mass) and intensely sheared intervals (deformation of a volume of sediment beneath a grounded ice mass). Thus, a strong glacial influence on deposition can be demonstrated.
- By analogy to microbialites in modern acid mine drainage environments, ironstone member stromatolites are likely to have been sustained by photosynthesis, and thus iron fixation and CO_2 drawdown may have occurred in tandem. Growth of stromatolites, and precipitation of ironstones, may thus potentially have promoted local cooling. This mechanism, whilst distinct from the burial model of Tziperman et al. (2011), adds credence to the idea of biologically mediated cooling.

Acknowledgements

The authors are very grateful to the owners of Ghaub Farm and Varianto Farm for permission to work on their land, and to Paulus N. Mungandjera and Ralph J.C.M. Muyamba for field assistance. We are also very grateful for the input of Grant Cox and Graham Shields-Zhou for feedback, to four anonymous reviewers, and to the editor, Finn Surlyk, for constructive criticism.

References

Abolins, M., Oskin, R., Prave, A., Summa, C., Corsetti, F.A., 2000. Neoproterozoic glacial record in the Death Valley region, California and Nevada (in Great Basin and Sierra Nevada), Field Guide. Geological Society of America 2, 319–335.
Awramik, S.M., Grey, K., 2005. Stromatolites: biogenicity, biosignatures, and bioconfusion. Proceedings of SPIE 5906 http://dx.doi.org/10.1117/12.625556 (59060P1–5906P9).
Badenhorst, F.P., 1988. The lithostratigraphy of the Chuos mixtite in part of the southern central zone of the Damara orogen, South-West Africa. Communications of the Geological Survey of SW Africa/Namibia 4, 103–110.
Bechstädt, T., Jäger, H., Spence, G., Werner, G., 2009. Late Cryogenian (Neoproterozoic) glacial and post-glacial successions at the southern margin of the Congo Craton, northern Namibia: facies, palaeogeography and hydrocarbon perspective. In: Craig, J., Thurow, J., Thusu, B., Whitham, A., Abutarruma, Y. (Eds.), Global Neoproterozoic Petroleum Systems: The Emerging Potential in North Africa: Geological Society, London, Special Publications, 326, pp. 255–287.
Bekker, A., Slack, J.S., Planavsky, N., Krapez, B., Konhauser, K.O., Rouxel, O.J., 2010. Iron formation: the sedimentary product of a complex interplay among mantle, tectonic, oceanic, and biospheric processes. Economic Geology 105, 467–508.
Brake, S.S., Hasiotis, S.T., 2008. Eukaryote-dominated biofilms in extreme environments: overlooked sources of information in the geologic record. Palaios 23, 121–123.
Brake, S.S., Hasiotis, S.T., Dannelly, H.K., Connors, K.A., 2002. Eukaryotic stromatolite builders in acid mine drainage: implications for Precambrian iron formations and oxygenation of the atmosphere? Geology 30, 599–602.
Bühn, B., Stanistreet, I.G., Okrusch, M., 1992. Late Proterozoic outer shelf manganese and iron deposits at Otjosondu (Namibia) related to the Damaran oceanic opening. Economic Geology 87, 1393–1411.
Buick, R., Dunlop, J.S.R., Groves, D.I., 1981. Stromatolite recognition in ancient rocks: An appraisal of irregularly laminated structures in an Early Archaen chert-barite unit from North Pole, Western Australia. Alcheringa 5, 161–181.
Chang, S.-B.R., Stolz, J.F., Kirschvink, J.L., Awramik, S.M., 1989. Biogenic magnetite in stromatolites. II. Occurrence in ancient sedimentary environments. Precambrian Research 43, 305–315.
Corsetti, F.A., Kaufman, A.J., 2003. Stratigraphic investigations of carbon isotope anomalies and Neoproterozoic ice ages in Death Valley, California. GSA Bulletin 115, 916–932.
De Kock, W.P., Gevers, T.W., 1933. The Chuos tillite in the Rehoboth and Windhoek Districts, South-West Africa. Transactions of the Geological Society of South Africa 35, 115–118.
De Vries Klein, G., 1970. Depositional and dispersal dynamics of intertidal sand bars. Journal of Sedimentary Petrology 40, 1095–1127.
Domack, E.W., Hoffman, P.F., 2011. An ice grounding-line wedge from the Ghaub glaciation (635 Ma) on the distal foreslope of the Otavi carbonate platform, Namibia, and its bearing on the snowball Earth hypothesis. Geological Society of America Bulletin 123, 1448–1477.
Eisbacher, G.H., 1985. Late Proterozoic rifting, glacial sedimentation and sedimentary cycles in the light of Windermere deposition, western Canada. Palaeogeography, Palaeoclimatology, Palaeoecology 51, 231–254.
España, J.-S., Pastor, E.S., López Pamo, E., 2007. Iron terraces in acid mine drainage systems: a discussion about the organic and inorganic factors involved in their formation through observations from the Tintillo acidic river (Riotinto mine, Huelva, Spain). Geosphere 3, 133–151.
Eyles, N., 2008. Glacio-epochs and the supercontinent cycle after ~3.0 Ga: tectonic boundary conditions for glaciation. Palaeogeography, Palaeoclimatology, Palaeoecology 258, 89–129.
Eyles, N., Januszcak, N., 2004. 'Zipper-rift': a tectonic model for Neoproterozoic glaciations during the breakup of Rodinia after 750 Ma. Earth-Science Reviews 65, 1–73.
Eyles, N., Januszczak, N., 2007. Syntectonic subaqueous mass flows of the Neoproterozoic Otavi Group, Namibia: where is the evidence of global glaciation? Basin Research 19, 179–198.
Geological Survey of Namibia, 2008. Sheet 1916- Tsumeb (1:250,000). Ministry of mines and Energy, Windhoek.
Gevers, T.W., 1931. An ancient tillite in South-West Africa. Transactions of the Geological Society of South Africa 34, 1–17.
Hedberg, R.M., 1979. Stratigraphy of the Ovamboland Basin, South West Africa. Bulletin - University of Cape Town, Precambrian Research Unit 24, 325.
Henry, G., Stanistreet, I.G., Maiden, K.J., 1986. Preliminary results of a sedimentological study of the Chuos Formation in the central zone of the Damara Orogen: evidence

for mass flow processes and glacial activity. Communications of the Geological Survey of South-West Africa/Namibia 2, 75–92.
Hoffman, P.F., Halverson, G.P., 2008. Otavi Group of the western Northern Platform, the eastern Kaoko Zone and the western Northern Margin Zone. In: Miller, R.McG. (Ed.), The Geology of Namibia: Neoproterozoic to Lower Palaeozoic. Ministry of Mines and Energy, vol. 2, pp. 13.69–13.136.
Hoffman, P.F., Halverson, G.P., 2011. Neoproterozoic glacial record in the Mackenzie Mountains, northern Canadian Cordillera. In: Arnaud, E., Halverson, G.P., Shields-Zhou, G. (Eds.), The Geological Record of Neoproterozoic Glaciations: Geological Society Memoirs, 36, pp. 397–411.
Hoffman, P.F., Schrag, D.P., 2002. The snowball Earth hypothesis: testing the limits of global change. Terra Nova 14, 129–155.
Hoffman, P.F., Hawkins, D.P., Isachsen, C.E., Bowring, S.A., 1996. Precise U–Pb zircon ages for early Damaran magmatism in the Summas Mountains and Welwitschia Inlier, northern Damara belt, Namibia. Communications of the Geological Survey of Namibia 11, 47–52.
Hoffman, P.F., Macdonald, F.A., Halverson, G.P., 2011. Chemical sediments associated with Neoproterozoic glaciation: iron formation, cap carbonate, barite and phosphate. In: Arnaud, E., Halverson, G.P., Shields-Zhou, G. (Eds.), The Geological Record of Neoproterozoic Glaciations: Geological Society Memoirs, 36, pp. 67–80.
Hoffmann, K.-H., Prave, A.R., 1996. A preliminary note on a revised subdivision and regional correlation of the Otavo Group based on glaciogenic diamictites and associated cap dolostones. Communications of the Geological Survey of Namibia 11, 77–82.
Hoffmann, K.H., Condon, D.J., Bowring, S.A., Crowley, J.L., 2004. U–Pb zircon date from the Neoproterozoic Ghaub formation, Namibia: constraints on Marinoan glaciation. Geology 32, 817–820.
Hofmann, H.J., Grey, K., Hickman, A.H., Thorpe, R.I., 1999. Origin of 3.45 Ga coniform stromatolites in Warrawoona Group, Western Australia. Geological Society of America Bulletin 111, 1256–1262.
Kamona, A.F., Günzel, A., 2007. Stratigraphy and base metal mineralization of the Otavi Mountain Land, Northern Namibia — a review and regional interpretation. Gondwana Research 11, 396–413.
Kirschvink, J.L., 1992. Late Proterozoic low-latitude glaciation: the snowball Earth. In: Schopf, J.W., Klein, C. (Eds.), The Proterozoic Biosphere. Cambridge University Press, Cambridge, pp. 51–52.
Konhauser, K.O., Hamade, T., Raiswell, R., Morris, R.C., Ferris, F.G., Southam, G., Canfield, D.E., 2002. Could bacteria have formed the Precambrian banded iron formations? Geology 30, 1079–1082.
Konhauser, K.O., Newman, D.K., Kappler, A., 2005. The potential significance of microbial Fe (III)-reduction during Precambrian banded iron formations. Geobiology 3, 167–177.
Konhauser, K.O., Kappler, A., Roden, E.E., 2011. Iron in microbial metabolisms. Elements 7, 89–93.
Le Heron, D.P., 2012. The Cryogenian record of glaciation and deglaciation in South Australia. Sedimentary Geology 243–244, 57–69.
Le Heron, D.P., Sutcliffe, O.E., Whittington, R.J., Craig, J., 2005. The origins of glacially related soft-sediment deformation structures in Upper Ordovician glaciogenic rocks: implication for ice sheet dynamics. Palaeogeography, Palaeoclimatology, Palaeoecology 218, 75–103.
Le Heron, D.P., Cox, G.M., Trundley, A.E., Collins, A., 2011. Sea-ice free conditions during the early Cryogenian (Sturt) glaciation, South Australia. Geology 39, 31–34.
Link, P.K., Gostin, V.A., 1981. Facies and palaeogeography of Sturtian glacial strata (Late Precambrian), South Australia. American Journal of Science 281, 353–374.
Macdonald, F.A., Strauss, J.V., Rose, C.V., Dudás, F.Ő., Schrag, D.P., 2010. Stratigraphy of the Port Nolloth Group of Namibia and South Africa and implications for the age of Neoproterozoic iron formations. American Journal of Science 310, 862–888.
Martin, H., 1965. Observations concerning the problem of the late Precambrian glacial deposits in South West Africa. Geologische Rundschau 54, 115–127.
Martin, H., Porada, H., Walliser, O.H., 1985. Mixtite deposits of the Damara sequence, Namibia, problems of interpretation. Palaeogeography, Palaeoclimatology, Palaeoecology 51, 159–196.
McCabe, C., van der Voo, R., Peacor, D.R., Scotese, C.R., Freeman, R., 1983. Diagenetic magnetite carries ancient yet secondary remanence in some Paleozoic sedimentary carbonates. Geology 11, 221–223.
Miller, R.McG. (Ed.), 2008. The Geology of Namibia: Neoproterozoic to Lower Palaeozoic. Ministry of Mines and Energy, vol. 2.
Mrofka, D., Kennedy, M., 2011. The Kingston Peak Formation in the eastern Death Valley region. In: Arnaud, E., Halverson, G.P., Shields-Zhou, G. (Eds.), The Geological Record of Neoproterozoic Glaciations: Geological Society, London, Memoirs, 36, pp. 449–458.
Pecoits, Aubet, N.R., Gingras, M.K., Poulton, S.W., Bekker, A., Veroslavsky, G., Konhauser, K.O., in press. An Ediacaran iron formation: New evidence for ferruginous late Neoproterozoic seawater. Precambrian Research. DOI: 10.1016/j.precamres.2011.10.002.
Petterson, R., Prave, A.R., Wernicke, B.P., 2011. Glaciogenic and related strata of the Neoproterozoic Kingston Peak Formation in the Panamint Range, Death Valley region, California. In: Arnaud, E., Halverson, G.P., Shields-Zhou, G. (Eds.), The Geological Record of Neoproterozoic Glaciations: Geological Society, London, Memoirs, 36, pp. 449–458.
Pierson, B.K., Parenteau, M.N., Griffin, B.M., 1999. Phototrophs in high-iron-concentration microbial mats: physiological ecology of phototrophs in an iron-depositing hot spring. Applications of Environmental Microbiology 65, 5474–5483.
Prave, A.R., 1999. Two diamictites, two cap carbonates, two $\delta^{13}C$ excursions, two rifts: the Neoproterozoic Kingston Peak Formation, Death Valley, California. Geology 27, 339–342.
Riding, R., 2011. The nature of stromatolites: 3,500 million years of history and a century of research. In: Reitner, J., Quéric, N.-V., Arp, G. (Eds.), Advances in Stromatolite Geobiology: Lecture Notes in Earth Sciences, 131. Springer-Verlag, Belin, Germany, pp. 29–74.
Stewart, M.A., Lonergan, L., 2011. Seven glacial cycles in the middle–late Pleistocene of northwest Europe: geomorphic evidence from buried tunnel valleys. Geology 39, 283–286.
Stolz, J.F., Chang, S.-B.R., Kirschvink, J.L., 1989. Biogenic magnetite in stromatolites. I. Occurrence in modern sedimentary environments. Precambrian Research 43, 295–304.
Sutcliffe, O.E., Theron, J.A., Whittington, R.J., Theron, J.N., Craig, J., 2000. Calibrating the Late Ordovician glaciation and mass extinction by the eccentricity cycles of the Earth's orbit. Geology 23, 967–970.
Tang, J.-F., Fu, H.-Q., Yu, Z.-Q., 1987. The stratigraphic horizon, type, and formation condition of Precambrian siliceous iron formation in south China. Ore Geology 6, 1–10 (in Chinese).
Tewari, V., Seckbach, J., 2011. Stromatolites: Interaction of Microbes with Sediments. Springer . 751 pp.
Trompette, R., Alvarenga, C.J.S., Walde, D., 1998. Geological evolution of the Neoproterozoic Corumbá graben system (Brazil). Depositional context of the stratified Fe and Mn ores of Jacadigo Group. Journal of South American Earth Sciences 11, 587–597.
Troxel, B.W., 1982. Description of the uppermost part of the Kingston Peak Formation, Amargosa Rim canyon, Death Valley region, California. In: Cooper, J.D., Troxel, B.W., Wright, L.A. (Eds.), Geology of Selected Areas in the San Bernadino Mountains, Western Mojave Desert, and Southern Great Basin, California. : Geological Society of America Cordilleran Section volume and guidebook. Death Valley Publi. Co., Shoshone, CA, pp. 61–70.
Tziperman, E., Halevy, I., Johnston, D.T., Knoll, A.H., Schrag, D., 2011. Biologically induced initiation of Neoproterozoic snowball Earth events. PNAS 108, 15091–15096.
Urban, H., Stribny, B., Lippolt, H., 1992. Iron and manganese deposits of the Urucum district, Mato Grosso do Sul, Brazil. Economic Geology 87, 1375–1392.
Van der Wateren, F.M., Kluiving, S.J., Bartek, L.R., 2000. Kinematic indicators of subglacial shearing. In: Maltman, A.J., Hubbard, B., Hambrey, M.J. (Eds.), Deformation of Glacial Materials: Geological Society Special Publication, 176, pp. 259–278.
Walker, J.C.G., 1987. Was the Archaean biosphere upside-down? Nature 329, 710–712.
Yeo, G.M., 1981. The Late Proterozoic Rapitan glaciation in the northern Cordillera. In: Campbell, F.H. (Ed.), Proterozoic Basins of Canada: Geological Survey of Canada Paper 81–10, pp. 25–46.
Young, G.M., 1976. Iron-formation and glaciogenic rocks of the Rapitan Group, Northwest Territories, Canada. Precambrian Research 3, 137–158.
Zhang, Q.-R., Chu, X.-L., Feng, L.-J., 2011. Neoproterozoic glacial records in the Yangtze Region, China. In: Arnaud, E., Halverson, G.P., Shields-Zhou, G. (Eds.), The Geological Record of Neoproterozoic Glaciations: Geological Society Memoirs, 36, pp. 357–366.

3.3. Chuos glacitectonite, Otavi Mountainland

Glacitectonic deformation in the Chuos Formation of northern Namibia: implications for Neoproterozoic ice dynamics

Busfield, M.E. & Le Heron, D.P.

Proceedings of the Geologists' Association 2013, v. 124, 778-789.
doi:10.1016/j.pgeola.2012.10.005

Statement of contribution

- ***Data collection***
  - Busfield logged the section and collected structural data throughout e.g. bedding, fold vergence.
  - Busfield chose the sampling strategy (at distinct changes in macro-scale deformation fabric/character), sampled the section and measured the orientation of the sampled blocks. Busfield later analysed and interpreted all sediment thin sections.
  - Le Heron assisted with sample collection.
- ***Manucript text***
  - Busfield was responsible for macro- and micro-scale lithofacies and structural interpretations, for identifying the distinct ductile and brittle deformation regimes, the palaeoenvironmental interpretation and the conceptual model for distinguishing sediment flow and glaciotectonic deformation.
  - Busfield authored all drafts of the manuscript, modified following reviews by Le Heron.
- ***Figures***
  - Busfield illustrated all figures in the manuscript, and provided both the macro-scale and micro-scale photographs.

Proceedings of the Geologists' Association 124 (2013) 778–789

Contents lists available at SciVerse ScienceDirect

Proceedings of the Geologists' Association

journal homepage: www.elsevier.com/locate/pgeola

Glacitectonic deformation in the Chuos Formation of northern Namibia: implications for Neoproterozoic ice dynamics

Marie E. Busfield *, Daniel P. Le Heron

Department of Earth Sciences, Royal Holloway, University of London, Egham, Surrey TW20 0EX, United Kingdom

ARTICLE INFO

Article history:
Received 20 April 2012
Received in revised form 29 October 2012
Accepted 30 October 2012
Available online 4 December 2012

Keywords:
Neoproterozoic
Glacitectonism
Ductile deformation
Snowball Earth
Otavi Mountainland

ABSTRACT

The Chuos Formation is a diamictite-dominated succession of Cryogenian age, variously interpreted as the product of glaciomarine deposition, glacially related mass movement, or rift-related sediment remobilisation in a non-glacial environment. These interpretations have wide ranging implications for the extent of ice cover during the supposedly pan-global Neoproterozoic icehouse. In the Otavi Mountainland, northern Namibia, detailed analysis of soft-sediment deformation structures on the macro- and micro-scale support glacitectonic derivation in response to overriding ice from the south/south-east. Overall, the upward increase in strain intensity, predominance of ductile deformation features (e.g. asymmetric folds, rotational turbates and necking structures, clast boudinage, unistrial plasmic fabrics) and pervasive glacitectonic lamination support subglacial deformation under high and sustained porewater pressures. In contrast, soft-sediment structures indicative of mass movements, including flow noses, tile structures, and basal shear zones, are not present. The close association of subglacial deformation, abundant ice-rafted debris and ice-contact fan deposits indicate subaqueous deposition in an ice-proximal setting, subject to secondary subglacial deformation during oscillation of the ice margin. These structures thus reveal evidence of dynamic grounded ice sheets in the Neoproterozoic, demonstrating their key palaeoclimatic significance within ancient sedimentary successions.

1. Introduction

The concept of a Neoproterozoic icehouse has remained contentious since its inception in the early 19th century ('*die Eiszeit*' of Agassiz, 1837; cf. Allen and Etienne, 2008), with renewed deliberation in recent years following proposal of the 'snowball Earth' hypothesis (Kirschvink, 1992; Hoffman et al., 1998; Hoffman and Schrag, 2002). This hypothesis has centred on the recognition of broadly age-equivalent diamictite-dominated successions on each continent, which are argued to be glaciogenic in origin (Hoffman et al., 1998; Hoffman and Schrag, 2002). Many diamictites are sharply overlain by dolomotized carbonates, interpreted as the record of rapid post-glacial climatic recovery (Shields, 2005). Compared to younger icehouse intervals, diagnostic glacial indicators, including striated and faceted clasts, subglacially striated pavements and extrabasinal clast assemblages, are notably scarce in the Neoproterozoic (Etienne et al., 2007), and rarely occur together in any one glacial succession. Consequently, Neoproterozoic diamictites have been argued to represent non-glacial, syn-tectonic sediment gravity flows (e.g. Eyles and Januszczak, 2004, 2007), associated with widespread rift activity during break-up of the Rodinia supercontinent.

In Quaternary studies, detailed analysis of soft-sediment deformation structures has received significant credence in discriminating between glacial and non-glacial successions (e.g. Lachniet et al., 2001; Menzies and Zaniewski, 2003; van der Meer and Menzies, 2011). However, with a few notable exceptions (e.g. Benn and Prave, 2006; Arnaud, 2008, 2012), such analyses are scarcely applied to Neoproterozoic deposits. To redress this, we present a new macro- and micro-scale structural analysis of the Chuos Formation of Cryogenian age in the Otavi Mountainland, northern Namibia (Fig. 1a). The study will utilise standard sedimentological and structural analysis of the diamictite succession in order to determine the genetic origin of the Chuos Formation, and assess the significance of soft-sediment deformation structures as palaeoclimate proxies during Neoproterozoic glaciation.

1.1. Geological background

The Otavi Group is a carbonate-dominated succession of Neoproterozoic age housing two diamictite horizons, the older Chuos and younger Ghaub formations (Fig. 1b), each sharply overlain by fine-grained carbonate deposits (Hoffmann and Prave,

* Corresponding author. Tel.: +44 7756819341.
E-mail address: Marie.Busfield.2011@live.rhul.ac.uk (M.E. Busfield).

0016-7878/$ – see front matter © 2012 The Geologists' Association. Published by Elsevier Ltd. All rights reserved.
http://dx.doi.org/10.1016/j.pgeola.2012.10.005

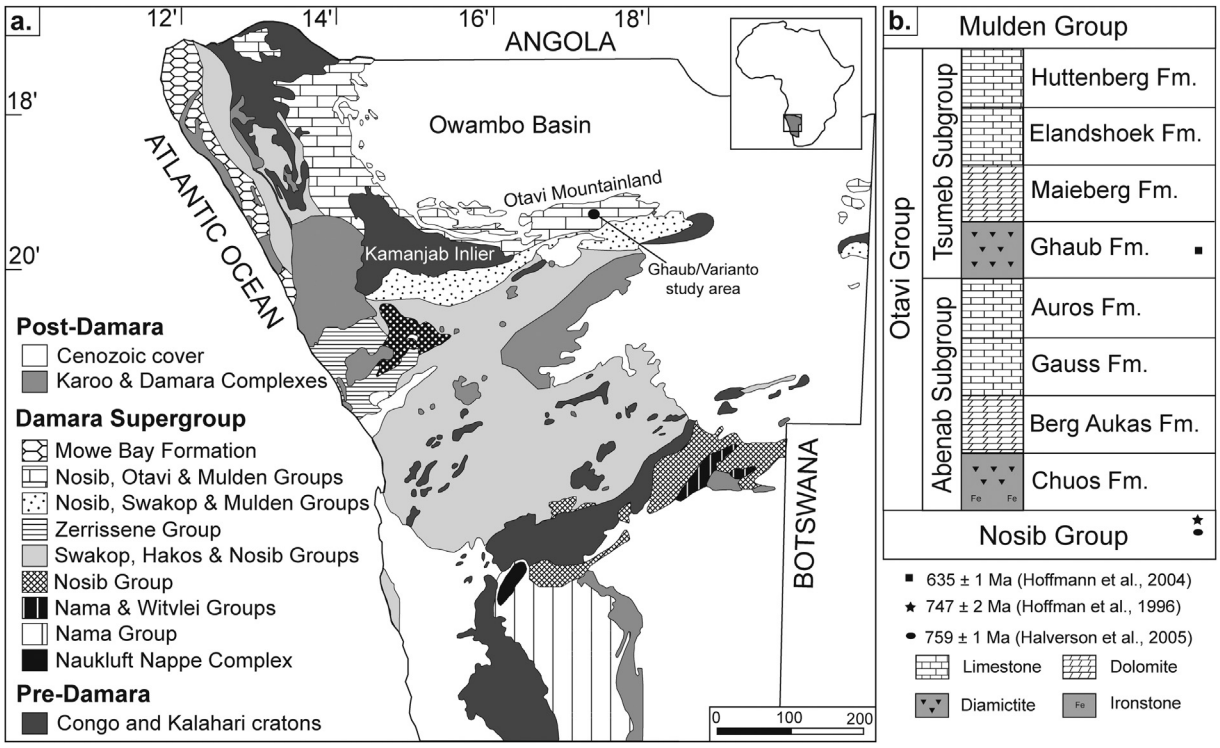

Fig. 1. (a) Map outlines stratigraphic framework of Namibia, and the location of the study sites in the Otavi Mountainland, along the south-eastern flank of the Owambo Basin, after Miller (2008). (b) Stratigraphy of the Cryogenian succession exposed in the study area, after Hoffmann and Prave (1996).

1996; Hoffman and Halverson, 2008; Miller, 2008). These horizons have been dated in turn to <746 ± 2 Ma (Hoffman et al., 1996) and 635.5 ± 1.2 Ma (Hoffmann et al., 2004), through U–Pb zircon ages of underlying and interbedded volcanic ash beds, leading to correlation with the purportedly global Sturtian and Marinoan glaciations, respectively (Kennedy et al., 1998). In light of the argued syn-rift derivation of the diamictite assemblages (e.g. Eyles and Januszczak, 2004, 2007), proponents of the glacial hypothesis have focussed largely on the younger Ghaub Formation, considered to have accumulated during the 'drift' stage of post-rift subsidence (Hoffman and Halverson, 2008). The older Chuos Formation, by comparison, has received less attention.

The glacial origin of the Chuos Formation was first proposed by Gevers (1931) due to its lithological similarity to the Late Palaeozoic Dwyka Tillite (cf. Henry et al., 1986), and its abundance of faceted and extrabasinal clasts. The stratigraphic position of the Chuos between carbonate successions was used to support a glaciomarine origin (Martin, 1965a,b; Hedberg, 1979), in-keeping with the regional absence of subglacial striated pavements (Kroner and Rankama, 1973). Alternative studies conversely describe the textural immaturity of the diamictites, abundance of locally derived erratic lithologies and their spatial and temporal association with faults as evidence of high energy, rift-related submarine gravity flow deposition (e.g. Hedberg, 1979; Miller, 1983; Porada, 1983; Porada and Wittig, 1983a,b; Martin et al., 1985). Under this scenario, the abundant outsized clasts, frequently cited as evidence of ice-rafting (e.g. Hoffman et al., 1998), are interpreted as the product of local mass flow 'rafting', or gravitational settling from overlying diamictites (Martin et al., 1985; Eyles and Januszczak, 2007). Further models propose a compromise between these two hypotheses, wherein both glacigenic deposition and gravitationally driven mass flows interact within an ice marginal, glaciomarine environment (Hoffmann, 1983; Henry et al., 1986).

Three interpretations of the diamictites are thus possible: (1) those generated directly by glacial processes; (2) those of primary glacial origin but re-worked by gravitational mass transport; and (3) those generated by mass flow or slope failure without glacial influence. Consequently, criteria to correctly distinguish these environments remain pivotal to the debate surrounding the origin of the Chuos Formation. These criteria, in turn, have wide implications for interpretations of Neoproterozoic diamictites from a global perspective.

1.2. Study area and stratigraphy

The Otavi Mountainland in northern Namibia exposes a thick succession of Neoproterozoic strata flanking the southern margin of the Owambo Basin (Fig. 1). The Chuos Formation exhibits considerable lateral thickness variations across the region, reaching up to 130 m in the central and western sectors, and pinching out towards the south-east (Hoffmann and Prave, 1996). In the study area, on Ghaub and Varianto farms (Fig. 2), it rests with angular unconformity on sandstones and conglomerates of the Nosib Group (here the Nabis Formation; Miller, 2008), and is sharply overlain by fine-grained carbonate mudstone of the Berg Aukas Formation. The study area is ideally situated in the least deformed northern margin of the Damara Orogenic Belt, characterised by a low shear, fold-thrust zone and sub-greenschist facies metamorphism (Gray et al., 2008; Miller, 2008). These characteristics permit detailed sedimentological and structural analysis of the diamictite horizons as they have suffered minimal tectonic and metamorphic overprint.

2. Methodology

Sedimentary logging of the Chuos Formation was undertaken at several exposures across the Ghaub and Varianto Farms at a metre-scale resolution. This process determined upper and lower boundary relationships, enabling thickness changes to be documented across the area, and the internal architecture of the

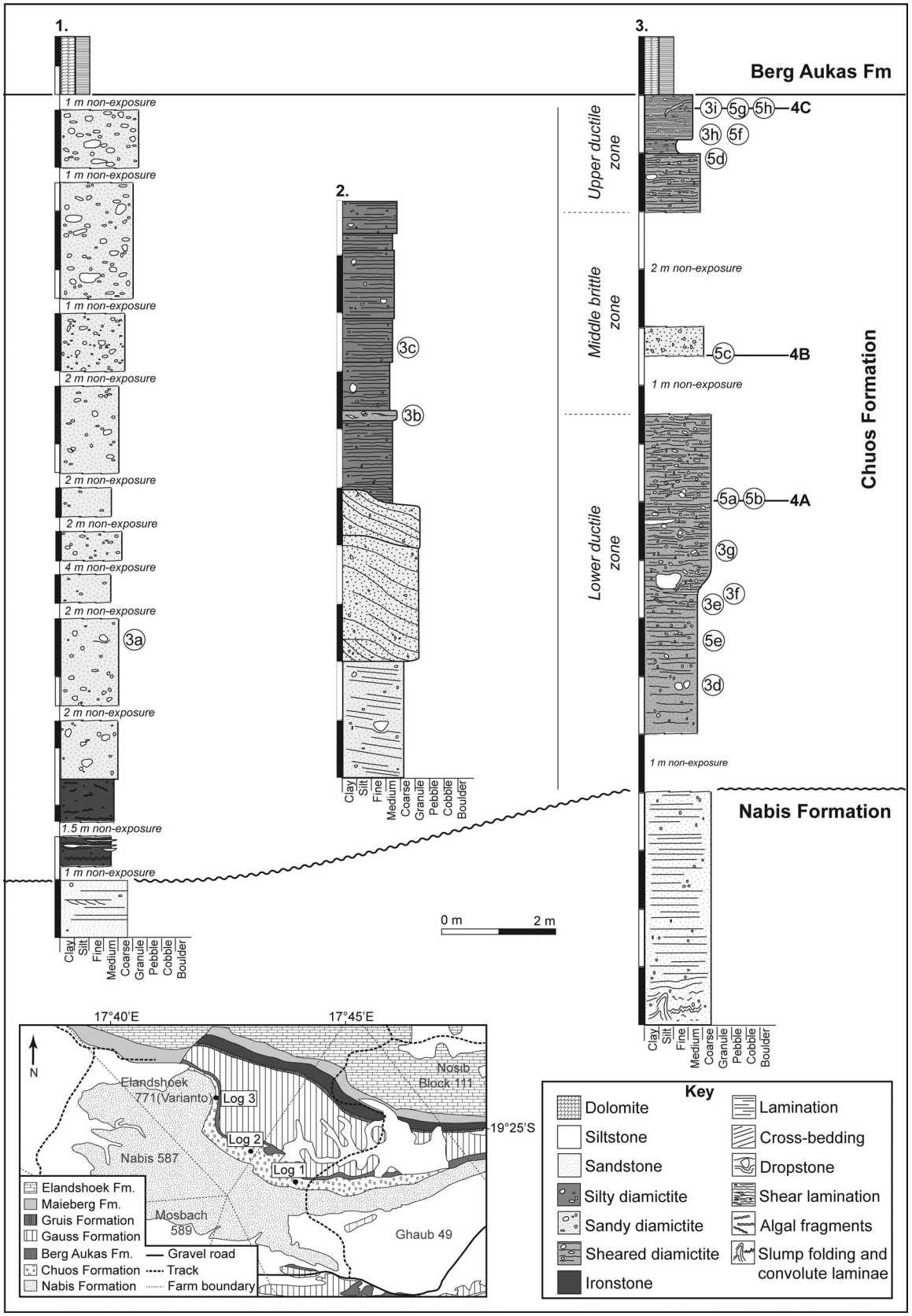

Fig. 2. Logged sections of the Chuos Formation, located on inset geological map of Ghaub and Varianto Farm study areas. Note the overall lateral transition from massive to stratified diamictites towards the west/north-west. The stratigraphic location of images shown in Figs. 3–5 are indicated by their corresponding numbers adjacent to the logs. Map modified after Geological Survey of Namibia (2008).

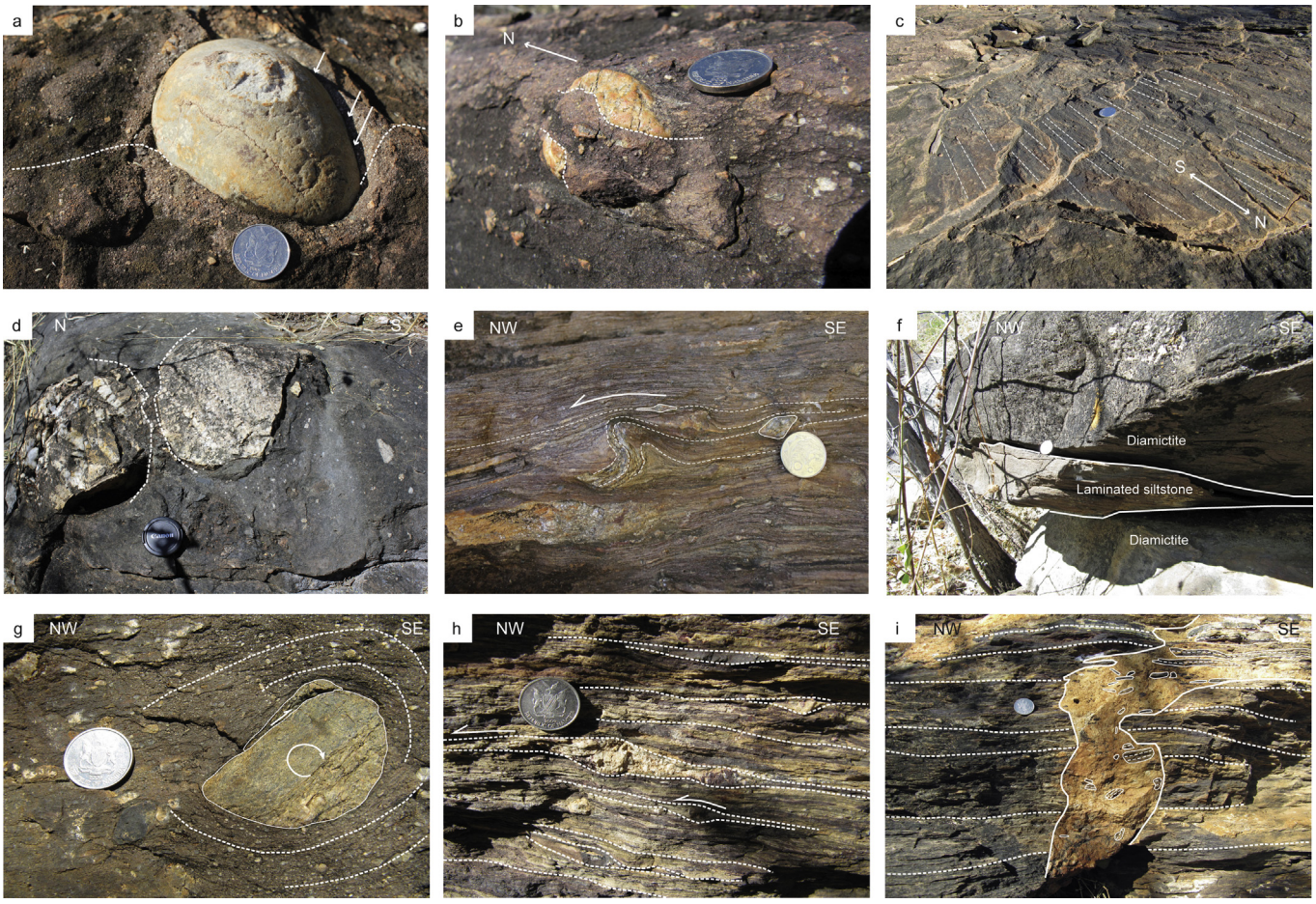

Fig. 3. Macro-scale sedimentary and deformation structures. Coin and lens cap for scale measure 2 cm and 5 cm, respectively. (a) Outsized clast with impact-related deformation structure, indicated by white arrows. (b) Fractured clast infilled by diamictite. (c) North–south trending linear grooves and ridges interpreted as soft-sediment striated surfaces. (d) Fractured outsized clast within the comparatively undeformed base of Log 3 (Fig. 2). (e) Asymmetric fold demonstrating top-to-the-NW vergence. Note clast attenuation parallel to deformed laminae. (f) Laminated siltstone lens, interpreted as ice-bed separation feature, restricted to the south-eastern margin of the exposed section (Log 3; Fig. 2). (g) Rotational turbate structure showing preferential alignment of smaller clasts around the margins of the central obstacle clast (picked out by white dashed lines). Note top-to-the-SE shearing and abrasion of core stone. (h) Pervasive tectonic lamination. Asymmetric clast boudinage and S-C structures define a top-to-the-NW shear sense. (i) Carbonate dyke cross-cuts sheared diamictite (g). Note brecciated fragments of deformed diamictite within the dyke.

formation to be characterised in detail. Lithofacies were described on the macro-scale, including clast fabrics, bedding relationships, and the presence and orientation of deformation structures.

For the purpose of this study, micro-scale analysis is restricted to an exposure of highly deformed diamictite, where vertical changes in deformation style could be documented in detail. Oriented samples were collected at appropriate intervals for thin section analysis, determined where macro-scale changes in sedimentary or structural features were apparent. Thin section analysis was undertaken using a petrographic microscope at low magnification (1× and 2×), under plane and cross-polarized light, as well as examining high resolution photographs and digital scans. Micro-scale features were described using standard structural terminology and micromorphological techniques (*sensu* van der Meer, 1987, 1993; Menzies, 2000; Carr, 2004).

3. Sedimentology

3.1. Description

Three principal facies can be recognised comprising: (1) stratified diamictite facies, (2) sheared and laminated diamictite, and (3) massive diamictite facies. In the south-east of the study area the latter facies dominates (Fig. 2), with intercalated and overlying units of stratified and sheared diamictite becoming more abundant northwards. At outcrop scale, diamictite units typically coarsen upwards, although grading is rarely observed within individual beds. Clast lithologies consist predominantly of well rounded quartzite, with minor sub-angular to rounded mudstone, mica schist, granite gneiss and andesite. Striated and faceted clasts were not observed. Evidence of impact-related deformation beneath some of the larger outsized clasts is typically restricted to the stratified units, expressed through puncturing and down-warping of the underlying laminae (Fig. 3a). This facies also preserves large-scale (1–2 m) eastward-dipping foreset structures (Log 2; Fig. 2), overlain by a sheared diamictite horizon (Fig. 3b), which is in turn succeeded by a series of soft-sediment striated surfaces, comprising centimetre-scale linear grooves and ridges which trend approximately north–south along exposed bedding planes (Fig. 3c). Detailed description of deformation structures within the sheared and laminated facies will be discussed in Section 4 below.

4. Deformation structures

A spectacularly well exposed vertical section of the Chuos Formation containing approximately 30 m of highly deformed and attenuated diamictite crops out on Varianto Farm (19°24.415′S, 17°42.443′E; Fig. 2), in the central portion of the Otavi Mountainland. The sequence overlies coarse sandstone of the Nabis

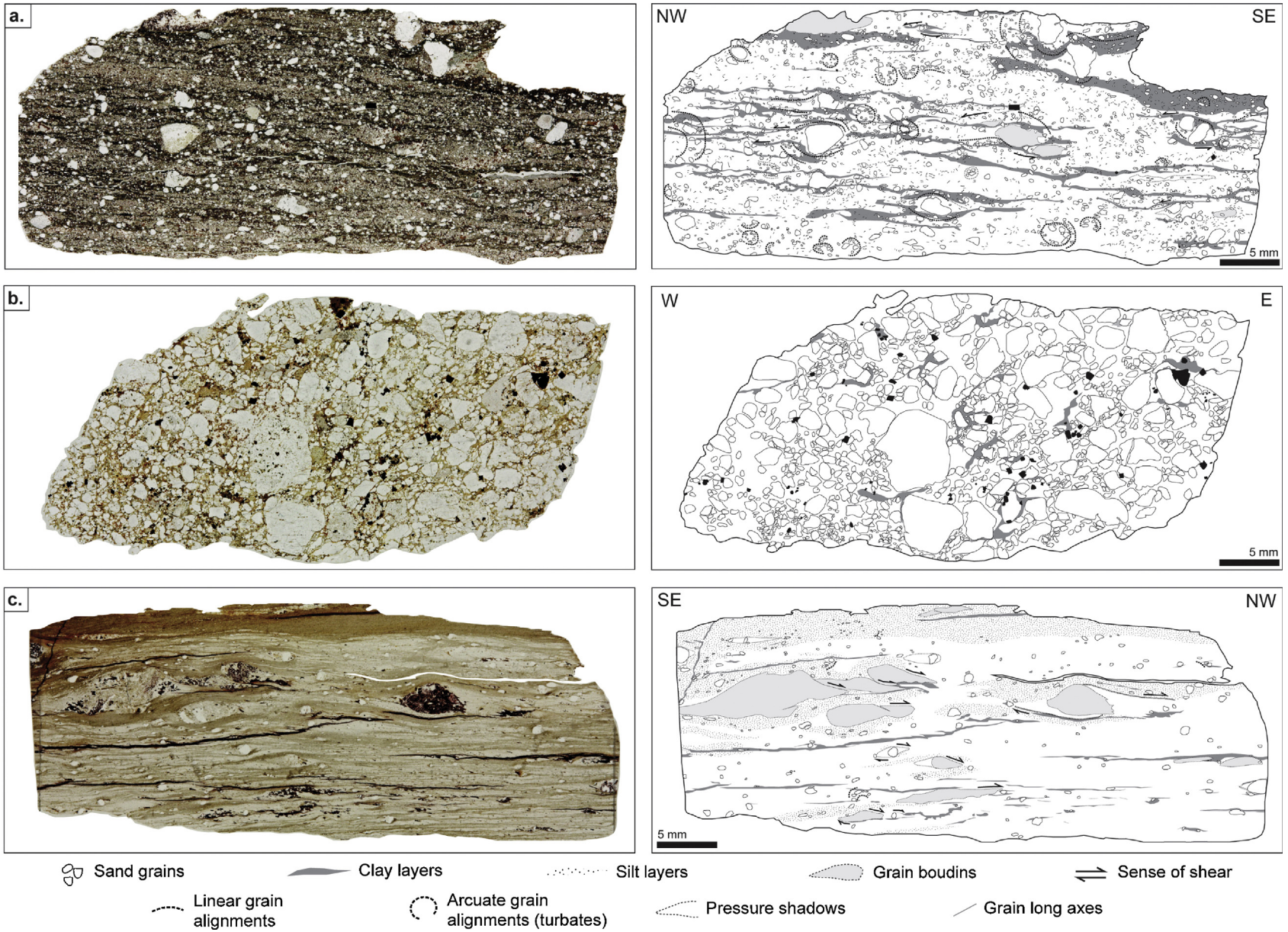

Fig. 4. Paired thin section photograph and interpretation of Chuos Formation microstructures. *Lower ductile zone*: (a) well developed sub-horizontal fabric and abundant rotational deformation structures (turbate structures, asymmetric boudins, clast dispersion tails and asymmetric pressure shadows). Microstructures support top-to-the-NW shear sense. *Middle brittle zone*: (b) section characterised by fractured and crushed quartz grains (white) and magnetite crystals (black). Fractured surfaces can be traced between adjacent clasts, akin to a 'jig-saw' pattern, indicating in situ clast breakage. Sense of deformation cannot be ascertained. *Upper ductile zone*: (c) microstructures are highly attenuated, defined by the predominance of sheared clast boudins. These features, alongside asymmetrical pressure shadows and rare rotational turbates support top-to-the-NW deformation. Note sub-horizontal clay layers cutting oblique to tectonic lamination, with flame-like structures on their upper boundary.

Formation, which exhibit well developed convolute bedding and soft-sediment fold structures approximately 6 m below the boundary with the Chuos, passing upwards into undeformed, well-bedded sediments (Log 3; Fig. 2). Likewise, finely laminated carbonate mudstone of the Berg Aukas Formation, sharply overlying the Chuos Formation, is undeformed.

Lateral exposure of the Chuos Formation at this locality is limited, and thus descriptions of the macro- and micro-scale structures below will focus on upsection evolution of the deformation regime. For ease of description, the section has been divided into three structural zones, shown on Fig. 2. The lower and upper zones are dominated by ductile deformation structures (e.g. rotational features, dispersion tails, clast boudinage). The intermediate zone, meanwhile, is dominated by brittle deformation styles (e.g. fractured and crushed grains). Micromorphological terminology follows the style of Brewer (1976), as adapted by Menzies (2000), Zaniewski and van der Meer (2005) and Phillips et al. (2011) (see Glossary).

4.1. Lower ductile zone (0–21 m)

4.1.1. Macroscale description

The basal 3 m of the Chuos Formation in Log 3 (Fig. 2) is characterised by massive to crudely laminated, poorly sorted diamictite. Evidence of deformation in this horizon is restricted to fractures traversing the larger outsized clasts (Fig. 3d). These sediments pass gradually upwards through moderately to well-laminated diamictites. Approximately 14 m above the base of the section, these well-laminated units exhibit asymmetric folds (Fig. 3e), clast attenuation and development of asymmetric pressure shadows. These features collectively record top-to-the-NW sense of shear.

At the south-eastern margin of the outcrop, these shear structures are overlain by a finely laminated siltstone (Fig. 3f), which coarsens upwards with the input of granule to small pebble sized clasts. The siltstone exhibits a concave-upward basal surface and planar upper surface, and pinches out laterally (to the NW), where no disconformity in the diamictite is visible. Above, the diamictite remains well-laminated with deformation features including rotational turbate structures (Fig. 3g), clast dispersion tails and pervasive lineations on the clast surfaces, trending NNW (344°).

4.1.2. Microscale description

Micro-scale observations support a crudely developed lamination in the basal 3 m of the logged section, passing gradually upwards into more delicately laminated intervals (Fig. 4a). Rounded to sub-angular grains consist predominantly of quartzite, with minor feldspar, siltstone and clay intraclasts. Clast long axis orientations are variable, although a high proportion of grains exhibit a sub-horizontal microfabric (oriented N/NW to S/SE).

Planar features (e.g. linear grain alignments, symmetrical pressure shadows) are restricted to the base of this zone, whereas rotational deformation structures (e.g. turbate structures, dispersion tails, asymmetric pressure shadows and clast boudinage) are dominant throughout (Figs. 4a, 5a and b), and become progressively more abundant upsection. This is reflected in the development of necking structures between adjacent turbates (Fig. 5a). Bands of birefringent clay material (plasmic fabric) also become more distinct and pervasive upsection, varying from skel-masepic to skelsepic and unistrial. In places, this clay birefringence also outlines distinct S-C fabrics (Fig. 5e). These features, alongside the rotational structures, support a top-to-the N/NW shear sense. Towards the top of this zone, these structures and plasmic fabrics are cross-cut by sub-horizontal, non-birefringent clays, which in places demonstrate vertical, flame-like structures along their upper boundary.

4.2. Middle brittle zone

4.2.1. Macroscale description

At 21 m, poor exposure precludes detailed observation. At this interval, a metre thick unit of massive diamictite crops out, without evidence of macro-scale deformation.

4.2.2. Microscale description

The thin section is composed of poorly sorted, angular to sub-rounded quartz and feldspar grains which demonstrate no preferred orientation (Fig. 4b). Brittle deformation features, including crushed quartz and fractured clasts (Fig. 5c), are common throughout, whereas ductile features were not observed. The abundant fracture surfaces can be correlated between adjacent grains across most of the section, resembling a 'jig-saw fit' pattern (Figs. 4b and 5c). A distinct birefringent fabric between the grains cannot be discerned.

4.3. Upper ductile zone

4.3.1. Macroscale description

Well-laminated diamictite returns at 28 m, wherein a high proportion of clast long axes parallel the sub-horizontal lamination, and are in places attenuated along this fabric. Deformation is again dominated by rotational features including asymmetric boudins, S-C fabrics and turbate structures (Fig. 3g and h). This interval is cross-cut by a carbonate sedimentary dyke, consisting of brecciated fragments of the surrounding laminated diamictite, set in a carbonate mudstone matrix (Fig. 3i).

4.3.2. Microscale description

This zone is characterised by a much smaller clast population than the underlying lower ductile and middle brittle zones, and becomes progressively more matrix-rich upsection accompanied by more distinct horizontal lamination (Fig. 4c). As in the lower ductile zone, rotational deformation features dominate, although conversely no planar features are present (e.g. linear grain alignments, symmetrical pressure shadows). Turbate structures and dispersion tails are abundant at the base of this zone (Fig. 5d), but diminish upsection where asymmetric pressure shadows and clast boudins are more prevalent (Fig. 5f–h). These features support a top-to-the NW sense of shear. Unistrial and skelsepic plasmic fabrics are highly developed throughout. In places, these fabrics are cross cut by sub-horizontal clay-rich layers (Fig. 5f–h), which exhibit flame structures along their upper boundary, as seen in the lower ductile zone.

5. Discussion

5.1. Syn-sedimentary evolution of the Chuos Formation

Within the stratified diamictite facies, the widespread occurrence of outsized clasts with impact-related deformation structures (Fig. 3a) is interpreted as evidence of ice-rafted debris (IRD) (Thomas and Connell, 1985; Bennett et al., 1996; Condon et al., 2002), whereby derivation via sediment gravity flow rafting is rejected owing to the absence of characteristic clast imbrication, or correlation between bed thickness and maximum clast size (e.g. Martin et al., 1985; Postma et al., 1988). Water depths were sufficient to accumulate IRD at repeated stratigraphic intervals throughout deposition, but in the absence of diagnostic indicators, accumulation within a glaciomarine or glaciolacustrine basin cannot be ascertained. Large-scale cross-bed foresets within this

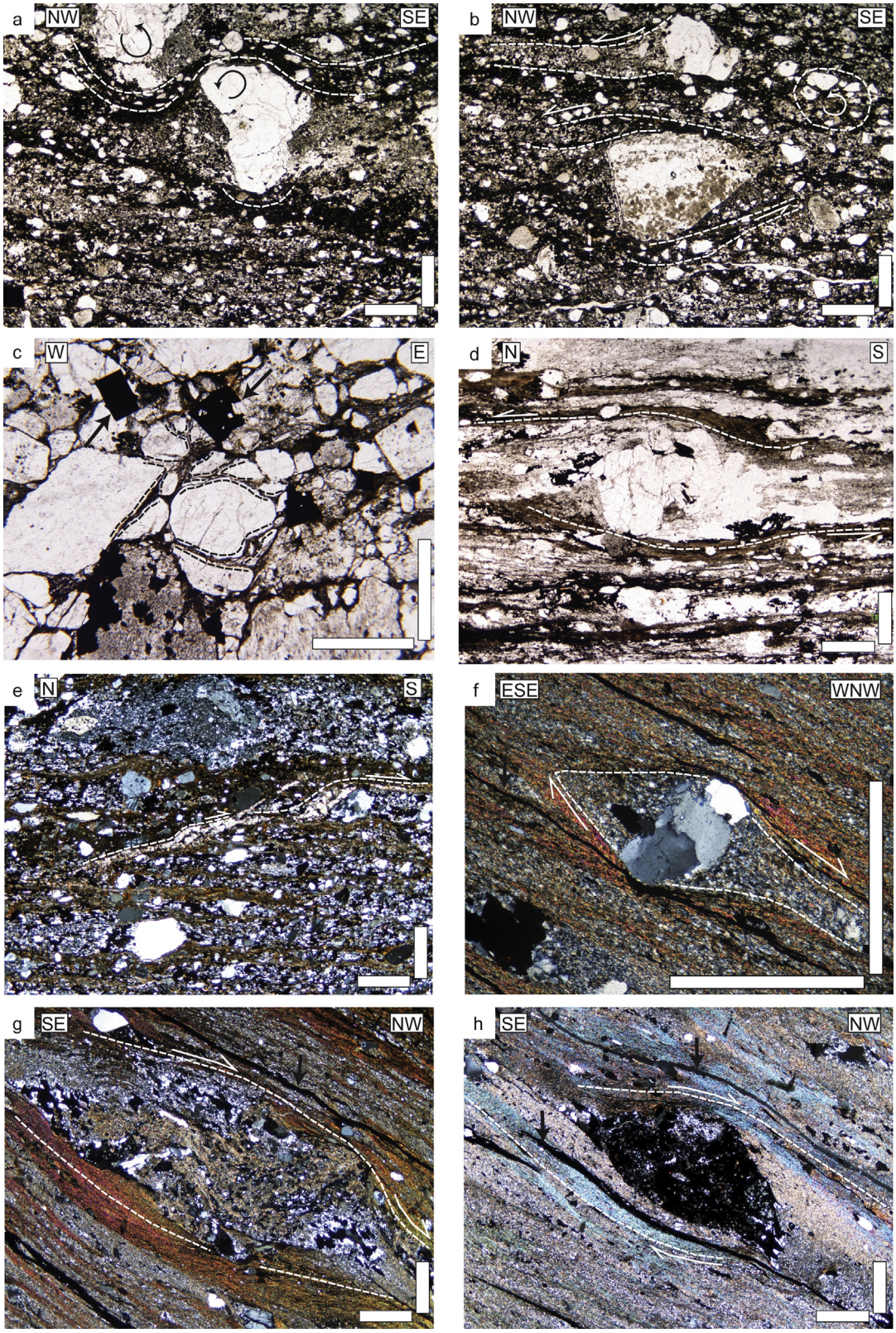

Fig. 5. Micro-scale deformation structures. Photos a–d: plane polarized light, photos e–h: cross-polarized light. White bar = 1 mm. *Lower ductile zone*: (a) necking structure developed between adjacent turbate structures. (b) Central rotational deformation structure with associated 'tails' of silt-grade sediment and small sand clasts. Top-to-the-NW shear sense also supported by asymmetric pressure shadow in the uppermost portion of the image. *Middle brittle zone*: (c) dashed lines highlight 'jig-saw fit' fractured grain surfaces. *Upper ductile zone*: (d) rotational structure with fabric-parallel 'tails' of clay-grade sediment and small sand grains. Abrasion and fracturing of core stone interpreted as product of pervasive shearing. (e) Birefringent clay particles outline S-C fabrics, supporting top-to-the-N shear sense. (f) Asymmetric pressure shadow outlined by skelsepic-unistrial plasmic fabric. Note discontinuous clay layers trending both parallel and oblique to the plasmic fabric (black arrow). (g and h) Well developed unistrial to skelsepic plasmic fabric surrounding boudinaged skeleton grains. Note discontinuous clay layers cutting oblique to the plasmic fabric (black arrow).

facies (Log 2; Fig. 2) record tractive deposition and development of a simple barform, prograding towards the east. In view of the evidence favouring ice-rafting, these features are interpreted as ice-proximal subaqueous fan deposits (e.g. Powell and Domack, 1995; Powell, 2003; Hornung et al., 2007). The overlying soft-sediment striated surfaces (Fig. 3c), identical in morphology to those of the Hirnantian glacial record of North Africa (Sutcliffe et al., 2000; Le Heron et al., 2005), support the intrastratal transmission of shear stresses and subglacial deformation following subaqueous fan progradation. The absence of slickencrysts and polish on these surfaces discounts a later tectonic origin (Petit and Laville, 1987; Eyles and Boyce, 1998).

In the massive diamictite facies, glacial indicators are typically absent (Fig. 2). This is considered to reflect glaciogenic debris flow remobilisation, consistent with the proposed ice-proximal environment. In this setting, dynamic grounding-line oscillations would contribute to high rates of sediment supply, supported by the presence of subaqueous fan deposits and common coarsening upward profile of the diamictites (e.g. Benn, 1996; Evans et al., 2012), leading to rapid accumulation and oversteepening of the sediment pile. Clast abrasion and erosion during resultant re-working of the glaciogenic sediments could therefore account, at least in part, for the unusual absence of striated and faceted clasts within the Chuos Formation.

In light of the location of the study area at the northern margin of an intracratonic fold belt (Miller, 2008), distinguishing the effects of soft-sediment or tectonogenetic deformation within the sheared and laminated diamictite facies remains paramount. Overall, the lack of bedding-discordant fabric development or metamorphic mineral overprint, and largely undeformed nature of the underlying and overlying formations indicate a soft-sediment genesis. In support, towards the top of Log 3 (Fig. 2) a carbonate dyke intrudes and brecciates the sheared diamictite (Fig. 3i), with evidence of liquefaction of clay and silt grade material along the intrusive contact. This is used to support a porewater-induced origin for the dyke, representing hydrofracturing of the sediment pile (e.g. van der Meer et al., 2009), and thus acts to support continued syn-sedimentary deformation *after* pervasive shearing and attenuation of the diamictite. Moreover, kinematic indicators throughout the section, all demonstrate top-to-the N/NW sense of shear (Figs. 3–5), consistent with the N-S strike of the grooves on the soft-sediment striated surfaces. Conversely, the dominant structural grain produced during Damaran orogenesis generated ENE-trending structures (Miller, 1983; Gray et al., 2008), cutting oblique to the trend of the sedimentary structures within the Chuos Formation.

5.2. Glacial vs. non-glacial deformation history

A striking feature of the described section, both on macro- and micro-scale, is the upsection increase in deformation intensity, reflected in the increased abundance and lateral attenuation of individual deformation structures (Figs. 3–5). This incremental strain profile is a common feature within subglacial regimes (Boulton and Hindmarsh, 1987; Hart and Boulton, 1991; Benn and Evans, 1996; Evans et al., 2006; Hart, 2007), where the highest stress conditions are encountered at the ice-bed interface and diminish downwards. In contrast, deformation structures in a mass flow deposit exhibit the highest stress characteristics at base (see Fig. 6), where friction between the flow and the underlying substrate is greatest, thereby resulting in development of a basal shear zone accompanied by an upward decrease in strain intensity (Nardin et al., 1979; Nemec, 1990; Hart and Roberts, 1994; Mulder and Alexander, 2001).

Features considered diagnostic of sediment remobilisation, including flow noses and tile structures (Hart and Roberts, 1994; Bertran and Texier, 1999; Lachniet et al., 2001; Menzies and Zaniewski, 2003), are conspicuously absent from the Chuos Formation (Fig. 6). The former are indicative of low shear, downslope slumping, and are hence rarely preserved under the relatively higher stress conditions encountered during subglacial deformation (Lowe, 1982; Hart and Roberts, 1994). Meanwhile, the latter appear to be a unique feature associated with deceleration and dewatering of sediment gravity flows (Menzies and Zaniewski, 2003; van der Meer and Menzies, 2011). Similarly, clasts with coatings of diamictite on the macro-scale, or concentrically laminated grain coatings on the micro-scale, though not diagnostic, would support sediment re-working if present (Phillips, 2006; Kilfeather et al., 2009). Furthermore, the absence of load structures and rare evidence of vertical to sub-vertical water escape structures may be considered atypical of mass flow deposition (Lowe, 1982; Visser et al., 1984; Hart and Roberts, 1994; Menzies and Zaniewski, 2003).

Rotational deformation structures are ubiquitous in the Chuos Formation, particularly on the micro-scale (Figs. 4 and 5), and are encountered in both subglacial settings and sediment gravity flows (Fig. 6; Lachniet et al., 2001; Menzies and Zaniewski, 2003; Phillips, 2006). In the former, these features are interpreted as the product of shearing within the deforming bed (van der Meer, 1993, 1997), whereby stress is accommodated around a rotating nucleus (consisting of a core stone or stiff matrix), leading to preferential alignment of smaller clasts at the nucleus periphery. Similar mechanisms are envisaged in sediment gravity flows, although rotation acts as a product of transient turbulent cells within the depositing flow (Phillips, 2006). Although the latter mechanism cannot be excluded, the absence of other features indicative of turbulence (e.g. normally graded beds), as compared to abundant evidence of pervasive shearing, is compatible with a glacitectonic origin for the turbates. This is also supported by their association with planar shear fabrics and structures throughout (cf. Hiemstra and Rijsdijk, 2003).

Additional deformation structures frequently cited as evidence of subglacial processes are prevalent throughout (see Fig. 6), including pervasive tectonic lamination, unidirectional folding, pressure shadows and clast dispersion tails (e.g. van der Meer, 1993; Hart and Roberts, 1994; Benn and Evans, 1996; Menzies et al., 1997; Lachniet et al., 2001; Carr et al., 2006; Menzies et al., 2006). These features are characteristic of relatively high strain ductile deformation, facilitated by elevated porewater pressures, which succeed in lowering the effective stress of the sediment (Menzies, 2000; Phillips et al., 2007; Lee and Phillips, 2008). These conditions are commonly encountered in subglacial settings under the high overburden pressure of ice and abundant basal meltwater supply (see Section 5.3). This is also supported by the presence of fractured and crushed grains, which frequently develop in zones of high hydrostatic pressure near the ice-bed interface (Hiemstra and van der Meer, 1997; Menzies, 2000; Carr et al., 2006).

5.3. Hydrology of the subglacial bed

In view of the sedimentological evidence of primary deposition as a subaqueous diamictite, it would be plausible to consider the sediments as water-saturated, and thus with elevated porewater contents, prior to subglacial deformation. Nonetheless, the observed upsection increase in strain intensity, alongside attenuation and lateral isolation of individual microstructures, reflects sustained and increasing high porewater pressures throughout deformation.

In a subglacial environment, the effect of overriding ice on porewater state will be three-fold: (1) overburden pressure will increase confining pressure on the deforming bed, (2) the ice will

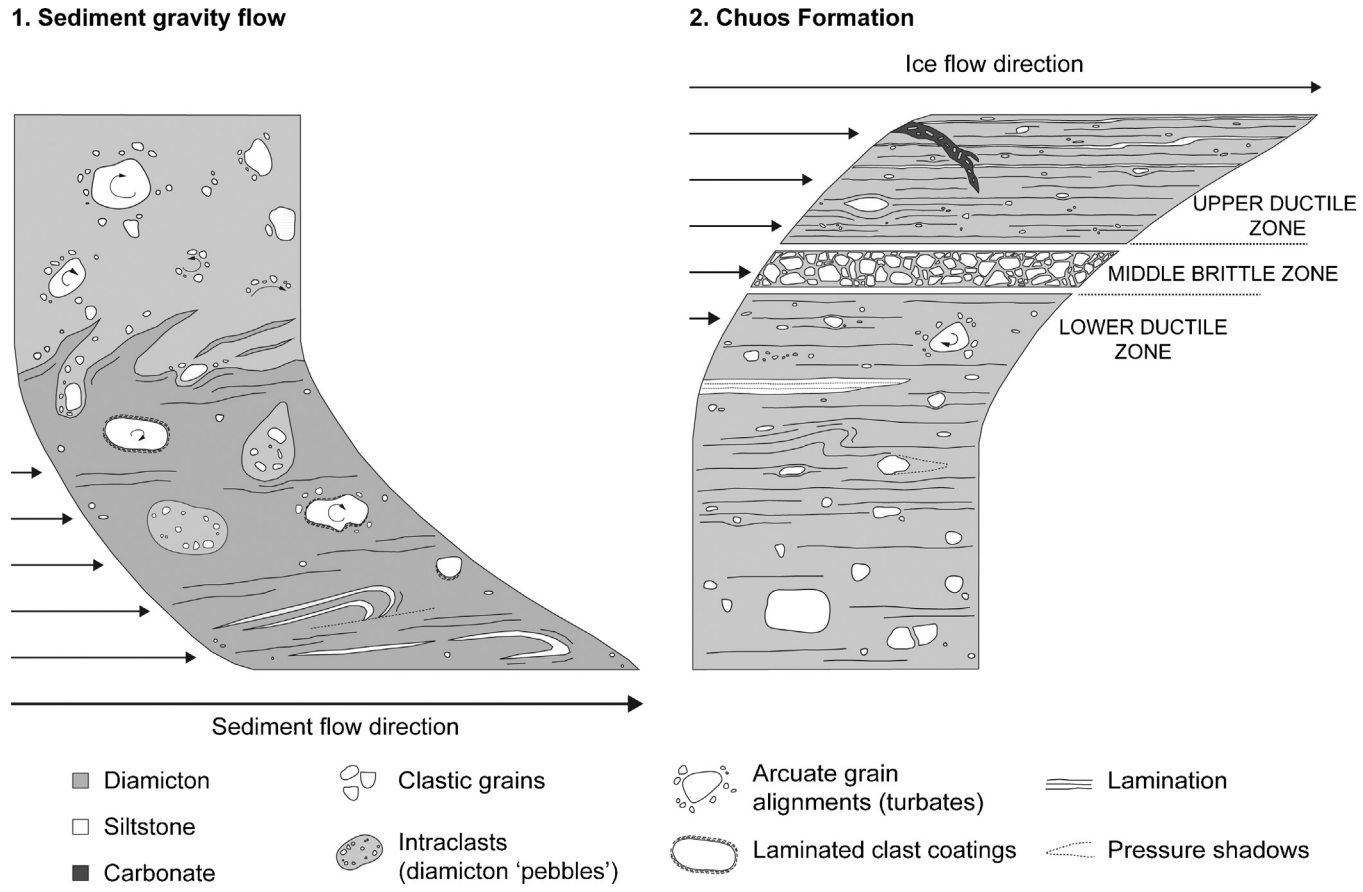

Fig. 6. Schematic diagram highlights dominant style and association of deformation structures typically encountered within a sediment gravity flow as compared to the assemblage identified in the Chuos Formation. Length of black arrow corresponds to strain intensity, wherein the former would be expected to demonstrate a basal shear zone with upward decreasing strain intensity, vertical water-escape structures and abundant evidence of re-working (e.g. diamictite intraclasts, laminated clast coatings, slump folds). In contrast, the observed upsection increase in strain intensity, abundance of ductile deformation features, pervasive tectonic lamination, and sub-horizontal water-escape features act to support subglacial deformation under high cumulative stress and elevated porewater pressures.
Adapted after Evans et al. (2012) and Phillips (2006).

act as an impermeable seal inhibiting vertical water escape, and (3) friction at the ice-bed interface will generate abundant basal meltwater, thereby increasing porewater content (Evans and Hiemstra, 2005; Phillips et al., 2007; Lee and Phillips, 2008, 2011). A common process in this scenario will be the development of lateral water escape features (Roberts and Hart, 2005; Lee and Phillips, 2008), in this succession generating abundant sub-horizontal clay-filled conduits. These features, in conjunction with well developed plasmic fabrics throughout (Fig. 5), support high concentrations of impermeable clay minerals within the sediment, which act to further retard water escape from the deforming bed (Denis et al., 2009; Lesemann et al., 2010). These factors will thus enable increased dilation of the sediment, whereby the zone of subglacial shearing can extend deeper within the deforming sediment pile (Lee and Phillips, 2008).

If porewater pressures continue to rise, stress at the ice-bed interface will reach critical levels enabling the ice to decouple from its substrate (Evans et al., 2006), especially in contact with underlying bed irregularities. This will typically result in infill of fine grained sediments within the subglacial cavity, preserved as discontinuous lens-shaped beds (Evans and Benn, 2004; Lesemann et al., 2010). This interpretation is favoured for the finely laminated siltstone (Fig. 3f) recorded at the south-eastern margin of Log 3 (Fig. 2). In contrast, when porewater pressures are reduced, e.g. in response to enhanced water escape or freezing of the subglacial bed, porewater influenced deformation will be inhibited, potentially leading to 'locking-up' of the deforming material (Evans et al., 2006; Lee and Phillips, 2008). As a result, the previously water-saturated sediment may undergo brittle brecciation, as recorded in the middle brittle zone (Fig. 4b). The jig-saw fit pattern of adjacent fractured surfaces (Fig. 5c) supports in situ brecciation of this unit, consistent with rapid de-watering and deceleration of the mobile deforming bed.

5.4. Ice marginal model for the deposition and deformation of the Chuos Formation

Recent studies of stratified glacigenic diamictites within ice marginal environments have advocated accumulation of thick, variably deformed sediment piles through the combined effects of high sediment supply and glaciotectonic thrusting (e.g. Evans and Hiemstra, 2005; Ó Cofaigh et al., 2011; Evans et al., 2012). In these settings, pre-existing stratification within the sediment, commonly produced in response to the heterogeneous sediment inputs encountered at the ice margin, encourages deformation partitioning along bed surfaces. Repeated oscillations of the ice margin will therefore exploit these pre-existing structural weaknesses, leading to glaciotectonic thrusting and stacking, and hence incremental thickening of the succession. Depending on the extent of ice advance, these oscillations can also lead to overriding of the sediment pile (Ó Cofaigh et al., 2011), resulting in subglacial as well as ice marginal deformation.

A similar setting is envisaged to account for the sedimentological and structural features preserved within the Chuos Formation

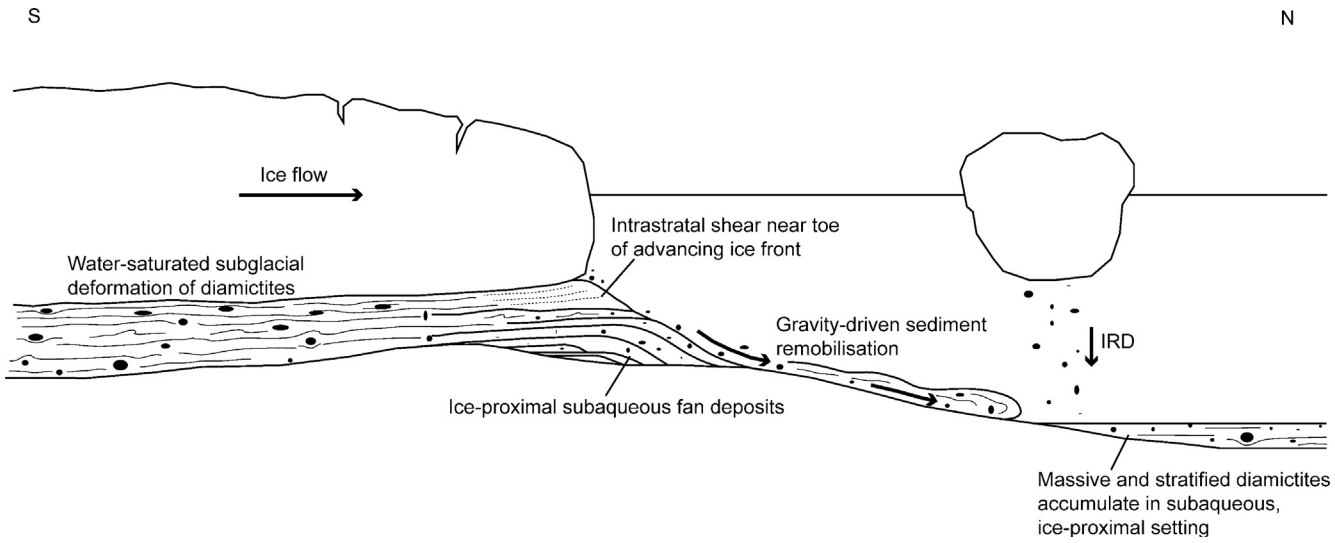

Fig. 7. Ice marginal model for the deposition and subsequent deformation of the Chuos Formation. Ice-proximal subaqueous deposition occurs through the combined input of ice-rafted, englacial, supraglacial and subglacial debris, building out as ice-contact subaqueous fans. During grounding-line oscillations, these sediments undergo subglacial deformation processes behind the ice front, periodic mass wasting in advance of the ice front, as well as proglacial to ice marginal intrastratal shear. Modified after Ó Cofaigh et al. (2011) and Evans et al. (2012).

(see Fig. 7). The development of sub-horizontal lamination at the relatively less deformed base of Log 3 (Fig. 2), alongside the widespread occurrence of stratified diamictites throughout the Chuos Formation, support the generation of a syn-depositional, or 'pre-existing' stratification. Subsequent deformation of the sediment pile clearly resulted in deformation partitioning along bed/lamina contacts since tectonic lamination, shear structures and plasmic fabrics are bed-parallel throughout. These layer-parallel detachments would therefore encourage lateral attenuation and 'smearing' of the deforming sediment, in contrast to the thrust-related aggradation recorded in previous studies (e.g. Evans and Hiemstra, 2005; Ó Cofaigh et al., 2011; Evans et al., 2012). This may also reflect the subglacial position of the sediment throughout deformation, where it would have been sheltered from proglacial and ice marginal tectonics (Fig. 7).

6. Conclusions

The Chuos Formation in the Otavi Mountainland, northern Nambia, accumulated in an ice-proximal subaqueous environment prior to secondary subglacial deformation. Detailed analysis of soft-sediment deformation structures was critical in determining the presence and influence of grounded ice at this time. These features, in conjunction with the deposition of ice-proximal subaqueous fan deposits, and abundant ice-rafted debris at recurrent stratigraphic intervals throughout the Chuos diamictites act to support dynamic oscillations of the ice grounding-line. Therefore, the unusual paucity of 'classic' glacial indicators (i.e. striated and facteted clasts, striated pavements) does not preclude Neoproterozoic glaciation, as frequently argued under sediment gravity follow hypotheses. Soft-sediment deformation structures are thus considered as key, and largely under-considered, palaeoclimate proxies, with significant implications for determining the glacigenic origin of pan-global diamictite successions, as well as the nature of subglacial bed conditions during the Neoproterozoic icehouse.

Acknowledgments

The authors wish to thank Paulus N. Mungandjera and Ralph J.C.M. Muyamba, UNAM, for their invaluable field assistance, and the owners of Ghaub and Varianto Farms for granting permission to examine these sections on their land. Many thanks also to John Menzies, Bob Thomas and Emrys Phillips for very constructive comments on an earlier draft of this manuscript.

References

Allen, P.A., Etienne, J.L., 2008. Sedimentary challenge to Snowball Earth. Nature Geoscience 1, 817–825.
Arnaud, E., 2008. Deformation in the Neoproterozoic Smalfjord Formation, northern Norway: an indicator of glacial depositional conditions? Sedimentology 55, 335–356.
Arnaud, E., 2012. The paleoclimatic significance of deformation structures in Neoproterozoic successions. Sedimentary Geology 243–244, 33–56.
Benn, D.I., 1996. Subglacial and subaqueous processes near a glacier grounding line: sedimentological evidence from a former ice-dammed lake, Achnasheen Scotland. Boreas 25, 23–36.
Benn, D.I., Evans, D.J.A., 1996. The interpretation and classification of subglacially deformed materials. Quaternary Science Reviews 15, 23–52.
Benn, D.I., Prave, A.R., 2006. Subglacial and proglacial glacitectonic deformation in the Neoproterozoic Port Askaig Formation, Scotland. Geomorphology 75, 266–280.
Bennett, M.R., Doyle, P., Mather, A.E., 1996. Dropstones: their origin and significance. Palaeogeography, Palaeoclimatology, Palaeoecology 121, 331–339.
Bertran, P., Texier, J.-P., 1999. Facies and microfacies of slope deposits. Catena 35, 99–121.
Boulton, G.S., Hindmarsh, R.C.A., 1987. Sediment deformation beneath glaciers: rheology and geological consequences. Journal of Geophysical Research 92, 9059–9082.
Brewer, R., 1976. Fabric and Mineral Analysis of Soils. Krieger, Huntington, 482 pp.
Carr, S.J., 2004. Micro-scale features and structures. In: Evans, D.J.A., Benn, D.I. (Eds.), A Practical Guide to the Study of Glacial Sediments. Arnold, New York, pp. 115–144.
Carr, S.J., Holmes, R., van der Meer, J.J.M., Rose, J., 2006. The last glacial maximum in the North Sea Basin: micromorphological evidence of extensive glaciation. Journal of Quaternary Science 21, 131–153.
Condon, D.J., Prave, A.R., Benn, D.I., 2002. Neoproterozoic glacial-rainout intervals: observations and implications. Geology 30, 35–38.
Denis, M., Guiraud, M., Konaté, M., Buoncristiani, J.F., 2009. Subglacial deformation and water-pressure cycles as a key for understanding ice stream dynamics: evidence from the Late Ordovician succession of the Djado Basin (Niger). International Journal of Earth Sciences 99, 1399–1425.
Etienne, J.L., Allen, P.A., Rieu, R., Le Guerroué, E., 2007. Neoproterozoic glaciated basins: a critical review of the Snowball Earth hypothesis by comparison with Phanerozoic glaciations. In: Hambrey, M.J., Christoffersen, P., Glasser, N.F., Hubbard, B. (Eds.), Glacial Sedimentary Processes and Products. Blackwell Publishing Ltd., Oxford, pp. 343–399.
Evans, D.J.A., Benn, D.I., 2004. A Practical Guide to the Study of Glacial Sediments. Arnold, New York, 266 pp.
Evans, D.J.A., Hiemstra, J.F., 2005. Till deposition by glacier submarginal, incremental thickening. Earth Surface Processes and Landforms 30, 1633–1662.

Evans, D.J.A., Hiemstra, J.F., Cofaigh, C.Ó., 2012. Stratigraphic architecture and sedimentology of a Late Pleistocene subaqueous moraine complex, southwest Ireland. Journal of Quaternary Science 27, 51–63.
Evans, D.J.A., Phillips, E.R., Hiemstra, J.F., Auton, C.A., 2006. Subglacial till: formation, sedimentary characteristics and classification. Earth Science Reviews 78, 115–176.
Eyles, N., Boyce, J.I., 1998. Kinematic indicators in fault gouge: tectonic analog for soft bedded ice sheets. Sedimentary Geology 116, 1–12.
Eyles, N., Januszczak, N., 2004. 'Zipper-rift': a tectonic model for Neoproterozoic glaciations during the breakup of Rodinia after 750 Ma. Earth Science Reviews 65, 1–73.
Eyles, N., Januszczak, N., 2007. Syntectonic subaqueous mass flows of the Neoproterozoic Otavi Group, Namibia: where is the evidence of global glaciation? Basin Research 19, 179–198.
Geological Survey of Namibia, 2008. Sheet 1916 – Tsumeb (1:250,000). Ministry of mines and Energy, Windhoek.
Gevers, T.W., 1931. An ancient tillite in South-West Africa. Transactions of the Geological Society of South Africa 34, 1–17.
Gray, D.R., Foster, D.A., Meert, J.G., Goscombe, R., et al., 2008. A Damara orogen perspective on the assembly of southwestern Gondwana. Geological, Society, London, Special Publication 294, 257–278.
Hart, J.K., 2007. An investigation of subglacial shear zone processes from Weybourne, Norfolk, UK. Quaternary Science Reviews 26, 2354–2374.
Hart, J.K., Boulton, G.S., 1991. The interrelation of glaciotectonic and glaciodepositional processes within the glacial environment. Quaternary Science Reviews 10, 335–350.
Hart, J.K., Roberts, D.H., 1994. Criteria to distinguish between subglacial glaciotectonic and glaciomarine sedimentation. 1: deformation styles and sedimentology. Sedimentary Geology 91, 191–213.
Hedberg, R.M., 1979. Stratigraphy of the Ovamboland Basin, South West Africa Bulletin. Precambrian Research Unit, Cape Town, 325 pp.
Henry, G., Stanistreet, I.G., Maiden, K.J., 1986. Preliminary results of a sedimentological study of the Chuos Formation in the central zone of the Damara Orog: evidence for mass flow processes and glacial activity. Communications of the Geological Survey of South-West Africa/Namibia 2, 75–92.
Hiemstra, J.F., Rijsdijk, K.F., 2003. Observing artificially induced stra: implications for subglacial deformation. Journal of Quaternary Science 18, 373–383.
Hiemstra, J.F., van der Meer, J.J.M., 1997. Pore-water controlled grain fracturing as an indicator for subglacial shearing in tills. Journal of Glaciology 43, 446–454.
Hoffman, P.F., Hawkins, D.P., Isachsen, C.E., Bowring, S.A., 1996. Precise U–Pb zircon ages for early Damaran magmatism in the Summas Mountains and Welwitschia Inlier, northern Damara belt, Namibia. Communications of the Geological Survey of Namibia 11, 47–52.
Hoffman, P.F., Kaufman, A.J., Halverson, G.P., Schrag, D.P., 1998. A Neoproterozoic snowball earth. Science 281, 1342–1346.
Hoffman, P.F., Schrag, D.P., 2002. The snowball Earth hypothesis: testing the limits of global change. Terra Nova 14, 129–155.
Hoffman, P.F., Halverson, G.P., 2008. Otavi Group of the western Northern Platform, southern Damara Belt, SWA/Namibia. In: Miller, R.McG. (Ed.), The Geology of Namibia. Volume 2: Neoproterozoic to Lower Palaeozoic. Ministry of Mines and Energy, Windhoek, pp. 13.69–13.136.
Hoffmann, K.-H., 1983. Lithostratigraphy and facies of the Swakop Group of the southern Damara Belt, SWA/Namibia. In: Miller, R.McG. (Ed.), Evolution of the Damara Orogen of Southwest Africa/Namibia. Geological Society of South Africa Special Publication, 11, Johannesburg, pp. 43–63.
Hoffmann, K.-H., Prave, A.R., 1996. A preliminary note on a revised subdivision and regional correlation of the Otavi Group based on glaciogenic diamictites and associated cap dolostones. Communications of the Geological Survey of Namibia 11, 77–82.
Hoffmann, K.H., Condon, D.J., Bowring, S.A., Crowley, J.L., 2004. U–Pb zircon date from the Neoproterozoic Ghaub Formation, Namibia: constraints on Marinoan glaciation. Geology 32, 817–820.
Hornung, J.J., Asprion, U., Winsemann, J., 2007. Jet-efflux deposits of a subaqueous ice-contact fan, glacial Lake Rinteln, northwestern Germany. Sedimentary Geology 193, 167–192.
Kennedy, M.J., Runnegar, B., Prave, A.R., Hoffmann, K.H., Arthur, M.A., 1998. Two or four Neoproterozoic glaciations? Geology 26, 1059–1063.
Kilfeather, A.A., ÓCofaigh, C., Dowdeswell, J.A., Meer, J.J.M., Evans, D.J.A., 2009. Micromorphological characteristics of glacimarine sediments: implications for distinguishing genetic processes of massive diamicts. Geo-Marine Letters 30, 77–97.
Kirschvink, J.L., 1992. Late Proterozoic low-latitude glaciation: the snowball Earth. In: Schopf, J.W., Klein, C. (Eds.), The Proterozoic Biosphere. Cambridge University Press, Cambridge, pp. 51–52.
Kroner, A., Rankama, K., 1973. Late Precambrian glaciogenic sedimentary rocks in southern Africa: a compilation with definitions and correlations. Bulletin of the Geological Society of Finland 45, 79–102.
Lachniet, M.S., Strasser, J.C., Lawson, D.E., Evenson, E.B., Alley, R.D., 1999. Microstructures of glacigenic sediment-flow deposits, Matanuska Glacier, Alaska. In: Mickelson, D.M., Attig, J.W. (Eds.), Glacial Processes Past and Present. Geological Society of America Special Paper 337, Boulder, Colorado, pp. 45–57.
Lachniet, M.S., Larson, G.J., Lawson, D.E., Evenson, E.B., Alley, R.B., 2001. Microstructures of sediment flow deposits and subglacial sediments: a comparison. Boreas 30, 254–264.
Lee, J.R., Phillips, E.R., 2008. Progressive soft sediment deformation within a subglacial shear zone—a hybrid mosaic-pervasive deformation model for Middle Pleistocene glaciotectonised sediments from eastern England. Quaternary Science Reviews 27, 1350–1362.
Lee, J.R., Phillips, E., 2011. Development of a 'soft deforming bed' within a subglacial shear zone: an example from Bacton Green. In: Phillips, E., Lee, J.R., Evans, H.M. (Eds.), Glacitectonics – Field Guide. Quaternary Research Association, UK, pp. 130–142.
Le Heron, D.P., Sutcliffe, O.E., Whittington, R.J., Craig, J., 2005. The origins of glacially related soft-sediment deformation structures in Upper Ordovician glaciogenic rocks: implication for ice sheet dynamics. Palaeogeography, Palaeoclimatology, Palaeoecology 218, 75–103.
Lesemann, J.-E., Alsop, G.I., Piotrowski, J.A., 2010. Incremental subglacial meltwater sediment deposition and deformation associated with repeated ice-bed decoupling: a case study from the Island of Funen, Denmark. Quaternary Science Reviews 29, 3212–3229.
Lowe, D.R., 1982. Sediment gravity flows. II: depositional models with special reference to the deposits of high-density turbidity currents. Journal of Sedimentary Petrology 52, 279–297.
Martin, H., 1965a. Beobachtungen zum problem der jung-präkambrischen glazialen Ablagerungen in Südwestafrika. Geologische Rundschau 54, 115.
Martin, H., 1965b. The Precambrian Geology of South West Africa and Namaqualand. Precambiran Research Unit, University of Cape Town, Cape Town.
Martin, H., Porada, H., Walliser, O.H., 1985. Mixtite deposits of the Damara Sequence, Namibia, problems of interpretation. Palaeogeography, Palaeoclimatology, Palaeoecology 51, 159–196.
Menzies, J., 2000. Micromorphological analyses of microfabrics and microstructures indicative of deformation processes in glacial sediments. In: Maltman, A.J., Hubbard, B., Hambrey, M.J. (Eds.), Deformation of Glacial Materials. Geological Society Special Publication 176, London, pp. 245–257.
Menzies, J., van der Meer, J.J.M., Rose, J., 2006. Till—as a glacial "tectomict", its internal architecture, and the development of a "typing" method for till differentiation. Geomorphology 75, 172–200.
Menzies, J., Zaniewski, K., 2003. Microstructures within a modern debris flow deposit derived from Quaternary glacial diamicton—a comparative micromorphological study. Sedimentary Geology 157, 31–48.
Menzies, J., Zaniewski, K., Dreger, D., 1997. Evidence, from microstructures, of deformable bed conditions within drumlins, Chimney bluffs, New York State. Sedimentary Geology 111, 161–175.
Miller, R.McG., 1983. Tectonic implications of the contrasting geochemistry of Damaran mafic volcanic rocks, South West Africa/Namibia. In: Miller, R.McG. (Ed.), Geodynamic Evolution of the Damara Orogen. Geological Society of South Africa Special Publication 11, Johannesburg, pp. 115–138.
Miller, R.McG. (Ed.), 2008. The Geology of Namibia. Volume 2: Neoproterozoic to Lower Palaeozoic. Ministry of Mines and Energy, Windhoek.
Mulder, T., Alexander, J., 2001. The physical character of subaqueous sedimentary density flows and their deposits. Sedimentology 48, 269–299.
Nardin, T.R., Hein, F.J., Gorsline, D.S., Edwards, B.D., 1979. A review of mass movement processes, sediment and acoustic characteristics and contrasts in slope and base of slope systems versus canyon-fan basin floor systems. In: Doyle, L.J., Pilkey, O.H. (Eds.), Geology of Continental Slopes. SEPM Special Publication, Tulsa, Oklahoma, pp. 61–73.
Nemec, W., 1990. Aspects of sediment movement on steep delta slopes. In: Colella, A., Prior, D. (Eds.), Coarse Grained Deltas. International Association of Sedimentologists, Special Publication, 10, Oxford, pp. 29–73.
Ó Cofaigh, C., Evans, D.J.A., Hiemstra, J.F., 2011. Formation of a stratified subglacial 'till' assemblage by ice-marginal thrusting and glacier overriding. Boreas 40, 1–14.
Petit, J.-P., Laville, E., 1987. Morphology and microstructures of hydroplastic slickensides in sandstone. In: Jones, M.E., Preston, R.M.F. (Eds.), Deformation of Sediments and Sedimentary Rocks, Geological Society of London Special Publication 29, pp. 107–121.
Phillips, E., 2006. Micromorphology of a debris flow deposit: evidence of basal shearing, hydrofracturing, liquefaction and rotational deformation during emplacement. Quaternary Science Reviews 25, 720–738.
Phillips, E., Merritt, J., Auton, C., Golledge, N., 2007. Microstructures in subglacial and proglacial sediments: understanding faults, folds and fabrics, and the influence of water on the style of deformation. Quaternary Science Reviews 26, 1499–1528.
Phillips, E., van der Meer, J.J.M., Ferguson, A., 2011. A new 'microstructural mapping' methodology for the identification, analysis and interpretation of polyphase deformation within subglacial sediments. Quaternary Science Reviews 30, 2570–2596.
Porada, H., 1983. Geodynamic model for the geosynclinal development of the Damara Orogen, Namibia, South West Africa. In: Martin, H., Eder, F.W. (Eds.), Intracontinental Fold Belts – Case Studies in the Variscan Belt of Europe and the Damara Belt in Namibia. Springer, Heidelberg, pp. 503–540.
Porada, H., Wittig, R., 1983a. Turbidites in the Damara Orogen. In: Martin, H., Eder, F.W. (Eds.), Intracontinental Fold Belts – Case Studies in the Variscan Belt of Europe and the Damara Belt in Namibia. Springer, Heidelberg, pp. 543–576.
Porada, H., Wittig, R., 1983b. Turbidites and their significance for the geosynclinal evolution of the Damara Orogen, South West Africa/Namibia. In: Miller, R.McG. (Ed.), Evolution of the Damara Orogen of South West Africa/Namibia. Geological Society of South Africa Special Publication 11, Johannesburg, pp. 21–36.
Postma, G., Nemec, W., Kleinspehn, K.L., 1988. Large floating clasts in turbidites – a mechanism for their emplacement. Sedimentary Geology 58, 47–61.
Powell, R.D., 2003. Subaquatic landsystems: fjords. In: Evans, D.J.A. (Ed.), Glacial Landsystems. Arnold, London, pp. 313–347.

Powell, R., Domack, E., 1995. Modern glaciomarine environments. In: Menzies, J. (Ed.), Modern Glaciomarine Environments – Processes, Dynamics and Sediments, vol. 1. Butterworth-Heinemann, Oxford, pp. 445–486.
Roberts, D.H., Hart, J.K., 2005. The deforming bed characteristics of a stratified till assemblage in north East Anglia, UK: investigating controls on sediment rheology and strain signatures. Quaternary Science Reviews 24, 123–140.
Shields, G.A., 2005. Neoproterozoic cap carbonates: a critical appraisal of existing models and the plumeworld hypothesis. Terra Nova 17, 299–310.
Sutcliffe, O.E., Theron, J.A., Whittington, R.J., Theron, J.N., Craig, J., 2000. Calibrating the Late Ordovician glaciation and mass extinction by the eccentricity cycles of the Earth's orbit. Geology 23, 967–970.
Thomas, G.S.P., Connell, R.J., 1985. Iceberg drop, dump, and grounding structures from Pleistocene Glacio-Lacustrine Sediments, Scotland. Journal of Sedimentary Petrology 55, 243–249.
van der Meer, J.J.M., 1987. Micromorphology of glacial sediments as a tool in distinguishing genetic varieties of till. Geological Survey of Finland, Special Paper 3, 77–89.
van der Meer, J.J.M., 1993. Microscopic evidence of subglacial deformation. Quaternary Science Reviews 12, 553–587.
van der Meer, J.J.M., 1997. Subglacial processes revealed by the microscope: particle and aggregate mobility in till. Quaternary Science Reviews 16, 827–831.
van der Meer, J.J.M., Kjær, K.H., Krüger, J., Rabassa, J., Kilfeather, A.A., 2009. Under pressure: clastic dykes in glacial settings. Quaternary Science Reviews 28, 708–720.
van der Meer, J.J.M., Menzies, J., 2011. The micromorphology of unconsolidated sediments. Sedimentary Geology 238, 213–232.
Visser, J.N.J., Colliston, W.P., Terblanche, J.C., 1984. The origin of soft sediment deformation structures in Permo-Carboniferous glacial and proglacial beds, South Africa. Journal of Sedimentary Petrology 54, 1183–1196.
Zaniewski, K., van der Meer, J.J.M., 2005. Quantification of plasmic fabric through image analysis. Catena 63, 109–127.

Glossary

Based on Brewer (1976), as adapted by Menzies (2000), and Zaniewski and van der Meer (2005) unless otherwise stated.

Dispersion tail: concentration of smaller grains or plasma in the lee of a larger grain.

Necking structure (Lachniet et al., 1999): variety of turbate structure. Alignment of smaller grains occurs between adjacent larger grains.

Plasma: particles of colloidal size (<20 μm), including mineral and organic material, within which individual grains cannot be discerned.

Plasmic fabric: orientation of plasma domains based on the optical properties (birefringence) of aligned plasma particles. Common varieties include:

- *Asepic:* anisotropic plasma domains with little to no preferred orientation. Sub-varieties include Argillasepic (dominantly clay-sized particles) and Silasepic (dominantly silt-sized particles).
- *Masepic:* short plasmic fabric domains with a single preferred orientation.
- *Bimasepic:* plasma particles exhibit two dominant preferred orientations. Termed *Lattisepic* where these directions are perpendicular.
- *Insepic:* small clusters of oriented plasma particles where clusters show no preferred orientation.
- *Multisepic:* multiple (>2) preferred plasmic fabric orientations.
- *Skelsepic:* plasmic particles preferentially oriented around skeleton grains.
- *Omnisepic:* random orientation of various plasmic fabric domains.
- *Unistrial:* elongate, discrete bands of birefringent clay plasma.

Pressure shadow (Phillips et al., 2011): Typically massive domain of lower strain adjacent to a clast. Synonymous with strain shadow.

Turbate structure (Hiemstra and Rijsdijk, 2003): circular arrangement of grains around a core stone or stiff matrix. Long axes of oriented grains exhibit a parallel or radial orientation relative to the margins of the core stone.

3.4. Dynamic glacial cycles, Omutirapo palaeovalley

An interglacial on snowball Earth? Dynamic ice behaviour revealed in the Chuos Formation, Namibia

Le Heron, D.P., Busfield, M.E. and Kamona, A.F.

Sedimentology 2013b, v. 60, 411-427.
doi:10.1111/j.1365-3091.2012.01346

Statement of contribution

- ***Data collection***
  - Busfield and Le Heron both logged the sections, and collected palaeocurrent and structural data e.g. bedding, fold vergence. Busfield designed a sampling strategy for the 'shear zones' and measured the orientation of the sampled blocks.
  - Le Heron took 'panoramic' photographs of the outcrop.
  - Busfield and Le Heron discussed preliminary facies analysis in the field, the nature of the palaeovalley and its fill, and the glaciotectonic origin of the deformation structures. The significance of evidence favouring glacial retreat, and extent of these facies, was also explored in the field.
- ***Manuscript text***
  - Le Heron authored the first draft of the manuscript and assigned lithofacies nomenclature based on the ideas of Busfield and Le Heron developed in the field.
  - Busfield modified the text throughout in all subsequent drafts of the manuscript.
  - Kamona reviewed the first draft.
- ***Figures***
  - Le Heron illustrated all figures in the manuscript.
  - Busfield and Le Heron contributed photographs to figures throughout.

SEDIMENTOLOGY the journal of the International Association of Sedimentologists

Sedimentology (2013) **60,** 411–427 doi: 10.1111/j.1365-3091.2012.01346.x

An interglacial on snowball Earth? Dynamic ice behaviour revealed in the Chuos Formation, Namibia

DANIEL P. LE HERON*, MARIE E. BUSFIELD* and FRED KAMONA†
**Department of Earth Sciences, Queen's Building, Royal Holloway University of London, Egham, Surrey TW20 0BY, UK (E-mail: d.leheron@es.rhul.ac.uk)*
†Geology Department, University of Namibia, Windhoek, Namibia

ABSTRACT

The Sturtian is the oldest (*ca* 716 Ma) of three pan-global glaciations in the Cryogenian. At Omutirapo, in northern Namibia, a 2 km wide, 400 m deep palaeovalley is filled by glaciogenic strata of the Chuos Formation, which represents the Sturtian glacial record. Sedimentary logging of an exceptionally high-quality exposure permits detailed stratigraphic descriptions and interpretations, allowing two glacial cycles to be identified. At the base of the exposed succession, strong evidence supporting glaciation includes diamictites, ice-rafted dropstones and intensely sheared zones of interpreted subglacial origin. These facies collectively represent ice-proximal to ice-rafted deposits. Upsection, dropstone-free mudstones in the middle of the succession, and the absence of diamictites, imply sedimentation free from glacial influence. However, the reappearance of glacial deposits above indicates a phase of Sturtian glacial re-advance. Comparison with age-equivalent strata in South Australia, where evidence for sea-ice free sedimentation has been established previously, suggests that a Sturtian interglacial may have been extensive, implying global-scale waxing and waning of ice sheets during a Cryogenian glacial event.

Keywords Cryogenian, glacial, Namibia, Neoproterozoic, Sturtian.

INTRODUCTION

The snowball Earth hypothesis proposes a global cover of ice at multiple times during the Cryogenian (850 to 630 Ma) period of the Neoproterozoic (Hoffman *et al.*, 1998; Hoffman & Schrag, 2002). The hypothesis has received support from climate modellers owing to the mathematically attractive solution of accumulating ice masses in the warm subtropics (Pollard & Kasting, 2005; Boyle *et al.*, 2007). Another interpretation is that pockets of open ocean persisted, and the term 'slushball' is often used to describe this scenario. However, the 'slushball' models assume that there were low evaporation rates in the tropics and opaque tropical sea ice: two assumptions that are at odds with contemporary understanding of climate (Pollard & Kasting, 2005).

A wealth of sedimentological data including ice-rafted debris (IRD; Condon *et al.*, 2002), thick diamictite successions recording a substantial sediment flux from dynamic ice sheets (Leather *et al.*, 2002), wave-rippled surfaces intercalated with diamictites (Allen & Etienne, 2008) and hummocky cross-stratification (HCS) in glaciomarine sequences (Le Heron *et al.*, 2011a) is in strong support of either small pockets, or large zones, of open water as first proposed in the 'slushball' interpretation of Hyde *et al.* (2000). Indeed, based on such empirical data, it is clear that ice sheets were very dynamic (Allen & Etienne, 2008). The present study presents strong evidence for substantive wasting then re-growth of ice sheets during the *ca* 715 Ma 'Sturtian' glaciation of Namibia. A high-quality sedimentological dataset is presented from the Chuos

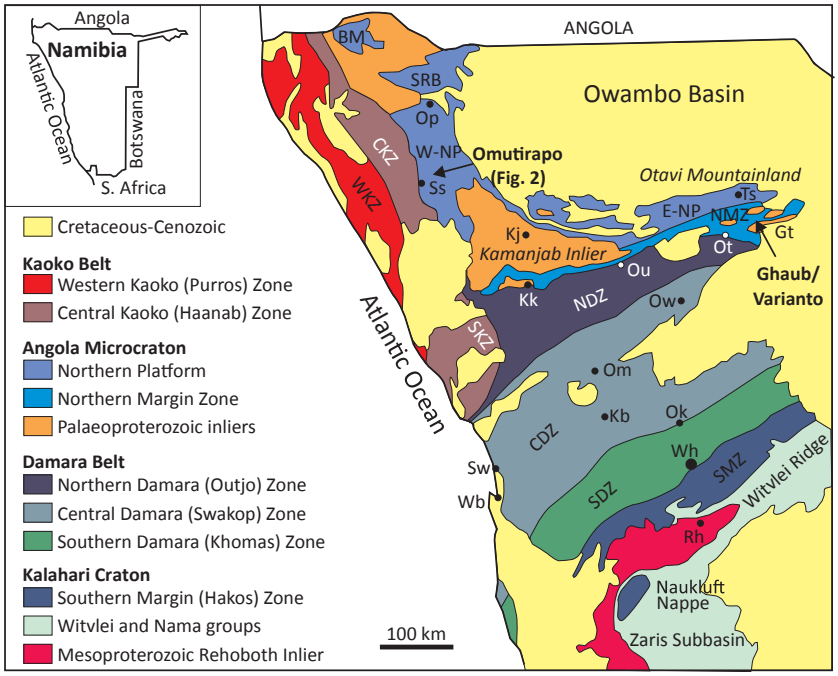

Fig. 1. Geotectonic framework of Namibia and the location of the data presented in this study, primarily from Omutirapo at the western flank of the Owambo Basin. Map after Hoffman & Halverson (2008). Abbreviations for town names are as follows: Rh - Rehoboth; Wb - Walvis Bay; Sw- Swakopmund; Wh - Windhoek; Ok - Okahandja; Kb - Karibib; Om - Omaruru; Ow - Otjiwarongo; Kk - Khorixas; Ou - Outjo; Ot - Otavi; Gt - Grootfontein; Ts - Tsumeb; Kj - Kamanjab; Ss - Sesfontein; Op - Opuwo.

Formation of northern Namibia (Fig. 1) from a hitherto little described but spectacularly exposed succession at Omutirapo (Fig. 2). By comparing the Namibian deposits with age-equivalent Australian counterparts, non-glacial deposits are highlighted within Sturtian successions, pointing to interglacial conditions. Based on these new sedimentological data, it is inferred here that Sturtian ice sheets waxed, waned and re-advanced, with multiple glacial cycles potentially recorded in this severe glacial event.

GEOLOGICAL BACKGROUND

The Neoproterozoic Otavi Group in northern Namibia preserves two diamictite-rich successions (Fig. 3), each overlain by a deglacial cap carbonate (Hoffmann & Prave, 1996), considered in turn to record intense glaciation and rapid climatic recovery (Hoffman *et al.*, 1998). U–Pb ages from the underlying Nauuwport volcanics place the maximum age of the older diamictite succession (Chuos Formation: Fig. 3) at

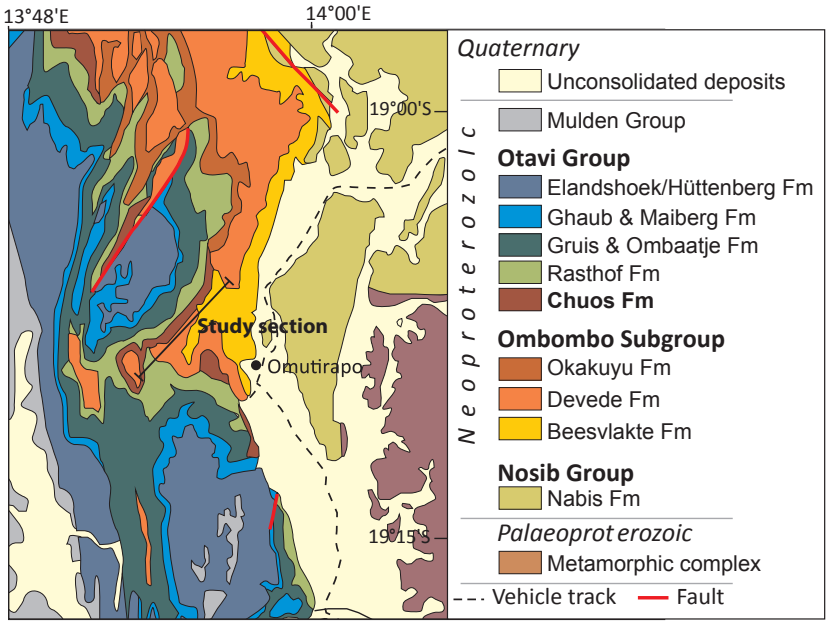

Fig. 2. Geological sketch map of the Omutirapo area in the Khowarib Fold Belt of northern Namibia, *ca* 15 km to the north-east of the village of Warmquelle. Map after Hoffman & Halverson (2008).

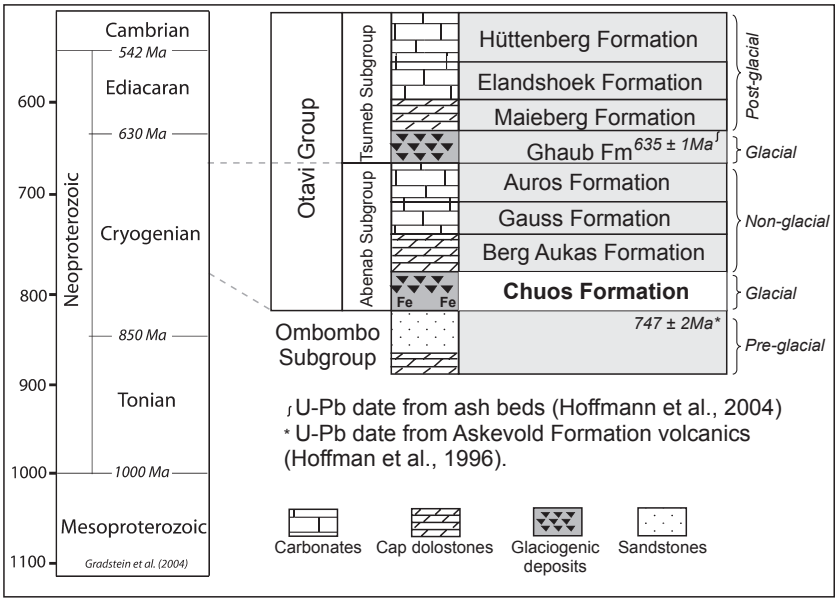

Fig. 3. Stratigraphy on the Cryogenian succession exposed in the Omutirapo area. Stratigraphic hierarchy and formation names adopted from Hoffmann & Prave (1996).

747 ± 2 Ma (Hoffman *et al.*, 1996), and the younger Ghaub Formation (Fig. 3) diamictite is constrained to 635·5 ± 1·2 Ma through U–Pb dating of interbedded volcanic ash beds (Hoffmann *et al.*, 2004). Most recent research has focused on this younger interval, with studies advocating either palaeo-ice stream activity or dynamic floating ice margin systems (Domack & Hoffman, 2011) or, conversely, rejecting the glacial hypothesis in favour of a mass flow origin (Eyles & Januszczak, 2007). The older glaciogenic succession, however, remains comparatively neglected, as exposure quality is lower than its younger counterpart.

Based on studies in the central zone of the Damara orogen (Fig. 1), Gevers (1931) first contended that the massive nature of diamictites in the Chuos, their areal extent and local occurrence of varves, supported a glacial interpretation. Martin *et al.* (1985) and Porada (1983), meanwhile, discarded this long-held view and interpreted the central Damaran successions as non-glacial gravity flow deposits. In support, the latter author cited: (i) local clast derivation; (ii) proximity to syn-sedimentary faults; and (iii) intercalated quartzites, interpreted as turbidite pulses.

Eyles & Januszczak (2007) developed similar arguments to Martin *et al.* (1985) and Porada (1983) to side against the glacial hypothesis for the Chuos as well as the second, younger, Cryogenian glacial succession (the Ghaub Formation). For the Chuos, these workers note that the Omutirapo section lies at the immediate juncture between the Congo Craton and the Damara Belt, which was cited to explain syntectonic mass flows (the diamictites). The problem with this argument, however, is one of timing. Separation of the Congo and Kalahari cratons, which might conceivably produce slopes to yield mass-flows, occurred long before Chuos deposition, with alluvial fanglomerates of the Nosib Group recording the rift phase (Hoffman & Halverson, 2008; Miller, 2008). Thus, the rift to drift transition, and accompanying passive-margin development, is represented by Otavi Group sedimentation (Fig. 3) (Miller, 2008). Compressional deformation, producing slopes to generate further mass flows and to juxtapose the Damara Belt with the Congo Craton, occurred much later when molasse of the Mulden Group was deposited (Miller, 2008).

The present study presents new data, including logged sections totalling *ca* 1000 m from four traverses, which demonstrate a strong glacial influence on sedimentation. The data permit detailed insight into the dynamics of older Cryogenian ice sheets (716·5 Ma, Sturtian: Macdonald *et al.*, 2010a). Furthermore, clear evidence for non-glaciogenic sedimentation within the middle of the succession, pointing to intra-Sturtian ice-free conditions, is presented.

STUDY AREA

In the Khowarib Fold Belt, the Chuos Formation wedges from *ca* 80 to 347 m in a north-east/south-

west direction along a 3 km long continuous cliff section to form a palaeovalley geometry, exposed *ca* 15 km north-east of the village of Warmquelle (Fig. 4). Evidence for a palaeovalley at Omutirapo is three-fold: (i) progressive incision and truncation of the Ombombo Subgroup occurs beneath the Chuos in a south-westerly direction; (ii) dramatic thickness changes in the Chuos are apparent from detailed sedimentary sections; and (iii) clear onlap relationships of the Chuos onto the Ombombo Subgroup can be demonstrated (Figs 4 and 5). The diamictite assemblage rests unconformably upon a mixed succession of clastic and carbonate formations of the Ombombo Subgroup (Fig. 3), shows significant lateral thickness variations, and is disconformably overlain by stratified and stromatolitic dolostones of the Rasthof Formation (Hoffman & Halverson, 2008) (Fig. 4). Northward thickening of the formations of the Ombombo Subgroup beneath the sub-Chuos unconformity allows approximately east/west striking growth faults to be inferred (Hoffman & Halverson, 2008). Furthermore, the region (Khowarib Fold Belt) is ideally situated in the least deformed northern margin of the Damara-Kaoko orogenic belt, subject only to sub-greenschist facies metamorphism (Miller, 2008), and thereby permitting detailed facies analysis with minimal tectonic overprint. This interpretation lies in contrast to many earlier studies of the older Cryogenian sequence (e.g. Gevers, 1931; Martin, 1965; Henry *et al.*, 1986; Badenhorst, 1988), undertaken in the highly deformed central Damara Zone to the south (Fig. 1).

Detailed sedimentary logging enables a correlation panel to be presented throughout the Chuos Formation that illustrates the internal architecture (Fig. 5). The correlation adopts the base-Rasthof Formation disconformity as a datum, emphasizing the degree of downcutting beneath the Chuos Formation at the base of the palaeovalley, and complete truncation of the Okakuyu Formation (top Ombombo Subgroup) to the south-west. The basal succession of the Chuos Formation is not preserved at the north-easternmost (thinnest) part of the exposure (Fig. 5, Log 4), but comprises a sandy diamictite in thicker sections of the Chuos Formation (Fig. 5, Logs 1 to 3).

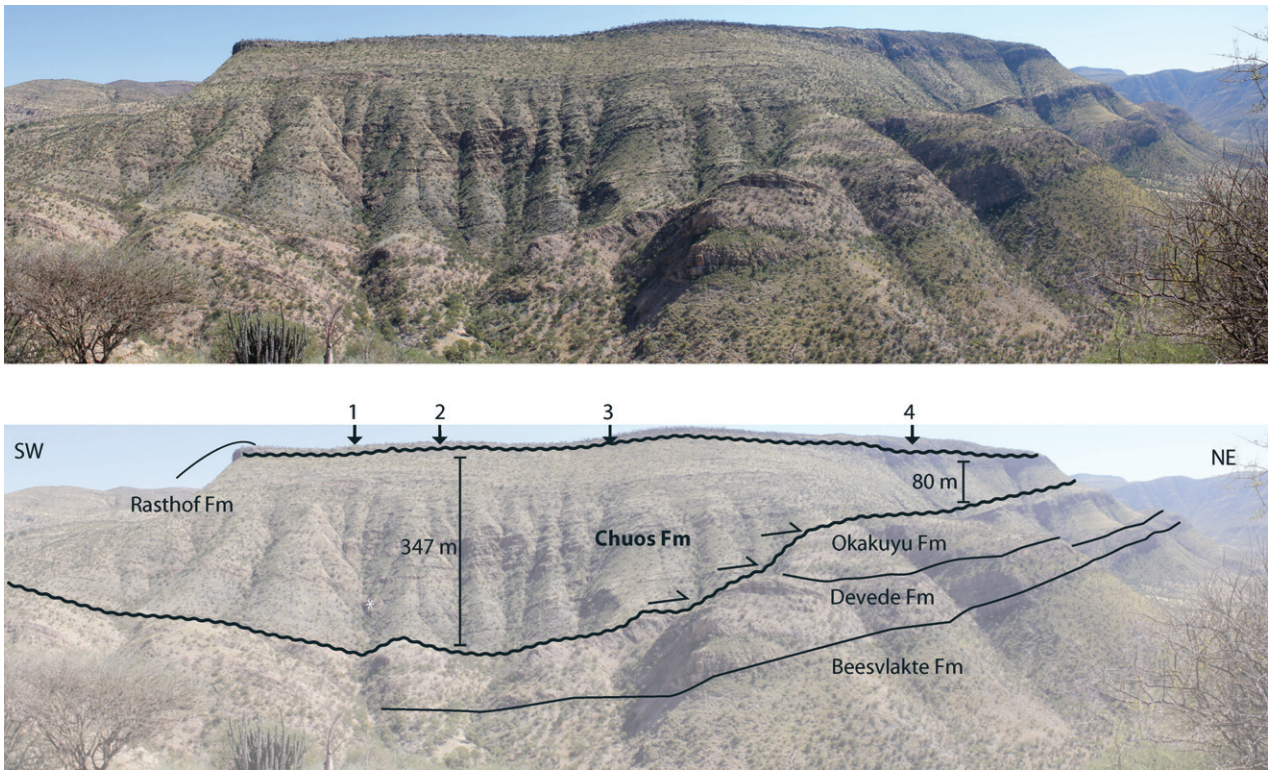

Fig. 4. Panoramic photograph, with accompanying sketch overlay/interpretation, of the Omutirapo palaeovalley. Note the pronounced downcutting at the base of the Chuos Formation, representing the base of the palaeovalley, onlap geometries in the palaeovalley fill and the location of measured sections presented on Fig. 5. Palaeovalley closure is towards the south-west.

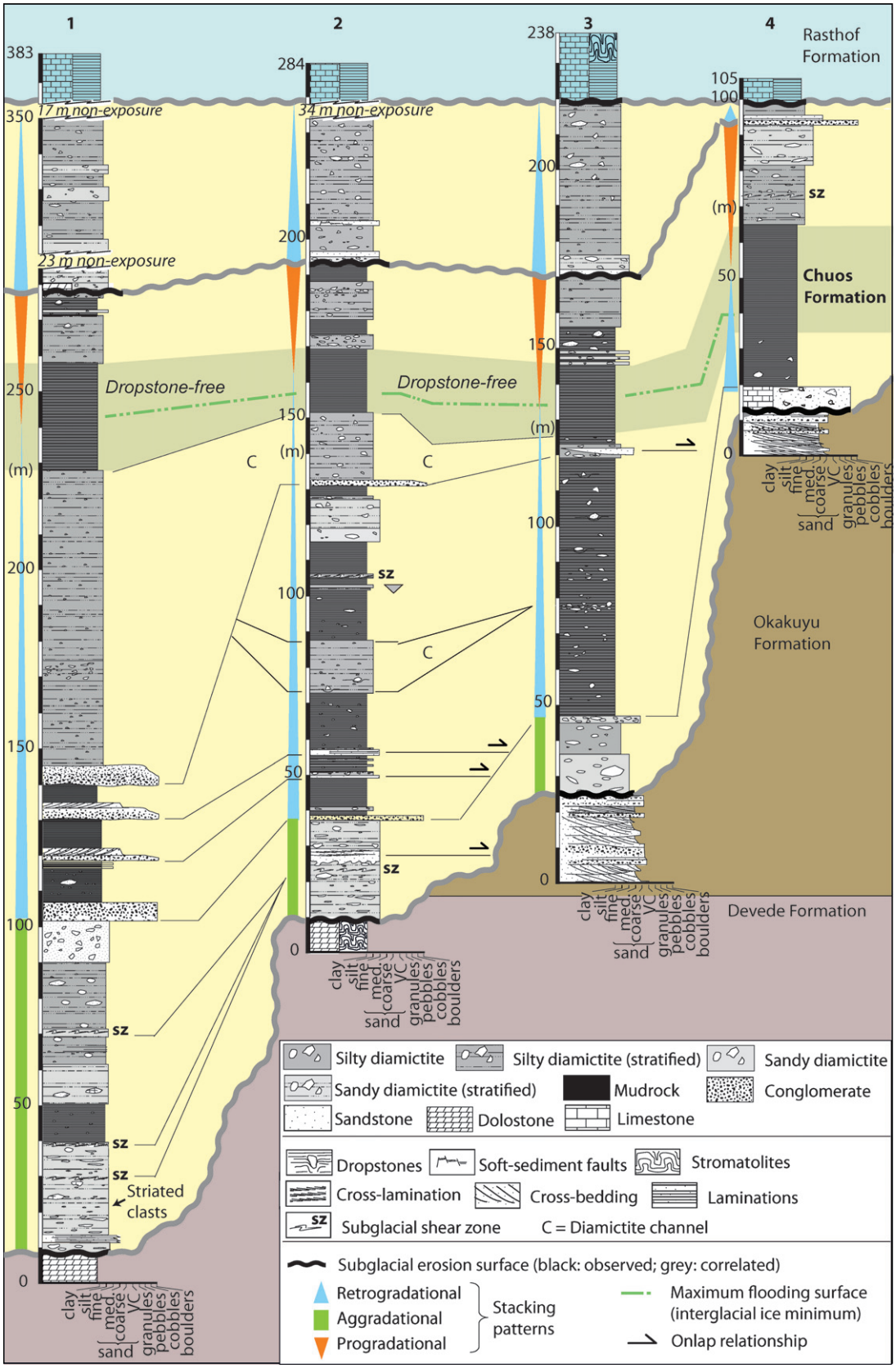

Fig. 5. Logged sections, facies and interpreted stratal architecture of the fill to the Omutirapo palaeovalley. Note the clear evidence for non-glacial facies (dropstone free shales, shown in green shading) in each of the measured sections.

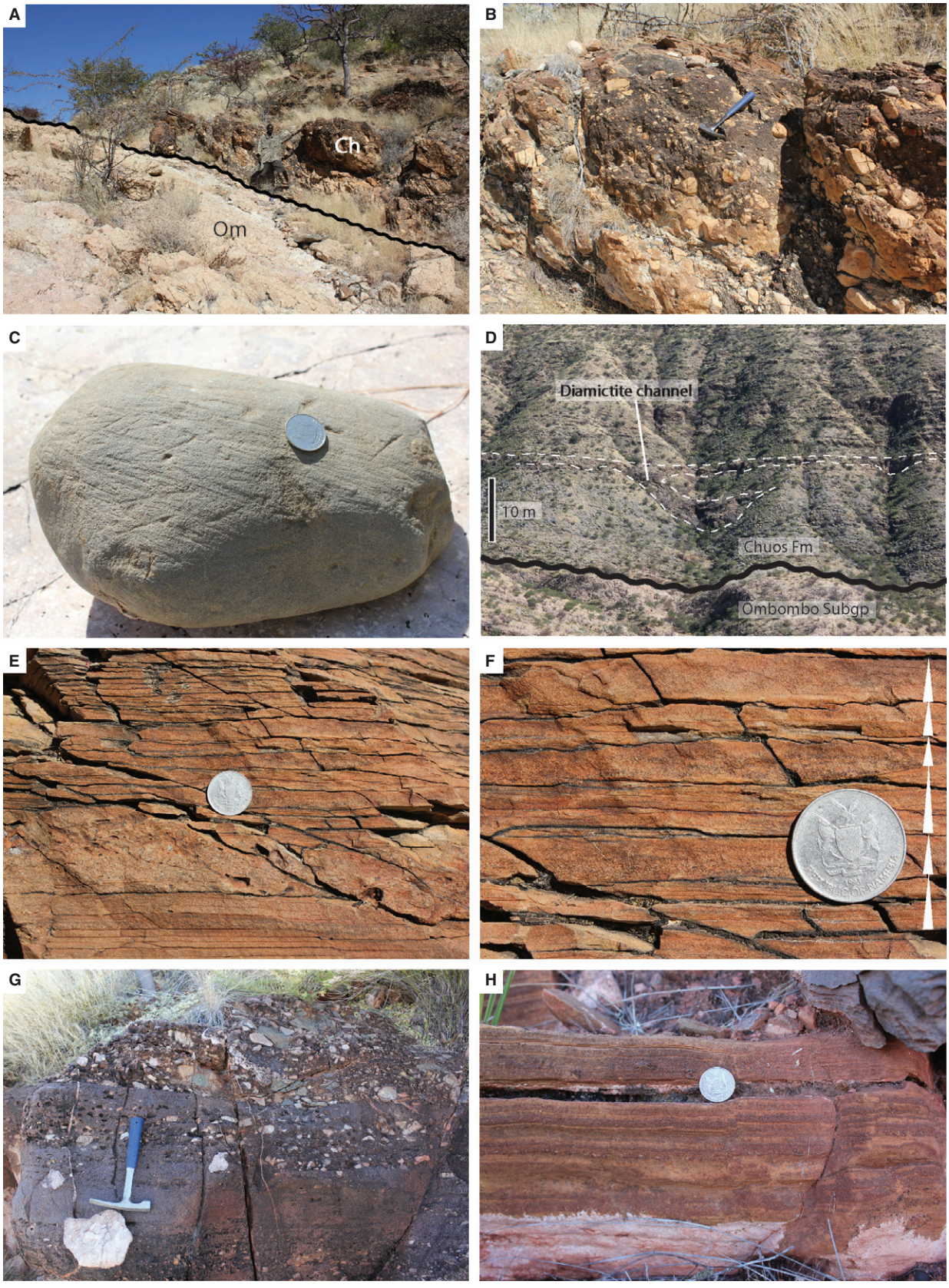
A
Ch
Om
B
C
D
Diamictite channel
10 m
Chuos Fm
Ombombo Subgp
E
F
G
H

FACIES ANALYSIS

Within the Omutirapo palaeovalley, five facies associations are recognized, namely: (i) massive and graded diamictites; (ii) pebbly cross-stratified sandstones; (iii) sheared diamictites; (iv) lonestone-bearing shale; and (v) clast-free shale.

Massive and graded diamictite facies association

Description

Two distinct constituent facies comprise the massive and graded facies association, both of which make multiple stratigraphic appearances in the Chuos Formation. The first of these is a clast-rich, sandy diamictite, typically brown-orange in colour, which is well-developed at the very base of the Chuos Formation (Fig. 6A and B). Clasts in this facies range from granule to boulder size, are sub-angular to rounded, typically equant and show no preferred orientation. Erratic lithologies include orange-yellow dolostone (particularly near the contact with the underlying Ombombo Subgroup) quartzite, andesite, amygdaloidal basalt, vein quartz, greenschist-facies pelites, leucogranite and sandstone. Locally, clasts are striated (Fig. 6C): these are restricted to the basal 10 m of the Chuos Formation. Bed thicknesses range from 0·3 to 2 m. At the outcrop scale, the massive diamictite facies association is organized into *ca* 10 m deep, *ca* 25 m wide channels and interchannel overspills (Fig. 6D). The second facies comprises two end members: a normally graded clast-poor sandy diamictite, and better differentiated, normally graded sandstone (Fig. 6E). These sub-facies are intercalated on the decimetre scale: 'floating' 2 cm diameter clasts are common to both. Graded intervals are on the lamination scale (0·7 to 1·5 cm), flat-based to slightly irregular, and repetitively stacked (Fig. 6F). These normally graded laminations form beds up to 0·75 m thick and are a comparatively minor component of the massive and graded diamictite facies association.

Interpretation

The massive diamictites are interpreted as a series of subaqueous glaciogenic debris flow (GDF) deposits, with the graded diamictites and sandstones interpreted as subordinate underflow deposits. Texturally, the massive diamictites are comparable with 'plug flow' deposits released from meltwater point sources on a grounding line fan (Powell, 1990). Flows hug the sea bed before becoming buoyant and detached, thus transforming into an underflow (Powell, 1990). In this context, equant clasts and lack of internal structure in bedding are expected. The organization of the GDF deposits into channel and interchannel areas, together with their thicknesses, is comparable with many Quaternary examples such as those found offshore Newfoundland (Tripsanas & Piper, 2008).

It is notable that the very substantial topography on the Ombombo Subgroup records stepwise incision to progressively deeper stratigraphic levels towards the south-west (Fig. 4), through a series of siliciclastic, and then carbonate, deposits (Fig. 5). The large number of non-sedimentary clasts implies that these are not derived locally. The stratigraphic concentration of striated clasts in the basal 10 m of the Chuos Formation is also noteworthy. No striated clasts were described by Eyles & Januszczak (2007): ''despite observation of many hundreds of metres of thickness'', including Omutirapo. Otherwise identical occurrences of the massive and graded diamictite facies association further upsection (Fig. 5) imply that subsequent debris flows may have completely eradicated striations on clast surfaces.

The 'floating clasts' in the graded diamictites are explained adequately by the Postma *et al.* (1988) model. In this model, larger clasts are supported on a pseudo-laminar inertia flow layer and are moved downslope in response to shear stresses in the overlying turbulent part of the

Fig. 6. Photographs (A) to (F) show various facies in the massive and graded diamictite facies association, interpreted as glaciogenic debris flow deposits. (A) Stratigraphic contact between dolostones of the Devede Formation (at Log 1, Fig. 4) and the Chuos Formation. Note 1·75 m tall geologist for scale. (B) Detail of the basal deposits – orange weathering, massive, pebbly diamictites. Hammer for scale is 30 cm long. (C) Striated sandstone cobble within the lower 10 m of the Chuos Formation. Namibian 50 c coin for scale (24 mm diameter). (D) Diamictite channel incising older diamictites. (E) Graded diamictite bed (below coin) encased in normally graded sandstone laminae. Namibian 50 c coin for scale. (F) Detail of stacked fining upward laminae in sandstone (indicated by upward tapering arrows). Namibian 50 c coin for scale. Photographs (G) and (H) show facies within the pebbly sandstone facies association interpreted as jet efflux deposits. (G) Typically well-differentiated pebble conglomerates and sandstones. The first pebbly bed above the hammer tip is planar cross-bedded, with foresets dipping at 20° towards the south-west (left in the direction of view). Hammer is 30 cm long. (H) Well-differentiated sandstone laminae, some inversely graded, others normally graded. Namibian 50 c coin for scale.

flow. Thus, the large clasts in this facies association are not interpreted as dropstones; rather, a within-flow sorting mechanism is envisaged to explain this texture. This interpretation is favoured owing to the lack of deformation/impact structures beneath the clasts typically associated with dropstones. Based on evidence from the pebbly cross-stratified sandstone facies association (see below), it is possible to infer that the basement clasts may have been sourced from the east (i.e. from the Congo Craton). In the Chuos of the central Damara Belt, Henry *et al.* (1986) contended that the presence of extrabasinal clasts, together with dropstone textures, were two of the strongest pieces of evidence for a glacial influence on deposition. At Omutirapo, parallels can be drawn between the massive and graded diamictites at the base of the palaeovalley with ice-proximal sediments in subglacially cut 'tunnel valley' networks (>1 km wide meltwater channels) where matrix-supported conglomerates and diamictites pass laterally and vertically into better differentiated underflow deposits or turbidites (e.g. Lang *et al.*, 2012). This possibility is given full consideration later, in the context of palaeovalley genesis and fill.

Pebbly cross-stratified sandstone facies association

Description

These deposits comprise red-coloured, clast-supported pebble conglomerates and sandstones in beds of 0·5 to 2 m thickness. Conglomerate beds are normally graded. Pebbles typically are moderately rounded to rounded, and a north-east dipping imbrication fabric of discoid quartz clasts (Fig. 6G) can be demonstrated locally. Low-angle cross-stratification is also developed. Owing to the poor exposure of this facies association, it was not possible to obtain palaeoflow measurements, although low-angle (<15°) planar foresets dip towards the south-west (Fig. 6G). The conglomerate and sandstone intervals are well-differentiated. At a centimetre-scale, coarse-grained and fine-grained sandstones alternate (Fig. 6G). The laminae exhibit both normal and reverse grading. In a typical exposure of this facies association, three or four stacked beds occur: these show an overall upward diminution in clast size in the conglomerates.

Interpretation

The pebbly cross-stratified sandstone facies association is interpreted as a series of jet efflux deposits released in proximity to a subglacial conduit. In ice-proximal settings, over a distance of several kilometres, a zone of flow establishment (characterized by debrites) typically passes into a zone of flow transition (clast-supported, cross-stratified gravels) and distally/downcurrent to upper flow regime conditions (antidune-bearing sands) (Hornung *et al.*, 2007). Thus, in this way, the clast-supported, cross-stratified, imbricated pebble conglomerates are interpreted to represent a gravelly bedform deposited in the zone of flow establishment. The imbricate clasts, together with the south-west dipping low-angle planar foresets, imply sediment transport to the south-west. Thus, in the pebbly cross-stratified sandstone facies association, sediments are interpreted to have been sourced from a meltwater conduit to the north-east.

In the interbedded sandstones, the distinction between coarsening-upward and fining-upward laminae within these beds may suggest that these structures formed through the 'burst/sweep process' (Cheel & Middleton, 1986). In this process, fining upward laminae originate through the gravitational fall out of grains that have been carried upward into suspension by a current 'burst', whereas coarsening upward laminae evolve in response to dispersive pressures operating near the base of the boundary layer due to the passage or 'sweep' of high-speed fluid near the base of the bed (Cheel & Middleton, 1986). These processes are typical of a rapid current, upper flow regime (Ashley, 1990), potentially the downcurrent equivalents of the cross-stratified conglomerates (Hornung *et al.*, 2007). Note that the alternating fine-grained and coarser-grained sand laminae could superficially be mistaken for varvites, a preferred interpretation of Gevers (1931) from the Chuos of the Damara Belt.

Sheared diamictite facies association

Description

Multiple horizons in the Chuos Formation exhibit diamictites that are stratified, deformed and attenuated. Continuously stratified sections of clast-poor diamictite occur over several metres, with clear separation of more argillaceous and more arenaceous layers (Fig. 7A). A slaty cleavage is observed (Fig. 7B), particularly in the finer-grained layers, which cross-cuts the soft-sediment deformation structures described below. By contrast with the massive and graded diamictite facies association, attenuated and elongate clasts

are common, and these are locally injected and fractured by bedding parallel sandstone sheets (Fig. 7C). Rotational deformation structures are commonplace, with an abundance of galaxy structures (Phillips, 2006; Phillips *et al.*, 2011) and necking structures observed at the macroscale (Fig. 7D and E). These structures indicate a top to the south-west sense of rotation. Dispersion tails are also commonly observed adjacent to highly attenuated siltstone clasts (Fig. 7F). No clasts were observed to protrude from an underlying bed into an overlying bed. Finally, pervasive lineations are developed in sandy diamictite intervals where prolate/rod geometries are conspicuous and trend approximately north-east/south-west. Within each stratigraphic occurrence (Fig. 5), the intensity of deformation in each shear zone usually increases upsection.

Interpretation

Layering in sheared diamictites is attributable to stratification of primary sedimentary origin, and pervasive attenuation of, for example, soft-sediment clasts and rootless folds (e.g. Roberts & Hart, 2005). At Omutirapo, clearly developed stratification within the sheared diamictite facies association is interpreted as primary subaqueous in origin. The multiple occurrences of sheared diamictite throughout the succession are interpreted to record subglacial deformation beneath an oscillating ice margin for the following reasons. The cross-cutting cleavage at a high angle to bedding and deformation structures demonstrates that the latter are soft-sediment in nature, and hence a tectonogenetic origin for the shear zones can be rejected. Thus, two interpretations remain: (i) shearing within a mass flow; or (ii) subglacial deformation. It should be emphasized that, in most analyses of Quaternary deformation structures, microscale observations normally inform interpretations (e.g. van der Meer, 1993; Phillips, 2006; Phillips *et al.*, 2011), yet the following necessarily derives from macroscopic features.

Clast fracture and injection (sedimentary dykes and sills) are common in debrites (Menzies & Zaniewski, 2003) but they also occur subglacially (Le Heron & Etienne, 2005). The presence of galaxy structures, necking structures and dispersion tails (Phillips, 2006) implies the attenuation of soft (non-consolidated) clasts. Turbate/galaxy structures can record clast rotation during simple shear of subglacial sediment, but may also occur in mass flows provided that turbulence can develop (Phillips, 2006). Thus, the top to the south-west sense of shear in the galaxy structures could equally be interpreted as glacial advance or downslope instability in this direction.

Fortunately, the other features permit less equivocal interpretations. Firstly, the observed dispersion tails are ubiquitous in subglacial shear zones but rare in debrites (van der Meer, 1993; Hart & Roberts, 1994; Menzies *et al.*, 1997; Lachniet *et al.*, 2001; Evans & Benn, 2004). Secondly, protruding clasts typically occur on the exposed surface of debrites, which in the rock record pierce overlying beds (Arnaud, 2012): none are observed in this facies association. Thirdly, pervasive lineations, directly comparable with those developed in Omutirapo, occur in the Late Ordovician glacial record of Libya, where they are capped by soft-sediment-striated surfaces of subglacial origin (Le Heron *et al.*, 2005). These features have not been described in debrites. Finally, the upward increase in deformation intensity in each occurrence of the sheared diamictite facies association is compatible with a subglacial glacitectonic shear zone. An upward increase in deformation within Quaternary glacitectonites is observed in many cases because strain is greatest near the ice–bed interface (e.g. Hart & Roberts, 1994; McCarroll & Rijsdijk, 2003; Arnaud, 2008, 2012; Weaver & Arnaud, 2011), although it is recognized that, in some instances, deformation may be partitioned at multiple levels. By contrast, in a debris flow, deformation intensity typically is greatest at the base (Nardin *et al.*, 1979; Lowe, 1982; Mulder & Alexander, 2001). Overall, the intensity of deformation contrasts vividly with the total absence of deformation in the debris flows and subordinate underflow deposits of the massive and graded diamictite facies association, which also appear recurrently throughout the Chuos Formation (Fig. 5). The repeated occurrence of subglacial shear zones in the stratigraphy of the Chuos Formation may suggest, by analogy to Cenozoic glaciomarine sequences of the south-west Ross Sea, Antarctica (Hambrey *et al.*, 2002), repeated grounding of a periodically buoyant tidewater ice sheet.

Lonestone-bearing shale facies association

Description

Green, brown and grey lonestone-bearing shale, in successions up to 70 m thick (Fig. 5, Log 3, 50 to 120 m), is represented in multiple stratigraphic occurrences at Omutirapo. Two end-member facies are recognized, *viz.* pure shale and silty shale that are intercalated on the centimetre scale; in both, lonestones are of granule to cobble-size,

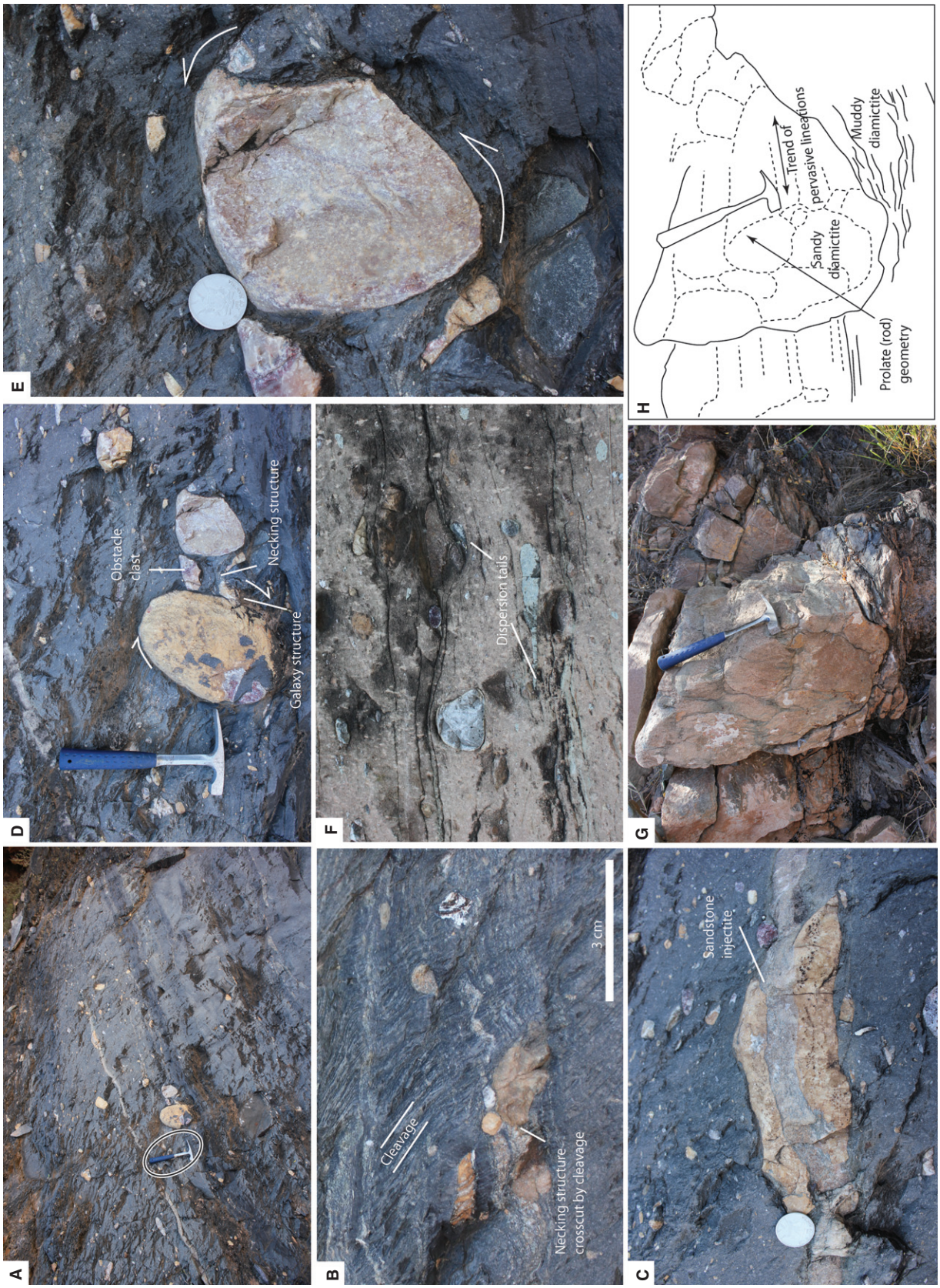
A
B
Cleavage
Necking structure crosscut by cleavage
3 cm
C
Sandstone injectite
D
Obstacle clast
Necking structure
Galaxy structure
E
F
Dispersion tails
G
H
Trend of pervasive lineations
Muddy diamictite
Sandy diamictite
Prolate (rod) geometry

and include the same lithologies as the massive and graded diamictite facies association. Clasts are of the same range of lithologies found in the massive and graded diamictite facies association. These clasts range from angular to sub-rounded; their lower contacts typically depress and punctuate shale laminae to form an impact structure (Fig. 8A and B). Laminae are deformed/deflected to a much lesser extent above than below the clasts (Fig. 8A and B).

Interpretation

The lonestone-bearing shale facies association is interpreted as paraglacial hemipelagic muds interrupted by IRD. The observation that the greatest deflection (and locally puncturing) of laminae occurs beneath clasts rather than above them strongly implies that these are released through iceberg meltout (Condon *et al.*, 2002; Leather *et al.*, 2002; Le Heron *et al.*, 2011b). Alternatively, given the south-west-oriented palaeoslope clearly recognized beneath the Chuos Formation, these deposits could record deposits from shorefast ice (e.g. Halverson *et al.*, 2004). The absence of shear textures/deformation structures in the lonestone-bearing shale facies association allows debris-flow rafting of large clasts to be discounted. These interpretations are incompatible with the overall conclusions of Eyles & Januszczak (2007), which did not recognize dropstones, and which, in shale, chart a very strong case for a glacial influence.

Clast-free shale facies association

Description

Light green to brown shale, devoid of clasts, occurs in each of the logged sections, representing the medial part of the palaeovalley fill at Omutirapo (Fig. 5). Unlike argillaceous deposits in the lonestone-bearing shale facies association, the clast-free shale does not include a silty-shale end member. Owing to the recessive character of shale, this facies is only intermittently exposed (Fig. 8C to E).

Interpretation

Unlike each of the facies associations described above, the clast-free shale facies is unique in lacking evidence for glacial processes, or processes associated with glacial activity. The homogenous nature of these deposits makes them difficult to interpret but the absence of siltstone discounts sedimentation via very distal underflows. Therefore, a hemipelagic fallout interpretation is preferred. The absence of either HCS or wave ripples precludes water depth estimation. Thus, greatest emphasis is placed on the wider context of these clast-free facies, set against the stratigraphic evolution of the Chuos Formation below.

STRATIGRAPHIC ARCHITECTURE AND ICE SHEET DYNAMICS

The preceding analysis has established a strong glacial influence on sedimentation in the Chuos Formation of northern Namibia that can be summarized as subglacial deformation (sheared diamictite), glaciogenic debris flows interspersed with underflows (massive and graded diamictite), ice-proximal jet efflux deposits (pebbly cross-stratified sandstone), IRD (lonestone-bearing shale) and non-glacial, hemipelagic fallout (clast-free shale). A schematic depositional model showing the interpreted inter-relationships of the facies associations during ice sheet re-advance is shown in Fig. 9. Below, the vertical and lateral stacking patterns of facies at Omutirapo are considered to infer ice sheet advance and retreat cycles. On the basis of the present data, the 1000 m thickness quoted in Eyles & Januszczak (2007) for the Omutirapo section is clearly an over-estimation (Fig. 4).

There are several possible interpretations of palaeovalley genesis. Growth sequences in the Ombombo suggest that an east/west growth fault controlled the location of the palaeovalley (Hoffman & Halverson, 2008). The palaeovalley may represent: (i) a large incision of fluvial or

Fig. 7. The sheared diamictite facies association. (A) General view of the well-bedded aspect of these deposits, with hammer for scale circled (30 cm long). (B) Fold structures in a buff coloured sandy diamictite layer encased within dark-grey muddy diamictite. Note that the fold structures are cut by a cleavage, demonstrating that the fold structures formed in a pre-tectonic phase, thus affecting unconsolidated sediments. (C) Sandstone sheet cross-cutting an attenuated dolostone clast, thus interpreted as a sandstone injectite. Namibian 50 c coin for scale (24 mm diameter). (D) Evidence of rotational deformation – a galaxy structure (Phillips, 2006; Phillips *et al.*, 2011) identified by the 'wings' on the perimeter of the clast, indicating that it was unconsolidated during deformation, and a necking structure indicated pre-boudinage extension of the clast 'wing'. (E) Detail of the galaxy structure developed in (D). (F) Highly attenuated green siltstone clasts with dispersion tails. Field of view is *ca* 10 cm wide. (G) and (H) Photograph and sketch of pervasive lineations, with characteristic prolate geometries, in a sandy part of a sheared diamictite.

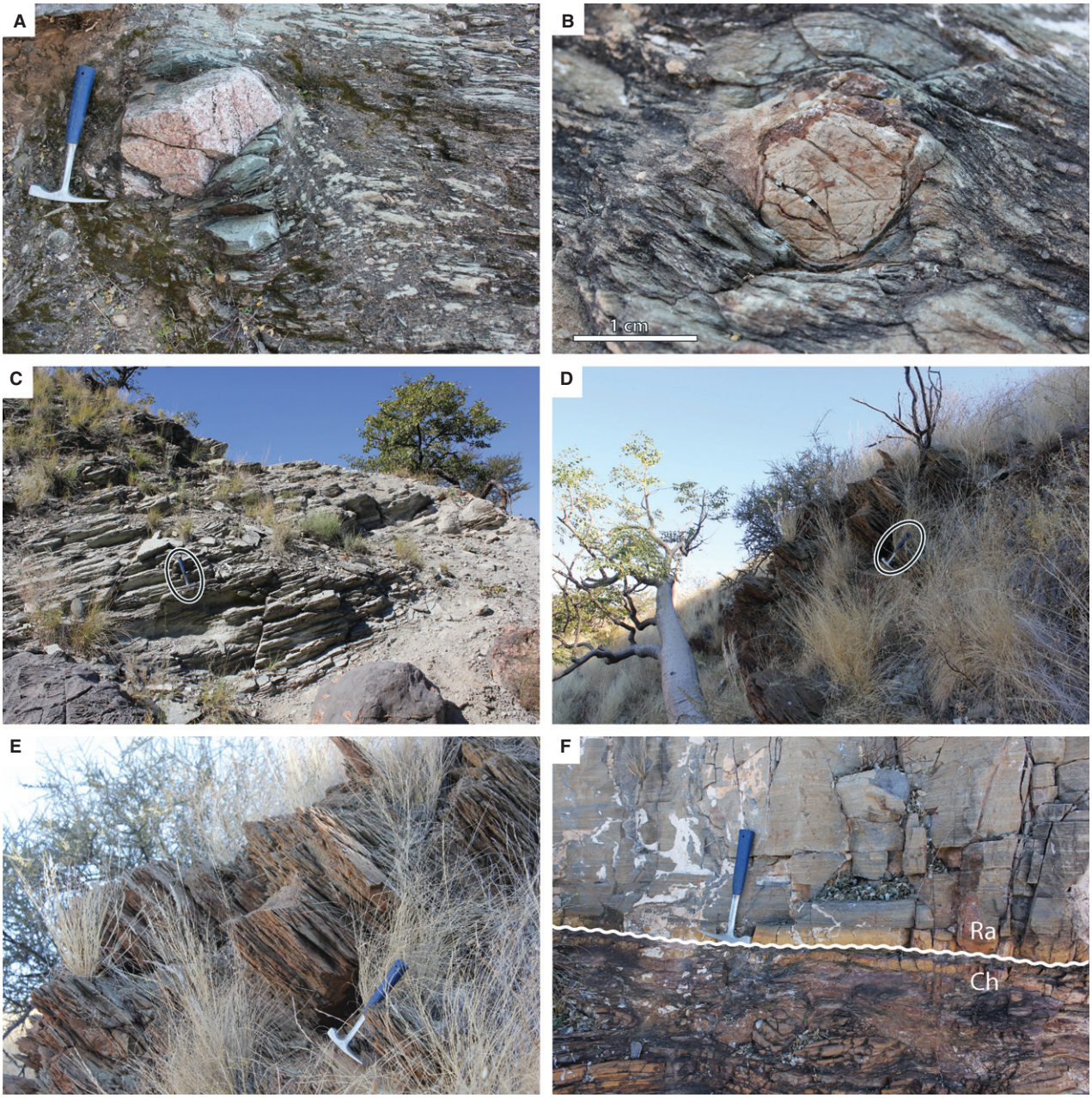

Fig. 8. (A) and (B) Examples of lonestones of pink quartzite punctuating, with impact structures, green shale: the lonestone-bearing shale facies association. These deposits are interpreted as ice-rafted debris (IRD). Hammer for scale is 30 cm long. (C) Basal outcrop of the clast-free shale facies association, showing fairly continuous exposure of grey shale. (D) and (E) General view and close-up of the upper part of the clast-free shale facies association in the middle part of the palaeovalley. The interval figured in (C) and (D)/(E) corresponds to the base and top of the 'dropstone-free interval' in Fig. 5.

submarine origin; (ii) an ice-carved incision (i.e. part of a sub-ice stream, cross-shelf trough: e.g. Andreasson *et al.*, 2004); or (iii) a tunnel valley (subglacial meltwater incision cut under elevated hydrostatic pressures: O'Cofaigh, 1996). The depth of the incision (*ca* 267 m) is an order of magnitude greater than lowstand fluvial incised valleys (e.g. Allen & Posamentier, 1993; Thomas & Anderson, 1994), but compares closely with deep tunnel valleys described from the Late Ordovician of Algeria (Lang *et al.*, 2012). Although folding/deformation beneath the Ombombo-Chuos contact is not observed (unlike many tunnel valley incisions: O'Cofaigh, 1996), the GDF deposits (massive and graded diamictite facies association) imply ice-proximal sedimentation

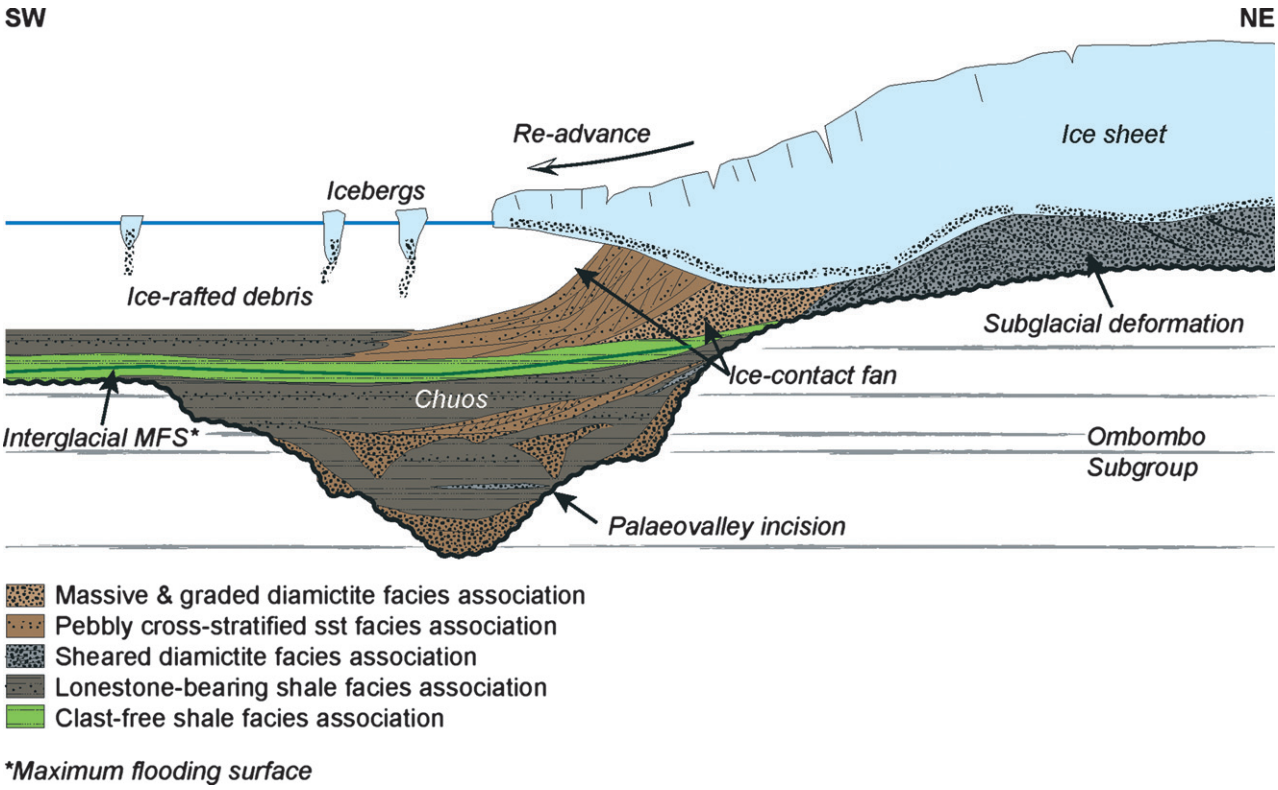

Fig. 9. A simple depositional model for the Chuos Formation at Omutirapo during re-advance of the ice sheet following deposition of the clast-free shale facies association. An ice margin grounded in a subaqueous environment is envisaged. Note that during re-advance, the basal and medial palaeovalley fill succession, deposited during the first glacial retreat, is protected from cannibalization. For clarity, this model shows the sheared diamictite facies association beneath the re-advancing ice in the intervalley area: it should be noted that, with continuing advance, ice-contact fan deposits will become deformed by subglacial shear.

comparable with that developed in the early stages of tunnel valley fill (Lang *et al.*, 2012). Thus, the Omutirapo structure is tentatively interpreted as a tunnel valley incision.

In accordance with sequence stratigraphic methodologies developed for ancient glacial sequences (e.g. Ghienne *et al.*, 2007), coarsening versus fining upward motifs in the Omutirapo palaeovalley fill may allow ice sheet advance/retreat cycles to be inferred. The basal series shows little to no vertical grain-size variation upward (massive and graded diamictite: an aggradational stacking pattern). In the thickest logged sections, the sheared diamictite facies association ('Shear Zones': Logs 1 and 2; Fig. 5) is well-developed. These intervals are more numerous towards the south-west (Log 1, 10 to 40 m; Fig. 5). The aggradational, basal series is capped by a conglomerate/sandy diamictite in each logged section, and this passes upward into the lonestone-bearing shale facies association that represents the base of a generally retrogradational medial series (Fig. 5). These latter deposits are characterized by dramatic lateral and vertical facies variations. These features include: (i) fining-up cycles of conglomerate through cross-bedded sandstone (Log 1, 120 m and 130 m; Fig. 5); (ii) diamictite channels, with evidence of channel–channel truncation (Log 1, 140 m and Log 2, 72 m; Fig. 5); and (iii) onlap relationships against the basal fill (Figs 4 and 5, between Logs 2 and 3). The massive and graded diamictite facies association is intercalated with the lonestone-bearing shale facies association in this part of the Chuos Formation (for example, Log 3, 90 to 100 m; Fig. 5).

Towards the top of the retrogradational, medial series, diamictites and dropstone-bearing intervals pass upward into green shales that are devoid of lonestones (i.e. the clast-free shale facies association) (Fig. 9). The dropstone-free zone can be recognized in each of the logged sections and correlated between them (Fig. 5). Upward, above the dropstone-free interval, a coarsening upward (thus progradational) succession is observed in each of the sections, locally culminating in a sheared diamictite (Log 4, 73 m; Fig. 5). The coarsening upward package consists

of increasingly numerous dropstones in siltstone and shale, transitional into silty sandstone and occasionally diamictites. This latter succession is sharply truncated by either an occurrence of the massive and graded diamictite facies association (Log 1, 280 m; Fig. 5) or the pebbly cross-stratified sandstone facies association (Log 4, 94 m; Fig. 5). This diamictite thus rests on an intra-Chuos disconformity that can be correlated between each of the logs (Fig. 5).

Above the intra-Chuos disconformity, the final, uppermost part of the succession comprises silty and sandy diamictites broadly organized into a fining-up (hence retrogradational) package. The finer-grained intervals in the uppermost part of the Chuos are recessive and intermittently exposed, and thus non-exposure characterizes the transition into the Rasthof Formation in two instances (Logs 1 and 2; Fig. 5). The overlying Rasthof Formation, which rests in sharp contact on the Chuos where observed, is divisible into two main facies: (i) laminated limestones; and (ii) stromatolitic limestones (Log 3, 220 to 238 m; Fig. 5).

At Omutirapo, the interpretation by the present authors of the stratigraphic evolution of the Chuos Formation is as follows. Striated cobbles, in the basal part of the palaeovalley, imply an ice-contact setting. The organization of some diamictites into channels (Fig. 6D) is consistent with abundant meltwater availability in this setting, or perhaps gravity-induced re-mobilization of glacial sediments (Eyles & Januszczak, 2007) at the steep palaeovalley margins. Some occurrences of the sheared diamictite facies association are restricted and cannot be traced along strike (cf. Logs 1 and 2; Fig. 5), implying that they formed during restricted re-advance across the palaeovalley and/or local grounding of a floating ice margin. The occurrence of this facies association within an aggradational stacking pattern supports the interpretation of a stable ice margin. Together, the massive and graded diamictites and the pebbly cross-stratified sandstone facies association represent ice-contact fan sedimentation at a subaqueous ice margin (Fig. 9). In this model, the textural differences in these facies associations relates to the position of the jet efflux conduit, prevailing hydraulic conditions on the sediment surface and sediment composition (e.g. Hornung *et al.*, 2007). The conglomerate/sandy diamictite that caps the basal succession represents such an ice-contact fan deposit.

The upward transition into lonestone-bearing mudrocks in the medial series of the palaeovalley, in tandem with onlap relationships demonstrable on the panoramic photograph (Fig. 4) and the retrogradational stacking pattern, are interpreted as the signature of ice-front recession. Given that the thick diamictite channels (for example, Log 1, 145 to 228 m; Fig. 5) are immediately followed by deposits of the lonestone-bearing shale facies association (IRD), it is suggested that the rapid ice sheet retreat ensued. This stacking pattern is compatible with sequence-stratigraphic models specifically developed for ice sheets rapidly retreating from palaeovalleys (Ghienne *et al.*, 2007). Given the context of ice sheet retreat, the dropstone-free zone potentially implies IRD-free seas, and thus interglacial conditions. A maximum flooding surface is thus placed within the dropstone-free zone, which is tentatively interpreted to record an interglacial sea-level maximum (Figs 5 and 9).

Resumption of progradation within the Omutirapo palaeovalley – including the progressive re-appearance of IRD-bearing siltstones and shales, and increase in volume of diamictite – is interpreted as the transition from interglacial conditions to a glacial re-advance scenario. An occurrence of the sheared diamictite towards the top of this progradational package is compatible with renewed ice sheet grounding and subglacial deformation (Fig. 9). Thus, the unconformity that truncates this package is tentatively interpreted as a subglacial erosion surface (Fig. 5). This stratigraphic motif compares with the 'sequence boundaries' recognized by Fielding *et al.* (2000) from the Cenozoic glaciomarine succession of the south-west Ross Sea, Antarctica, which were suggested by Hambrey *et al.* (2002) to record periodic ice-sheet grounding at a tidewater margin. The fining-upward diamictite package above (for example, Log 1, 278 to 357 m; Fig. 5) is interpreted as a grounding line moraine: its lateral extent across the palaeovalley stands in contrast to the diamictite channels beneath. The retrogradational nature of this uppermost unit is compatible with ice sheet recession. Thus, although the contact with the overlying Rasthof Formation is sharp where observed (Logs 2 and 4; Fig. 5), terminal ice sheet recession appears to have been more gradual than initial retreat at the onset of the interglacial phase. This observation can simply be explained by an ice front retreating over a topographically subdued shelf (Ghienne *et al.*, 2007). This behaviour is to be expected given glacial re-advance over a palaeovalley already largely filled with sediment.

DISCUSSION AND CONCLUSIONS

The above analysis has demonstrated that the Omutirapo palaeovalley fill contains a clear glacial retreat–re-advance–retreat signature (Fig. 9). The well-developed, dropstone-free interval is herein suggested to represent interglacial sedimentation, in which a maximum flooding surface is recognized, representing an interglacial sea-level high. The snowball Earth hypothesis recognizes three putative glacial episodes: the Sturtian, Marinoan and Gaskiers events (Hoffman & Schrag, 2002). If it were assumed that, on the basis of geochemical signatures, the Sturtian glaciation was isochronous and global (*ca* 716·5 Ma: Macdonald *et al.*, 2010b), rather than one of several diachronous ice house events (Allen & Etienne, 2008), internal correlation might be possible between diamictite-prone successions of Sturtian age on different continents. It should be emphasized that, in Namibia, the outcrop quality of Omutirapo is exceptional and that the Chuos is patchy elsewhere (Hoffman & Halverson, 2008). The Omutirapo succession is also exceptionally thick in comparison with neighbouring sections (Hoffman & Halverson, 2008) implying that substantial accommodation space during deposition protected interglacial deposits from cannibalization by re-advancing ice sheets. This implication is also supported by the observation here that the interpreted subglacial erosion surface at the top of the palaeovalley is essentially a disconformity (Fig. 5) and not a deeply channelled discontinuity. Furthermore, at Omutirapo, onlap geometries are clearly expressed throughout (Fig. 4), clearly demonstrating excellent stratal preservation. The present authors envisage a tidewater ice margin that, in addition to a major retreat–re-advance cycle, was subject to periodic oscillations. Buoyancy, perhaps as a result of tidal effects, resulted in repeated floating and grounding of the ice margin; this would account for the mismatch in the number of subglacial shear zones across the palaeovalley (Figs 5 and 9).

Under the snowball Earth model, the Chuos Formation correlates perfectly with the Sturt Tillite and its lateral equivalents in South Australia (Hoffman & Schrag, 2002). During the Sturtian glaciation at *ca* 716·5 Ma (Macdonald *et al.*, 2010b), northern Namibia and South Australia lay at opposite ends of the Rodinia supercontinent (Collins & Pisarevsky, 2005). Le Heron *et al.* (2011a,b) provided detailed descriptions of these strata at the Holowilena South homestead in the central Flinders Ranges. At Holowilena, the Sturtian succession comprises the Pualco Tillite (glaciogenic debris flows), overlain by the Holowilena Ironstone (glacioturbidites); these pass up into pebbly diamictite of the lowermost Wilyerpa Formation (glaciogenic debris flows), succeeded by hummocky cross-stratification-bearing sandstones and siltstones (storm deposits). These latter deposits are capped by a *ca* 2 km thick ice-rafted debris-rich unit, deposited during ice sheet re-advance, in which hummocky cross-stratification is lacking. Storm waves are required to generate hummocky cross-stratification, thus implying sea-ice free conditions prior to glacial re-advance (Le Heron *et al.*, 2011a). The hummocky cross-stratification-bearing interval appears *ca* 2 km below the Tindelpina Shale member of the Tapleys Hill Formation, which records post-glacial flooding and non-glacial hemipelagic shale and underflow deposition. In South Australia, a significant phase of rifting preceded glaciation, and diamictite-rich successions were deposited in local 'troughs', grabens and palaeo-lows (Le Heron, 2012 and references therein). On this basis, correlation between the dropstone-free interval of the Chuos Formation with interglacial, hummocky cross-stratified sandstones of the Yudnamutana Subgroup in Holowilena, South Australia (Le Heron *et al.*, 2011a) may be proposed.

In any glacial succession, cannibalization of earlier glacial cycles by successive advances can never be fully discounted. However, considering the high accommodation space settings of Omutirapo (Fig. 9) and Holowilena, and hence preservation potential, it can be argued that these regions provide an excellent opportunity to identify intra-Sturtian global events. Considering evidence from Omutirapo (the clast-free shale facies association) and Australia (the hummocky cross-stratification-bearing interval in the middle of the Wilyerpa Formation) in tandem identifies clear non-glacial facies in the middle of each succession. Existing chronostratigraphic frameworks for the Cryogenian glaciations (Macdonald *et al.*, 2010b) are permissible of a global-scale interglacial, although the concept of major ice-free interglacials during the supposedly global ice cover may be difficult to reconcile with current interpretations of snowball Earth (Hoffman & Schrag, 2002).

ACKNOWLEDGEMENTS

The authors are grateful to two very able field assistants – Mr Ralph Muyamba and Mr Paulus

Mungandjera – from the Geology Department of the University of Namibia, Windhoek, and to Mr Gerd Winterleitner for logistical assistance in arranging fieldwork in July 2011. The authors would also like to thank Emrys Phillips and Guy Desaubliaux for very constructive reviews, and the *Sedimentology* Chief Editor, Stephen Rice, for persistence in securing reviewers.

REFERENCES

Allen, P.A. and **Etienne, J.L.** (2008) Sedimentary challenge to snowball Earth. *Nat. Geosci.*, **1,** 817–825.

Allen, G.P. and **Posamentier, H.W.** (1993) Sequence stratigraphy and facies models of an incised valley fill: the Gironde Estuary, France. *J. Sed. Petrol.*, **63,** 378–391.

Andreasson, K., Nilssen, L.C., Rafaelsen, B. and **Kuilman, L.** (2004) Three dimensional seismic data from the Barents Sea margin reveal evidence of past ice streams and their dynamics. *Geology*, **32,** 729–732.

Arnaud, E. (2008) Deformation in the Neoproterozoic Smalfjord Formation, northern Norway: an indicator of glacial depositional conditions? *Sedimentology*, **55,** 335–356.

Arnaud, E. (2012) The paleoclimatic significance of deformation structures in Neoproterozoic successions. *Sed. Geol.*, **243–244,** 33–56.

Ashley, G.M. (1990) Classification of large-scale subaqueous bedforms: a new look at an old problem. *J. Sed. Res.*, **60,** 161–172.

Badenhorst, F.P. (1988) The lithostratigraphy of the Chuos Mixtite in part of the southern central zone of the Damara Orogen, South-West Africa. *Commun. Geol. Surv. SW Africa/Namibia*, **4,** 103–110.

Boyle, R.A., Lenton, T.M. and **Williams, H.T.P.** (2007) Neoproterozoic 'snowball Earth' glaciations and the evolution of altruism. *Geobiology*, **5,** 337–349.

Cheel, R.J. and **Middleton, G.V.** (1986) Horizontal laminae formed under upper flow regime plane bed conditions. *J. Geol.*, **94,** 489–504.

Collins, A.S. and **Pisarevsky, S.A.** (2005) Amalgamating eastern Gondwana: the evolution of the Circum-Indian Orogens. *Earth Sci. Rev.*, **71,** 229–270.

Condon, D.J., Prave, A.R. and **Benn, D.I.** (2002) Neoproterozoic glacial-rainout intervals: observations and implications. *Geology*, **30,** 35–38.

Domack, E.W. and **Hoffman, P.F.** (2011) An ice grounding-line wedge from the Ghaub glaciation (635 Ma) on the distal foreslope of the Otavi carbonate platform, Namibia, and its bearing on the snowball Earth hypothesis. *Geol. Soc. Am. Bull.*, **123,** 1448–1477.

Evans, D.J.A. and **Benn, D.I.** (2004) *A Practical Guide to the Study of Glacial Sediments*. Arnold, New York, 266 pp.

Eyles, N. and **Januszczak, N.** (2007) Syntectonic subaqueous mass flows of the Neoproterozoic Otavi Group, Namibia: where is the evidence of global glaciation? *Basin Res.*, **19,** 179–198.

Fielding, C.R., Naish, T.R., Woolfe, K.J. and **Lavelle, M.A.** (2000) Facies analysis and sequence stratigraphy of CRP-2/2A, Victoria Land Basin, Antarctica. *Terra Antart.*, **7,** 323–338.

Gevers, T.W. (1931) An ancient tillite in South-West Africa. *Trans. Geol. Soc. S. Afr.*, **34,** 1–17.

Ghienne, J.-F., Le Heron, D.P., Moreau, J. and **Deynoux, M.** (2007) The Late Ordovician glacial sedimentary system of the West Gondwana platform. In: *Glacial Sedimentary Environments – Processes and Products* (Eds M.J. Hambrey, P. Cristofferson, N. Glasser and B. Hubbard), *IAS Spec. Publ.*, **39,** 295–319.

Halverson, G.P., Maloof, A.C. and **Hoffman, P.F.** (2004) The Marinoan glaciation (Neoproterozoic) in northeast Svalbard. *Basin Res.*, **16,** 297–324.

Hambrey, M.J., Barrett, P.J. and **Powell, R.D.** (2002) Late Oligocene and early Miocene glacimarine sedimentation in the SW Ross Sea, Antarctica: the record from offshore drilling. In: *Glacier-Influenced Sedimentation on High-Latitude Continental Margins* (Eds J.A. Dowdeswell and C. O'Cofaigh), *Geol. Soc. London Spec. Publ.*, **203,** 105–128.

Hart, J.K. and **Roberts, D.H.** (1994) Criteria to distinguish between subglacial glaciotectonic and glaciomarine sedimentation, I. Deformation styles and sedimentology. *Sed. Geol.*, **91,** 191–213.

Henry, G., Stanistreet, I.G. and **Maiden, K.J.** (1986) Preliminary results of a sedimentological study of the Chuos Formation in the central zone of the Damara Orogen: evidence for mass flow processes and glacial activity. *Commun. Geol. Surv. SW Africa/Namibia*, **2,** 75–92.

Hoffman, P.F. and **Halverson, G.P.** (2008) Otavi Group of the western Northern Platform, the eastern Kaoko Zone and the western Northern Margin Zone. In: *The Geology of Namibia Volume 2 – Neoproterozoic to Lower Palaeozoic* (Ed. R. McG Miller), pp. 13.69–13.136. Ministry of Mines and Energy, Windhoek, Namibia.

Hoffman, P.F. and **Schrag, D.P.** (2002) The snowball Earth hypothesis: testing the limits of global change. *Terra Nova*, **14,** 129–155.

Hoffman, P.F., Hawkins, D.P., Isachsen, C.E. and **Bowring, S.A.** (1996) Precise U-Pb zircon ages for early Damaran magmatism in the Summas Mountains and Welwitschia Inlier, northern Damara belt, Namibia. *Commun. Geol. Surv. SW Africa/Namibia*, **11,** 47–52.

Hoffman, P.F., Kaufman, A.J., Halverson, G.P. and **Schrag, D.P.** (1998) A Neoproterozoic snowball Earth. *Science*, **281,** 1342–1346.

Hoffmann, K.-H. and **Prave, A.R.** (1996) A preliminary note on a revised subdivision and regional correlation of the Otavo Group based on glaciogenic diamictites and associated cap dolostones. *Commun. Geol. Surv. SW Africa/Namibia*, **11,** 77–82.

Hoffmann, K.H., Condon, D.J., Bowring, S.A. and **Crowley, J.L.** (2004) U-Pb zircon date from the Neoproterozoic Ghaub formation, Namibia: constraints on Marinoan glaciation. *Geology*, **32,** 817–820.

Hornung, J.J., Asprion, U. and **Winsemann, J.** (2007) Jet efflux deposits of a subaqueous ice contact fan, glacial Lake Rinteln, northwestern Germany. *Sed. Geol.*, **193,** 167–192.

Hyde, W.T., Crowley, T.J., Baum, S.K. and **Peltier, W.R.** (2000) Neoproterozoic 'snowball Earth' simulations with a coupled climate/ice sheet model. *Nature*, **405,** 425–429.

Lachniet, M.S., Larson, G.J., Lawson, D.E., Evenson, E.B. and **Alley, R.B.** (2001) Microstructures of sediment flow deposits and subglacial sediments: a comparison. *Boreas*, **30,** 254–262.

Lang, J., Dixon, R.J., Le Heron, D.P. and **Winsemann, J.** (2012) Depositional architecture and sequence stratigraphic correlation of Upper Ordovician glaciogenic deposits, Illizi Basin, Algeria. In: *Glaciogenic Reservoirs and Hydrocarbon Systems* (Eds M. Huuse, J. Redfern, D.P. Le Heron, R.J.

Dixon, A. Moscariello and J. Craig), *Geol. Soc. London. Spec. Publ.*, **368,** doi: 10.1144/SP368.1.

Le Heron, D.P. (2012) The Cryogenian record of glaciation and deglaciation in South Australia. *Sed. Geol.*, **243–244,** 57–69.

Le Heron, D.P. and **Etienne, J.L.** (2005) A complex subglacial clastic dyke swarm, Sólheimajökull, southern Iceland. *Sed. Geol.*, **181,** 25–37.

Le Heron, D.P., Sutcliffe, O.E., Whittington, R.J. and **Craig, J.** (2005) The origins of glacially related soft-sediment deformation structures in Upper Ordovician glaciogenic rocks: implication for ice sheet dynamics. *Palaeogeogr. Palaeoclimatol. Palaeoecol.*, **218,** 75–103.

Le Heron, D.P., Cox, G.M., Trundley, A.E. and **Collins, A.** (2011a) Sea-ice free conditions during the early Cryogenian (Sturt) glaciation, South Australia. *Geology*, **39,** 31–34.

Le Heron, D.P., Cox, G.M., Trundley, A.E. and **Collins, A.S.** (2011b) Two Cryogenian glacial successions compared: aspects of the Sturt and Elatina sediment records of South Australia. *Precamb. Res.*, **186,** 147–168.

Leather, J., Allen, P.A., Brasier, M.D. and **Cozzi, A.** (2002) Neoproterozoic snowball Earth under scrutiny: evidence from the Fiq glaciation of Oman. *Geology*, **30,** 891–894.

Lowe, D.R. (1982) Sediment gravity flows: II. Depositional models with special reference to the deposits of high--density turbidity currents. *J. Sed. Petrol.*, **52,** 279–297.

Macdonald, F.A., Strauss, J.V., Rose, C.V., Dudás, F.Õ. and **Schrag, D.P.** (2010a) Stratigraphy of the Port Nolloth Group of Namibia and South Africa and implications for the age of Neoproterozoic iron formations. *Am. J. Sci.*, **310,** 862–888.

Macdonald, F.A., Schmitz, M.D., Crowley, J.L., Roots, C.F., Jones, D.S., Maloof, A.C., Strauss, J.V., Cohen, P.A., Johnson, D.T. and **Schrag, D.P.** (2010b) Calibrating the Cryogenian. *Science*, **327,** 1241–1243.

Martin, H. (1965) Observations concerning the problem of the late Precambrian glacial deposits in South West Africa. *Geol. Rundsch.*, **54,** 115–127.

Martin, H., Porada, H. and **Walliser, O.H.** (1985) Mixtite deposits of the Damara sequence, Namibia, problems of interpretation. *Palaeogeogr. Palaeoclimatol. Palaeoecol.*, **51,** 159–196.

McCarroll, D. and **Rijsdijk, K.** (2003) Deformation styles as a key for unlocking glacial depositional environments. *J. Quatern. Sci.*, **18,** 473–489.

van der Meer, J.J.M. (1993) Microscopic evidence of subglacial deformation. *Quatern. Sci. Rev.*, **12,** 553–587.

Menzies, J. and **Zaniewski, K.** (2003) Microstructures within a modern debris flow deposit derived from Quaternary glacial diamicton – a comparative micromorphological study. *Sed. Geol.*, **157,** 31–48.

Menzies, J., Zaniewski, K. and **Dreger, D.** (1997) Evidence from microstructures of deformable bed conditions within drumlins, Chimney Bluffs, New York State. *Sed. Geol.*, **111,** 161–176.

Miller, R.Mc.G. (2008) *The Geology of Namibia Volume 2 – Neoproterozoic to Lower Palaeozoic*. Ministry of Mines and Energy, Windhoek, Namibia.

Mulder, T. and **Alexander, J.** (2001) The physical character of subaqueous sedimentary density flows and their deposits. *Sedimentology*, **48,** 269–299.

Nardin, T.R., Hein, F.J., Gorsline, D.S. and **Edwards, B.D.** (1979) A review of mass movement processes, sediment and acoustic characteristics and contrasts in slope and base of slope systems versus canyon-fan basin floor systems. In: *Geology of Continental Slopes* (Eds L.J. Doyle and O.H. Pilkey), **27,** 61–73, SEPM Spec. Publ., Tulsa, Oklahoma, USA.

O'Cofaigh, C. (1996) Tunnel valley genesis. *Prog. Phys. Geog.*, **20,** 1–19.

Phillips, E. (2006) Micromorphology of a debris flow deposit: evidence of basal shearing, hydrofracturing, liquefaction and rotational deformation during emplacement. *Quatern. Sci. Rev.*, **30,** 720–738.

Phillips, E., van der Meer, J.J.M. and **Ferguson, A.** (2011) A new 'microstructural mapping' methodology for the identification, analysis and interpretation of polyphase deformation within subglacial sediments. *Quatern. Sci. Rev.*, **30,** 2570–2596.

Pollard, D.P. and **Kasting, J.F.** (2005) Snowball Earth: a thin-ice solution with flowing sea glaciers. *J. Geophys. Res.*, **110,** C07010.

Porada, H. (1983) Geodynamic model for the geosynclinal development of the Damara Orogen, Namibia, South West Africa. In: *Intracontinental Fold Belts, Case Studies in the Variscan Belt of Europe and the Damara Belt in Namibia* (Eds H. Martin and F.W. Eder), pp. 503–541, Springer-Verlag, Berlin.

Postma, G., Nemec, W. and **Kleinspehn, K.L.** (1988) Large floating clasts in turbidites: a mechanism for their emplacement. *Sed. Geol.*, **58,** 47–61.

Powell, R.D. (1990) Glacimarine processes at grounding-line fans and their growth to ice-contact deltas. In: *Glacimarine Environments: Processes and Sediments* (Eds J.A. Dowdeswell and J.D. Scourse), *Geol. Soc. London Spec. Publ.*, **53,** 53–73.

Roberts, D.H. and **Hart, J.K.** (2005) The deforming bed characteristics of a stratified till assemblage in north East Anglia, UK: investigating controls on sediment rheology and strain signatures. *Quatern. Sci. Rev.*, **24,** 123–140.

Thomas, M.A. and **Anderson, J.B.** (1994) Sea-level controls on the facies architecture of the Trinity-Sabine incised-valley system, Texas continental shelf. *Soc. Econ. Paleontol. Mineral. Spec. Publ.*, **51,** 63–82.

Tripsanas, E.K. and **Piper, D.J.W.** (2008) Glaciogenic Debris-Flow Deposits of Orphan Basin, Offshore Eastern Canada: Sedimentological and Rheological Properties, Origin, and Relationship to Meltwater Discharge. *J. Sed. Res.*, **78,** 724–744.

Weaver, L. and **Arnaud, E.** (2011) Polyphase glacigenic deformation in the Waterloo Moraine, Kitchener, Ontario, Canada. *Sed. Geol.*, **235,** 292–303.

Manuscript received 7 March 2012; revision accepted 18 June 2012

4. South Australia

4.1. Introduction

The Sturt Gorge in Adelaide's outer suburbs is the type area of the Sturtian glaciation, and where the name was first coined in 1920 (Howchin, 1920; Cooper, 2010), with the younger Marinoan glaciation so-named after the nearby Marino Rocks (Preiss et al., 1998). These two horizons are exposed throughout the Adelaide Fold Belt, with the thickest preserved successions in the Flinders and Mount Lofty Ranges. Stratigraphic nomenclature of the older 'Sturtian' interval is highly variable across this region. Housed within the Yudnamutana Subgroup, the succession typically comprises a lower diamictite-dominated unit, named the Bolla Bollana Formation in the northern Flinders Ranges, the Pualco Tillite in the central regions, the Appila Tillite further south, or the Sturt Tillite in its type area, and overlain by more heterolithic deposits of the Wilyerpa Formation in the central and southern regions, or its stratigraphic equivalent the Lyndhurst Formation further north (see Fig. 3, Chapter 4.3). The post-glacial shale succession is widely recognised as the Tapley Hill Formation.

The glacial origin of these sediments was first recognised by Howchin (1901), although subsequent debates have disputed their terrestrial (Mawson, 1941, 1949) or glaciomarine (Young & Gostin, 1991) deposition. Detailed work by Young and Gostin (1988, 1989, 1990, 1991) in the northern Flinders Basin provided a strong case for interpreting these successions as glaciomarine, as well as highlighting clear evidence for sequences of glacial advance or retreat. These ideas were re-enforced by Le Heron et al. (2011) some 20 years later through examination of the Holowilena Creek section in the central Flinders Ranges, where evidence of interglacial conditions interrupting the Sturtian glacial interval, including testament to open water conditions, cast significant doubt on earlier arguments for a prolonged, severe glaciation (e.g. Hoffman et al., 1998; Hoffman & Schrag, 2002).

This chapter includes two studies which re-examine sections in the Arkaroola and Orroroo regions of the northern and central Flinders Ranges, respectively, which have not been subject to detailed re-examination for decades. In the Arkaroola region, exceptionally thick exposures of the diamictite-dominated Bolla Bollana Formation allow a critical evaluation of the diagnostic criteria to recognise glacially-influenced diamictite sequences, and their stratigraphic architecture to be explored in detail (Chapter 4.2). Meanwhile, building on Le Heron et al.'s (2011a,b) earlier work in the Holowilena Creek, examination of correlative sections in the central Flinders Ranges enables a comparison of the evidence for, and nature of glacial advance-retreat sequences, and the influence of underlying palaeotopography on their preservation (Chapter 4.3).

4.2. Bolla Bollana Trough Mouth Fan, northern Flinders Ranges

Bolla Bollana boulder beds: A Neoproterozoic trough mouth fan in South Australia

Le Heron, D.P., Busfield, M.E. & Collins, A.S.

Sedimentology 2014a, v. 61, 978-995.
doi:10.1111/sed.12082

Statement of contribution

- ***Data collection***
  - Busfield and Le Heron logged the studied sections.
  - Busfield collected samples for hand specimen and micro-scale analysis. Micro-scale analysis did not reveal significant additional data and therefore was not included in the final manuscript.
- ***Manuscript text***
  - Preliminary ideas on lithofacies interpretation, evidence for glacial influence and the depositional model as a trough mouth fan were discussed by Le Heron and Busfield in the field. Le Heron authored the first draft of the manuscript following these discussions.
  - Busfield modified the manuscript in all subsequent drafts, specifically with reference to the correlative central Flinders Ranges sections (Chapter 4.3).
  - Collins reviewed the first draft of the manuscript.
- ***Figures***
  - Le Heron illustrated all figures in the manuscript. Figure 1 was re-drawn by Busfield.
  - Busfield and Le Heron contributed photographs to figures throughout.

SEDIMENTOLOGY the journal of the International Association of Sedimentologists

Sedimentology (2014) **61**, 978–995 doi: 10.1111/sed.12082

Bolla Bollana boulder beds: A Neoproterozoic trough mouth fan in South Australia?

DANIEL P. LE HERON*, MARIE E. BUSFIELD* and ALAN S. COLLINS†
**Department of Earth Sciences, Queen's Building, Royal Holloway University of London, Egham TW200EX, UK (E-mail: le_herondaniel@hotmail.com)*
†TRAX, School of Earth and Environmental Sciences, University of Adelaide, Adelaide, SA 5005, Australia

Associate Editor – Nick Eyles

ABSTRACT

The Bolla Bollana Formation is an exceptionally thick (*ca* 1500 m), rift-related sedimentary succession cropping out in the northern Flinders Ranges, South Australia, which was deposited during the Sturtian (mid Cryogenian) glaciation. Lithofacies analysis reveals three distinct facies associations which chart changing depositional styles on an ice-sourced subaqueous fan system. The diamictite facies association is dominant, and comprises both massive and stratified varieties with a range of clast compositions and textures, arranged into thick beds (1 to 20 m), representing stacked, ice-proximal glaciogenic debris-flow deposits. A channel belt facies association, most commonly consisting of normally graded conglomerates and sandstones, displays scour and fill structure of *ca* 10 m width and 1 to 3 m depth: these strata are interpreted as channelized turbidites. Rare mud-filled channels in this facies association bear glacially striated lonestones. Finally, a sheet heterolithics facies association contains a range of conglomerates through sandstones to silty shales arranged into clear, normally graded cycles from the lamina to bed scale. These record a variety of non-channelized turbidites, probably occupying distal and/or inter-channel locations on the subaqueous fan. Coarsening and thickening-up cycles, capped by dolomicrites or mudstones, are indicative of lobe build out and abandonment, potentially as a result of ice lobe advance and stagnation. Dropstones, recognized by downwarped and punctured laminae beneath pebbles to boulders in shale, or in delicate climbing ripple cross-laminated siltstones, are clearly indicative of ice rafting. The co-occurrence of ice-rafted debris and striated lonestones strongly supports a glaciogenic sediment source for the diamictites. Comparison to Pleistocene analogues enables an interpretation as a trough mouth fan, most probably deposited leeward of a palaeo-ice stream. Beyond emphasizing the highly dynamic nature of Sturtian ice sheets, these interpretations testify to the oldest trough mouth fan recorded to date.

Keywords Flinders Ranges, glaciation, ice stream, Neoproterozoic, snowball Earth, Sturtian, trough mouth fan.

INTRODUCTION

The northern Flinders Ranges of South Australia expose an extremely thick succession of diamictites that were deposited during the Sturt glaciation (Young & Gostin, 1991; Preiss *et al.*, 2011) at *ca* 715 Ma (Macdonald *et al.*, 2010). In Arkaroola (Fig. 1), these deposits were first described by Mawson (1941, 1949) and interpreted as terrestrial glacial deposits. By contrast, glaciomarine interpretations were offered by Young & Gostin (1991) by the recognition of dropstone fabrics. The deposits are highly contentious and significant to debates focused on the intensity and extent of Cryogenian glaciations (e.g. Etienne *et al.*, 2007; Fairchild & Kennedy, 2007; Allen & Etienne, 2008), particularly because South Australia can be regarded as a type area for the 'Sturtian' pan-glacial event (Hoffman & Schrag, 2002).

For some, scepticism surrounds the interpretation of many Cryogenian diamictite-bearing successions, such as those in the Flinders Ranges. A mechanism of diachronous rift shoulder glaciation, during the fragmentation of Rodinia, was proposed by Eyles & Januszczak (2004). In that model, debris flows were fluxed into rift basins. In Namibia, for example, it was proposed that some diamictites were deposited by non-glacially influenced gravity flow deposits (Eyles & Januszczak, 2007), amplifying the earlier non-glacial interpretations by Schermerhorn (Schermerhorn & Stanton, 1963; Schermerhorn, 1974). Such studies have hence stimulated questions about the clarity of the glacial signature in Neoproterozoic sedimentary successions. Recent examples worldwide, however, highlight the diverse range of reliable glaciogenic proxies preserved, despite tectonically active basin configurations (e.g. Arnaud, 2012; Busfield & Le Heron, 2013; Le Heron *et al.*, 2011; Le Heron, 2012; Uhlein *et al.* 2011). These studies provide substantive evidence for glacial processes during the Neoproterozoic, irrespective of the scale of interpreted ice sheets (cf. Allen & Etienne, 2008).

In this study, a detailed facies analysis of the Bolla Bollana Formation in the northern Flinders Ranges (Figs 1 and 2) is undertaken, presenting data from three outstanding exposures. The succession is part of a classic diamictite succession which has not been subjected to detailed investigation for over 20 years. The data

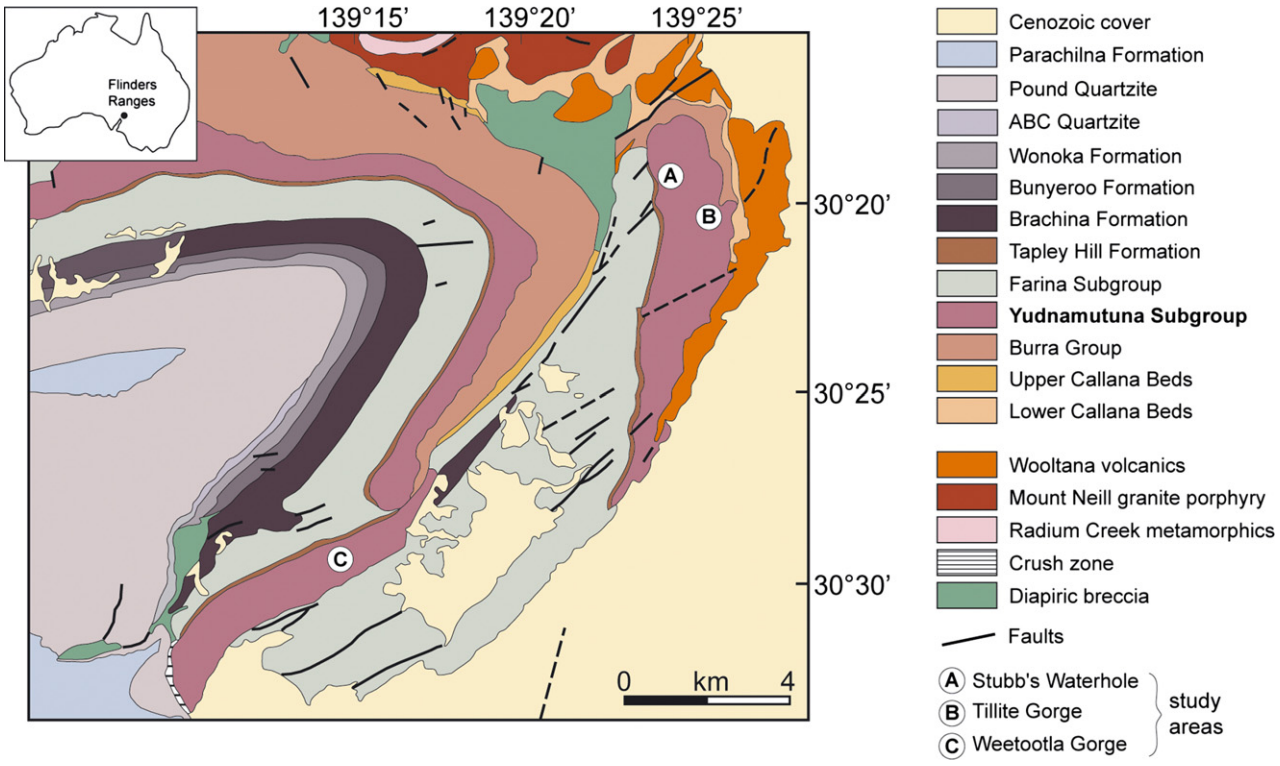

Fig. 1. Geological sketch map of the Arkaroola region (modified and simplified after Coats, 1973). Note the location of the Tillite Gorge, Stubb's Waterhole and Weetootla Gorge sections which are shown in Fig. 4.

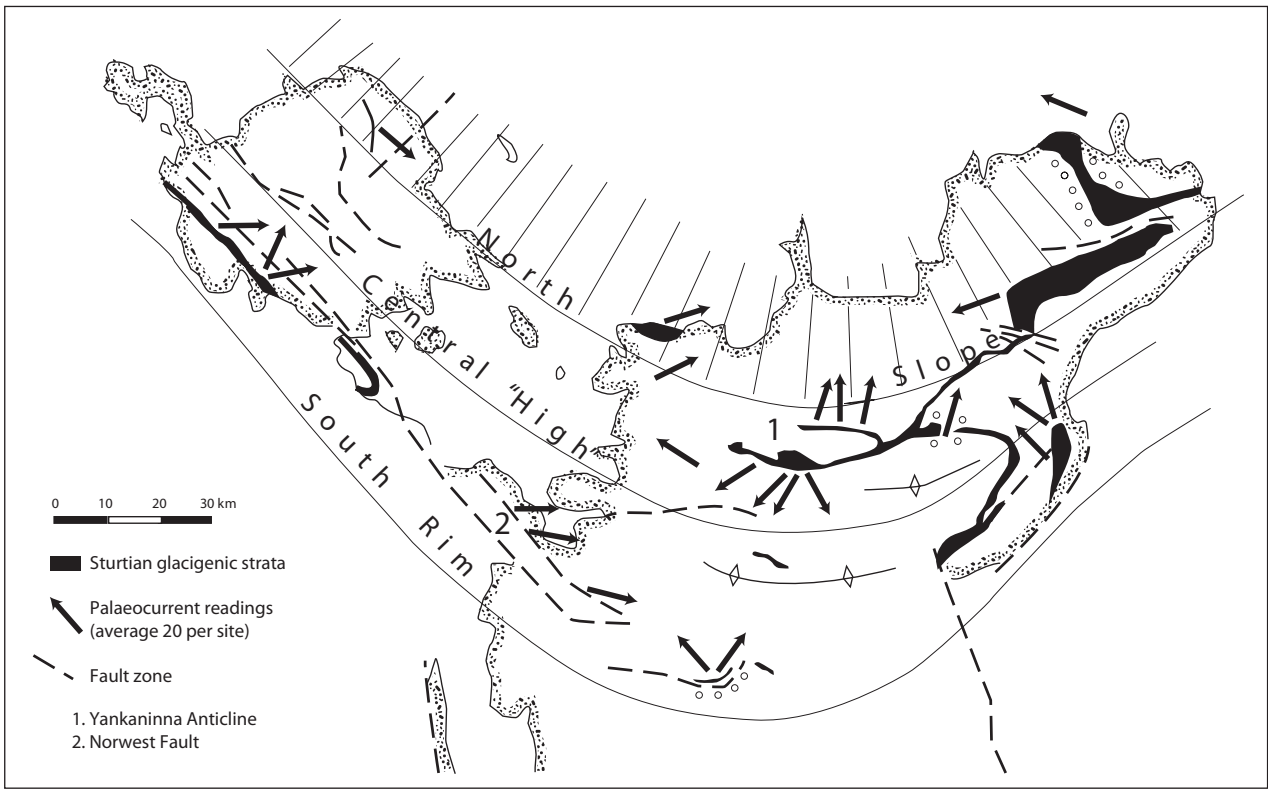

Fig. 2. Northern Flinders Basin map, reproduced from Young & Gostin (1991). The palaeocurrent data, shown here schematically, derive from a variety of sources (flute casts and ripple cross-laminae) and have been used to infer the development of syn-glacial horst and graben topography (Young & Gostin, 1991). The outlines of various sub-basins are shown with a solid line, with stippling marking the internal margins of these sub-basins.

were collected as part of a six week field campaign in August 2012.

STUDY AREA AND STRATIGRAPHY

In the Arkaroola district of the northern Flinders Ranges, the lowermost of two Neoproterozoic diamictite-bearing intervals is exposed. These rocks belong to the Yudnamutana Subgroup (Fig. 3). A three-fold subdivision of this subgroup is recognized: the Fitton Formation occurs at the base, the Bolla Bollana Formation in the middle and the Lyndhurst Formation is the uppermost unit (Fig. 3). The Bolla Bollana Formation was first examined in the Arkaroola district by Mawson (1941, 1949). This pioneering work offered a terrestrial glacial origin for the diamictites. The formation itself was defined by Coats (in Thomson *et al.*, 1964) as a sub-greywacke tillite of massive character with intercalated quartzite and siltstone. Young & Gostin (1988, 1989, 1990, 1991) studied the Sturtian succession within the North Flinders Basin (NFB), a sub-basin within the Adelaide Fold Belt that Preiss (1987, 1999) argued was probably disconnected from depocentres in the central and southern Flinders Ranges. Each paper presented a series of sedimentary logs and facies descriptions, recognizing a comparable stratigraphic subdivision across the area. The dramatic increase in knowledge of sedimentary processes at tidewater ice margins since the time of Mawson motivated Young & Gostin (1989, 1991) to re-interpret the Bolla Bollana Formation as glaciomarine. Regional mapping (Coats, 1973) demonstrates that the Bolla Bollana Formation is extensive in the eastern part of the Copley Sheet, and is particularly well-exposed to the east and south of Arkaroola (Fig. 1). When summarizing the regional stratigraphy, Young & Gostin (1991) published a map showing how sediment dispersal, surmised from a variety of palaeocurrent indicators, testifies to the interplay of extensional tectonics, forming graben-like minibasins and palaeohighs (Fig. 2).

The Bolla Bollana Formation trends towards massive in character in the south of the NFB,

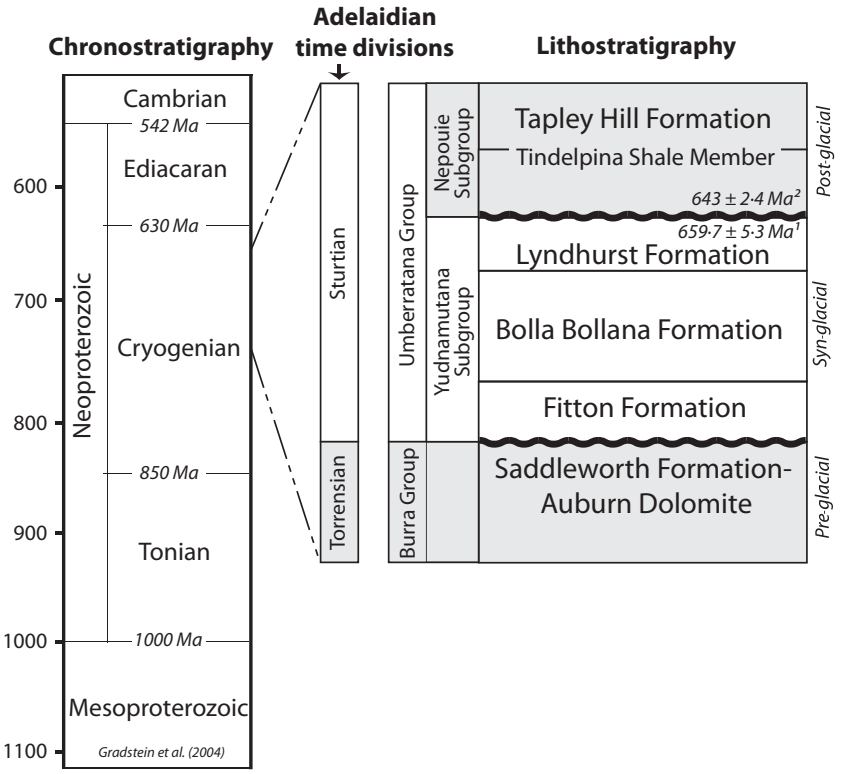

Fig. 3. Stratigraphy of the Neoproterozoic of the Arkaroola area, with subdivisions of the Sturt glacial succession based on Young & Gostin (1989). The internal lithostratigraphy of the Sturt glacial succession varies dramatically even over the comparatively small region of the northern Flinders Ranges (cf. Young & Gostin, 1988, 1989, 1990, 1991). In the Arkaroola district, a three-fold division is recognized with the Fitton Formation at the base, the Bolla Bollana Formation in the middle, and the Lyndhurst Formation as the uppermost unit within the Yudnamutana Subgroup. This paper specifically examines the Bolla Bollana Formation.

becoming stratified in the north. To explain this, Young & Gostin (1988) suggested that ice-rafted debris (IRD) deposition was predominant in the south, with reworking processes more important northward. No unequivocal glacially striated surfaces are reported in Cryogenian successions of Australia, with the exception of those in Western Australia (Corkeron, 2007). However, the "cast of striations" is reported to occur "on the underside of basal Sturt silty mudstones near Merinjina Well" (Young & Gostin, 1991); these were interpreted as tectonic by Daily *et al.* (1973) and glaciogenic by others (Preiss, 1987; Young & Gostin, 1991; Preiss *et al.*, 2011).

In the present study, detailed facies descriptions and interpretations are provided from three new sections at Stubb's Waterhole, Tillite Gorge and Weetootla Gorge. None of these sections were investigated by Young & Gostin (1991), yet they yield exceptionally high-quality exposure. The sections are situated ideally in a region subject to only low-grade metamorphism during the Early Palaeozoic Delamerian Orogeny (Preiss, 1987), whereas mid-amphibolite facies affect correlative sediments in the Adelaide region. The objectives of this study are: (i) to highlight a clear glaciogenic source for the Bolla Bollana Formation; (ii) to reject a rift-only origin for diamictites; and (iii) to present a new depositional model for the sequence as a trough-mouth fan (TMF) succession.

FACIES ANALYSIS

The thickness of the Yudnamutana Subgroup in the North Flinders Basin is estimated to reach 6000 m in the Yudnamutana Trough (Young & Gostin, 1991), *ca* 30 km north-west of the study area. Herein, exceptionally well-preserved, high-quality sections are focused on rather than attempting a complete stratigraphic traverse. Each of the three facies associations described and interpreted below occurs in multiple locations in the Arkaroola district. A diamictite facies association, a channel belt facies associa-

tion and a sheet heterolithics facies association are recognized. Below, data from three detailed logged sections are presented (Fig. 4).

Diamictite facies association

Description

This facies association is highly heterogeneous and, in terms of volume, dominates the Bolla Bollana Formation (Fig. 5A). Uninterrupted accumulations >90 m thick are common (for example, Tillite Gorge: Figs 4B and 5A). Diamictites are sandy throughout, including both clast-poor and clast-rich varieties (*sensu* Moncrieff, 1989), with pebble to predominantly boulder-sized clasts. Bed thickness varies considerably between 1 m and 15 m (thus reaching megabed dimensions, *sensu* Marjanac, 1996) (Fig. 5B). With some exceptions, most bed contacts are parallel to one another with minimal evidence for erosive contacts.

Both massive and well-stratified diamictites occur as end-members of a continuum; most beds exhibit at least some diffuse stratification. In some cases, pronounced variations in clast content (20 to 60%) occur in successive beds (for example, Fig. 4A, 15 to 25 m; Fig. 5C). In thick beds, upward transitions from stratified through to massive facies occur, accompanied by an increase in clast size and content (Fig. 4B, 43 to 73 m). In stratified clast-poor diamictites, isolated clasts of pebble to boulder size downwarp and pierce underlying laminations; overlying laminae are unaffected (Fig. 5D). Sand lenses, or lens-shaped clast-free zones in the diamictite, occur both at the bottom and top of some beds. Throughout the facies association, clasts are typically equant, and sub-rounded to sub-angular. The base of the thickest observed bed in the Tillite Gorge section (Fig. 4B, 43 m) shows a highly undulose contact (Fig. 5E). Clasts with polished surfaces and cross-cutting striations occur locally (Fig. 5F).

Interpretation

The diamictite facies association is interpreted largely as a suite of glaciogenic debris flows (GDFs) deposited in a subaqueous setting. The organization of the diamictites into clearly defined beds indicates repeated emplacement of flows. The typical absence of erosive contacts is attributed to hydroplaning at the head of the flow, thereby lubricating the base of the flow and protecting the underlying bed from cannibalization (e.g. Laberg & Vorren, 2000). The upsection increase in clast abundance and size is consistent with kinetic sieving within the flow, to generate inverse grading (Talling *et al.*, 2012). The downwarping of laminae beneath pebbles in the stratified clast-poor diamictites (Fig. 5D) is interpreted as impact structures produced by falling dropstones. Whilst clasts sinking into water saturated sediment can produce dropstone-like texture in a debris flow, such clasts typically behave similarly to tectonic augen, with concomitant shearing of adjacent laminae as the flow evolves (Hart & Roberts, 1994). Thus, in addition to downslope mass flow, evidence for subaqueous sedimentation and ice-rafted debris accumulation is preserved. Given the compositional similarity of strata both below and above the undulose bed contacts, (Fig. 5E) it is likely that this feature developed through differential compaction rather than through erosion. The presence of clasts with cross-cutting striations (Fig. 5F) strongly supports a glacial derivation. Specifically, the cross-cutting striations indicate rotation of the clasts, either in basal ice, at the ice-bed interface, or within the deforming bed beneath an ice mass (Benn & Evans, 2010). The exceptional preservation of striations supports incorporation into the glaciogenic debris flows (GDFs) via ice rafting, thereby protecting clast surfaces from the erosion processes anticipated during downslope remobilization.

Channel belt facies association

Description

A variety of scour and fill structures, measuring 5 to 14 m wide and 2 to 3·5 m deep, are a key feature of this facies association (Fig. 4B, 95 to 113 m; Fig. 6A and B). The scours cross-cut, with multiple generations apparent over a few metres (Fig. 6A and B). Lithologies include pebble to granule conglomerates, sandstones and siltstones, together with subordinate sandy diamictites. Some of the scours are mud-filled and re-incised by an overlying channel (Fig. 6C). The base of most beds is irregular (Fig. 6D). Normally graded bedding is typical, with transitions from granule conglomerate through to planar-bedded sandstone well-expressed in Tillite Gorge as R1 to S3 turbidite divisions of Lowe (1982) (for example, Fig. 4B, 99 to 103 m; Fig. 7A). Soft-sediment deformation structures in sandstone include recumbent folds (Fig. 7B), curvilinear grooves on the upper surfaces of sandstone beds (Fig. 7C) and flame structures.

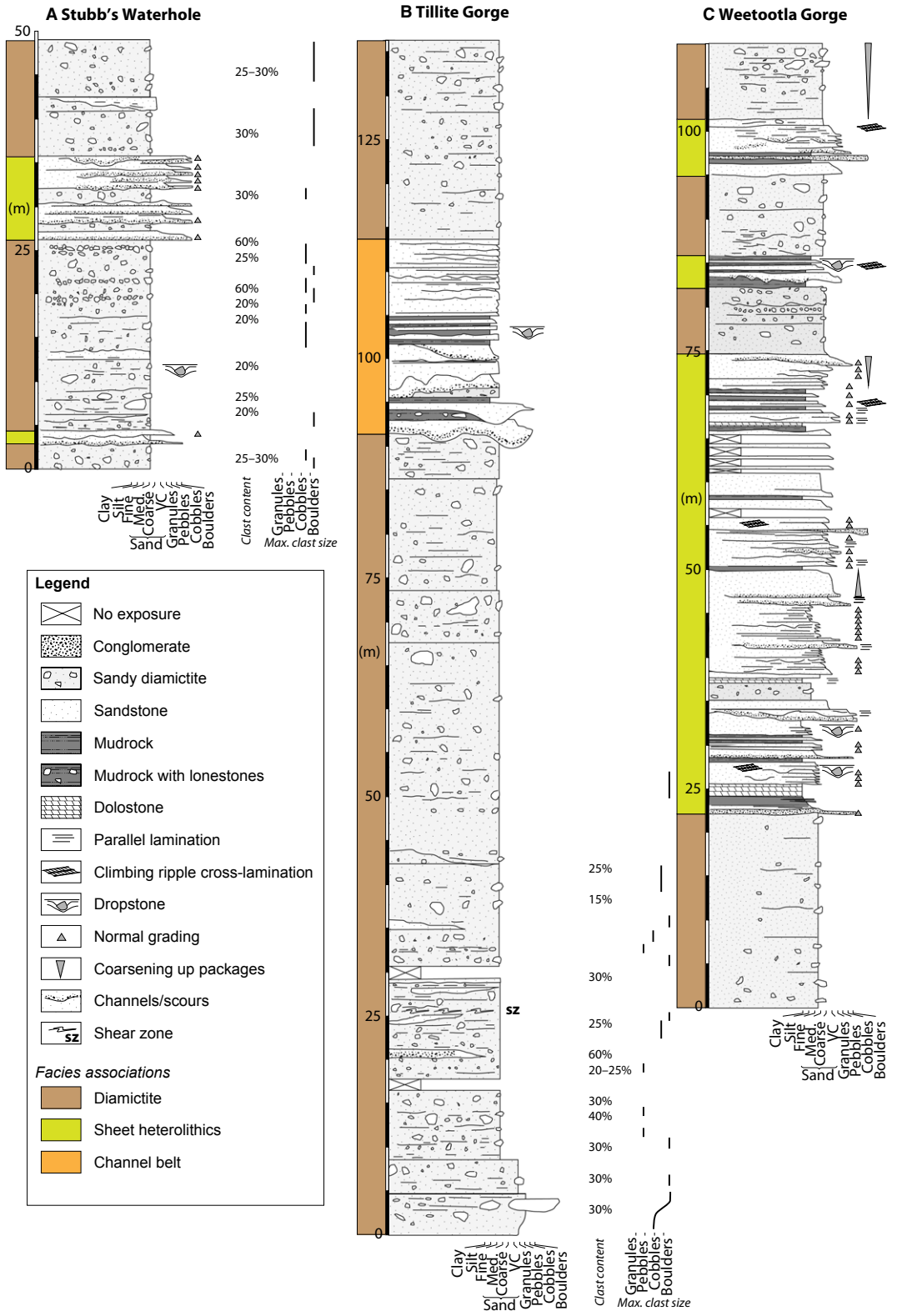

Fig. 4. Detailed sedimentary logs through the Bolla Bollana Formation in the Arkaroola district (see Fig. 1 for location of sections). Each is a partial section through the exposure at each locality rather than a complete section: (A) Stubb's Waterhole; (B) Tillite Gorge; (C) Weetootla Gorge. Note that in the case of the diamictites, the grain size in each of the logs refers to grain size of the matrix: maximum clast size, where possible, was also measured. These latter data are shown to the right of the logs.

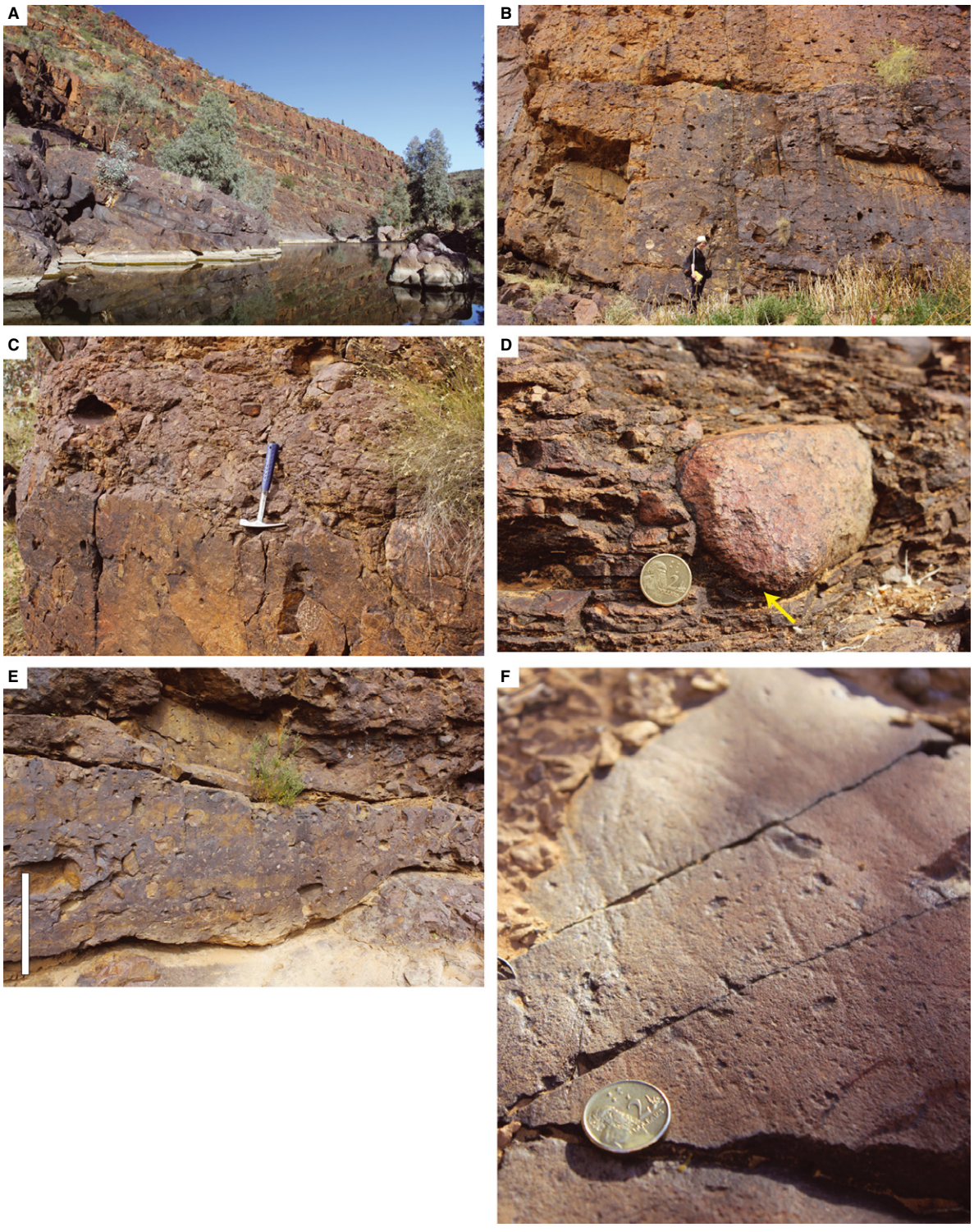

Fig. 5. Representative photographs of facies within the diamictite facies association. (A) Outcrop perspective of the Tillite Gorge locality, showing thickly bedded diamictites dipping towards the right of the photograph. Height of the cliff is *ca* 50 m. (B) Base of a diamictite megabed (42 to 67 m, Fig. 4B) with geologist for scale, *ca* 1.8 m tall. (C) Clast-poor diamictite overlain by clast-rich diamictite, with geological hammer for scale placed at the boundary. Hammer for scale is 250 mm long. (D) Impact structure beneath gneiss pebble in well-stratified diamictite. Rounded clasts are quite typical. Diameter of coin for scale is 20.5 mm. (E) Undulose contact at the base of a diamictite megabed. Note that this undulose character probably records differential compaction. Scale bar: 1 m. (F) Face of a polished and striated sandstone boulder, showing cross-cutting striation orientations.

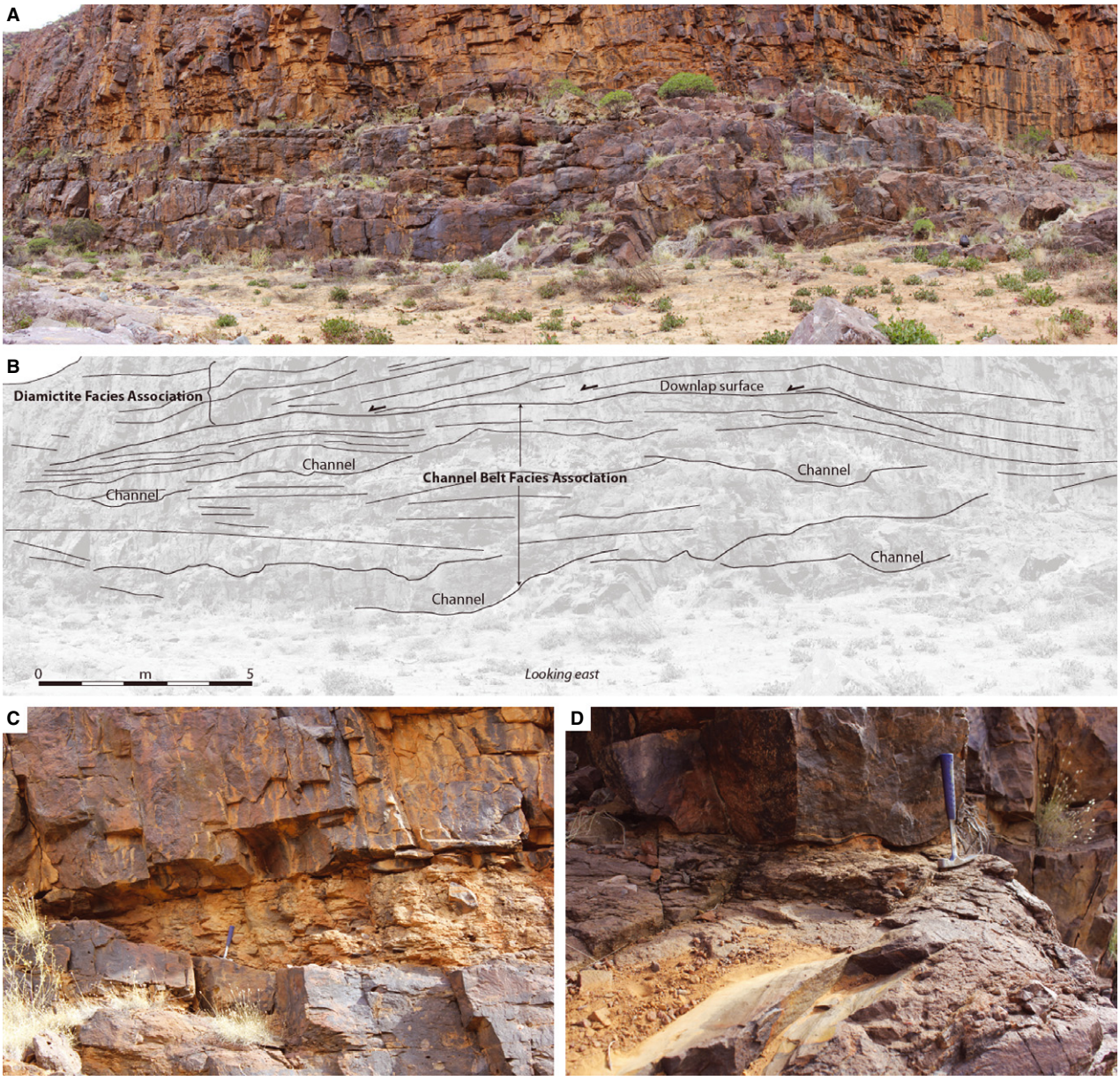

Fig. 6. (A) and (B) Panoramic photograph and corresponding sketch of stacked channel geometries in the channel belt facies association. Note also the downlapping strata of the diamictite facies association directly above. (C) Low-angle channel incision cutting down towards the left of the photograph (marked by solid white line), clearly truncating recessive siltstones, themselves infilling a channel scour. Hammer for scale is 250 mm long. (D) Low amplitude scour at the base of a sandstone bed: evidence for erosionally based beds even where clear channel geometries are not observed.

This suite of deformation structures is concentrated at a discrete stratigraphic interval ('shear zone' at 25 m, log B, Fig. 4). Sandy diamictites form sheet-like beds of 0·3 to 1 m, and contain sub-rounded to rounded clasts with striated faces (Fig. 7D). Siltstones occur both within channel structures, and as sheet-like lithosomes traceable for several tens of metres. In both cases, siltstones are poorly stratified, yet bear rare clasts of pebble to boulder size; these pierce and downwarp underlying laminations, with overlying laminations unaffected (Fig. 7E and F).

Interpretation

The scour and fill structures are interpreted as channels cut by turbidity currents and filled with turbidites. The coarse calibre of some of the channel fills, and the characteristic R1 to S3 turbidite motif (Lowe, 1982), implies a relatively

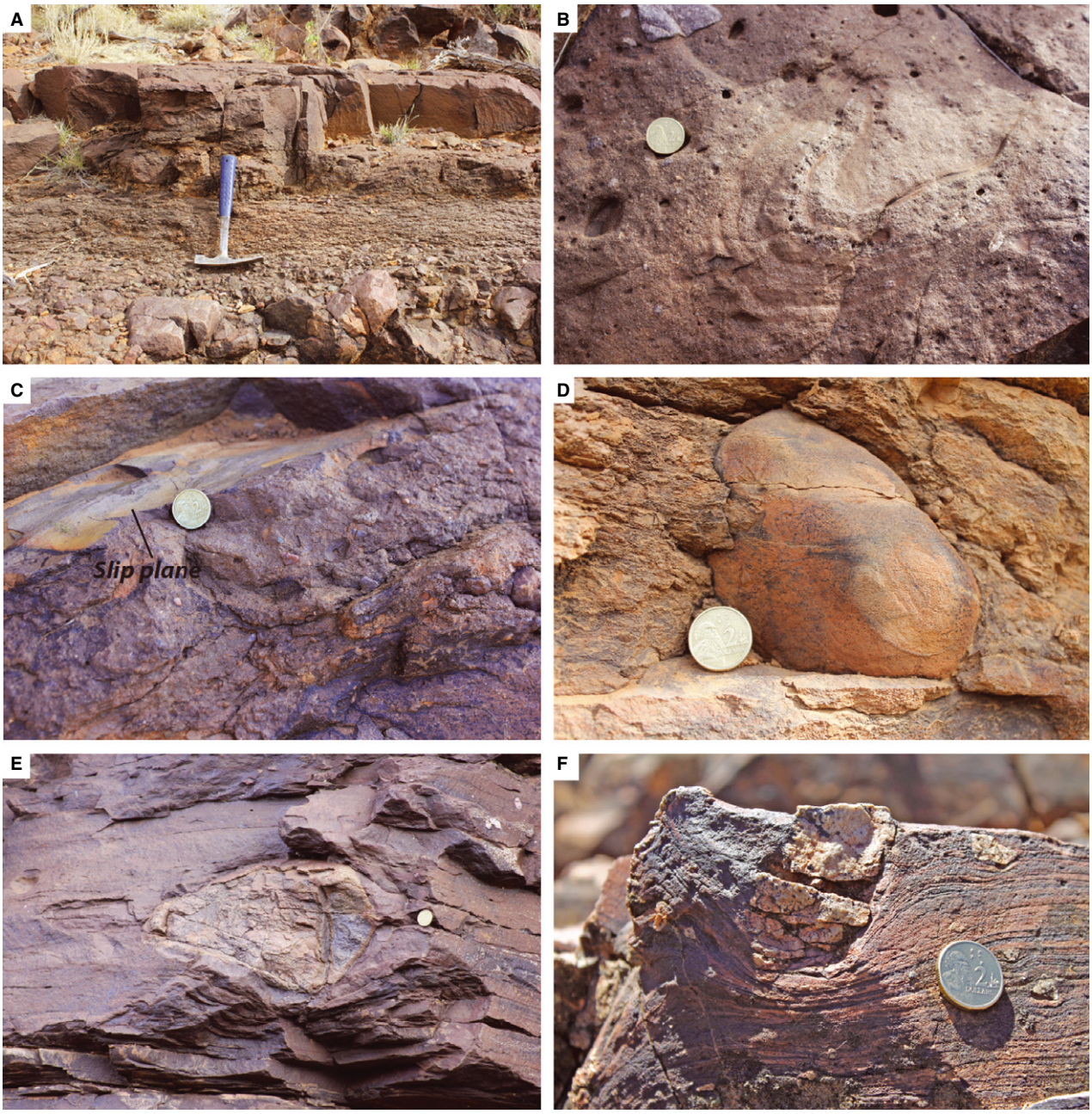

Fig. 7. (A) Typical fining-upward sequence, interpreted as a turbidite bed. In this example, pebble to cobble-grade clasts beneath the hammer pass upward over 10 cm into granular conglomerates, and finally well-differentiated, moderately to well-sorted sandstone above the hammer handle. Hammer for scale is 250 mm long. (B) Recumbent fold in a turbidite. Diameter of coin for scale is 20.5 mm. (C) Curvilinear grooves on a sandstone surface, interpreted to record intrastratal shear in sandstones. The absence of asperities or quartz/calcite mineralization discounts a tectonic origin. (D) Striated lonestone within siltstone: a putative dropstone emplaced towards the top of a Bouma sequence. (E) and (F) Two examples of dropstones with clear impact structures in laminated siltstone intervals.

proximal location on the fan (Reading & Richards, 1994). The particularly coarse-calibre (gravelly) material at the base of some channels is suggestive of a lag deposit (Alpak *et al.*, 2013). By comparison, the finer-grained channel fills are interpreted to record lower energy deposition in either a slightly more distal location on the fan or, alternatively, a finer-grained sediment source. Specifically, silt-plugged channels may suggest that the channels are filled by low-density turbidites (Talling *et al.*, 2012). These deposits represent off-axis/channel margin facies

(Camacho *et al.*, 2002) or coarse-grained sediment bypass (Talling *et al.*, 2012), and probably record deposition of these turbidites more distal to the sediment source than their coarser-grained counterparts.

The suite of soft-sediment deformation structures is compatible with rapid subaqueous deposition: recumbent folds can be indicative of gravitational instability and downslope slumping (Maltman, 1994), whereas flame structures are probably examples of Rayleigh–Taylor instabilities generated at a grain-size/bed interface (Allen, 1984; Collinson & Thompson, 1987). Numerical modelling of flame structures indicates that their genesis is promoted when relatively low viscosity, Newtonian fluids (the sand layer) rest on underlying clays (Harrison & Maltman, 2003). These conditions may be satisfied by rapid sedimentation or liquefaction. The curvilinear grooves on the upper surface of beds are interpreted as intra-bed slip planes, akin to hydroplastic slickensides (Petit & Laville, 1987) produced by the shearing of soft sediment in response to downslope movement. Shanmugam *et al.* (1995) described similar features from the Cretaceous and Palaeogene of the North Sea. A later tectonic origin can be dismissed on account of their local occurrence, curvilinear geometry, absence of asperities and lack of mineralization (cf. Petit & Laville, 1987).

The presence of 'impact structures' (curvature, deflection and puncturing of underlying laminations) beneath lonestones clearly points to ice-rafted debris (e.g. Eyles *et al.*, 2007). Moreover, the presence of polished and striated clast surfaces also indicates a clear glacial derivation. Despite the absence of impact structures in the sheet-like siltstones, the presence of lonestones may likewise indicate rafting from icebergs, or alternatively sub-ice shelf deposition (Benn & Evans, 2010). By analogy to comparable facies in the diamictite facies association, the diamictites in the channel belt facies association are also interpreted as the product of glaciogenic debris flows.

Sheet heterolithics facies association

Description

These deposits include a heterogeneous collection of lithologies ranging from granule conglomerates and diamictites, sandstones, siltstones, shales and dolostones. At outcrop, these lithologies are well-differentiated, forming tabular beds that can be traced for tens to hundreds of metres along strike. Decimetre to metre-scale fining-upward cycles are typical, with well-expressed examples in Weetootla Gorge (Fig. 4C, 23 to 75 m; Fig. 8A). Fining-upward cycles commence with sharp-based and locally scoured surfaces, overlain by granule-lags or massive sandstones (Fig. 8B), becoming parallel laminated upsection. Supercritical climbing ripple cross-laminated sandstones and siltstones (Fig. 8C) are typical in the upper part of many fining-upward cycles (for example, 56 m, 68 m, 85 m and 100 m at Weetootla Gorge; Fig. 4C). The crests of the ripple cross-laminae show an aggradational to weakly progradational character (Fig. 8C). Rarely, the fining-upward intervals are interrupted by clast-poor, sandy diamictites which do not exceed 1 m in thickness (Fig. 8D). Siltstone and shale occur at the top of the fining-upward cycles (Fig. 8E). Lonestones with impact structures occur in most facies, including the cross-laminated sandstone (for example, 102 m, Tillite Gorge: Figs 4B and 8B, arrowed clast) and in shale beds (Fig. 8E). The metre-scale fining-upward cycles are themselves organized into multi-metre thick coarsening and fining-upward motifs. At three intervals (25 m, 37 m and 66·5 m at Weetootla Gorge; Fig. 4C) buff-coloured, delicately parallel laminated, mud-grade dolostones were observed (Fig. 8F).

Interpretation

This facies association is interpreted to represent deposition in an inter-channel part of a subaqueous fan system, where the well-expressed, metre-scale fining-upward cycles are interpreted to record repeated emplacement of turbidity flows. A basal scour and lag, succeeded by a massive then parallel laminated sandstone interval, succeeded by climbing ripple cross-lamination, is a motif common to all models of turbidite genesis (cf. Bouma, 1963; Lowe, 1982; Mutti *et al.*, 1999; Talling *et al.*, 2012). Whilst the tabular geometry of the cycles is compatible with deposition as high-density turbidites (i.e. divisions T_A, $T_{B\text{-}2}$ and $T_{B\text{-}3}$ in the modified Bouma nomenclature: Talling *et al.*, 2012). The occurrence of lonestones with impact structures, interpreted as dropstones, in ripple cross-laminated siltstones is strong evidence for glacial influence. The supercritical styles of ripple cross-lamination testify to high rates of sediment delivery, and tractive velocities of $<0{\cdot}6$ m sec^{-1} (e.g. Bridge & Demicco, 2008). The occurrence of large clasts within these facies is at odds with the low velocities required for the formation of ripple cross-lamination,

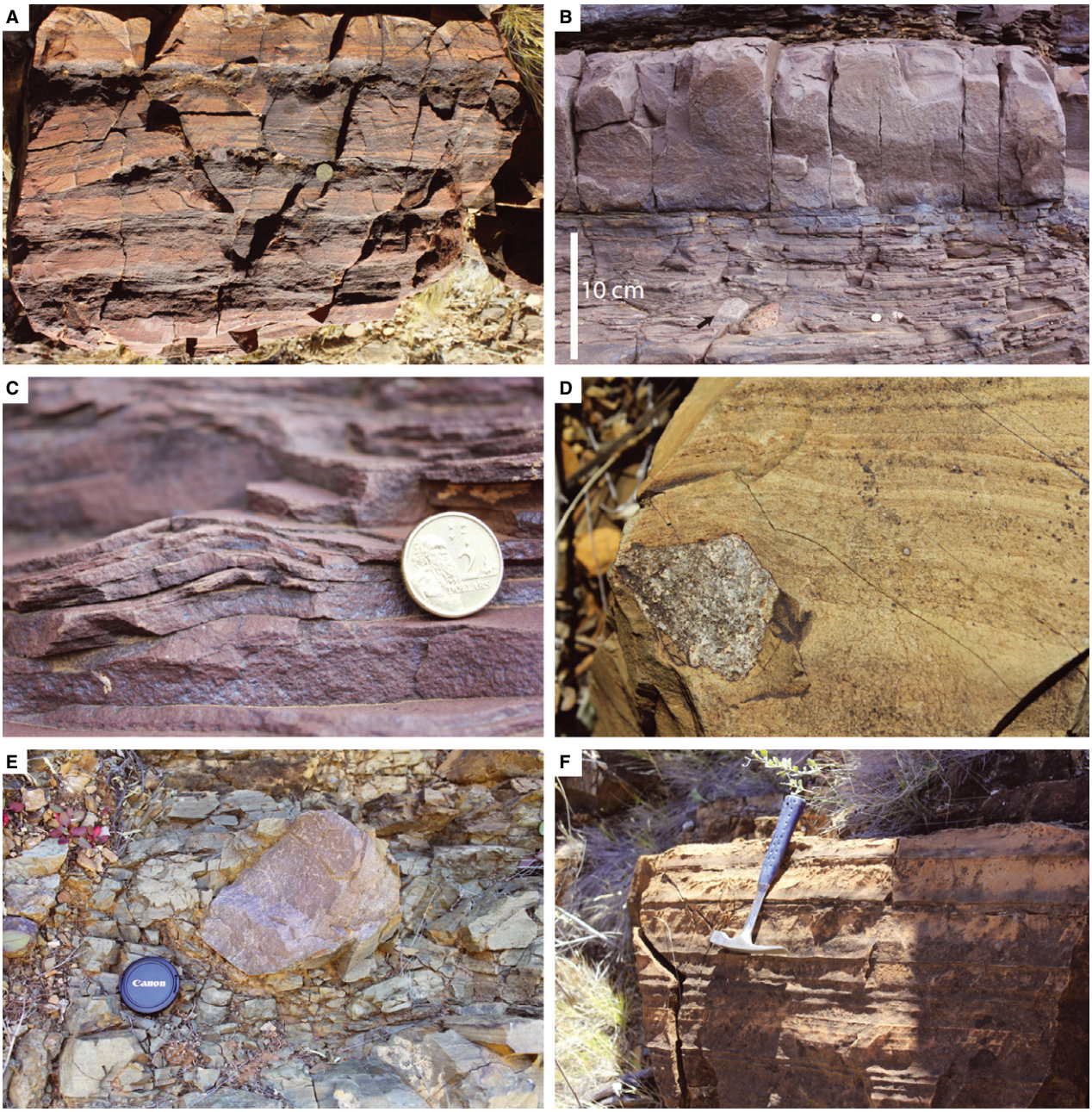

Fig. 8. Representative photographs of facies within the sheet heterolithics facies association. (A) Repetitively stacked, decimetric Bouma cycles. Note coin for scale. (B) Lonestones to the left of the coin within fine-grained, climbing ripple cross-laminated sandstone. (C) Detail of (B) showing the prograding crest (from right to left) of a climbing ripple. Note that tractive velocities predicted within the field of ripple formation (e.g. Bridge & Demicco, 2008) are insufficient to transport pebble-sized clasts. Thus, a dropstone origin is deduced. Diameter of coin for scale is 20.5 mm. (D) Lonestone with deflected laminations above the clast: possibly as a result of compaction. Field of view 7 cm. (E) Quartzite dropstone, with impact structure (truncation and piercing of shale laminae) beneath the lens cap (diameter is 58 mm). (F) Laminated dolostone (25 m, Fig. 4C). Hammer for scale is 250 mm long.

which are thus interpreted as ice-rafted debris. Furthermore, turbidity flows typically demonstrate low yield strength and cannot support clasts through buoyancy within the flow (Shanmugam, 2002). Although Lowe (1982) suggested that sand-dominated traction carpets in dense sandy turbidites were capable of periodically bouncing clasts as suspension load, these inferred processes have not been observed in turbidity currents (Talling *et al.*, 2012). The co-occurrence

of thin sandy diamictites, interpreted as the dilute distal fronts of glaciogenic debris flows, strengthens the interpretation of a glacial influence on sedimentation.

The organization of the Bouma cycles into both coarsening and fining-upward motifs at the multi-metre scale is, respectively, suggested to record the build out and abandonment of subaqueous fan lobes, in a similar manner to other glacially sourced subaqueous fan systems (Le Heron *et al.*, 2008). The delicately laminated dolostones at the top of some fining-upward cycles remain cryptic; they do not occur in finer-grained, turbidite-dominated systems of the central Flinders Ranges (e.g. Le Heron *et al.*, 2011; Busfield & Le Heron, in review), which probably indicates that the dolostones are of local significance. These dolostones are presently suggested to record chemical or biological precipitation during or following lobe abandonment, although the precise mechanisms of precipitation require further study. Their lonestone-free textures merit one further consideration, however. If subaqueous sedimentation rates of IRD were similar everywhere on the fan system at a given time, comparable deposits should form simultaneously. Given the absence of lonestones in the dolostones, intervals of IRD-free conditions might be proposed, thus suggesting that these might be associated with lower rates of deposition and therefore no floating ice.

STACKING PATTERNS

The vertical stacking motif of facies associations is an important consideration in a glacially sourced sedimentary system and may allow the dynamics of former ice sheets to be elucidated. At Stubb's Waterhole, the diamictite facies association predominates but those strata are intercalated with *ca* 5 m thick developments of the sheet heterolithics facies association. A considerably thicker example of that facies association is found interbedded with the diamictite facies association at Weetootla Gorge (23 to 75 m, Fig. 4C). Given the differences in thickness at both localities, it is proposed that the Stubb's Waterhole occurrence may represent the margins of a turbidite lobe system (e.g. Prélat *et al.*, 2010), whereas the Weetootla Gorge examples are more compatible with the core of a turbidite lobe system. Note, however, that the present data do not represent a complete traverse through the formation in either case. Interstratification of the diamictite facies association and the channel belt facies association, at the tens of metres scale at Tillite Gorge testifies to the likely synchronous co-development of turbidite channel belts and glaciogenic debris flow deposits. This interstratification implies that each sub-environment, recognized in the form of the three facies associations, co-existed during deposition of the Bolla Bollana Formation.

In the Arkaroola area, the Bolla Bollana Formation maps as a continuous stratigraphic unit around the north-eastern extremity of the Gammon Ranges. Preiss (1993, 1999, 2000), Preiss *et al.* (2011), interpret the North Flinders Basin as a region that experienced extension synchronous with glaciation by Sturtian ice sheets. Progressive thickness increases to the north are explained by the development of an en échelon half graben (Preiss *et al.*, 2011). Crustal extension, during the fragmentation of Rodinia, which accounted for the generation of substantive accommodation space, was also considered to be important by Young & Gostin (1988, 1989, 1990, 1991). However, the location of many of these faults remains unclear: the 1 : 250 000 sheet (Copley: Coats, 1973) reveals no faults specifically causing abrupt thickness changes in the Bolla Bollana Formation.

The present authors argue that the substantial thickness and sedimentary architecture of the Bolla Bollana Formation can be explained by ice-sheet dynamics alone. The diamictite facies association records glaciogenic debris flows with secondary ice rafting in the proximal part of a subaqueous basin (Fig. 9). The presence of facetted, polished and striated clasts in the Bolla Bollana Formation strongly implies direct glacial derivation; this is because cannibalized or reworked (second generation) debris flows tend to erode and smooth clast surfaces (Le Heron *et al.*, 2013). The glaciogenic debris flows probably became diluted basinward, developing into turbulent underflows, which built up a series of lobes and channel belts (i.e. channel belt facies association) on a large subaqueous fan (Fig. 9). The sheet heterolithics facies association represents lobe deposits (e.g. Prélat *et al.*, 2010) in the inter-channel part of a subaqueous fan system. These lobes were influenced by local ice rafting as a secondary sediment source (Fig. 9). Abandonment of the lobes locally resulted in some highly unusual laminated dolostone deposits; these superficially resemble 'cap dolostone' deposits (e.g. Rose & Maloof, 2010). As

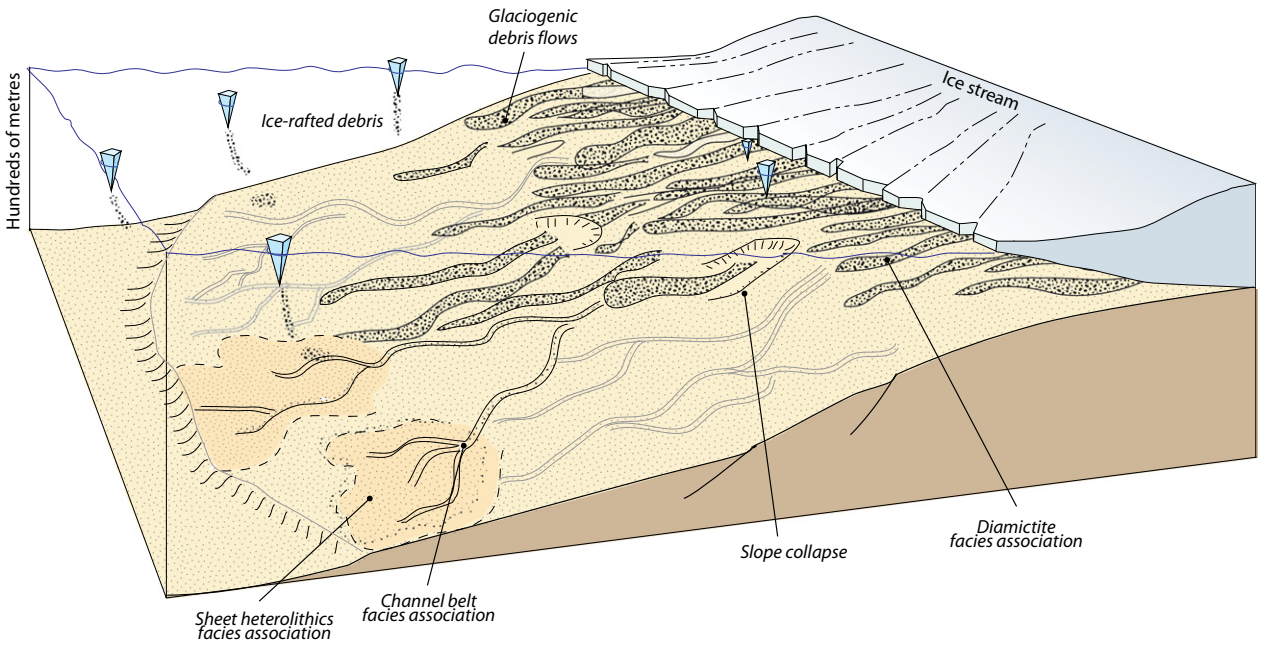

Fig. 9. Simple depositional model for the Bolla Bollana Formation. The interpretation here is a glaciomarine basin, a general setting consistent with previous work (e.g. Coats, 1981; Young & Gostin, 1989, 1991). Glaciogenic debris flows fed the basin, evolving into turbidites down depositional dip. Channel belts and inter-channel areas recording slightly finer-grained turbidites are recognized. Phases of fan-lobe build out and abandonment are recognized, with these processes probably a result of autocyclic switching of channel belts and sediment supply rather than basin-scale ice dynamics. The scale of the sedimentary system, and clear evidence for a strong glacial influence on sedimentation in all facies associations, suggest that the Bolla Bollana deposit is a trough mouth fan deposit, with huge volumes of glaciogenic debris supplied to a subaqueous setting. This is the first such interpretation from the Neoproterozoic record.

noted earlier, given their probable stratigraphic context as lobe abandonment facies, it is unlikely that they have any wider significance. The lack of evidence for IRD in these specific facies, – a texture which might be expected to appear more prominently once sediment supply is arrested – is also puzzling.

A NEOPROTEROZOIC TROUGH-MOUTH FAN?

It is suggested that the Bolla Bollana Formation is a trough-mouth fan (TMF) (Fig. 9) deposited seaward of a comparatively small palaeo-ice stream. This interpretation is fully consistent with: (i) clear evidence for glacial processes in every facies association of the Bolla Bollana Formation; (ii) the substantial thickness of the succession which compares closely to stacked mass flow deposits of the Bear Island Fan (Taylor *et al.*, 2002; Ó Cofaigh *et al.*, 2003); and (iii) the stratigraphic motif and nature of the facies associations preserved.

Evidence for glaciation throughout the Bolla Bollana Formation is pervasive and includes dropstone textures (in turbidites, as well as hemipelagic muds), together with facetted, polished and striated clasts throughout the succession. Boreholes sunk in the Uummannaq Fan (western Greenland) illustrate 300 m thick successions of diamicton that are sharply overlain by mud (Ó Cofaigh *et al.*, 2013). These successions are closely comparable to stacked examples of the diamictite facies association in Tillite Gorge. Intercalated debrites, turbidites and ice-rafted debris commonly occur together in depositional models of Pleistocene TMFs (Ó Cofaigh *et al.*, 2013).

In both the northern and southern hemispheres, TMFs were deposited during Pleistocene glaciations and consist of thick accumulations of glaciogenic detritus (Escutia *et al.*, 2000; Taylor *et al.*, 2002). In this process, fast-flowing ice streams excavate the subglacial substrate and deposit diamictite at the ice front, perched landward of the slope break. In Pleistocene examples, rapid sedimentation of water sat-

urated tills led to unstable slope angles and hence intermittent failure (Dowdeswell *et al.*, 2002). This failure, in turn, led to the generation of GDFs derived from collapsing tills (Taylor *et al.*, 2002). In the southern hemisphere, the Wilkes Land continental margin was fed by stacked GDFs, which evolved downslope into turbidites, building up a multi-kilometre thick pile of channelized proglacial detritus (Escutia *et al.*, 2000).

Regional mapping (Coats, 1973) shows that the Bolla Bollana Formation crops out over at least 1800 km^2. Assuming a conservative thickness of 1 km in the Arkaroola district, the Bolla Bollana Formation represents *ca* 1800 km^3 of glaciogenic sediment: impressive, yet substantially less volumetric than the modern Bear Island Fan (*ca* 340 000 km^3) (Dowdeswell *et al.*, 2002; and references therein). Part of the reason for this comparatively small volume may lie in the partitioning of the basin by syn-depositional faults (Preiss *et al.*, 2011). From both stratigraphic and facies perspectives, there is good reason to view the North Flinders Basin as a sub-basin disconnected from the central Flinders Ranges further to the south (Preiss *et al.*, 2011). Differences between Pleistocene TMF models and the interpretation herein (Fig. 9) include the absence of bioturbation and a lower volume of mud in the Bolla Bollana TMF deposit (cf. Ó Cofaigh *et al.*, 2002, 2003, 2013). In subaqueous fans, an increase in mud content improves the run-out efficiency of turbidites and increases fan size (Reading & Richards, 1994). Another obvious difference is the presence of dolostones in the Bolla Bollana Formation: such dolostones are absent in Pleistocene TMFs. They are, however, almost ubiquitous in the Cryogenian record, typically occurring immediately above the diamictite successions as cap carbonates (e.g. Shields, 2005).

The gentle regional dip of the Bolla Bollana Formation (Fig. 5A) precludes mapping of individual debrite megabeds, yet Quaternary analogues may allow some insight into possible maximum lateral dimensions. Debrites on the Bear Island Fan are elongate lobes with individual run-out distances of >40 km (Laberg & Vorren, 2000; Ó Cofaigh *et al.*, 2003); they commence at *ca* 1 km below sea-level, extending to *ca* 2·5 km depth. The up-dip termination of the debrite lobes approximates the palaeo-ice margin (Fig. 9). In addition to the generation of GDFs, the accumulation of thick piles of detritus on TMFs lends them prone to gravitational collapse (Dowdeswell *et al.*, 2002). Thus, many of the extensional faults and graben structures in the North Flinders Basin may represent seaward partial collapse of the fan.

Young & Gostin (1989) provided detailed descriptions and interpretations of comparable successions further north, in the Yudnamutana homestead and surrounds. There, a subaqueous fan system, dominated by boulder-bearing debrites with subordinate turbidites, was envisaged (Young & Gostin, 1989). This interpretation is fully compatible with that of the present authors and underscores that an identical range of sub-environments are recognized around the Bolla Bollana outcrop belt (Fig. 9). It is clear that the Bolla Bollana Formation contains excellent evidence for glacial sedimentary processes, reinforcing the original work of Mawson (1941, 1949) and making it difficult to argue for a rift-source alone, as has been suggested for similar Neoproterozoic diamictite successions (e.g. Eyles & Januszczak, 2004).

The connection between the Bolla Bollana depocentre and other sub-basins in the central Flinders Ranges is obscure. Rifting is an attractive mechanism to account for the different stratigraphic units preserved in the North Flinders Basin and depocentres further south, such as Baratta and Holowilena (Preiss, 2000). It should be stressed, however, that not all sub-basins in the Flinders Ranges preserve clear evidence for rifting. The Holowilena succession, for example, contains delicately interbedded siltstones, diamictites, sandstones and IRD-bearing shale (Le Heron, 2012; Busfield & Le Heron, in review). Internally, that succession contains disconformities and not angular relations between bedsets (Le Heron, 2012) which might be expected where undeformed sediments onlap rotated hangingwall strata. Nonetheless, correlative successions at Oladdie Creek and Hillpara Creek, in the central Flinders Ranges, reveal dramatic thickness changes along strike. These changes testify to an irregular underlying palaeotopography, which is probably attributed to the combined influence of pre-depositional and early syn-depositional rift activity and subglacial downcutting (Busfield & Le Heron, in review).

The Bolla Bollana Formation provides a unique window into the sedimentary architecture of a TMF. The interpretation of a TMF is doubly significant. Firstly, the authors are not aware of any previously described TMFs of pre-Pleistocene age, and thus the first documentation is provided herein. Secondly, the Bolla Bollana is the only known outcrop example thus far described of

such a fan. It is probably the case that the generally large scale of these fans (Ó Cofaigh *et al.*, 2013) has precluded their outcrop-scale interpretation in ancient strata. Whilst volumetrically less significant in the fan systems than GDFs, the Bolla Bollana succession also reveals the common occurrence of turbidite intervals, amplifying the importance of turbidity currents in TMF models (Escutia *et al.*, 2000). The occurrence of correlative turbidite and debrite-dominated successions is also well-reported from subsurface boreholes elsewhere in southern and central Australia (for example, Blinman 2 borehole, central Flinders Ranges; Nicholson 2 borehole, *ca* 500 km northwest of Arkaroola; Vines 1 borehole, Officer Basin) (Eyles *et al.*, 2007). A clear, glacial influence is reported from those sections on account of striated and outsized clasts in laminated facies (Eyles *et al.*, 2007), although it remains unclear how these underflow-dominated successions relate laterally to one another. In the light of the interpretations herein, it is possible that these deposits represent an amalgam of overlapping TMFs, line-sourced detritus, or somewhat more disconnected fan systems.

In the context of a Neoproterozoic snowball Earth model, Hoffman (2005) argued that palaeoice streaming – which Hoffman inferred on the basis of irregular topography within the Ghaub glacial succession of Namibia, and the occurrence of a large wedge of grainstone sediment – was "not incompatible with a frozen ocean". Etienne *et al.* (2007) and Allen & Etienne (2008), meanwhile, pointed out that the highly dynamic nature of tidewater ice sheets directly challenged this view. In particular, the issue of resupply of snow in the accumulation zone of ablating ice sheets – given the presumed arrested hydrological cycle – remains problematic.

Some 120 km to the south of Arkaroola, exceptionally exposed, age equivalent successions at Holowilena, Oladdie and Hillpara creeks, in the central Flinders Ranges (Le Heron *et al.*, 2011; Busfield & Le Heron, in review) reveal a highly comparable stratigraphic subdivision in a series of tectonically partitioned basins. These sections identify a clear non-glacial interval within the Wilyerpa Formation, which yields spectacularly preserved hummocky cross-strata, indicative of sea-ice free conditions (Le Heron *et al.*, 2011), followed by a glacial re-advance. Young & Gostin (1991) likewise identified a second major re-advance in the Sturtian, represented by accumulation of the Bolla Bollana Formation. These considerations suggest that the Bolla Bollana Formation may correlate with the re-advance succession in the central and southern Flinders Ranges and, if so, suggest deposition of the TMF at Arkaroola in seas which were at least periodically unfrozen.

CONCLUSIONS

The Bolla Bollana Formation is a spectacularly exposed glaciogenic succession of Sturtian age in the Arkaroola district. This formation was first investigated by Mawson (1941, 1949) but, subsequently, little work has been undertaken at the Tillite Gorge, Stubb's Waterhole or Weetootla Gorge locations. Detailed sedimentary logging at these locations, therefore, allows a detailed sedimentary model to be developed as follows:

1 Three facies associations are recognized in the Bolla Bollana Formation. These are a diamictite facies association (glaciogenic debris flows with subordinate ice-rafted debris), a channel belt facies association (channelized turbidites with subordinate ice-rafted debris) and a sheet heterolithics facies association (non-channelized turbidites and subordinate ice-rafted debris). A strong glacial influence on sedimentation is inferred, reinforcing previous interpretations of Young & Gostin (1991). A rift-related source for the diamictites is rejected.

2 A depositional model based on detailed observations and interpretations from all three facies associations proposes that the Bolla Bollana Formation was deposited as a trough-mouth fan (TMF), seaward of the terminus of a small ice stream. Rapid ice flux promoted high-erosion rates and sediment delivery. At the ice margin, glaciogenic debris flows deposited multi-storey stacks of diamictite, many of which were deposited as megabeds. Slope failure and/or dilution of these flows basinward ignited turbidites, which cut channel geometries onto the proximal and medial parts of the fan. Non-channelized turbidites demonstrate well-organized multi-metre coarsening and fining-upward motifs, interpreted to record build out and abandonment of fan lobes. Laminated dolostones are an unusual fan-lobe abandonment facies and bear superficial resemblance to post-glacial 'cap dolostones' elsewhere.

3 Previous models of tectonic compartmentalization resulting from rifting post-750 Ma (e.g. Young & Gostin, 1991; Preiss, 2000; Eyles & Januszczak, 2004) may help in explaining dra-

matic regional differences in facies and internal Sturtian stratigraphy. In the Bolla Bollana Formation, however, it is suggested that a tectonic mechanism is not required by reference to Cenozoic trough-mouth fan systems where substantive diamictite accumulations occur.

ACKNOWLEDGEMENTS

The authors wish to thank Doug Sprigg for sharing with us his knowledge of the pioneer's experiences in the Arkaroola area, for permission to work in the area and general helpfulness. We are very grateful to two anonymous referees whose comments significantly improved the manuscript. We also want to thank Professor Nick Eyles for additional comments which helped improve the final version of the paper, and Professor Stephen Rice, the handling editor, for assistance and carefully considered input. This work was funded by a National Geographic Explorer Fund grant to DPLeH.

REFERENCES

Allen, J.R.L. (1984) *Sedimentary Structures: Their Character and Physical Basis, Volumes I and II*. Elsevier, Amsterdam.

Allen, P.A. and **Etienne, J.L.** (2008) Sedimentary challenge to snowball earth. *Nature Geosci.*, **1**, 817–825.

Alpak, F., **Barton, M.D.** and **Naruk, S.J.** (2013) The impact of fine-scale turbidite channel architecture on deep-water reservoir performance. *AAPG Bull.*, **97**, 251–284.

Arnaud, E. (2012) The paleoclimatic significance of deformation structures in Neoproterozoic successions. *Sed. Geol.*, **243–244**, 33–56.

Benn, D.I. & **Evans, D.J.A.** (2010). *Glaciers and Glaciation*. Hodder Education London, 802 p.

Bouma, A.H. (1963) Sedimentary facies model of turbidites. *AAPG Bull.*, **47**, 351.

Bridge, J.S. and **Demicco, R.V.** (2008) *Earth Surface Processes, Landforms and Sediment Deposits*. Cambridge University Press, UK, 815 p.

Busfield, M.E. and **Le Heron, D.P**. (2013) Glacitectonic deformation in the Chuos Formation of northern Namibia: implications for Neoproterozoic ice dynamics. *Proc. Geol. Assoc.* **124**, 778–789.

Busfield, M.E. and **Le Heron, D.P**. (in review) Sequencing the Sturtian icehouse: dynamic ice behaviour in South Australia. *J. Geol. Soc. Lond.*,

Camacho, H., **Busby, C.J.** and **Kneller, B.** (2002) A new depositional model for the classical turbidite locality at San Clemente State Beach. *California. AAPG Bull.*, **86**, 1543–1560.

Coats, R.P. (1973) Copley, South Australia. Explanatory Notes. 1:250,000 Geological Series, Sheet SH/54-9. Geological Survey of South Australia, 38 pp.

Coats, R.P. (1981) Late Proterozoic (Adelaidian) tillites of the Adelaide Geosyncline. In: *Earth's Pre-Pleistocene Glacial Record* (Eds M.J. Hambrey and W.B. Harland), pp. 537–548. Cambridge University Press, Cambridge.

Collinson, J.D. and **Thompson, D.B.** (1987) *Sedimentary Structures*, 2nd edn. Chapman and Hall, London.

Corkeron, M.L. (2007) 'Cap carbonates' and Neoproterozoic glacigenic successions from the Kimberley region, northwest Australia. *Sedimentology*, **54**, 871–903.

Daily, B., **Gostin, V.A.** and **Nelson, C.A.** (1973) Tectonic origin for an assumed glacial pavement of Late Proterozoic age, South Australia. *J. Geol. Soc. Aust.*, **20**, 75–78.

Dowdeswell, J.A., **O'Cofaigh, C.**, **Taylor, J.**, **Kenyon, N.H.**, **Mienert, J.** and **Wilken, M**. (2002) On the architecture of high-latitude continental margins: the influence of ice-sheet and sea-ice processes in the Polar North Atlantic. In: *Glacier-Influenced Sedimentation on High-Latitude Continental Margins* (Eds J.A. Dowdeswell and C. O'Cofaigh), *Geol. Soc. London Spec. Publ.*, **203**, 33–54.

Escutia, C., **Eittreim, S.L.**, **Cooper, A.K.** and **Nelson, C.H.** (2000) Morphology and acoustic character of the Antarctic Wilkes Land turbidite systems: icesheet-sourced versus river-sourced fans. *J. Sed. Res.*, **70**, 84–93.

Etienne, J.L., **Allen, P.A.**, **Rieu, R.** and **Le Guerroue, E**. (2007) Neoproterozoic glaciated basins: a critical review of the Snowball Earth hypothesis by comparison with Phanerozoic glaciations. In: *Glacial Processes and Products* (Eds M.J. Hambrey, P. Christoffersen, N.F. Glasser and B. Hubbard), *Int. Assoc. Sedimentol. Spec. Publ.*, **39**, 436 pp.

Eyles, N. and **Januszczak, N.** (2004) 'Zipper-rift': a tectonic model for Neoproterozoic glaciations during the breakup of Rodinia after 750 Ma. *Earth Sci. Rev.*, **65**, 1–73.

Eyles, N. and **Januszczak, N.** (2007) Syntectonic subaqueous mass flows of the Neoproterozoic Otavi Group, Namibia: where is the evidence of global glaciation? *Basin Res.*, **19**, 179–198.

Eyles, C.H., **Eyles, N.** and **Grey, K.** (2007) Palaeoclimate implications from deep drilling of Neoproterozoic strata in the Officer Basin and Adelaide Rift Complex of Australia; a marine record of wet-based glaciers. *Palaeogeogr. Palaeoclimatol. Palaeoecol.*, **248**, 291–312.

Fairchild, I. and **Kennedy, M.J.** (2007) Neoproterozoic glaciation in the Earth System. *J. Geol. Soc. London*, **164**, 895–921.

Harrison, P. and **Maltman, A.J.** (2003) Numerical modelling of reverse-density structures in soft non-Newtonian sediments. In: *Subsurface Sediment Mobilization* (Eds P. van Rensbergen, R.R. Hillis, A.J. Maltman and C.K. Morley), *Geol. Soc. Spec. Publ.*, **216**, 35–50.

Hart, J.K. and **Roberts, D.H.** (1994) Criteria to distinguish between subglacial glaciotectonic and glaciomarine sedimentation, I. Deformation styles and sedimentology. *Sed. Geol.*, **91**, 191–213.

Hoffman, P.F. (2005) 28th DeBeers Alex Du Toit Memorial Lecture, 2004. On Cryogenian (Neoproterozoic) ice-sheet dynamics and the limitations of the glacial sedimentary record. *S. Afr. J. Geol.*, **108**, 557–576.

Hoffman, P.F. and **Schrag, D.P.** (2002) The snowball earth hypothesis: testing the limits of global change. *Terra Nova*, **14**, 129–155.

Laberg, J.S. and **Vorren, T.O.** (2000) Flow behaviour of the submarine glacigenic debris flows on the Bear Island Trough Mouth Fan, western Barents Sea. *Sedimentology*, **47**, 1105–1117.

Le Heron, D.P. (2012) The Cryogenian record of glaciation and deglaciation in South Australia. *Sed. Geol.*, **243–244**, 57–69.

Le Heron, D.P., **Khoukhi, Y.**, **Paris, F.**, **Ghienne, J.-F.** and **Hérissé, Le** (2008) Black shale, grey shale, fossils and glaciers: anatomy of the Upper Ordovician–Silurian succession in the Tazzeka Massif of eastern Morocco. *Gondwana Res.*, **14**, 483–496.

Le Heron, D.P., **Cox, G.M.**, **Trundley, A.E.** and **Collins, A.** (2011) Sea-ice free conditions during the early Cryogenian (Sturt) glaciation, South Australia. *Geology*, **39**, 31–34.

Le Heron, D.P., **Busfield, M.E.** and **Kamona, A.F.** (2013) Interglacial on snowball Earth? Dynamic ice behaviour revealed in the Chuos Formation, Namibia. *Sedimentology*, **60**, 411–427.

Lowe, D.R. (1982) Sediment gravity flows: II. Depositional models with special reference to the deposits of high-density turbidity currents. *J. Sed. Petrol.*, **52**, 279–297.

Macdonald, F.A., **Schmitz, M.D.**, **Crowley, J.L.**, **Roots, C.F.**, **Jones, D.S.**, **Maloof, A.C.**, **Strauss, J.V.**, **Cohen, P.A.**, **Johnson, D.T.** and **Schrag, D.P.** (2010) Calibrating the Cryogenian. *Science*, **327**, 1241–1243.

Maltman, A. (1994) *The Geological Deformation of Sediments*. Chapman and Hall, Cambridge, 384 pp.

Marjanac, T. (1996) Deposition of megabeds (megaturbidites) and sea-level change in a proximal part of the Eocene-Miocene flysch of central Dalmatia (Croatia). *Geology*, **24**, 543–546.

Mawson, D. (1941) Middle Proterozoic sediments in the neighbourhood of Copley. *Trans. Roy. Soc. S. Aust.*, **65**, 304–311.

Mawson, D. (1949) Sturt tillite of Mount Jacob and Mount Warren Hastings, north Flinders Ranges. *Trans. Roy. Soc. S. Aust.*, **72**, 244–251.

Moncrieff, A.C.M. (1989) Classification of poorly-sorted sedimentary rocks. *Sed. Geol.*, **65**, 191–194.

Mutti, E., **Tinterri, R.**, **Remacha, E.**, **Mavilla, N.**, **Angella, S.** and **Fava, L.** (1999) An introduction to the analysis of ancient turbidite basins from an outcrop perspective. American Association of Petroleum Geologists, Continuing Education Course Notes Series, 39. Oklahoma, USA.

Ó Cofaigh, C., **Taylor, J.**, **Dowdeswell, J.A.**, **Rosell-Melé, A.**, **Kenyon, N.H.**, **Evams, J.** and **Mienert, J.** (2002) Sediment reworking on high-latitude continental margins and its implications for palaeoceanographic studies: insights from the Norwegian-Greenland Sea. In: *Glacier-Influenced Sedimentation on High-Latitude Continental Margins* (Eds J.A. Dowdeswell and C. Ó Cofaigh), *Geol. Soc. London Spec. Publ.*, **203**, 325–348.

Ó Cofaigh, C, **Taylor, J**, **Dowdeswell, J.A.** and **Pudsey, C.J.** (2003) Palaeo-ice streams, trough mouth fans and high-latitude continental slope sedimentation. *Boreas*, **32**, 37–55.

Ó Cofaigh, C., **Andrews, J.T.**, **Jennings, A.E.**, **Dowdeswell, J.A.**, **Hogan, K.A.**, **Kilfeather, A.A.** and **Sheldon, C.** (2013) Glacimarine lithofacies, provenance and depositional processes on a West Greenland trough-mouth fan. *J Quatern. Sci.*, **28**, 13–26.

Petit, J.-P. and **Laville, E.** (1987) Morphology and microstructures of hydroplastic slickensides in sandstone. In: *Deformation of Sediments and Sedimentary Rocks* (Eds M.E. Jones and R.M.F. Preston), *Geol. Soc. London Spec. Publ.*, **29**, 107–121.

Preiss, W.V. (1987) A synthesis of palaeogeographic evolution of the Adelaide Geosyncline. In: *The Adelaide Geosyncline. Late Proterozoic Stratigraphy, Sedimentation, Palaeontology and Tectonics* (Ed. W.V. Preiss), *Geol. Surv. S. Aust. Bull.*, **53**, 315–409.

Preiss, W.V. (1993) Neoproterozoic. In: *The Geology of South Australia, Vol. 1, The Precambrian: South Australia* (Eds J.F. Drexel, W.V. Preiss and A.J. Parker), *Geol. Surv. Bull.*, **54**, 170–224.

Preiss, W.V. (1999) *Parachilna Sheet SH54-13. 1:250 000 scale Geological Map and Explanatory Notes, Primary Industries and Resources South Australia*, 2nd edn, 52 p. PIRSA (Primary Industry and Resources South Australia), Adelaide, South Australia.

Preiss, W.V. (2000) The Adelaide Geosyncline of South Australia and its significance in Neoproterozoic continental reconstruction. *Precambrian Res.*, **100**, 21–63.

Preiss, W.V., **Gostin, V.A.**, **McKirdy, D.M.**, **Ashley, P.M.**, **Williams, G.E.** and **Schmidt, P.W.** (2011) The glacial succession of Sturtian age in South Australia: the Yudnamutana Subgroup. *Geol. Soc. London Mem.*, **36**, 701–712. doi:10.1144/M36.69.

Prélat, A., **Covault, J.A.**, **Hodgson, D.M.**, **Fildani, A.** and **Flint, S.S.** (2010) Intrinsic controls on the range of volumes, morphologies, and dimensions of submarine lobes. *Sed. Geol.*, **232**, 66–76. doi:10.1016/j.sedgeo.2010.09.010.

Reading, H.G. and **Richards, M.** (1994) Turbidite systems in deep-water basin margins classified by grain size and feeder system. *AAPG Bull.*, **78**, 792–822.

Rose, C.V. and **Maloof, A.C.** (2010) Testing models for post-glacial 'cap dolostone' deposition: Nuccaleena Formation, South Australia. *Earth Planet. Sci. Lett.*, **296**, 165–180.

Schermerhorn, L.J.G. (1974) Late Precambrian mixtites: glacial and/or nonglacial. *Am. J. Sci.*, **274**, 673–824.

Schermerhorn, L.J.G. and **Stanton, W.I.** (1963) Tilloids in the West Congo Belt. *Q. J. Geol. Soc. London*, **119**, 201–241.

Shanmugam, G. (2002) Ten turbidite myths. *Earth Sci. Rev.*, **58**, 311–341.

Shanmugam, G., **Bloch, R.B.**, **Mitchell, S.M.**, **Beamish, G.W.J.**, **Hodgkinson, R.J.**, **Damuth, J.E.**, **Staume, T.**, **Syvertsen, S.E.** and **Shields, K.E.** (1995) Basin-floor fans in the North Sea; sequence stratigraphic models vs. sedimentary facies. *AAPG Bull.*, **79**, 477–512.

Shields, G.A. (2005) Neoproterozoic cap carbonates: a critical appraisal of existing models and the plumeworld hypothesis. *Terra Nova*, **17**, 299–310.

Talling, P.J., **Masson, D.G.**, **Sumner, E.J.** and **Malgesini, G.** (2012) Subaqueous sediment density flows: depositional processes and deposit types. *Sedimentology*, **59**, 1937–2003.

Taylor, J., **Dowdeswell, J.A.**, **Kenyon, N.H.** and **O'Cofaigh, C.** (2002) Late quaternary architecture of trough-mouth fans: debris flows and suspended sediments on the Norwegian margin. In: *Glacier-Influenced Sedimentation on High-Latitude Continental Margins* (Eds J.A. Dowdeswell and C. O'Cofaigh), *Geol. Soc. London Spec. Publ.*, **203**, 55–71.

Thomson, B.P., **Coats, R.P.**, **Mirams, R.C.**, **Forbes, B.G.**, **Dalgarno, C.R.** and **Johnson, J.E.** (1964) Precambrian rock groups in the Adelaide Geosyncline: a new subdivision. *Q. Geol. Notes Geol. Surv. S. Aust.*, **9**, 1–19.

Uhlein, A., **Alvarenga, C.J.S.**, **Dardenne, M.A.** and **Trompette, R.R.** (2011) The glaciogenic Jequitai Formation, southeastern Brazil. In: The Geological Record of Neoproterozoic Glaciations (Eds E. Arnaud, G.P. Halverson, G. Shields-Zhou). *Geol. Soc. Mem.*, **36**, 541–546.

Young, G.M. and **Gostin, V.A.** (1988) Stratigraphy and Sedimentology of Sturtian glaciogenic deposits in the western part of the North Flinders Basin, South Australia. *Precambrian Res.*, **39**, 151–170.

Young, G.M. and **Gostin, V.A.** (1989) An exceptionally thick upper Proterozoic (Sturtian) glacial succession in the Mount Painter area, South Australia. *Geol. Soc. Am. Bull.*, **101**, 834–845.

Young, G.M. and **Gostin, V.A.** (1990) Sturtian glacial deposition in the vicinity of the Yankaninna Anticline, North Flinders Basin, South Australia. *Aust. J. Earth Sci.*, **37**, 447–458.

Young, G.M. and **Gostin, V.A.** (1991) Late Proterozoic (Sturtian) succession of the North Flinders Basin, South Australia; an example of temperate glaciation in an active rift setting. In: *Glacial Marine Sedimentation: Palaeoclimatic Significance* (EdsJ.R. Anderson and G.M. Ashley), *Geol. Soc. Am. Spec. Pap.*, **261**, 207–222.

Manuscript received 7 May 2013; revision 23 July 2013; revision accepted 27 September 2013

4.3. Glacial sequence stratigraphy, central Flinders Ranges

Sequencing the Sturtian icehouse: dynamic ice behaviour in South Australia

Busfield, M.E. and Le Heron, D.P.

Journal of the Geological Society 2014, v. 171, 443-456.
doi:10.1144/jgs2013-067

Statement of contribution

- ***Data collection***
  - Busfield logged the Holowilena Creek section (Fig. 4, Log A), and both Busfield and Le Heron logged the Oladdie Creek and Hillpara Creek sections (Fig. 4, Logs B & C).
  - Numerous diamictite and ironstone horizons were sampled for micro-scale sedimentology by Busfield, who later analysed and interpreted the thin sections.
- ***Manuscript text***
  - Busfield authored the first draft of the manuscript, including developing and interpreting the lithofacies scheme, the evidence favouring varying palaeotopography across the studied sections, and the depositional model.
  - Le Heron reviewed the first draft and suggested exploring sequence stratigraphic schemes. Busfield developed the sequence stratigraphic scheme utilised herein, and modified the manuscript accordingly.
- ***Figures***
  - Busfield illustrated all figures and supplied all photographs used within the manuscript.

Journal of the Geological Society, London, Vol. **171**, 2014, pp. 443–456. http://dx.doi.org/10.1144/jgs2013-067
Published *Online First* on January 30, 2014

Sequencing the Sturtian icehouse: dynamic ice behaviour in South Australia

M. E. BUSFIELD* & D. P. LE HERON
Department of Earth Sciences, Royal Holloway, University of London, Egham TW20 0EX, UK
**Corresponding author (email: Marie.Busfield.2011@live.rhul.ac.uk)*

Abstract: The Cryogenian record of South Australia includes the type region of the Sturtian glaciation, the oldest of three pan-global icehouse intervals during the Neoproterozoic. Data are presented from previously little described sections at Holowilena Creek, Oladdie Creek and Hillpara Creek in the central and southern Flinders Ranges, where five facies associations are recognized. These are (1) diamictite and conglomerate, (2) interbedded heterolithic deposits, (3) hummocky cross-stratified sandstone, (4) lonestone-bearing siltstone, and (5) ferruginous siltstone and sandstone. The succession reveals significant lateral and vertical facies variation, which is linked to a complex inherited palaeotopography and distance from the sediment source. Repeated stratigraphic occurrences of striated clasts and abundant ice-rafted debris strongly support recurrent glacial influence on sedimentation. The intercalation of gravitationally reworked diamictites, dropstone-bearing siltstone and dropstone-free siltstone testifies to dynamic sedimentation within a periodically glacially influenced subaqueous environment. Sequence stratigraphic analysis identifies four glacial advance systems tracts, separated by three glacial retreat systems tracts, wherein hummocky cross-stratified sandstones attest to open water conditions. These findings support dynamic ice sheet behaviour in South Australia, and provide clear evidence for repeated intra-Sturtian ice sheet recession.

Two Neoproterozoic icehouse intervals have long been recognized in South Australia (Mawson & Sprigg 1950); namely, the older Sturtian and younger Marinoan glaciations, so named after the Sturt Gorge and Marino Rocks of Adelaide's outer suburbs (Preiss *et al*. 1998). The recognition of broadly age-equivalent deposits worldwide contributed to the development of the snowball Earth hypothesis (Hoffman *et al*. 1998; Hoffman & Schrag 2002), wherein two distinct episodes of severe pan-global glaciation allowed ice sheets to extend to low palaeolatitudes, resulting in a suppressed hydrological cycle. Recent studies, however, support a considerably more dynamic cryosphere, with fluctuating ice margins, open water areas, and abundant evidence of hydrological activity (e.g. Etienne *et al*. 2007; Arnaud *et al*. 2011, and references therein). Moreover, new age constraints, and their likely error bars, cast doubt on the pan-global synchronicity of these glacial events (e.g. Allen & Etienne 2008; Condon & Bowring 2011), and hence their two-fold subdivision as 'Sturtian' or 'Marinoan'. This has a significant bearing on the Neoproterozoic glacial deposits of South Australia, widely considered as the type area of the Sturtian icehouse period (Hoffman & Schrag 2002).

The Adelaide Fold Belt of South Australia (Figs 1 and 2) exposes an extremely thick succession of diamictite, sandstone and siltstone, thought to have accumulated during the Sturtian glaciation. The glacial affinity of these sediments was first proposed by Howchin (1901), who argued in favour of glaciomarine deposition (Howchin 1908), although correlative sections were subsequently interpreted as terrestrial glacial deposits by Mawson (1941, 1949). Detailed examination of sections in the northern Flinders Ranges and Mount Painter area by Link & Gostin (1981) and Young & Gostin (1988, 1989, 1990, 1991) heralded a return to the glaciomarine hypothesis. The latter studies identified a four-fold stratigraphic subdivision, consisting of two principal diamictite units, each overlain by a succession of siltstones and sandstones, interpreted to record two glacial cycles within the Sturtian interval. The thickness of studied sections varies considerably across the region from a few hundred metres to a purported 6000 m in the Yudnamutana Trough (Fig. 2), attributed to either the development of subglacial palaeovalleys or active extensional tectonics, or a combination of these (Young & Gostin 1990, 1991; Preiss 2000).

Comparatively few detailed sedimentological studies have been conducted on the Sturtian deposits of the central and southern Flinders Ranges. Regional mapping identifies a major fault-bound depocentre in the Barratta Trough (Fig. 2), where Sturtian sediments attain an estimated thickness of 4000 m (Preiss 1999, and references therein), thinning to a few hundred metres in adjacent shelf areas (Preiss *et al*. 1993). Recent work by Le Heron *et al*. (2011*a*,*b*) and Le Heron (2012) at Holowilena Creek, in the central Flinders Ranges, records a thick (>800 m) succession of heterogeneous glacigenic strata, with abundant evidence of striated erratic clasts and ice-rafted debris (IRD). Significantly, the occurrence of dropstone-free, hummocky cross-stratified sediments punctuating the succession is interpreted as an interglacial sequence during the Sturtian interval, pointing to major ice sheet fluctuation.

This paper will build upon earlier work by Le Heron *et al*. (2011*a*,*b*) and Le Heron (2012) at Holowilena Creek, and present high-resolution datasets for correlative sections at Oladdie Creek and Hillpara Creek, approximately 60 km further south and SE (Fig. 1), previously described only at the reconnaissance level by Binks (1968). These sections allow the facies variability of ice-proximal to more ice-distal settings to be examined, and the influence of pre-existing topographic relief to be tested. A new sedimentary model is presented, which frames the development of the diamictite-bearing successions in a glacial sequence stratigraphic context.

Study area and stratigraphy

The studied sedimentary successions belong to the mid-Cryogenian Yudnamutana Subgroup, at the base of the Umberatana Group (Fig. 3). In the Adelaide Fold Belt, these sediments rest with angular unconformity upon sandstones and siltstones of the underlying Burra Group (Coats & Preiss 1987). Stratigraphic nomenclature is highly variable across the region, but typically includes a basal diamictite-dominated unit; namely, the Bolla Bollana Formation to the north, the Pualco Tillite in the central regions, the Appila Tillite

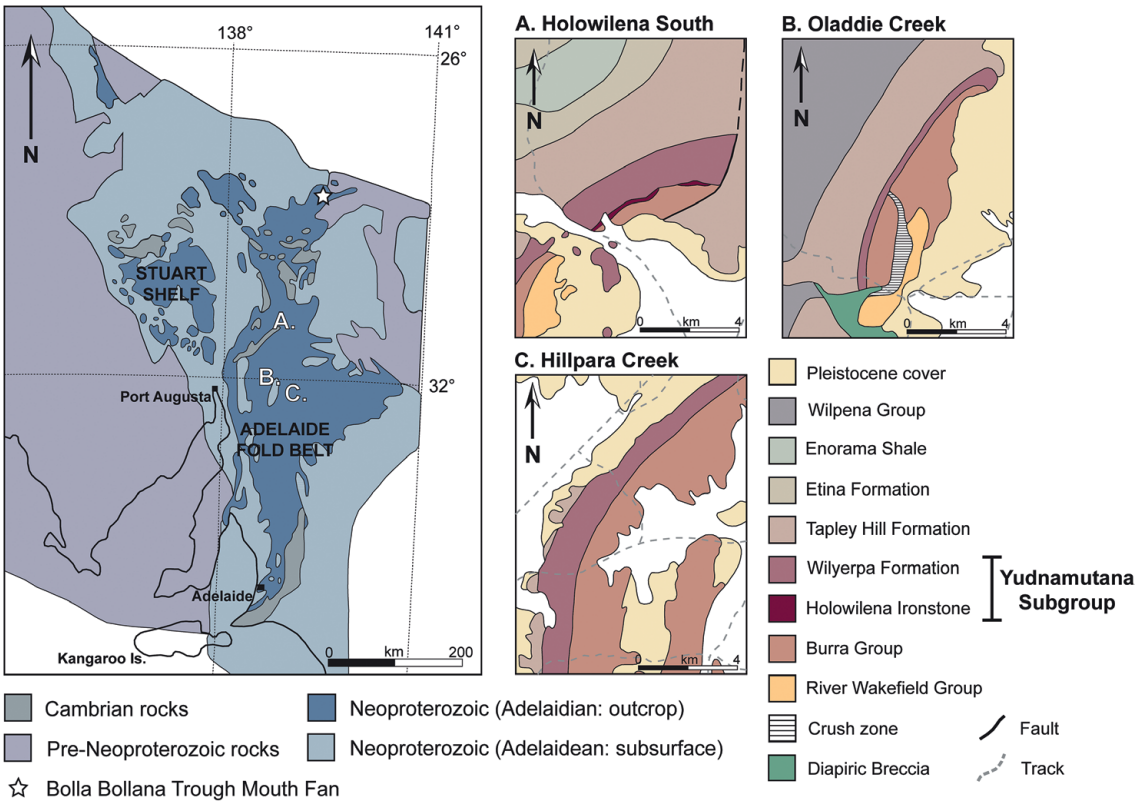

Fig. 1. Geological sketch map of the Adelaide Fold Belt, modified after Preiss *et al.* (1993), showing location of studied sections. Detailed geological maps of study areas are shown in insets; Log A, Holowilena Creek, modified after Preiss (1999); Log B, Oladdie Creek; Log C, Hillpara Creek modified after Binks (1968).

further south, or the Sturt Tillite in the type-section of the Adelaide Hills. These pass upwards into more heterogeneous diamictite, sandstone and siltstone facies of the Wilyerpa Formation in the central region, or the Lyndhurst Formation to the north. These deposits are in turn blanketed by the post-glacial Tindelpina Shale Member of the Tapley Hill Formation throughout the Adelaide Fold Belt (Fig. 3). Re–Os dating of the Tindelpina Shale Member provides a minimum age constraint of 643 ± 2.4 Ma for the Yudnamutana Subgroup (Kendall *et al*. 2006), further corroborated by a U–Pb zircon date of 659 ± 6 Ma derived from a volcaniclastic horizon towards the top of the Wilyerpa Formation (Fanning & Link 2006).

In places, ironstone facies characterize the lower Yudnamutana Subgroup, ascribed to the Holowilena Ironstone Formation in the study area (Fig. 3), or its correlative the Braemar Ironstone Formation to the east (Forbes 1989). The Holowilena Ironstone is variously interpreted as overlying the Pualco Tillite, (and equivalent Appila Tillite), or alternatively considered as laterally correlative (Preiss *et al*. 1993, and references within). In view of this, we adopt the term 'Holowilena Ironstone' in reference to the distinctly ferruginous facies. The terms 'Pualco Tillite' and 'Wilyerpa Formation' will be adopted to describe the underlying and overlying sedimentary facies, respectively.

The study areas occur within broadly NE–SW-trending outcrop belts that span the Parachilna and Orroroo map sheets (Fig. 1; Binks 1968; Preiss 1999). The orientation of these outcrops is considered to reflect widespread Willouran to early Sturtian rifting (*c.* 830 Ma to <660 Ma; Preiss *et al*. 2011), in this region culminating in development of the Barratta Trough depocentre (Fig. 2). The studied sections to the west and SW of this trough may thus be considered shallower 'shelf' deposits (Preiss *et al*. 1993), accumulating within neighbouring sub-basins. The sediments subsequently underwent intracratonic deformation during the Cambrian–Ordovician Delamerian Orogeny, becoming incorporated in a series of continuous, relatively upright fold structures at the northern margin of the Nackara Arc (Preiss 2000). The rocks of the study area are characterized by low-grade, greenschist-facies metamorphism (Preiss 1995). The minimal metamorphic overprint thus permits detailed study of primary sedimentary facies and structures.

Facies analysis

Data are presented from three detailed logged sections at Holowilena Creek, Oladdie Creek and Hillpara Creek (Fig. 4). Exposure of the underlying Burra Group sediments permits regional correlation, whereas the overlying Tapley Hill Formation is recorded only at Oladdie Creek. Therefore, only minimum thicknesses are observed at Holowilena and Hillpara Creeks, although considerable thickness variations across the logged sections are demonstrable by correlation. Five facies associations are recognized: (1) diamictite and conglomerate; (2) interbedded heterolithic deposits; (3) hummocky cross-stratified sandstone; (4) lonestone-bearing siltstone; (5) ferruginous siltstone and sandstone.

Diamictite and conglomerate facies association

This facies association makes up almost the entire section at Hillpara Creek, is notably dominant at Oladdie Creek, and constitutes less than 50% of the succession at Holowilena Creek. It is sandy throughout,

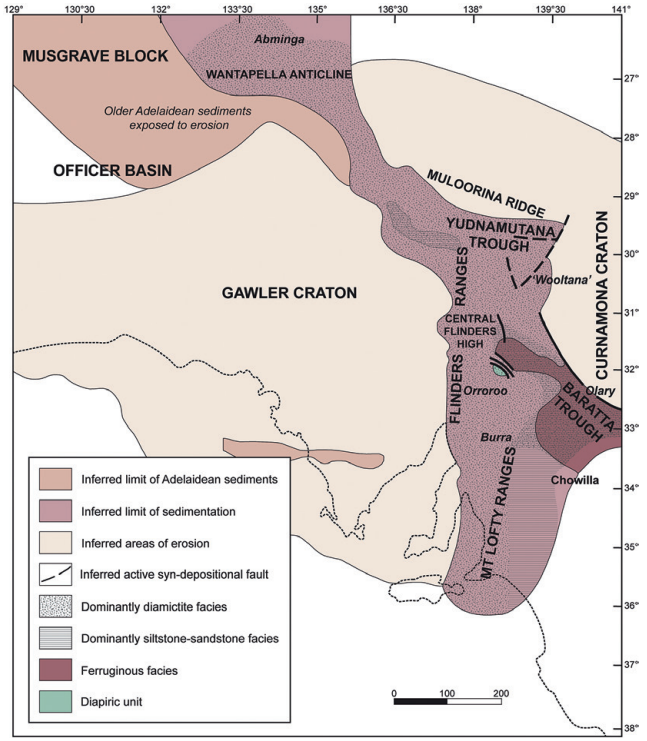

Fig. 2. Sketch map showing distribution of Sturtian sedimentary deposits and depositional basins throughout the Adelaide Fold Belt, modified after Preiss *et al*. (1998). (Note location of Barratta Trough and Yudnamutana Trough, representing the principal depocentres during Sturtian glaciation.)

and predominantly crudely stratified, with subsidiary massive and well-stratified varieties. The conglomerate deposits commonly display normal grading, fining into diamictite deposits, whereas the latter include normal, reverse and non-graded varieties (Fig. 4). Erosive contacts are prevalent at the base of conglomerates and clast-rich diamictites (Fig. 5a). Outsized clasts range from *c.* 3 to 80 cm in size, typically 15–20 cm, and comprise limestone, dolostone, metasediments, basalt and granite. Clasts are predominantly sub-angular to sub-rounded in shape; striated forms locally occur.

Downwarping and puncturing of laminae beneath pebble- to boulder-sized clasts is common (Fig. 5b and c), particularly in the crudely stratified diamictites. Other outsized clasts frequently form turbate structures, where smaller clasts form circular alignments around a core stone or rigid matrix (Fig. 5d and e), and are especially common where downwarping structures are rare. Lenticular siltstone and sandstone bodies locally occur, and are typically bed-parallel. However, in places these lenses are highly deformed, forming tight to recumbent intrabed fold structures.

Interpretation. The diamictite and conglomerate facies association is interpreted as a series of glacially influenced, subaqueous sediment flow deposits. The common fining-upward motif and internal organization of stacked conglomerate and diamictite deposits is typical of turbulence within the flow (Talling *et al*. 2012), representing high-density and more dilute turbidites, respectively. This is supported by the abundance of turbate structures, attributed to the generation of transient rotational eddies during turbulent flow (Phillips 2006). Similar structures can be generated during subglacial shearing of diamictites (e.g. Busfield & Le Heron 2013, and references within), but this interpretation is deemed unlikely in the absence of other shear-related features (e.g. attenuated clasts, pressure shadows, galaxy structures). Massive and reverse graded diamictite deposits are interpreted as the product of glaciogenic debris flows (GDFs), which commonly generate inverse grading patterns through the combined influence of upward clast migration and kinetic sieving (Legros 2002; Benn & Evans 2010; Talling *et al*. 2012). Erosive contacts at the base of many conglomerate and clast-rich diamictite units reflect repeated sediment flow emplacement, and resultant cannibalization of underlying sediments.

The close association of GDFs and turbidites probably reflects flow transformation during downslope movement, whereby mixing of the subaqueous debris flow with the overlying water body results in flow dilution (Benn & Evans 2010; Talling *et al*. 2012), and hence a tendency towards more turbulent flow conditions. The generation of these 'linked' turbidity currents frequently occurs through transformation of moderate strength debris flows (Talling *et al*. 2012), and is a common process within ice-proximal and ice-contact regimes under rates of high sedimentation (Benn & Evans 2010). This is consistent with the occurrence of tight to recumbent folded sand lenses, associated with slumping and sediment failure in response to rapid sediment delivery (Maltman 1994). Outsized clasts that downwarp and puncture underlying laminae are interpreted as IRD, wherein the preserved examples probably accumulated as sediment flows waned, thus restricting overprint of the structures under downslope remobilization. The local occurrences of striated clasts provide further credence to the proposed glacigenic origin.

Interbedded heterolithic facies association

This facies association comprises a series of well-stratified, dominantly interbedded siltstones, fine sandstones and coarse quartz arenites. It is most prominent in the Holowilena Creek section, constituting *c.* 30% of the succession, diminishing to <10% in the Oladdie Creek deposits and *c.* 2% at Hillpara Creek (Fig. 4). No lonestones occur within this facies association. The deposits exhibit minimal grading; rarely sandstone interbeds fine upward into the overlying siltstone. Current ripple cross-lamination is common within the fine sandstone–siltstone interbeds (Fig. 6a), predominantly demonstrating palaeoflow towards the north. An isolated example of climbing ripple cross-lamination is recorded at Oladdie Creek. In places, the fine sandstone interbeds are deformed into largely bed-parallel discontinuous fold structures (Fig. 6b); other beds contain highly convolute lamination as well as load and flame structures (Fig. 6c). Conversely, the coarser quartzite interbeds are planar throughout, and exhibit no sedimentary structures at Holowilena or Oladdie, with limited evidence of small-pebble lined cross-bedding in the Hillpara Creek section (at *c.* 75 m Log C, Fig. 4).

Interpretation. The interbedded heterolithic facies association is interpreted as a finer-grained series of sediment flow deposits, wherein the enhanced preservation of bedforms probably reflects reduced sediment concentrations compared with the coarser diamictite and conglomerate facies association. This may be a product of diminished sediment supply, which in tandem with the loss of the ice-rafting signature can be used to support periods of relative ice margin stability or retreat during deposition of the interbedded heterolithic material. Within the coarser-grained diamictite and conglomerate facies association, higher sediment concentrations and fall-out rates suppress the migration and preservation of delicate ripple structures (Sumner *et al*. 2008; Talling *et al*. 2012). However, as they move downslope, flows become more dilute through mixing with the water column, generating fully turbulent, low-density flows that allow the development of

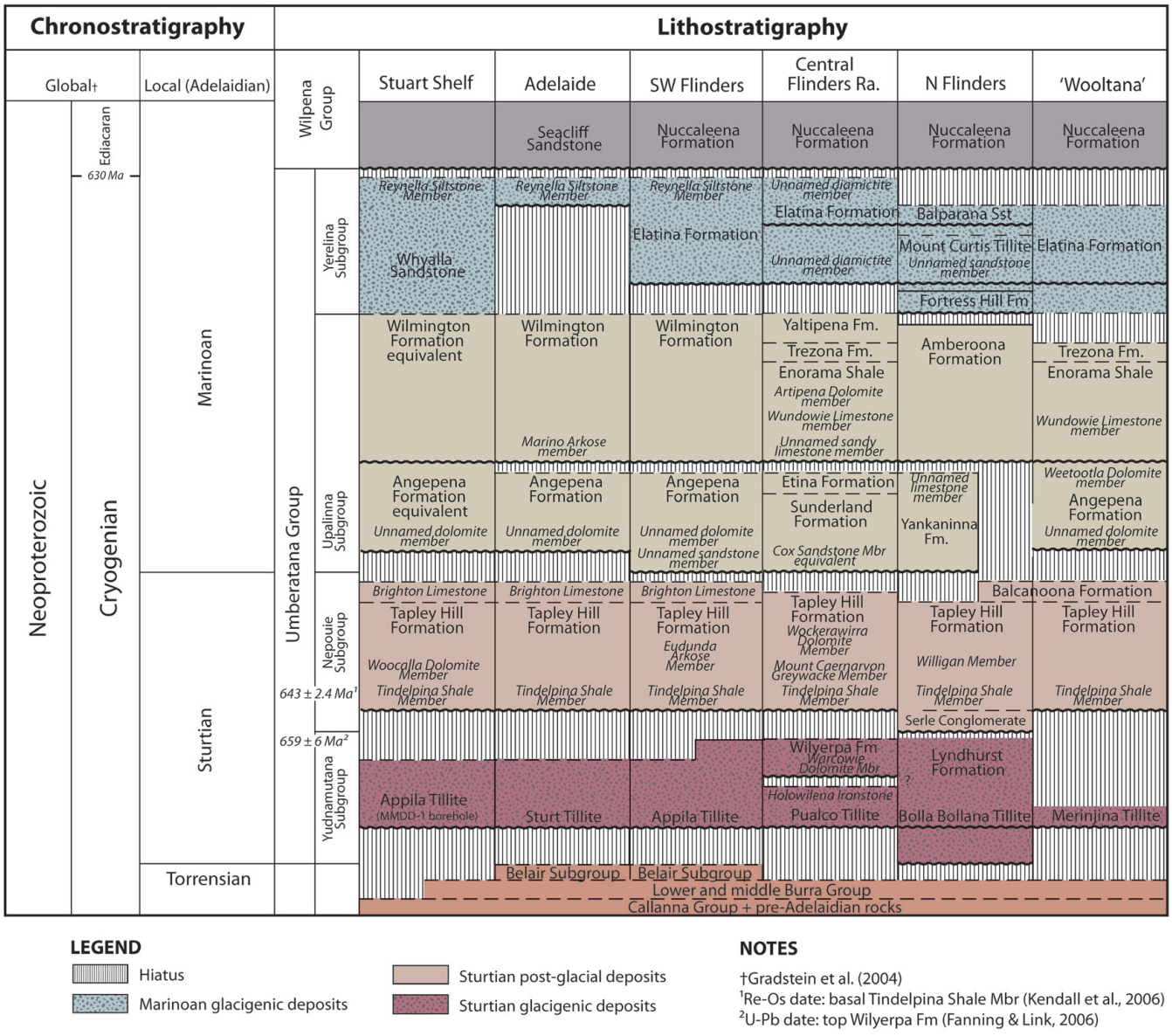

Fig. 3. Cryogenian stratigraphy and geochronology of the Adelaide Fold Belt and Stuart Shelf, after Preiss *et al*. (1998). Disparity in stratigraphic nomenclature of 'Sturtian' glacigenic deposits across South Australia should be noted. In this paper data are presented from the Yudnamutana Subgroup of the central and SW Flinders Ranges.

ripple cross-lamination (Baas *et al*. 2011; Talling *et al*. 2012). Rare normally graded sandstone interbeds are likewise interpreted to record deposition from turbulent underflows, succeeded by settling of hemipelagic silt material as the flows waned (e.g. Allen *et al*. 2004). The preservation of convolute lamination and climbing ripple cross-lamination at intervals reflects periods of more rapid turbidite deposition (Kuenen & Humbert 1969; Allen 1991; Baas 2000; Jobe *et al*. 2012; Talling *et al*. 2012). Similarly, folded sandstone and siltstone beds or lenses attest to downslope slumping and sediment instability induced by rapid sedimentation (Maltman 1994). Load and flame structures attest to Rayleigh–Taylor instabilities initiated at a grain-size or bed interface (Allen 1984; Collinson & Thompson 1987).

The coarser quartz arenite beds typically lack internal organization, and are thus interpreted as non- or poorly cohesive, clean sand debrites (Talling *et al*. 2012). An alternative mechanism of incremental accumulation via high-density turbidity currents is rejected owing to the absence of vertical and lateral grading (Kneller & Branney 1995; Talling *et al*. 2012). Moreover, the prominent cross-bedded quartzite bed at Hillpara Creek (at *c*. 75 m Log C, Fig. 4) pinches out sharply as opposed to gradationally, considered a characteristic feature of debris-flow deposition (Johnson 1970; Major & Iverson 1999; Amy *et al*. 2005; Amy & Talling 2006). The generation of dune-scale traction bedforms is also incompatible with rapid deposition from a high-density turbidity current (Kuenen 1966; Middleton & Hampton 1973; Talling *et al*. 2012). The prominent quartzite bed at Hillpara has been previously interpreted as a large ice-rafted erratic (Binks 1968). However, in light of its bed-parallel orientation, the absence of associated impact-related deformation and its textural similarity to other quartzite interbeds at Holowilena and Oladdie, we prefer interpretation as a laterally discontinuous debrite.

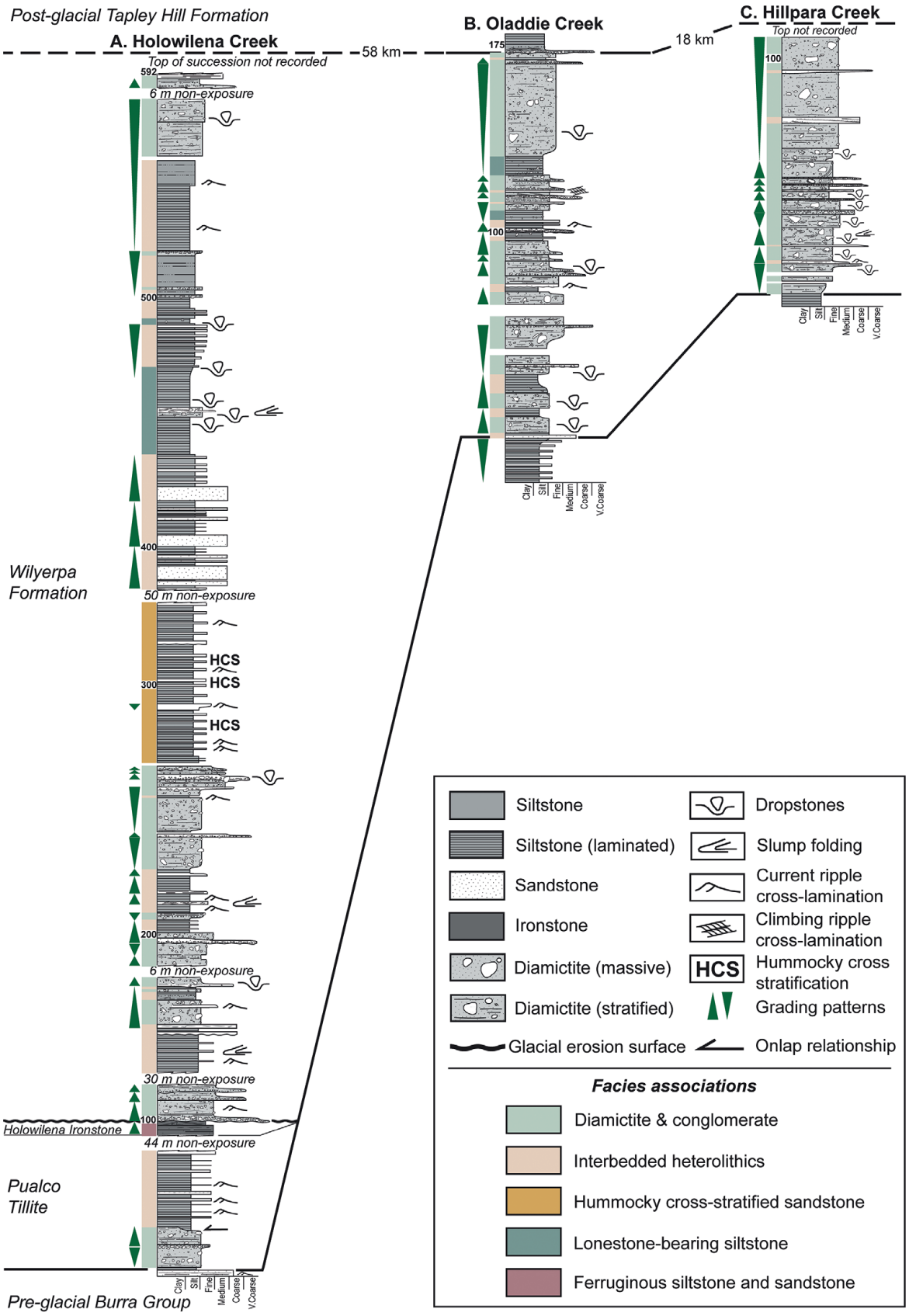

Fig. 4. Logged sections of the Yudnamutana Subgroup in the central and southern Flinders Ranges: Log A, Holowilena Creek (base of log: 31°59.232'S, 138°51.052'E); Log B, Oladdie Creek (base of log: 32°28.039'S, 138°38.285'E); Log C, Hillpara Creek (base of log: 32°33.777'S, 138°47.302'E). The variable thickness and lateral distribution of the five facies associations across the logged sections should be noted. Significant thickness changes from north to south attest to irregular palaeotopographic relief during deposition.

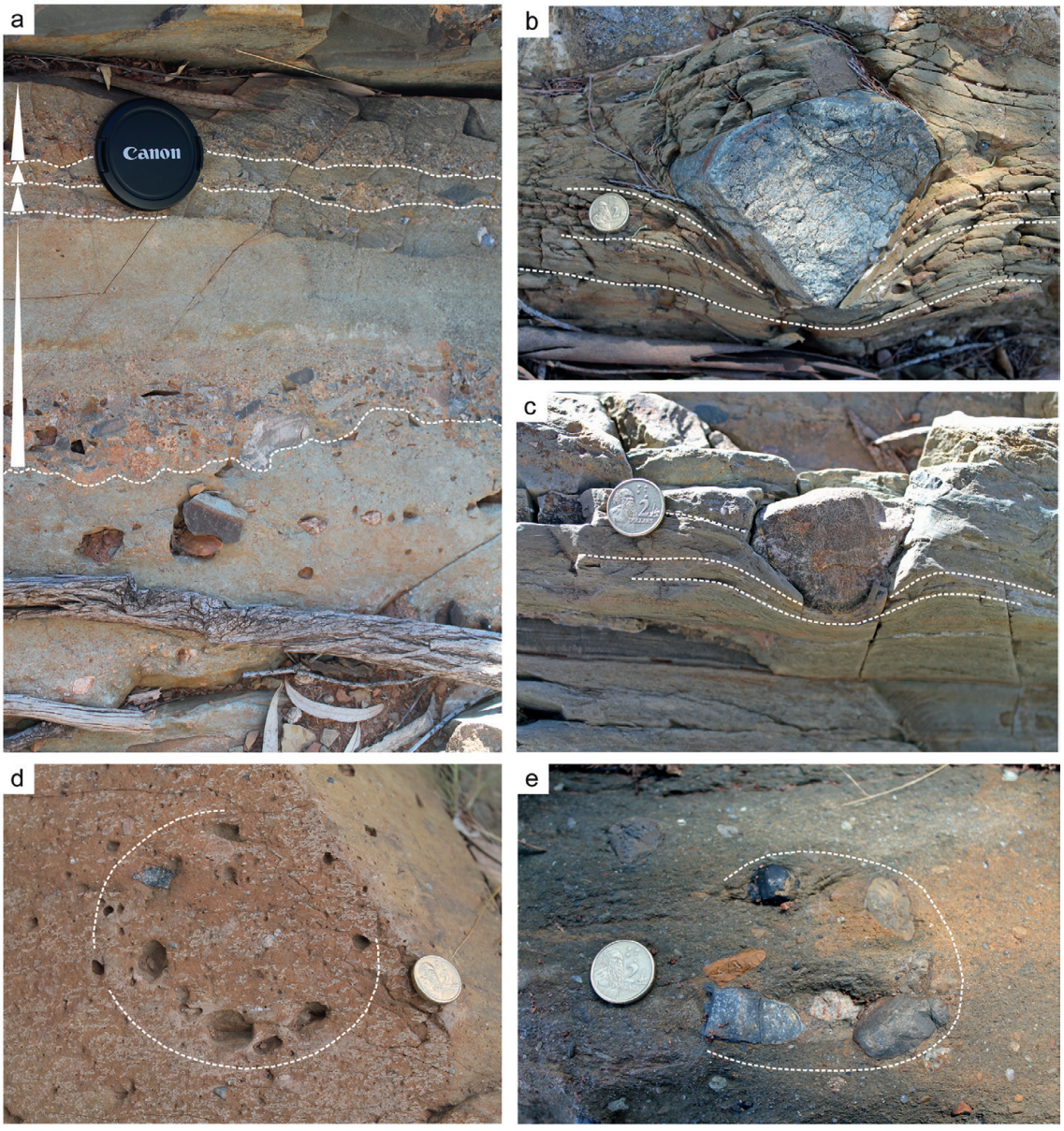

Fig. 5. Representative photographs of the diamictite and conglomerate facies association. (**a**) Erosive scour at base of normally graded conglomerate–sandstone interbeds (white triangles demonstrate grading patterns). (**b**) Ice-rafted dropstone, puncturing and downwarping the underlying laminae. Compaction-related deflection above lonestone significantly lower in amplitude than below. (**c**) Ice-rafted debris with impact-related deformation. (**d**, **e**) Profile view of rotational turbate structures (circular alignment of clasts around a core stone or rigid matrix). Coin and lens cap for scale measure 2 cm and 5 cm, respectively.

Hummocky cross-stratified sandstone facies association

This facies association is restricted to the Holowilena Creek section (Log A, Fig. 4). Overall, the facies resemble those of the interbedded heterolithic facies association in that they comprise well-stratified, non-graded fine sandstone and siltstone interbeds. They are distinguished, however, by the occurrence of hummocky cross-stratification (HCS) within many of the sandstone units (Fig. 6d and e). The bedforms are predominantly isotropic, with subsidiary anisotropic components. Current ripple cross-laminated and convolute laminated sandstones are also intercalated within this facies association. Lonestones were not observed.

Interpretation. The interbedded current rippled sandstones and laminated siltstones are interpreted to record turbulent underflow deposition and settling of hemipelagic fine material, respectively, in concert with the interbedded heterolithic facies association. However, the presence of HCS attests to the interplay of storm wave oscillatory flow during deposition, within a shallow shelf environment (Duke *et al*. 1991; Cheel & Leckie 1993; Johnson & Baldwin 1996; Dumas & Arnott 2006). Le Heron *et al*. (2011*a*,*b*) argued in favour of sea ice-free conditions at this time, as sea ice would inhibit the efficacy of storm wave agitation. Certainly these features attest to a sea ice minimum zone, where sufficient expanses of open water allow storm wave agitation, although the extent of ice meltback remains unclear. The absence of lonestones within this facies association is consistent with a lack of glacial influence on deposition.

Lonestone-bearing siltstone facies association

This facies association consists predominantly of planar laminated siltstone, with notably fewer sandstone beds than the interbedded heterolithic facies association. It is restricted to the Holowilena and

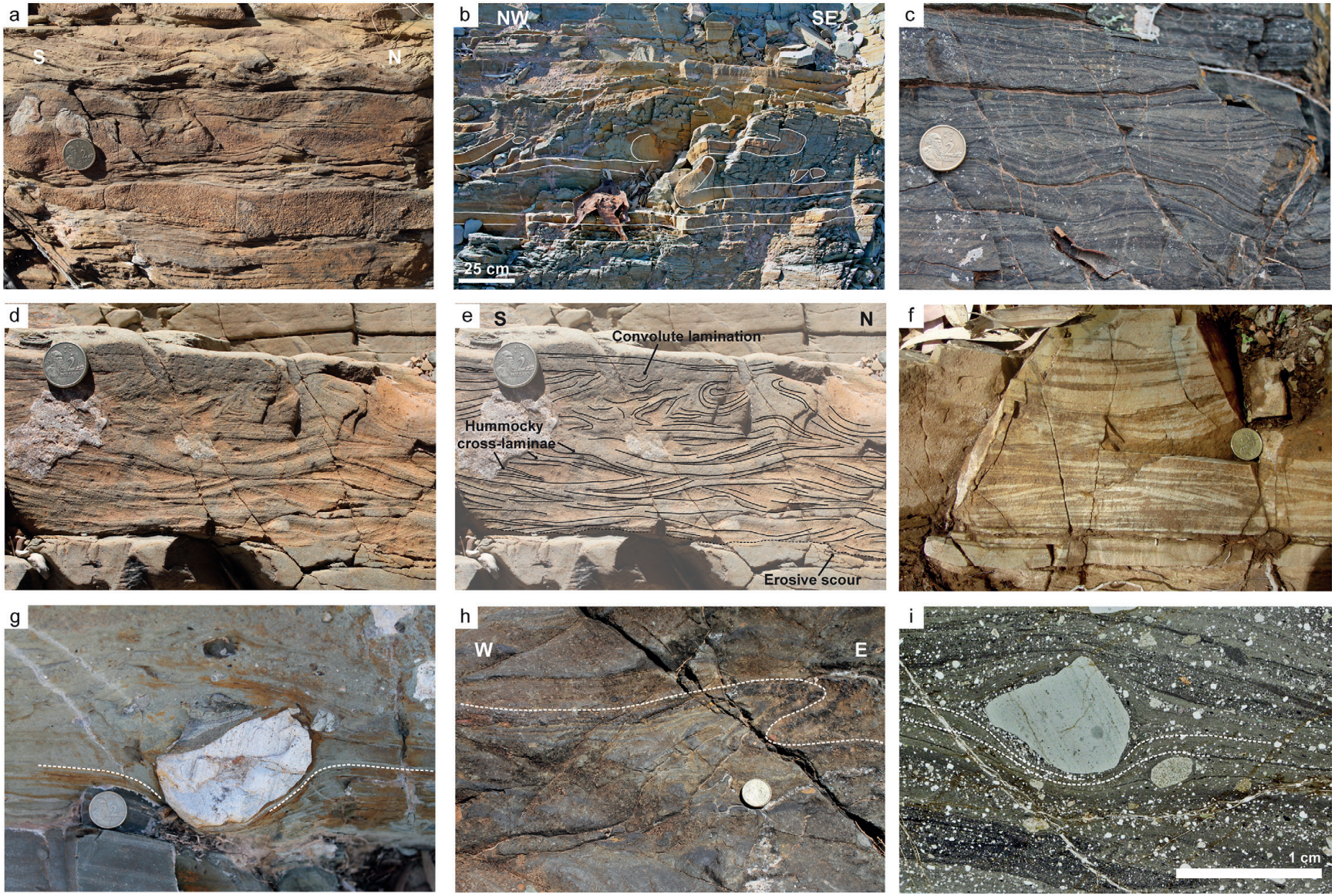

Fig. 6. Interbedded heterolithic facies association: (**a**) fine-grained current ripple cross-laminated sandstone and coarse to granule erosive based sandstone interbeds; (**b**) soft-sediment slump folded sandstone interbeds; (**c**) trough cross-lamination, convolute laminae and load and flame structures in beds that onlap the underlying Pualco Tillite (see Fig. 8a). Hummocky cross-stratified sandstone facies association: (**d**) dominantly isotropic hummocky cross-stratified sandstone interbeds, interpretive overlay in (**e**); (**f**) amalgamated sets of isotropic cross strata, with truncation of laminae to the left and above coin. Lonestone-bearing siltstone facies association: (**g**) ice-rafted debris downwarps and punctures underlying silt. Ferruginous siltstone and sandstone facies association: (**h**) distinct, sharp banding within the Holowilena Ironstone interpreted as possible algal laminites; irregular fold structure or possible domed algal laminite, verging towards the SE, should be noted; (**i**) micro-scale ice-rafted debris that punctures and downwarps underlying laminae. Coin for scale measures 2 cm.

Oladdie Creek sections, constituting <10% and <5% of the succession, respectively (Fig. 4). Downwarping of laminae beneath the outsized lonestones is common, in places piercing the laminae also (Fig. 6f). Rarely, lamina-parallel trains of lonestones are recorded, coincident with the absence of downwarping features.

Interpretation. The predominance of planar laminated siltstone alongside minor sandstone interbeds is interpreted to record settling of hemipelagic fine material, interrupted by isolated sand-rich sediment underflows. The presence of outsized lonestones that puncture and downwarp underlying laminae provides clear evidence of ice-rafting during deposition. Sediment flow 'rafting' of the lonestones (e.g. Postma *et al*. 1988; Eyles & Januszczak 2007) is discounted on the basis of the fine grain size of the supporting material, which would lack the cohesive strength to transport cobble- to boulder-sized material.

Ferruginous siltstone and sandstone facies association

This facies association is again restricted to Holowilena Creek, and attains only 6 m in thickness in the studied section (Log A, Fig. 4). It comprises both massive and crudely stratified fine sandstone and siltstone, with few granule- to small pebble-sized clasts, which are locally associated with impact-related deformation at the micro-scale (Fig. 6g). No pebble- or boulder-sized lonestones were observed within this facies association. Sharp, undulose, bed-parallel layering is apparent in the siltstone unit (Fig. 6h), alongside an isolated asymmetric fold structure verging towards the SE (Fig. 6i).

Interpretation. The ferruginous siltstone and sandstone facies association is tentatively interpreted to record similar styles of hemipelagic silt deposition and underflow sand emplacement as the lonestone-bearing siltstone facies association. However, impact-related deformation beneath granule-sized clasts at the micro-scale is interpreted to record early onset of ice-rafting processes. It is possible that the bed-parallel, undulose layering (Fig. 6h) may represent horizontal algal laminites, and by association an algal growth structure preserved in the asymmetric fold. This tentative interpretation is based on recognition of similar features observed in age-equivalent deposits of northern Namibia (Le Heron *et al*. 2013*b*), but requires further investigation.

The source of iron minerals within Neoproterozoic glacial successions remains highly contentious, and is considered beyond the scope of this study given its limited outcrop occurrence. Recent studies in South Australia support the intermixing of detrital terrestrial sediment and hydrothermal fluids (Lottermoser & Ashley 2000; Cox *et al*. 2013). In contrast to previous studies that advocate globally widespread seawater anoxia (e.g. Kirschvink 1992), the accumulation of abundant soluble iron, and hence deposition of iron-enriched sediments, is thought to occur under enhanced, not extreme anoxia and elevated Fe:S ratios (Cox *et al*. 2013).

Depositional cycles and glacial sequence stratigraphy

The preceding facies analysis reveals a diverse accumulation of sediments both with and without evidence of glacial influence on deposition. Examination of the vertical grading of these facies associations, alongside changes in their lateral distribution, provides insight into their depositional history, and allows a sequence stratigraphic framework to be constructed. Sequence stratigraphic concepts are scarcely applied to glacial depositional systems (e.g. Proust & Deynoux 1994; Brookfield & Martini 1999; Powell & Cooper 2002; El-ghali 2005; Pedersen 2012), largely owing to the complexity of deciphering the influence of glacial fluctuations from changes in relative lake or sea level. The term 'glacial sequence stratigraphy' is therefore used to denote a sequence stratigraphic model driven by glacier dynamics (Powell & Cooper 2002), the effects of which are preserved independently of other external forces (e.g. eustacy, isostacy). Glacial systems tracts (GST) are defined following the scheme of Powell & Cooper (2002). Systems tracts are subdivided into glacial advance (GAST) and glacial retreat (GRST) sequences, which may also include ice maximum (GMaST) and ice minimum (GMiST) systems tracts, respectively. Ten glacial systems tracts are recognized (Fig. 7), separated either by a glacial erosion surface (GES) or glacial bounding surface (GBS), the latter including the glacial advance surface (GAS) representing the onset of advance systems tracts, and the iceberg-rafting termination surface (ITS) representing the onset of retreat.

The first sequence is restricted to the base of the Holowilena Creek section (Fig. 7), and constitutes striated clast-bearing sediment gravity-flow deposits of the diamictite and conglomerate facies association, correlated to the Pualco Tillite. This sequence is attributed to the glacial advance systems tract (GAST 1) owing to its characteristically thin exposure, and coarsening-upward motif (Powell & Cooper 2002). The sequence is capped by an onlap surface, representing the first glacial bounding surface (GBS1), beneath sediments of the interbedded heterolithic facies association (Fig. 8a). This onlap surface is interpreted to reflect transgression following local ice meltback, demarcating the base of the first glacial retreat systems tract (GRST 1), consistent with the absence of glacigenic indicators (e.g. IRD) in the overlying heterolithic facies (Fig. 7). These sediments are overlain by the ferruginous siltstone and sandstone facies association, the Holowilena Ironstone. The first appearance of micro-scale IRD at this interval is interpreted as the glacial advance surface (GAS1; Powell & Cooper 2002), and thus the overlying Holowilena Ironstone is interpreted as a thinly exposed remnant of the second GAST.

The top of the Holowilena Ironstone is sharply truncated by a glacial erosion surface (GES1) in the Holowilena Creek section (Figs 7 and 8b), a widely recognized disconformity throughout the Flinders Ranges (e.g. Coats 1981; Preiss *et al*. 1993). The thin exposure of the underlying GAST 2 probably reflects significant downcutting during development of the GES. The surface is correlated to the top of the pre-glacial Burra Group sediments at Oladdie Creek and Hillpara Creek based upon the absence of the underlying Pualco Tillite and Holowilena Ironstone, although no significant erosion surface was observed. The absence of a significant erosion surface in the proximal sections is probably the result of reworking and erosion during subsequent sediment flow emplacement (during GRST 2), as opposed to marine ravinement, the effects of which would be expected to be more prominent in the distal sections, and accompanied by a transgressive lag, which is not present. Deposits of the glacial maximum systems tract (GMaST) are not recorded above the GES, as is typical of many temperate glacial systems (Powell & Cooper 2002). Instead, at Holowilena and Oladdie, the overlying sediments of the Wilyerpa Formation correspond to a second phase of glacial retreat (GRST 2, Fig. 7). These comprise stacked, dominantly fining-upward deposits of the diamictite and conglomerate facies association and interbedded heterolithic facies association. The former contains repeated intervals of IRD, which are typically absent in the latter. This is interpreted as the product of pulsed collapse events at the ice front, driving coarser-grained gravity flows and iceberg distribution into the basin, followed by periods of relative ice margin stability or retreat. During these intervals, the shelf becomes starved of coarser

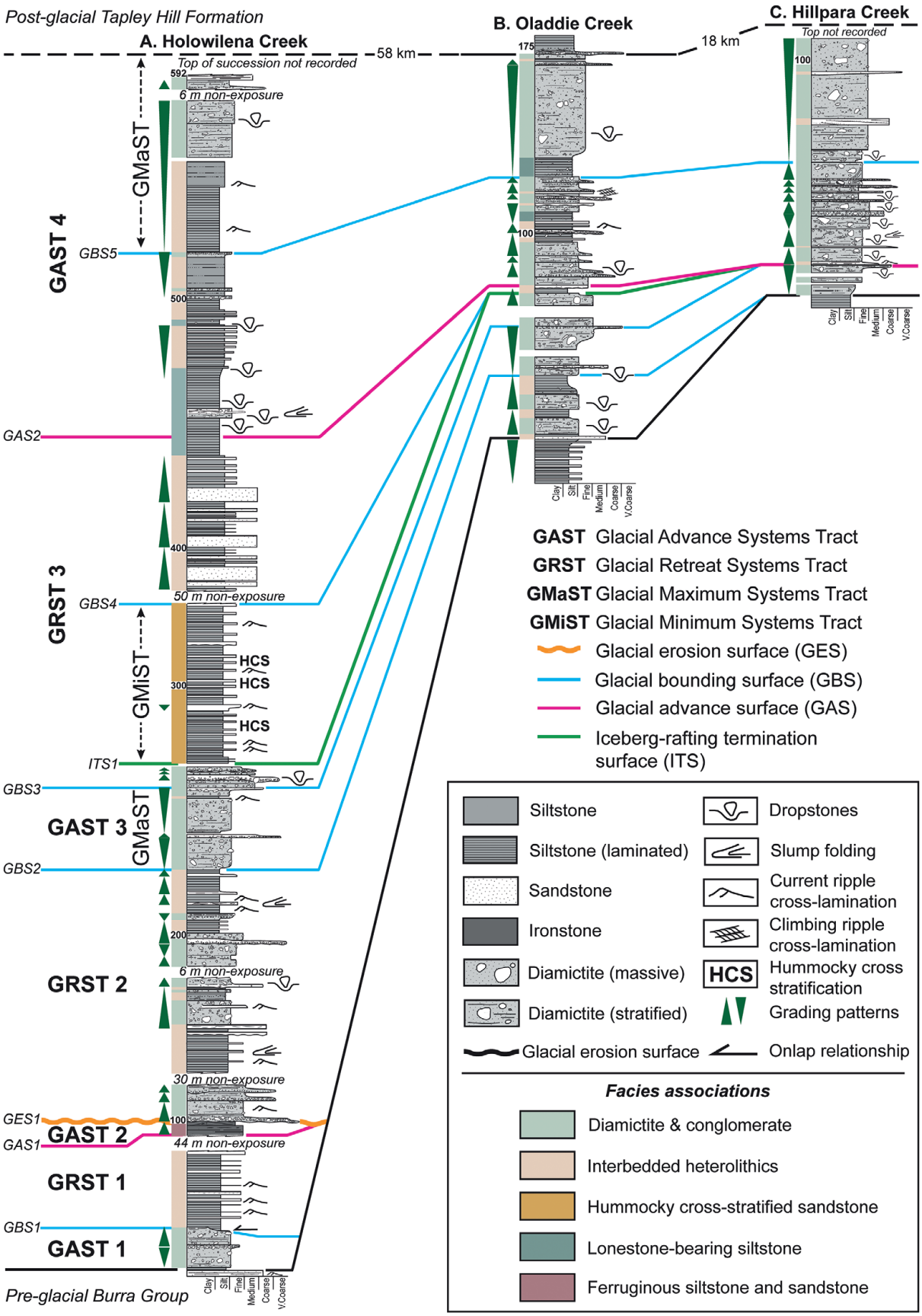

Fig. 7. Sequence stratigraphic framework for the studied sections. Glacial systems tracts are separated either by a glacial erosion surface (GES) or glacial bounding surface (GBS), the latter including the glacial advance surface (GAS) and iceberg-rafting termination surface (ITS).

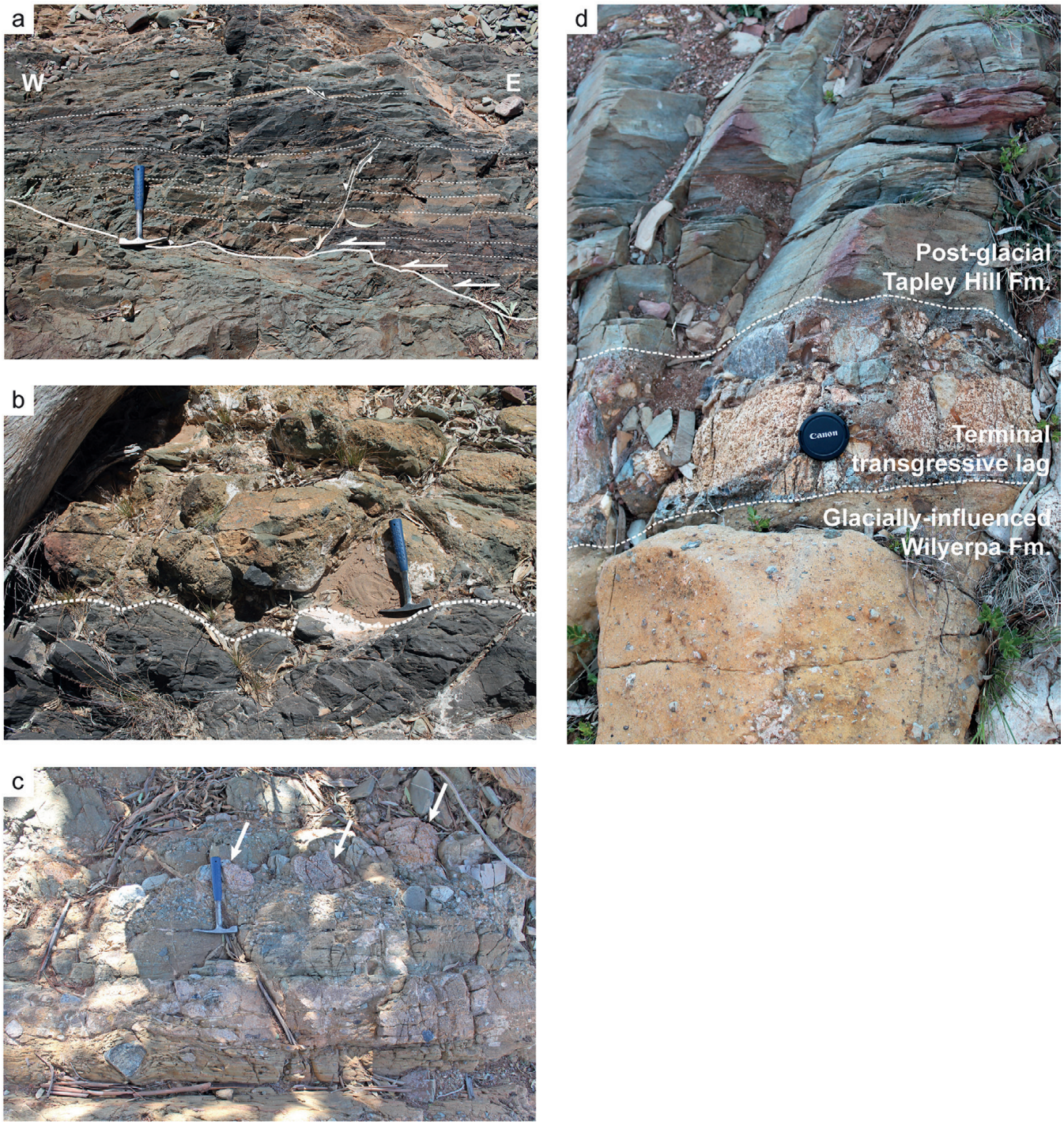

Fig. 8. Photographs of significant depositional boundaries within the studied succession: (**a**) glacially influenced Pualco Tillite onlapped by non-glacially influenced interbedded heterolithic deposits (see Fig. 6c); (**b**) glacial erosion surface at the base of the Wilyerpa Formation, downcutting into the Holowilena Ironstone; (**c**) influx of extrabasinal granite clasts, indicated by white arrows, at inferred glacial maximum; (**d**) conglomeratic transgressive lag records terminal glacial conditions at the top of the Wilyerpa Formation, succeeded by post-glacial siltstone of the Tapley Hill Formation. Hammer and lens cap for scale measure 26 cm and 5 cm, respectively.

sediment, leading to deposition of finer-grained sediment flow deposits, and ice-rafting processes are inhibited.

Transition to an advance systems tract (GAST 3) is recorded above this sequence (at GBS2, Fig. 7), where coarser-grained sediments of the diamictite and conglomerate facies association predominate, concomitant with a switch to a coarsening-upward motif. A pronounced inverse-grading event can be correlated across all three logged sections (Fig. 7: 260 m Log A, 62 m Log B, 18 m Log C), and at Holowilena is accompanied by a sudden influx of exotic pebble- to boulder-sized granite clasts (Fig. 8c). This

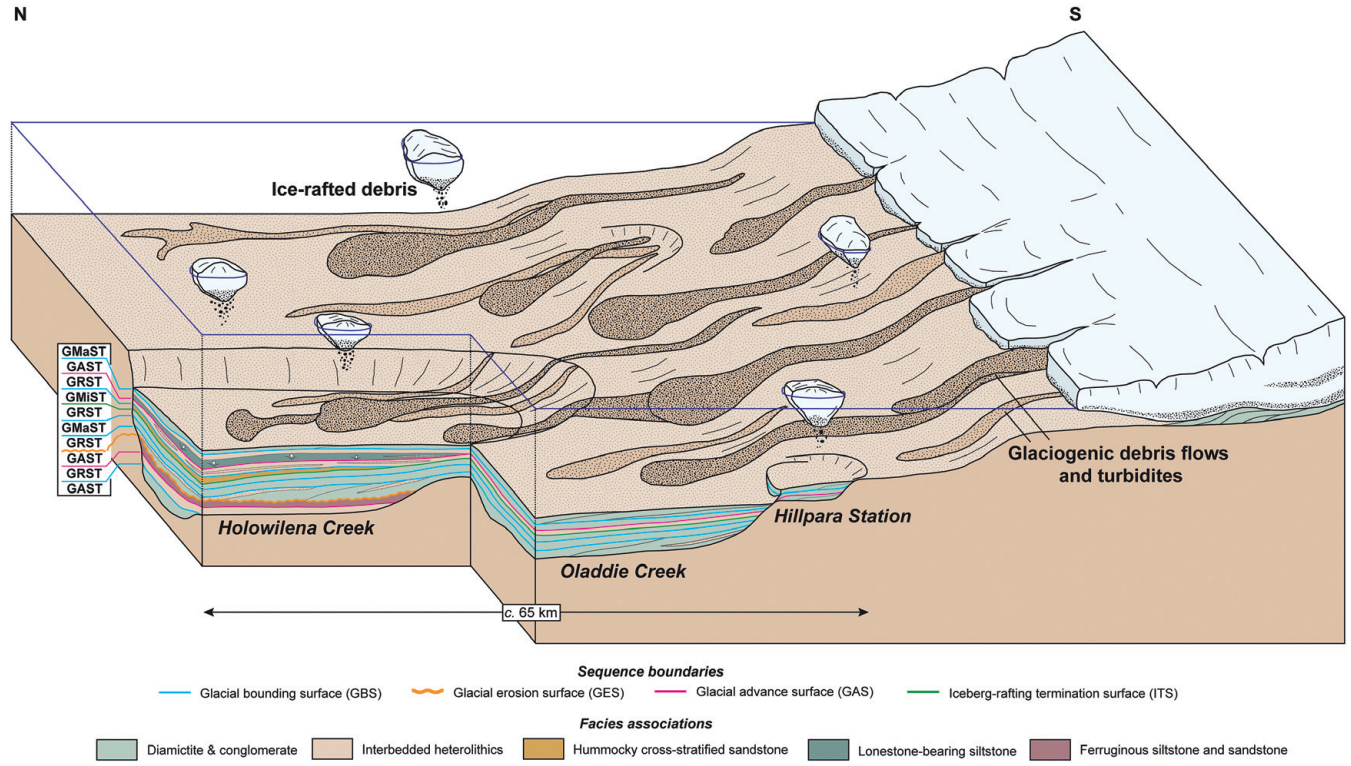

Fig. 9. Simple depositional model for the studied sections in the central and southern Flinders Ranges. Sequence stratigraphic analysis identifies four glacial advance sequences, separated by three intervals of ice meltback. During glacial advance, dynamic ice sheet oscillations drive delivery of glaciogenic debris flows and glacioturbidites downslope, subject to secondary ice-rafting. During glacial retreat, the ice-rafting signature is lost, and ice minimum conditions permit storm-wave agitation of the water column, and generation of hummocky cross-stratified sandstones. Thickness variations across the logged sections attest to significant palaeotopographic relief during deposition, creating progressively greater accommodation space downslope (Hillpara–Oladdie–Holowilena) through the combined effects of pre- and early syn-depositional rift activity and subglacial downcutting. Key for glacial systems tracts codes: GAST, glacial advance systems tract; GRST, glacial retreat systems tract; GMaST, glacial maximum systems tract; GMiST, glacial minimum systems tract.

event is interpreted to record ice maximum conditions (GMaST), resulting in high rates of sediment supply and delivery of extrabasinal erratic lithologies. At Holowilena and Oladdie a thin succession of normally graded diamictite and conglomerate facies above GBS3 marks a return of the GRST (3), capped by an abrupt facies dislocation to thinly laminated siltstones (Fig. 7). This facies change is concurrent with the disappearance of IRD, and is thus identified as the iceberg-rafting termination surface (ITS1; Powell & Cooper 2002).

The retreat sequence above ITS1 is largely restricted to the Holowilena Creek section (Fig. 7), and comprises the hummocky cross-stratified sandstone facies association at the base, and interbedded heterolithic facies association above. The occurrence of hummocky cross-stratification in the basal sediments, requiring sufficient open waters and hence sea ice meltback to permit storm wave agitation (Le Heron *et al.* 2011*a*,*b*), is used to support ice minimum conditions (GMiST). Moreover, HCS is typically encountered within a shallow shelf setting (Duke *et al.* 1991; Cheel & Leckie 1993; Johnson & Baldwin 1996; Dumas & Arnott 2006), and thus the absence of this facies association in the more proximal, shallower Oladdie Creek and Hillpara Creek sections may reflect a period of subaerial exposure and non-deposition in the proximal reaches during this retreat phase. The overlying interbedded heterolithic facies above GBS4 records an influx of coarser-grained sand underflows within the Oladdie and Holowilena Creek sections, interpreted as the product of increased sediment instability in the source region, perhaps in response to initial, more proximal ice movement, which may correspond to early GAST. However, the first appearance of IRD in the overlying laminated siltstones is taken as a more reliable indicator of initial advance (Powell & Cooper 2002), identified as the second glacial advance surface (GAS2; Fig. 7).

The overlying GAST 4 is initially characterized by stacked, thickly bedded IRD-bearing diamictite and conglomerate at Hillpara Creek, normally graded and thinly bedded diamictite and conglomerate separated by IRD-bearing siltstone at Oladdie Creek, and by IRD-bearing siltstone only at Holowilena Creek (Fig. 7). These facies associations reflect initial advance of the ice front, where coarse-grained glacially influenced sediment flows are deposited in the more proximal regions (Hillpara), further downslope these sediment flows occur as pulsed events separated by periods of quiescence where ice-rafting processes dominate (Oladdie), and the distal regions remain starved of coarser-grained sediment, preserving only the ice-rafting signature (Holowilena). Towards the top of the succession, above GBS5, thickly bedded and dominantly inverse graded diamictites, conglomerates and coarse-grained sandstones are preserved across all three logged sections, reflecting full glacial advance during late-stage GAST 4, identified as the GMaST (Fig. 7).

The upper contact of the Wilyerpa Formation, and cessation of glacially influenced sedimentation, was observed only in the Oladdie Creek section (Fig. 7). Here, an erosional contact occurs at the base

of a pebble- to boulder-bearing conglomerate, with a distinct dark grey silt matrix, notably dissimilar to the pale brown sandy matrix of the underlying Wilyerpa Formation (Fig. 8d). The conglomerate is interpreted as a post-glacial transgressive lag, and is succeeded by a thick succession of laminated dark grey siltstones of the Tindelpina Shale Member, the basal unit of the Tapley Hill Formation.

Discussion

Sequence stratigraphic analysis of the studied sections in the central and southern Flinders Ranges identifies four distinct glacial advance sequences, separated by three intervals of ice meltback (Fig. 7). The glacial influence on deposition (IRD) is pervasive throughout the Hillpara and Oladdie Creek sections. This is consistent with their more proximal position relative to the ice front (see Fig. 9), corroborated by the predominance of coarser-grained facies associations, as well as ripple cross-lamination and soft sediment slump folding indicative of sediment supply from the south. The Holowilena Creek section represents the most ice-distal position, as indicated by the clear increase of fine-grained facies. Deposition in the ice-proximal zone is proposed owing to the dominance of sediment gravity flow and ice-rafting processes (Benn & Evans 2010), with sediment accumulation on the shelf at Hillpara and Oladdie, and the slope at Holowilena (Fig. 9).

The studied sections demonstrate considerable thickness variations, thickening by a few tens of metres from Hillpara to Oladdie, and by several hundred metres to Holowilena Creek (Fig. 7). This is attributed to significant palaeotopographic relief during deposition (see Fig. 9), the origin of which remains obscure. Previous studies have advocated accumulation of Sturtian glacigenic sediments within pre- and early syn-depositional rift basins (e.g. Preiss 2000), whereas the presence of a distinct glacial erosion surface immediately above the Holowilena Ironstone may be used to support the interplay of subglacial downcutting (*sensu* Young & Gostin 1990, 1991). None the less, the palaeotopographic depression at Holowilena provided enhanced accommodation space for the preservation of non-glacially influenced regressive systems tracts, alongside protection from cannibalization under repeated sediment flow emplacement. In contrast, on the palaeotopographic highs at Oladdie and Hillpara (Fig. 9), relatively thin successions of stacked coarse-grained sediment flows probably underwent significant cannibalization and reworking during subsequent downslope movements, and were redeposited basinward as flows waned, and hence glacial advance systems tracts are preferentially preserved.

Previous studies in South Australia have also identified multiple advance–retreat sequences within the Sturtian record (e.g. Forbes 1970; Forbes & Cooper 1976; Coats & Preiss 1987; Young & Gostin 1988, 1989, 1990, 1991; Le Heron *et al*. 2011*b*). The four-fold stratigraphic subdivision of Young & Gostin (1990, 1991) comprises two diamictite-dominated intervals, each overlain by mudstone-dominated facies, interpreted as glacial advance and retreat sequences, respectively. The uppermost mudstone-dominated interval, Unit 4 of Young & Gostin (1990), is regarded as a transitional unit between the diamictic deposits of Unit 3 and the shale-rich deposits of the post-glacial Tapley Hill Formation. These considerations suggest that the diamictites of the upper GMaST in the central and southern Flinders Ranges, overlain by the Tapley Hill Formation at Oladdie Creek (Fig. 7), correlate with Unit 3 of Young & Gostin (1990, 1991), and therefore Unit 4 is absent. The absence of Unit 4 from sequences in the Northern Flinders Basin (Young & Gostin 1990) is attributed to non-deposition on topographically elevated regions, possibly in response to local tectonic and/or isostatic readjustments. This is considered plausible following the significant glacial advance recorded in the upper GMaST (this study) and Unit 3 (Young & Gostin 1990, 1991). Furthermore, the basal GAST 1 and GRST 1 identified in the Holowilena Creek section were not recorded by Young & Gostin (1990, 1991). Previous studies in the Olary region to the east of the Orroroo map sheet, however, also recognized the basal Pualco Tillite as recording the glacial maximum of the first Sturtian glaciation (Coats & Preiss 1987; Forbes 1989). The absence of these depositional sequences in the Northern Flinders Basin may reflect erosion during subglacial downcutting, coeval with GES1 at the top of the Holowilena Ironstone (Figs 7–9).

In the North Flinders Basin, Le Heron *et al*. (2013*a*) recently interpreted a trough mouth fan (TMF) in the Sturtian glacigenic record, building out seaward of a small palaeo-ice stream. Three facies associations are recognized, comprising a diamictite facies association accumulating via glaciogenic debris flows and ice-rafting processes at the ice margin, a channel belt facies association recording channelized turbidity currents subject to ice-rafting on the proximal and medial areas of the fan, and a sheet heterolithic facies association, deposited as non-channelized turbidites and ice-rafted debris. The overriding signature of sediment gravity-flow deposition subject to ice-rafting processes closely mirrors the depositional sequences described in this study. The sequences are readily differentiated, however, by the abundance of coarse-grained material. The Bolla Bollana Formation (Le Heron *et al*. 2013) is dominated by coarse-grained diamictite and conglomerate facies, with a subordinate fine-grained component throughout, and hence records deposition principally as sediment concentrated glaciogenic debris flows (GDFs). Our present study, however, demonstrates significantly greater facies variability, a more diverse range of grain sizes throughout, and a notably more abundant component of fine material. As a result, the dominant mode of deposition is via less concentrated turbulent sediment flows. Le Heron *et al*. (2013) correlated the Bolla Bollana Formation to the second glacial advance (Unit 3) of Young & Gostin (1991), which would therefore equate to the upper GMaST of this study. This is consistent with build-out of TMFs during glacial advance (e.g. Powell & Cooper 2002; Ó'Cofaigh *et al*. 2012). The North Flinders Basin is, however, widely considered as a separate sub-basin, disconnected from the depocentres of the central and southern Flinders Ranges (Preiss 1987, 2000; Preiss *et al*. 2011). Arguably, therefore, separate ice masses may have fed each depocentre, where the evidence for concomitant advance phases, each following a period of significant ice meltback, may testify to regional warming and cooling events.

To summarize, this study proposes multiple, clear-cut cycles within the Sturtian glaciation of South Australia. Although the concept of hydrological shutdown under the snowball Earth hypothesis (Hoffman *et al*. 1998; Hoffman & Schrag 2002) is readily dismissed from sedimentological evidence (Allen & Etienne 2008), the true nature of ice sheet dynamics has awaited clarification. Despite there being very few attempts to apply it in the Cryogenian, sequence stratigraphic analysis is clearly a valuable tool to elucidate glacial cycles, including recognition of open water during glacial minima. Detailed examination of the sections at Holowilena Creek, Oladdie Creek and Hillpara Creek therefore contribute to the growing body of research supporting a dynamic Neoproterozoic cryosphere, akin to the numerous Phanerozoic icehouse events recorded throughout Earth's history (e.g. Etienne *et al*. 2007; Allen & Etienne 2008; Arnaud *et al*. 2011, and references therein). Contingent on an adequate chronostratigraphic framework, detailed facies and sequence stratigraphic analysis of pan-global 'Sturtian' successions may even allow the glaciodynamic signature of these successions to be assessed on a global scale.

Conclusions

Detailed sedimentary logging of previously little described sections in Holowilena Creek, Oladdie Creek and Hillpara Creek in the central and southern Flinders Ranges reveals significant lateral

and vertical facies variation within the Yudnamutana Subgroup. Repeated occurrences of ice-rafted debris and subglacially striated clasts attest to a strong glacial influence on sedimentation. The application of glacial sequence stratigraphy allows the dynamics of the Sturtian ice sheet to be elucidated, as follows.

Five facies associations are recognized: (1) diamictite and conglomerate facies association (glaciogenic debris flows and turbidites subject to secondary ice-rafting); (2) interbedded heterolithic facies association (debrites, low-density turbidites and hemipelagic fine-grained material); (3) hummocky cross-stratified sandstone facies association (storm-wave agitation of low-density turbidity currents and settling of hemipelagic fine-grained material); (4) lonestone-bearing siltstone facies association (settling of hemipelagic fine-grained material and isolated sand-rich turbulent underflows); (5) ferruginous siltstone and sandstone facies association (settling of hemipelagic fine-grained material and sand-rich turbulent underflows under enhanced anoxia, subject to subordinate ice-rafting).

Thickness variations across the logged sections attest to an irregular underlying palaeotopography during deposition, attributed to the combined influence of pre- and early syn-depositional rift activity and subglacial downcutting.

Glacial sequence stratigraphic analysis identifies four glacial advance systems tracts (GAST), separated by three glacial retreat systems tracts (GRST), the uppermost, GRST 3, testifying to open water conditions. These findings support dynamic advance and retreat of the Sturtian ice sheet, requiring an active hydrological cycle.

The authors are extremely grateful to A. S. Collins (University of Adelaide) and B. L. Moorhouse (University of Otago) for their assistance in the field. We would like to thank the two anonymous reviewers for suggestions that allowed us to improve the paper, A. Spencer for constructive comments on an earlier draft of the paper, and P. Hughes for editorial input. This work was funded by the National Geographic Explorer Fund, Novas Consulting Research Grant (Geological Society, London), Gill Harwood Memorial Fund (BSRG) and the Helen Shackleton Award (RHUL).

References

Allen, J.R.L. 1984. *Sedimentary Structures: Their Character and Physical Basis, Volumes I and II*. Elsevier, Amsterdam.

Allen, J.R.L. 1991. The Bouma A division and the possible duration of turbidity currents. *Journal of Sedimentary Petrology*, **61**, 291–295.

Allen, P.A. & Etienne, J.L. 2008. Sedimentary challenge to Snowball Earth. *Nature Geoscience*, **1**, 817–825.

Allen, P.A., Leather, J. & Brasier, M.D. 2004. The Neoproterozoic Fiq glaciation and its aftermath, Huqf supergroup of Oman. *Basin Research*, **16**, 507–534.

Amy, L.A. & Talling, P.J. 2006. Anatomy of turbidite and debrite sandstones based on long distance (120×35 km) bed correlation, Marnoso-arenacea Formation, Northern Apennines, Italy. *Sedimentology*, **53**, 161–212.

Amy, L.A., Talling, P.J., Peakall, J., Wynn, R.B. & Arzola Thynne, R.G. 2005. Bed geometry used to test recognition criteria of turbidites and (sandy) debrites. *Sedimentary Geology*, **79**, 163–174.

Arnaud, E., Halverson, G.P. & Shields-Zhou, G. (eds) 2011. *The Geological Record of Neoproterozoic Glaciations*. Geological Society, London, Memoirs, **36**.

Baas, J.H. 2000. Duration of deposition from decelerating high-density turbidity currents. *Sedimentary Geology*, **136**, 71–88.

Baas, J.H., Best, J.L. & Peakall, J. 2011. Depositional processes, bedform development and hybrid flows in rapidly decelerated cohesive (mud–sand) sediment flows. *Sedimentology*, **58**, 1953–1987.

Benn, D.I. & Evans, D.J.A. 2010. *Glaciers and Glaciation*. Hodder, London.

Binks, P.J. 1968. *Orroroo Sheet SI54-1. 1:250,000 Scale Geological Map and Explanatory Notes*. Primary Industries and Resources South Australia, Adelaide.

Brookfield, M.E. & Martini, I.P. 1999. Facies architecture and sequence stratigraphy in glacially influenced basins: Basic problems and water-level/glacier input-point controls (with an example from the Quaternary of Ontario, Canada). *Sedimentary Geology*, **123**, 183–197.

Busfield, M.E. & Le Heron, D.P. 2013. Glacitectonic deformation in the Chuos Formation of northern Namibia: Implications for Neoproterozoic ice dynamics. *Proceedings of the Geologists' Association*, **124**, 778–789.

Cheel, R.J. & Leckie, D.A. 1993. Hummocky cross-stratification. *In*: Wright, V.P. (ed.) *Sedimentology Review Volume 1*. Wiley Blackwell, London, 103–122, http://dx.doi.org/10.1002/9781444304534.ch7.

Coats, R.P. 1981. Late Proterozoic (Adelaidean) tillites of the Adelaide Geosyncline. *In*: Hambrey, M.J. & Harland, W.B. (eds) *Earth's Pre-Pleistocene Glacial Record*. Cambridge University Press, Cambridge, 537–548.

Coats, R.P. & Preiss, W.V. 1987. Stratigraphy of the Umberatana Group. *In*: Preiss, W.V. (ed.) *The Adelaide Geosyncline: Late Proterozoic Stratigraphy, Sedimentation, Palaeontology and Tectonics*. Geological Survey of South Australia, Bulletin, **53**, 125–210.

Collinson, J.D. & Thompson, D.B. 1987. *Sedimentary Structures*, 2nd edn. Chapman & Hall, London.

Condon, D.J. & Bowring, S.A. 2011. A user's guide to Neoproterozoic geochronology. *In*: Arnaud, E., Halverson, G.P. & Shields-Zhou, G. (eds) *The Geological Record of Neoproterozoic Glaciations*. Geological Society, London, Memoirs, **36**, 135–149.

Cox, G.M., Halverson, G.P., Minarik, W.G., Le Heron, D.P., MacDonald, F.A., Bellefroid, E.J. & Strauss, J.V. 2013. Neoproterozoic Iron Formation: An evaluation of its temporal, environmental and tectonic significance. *Chemical Geology*, **362**, 232–249, http://dx.doi.org/10.1016/j.chemgeo.2013.08.002.

Duke, W.L., Arnott, R.W.C. & Cheel, R.J. 1991. Shelf sandstones and hummocky cross-stratification: New insights into a stormy debate. *Geology*, **19**, 625–628.

Dumas, S. & Arnott, R.W.C. 2006. Origin of hummocky and swaley cross-stratification—the controlling influence of unidirectional current strength and aggradation rate. *Geology*, **34**, 1073–1076.

El-ghali, M.A.K. 2005. Depositional environments and sequence stratigraphy of the paralic glacial, para-glacial and postglacial Upper Ordovician siliciclastic deposits of the Murzuq Basin, SW Libya. *Sedimentary Geology*, **177**, 145–173.

Etienne, J.L., Allen, P.A., Rieu, R. & Le Guerroué, E. 2007. Neoproterozoic glaciated basins: A critical review of the Snowball Earth hypothesis by comparison with Phanerozoic glaciations. *In*: Hambrey, M.J., Christoffersen, P., Glasser, N.F. & Hubbard, B. (eds) *Glacial Sedimentary Processes and Products*. Blackwell, Oxford, 343–399.

Eyles, N. & Januszczak, N. 2007. Syntectonic subaqueous mass flows of the Neoproterozoic Otavi Group, Namibia: Where is the evidence of global glaciation? *Basin Research*, **19**, 179–198.

Fanning, C.M. & Link, P.K. 2006. Constraints on the timing of the Sturtian glaciogene event from southern Australia; i.e. for the true Sturtian. *Geological Society of America, Abstracts with Programs*, **38**, 115.

Forbes, B.G. 1970. Benda Siltstones. *Geological Survey of South Australia, Quarterly Notes*, **33**, 1–2.

Forbes, B.G. 1989. *Olary Sheet SI54-2. 1:250,000 scale Geological Map and Explanatory Notes*. Primary Industries and Resources South Australia, Adelaide.

Forbes, B.G. & Cooper, R.S. 1976. The Pualco Tillite of the Olary region, South Australia. *Geological Survey of South Australia, Quarterly Notes*, **60**, 2–5.

Gradstein, F.M., Ogg, J.G. & Smith, A.G. (eds) 2004. *A Geologic Time Scale*. Cambridge University Press, Cambridge.

Hoffman, P.F. & Schrag, D.P. 2002. The snowball Earth hypothesis: Testing the limits of global change. *Terra Nova*, **14**, 129–155.

Hoffman, P.F., Kaufman, A.J., Halverson, G.P. & Schrag, D.P. 1998. A Neoproterozoic snowball Earth. *Science*, **281**, 1342–1346.

Howchin, W. 1901. Preliminary note on the existence of glacial beds of Cambrian age in South Australia. *Transactions of the Royal Society of South Australia*, **25**, 10–13.

Howchin, W. 1908. Glacial beds of Cambrian age in South Australia. *Quarterly Journal of the Geological Society of London*, **64**, 234–259.

Jobe, Z.R., Lowe, D.R. & Morris, W.R. 2012. Climbing-ripple successions in turbidite systems: Depositional environments, sedimentation rates and accumulation times. *Sedimentology*, **59**, 867–898.

Johnson, A.M. 1970. *Physical Processes in Geology*. Freeman Cooper, San Francisco.

Johnson, H.D. & Baldwin, C.T. 1996. Shallow clastic seas. *In*: Reading, H.G. (ed.) *Sedimentary Environments*. Blackwell, London, 236–286.

Kendall, B., Creaser, R.A. & Selby, D. 2006. Re–Os geochronology of postglacial black shales in Australia: Constraints on the timing of 'Sturtian' glaciation. *Geology*, **34**, 729–732.

Kirschvink, J.L. 1992. Late Proterozoic low-latitude glaciation: The snowball Earth. *In*: Schopf, J.W. & Klein, C. (eds) *The Proterozoic Biosphere*. Cambridge University Press, Cambridge, 51–52.

Kneller, B.C. & Branney, M.J. 1995. Sustained high-density turbidity currents and the deposition of thick massive sands. *Sedimentology*, **42**, 607–616.

Kuenen, P.H. 1966. Experimental turbidite lamination in a circular flume. *Journal of Geology*, **74**, 523–545.

Kuenen, P.H. & Humbert, F.L. 1969. Grain size of turbidite ripples. *Sedimentology*, **13**, 253–261.

Legros, F. 2002. Can dispersive pressure cause inverse grading in grain flows? *Journal of Sedimentary Research*, **72**, 166–170.

Le Heron, D.P. 2012. The Cryogenian record of glaciation and deglaciation in South Australia. *Sedimentary Geology*, **243-244**, 57–69.

Le Heron, D.P., Cox, G.M., Trundley, A.E. & Collins, A. 2011*a*. Sea ice-free conditions during the Sturtian glaciation (early Cryogenian), South Australia. *Geology*, **39**, 31–34.

Le Heron, D.P., Cox, G.M., Trundley, A.E. & Collins, A. 2011*b*. Two Cryogenian glacial successions compared: Aspects of the Sturt and Elatina sediment records of South Australia. *Precambrian Research*, **186**, 147–168.

Le Heron, D.P., Busfield, M.E. & Collins, A.S. 2013*a*. Bolla Bollana boulder beds: A Neoproterozoic trough mouth fan in South Australia? *Sedimentology*, first published online December 17, 2013, http://dx.doi.org/10.1111/sed.12082.

Le Heron, D.P., Busfield, M.E., Le Ber, E. & Kamona, A.F. 2013*b*. Neoproterozoic ironstones in northern Namibia: Biogenic precipitation and Cryogenian glaciation. *Palaeogeography, Palaeoclimatology, Palaeoecology*, **369**, 48–57.

Link, P.K. & Gostin, V.A. 1981. Facies and paleogeography of Sturtian glacial strata (late Precambrian), South Australia. *American Journal of Science*, **281**, 353–374.

Lottermoser, B.G. & Ashley, P.M. 2000. Geochemistry, petrology and origin of Neoproterozoic ironstones in the eastern part of the Adelaide Geosyncline, South Australia. *Precambrian Research*, **101**, 49–67.

Major, J.J. & Iverson, R.M. 1999. Debris-flow deposition: Effects of pore-fluid pressure and friction concentrated at flow margins. *Geological Society of America Bulletin*, **111**, 1424–1434.

Maltman, A. 1994. *The Geological Deformation of Sediments*. Chapman & Hall, Cambridge.

Mawson, D. 1941. Middle Proterozoic sediments in the neighbourhood of Copley. *Transactions of the Royal Society of South Australia*, **65**, 304–311.

Mawson, D. 1949. Sturt tillite of Mount Jacob and Mount Warren Hastings, north Flinders Ranges. *Transactions of the Royal Society of South Australia*, **72**, 244–251.

Mawson, D. & Sprigg, R.C. 1950. Subdivision of the Adelaide System. *Australian Journal of Science*, **13**, 69–72.

Middleton, G.V. & Hampton, M.A. 1973. Sediment gravity flows: mechanisms of flow and deposition. *In:* Middleton, G.V. & Bouma, A.H. (eds) *Turbidites and Deep-water Sedimentation*. SEPM Pacific Section, Short Course Lecture Notes, 1–38.

Ó'Cofaigh, C., Andrews, J.T., Jennings, A.E., Dowdeswell, J.A., Hogan, K.A., Kilfeather, A.A. & Sheldon, C. 2012. Glacimarine lithofacies, provenance and depositional processes on a West Greenland trough-mouth fan. *Journal of Quaternary Science*, **28**, 13–26.

Pedersen, S.A.S. 2012. Glaciodynamic sequence stratigraphy. *In*: Huuse, M., Redfern, J., Le Heron, D.P., Dixon, R.J., Moscariello, A. & Craig, J. (eds) *Glaciogenic Reservoirs and Hydrocarbon Systems*. Geological Society, London, Special Publications, **368**, 29–51.

Phillips, E. 2006. Micromorphology of a debris flow deposit: Evidence of basal shearing, hydrofacturing, liquefaction and rotational deformation during emplacement. *Quaternary Science Reviews*, **25**, 720–738.

Postma, G., Nemec, W. & Kleinspehn, K.L. 1988. Large floating clasts in turbidites—a mechanism for their emplacement. *Sedimentary Geology*, **58**, 47–61.

Powell, R.D. & Cooper, J.M. 2002. A glacial sequence stratigraphic model for temperate, glaciated continental shelves. *In*: Dowdeswell, J.A. & O'Cofaigh, C. (eds) *Glacier-Influenced Sedimentation on High-Latitude Continental Margins*. Geological Society, London, Special Publications, **203**, 215–244.

Preiss, W.V. 1987. A synthesis of palaeogeographic evolution of the Adelaide Geosyncline. *In*: Preiss, W.V. (ed.) *The Adelaide Geosyncline. Late Proterozoic Stratigraphy, Sedimentation, Palaeontology and Tectonics*. Geological Survey of South Australia, Bulletin, **53**, 315–409.

Preiss, W.V. 1995. Delamerian Orogeny. *In*: Drexel, J.F. & Preiss, W.V. (eds) *The Geology of South Australia. Vol. 2, The Precambrian*. Geological Survey of South Australia, Bulletin, **54**, 45–57.

Preiss, W.V. 1999. *Parachilna Sheet SH54-13. 1:250,000 scale Geological Map and Explanatory Notes*. Primary Industries and Resources South Australia, Adelaide.

Preiss, W.V. 2000. The Adelaide Geosyncline of South Australia and its significance in Neoproterozoic continental reconstruction. *Precambrian Research*, **100**, 21–63.

Preiss, W.V., Belperio, A.P., Cowley, W.M. & Rankin, L.R. 1993. Neoproterozoic. *In*: Drexel, J.F., Preiss, W.V. & Parker, A.J. (eds) *The Geology of South Australia. Vol. 1, The Precambrian*. Geological Survey of South Australia, Bulletin, **54**, 171–203.

Preiss, W.V., Dyson, I.A., Reid, P.W. & Cowley, W.M. 1998. Revision of lithostratigraphic classification of the Umberatana Group. *MESA Journal*, **9**, 36–42.

Preiss, W.V., Gostin, V.A., McKirdy, D.M., Ashley, P.M., Williams, G.E. & Schmidt, P.W. 2011. The glacial succession of Sturtian age in South Australia: The Yudnamutana Subgroup. *In*: Arnaud, E., Halverson, G.P. & Shields-Zhou, G. (eds) *The Geological Record of Neoproterozoic Glaciations*. Geological Society, London, Memoirs, **36**, 701–712.

Proust, J.N. & Deynoux, M. 1994. Marine to non-marine sequence architecture of an intracratonic glacially-related basin. Late Proterozoic of the West African platform in western Mali. *In*: Deynoux, M., Miller, J.M.G., Domack, E.W., Eyles, N., Fairchild, I.J. & Young, G.M. (eds) *The Earth's Glacial Record: Facies Models and Geodynamic Evolution*. Cambridge University Press, Cambridge, 121–145.

Sumner, E.J., Amy, L. & Talling, P.J. 2008. Deposit structure and processes of sand deposition from a decelerating sediment suspension. *Journal of Sedimentary Research*, **78**, 529–547.

Talling, P.J., Masson, D.G., Sumner, E.J. & Malgesini, G. 2012. Subaqueous sediment density flows: Depositional processes and deposit types. *Sedimentology*, **59**, 1937–2003.

Young, G.M. & Gostin, V.A. 1988. Stratigraphy and sedimentology of Sturtian glaciogenic deposits in the western part of the North Flinders Basin, South Australia. *Precambrian Research*, **39**, 151–170.

Young, G.M. & Gostin, V.A. 1989. An exceptionally thick upper Proterozoic (Sturtian) glacial succession in the Mount Painter area, South Australia. *Geological Society of America Bulletin*, **101**, 834–845.

Young, G.M. & Gostin, V.A. 1990. Sturtian glacial deposition in the vicinity of the Yankaninna Anticline, North Flinders Basin, South Australia. *Australian Journal of Earth Sciences*, **37**, 447–458.

Young, G.M. & Gostin, V.A. 1991. Late Proterozoic (Sturtian) succession of the North Flinders Basin, South Australia; An example of temperate glaciation in an active rift setting. *In*: Anderson, J.R. & Ashley, G.M. (eds) *Glacial Marine Sedimentation: Palaeoclimatic Significance*. Geological Society of America, Special Papers, **261**, 207–222.

Received 4 June 2013; revised typescript accepted 31 October 2013.
Scientific editing by Philip Hughes.

5. Western USA

5.1. Introduction

The Death Valley region in eastern California is home to some of the thickest and most sedimentologically diverse 'Sturtian' equivalent strata in the Neoproterozoic record. In tandem with other Cryogenian sequences, the succession records two glacial intervals, although the preservation of the younger 'Marinoan' horizon is extremely variable (Mrofka & Kennedy, 2011; Petterson et al., 2011). Unusually, by comparison to other Cryogenian sequences worldwide, both horizons occur within the same stratigraphic unit: the Kingston Peak Formation. Traditionally this formation has been subdivided into four constituent units, numbered sequentially KP1-4 (Prave, 1999; Macdonald et al., 2013). It is now widely recognised that KP1 is a pre-glacial succession, with some authors advocating re-assignment to the underlying (Beck Spring Dolomite) depositional cycle (Macdonald et al., 2013). KP2 and KP3 represent the most widespread evidence of glaciogenic deposition, considered equivalent to the 'Sturtian' interval, whilst the younger 'Marinoan' occurs as laterally impersistent outcrops of the KP4, and is more prevalent in the neighbouring Panamint Range (Petterson et al., 2011).

The Kingston Peak Formation is considered to have been deposited in a glaciomarine environment beyond the grounded ice margin (Hazzard, 1939; Wright et al., 1976; Miller, 1985; Mrofka & Kennedy, 2011), although arguments have been made favouring deposition via terrestrial fanglomerates (Mrofka & Kennedy, 2011), whilst others dispute its glacial origin (Troxel, 1982). Considering the vast thickness and exceptional exposure of these sedimentary rocks, surprisingly few studies have attempted detailed sedimentological analysis, with many authors concentrating on the broader scale stratigraphy and geological mapping (e.g. Macdonald et al., 2013). As such, vast quantities of the Kingston Peak Formation await detailed analysis.

This chapter includes three studies of the Kingston Peak Formation, two in its type area of the Kingston Range (Chapter 5.2, 5.3) and one at the Sperry Wash section in a neighbouring outcrop belt (Chapter 5.4). These studies permit the broad spectrum of glaciomarine depositional environments in the Death Valley region to be characterised in detail, alongside an assessment of glacier advance-retreat cyclicity (Chapter 5.2), the controls modulating the distribution of ice-rafted debris throughout the ice catchment to be explored (Chapter 5.3), and the sedimentological and structural characteristics of an archetypal glacial advance sequence to be examined (Chapter 5.4). Cumulatively, they enable generation of detailed palaeoenvironmental reconstructions of the glaciated basin, alongside inferences on the topographic controls on ice mass scale and behaviour.

5.2. Proximal glacier-fed shelf, northern Kingston Range

Neoproterozoic ice sheets and olistoliths: multiple glacial cycles in the Kingston Peak Formation, California

Le Heron, D.P., Busfield, M.E. and Prave, A.R.

Journal of the Geological Society 2014b, v. 171, 525-538.
doi:10.1144/jgs2013-130

Statement of contribution

- ***Data collection***
  - Busfield and Le Heron logged all studied sections, collected palaeocurrent and structural data, and sampled deformed horizons for thin section analysis. Preliminary facies association schemes were developed by Busfield and Le Heron in the field, alongside early ideas on olistolith emplacement during a glacial minimum.
  - Prave shared the location of several of the studied sections, through both grid co-ordinates and directing Busfield and Le Heron to the sections in person.
  - Busfield described and interpreted the thin sections. Le Heron mapped the outcrops using field data and satellite imagery (Google Earth).
- ***Manuscript text***
  - Busfield and Le Heron further developed the preliminary facies association schemes and their glaciological significance, and honed the model of glacial retreat and isostatic rebound driving olistolith remobilisation.
  - Le Heron authored the first draft of the manuscript, and several iterations occurred between Busfield and Le Heron.
  - Prave offered detailed reviews on the first draft of the manuscript, suggesting a removal of earlier sequence stratigraphic analyses, and a more detailed focus on the sedimentology instead. Le Heron and Busfield modified the text following these suggestions.
- ***Figures***
  - Le Heron illustrated Figures 1-2, 6 and 9. Busfield illustrated Figures 3F and 8.
  - Le Heron and Busfield contributed photographs to figures throughout.

Journal of the Geological Society, London, Vol. **171**, 2014, pp. 525–538. http://dx.doi.org/10.1144/jgs2013-130
Published *Online First* on May 28, 2014

Neoproterozoic ice sheets and olistoliths: multiple glacial cycles in the Kingston Peak Formation, California

DANIEL P. LE HERON[1*], MARIE E. BUSFIELD[1] & ANTHONY R. PRAVE[2]
[1]*Department of Earth Sciences, Queen's Building, Royal Holloway University of London, Egham TW20 0BY, UK*
[2]*Department of Earth and Environmental Sciences, University of St. Andrews, St. Andrews KY16 9AL, UK*
**Corresponding author (e-mail: daniel.le-heron@rhul.ac.uk)*

Abstract: The Kingston Peak Formation is a diamictite-bearing succession that crops out in the Death Valley region, California, USA. An exceptionally thick (>1.5 km) outcrop belt in its type area (the Kingston Range) provides clear insights into the dynamics of mid-Cryogenian ('Sturtian') ice sheets in Laurentia. Seven detailed logs allow the lateral and vertical distribution of facies associations to be assessed. We recognize (1) diamictite facies association (ice-proximal glacigenic debris flows), (2) lonestone-bearing facies association (ice-marginal hemipelagic deposits and low-density gravity flows with iceberg rafting), (3) pebble to boulder conglomerate facies association (ice-proximal cogenetic glacigenic debris flows and high-density turbidites), (4) megaclast facies association (olistostrome and hemipelagic sediments subject to ice-rafting), and (5) interbedded heterolithics facies association (low-density turbidites and hemipelagic deposits). The stratigraphic motif allows three glacial cycles to be inferred across the range. Ice-minimum conditions interrupting the Kingston Peak succession are associated with the development of an olistostrome complex, succeeded by a thick accumulation of boulder conglomerates deposited during ice readvance. The data testify to a strong glacial influence on sedimentation within this ancient subaqueous succession, and to highly dynamic ice sheet behaviour with clear glacial cycles during the Sturtian glaciation.

The snowball Earth hypothesis (Hoffman *et al.* 1998) postulates that pan-global ice sheets covered the Earth's surface at multiple intervals in the Cryogenian (850–635 Ma), traditionally correlated to an older 'Sturtian' and younger 'Marinoan' glaciation. Evidence for a 'hard' snowball Earth has become difficult to support in recent years, as evidence has emerged of highly dynamic ice sheets, including evidence for open water (e.g. Leather *et al.* 2002; Arnaud 2004; Allen & Etienne 2008; Le Heron *et al.* 2011). The extent to which Neoproterozoic ice sheets mirrored the behaviour of their Phanerozoic counterparts has remained hotly debated (Etienne *et al.* 2007). However, detailed study of the sedimentary architecture of many Cryogenian glacial successions is long overdue. Such studies provide insight into Earth surface environments during the Cryogenian, shedding light on the scale and intensity of glacial cycles, and, importantly, the link between the break-up of the Rodinia supercontinent and glaciation (Eyles & Januszczak 2004).

Although the task is important, determining the dimensions and behavioural characteristics of Neoproterozoic ice sheets is challenging. The snowball Earth hypothesis (Hoffman *et al.* 1998) requires globally extensive ice, yet the location of ice sheet grounding lines remains poorly defined. In the Death Valley region, California, the 'Sturtian'-equivalent Kingston Peak Formation is commonly interpreted as the product of glaciomarine deposition beyond the grounded ice margin (Hazzard 1939; Wright *et al.* 1974; Miller 1985; Mrofka & Kennedy 2011), although a solely glacial derivation is not accepted by all (e.g. Troxel 1982). Outcrop belts have been tectonically dismembered by Tertiary extensional deformation but single fault blocks can be reconstructed to reveal laterally and vertically variable lithofacies assemblages comprising strata that include several kilometres of turbidites, diamictites of mass-flow affinity and boulder-size lonestones (Troxel 1982; Miller 1985, 1987; Prave 1999; Mrofka & Kennedy 2011), many interpreted as dropstones (Abolins *et al.* 2000; Corsetti & Kaufman 2003).

This paper provides a thorough sedimentological analysis of the Kingston Peak Formation in its type area, the Kingston Range (Fig. 1), and includes detailed descriptions of facies and facies associations, documents their distribution in map view, and presents a glacial depositional model for their accumulation. In doing so we propose three glacial cycles within the mid-Cryogenian succession, and offer a refined interpretation for the origin of kilometre-scale megaclasts. This study therefore provides a stratigraphic framework to facilitate comparison with other 'Sturtian' sequences elsewhere in the Cordillera.

Study area and lithostratigraphy

The Kingston Range exposes a superb outcrop belt of the Kingston Peak Formation, a 300–2400 m thick heterolithic, predominantly siliciclastic succession preserving a record of Cryogenian glaciation (Fig. 1). The Kingston Peak Formation overlies microbial carbonates of the Beck Spring Dolomite and is truncated by the Noonday Dolomite (Fig. 1). Following on from the mapping of Wright and Troxel and their colleagues (as synthesized in Calzia *et al.* 2000), Prave (1999) applied a fourfold subdivision of the Kingston Peak Formation, with units termed KP1–KP4. KP1 is now known to be genetically unrelated to the glaciogenic portion of the Kingston Peak Formation (Prave 1999; Macdonald *et al.* 2013), and is thus excluded from this study. Units KP2 and KP3 account for almost all the remaining stratigraphy in the Kingston Peak Formation across the southern Death Valley region and the Kingston Range (Macdonald *et al.* 2013), with only thin, patchy development of the fourth unit termed KP4. Units KP2 and KP3 are tentatively assigned to an older Cryogenian ('Sturtian') glaciation, and KP4 is attributed to the younger Cryogenian ('Marinoan') glaciation (Prave 1999; Petterson *et al.* 2011*a*,*b*; Macdonald *et al.* 2013), with an interglacial stratigraphy well developed in the Panamint Range (Miller 1985; Petterson *et al.* 2011*b*). Although

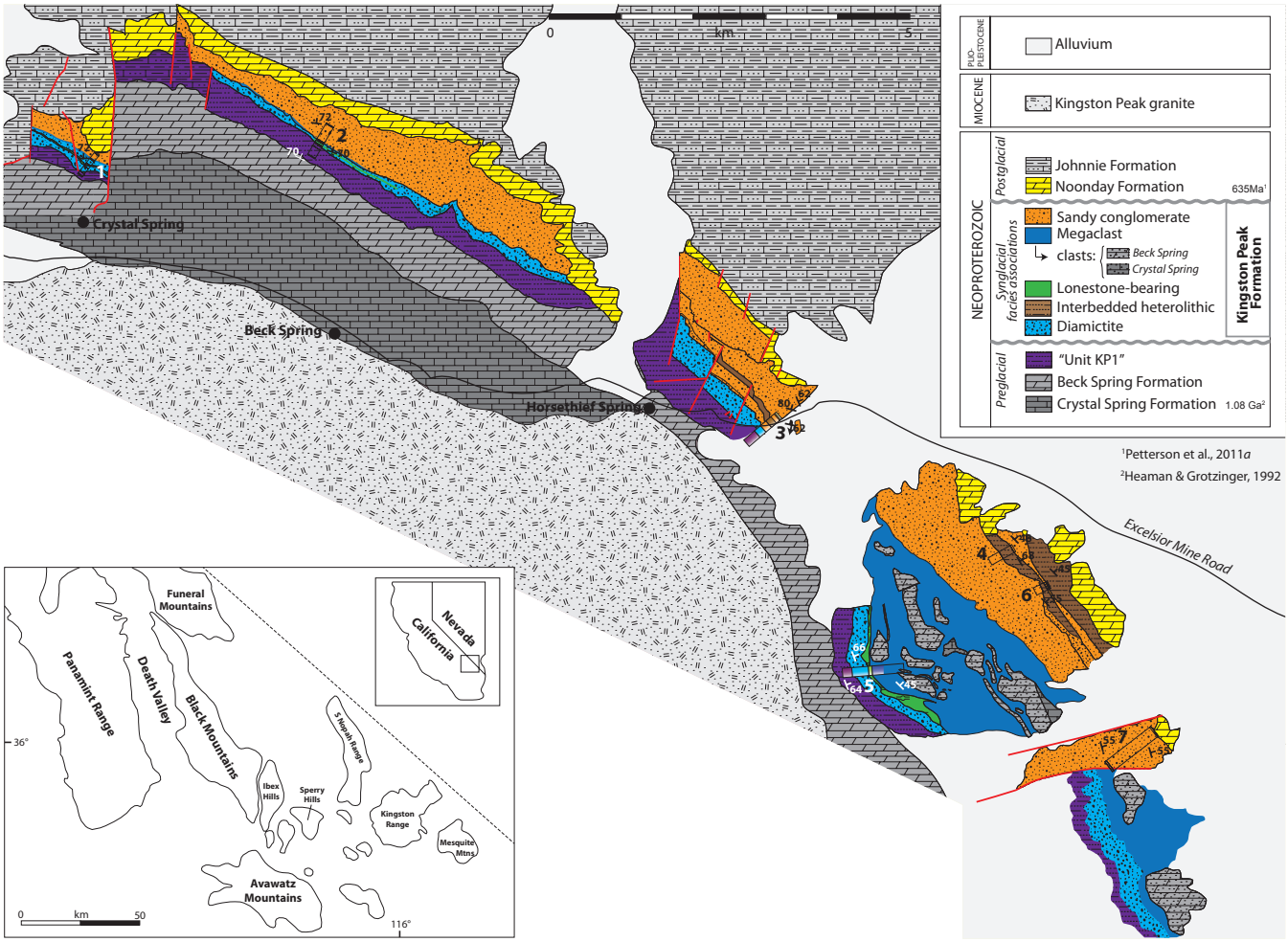

Fig. 1. Geological map of the NE Kingston Range, compiled from field observations in concert with satellite image interpretation. Distribution of the olistoliths in the vicinity of section 5 is after Macdonald *et al.* (2013). The map shows the distribution of those facies associations described and interpreted in this paper. Stratigraphic dips of the Beck Spring Dolomite and the overlying Kingston Peak Formation fan around the periphery of the granite intrusion that dominates the range. The substantial lateral thickness variations of the Kingston Peak Formation, with a general increase toward the SE, should be noted. This trend is interrupted by a comparatively reduced thickness in the vicinity of the Horsethief Spring (section 3), where en echelon faults transecting the succession can be clearly observed. Inset map shows the location of the Kingston Range in its regional context.

absolute age dates are lacking, carbon isotope stratigraphy of the overlying Noonday Dolomite is closely comparable with basal Ediacaran cap carbonates worldwide, dated at 635 Ma (Kennedy *et al.* 1998; Prave 1999; Corsetti & Kaufman 2003; Petterson *et al.* 2011*a*,*b*; Macdonald *et al.* 2013), and the work of Petterson *et al.* (2011*a*,*b*) supports strongly the inference that it is the younger Cryogenian (Marinoan) cap. Other stratigraphies have been proposed but these are variations on the overall framework noted above. For example, Mrofka (2010) proposed subdividing the Kingston Peak Formation into, from the base up, the Saratoga Hills Sandstone (KP1), the Alexander Hills Diamictite (KP2), the Silver Rule Mine Member (basal KP3) and the Jupiter Mine Member (upper KP3). Macdonald *et al.* (2013) highlighted the likely linkages between the Death Valley succession and those elsewhere in western Laurentia and defined four inter-regionally developed, unconformity-bound tectonostratigraphic units (TU1–4) as a means of establishing a craton-margin stratigraphic framework. The present paper deals almost exclusively with rocks contained within units KP2 and KP3, which are components of TU3a and TU3b of Macdonald *et al.* (2013).

In the vicinity of section 3 at Horsethief Spring (Fig. 1), the outcrop belt is cut by a series of en echelon, NE–SW-trending faults.

Fig. 2. Correlation panel for seven detailed sections (locations shown in Fig. 1). This NW–SE traverse is hung from the Noonday Dolomite as a datum. The top of measured section 5 is at least 1 km stratigraphically below the Noonday Dolomite (see Fig. 1) and thus the total thickness of the Kingston Peak Formation is at least 1200 m in this part of the range. The apparent continuity of the lonestone-bearing facies association is arrested by truncation beneath a thick accumulation of boulder conglomerates (section 2). Co-ordinates of sections are as follows: (1) 35°47.924′N, 115°57.773′W (base), 35°48.074′N, 115°57.673′W (top and Noonday contact); (2) 35°47.795′N, 115°55.628′W (base Kingston Peak Fm), 35°48.253′N, 115°55.635′W (top; base of Noonday); (3) 35°46.201′N, 115°52.577′W (base), 35°46.315′N, 115°52.207′W (top); (4) 35°45.489′N, 115°50.603′W (base), 35°45.528′N, 115°50.497′W (top); (5) 35°44.810′N, 115°51.612′W (base of diamictite), 35°44.843′N, 115°51.137′W (top of olistolith); (6) 35°45.282′N, 115°50.053′W (top), 35°45.235′N, 115°50.167′W (base); (7) 35°44.034′N, 115°49.325′W (base and contact with olistolith), 35°44.291′N, 115°49.057′W (top and Noonday contact).

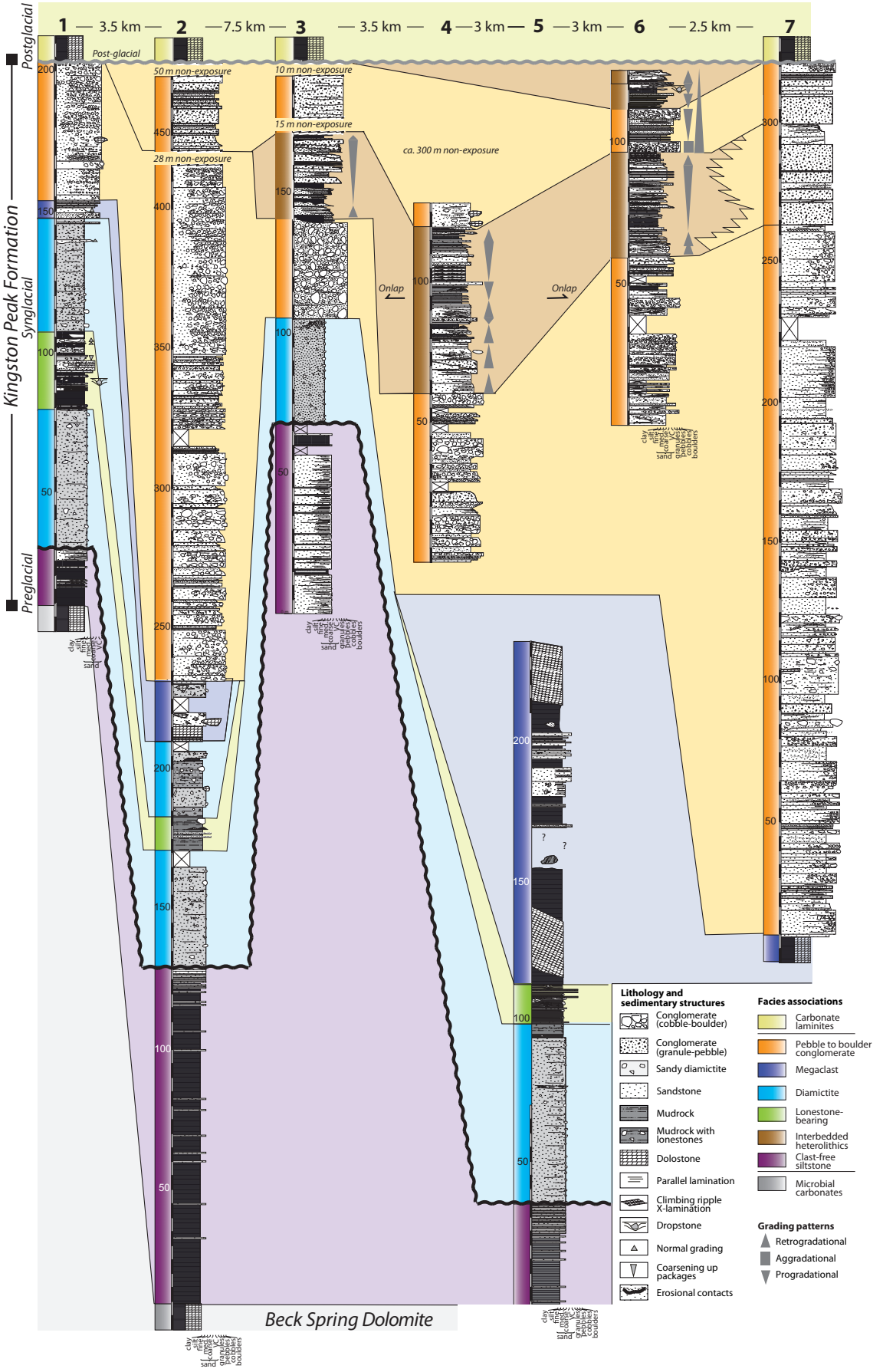

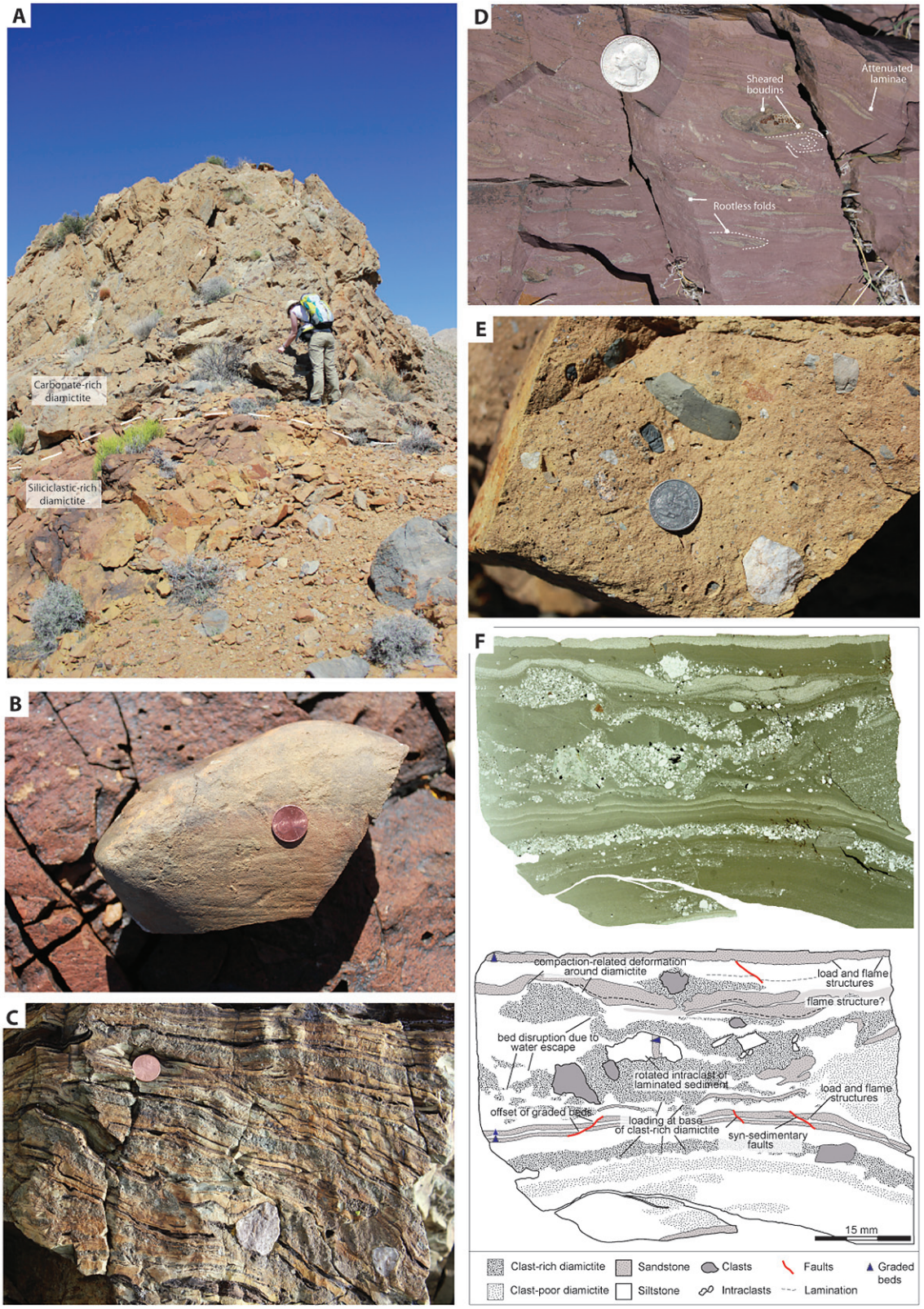

Fig. 3. Aspects of the diamictite facies association. (**a**) Interbedded carbonate-rich and siliciclastic-rich diamictites on the multi-metre scale (section 1, 60–65 m, Fig. 2). (**b**) Typical example of a striated cobble from the Kingston Peak Formation, collected from *c*. 40 m from the base of section 1. Striated clasts are very common, and were recovered from each studied outcrop of this facies association. (**c**) Stratified diamictite with 2 cm diameter lonestones (section 5, 45 m, Fig. 2). (**d**) Stratified diamictite composed of highly attenuated laminae in the brown strata and showing intercalations of granular and clast-free siltstone horizons on the centimetre scale (section 5, 46 m, Fig. 2). (**e**) Fresh face of massive diamictites (section 3, 90 m, Fig. 2). (**f**) Thin-section micromorphology of the stratified diamictite facies (section 5, 48 m, Fig. 2).

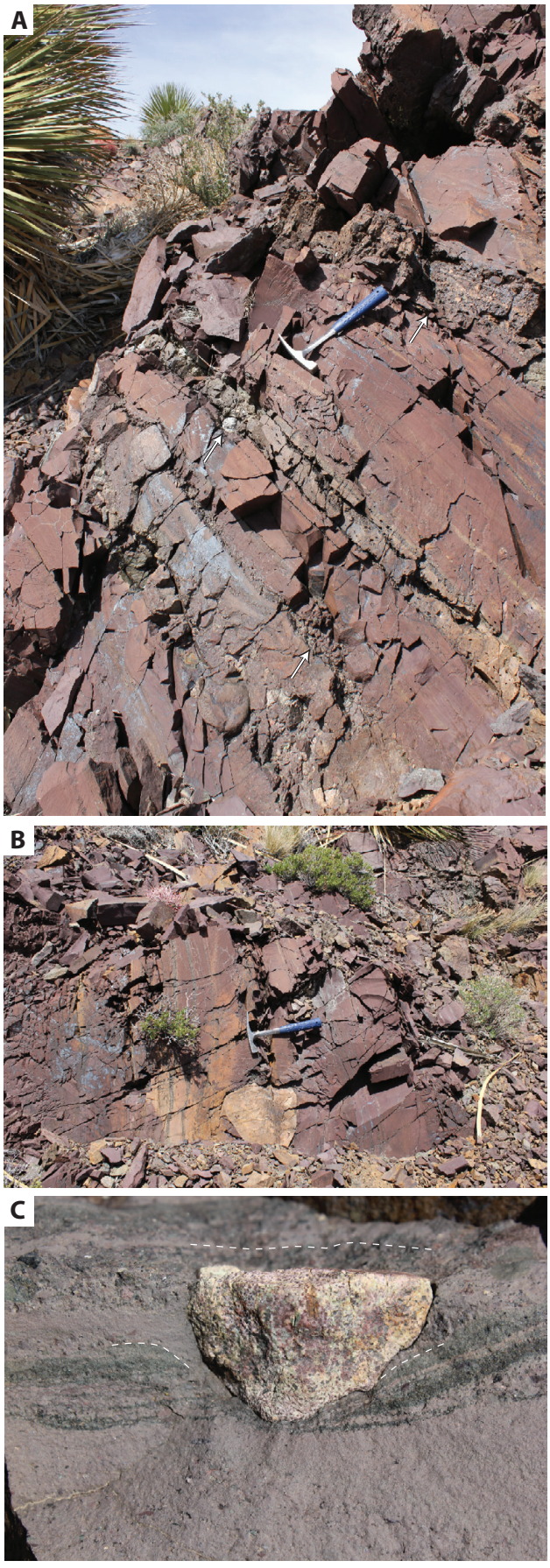

Some of these faults were active during sedimentation, evidenced by the abrupt termination of some facies against them, as well as thickness increases of others across them. They are interpreted as an array of normal faults that essentially partitioned the basin into horst–graben structures (Fig. 1, section 3) superimposed on the regional southward dipping palaeoslope. Studied sections were carefully examined away from these fault surfaces to avoid stratigraphic repetition and fault-related deformation.

Facies analysis

The high degree of lateral and vertical continuity of strata across the Kingston Range allows detailed lithofacies analysis. Five lithofacies associations (Fig. 1) are distinguished: (1) diamictite, (2) lonestone-bearing, (3) megaclast, (4) pebble to boulder conglomerate, and (5) interbedded heterolithics facies associations. The following descriptions cross-reference the correlation panel (Fig. 2).

Diamictite facies association: description

These deposits encompass sandy and silty, grey, buff-weathering diamictites, with a range of clast-rich to clast-poor varieties recorded. The diamictite facies association occurs at two stratigraphic levels in the Kingston Range (Fig. 2), locally with uninterrupted stratigraphic thicknesses of up to 65 m (section 5). At the outcrop scale, clear intercalation of carbonate-matrix diamictites with siliciclastic-matrix diamictites is observed (e.g. section 1, Figs 2 and 3a). Clast lithologies include massive and laminated dolostone (Crystal Spring Formation and Beck Spring Dolomite), schist, leucogranite, siltstone (basal Kingston Peak), quartzite, and chloritized diabase. Striated clasts (Fig. 3b) are common.

Interbedded silty, stratified diamictites and sandy, massive diamictites are recognized locally at the metre scale (e.g. section 2, 180–200 m, Fig. 2). The former are typically ungraded and tend towards more clast-poor varieties, but in places preserve lonestones with impact-related deformation structures (Fig. 3c). Finer-grained intervals show intercalations of granular and clast-free siltstone layers on the centimetre scale, where isolated examples of millimetre- to centimetre-scale rootless folds and sheared boudins also occur (Fig. 3d). Massive diamictites (Fig. 3e) are also commonly ungraded, with local evidence of increased clast abundance upsection within single beds. Such intervals also include cut-and-fill geometries, with 2–3 m wide incisions, filled with sandy, massive diamictite truncating silty, stratified varieties (e.g. section 2, 203 m, Fig. 2). Rarely, discrete, erosively based sandstone lenses interrupt massive diamictites (e.g. section 1, 139 m, Fig. 2). Micromorphological investigation reveals comparatively clast-rich and clast-poor stratified diamictites (Fig. 3f), intercalated with 1–2 mm thick graded beds. This approach also reveals normal faults with millimetre-scale throws, flame structures, rotated intraclasts, and the effects of loading or differential compaction beneath clast-rich diamictites (Fig. 3f).

Diamictite facies association: interpretation

Macdonald *et al.* (2013) described unit KP2 as a 'massive diamictite' and unit KP3 as a stratified diamictite, but we emphasize that only

Fig. 4. Aspects of the lonestone-bearing facies association. (**a**) Typical example of a ferruginous facies, with well-stratified siltstones and well-expressed bedding. Pebble trains, defining some of the bed bases, are arrowed. (**b**) Boulder-sized, buff-coloured dolostone clast; an isolated lonestone, without associated pebble train. (**c**) A lonestone downwarping and piercing siltstone laminae beneath it. It should be noted that overlying laminae are undeformed. All examples are from section 5, *c*. 105 m from base (see Fig. 2).

those strata of our diamictite facies association (unit KP2) can texturally be described as diamictite (Moncrieff 1989; Hambrey & Glasser 2003). The massive diamictite lithofacies in this study are interpreted as a series of glacigenic debris flows (GDFs) derived via downslope reworking of inherently unstable sediment delivered to the ice-grounding line (e.g. Elverhøi *et al.* 2002; Ó Cofaigh *et al.* 2002; Benn & Evans 2010). Beds that exhibit inverse grading are interpreted to result from a combination of kinetic sieving and upward clast migration; common processes during laminar sediment remobilization (Bagnold 1954; Talling *et al.* 2012). Erosive contacts and cut-and-fill structures are interpreted to record cannibalization of underlying sediments during repeated sediment gravity flow emplacement. Conversely, the predominance of planar, non-erosive contacts is attributed to hydroplaning during flow emplacement, whereby elevated fluid contents both lubricate and sustain the flow, and simultaneously protect the underlying bed from cannibalization (e.g. Laberg & Vorren 2000). This process also allows greater run-out distances, which may contribute to the absence of subglacial or ice-contact deformation features. Both stratified and massive diamictites are thought to accumulate within the ice-proximal zone, as more distally they would probably undergo flow transformation to more dilute, cogenetic turbidity flows (Hampton 1972; Talling *et al.* 2012). This is consistent with the preservation of clast striations, which would be expected to be removed during clast-on-clast abrasion under prolonged sediment reworking.

Isolated lonestones with impact-related deformation structures are interpreted as iceberg-rafted debris, wherein debris-laden icebergs are released from the ice front, leading to rain-out in the ice-proximal zone as the basal debris layer melts. The diverse size and lithology of ice-rafted clasts is considered more characteristic of iceberg than ice-shelf rafting (Pudsey *et al.* 2006; Reinardy *et al.* 2009; Domack & Hoffman 2011), wherein freeze-on of the basal debris layer would also inhibit widespread rain-out (e.g. Anderson *et al.* 1991; Hambrey & Glasser 2012). In addition, sub-ice shelf diamicton facies are reportedly characterized by numerous intraformational sediment clasts derived through subglacial deformation near the grounding line ('till pellets'; e.g. Domack & Harris 1998; Khatwa & Tulaczyk 2001; Evans & Pudsey 2002), which are absent from the diamictite facies association described herein.

At the outcrop scale, the presence of rootless folds and sheared boudins might be argued to indicate sediment shearing, either in response to ice-sheet grounding (Arnaud 2012, and references therein), or potentially a shearing basal layer in a debris flow (Phillips 2006). At the thin-section scale, the primary source of the stratification is clearly sedimentary, rather than of shear origin, with intercalated clast-rich and clast-poor diamictites on the lamina scale, and graded sandstone laminae. The suite of deformation features (flame structures, load structures, extensional microfaults) is more suggestive of post-depositional loading in concert with local fluid escape. None of the rotational structures characteristic of Sturtian glacitectonites in northern Namibia (Busfield & Le Heron 2013) were observed in the Kingston Range sections.

Lonestone-bearing facies association: description

These deposits are typically thin, ranging in thickness from 12 m (section 5, Fig. 2) to 27 m (section 1, Fig. 2). The dominant lithology is well-stratified grey siltstone and shale, punctuated by 10–20 cm thick sandstone beds, 5–40 cm thick pebbly conglomerate layers, and massive, silty diamictites. The siltstone and shale intervals are well laminated throughout, with isolated examples of current ripple cross-lamination. These intervals bear lonestones, typically of pebble to cobble size, of dolostone, siltstone, quartzite, and rarely chloritized metabasite. In places, clasts occur as bedding-parallel trains of pebbles and cobbles (Fig. 4a), but more commonly as outsized clasts (lonestones) (Fig. 4b). The lonestones typically puncture underlying laminae; overlying laminae are undeformed, draping the lonestones (Fig. 4c).

Lonestone-bearing facies association: interpretation

The well-stratified siltstones and shales are interpreted as hemipelagic deposits, largely derived from fine-grained sediment plumes triggered by associated silt and sand underflows. The latter, including the thick sandstone interbeds and ripple cross-laminated siltstones, are interpreted as the product of dilute, low-density turbidity currents (Bouma T_{c-e}: e.g. Talling *et al.* 2012), where fully turbulent conditions are required for ripple development (Baas *et al.* 2011). Thin beds of massive diamictite are interpreted as glacigenic debris flow deposits, in a similar manner to their thicker counterparts in the diamictite facies association. Lonestones with clear impact structures indicate ice-rafting, with the diversity of clast lithologies indicative of iceberg- as opposed to ice-shelf-rafted debris (Pudsey *et al.* 2006; Reinardy *et al.* 2009; Domack & Hoffman 2011). The finer-grained nature of the host sediments, and greater abundance of dilute turbidites than their less evolved cogenetic debrites supports accumulation in an ice-marginal setting, rather than the ice-proximal setting of the diamictite facies association.

Pebble to boulder conglomerate facies association: description

These deposits are dominated by clast- and matrix-supported conglomerates with a sandy matrix, with uninterrupted stratigraphic thicknesses that can be as much as >250 m (e.g. section 7, Fig. 2). The total thickness of the facies association is highly variable across the range, not exceeding 40 m at section 3 (Fig. 2). Maximum clast size is typically cobble to boulder dimensions (Fig. 5a); we differentiate these from pebbly conglomerates in our logged sections (Fig. 2). Clasts are typically equant to irregular, ranging from angular to rounded, with sub-rounded clasts predominant. Compositionally, clasts are dominated by dolostones derived from the Beck Spring Dolomite, including microbial laminites and crystalline dolostone, with sandstone clasts also common. Bed thicknesses range from *c.* 20 cm to >10 m. Bed contacts are typically diffuse wherein normally graded, finer-grained beds pass vertically into massive, ungraded boulder conglomerates (e.g. section 7, 175 m, Fig. 2). In the same section, both fining- and coarsening-upward motifs are apparent, and are partitioned by clast-poor sandstone (Fig. 5b); otherwise, many beds are structureless at the base, passing upwards into plane-bedded gravels (e.g. section 7, 233 m: Fig. 2). Trough cross-strata are also locally developed at the metre scale, within both pebble conglomerates and intercalated coarse-grained sandstones (Fig. 5c). On the decametre scale, thick packages dominated by stratified, pebbly conglomerates (Fig. 2, section 2, 320–350 m) alternate with cobble- and boulder-dominated units (Fig. 2, section 2, 350–415 m; Fig. 5d).

Pebble to boulder conglomerate facies association: interpretation

This facies association is interpreted as the product of glaciogenic debris flows and associated high-density turbidites. Limited palaeocurrent data from cross strata and cross laminae support southward dipping palaeoslopes. The considerable uninterrupted thickness (>250 m in single sections) testifies to a sustained interval of high sediment influx. The clear differentiation into predominantly cobble- to boulder-bearing beds and pebbly beds implies variations in energy levels or sediment supply, interpreted as the product of pulsed sediment delivery from the ice-grounding line.

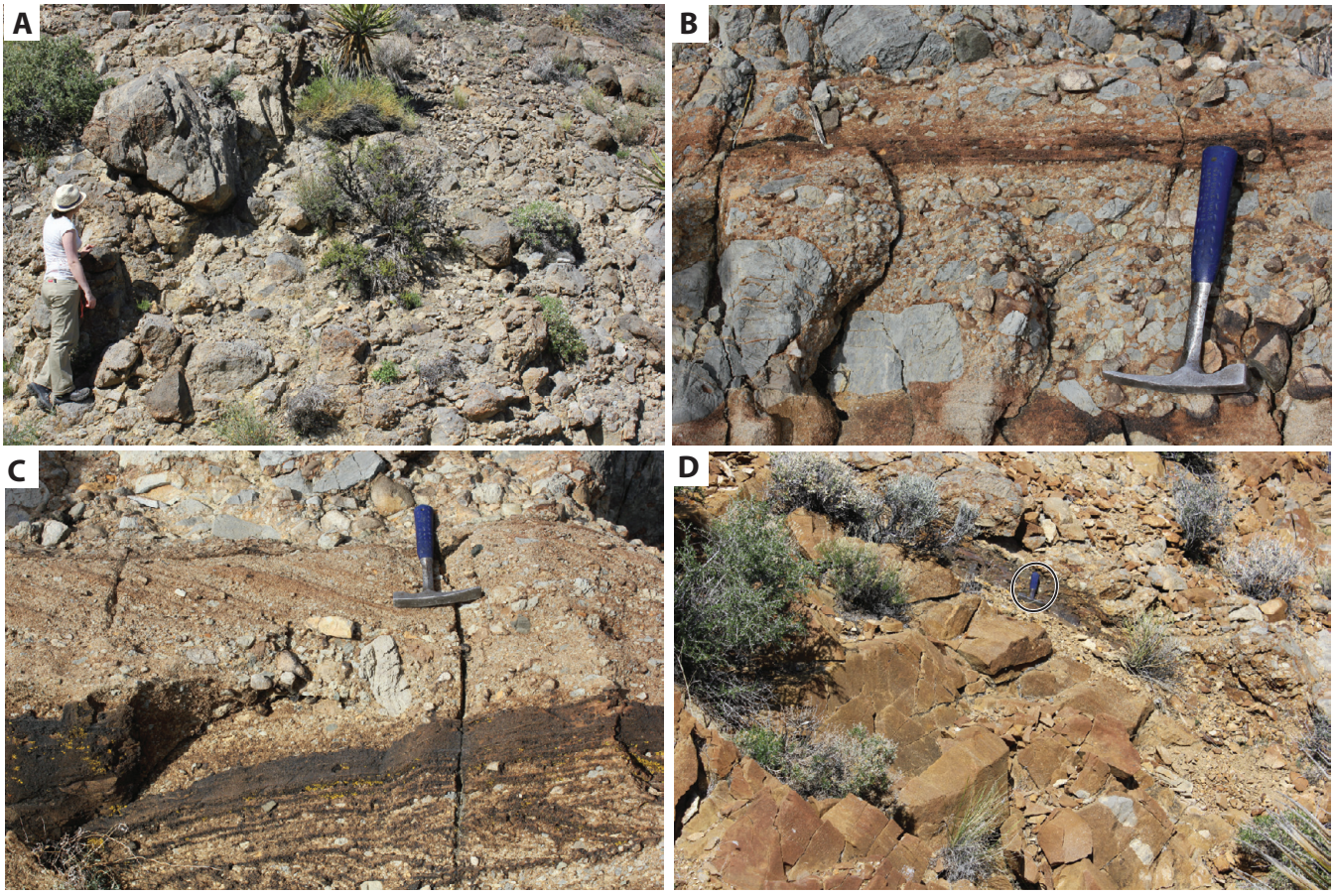

Fig. 5. Boulder conglomerate facies association. (**a**) Boulder conglomerate (110 m on section 3: see Fig. 2 for stratigraphic position). (**b**) Fining-upward motif (approximately delineated by hammer), with an overlying coarsening-upward motif. (**c**) Decimetre-scale trough cross-strata downlapping onto differentially silicified sandstones. (**d**) Dramatic vertical facies shift from conglomerate beds to overlying black, silicified shales and sandstones (113–115 m, section 6).

In this setting, high rates of sedimentation promote instability and repeated slope failure (e.g. Vorren *et al.* 1998; Dimakis *et al.* 2000; Benn & Evans 2010), triggering downslope sediment remobilization. The coarsening-upward, structureless beds are interpreted as debrites, reflecting processes of upward clast migration and kinetic sieving (e.g. Talling *et al.* 2012), as recorded in the diamictite facies association. The clast angularity may imply a short transport interval, although the predominance of sub-rounded clasts underscores the importance of intra-flow clast abrasion. The fining-upwards conglomerates are interpreted as cogenetic high-density turbidites (Hampton 1972; Talling *et al.* 2012). This is supported by the overall absence of bedforms, hindered by both rapid deposition and dampening of turbulence under high sediment concentrations (Talling *et al.* 2012). Both outcrop (Amy & Talling 2006) and experimental approaches increasingly emphasize the cogenetic (bipartite; Tinterri *et al.* 2003) link between turbidity flows and debris flows. This process frequently occurs through transformation of moderate strength debris flows into more dilute ('linked') turbulent flows during mixing with the overlying water body (Talling *et al.* 2012), and commonly occurs within ice-proximal zones under high sedimentation rates (Benn & Evans 2010). This setting is further supported by the occurrence of striated pebbles, reported by Mrofka & Kennedy (2011) and Macdonald *et al.* (2013), which would be unlikely to survive significant reworking and clast abrasion beyond the ice-proximal zone. The cogenetic nature of debrites and turbidites may also account for the diffuse boundaries between beds.

The association of debrites and turbidites is strong evidence that they were deposited in a marine setting. Thus, earlier interpretations of these strata as 'terrestrial fanglomerates' are rejected (Mrofka 2010; Mrofka & Kennedy 2011). It is recognized that high concentrations of boulder-bearing gravels could be produced by terrestrial jökulhlaup outbursts onto sandur plains, associated with catastrophic release of turbulent meltwater (Marren *et al.* 2009). However, these are typically marked by a suite of sedimentary structures such as metre-scale antidunes and megaripples, even in gravels, as a result of sustained flow over several hours or more (Duller *et al.* 2008). These characteristics are lacking in the pebble to boulder conglomerate facies association. Moreover, features characterizing subaerial exposure such as palaeosols (Sheldon & Tabor 2009), desiccation cracks or aeolian deflation surfaces are lacking.

Megaclast facies association: description

This facies association consists of metre- to hundreds-of-metre-scale blocks (megaclasts) that occur at a number of levels over a *c.* 1000 m interval. The scale of the blocks is amply demonstrated in panoramic view (Fig. 6a and b), and the facies association is particularly well expressed in section 5 (Fig. 2). First described by Troxel (1966), the blocks are tabular bodies with highly irregular edges (Figs 2 and 6a, b); most are carbonate lithologies derived from the Crystal Spring Formation and Beck Spring Dolomite, but also comprise arkosic sandstones and granular conglomerates (Fig. 2, section 5, 180–190 m), intensely sheared, carbonate-dominated diamictite beds

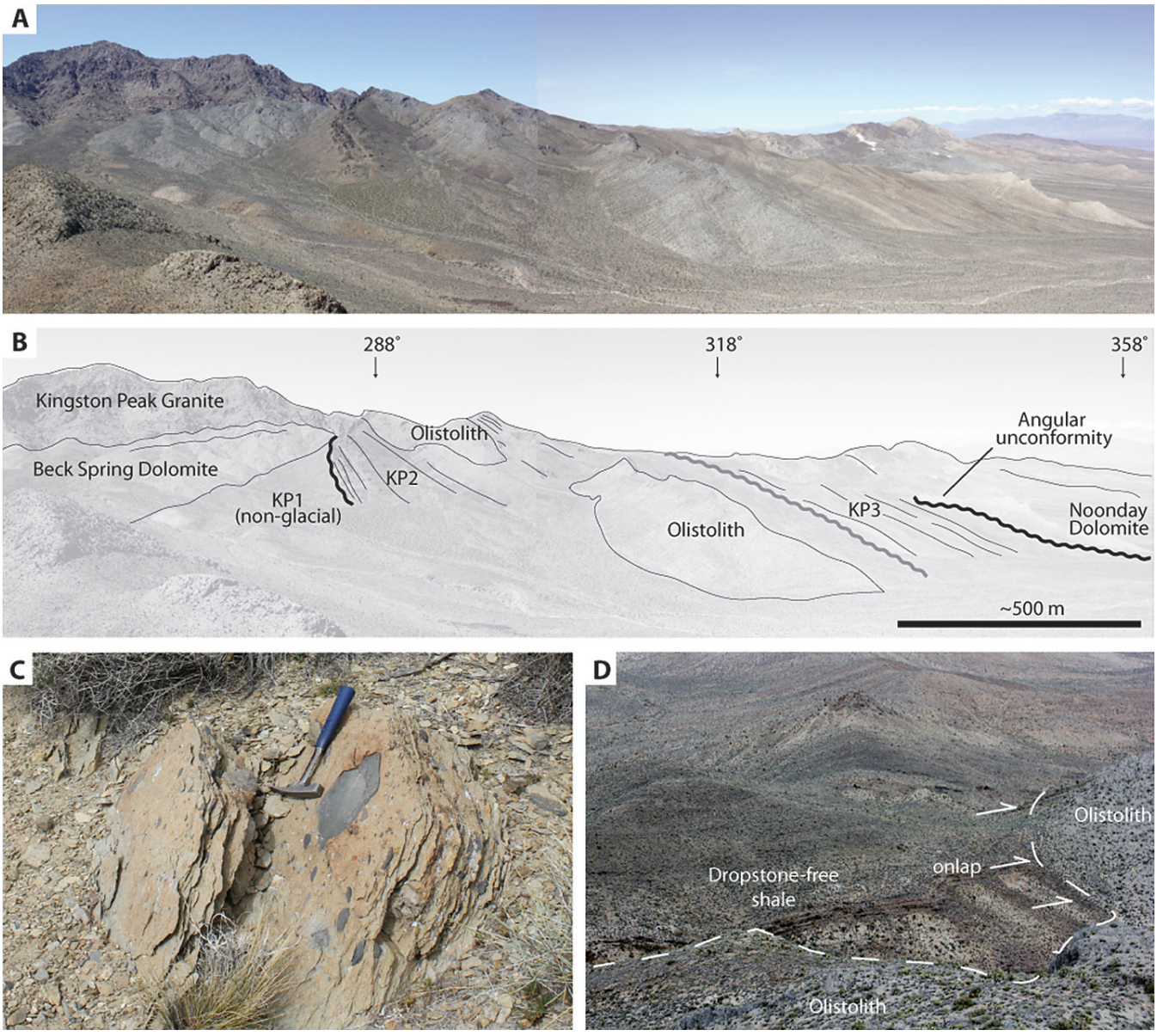

Fig. 6. Megaclast facies association. (**a**) Photograph taken looking north whilst completing log 5, and taken from the top of an olistolith (in foreground, and at 140 m on log: see Fig. 2). Field of view is *c*. 3 km in midground. (**b**) Line drawing over photograph of (**a**), illustrating the geometry of the olistoliths, their blocky character at the kilometre scale, the outcrop width of the olistostrome in general, and the disconnected Noonday Dolomite peaks capping the Kingston Peak Formation in the distance. The shale beds onlapping the cliff-forming olistolith in the middle of the photograph should also be noted. (**c**) Blocky, angular carbonate boulder of the Beck Spring Dolomite (226 m on log 2: see Fig. 2), encased within red siltstone. These deposits are interpreted as lateral equivalents of the olistostrome shown in (**a**) and (**b**). (**d**) Carbonate-rich diamictite, with highly attenuated clasts of Crystal Spring Formation stromatolite. The diamictite is well stratified, with the fabric dipping steeply toward the left of the photograph. (**e**) Arkose megaclast, with hammer for scale. (**f**) Onlap of shale against olistolith. The photograph is an area of detail shown in (**a**) and (**b**).

(Fig. 2, section 5, 157 m; Fig. 6c) and gneissic basement. Internally they commonly comprise coherent beds, some of which are stratigraphically inverted (i.e. upside down; Macdonald *et al.* 2013). Between the blocks, exposure is often poor. In places, however, well-stratified shales are preserved in continuous sections more than 10 m thick (Fig. 2), which onlap single dolostone megaclasts (Fig. 6d).

Megaclast facies association: interpretation

The megaclast facies association is interpreted as an olistostrome (also see Macdonald *et al.* 2013), with the blocks representing constituent olistoliths and the interstitial shale representing background sedimentation. The planform distribution of the blocks (Fig. 1) demonstrates that whereas their strike is approximately bedding-parallel, each is an isolated fragment. Their size and angularity implies a short transport distance, and their source has been proposed to lie a few kilometres to the north of the outcrop belt (Macdonald *et al.* 2013). The presence of stratigraphically inverted olistoliths supports deposition via downlope gravity sliding (Robertson 1977) and toppling, rather than debris flow slumping (Heck & Speed 1987; Wendorff 2005).

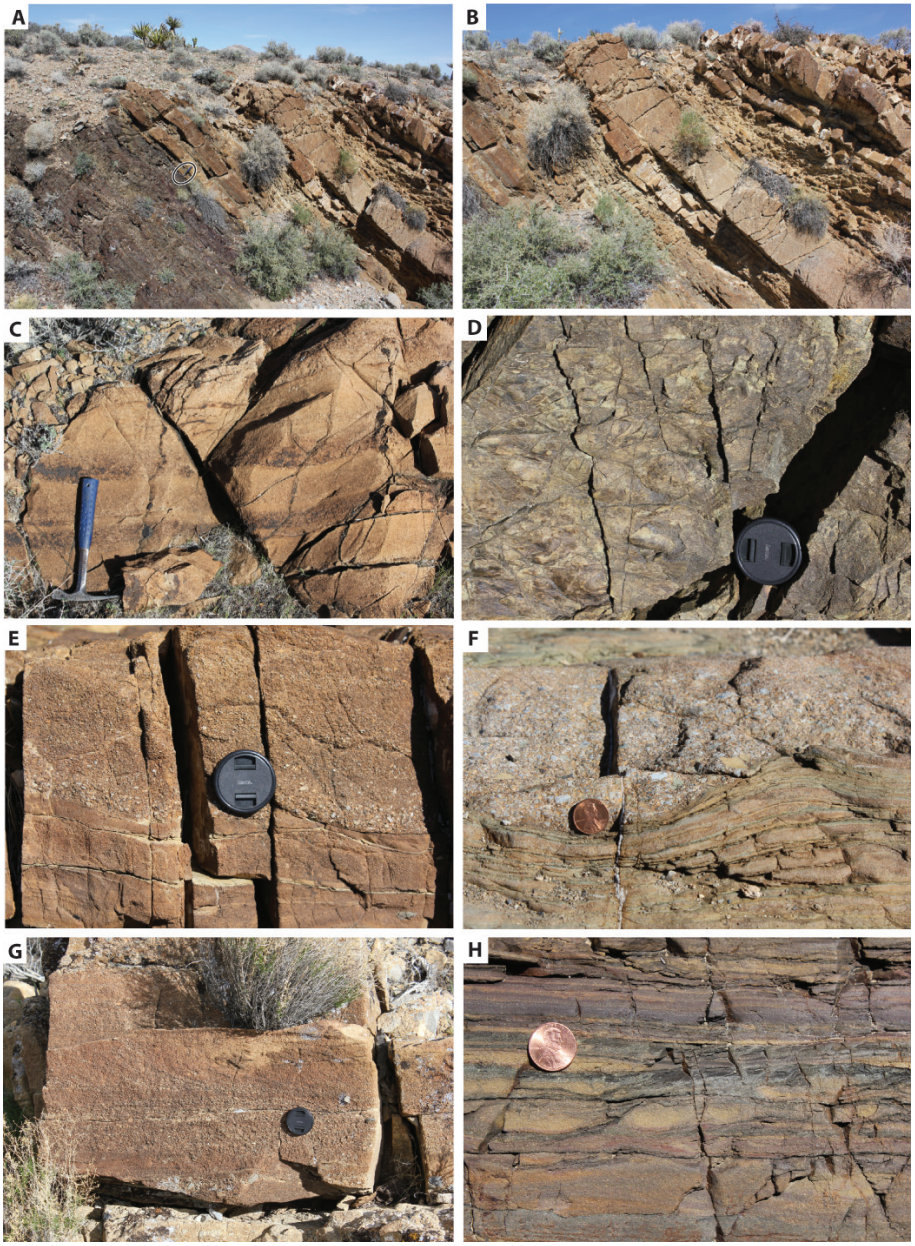

Fig. 7. Interbedded heterolithics facies association. (**a**) Coarsening-upward shales and siltstones to the left of the hammer (circled) and thickening-upward sandstones and conglomerates (right of the hammer). (**b**) Detail of (**a**), with thick sandstone bed clearly showing truncation of underlying strata. (**c**) Stacked fining-upward successions developed in a sandstone package. (**d**) Flute casts at the base of a bed. Palaeocurrent was moving toward 030°. (**e**) Normal grading: fining upward from a granular conglomerate at the base of the lens cap to medium-grained sandstone at the top of the bed. (**f**) Granular conglomerate, with an undulose base, cutting into siltstone. (**g**) Trough-cross stratification in coarse-grained sandstone. (**h**) Interlaminated siltstone (dark grey) and shale (light grey or brown) with low-amplitude load structures in the lamina beneath the coin. (**a**), (**b**) and (**e**–**h**) are from section 6 (60–110 m); (**c**) from section 4 (105–110 m); (**d**) from section 3 (145 m) .

The onlap relationship of the shales against the olistoliths demonstrates that they represent background sedimentation prior to, during, and following olistolith emplacement. Comparable hemipelagic intervals have been encountered in other olistostromes (Heck & Speed 1987). Isolated lonestones within the shale facies are interpreted as ice-rafted debris, suggesting deposition of the olistostrome concurrent with disintegration of the ice front. This process would be expected to destabilize a marine-terminating ice mass, thereby providing a plausible mechanism for inducing catastrophic slope failure. Under this scenario, icebergs may be calved from the ice front, releasing debris into the interstitial shales. An alternative explanation is that the megaclasts are themselves ice-rafted, but the absence of impact-related deformation features within the underlying shales, the sheer scale of the megaclasts, and the evidence for inversion during downslope movement are considered incompatible with this scenario.

It has long been recognized that syndepositional extensional tectonism occurred concomitant with sedimentation (e.g. Prave 1999, and references therein), and is considered to be a key factor in formation of the olistostrome (e.g. Macdonald *et al.* 2013, and references therein). In light of the evidence for ice-rafting accompanying accumulation of the olistoliths, the role of glaciation in triggering their remobilization can be invoked. Prior to deposition, ice cover in the source area of the megaclasts may have contributed to break-up of the bedrock through processes of freeze–thaw, whereby the exploitation of joints by meltwater and permafrost development resulted in *in situ* fracturing. With the overburden of the ice cover, the fractured bedrock would be held in place as tabular blocks. As ice retreated, unloading accompanied by isostatic rebound destabilized the fractured substrate. Therefore, the combined influence of removal of the ice buttress and synsedimentary tectonism, potentially during isostatic rebound, allowed excavation of the fractured substrate, and downslope remobilization of the megaclasts.

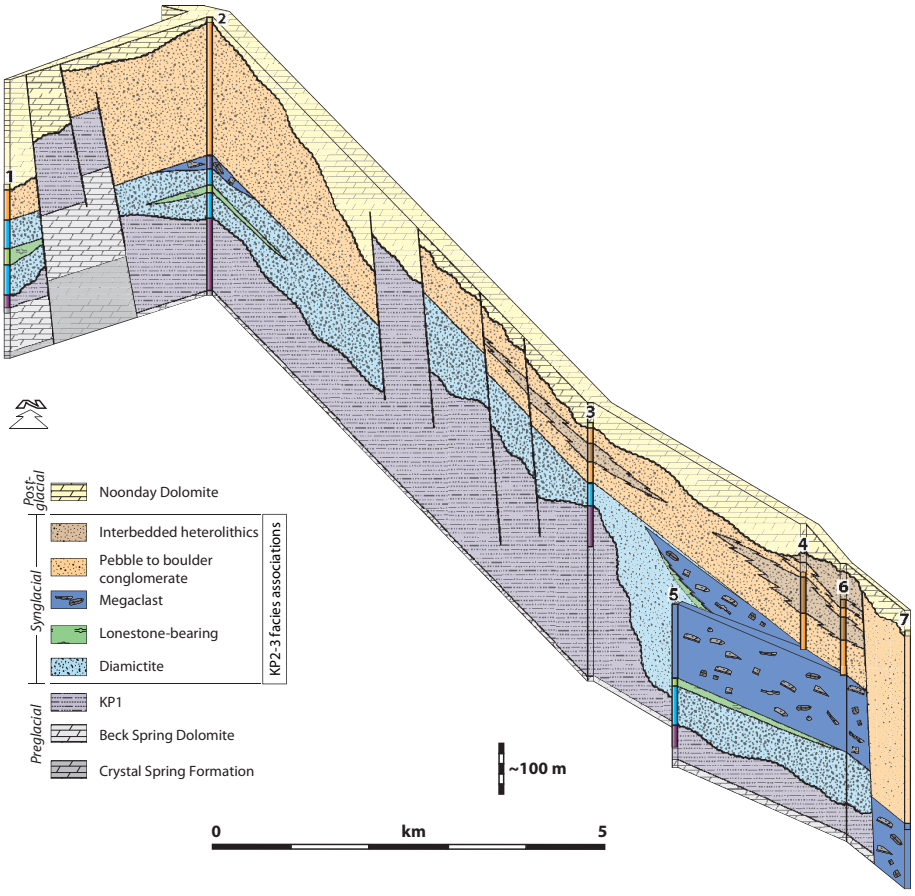

Fig. 8. Fence diagram based on Figure 2, attempting to show the 3D organization of facies association based on the relative map positions of the correlated sections as shown in Figure 1.

Interbedded heterolithics facies association: description

These deposits are well exposed in measured sections 3, 4 and 6 (Fig. 2) where they comprise a series of pebbly sandstones, sandstones, siltstones and shale (Fig. 7a and b). Beds range from 5 to 75 cm in thickness for the sandstones, and from 10 to 50 cm for the siltstones and shale. In vertical section, beds are organized into clear coarsening- and thickening-upwards (Fig. 7a and b) and fining- and thinning-upwards packages (Fig. 7c); a small proportion is ungraded. Single coarsening-upwards packages reach 20 m thicknesses and can be traced for at least 4 km (Figs 1 and 2).

The base to all sandstone beds is sharp, and flute casts are locally preserved (Fig. 7d). Stacked sandstone beds commonly display a planar, parallel bed top and base (Fig. 7c), whereas pebbly sandstone beds resting on siltstones and shales show an irregular to undulose base (Fig. 7e and f). Structureless and parallel-laminated sandstone beds are common; in places single beds show a vertical transition from the former to the latter. Current-ripple cross-lamination and small-scale trough cross-bedding (Fig. 7g) are developed both toward the top of fining-upward cycles and in ungraded beds. Whereas palaeocurrent data are few, dip-corrected ripple foreset azimuths indicate south to SW palaeoflows. Convolute bedding, ball and pillow structures (Fig. 7h) and flame structures are prevalent.

Interbedded heterolithics facies association: interpretation

The normally graded sandstone beds record classic T_{abc} turbidites (Talling *et al.* 2012), consistent with the preservation of flute casts on bed bases, with interbedded siltstone and shale interpreted as the hemipelagic product of waning flow (e.g. Allen *et al.* 2004). These deposits are considered to be lateral equivalents of the pebble to boulder conglomerate facies association. Downslope evolution of high-density turbidity currents and hyperconcentrated flows results in their dilution as they mix with ambient waters, generating turbulent, lower density flows (Hampton 1972; Baas *et al.* 2011; Talling *et al.* 2012). The generation of these facies via flow transformation of ice-proximal turbidites and debrites is used to argue in favour of a more distal depositional setting, whereas the coarser calibre of the sediment indicates a more proximal setting than that for comparable low-density turbidites of the lonestone-bearing facies association. As such, accumulation in the distal reaches of the ice-proximal zone is supported.

Irregular, undulose bed bases indicate cannibalization of underlying sediments during subsequent turbidity flows, whereas the predominance of planar, non-erosive contacts supports hydroplaning during flow emplacement (e.g. Laberg & Vorren 2000), in a similar manner to the diamictite facies association. This is consistent with the elevated fluid contents anticipated during downslope flow dilution. The presence of convolute lamination and climbing ripple cross-lamination is indicative of rapid deposition under fully turbulent conditions (Allen 1991; Baas 2000; Baas *et al.* 2011; Jobe *et al.* 2012; Talling *et al.* 2012). Load and flame structures are indicative of Rayleigh–Taylor instabilities at a grain-size boundary (Allen 1984).

The stratigraphic arrangement of beds into packages that display clear fining- and coarsening-upwards profiles may imply either autocyclic or allocyclic processes at work. Prélat *et al.* (2010) recognized a hierarchy of stratigraphic organization in

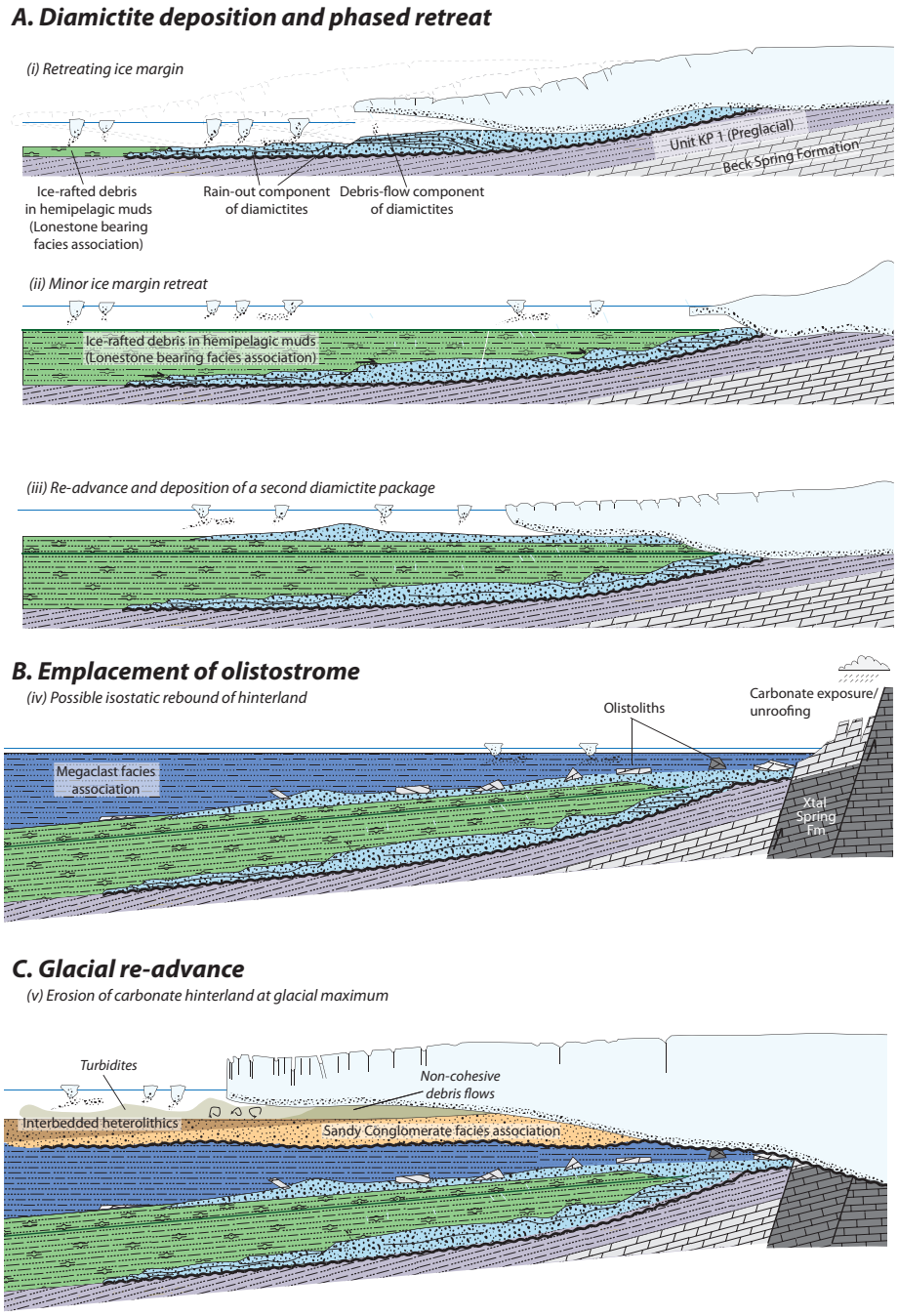

Fig. 9. (**a**–**c**) Sequence of models illustrating the evolution of the Kingston Peak Formation in the context of glacial cycles in the Kingston Range.

subaqueous turbidite systems of the Karoo Basin. In descending hierarchical order, lobe complexes are built from lobe elements, in turn built from bedsets and beds. A single subaqueous lobe consists of several vertically stacked lobe elements. The alternation of fine- and coarser-grained packages of multi-metre-scale lobe elements in the Kingston Range might thus be suggestive of upstream avulsion of feeder channels (e.g. Prélat *et al.* 2010). The stratigraphic arrangement of coarsening- and fining-upward cycles (i.e. lobe elements) within this facies association compares closely with similar cycles identified within the pebble to boulder conglomerate facies association (Fig. 2, compare sections 6 and 7), thus affirming a genetic connection between these deposits.

Evolution of the Kingston Peak Formation

Stacking patterns and inferred glacial cycles

Combining the map distribution of facies associations and their vertical stacking patterns, their 3D distribution can be visualized with the aid of a simple fence diagram (Fig. 8). The stratigraphic surface immediately underlying the first occurrence of diamictite (i.e. the KP1–KP2 contact; Prave 1999) (Figs 2 and 8) is a significant unconformity. The overlying diamictite facies association is interpreted as a series of ice-proximal glaciogenic debris flows subject to secondary ice-rafting, and as such represents the onset of glaciation in this region (Fig. 8). Arguably, therefore, the basal unconformity that downcuts facies of KP1 may represent a glacial

erosion surface (GES). Given the lack of evidence for subglacial features (e.g. ice-contact deformation) within the diamictite facies association, this GES would probably represent subglacial erosion during initial ice advance, which subsequently becomes infilled by glaciogenic debris flows. In this scenario, the erosion surface can be used to support ice grounding in the Kingston Range (Fig. 9a). This is a widely recognized unconformity throughout the Death Valley region, defined at the base of the Virgin Spring Limestone owing to local angular truncation of the underlying strata (Mrofka 2010; TU3 of Macdonald *et al.* 2013). However, this unit is absent throughout the Kingston Range, where the unconformity is defined at the base of KP2. Therefore, the region-wide unconformable surface at the top of KP1 clearly has a tectonic origin in places (Macdonald *et al.* 2013), but is perhaps coincident with a GES in the Kingston Range (sections 1, 2 and 5, Figs 2 and 9a).

Macdonald *et al.* (2013) ascribed the diamictite of KP2 to a single tectonostratigraphic unit. Broadly, the stratigraphic position of that diamictite compares with the stratigraphic position of the diamictite facies association described herein, with one important caveat. We recognize two discrete stratigraphic occurrences of the diamictite facies association, clearly separated by a lonestone-bearing facies association (which is largely diamictite free) in sections 1, 2 and 5 (Figs 2 and 8). We are wary of overemphasizing the significance of this interval beyond the Kingston Range, although interestingly Mrofka & Kennedy (2011) also noted that the diamictite in KP2 is 'interrupted by a 5–20 m interval of finer-grained facies in the Saratoga Hills, southern Saddle Peak Hills and the Alexander Hills'. The lonestone-bearing facies association is interpreted to record deposition via dilute turbidity currents and thin glaciogenic debris flows, alongside ice-rafting in interbedded hemipelagic deposits, within an ice-marginal setting (Fig. 9a). It therefore reflects a minor retreat phase interrupting ice-proximal deposition of the diamictite facies association, attributed to oscillation of the grounding line as opposed to widespread ice meltback.

The second appearance of ice-proximal diamictites is succeeded by the olistostrome of the megaclast facies association (Figs 2 and 8). Release and downslope remobilization of the megaclasts is attributed to the cumulative effects of synsedimentary tectonism, removal of ice cover in the source area and isostatic rebound, triggering iceberg rafting concomitant with olistolith emplacement. It is therefore interpreted to record an ice minimum phase (Fig. 9b). Sufficient meltback to expose bedrock in the source area of the megaclasts, considered to lie a few kilometres north of the outcrop belt (Macdonald *et al.* 2013), is likely to be more significant than the minor oscillation interrupting accumulation of the diamictite facies association. However, further examination is required to assess the significance of this meltback beyond the Kingston Range, and thus it is important to stress that we do not argue for full interglacial conditions during this interval.

The first stratigraphic appearance of the pebble to boulder conglomerate facies association above the olistostrome complex is abrupt and often sharp-based (Figs 2 and 8). These deposits are interpreted to record a sudden influx of coarse debris debouched into the basin during an ice readvance (Fig. 9). The predominance of carbonate boulders derived from the Crystal Spring Formation and Beck Spring Dolomite (i.e. equivalent lithologies to the olistoliths) suggests that the exposed bedrock that supplied the megaclasts was equally exploited during the subsequent ice advance. Significant erosion and plucking of the carbonate bedrock would have therefore provided abundant debris for remobilization as debrites and high-density turbidites of the pebble to boulder conglomerate facies association. The presence of subglacially striated clasts, as reported both by Mrofka & Kennedy (2011) and Macdonald *et al.* (2013), strongly supports their glacial derivation. The thick, hyperconcentrated deposits are typical of rapid and high rates of sedimentation, commonly encountered within the ice-proximal zone (e.g. Benn & Evans 2010), corroborated by the preservation of clast striations, which would be removed under significant reworking and clast abrasion further downslope.

With increasing distance from the ice front, high-density flows of the pebble to boulder conglomerate facies association become diluted, and undergo flow transformation to low-density turbidites and hemipelagic deposits of the interbedded heterolithics facies association. These deposits could be interpreted to record back-stepping of the ice front, thereby preserving a retrogradational sequence of more ice-distal fines overlying ice-proximal conglomerates. However, in places deposits of the interbedded heterolithics and pebble to boulder conglomerate facies associations occur at comparable stratigraphic levels in different logged sections (Fig. 2), with no clear upslope to downslope trend (i.e. north to south). This pattern could reflect deposition of the coarser-grained facies as turbiditic lobes (*sensu* Prélat *et al.* 2009, 2010) with accumulation of finer-grained turbidites between coarser lobe elements. The finer-grained facies could then be succeeded by the coarser, high-density turbidites (e.g. section 3, Fig. 2) under lobe-switching and upstream avulsion. In the Kingston Range, the final deglaciation of the Death Valley region is obscured owing to the angular unconformity that truncates the topmost strata at the base of the Noonday Dolomite.

The wider significance of glacial cycles

Based on the stratigraphic organization of facies associations, we are able to infer advance and retreat of the ice sheets during deposition of the Kingston Peak Formation. The following should be regarded as preliminary, and awaits careful testing in other Death Valley outcrop belts.

Evidence of initial ice advance is proposed at the unconformable contact between the pre-glacial KP1 and glacial KP2, interpreted as a glacial erosion surface, at the same stratigraphic level as the more regionally significant tectonic unconformity (base TU3, Macdonald *et al.* 2013). The first evidence of glacially influenced sedimentation occurs in the overlying diamictite facies association, which records accumulation of glaciogenic debris flows and ice-rafted debris in the ice-proximal zone. A thin interval of ice-marginal turbidites and ice-rafted debris of the lonestone-bearing facies association interrupts this ice-proximal succession, interpreted to record a minor ice front oscillation. Resumed ice-proximal deposition of the diamictite facies association is then succeeded by a more substantial ice meltback during accumulation of the megaclast facies association, wherein ice retreats beyond the source region of the olistoliths to allow excavation of the carbonate bedrock. This retreat phase is also associated with disintegration of the ice front, calving icebergs into the basin, which feed debris into the hemipelagic deposits onlapping the olistoliths. A second major ice advance is then recorded in the accumulation of ice-proximal glaciogenic debris flows and turbidites of the pebble to boulder conglomerate facies association, fed by the eroded bedrock that sourced the carbonate megaclasts. Minor back-stepping of the ice front could account for accumulation of more distal low-density turbidites of the interbedded heterolithics facies association towards the top of some logged sections (Fig. 2), although evidence of terminal deglaciation is not recorded.

This stratigraphic motif can be used to infer advance and retreat of ice sheets during deposition of the Kingston Peak Formation, although the full extent of ice growth and meltback remains to be tested elsewhere in the Death Valley region, and throughout the Cordillera. The absence of time constraints within the Kingston Peak Formation currently precludes an objective analysis of the

cyclicity of these advance–retreat phases. However, recent Re–Os constraints on both the base and top of the Sturtian-equivalent Rapitan succession in NW Canada demonstrate that this glaciation, if global, may have been some 60 Ma in duration (Rooney *et al.* 2013). A *c*. 60 Ma glacial era could clearly incorporate multiple glacial cycles, and multiple glacial events, within the timeframe of a first-order global sequence (Catuneanu *et al.* 2005). Even if we assume that the glacial sedimentary record in the Kingston Range is only a partial record, with cannibalization of some units demonstrable (Fig. 9), the greatest potential for regional, and global, correlation lies within the thickest accumulations, which can be interpreted as major depocentres. Thus, for the purposes of global stratigraphic comparisons with other sections, the Kingston Range is an excellent reference section, even if the significance of the glacial cycles requires further investigation.

Classic 'Sturtian' successions in South Australia and northern Namibia both demonstrate evidence for advance and retreat of ice masses during Cryogenian glaciation (e.g. Le Heron *et al.* 2013; Busfield & Le Heron 2014), each with an interval of significant ice meltback possibly equating to interglacial conditions. Busfield & Le Heron (2014) proposed a high-resolution, glacial sequence stratigraphic framework for the central Flinders Ranges in Australia, in which four glacial advance sequences are recognized, separated by three intervals of glacial retreat. One retreat phase also includes evidence of open water conditions, allowing storm-wave agitation of the sediments and generation of hummocky cross-stratification (Le Heron *et al.* 2011; Busfield & Le Heron 2014). Sturtian-equivalent deposits of the Chuos Formation in the Omutirapo palaeovalley of northern Namibia likewise preserve evidence of a significant period of ice meltback, wherein a succession of shales lacking glacial influence interrupt the overall ice-proximal regime (Le Heron *et al.* 2013). It is possible that these intervals of major meltback correlate with the most pronounced retreat in the Kingston Peak succession. However, it is equally plausible that the glacial records are diachronous (e.g. Allen & Etienne 2008), and hence many more than three glacial cycles can be accommodated within the global 'Sturtian' record. Regardless of which is correct, substantial ice mass wasting and regrowth is necessary to explain the stratigraphy of the Kingston Peak Formation in the Kingston Range. The biggest challenge remains to compare the internal Sturtian record from continent to continent.

Conclusions

Based on mapping, sedimentary logging and facies analysis, the Kingston Peak Formation demonstrates a strong glacial influence throughout, subject to advance and retreat of the ice margin. Specific findings are as follows.

(1) Five facies associations are recognized in the Kingston Range: (1) diamictite facies association (glacigenic debris flows with secondary iceberg rafting); (2) lonestone-bearing facies association (hemipelagic deposits and low-density gravity flows with iceberg rafting); (3) pebble to boulder conglomerate facies association (cogenetic glacigenic debris flows and high-density turbidites); (4) megaclast facies association (olistostrome and hemipelagic sediments subject to ice-rafting); (5) interbedded heterolithics facies association (low-density turbidites and hemipelagic deposits). Collectively, these facies testify to the importance of mass flow processes on sedimentation, under an entirely subaqueous regime.

(2) Deposition of the olistostrome is associated with a period of ice meltback, allowing exposure of the subglacially fractured carbonate bedrock, and hence release of the olistoliths downslope via removal of the ice buttress, isostatic rebound and synsedimentary tectonism.

(3) The stratigraphic organization of facies associations allows the glacial history of units KP2 and KP3 of the Kingston Peak Formation to be elucidated, including multiple ice advance–retreat cycles. These are considered to record intra-Sturtian glacial cycles. Overall ice-proximal sedimentation is interrupted by a minor ice front oscillation, and a more significant meltback during deposition of the olistostrome. Terminal de-glaciation is not recorded in the Kingston Range.

This work was supported by a Fermor Fund grant from the Geological Society of London. The authors are very grateful to F. A. Macdonald, W. Preiss and M. Hambrey, who provided invaluable, thought-provoking suggestions that greatly improved this paper. We are also grateful to P. Hughes for his editorial work.

References

Abolins, M., Oskin, R., Prave, T., Summa, C. & Corsetti, F. 2000. Neoproterozoic glacial record in the Death Valley region, California and Nevada. In: Lageson, D.R., Peters, S.G. & Lahren, M.M. (eds) *Great Basin and Sierra Nevada*. Geological Society of America Field Guide, **2**, 319–336.

Allen, J.R.L. 1984. *Sedimentary Structures, their Character and Physical Basis*. Elsevier, Amsterdam.

Allen, J.R.L. 1991. The Bouma a division and the possible duration of turbidity currents. *Journal of Sedimentary Petrology*, **61**, 291–295.

Allen, P.A. & Etienne, J.L. 2008. Sedimentary challenge to Snowball Earth. *Nature Geoscience*, **1**, 817–825.

Allen, P.A., Leather, J. & Brasier, M.D. 2004. The Neoproterozoic Fiq glaciation and its aftermath, Huqf supergroup of Oman. *Basin Research*, **16**, 507–534.

Amy, L.A. & Talling, P. 2006. Anatomy of turbidites and linked debrites based on long distance (120 × 30 km) bed correlation, Marnoso Arenacea Formation, Northern Apennines, Italy. *Sedimentology*, **53**, 161–212.

Anderson, J.B., Kennedy, D.S., Smith, M.J. & Domack, E.W. 1991. Sedimentary facies associated with Antarctica's floating ice masses. *In*: Anderson, J.B. & Ashley, G.M. (eds) *Glacial–Marine Sedimentation: Paleoclimatic Significance*. Geological Society of America, Special Papers, **261**, 1–25.

Arnaud, E. 2004. Giant cross-beds in the Neoproterozoic Port Askaig Formation, Scotland: Implications for snowball Earth. *Sedimentary Geology*, **165**, 155–174.

Arnaud, E. 2012. The paleoclimatic significance of deformation structures in Neoproterozoic successions. *Sedimentary Geology*, **243–244**, 33–56.

Baas, J.H. 2000. Duration of deposition from decelerating high-density turbidity currents. *Sedimentary Geology*, **136**, 71–88.

Baas, J.H., Best, J.L. & Peakall, J. 2011. Depositional processes, bedform development and hybrid flows in rapidly decelerated cohesive (mud–sand) sediment flows. *Sedimentology*, **58**, 1953–1987.

Bagnold, R.A. 1954. Experiments on a gravity-free dispersion of large solid spheres in a Newtonian fluid under shear. *Proceedings of the Royal Society of London, Series A*, **225**, 49–63.

Benn, D.I. & Evans, D.J.A. (eds) 2010. *Glaciers and Glaciation*. Hodder Education, London.

Busfield, M.E. & Le Heron, D.P. 2013. Glacitectonic deformation in the Chuos Formation of northern Namibia: Implications for Neoproterozoic ice dynamics. *Proceedings of the Geologists' Association*, http://dx.doi.org/10.1016/j.pgeola.2012.10.005.

Busfield, M.E. & Le Heron, D.P. 2014. Sequencing the Sturtian icehouse: Dynamic ice behaviour in South Australia. *Journal of the Geological Society, London*, **124**, 778–789.

Calzia, J.P., Troxel, B.W., Wright, L.A., Burchfiel, B.C., Davis, G.A. & McMackin, M.R. 2000. *Geologic map of the Kingston Range, southern Death Valley, California*. USGS Open-File Report, **2000–412**.

Catuneanu, O., Martins-Neto, M.A. & Eriksson, P.G. 2005. Precambrian sequence stratigraphy. *Sedimentary Geology*, **176**, 67–95.

Corsetti, F.A. & Kaufman, A.J. 2003. Stratigraphic investigations of carbon isotope anomalies and Neoproterozoic ice ages in Death Valley, California. *Geological Society of America Bulletin*, **115**, 916–932.

Dimakis, P., Elverhøi, A., *et al.* 2000. Submarine slope stability on high-latitude glaciated Svalbard–Barents Sea margin. *Marine Geology*, **162**, 303–316.

Domack, E.W. & Harris, P. 1998. A new depositional model for ice shelves based upon sediment cores recovered in the Ross Sea and Mac. Robertson Shelf, Antarctica. *Annals of Glaciology*, **27**, 281–284.

Domack, E.W. & Hoffman, P.F. 2011. An ice grounding-line wedge from the Ghaub glaciation (635 Ma) on the distal foreslope of the Otavi carbonate platform, Namibia, and its bearing on the snowball Earth hypothesis. *Geological Society of America Bulletin*, **123**, 1448–1477.

Duller, R., Mountney, N.P., Russell, A.J. & Cassidy, N.C. 2008. Architectural analysis of a volcaniclastic jökulhlaup deposit, southern Iceland: Sedimentary evidence for supercritical flow. *Sedimentology*, **55**, 939–964.

Elverhøi, A., De Blasio, F.V., *et al.* 2002. Submarine mass-wasting on glacially influenced continental slopes—processes and dynamics. *In*: Dowdeswell, J.A. & Ó Cofaigh, C. (eds) *Glacier-Influenced Sedimentation on High-Latitude Continental Margins*. *Geological Society, London, Special Publications*, **203**, 73–87.

Etienne, P.L., Allen, P.A., Rieu, R. & Le Guerroué, E. 2007. Neoproterozoic glaciated basins: A critical review of the Snowball Earth hypothesis by comparison with Phanerozoic glaciations. *In*: Hambrey, M.J., Christoffersen, P., Glasser, N.F. & Hubbard, B. (eds) *Glacial Sedimentary Processes and Products*. Blackwell, Oxford, 343–399.

Evans, J. & Pudsey, C.J. 2002. Sedimentation associated with Antarctic Peninsula ice shelves: Implications for palaeoenvironmental reconstructions of glacimarine sediments. *Journal of the Geological Society, London*, **159**, 233–237.

Eyles, N. & Januszczak, N. 2004. 'Zipper-rift': A tectonic model for Neoproterozoic glaciations during the breakup of Rodinia after 750 Ma. *Earth-Science Reviews*, **65**, 1–73.

Hambrey, M.J. & Glasser, N.F. 2003. Glacial sediments: Processes, environments and facies. *In*: Middleton, G.V. (ed.) *Encyclopedia of Sediments and Sedimentary Rocks*. Kluwer, Dordrecht, 316–331.

Hambrey, M.J. & Glasser, N.F. 2012. Discriminating glacier thermal and dynamic regimes in the sedimentary record. *Sedimentary Geology*, **251**, 1–33.

Hampton, M.A. 1972. The role of subaqueous debris flow in generating turbidity currents. *Journal of Sedimentary Petrology*, **42**, 775–793.

Hazzard, J.C. 1939. Possibility of a pre-Cambric glaciation in southeastern California. *Pan-American Geologist*, **71**, 47–48.

Heaman, L.M. & Grotzinger, J.P. 1992. 1.08 Ga diabase sills in the Pahrump Group, California; implications for development of the Cordilleran miogeosyncline. *Geology*, **20**, 637–640.

Heck, F.R. & Speed, R.C. 1987. Triassic olistostrome and shelf–basin transition in the western Great Basin: Palaeogeographic implications. *Geological Society of America Bulletin*, **99**, 539–551.

Hoffman, P.F., Kaufman, A.J., Halverson, G.P. & Schrag, D.P. 1998. A Neoproterozoic Snowball Earth. *Science*, **281**, 1342–1346.

Jobe, Z.R., Lowe, D.R. & Morris, W.R. 2012. Climbing-ripple successions in turbidite systems: Depositional environments, sedimentation rates and accumulation times. *Sedimentology*, **59**, 867–898.

Kennedy, M.J., Runnegar, B., Prave, A.R., Hoffmann, K.H. & Arthur, M.A. 1998. Two of four Neoproterozoic glaciations? *Geology*, **26**, 1059–1063.

Khatwa, A. & Tulaczyk, S. 2001. Microstructural interpretations of modern and Pleistocene subglacially deformed sediments: The relative role of parent material and subglacial processes. *Journal of Quaternary Science*, **16**, 507–517.

Laberg, J.S. & Vorren, T.O. 2000. Flow behaviour of the submarine glacigenic debris flows on the Bear Island Trough Mouth Fan, western Barents Sea. *Sedimentology*, **47**, 1105–1117.

Leather, J., Allen, P.A., Brasier, M.D. & Cozzi, A. 2002. Neoproterozoic snowball Earth under scrutiny: Evidence from the Fiq glaciation of Oman. *Geology*, **30**, 891–894.

Le Heron, D.P., Cox, G.M., Trundley, A.E. & Collins, A. 2011. Sea ice-free conditions during the Sturtian glaciation (early Cryogenian), South Australia. *Geology*, **39**, 31–34.

Le Heron, D.P., Busfield, M.E. & Kamona, A.F. 2013. Interglacial on snowball Earth? Dynamic ice behaviour revealed in the Chuos Formation, Namibia. *Sedimentology*, **60**, 411–427.

Macdonald, F.A., Prave, A.R., *et al.* 2013. The Laurentian record of Neoproterozoic glaciation, tectonism, and eukaryotic evolution in Death Valley, California. *Geological Society of America Bulletin*, http://dx.doi.org/10.1130/B30789.1.

Marren, P.M., Russell, A.J. & Rushmer, E.L. 2009. Sedimentology of a sandur formed by multiple jökulhlaups, Kverkfjöll, Iceland. *Sedimentary Geology*, **213**, 77–88.

Miller, J.M.G. 1985. Glacial and syntectonic sedimentation: The upper Proterozoic Kingston Peak Formation, southern Panamint Range, California. *Geological Society of America Bulletin*, **96**, 1537–1553.

Miller, J.M.G. 1987. Paleotectonic and stratigraphic implications of the Kingston Peak–Noonday contact in the Panamint Range, eastern California. *Journal of Geology*, **95**, 75–85.

Moncrieff, A.C.M. 1989. Classification of poorly-sorted sedimentary rocks. *Sedimentary Geology*, **65**, 191–194.

Mrofka, D. 2010. Competing models for the timing of Cryogenian Glaciation: Evidence from the Kingston Peak Formation, southeastern California. PhD dissertation, University of California, Riverside.

Mrofka, D. & Kennedy, M. 2011. The Kingston Peak Formation in the eastern Death Valley region. *In*: Arnaud, E., Halverson, G.P. & Shields-Zhou, G. (eds) *The Geological Record of Neoproterozoic Glaciations*. Geological Society, London, Memoirs, **36**, 449–458.

Ó Cofaigh, C., Taylor, J., Dowdeswell, J.A., Rosell-Mele, A., Kenyon, N.H., Evans, J. & Mienert, J. 2002. Sediment reworking on high-latitude continental margins and its implications for palaeoceanographic studies: Insights from the Norwegian–Greenland Sea. *In*: Dowdeswell, J.A. & Ó Cofaigh, C. (eds) *Glacier-Influenced Sedimentation on High-Latitude Continental Margins*. Geological Society, London, Special Publications, **203**, 325–348.

Petterson, R., Prave, A.R., Wernicke, B.P. & Fallick, A.E. 2011*a*. The Neoproterozoic Noonday Formation, Death Valley region, California. *Geological Society of America Bulletin*, **123**, 1317–1336.

Petterson, R., Prave, A.R. & Wernicke, B.P. 2011*b*. Glaciogenic and related strata of the Neoproterozoic Kingston Peak Formation in the Panamint Range, Death Valley region, California. *In*: Arnaud, E., Halverson, G.P. & Shields-Zhou, G. (eds) *The Geological Record of Neoproterozoic Glaciations*. Geological Society, London, Memoirs, **36**, 449–458.

Phillips, E. 2006. Micromorphology of a debris flow deposit: Evidence of basal shearing, hydrofracturing, liquefaction and rotational deformation during emplacement. *Quaternary Science Reviews*, **25**, 720–738.

Prave, A.R. 1999. Two diamictites, two cap carbonates, two $\delta^{13}C$ excursions, two rifts: The Neoproterozoic Kingston Peak Formation, Death Valley, California. *Geology*, **27**, 339–342.

Prélat, A., Hodgson, D.M. & Flint, S.S. 2009. Evolution, architecture and hierarchy of distributary deep-water deposits: A high-resolution outcrop investigation from the Permian Karoo Basin, South Africa. *Sedimentology*, **56**, 2132–2154.

Prélat, A., Covault, J.A., Hodgson, D.M., Fildani, A. & Flint, S.S. 2010. Intrinsic controls on the range of volumes, morphologies, and dimensions of submarine lobes. *Sedimentary Geology*, **232**, 66–76.

Pudsey, C.J., Murray, J.W., Appleby, P. & Evans, J. 2006. Ice shelf history from petrographic and foraminiferal evidence, northeast Antarctic Peninsula. *Quaternary Science Reviews*, **25**, 2357–2379.

Reinardy, B.T.I., Pudsey, C.J., Hillenbrand, C.-D., Murray, T. & Evans, J. 2009. Contrasting sources for glacial and interglacial shelf sediments used to interpret changing ice-flow directions in the Larsen Basin, northern Antarctic Peninsula. *Marine Geology*, **266**, 156–171.

Robertson, A.H.F. 1977. The Moni Mélange, Cyprus: An olistostrome formed at a destructive plate margin. *Journal of the Geological Society, London*, **133**, 447–466.

Rooney, A.D., Macdonald, F.A., Strauss, J.V., Dudás, F. Ö., Hallmann, C. & Selby, D. 2013. Re–Os geochronology and coupled Os–Sr isotope constraints on the Sturtian snowball Earth. *Proceedings of the National Academy of Sciences of the USA*, **111**, 51–56.

Sheldon, N.D. & Tabor, N.J. 2009. Paleoenvironmental and paleoclimatic reconstruction using paleosols. *Earth-Science Reviews*, **95**, 1–52.

Talling, P.J., Masson, D.G., Sumner, E.J. & Malgesini, G. 2012. Subaqueous sediment density flows: Depositional processes and deposit types. *Sedimentology*, **59**, 1937–2003.

Tinterri, R., Drago, M., Consonni, A., Davoli, G. & Mutti, E. 2003. Modelling subaqueous bipartite sediment gravity flows on the basis of outcrop constraints: First results. *Marine and Petroleum Geology*, **20**, 911–933.

Troxel, B.W. 1966. *Sedimentary Features of the Later Precambrian Kingston Peak Formation, Death Valley, California*. Geological Society of America, Special Papers, **101**.

Troxel, B.W. 1982. Description of the uppermost part of the Kingston Peak Formation, Amargosa Rim canyon, Death Valley region, California. *In*: Cooper, J.D., Troxel, B.W. & Wright, L.A. (eds) *Geology of Selected Areas in the San Bernadino Mountains, Western Mojave Desert, and Southern Great Basin, California*. Geological Society of America (Cordilleran Section) Volume and Guidebook. Death Valley Publishing Company, Shoshone, CA, 61–70.

Vorren, T.O., Blaume, F., Dowdeswell, J.A., Laberg, J.S., Mienert, J., Rumohr, J. & Werner, F. 1998. The Norwegian–Greenland Sea continental margins: Morphology and late Quaternary sedimentary processes and environments. *Quaternary Science Reviews*, **17**, 273–302.

Wendorff, M. 2005. Lithostratigraphy of Neoproterozoic syn-rift sedimentary megabreccia from Mwambashi, Copperbelt of Zambia, and correlation with olistostrome succession from Mufulira. *South African Journal of Geology*, **108**, 505–524.

Wright, L.A., Troxel, B.W., Williams, E.G., Roberts, M.T. & Diehl, P.E. 1974. Precambrian sedimentary environments of the Death Valley region, eastern California. *In*: Troxel, B.W. & Wright, L.A. (eds) *Guidebook: Death Valley Region, California and Nevada*. Death Valley Publishing Company, Shoshone, CA, 27–35.

Received 6 November 2013; revised typescript accepted 23 February 2014.
Scientific Editing by Philip Hughes.

5.3. Distal glacier-fed shelf, southern Kingston Range

Pulsed iceberg delivery driven by Sturtian ice sheet dynamics: an example from Death Valley, California

Le Heron, D.P. and Busfield, M.E.

Sedimentology (2015-2016), *accepted*

Statement of contribution

- ***Data collection***
  - Busfield and Le Heron logged all studied sections, and collected both palaeocurrent and structural (bedding) data.
  - Le Heron mapped the outcrops using field data and satellite imagery.
- ***Manuscript text***
  - Busfield suggested following the facies associations scheme of Le Heron et al. 2014b (Chapter 5.2) for consistency. Both Busfield and Le Heron interpreted the facies associations in these studied sections and devised the depositional model.
  - Le Heron authored the first draft of the manuscript, and Busfield modified the manuscript in all subsequent drafts, particularly with reference to the sister paper by Busfield & Le Heron *in press* (Chapter 5.4).
- ***Figures***
  - Le Heron illustrated Figures 1-3, 6 and 8.
  - Le Heron and Busfield contributed photographs to figures throughout.

Sedimentology (2015) doi: 10.1111/sed.12225

Pulsed iceberg delivery driven by Sturtian ice sheet dynamics: an example from Death Valley, California

DANIEL P. LE HERON and MARIE E. BUSFIELD
Department of Earth Sciences, Royal Holloway University of London, Egham, Surrey TW20 0EX, UK (E-mail: daniel.leeron@rhul.ac.uk)

Associate Editor – Guy Spence

ABSTRACT

The Kingston Peak Formation is a Cryogenian sedimentary succession that crops out in the Death Valley area, California. It is widely accepted to record pre-glacial conditions (KP1), followed by two glaciations of pan-global extent, the older Sturtian (KP2 to KP3) and younger Marinoan glaciation (KP4). In the type area (the Kingston Range), detailed facies analysis of the Sturtian succession reveals that a basal diamictite unit and an upper boulder conglomerate were deposited by proglacial subaqueous sediment gravity flows. An olistostrome unit punctuating the succession is interpreted to result from tectonically induced downslope mobilization during isostatic rebound, triggered by significant ice-meltback. Focussing on strata onlapping the olistostrome, this article provides insight into the processes of glacial re-advance following an intra-Sturtian glacial minimum. The first 50 m of strata above the olistostrome are thinly bedded turbidites that are devoid of lonestones. A trend towards thicker graded beds upsection, in concert with the gradual appearance and then abundance of lonestones, testifies to the influence of ice rafting and to the resumption of a direct ice sheet influence upon sedimentation. Stratigraphic organization into thickening and coarsening upward bedsets over a multi-metre scale reveals a subaqueous gravity flow-dominated succession composed of a spectrum of high to low density turbidites, with thick graded boulder-conglomerates at intervals. The finer-grained facies assemblage is heterolithic: current ripple cross-laminated sandstones intercalated with shales that bear delicate granule to pebble-sized dropstones in abundance. Intervals of dropstone-bearing and dropstone-free strata are attributable to dynamic oscillation of the ice margin in the hinterland. Integrating palaeocurrent data with observations from neighbouring outcrop belts allow a detailed palaeogeographic map of the eastern Death Valley area to be compiled for the first time.

Keywords Cryogenian, Death Valley, Neoproterozoic, Pahrump Group, snowball earth.

INTRODUCTION

The Sturtian glaciation is the oldest of two major glacial intervals in the Cryogenian interval and considered to span approximately 60 Myr (Rooney *et al.*, 2014). In the Death Valley area, California, lower to middle levels of the Kingston Peak Formation are renowned as an excellent example of the interplay between extensional tectonics and glaciation (e.g. Basse, 1978; Miller, 1985; Link *et al.*, 1993; Prave, 1999; MacDonald *et al.*, 2013; Le Heron *et al.*, 2014), contributing to the debate on tectonic versus glaciogenic controls upon diamictites in the Neoproterozoic on a

global scale (Eyles & Januszczak, 2004). These deposits, of interpreted Sturtian age (Prave, 1999) have thus received a resurgence of interest since the early sedimentological models were developed (Basse, 1978; Miller, 1985), stemming ultimately from the interest stirred by the Snowball Earth hypothesis (Hoffman *et al.*, 1998). Neoproterozoic strata crop out in typically well-exposed but disconnected outcrop belts, providing detailed insight into ice sheet dynamics in the southern Cordillera. Understanding palaeo-ice sheet behaviour, via a detailed scrutiny of facies and stratigraphic architecture, provides valuable boundary conditions for climate models in the Sturtian icehouse world (Hyde *et al.*, 2000; Pierrehumbert, 2005; Le Hir *et al.*, 2007; Pierrehumbert *et al.*, 2011).

In eastern California, the Kingston Peak Formation (Fig. 1) preserves an exceptionally well-exposed, thick and laterally extensive succession that includes glaciogenic strata of both early Cryogenian (Sturtian) and late Cryogenian (Marinoan) age (MacDonald *et al.*, 2013; Le Heron *et al.*, 2014). This region, representing the type area of the Kingston Peak Formation, demonstrates clear evidence for a glacial influence on sedimentation (e.g. Mrofka & Kennedy, 2011; MacDonald *et al.*, 2013), including major advance–retreat cycles (Le Heron *et al.*, 2014). In the northern Kingston Range, both MacDonald *et al.* (2013) and Le Heron *et al.* (2014) described a >1 km thick olistostrome unit punctuating the Sturtian succession. This interval has been interpreted as a glacial minimum (Le Heron *et al.*, 2014), with retreat of the ice front triggering isostatic rebound, tectonism and unbuttressing of the carbonate bedrock. These processes led to remobilization of angular olistoliths downslope, accompanied by background ice-rafting following widespread ice sheet disintegration. Above this horizon, conglomerate and graded sandstone facies are interpreted to record subaqueous outwash during a glacial re-advance (Le Heron *et al.*, 2014). However, the contact between the olistostrome unit and overlying strata is largely obscure in the northern Kingston Range owing to the high proportion of muddy deposits that are typically recessive on hillsides.

This article targets the southern Kingston Range (Fig. 1), where outstanding gulley sections permit the olistostrome and supra-olistostrome units to be distinguished clearly. In contrast with other regions in the Death Valley area, mudstone-rich intervals are well-exposed, and demonstrate clear variations in the content

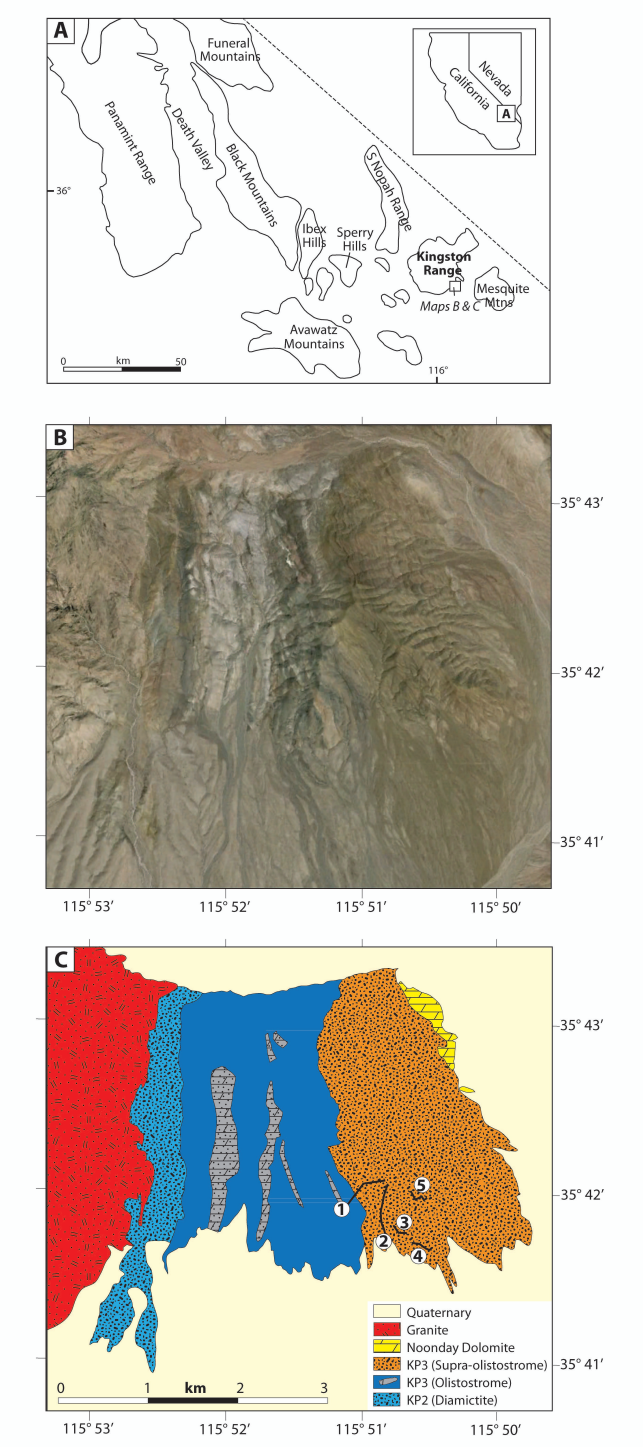

Fig. 1. (A) Overview map of the main outcrops of Neoproterozoic strata in Death Valley. (B) Satellite image of the southernmost part of the Kingston Range [see (A) for location]. (C) Simple geological map of the southern Kingston Range, covering the same geographic area as the satellite image (B). The colour scheme matches that of Le Heron *et al.* (2014) for comparison with strata further north in the range. Also shown on this map are the locations of detailed sedimentary logs which are presented in Fig. 2.

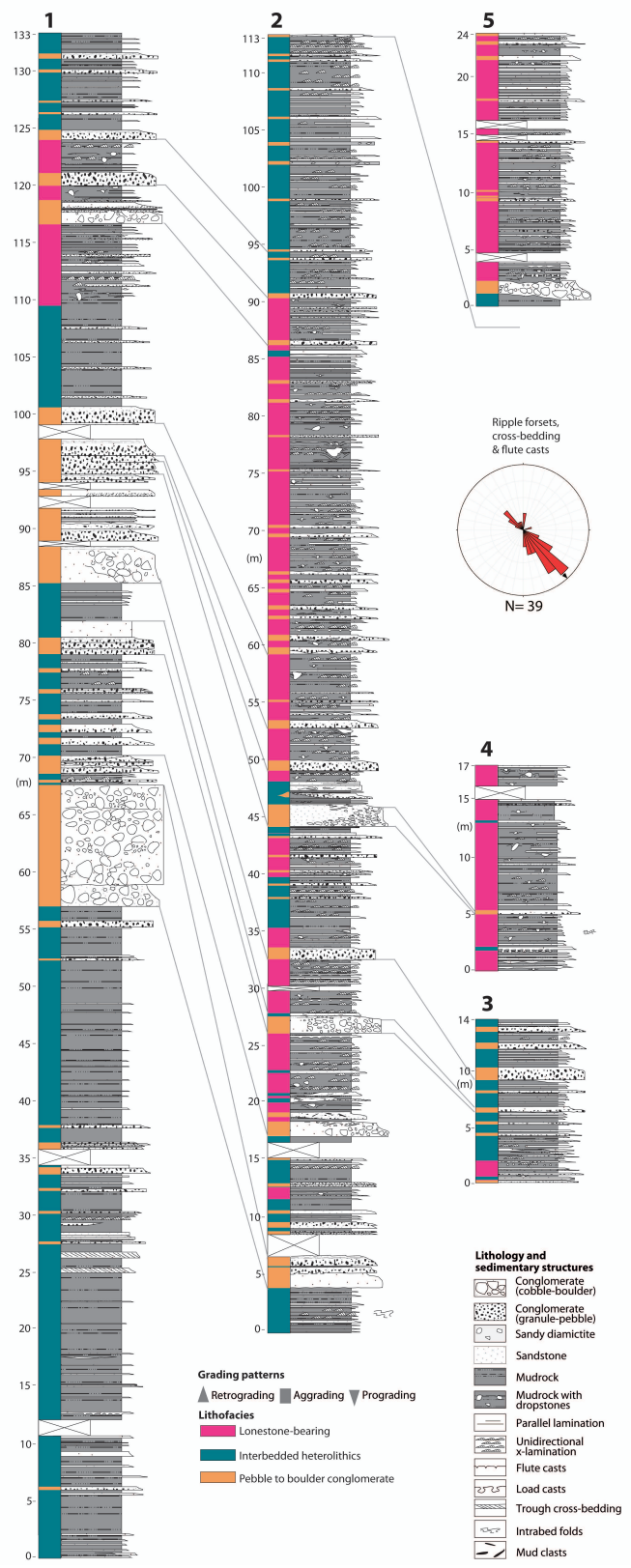

Fig. 2. Sedimentary logs corresponding to each of the locations that are shown in Fig. 1C. Note that three facies associations are recognized in this study. Three lines of evidence for a south-east dipping, major palaeoslope can be established: (i), palaeocurrents in the rose diagram, showing regional-dip corrected cross-laminations plus flute casts and grooves; (ii) consistent thinning and pinch out of the conglomerates on each of the logs in the same direction and (iii) based on previous evidence (Le Heron *et al.*, 2014), thickening of the entire Kingston Peak Formation away from growth faults in the Horsethief Spring area to the north-west. On the logs, note the clear alternation/differentiation of lonestone-bearing and lonestone-free thin bedded heterolithic deposits.

of ice-rafted debris (IRD). This paper therefore aims to: (i) document the facies associations preserved in the supra-olistostrome unit; (ii) comment on the distribution of IRD in the succession and its relation to ice sheet dynamics and (iii) assess the regional palaeogeography during deposition of part of the Kingston Peak Formation, as a first step towards constraining the geometry of the palaeo-ice margin.

REGIONAL GEOLOGY AND STRATIGRAPHY

In ascending order, the Pahrump Group traditionally comprises three subdivisions; the Crystal Spring Formation, the Beck Spring dolomite and the Kingston Peak Formation (Prave, 1999; MacDonald *et al.*, 2013). Recent detrital zircon ages constrain the upper Crystal Spring Member to younger than 787 ± 11 Ma, which Mahon *et al.* (2014a) use to propose a separate 'Horse Thief Springs Formation'. This offers a maximum depositional age for the Kingston Peak Formation, which is recognized as older than 635 Ma based upon angular truncation beneath the Noonday Dolomite (Petterson *et al.*, 2011; MacDonald *et al.*, 2013). No palaeomagnetic data are available from the Kingston Peak Formation itself, although Evans (2000) obtained a near-equatorial (01 ± 4°) palaeolatitude from the Johnnie Formation some hundreds of metres stratigraphically upsection.

The Kingston Peak Formation is considered to span two intracratonic rifting events, associated with break-up of the supercontinent Rodinia (Prave, 1999; Mahon *et al.*, 2014a). In the southern Panamint Range, mid-ocean ridge basalt type pillow lavas are intercalated with diamictites belonging to the lower part of the Kingston Peak Formation in Surprise Canyon (Labotka *et al.*, 1980; Miller, 1985). This key finding, taken together with evidence for 'buried faults' led

Prave (1999) to propose an early phase of rifting at about 700 Ma. In the Kingston Range, in the vicinity of Horsethief Spring, a series of spectacular *en echelon* normal faults, dissecting the upper part of the Kingston Peak Formation can be observed on satellite imagery (Le Heron, 2015).

A second phase of rifting during Kingston Peak times was proposed by Prave (1999) at about 600 Ma on account of an olistostrome mapped in Goler Wash, southern Panamint Range. This olistostrome, it was shown, progressively truncated underlying Kingston Peak Formation strata down to crystalline basement, and was itself capped by an upper diamictite termed the Wildrose Diamictite (Miller, 1985). Elsewhere in the Death Valley area, olistostromes with kilometre-scale blocks occur in the central and southern Kingston Range (MacDonald *et al.*, 2013; Le Heron *et al.*, 2014; this paper). Large, angular blocks of dolostone derived from the Crystal Spring Formation are mappable in the Silurian Hills (Kupfer, 1960) where crystalline basement fragments are also common (Basse, 1978).

Evidence for olistostromes in the Pahrump Group is confined to the Kingston Peak Formation. However, it is noted that arkosic sandstone and granular conglomerates – presumably implying downcutting to crystalline basement – occur at intervals in other units, notably in the Crystal Spring Formation (MacDonald *et al.*, 2013). Carbonate conglomerate intervals at the base of the Horse Thief Spring Formation record deposition following a 300 Myr duration hiatus (Mahon *et al.*, 2014a). Regional zircon data suggest an evolution in sediment routing systems, with provenance from the north-east (Colorado) during latest Tonian and early Cryogenian time, with progressive input from the south-east and east into the Cryogenian (Mahon *et al.*, 2014b).

MacDonald *et al.* (2013) adopted and refined the regional allostratigraphy for the Cryogenian Kingston Peak Formation developed by Prave (1999). In that framework, the formation is subdivided into four units; KP1 to KP4 in ascending stratigraphic order. Owing to the lack of glacial indicators in the lower part of the formation, KP1 is considered to predate the growth of ice sheets that deposited glaciogenic strata of KP2 to KP4. In the Panamint Range, an angular unconformity and package of non-glacial carbonate separates units KP3 and KP4, leading to their interpretation as products of the older Sturtian and younger Marinoan glaciation, respectively (Prave, 1999; Petterson *et al.*, 2011). Le Heron *et al.* (2014) did not find clear evidence for a KP4 unit in their study area in the northern Kingston Range, although a detailed sedimentary model for units KP2 to KP3 was developed in that paper. Unit KP2 consisted entirely of a dropstone-bearing diamictic unit, but the olistostrome and supra-olistostrome succession were restricted to unit KP3 (Le Heron *et al.*, 2014).

THE SOUTHERN KINGSTON RANGE

High quality exposure of unit KP3 is recorded within a series of north–south oriented gulleys that dissect the southern Kingston Range, providing the basis for both correlation (Fig. 2) and high resolution facies analysis (Fig. 3) that underpin the present paper. The contact between the olistostrome and supra-olistostrome succession is well-preserved and is sharply defined in the field by a colour change from dark grey weathering, manganiferous deposits to light brown strata (Fig. 4A). At the outcrop scale, the olistostrome succession bears very angular blocks of dolostone of boulder size (Fig. 4B), extending to kilometre-scale blocks in the northern Kingston Range (Le Heron *et al.*, 2014). This unit is succeeded by heterolithic facies of the supra-olistostrome succession (Fig. 4C).

Five detailed sedimentary logs in this area, supplemented by additional data from the northern Kingston Range, are presented herein. The location of logged sections is shown on the geological map (Fig. 1). A correlation panel for the strata (Fig. 2) clearly demonstrates that some beds can readily be traced (by carefully walking out the contacts in the field) but, in other cases, internal complexity is such that bed by bed correlation is sometimes impossible. The logged sections are partly simplified, thus an expanded, maximum-detail log is presented for the most important and continuous section (Log 2, Fig. 3). For ease of comparison, the facies scheme developed for the northern Kingston Range (Le Heron *et al.*, 2014) and Sperry Wash (Busfield & Le Heron, 2015, this volume) will be adopted herein. Focussing on the topmost unit in the succession (KP3), this study is restricted to three facies associations: (i) pebble to boulder conglomerate; (ii) interbedded heterolithics and (iii) lonestone-bearing. This locality is down palaeo-dip from the northern Kingston Range sections, which is evidenced in measured palaeocurrent orientations, and is further reflected in downslope changes in facies character, discussed below.

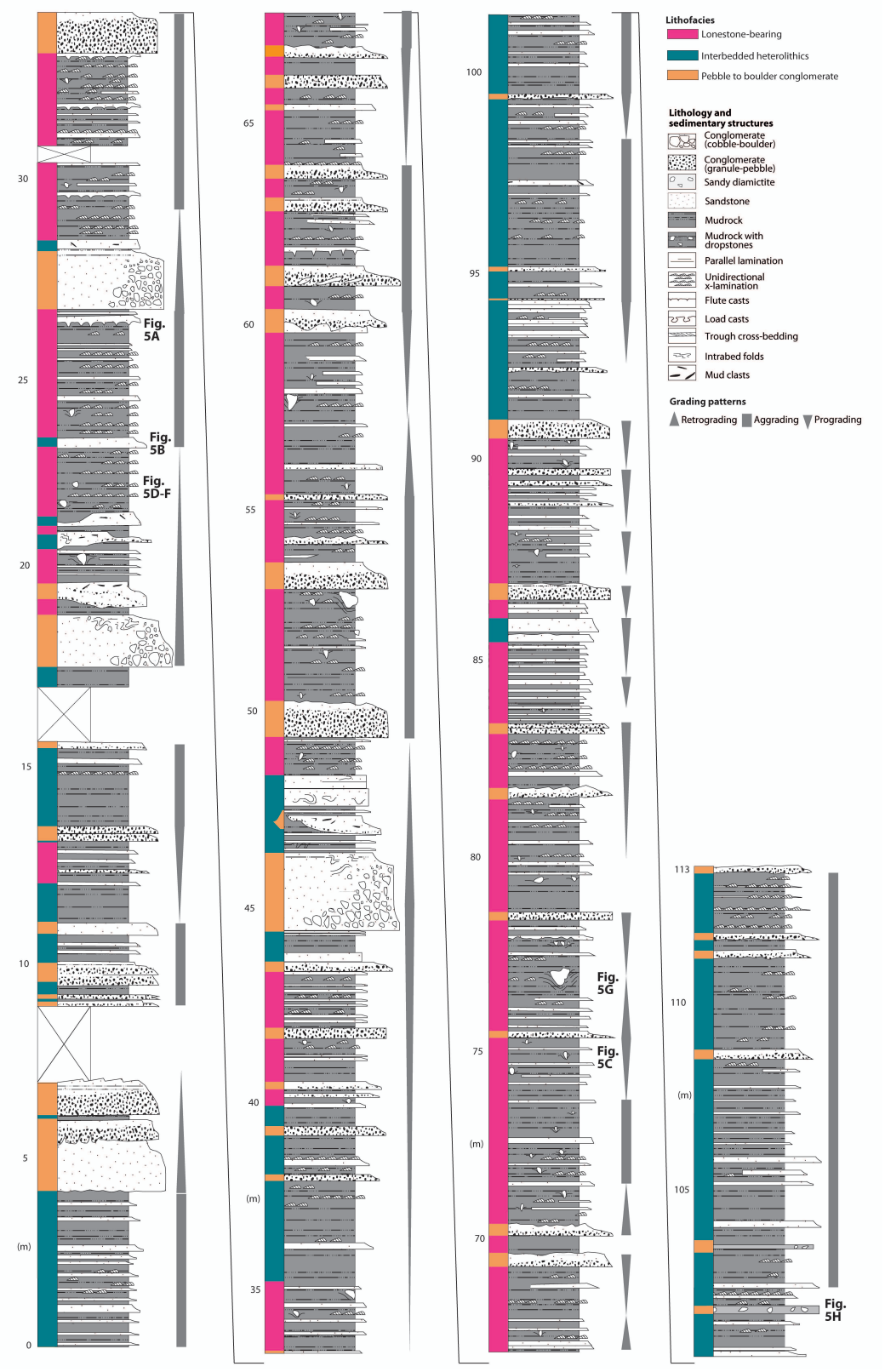

Fig. 3. Expanded version of logged section 2 (Fig. 2) at a higher resolution, without simplification, illustrating the vertical facies transitions at maximum-level detail. This log is a key section owing to almost continuous exposure of the finer-grained fraction in water-washed gullies, enabling the presence and absence of ice-rafted debris (IRD) to be documented to a high level of confidence.

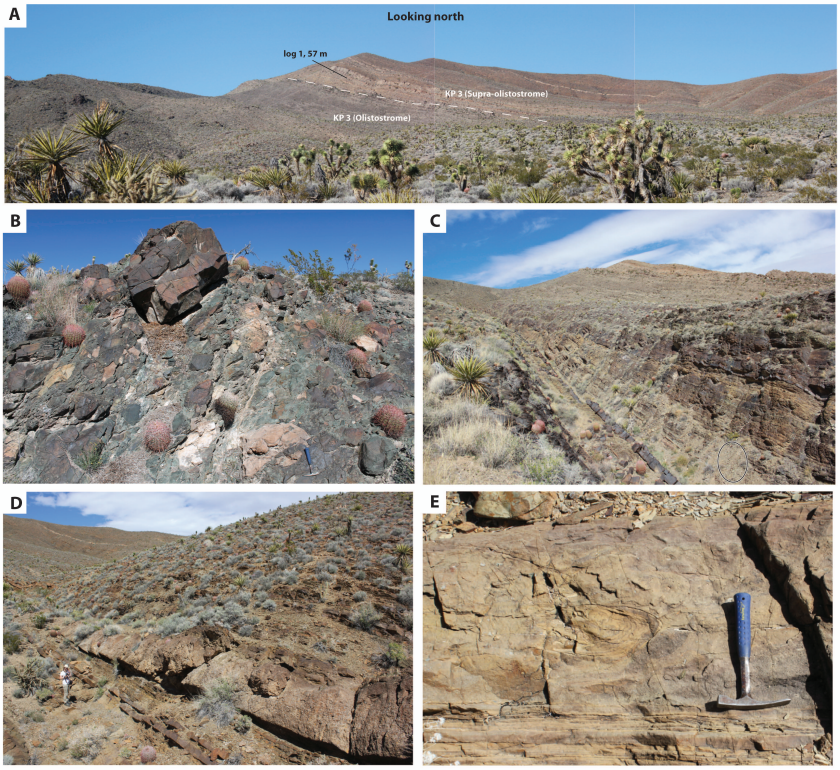

Fig. 4. Macroscale phenomena. (A) Landscape-scale view of the contact between the top of the olistostrome complex in KP3 and the base of the supra-olistostrome succession (see also Fig. 1C). (B) Olistostrome complex at the outcrop scale, with extremely angular blocks of dolostone embedded with a manganese-rich matrix. Kilometre-scale dolostone blocks also occur at intervals (Fig. 1C). (C) View of the basal part of the supra-olistostrome complex, characterized by well-stratified interbedded sandstones, conglomerates and heterolithic strata (documented in Fig. 2, log 1, 0 to 55 m). (D) Typical view of a series of thickly bedded sandstones (next to geologist, *ca* 1·8 m tall, in view) sharply overlain by a graded conglomerate bed (124 m, log 1, Fig. 2). (E) Top of a thickening-up, coarsening upward interval (87 m log 2; Figs 2 and 3), culminating in a normally graded conglomerate unit. Hammer for scale is 32 cm long.

Pebble to boulder conglomerate facies association

Description

On the basis of grain size and matrix content, several subfacies are distinguished, namely clast-supported cobble to boulder-rich conglomerates, clast-supported granule to pebble-rich conglomerates and matrix-supported conglomerates (Figs 2 and 3). Clasts are dominated by carbonates of the Crystal Spring and Beck Spring Dolomite, although sandstone intraclasts are also recognized, and are typically sub-rounded to rounded. Where discoid clasts are present, imbrication is developed in boulders at the base of beds. Stacked conglomeratic bedsets which thicken upwards occur at intervals (for example, 70 m, 80 m and 95 m, Log 1, Fig. 2).

Continuous intervals of cobble to boulder-rich conglomerates extend up to 11 m in thickness (for example, Fig. 2, log 1, 57 to 68 m), but typically occur in beds 1 to 2 m thick (multiple intervals in log 2, Figs 2, 3, and 4D). These facies are predominantly normally graded, with sharp bed bases in all cases. Some deposits occur above irregular basal contacts, defining lenticular lithosomes 5 m wide and 0·75 m thick (Fig. 4D). Granule to pebble-rich conglomerates share many of these characteristics with their coarser-grained counterparts, but tend to occur as thinner (*ca* 0·5 m beds). Furthermore, although the cobble to boulder-rich conglomerates are rare, the granule to pebble-rich varieties occur with greater regularity and over intervals of ≤5 m.

Matrix-supported conglomerates are comparatively rare, with bed thicknesses typically <30 cm, attaining clast-width in the case of boulder-bearing beds. In contrast with their pebble to boulder-rich counterparts, these conglomerates are ungraded. Internally, pebble-sized mud chips are observed, forming detached rootless folds in some instances (Fig. 4E).

Interpretation

The clast-supported pebble to boulder conglomerates are interpreted as hyperconcentrated flow deposits (massive) and high-density turbidites (normally graded) (cf. Lowe, 1982; Kneller, 1995; Mulder & Alexander, 2001; Winsemann *et al.*, 2009; Talling *et al.*, 2012). High sediment concentrations within these flows act to dampen turbulence, and thus hinder the development of bedforms (Talling *et al.*, 2012). The transition from massive to normally graded varieties is interpreted to reflect flow transformation from moderate cohesive strength debris flows to turbidity currents (Hampton, 1972; Tinterri *et al.*, 2003; Amy & Talling, 2006; Talling *et al.*, 2012). In this scenario, dilution and mixing with the overlying water column during downslope remobilization promotes increased turbulence and sorting, leading to deposition of normally graded beds. It is noteworthy that within the northern Kingston Range, massive hyperconcentrated flows dominate (Le Heron *et al.*, 2014), whereas downslope in the southern Kingston Range more dilute, turbidites are far better developed.

Thickening-upward conglomeratic bedsets are interpreted to record the build-up of lobe elements, the constituent 'building blocks' of depositional lobes which, in turn, stack to form a lobe complex (Prélat *et al.*, 2010; MacDonald *et al.*, 2011). An axis to off-axis position within the lobe complex is favoured by their coarse calibre and occurrence of amalgamated bedsets (Prélat *et al.*, 2010; Prélat & Hodgson, 2013). Stacked conglomeratic lobe elements are commonly overlain by siltstones of the interbedded heterolithics facies association, representing lobe switching/abandonment.

Matrix-supported conglomerates are interpreted as debris flows of a moderate cohesive strength. Pebble-sized mud chips are interpreted as rip-up clasts incorporated from underlying semi-lithified silt-grade sediments; their chaotic orientation is consistent with transport within a debris flow (Talling *et al.*, 2012). The rarity of these debrites in the succession of the southern Kingston Range is remarkable given that 6 km further north abundant, matrix-supported conglomerates interpreted as glaciogenic debris flows (GDFs) are preserved (Le Heron *et al.*, 2014). This provides further credence that the southern Kingston Range represents a more distal depositional setting. By analogy to Pleistocene glacier-fed deep marine environments, these sediments are interpreted as elongate debrite lobes interfingering with turbidites on the slope and into the basin plain (Escutia *et al.*, 2000; Taylor *et al.*, 2002).

Interbedded heterolithics facies association

Description

This facies association comprises closely interbedded siltstones and thick-bedded, normally graded sandstones; they occur either as isolated beds punctuating siltstone facies, or as the basal part of coarsening-upward and thickening-upward cycles that culminate in conglomerates (Fig. 5A). The sandstones exhibit classic sole mark structures at their bases, including flute marks and grooves (Fig. 5B), and sharp to irregular bed bases (Fig. 5C). Composite cross-laminations with climbing geometries are common. Additionally, flame structures occur at the contact between sandstones and underlying siltstones, and convolute bedding locally disrupts or obscures bed contacts. The graded sandstones occur with similar stratigraphic regularity to their granule to pebble-rich conglomerate counterparts. Two isolated examples of ungraded sandstones with dune-scale cross-stratification are also recorded, at 25 m and 27 m in Log 1 (Fig. 2). The beds are sharp-based and bounded by siltstone facies.

Lonestone-free siltstones constitute approximately 40% of the succession by volume studied in the southern Kingston Range. Intervals of thin-bedded and normally graded sandstones (2 to 10 cm thick) are intercalated with siltstone facies. Siltstone-dominated intervals contain variable thicknesses of associated fine to very fine-grained cross-laminated sandstones. These are expressed as both laterally continuous sets and as laterally disconnected to isolated lenses (Fig. 5E and F). Both morphologies exhibit principal palaeoflow towards the south-east. In vertical section, both cross-lamina cosets and stratigraphically isolated cross-lamina intervals occur. Some cosets express climbing ripple cross-stratification (Fig. 5E). Piled load casts occur between superposed laminae, and flame structures occur at the base of some of the thin sandstone intervals (Fig. 5E). Detached elliptical load-casts, composed of individual cross-lamina lenses, are also preserved (Fig. 5F).

Interpretation

The majority of the thick-bedded sandstones are interpreted as T_A, $T_{B\text{-}2}$ and T_C turbidites. The

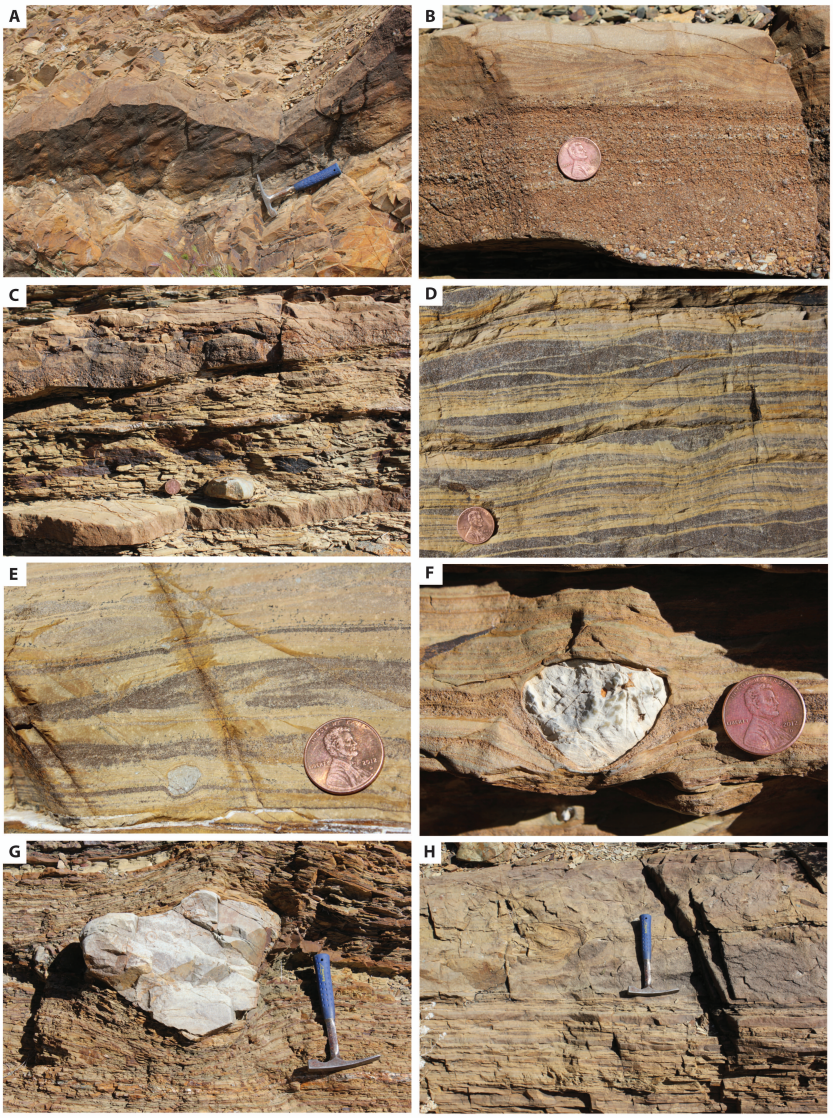

Fig. 5. Mesoscale phenomena. (A) Flute casts indicating south-easterly flow. (B) Classic T_{A-C} cycle. Note the characteristic sharp grain-size break between the parallel laminated T_B interval and the ripple cross-laminated T_C subdivision. (C) Intercalated graded sandstone beds and lonestone-bearing shales (indicated by arrows). (D) Climbing ripple sets, starved ripple lenses and shale laminae. Load clasts occur beneath the sandstone intervals. (E) 2 m along strike from image in (D), showing a small dolostone granule with classic impact structure (hence a dropstone) beneath. (F) Pebble-sized dropstone, clearing puncturing a centimetre-thick graded bed. (G) Boulder-sized dropstone, typical of the interval 55 to 80 m in log 2. (H) Matrix supported, muddy conglomerare with detached, rootless, recumbent fold within the bed. Scales: Hammer is 32 cm long, coin is 1 ·9 cm in diameter.

exception may be the cross-stratified sandstones, because the generation of dune-scale cross-stratification is rare in turbidites, possibly owing to the rapidity of sediment fallout suppressing their development (Talling *et al.*, 2012, and references therein). These sandstones are therefore more likely to originate through localized bottom-current reworking than from a primarily turbulent process.

Within the dominant turbidite facies, the contact between the T_{B-2} and T_C subdivisions is characterized by a grain-size break, recently summarized by Talling *et al.* (2012) as a commonplace phenomenon in high density turbidites. However, ripple cross-laminated intervals support fully turbulent conditions within low-density turbidity currents (T_C; Mulder & Alexander, 2001; Baas *et al.*, 2011; Talling *et al.*, 2012). Cross-lamination with climbing geometries also reflects fully turbulent conditions but under more rapid rates of sedimentation (Baas, 2000; Kane & Hodgson, 2010; Jobe *et al.*, 2012). The grain-size break between the T_{B-2} and T_C subdivisions there-fore probably records a bipartite structure to the flow in which comparatively higher and lower sediment concentration layers become differenti-ated as the flow evolves (Mutti, 1992; Mutti *et al.*, 2003). Cross-laminated intervals are bounded by planar laminated and massive siltstones, inter-preted to record dilute, low-density turbidity cur-rent deposits (T_D and T_{E-1}; Talling *et al.*, 2012) and hemipelagic fallout from the turbulent sus-pension during waning flow (e.g. Allen *et al.*, 2004). The range of ripple morphologies – both as laterally continuous sets and isolated lenses – indicates fluctuations in sand supply in the dilute

turbidity currents, alongside elevated tractional re-working (e.g. Talling *et al.*, 2007, 2012). The piled load casts, detached elliptical load casts and flame structures originate through density contrasts between rapidly deposited sand and underlying muds (Rayleigh-Taylor instabilities; Allen, 1984). The thick, uninterrupted accumulations of this facies over tens of metres suggest continuous input of dilute sediment into the basin.

Lonestone-bearing facies association

Description

Lonestone-bearing strata constitute approximately 30% of the studied sections. Lithologically the sediments are nearly identical to the lonestone-free siltstones of the interbedded heterolithic facies association, comprising massive, laminated and ripple-cross laminated siltstones and fine sandstones. Strata assigned to this facies association tend to exhibit lonestones over decimetre-scale stratigraphic intervals: note that centimetre-thick, lonestone-free beds occur within these intervals. The following considers 'outsize clasts' as granule-size and larger, i.e. the assignment was undertaken on the basis of macroscopic rather than microscopic textures.

The lonestone-bearing heterolithics contain granule to boulder-sized lonestones dominated by carbonate (both limestone and dolostone are represented), occasional siltstone and arkose, and rarely quartzite. Clear flexure of underlying laminae beneath these lonestones can be demonstrated (Fig. 5G and H). Most commonly, isolated clasts are found in the T_e subdivision, but at some levels, clast clusters are observed. In a large number of cases, puncturing and/or abrupt termination of laminae occurs against the margins of the clast, and non-deformed strata overlie the lonestone.

It should be noted that the size of lonestones varies considerably upsection: the greatest concentration of cobble-sized and boulder-sized clasts occurs towards the middle part of Log 2 (52 to 80 m; Fig. 3). At this stratigraphic level, it is estimated that pebble to cobble-grade lonestones account for approximately 8 to 10% by stratal volume. Lonestone frequency is considerably lower (2 to 6%) at most other stratigraphic levels. Rarely, concentrated intervals of small lonestones (i.e. granules to small pebbles) occur over 2 to 3 cm stratigraphic intervals. These thin belts of lonestones transcend clear-cut lithological boundaries in centimetre-thick graded beds.

In vertical section, four examples of a switch between interbedded heterolithics to the lonestone-bearing facies association are noted in the most complete study section herein (Fig. 2). Nevertheless, there are considerable lateral variations on this trend along strike. For example, lonestone-bearing facies in log 2 (27 to 33 m, Fig. 2) correlate with lonestone-free sediments in log 3 (7 to 10 m, Fig. 2). The basal section of Log 1 (Fig. 2), which based upon local correlation is not preserved at the base of the other logged sections, demonstrates a notable absence of lonestones.

Interpretation

The lonestone-bearing facies association, akin to comparable lonestone-free siltstones of the interbedded heterolithic facies, is interpreted as the product of fully turbulent, low-density turbidity currents. In this facies association, the deflected and pierced laminae beneath lonestones, in concert with undeformed laminae that drape them, is strong evidence that they are IRD. Bouncing clasts in a turbulent suspension load has long been predicted (Lowe, 1982) but this has not been reproduced experimentally (Talling *et al.*, 2012). Therefore, gravity flow processes should be dismissed as a possibility for forming the dropstone textures. Moreover, dilute, low-density flows would not have the cohesive strength to 'raft' up to boulder-sized lonestones. Their presence within delicate ripple cross-laminated siltstones and fine sandstones can only readily be explained by ice-rafting processes: other mechanisms for the generation of dropstones (attached to the roots of trees, seaward rafting and animal ingestion: Bennett *et al.*, 1996) are clearly inappropriate for Cryogenian strata.

The lateral and vertical variability of IRD is remarkable. By transcending lithological boundaries, the thin belts of granule to small pebble-sized lonestones demonstrate that these were also deposited as IRD. It is perhaps surprising that no occurrences of 'trains' of granule-grade lonestones (i.e. single-clast thick layers of material) are noted in the southern Kingston Range which might point to local winnowing. Correlation between closely spaced sections (Fig. 2) suggests that the absence of IRD in small, isolated sections should be treated with caution, highlighting that multiple traverses are important to properly document the trends. Clearly, the absence of IRD in a single section does not imply sedimentation free from glacial influence.

The four clear transitions from thin bedded heterolithics to lonestone-bearing facies associations observed in the study section imply that IRD delivery to the basin was pulsed. The potential mechanisms for this are considered in detail elsewhere (Le Heron, 2015). The lateral correlation between lonestone-free and lonestone-bearing deposits may simply imply that certain areas of the Southern Kingston Range escaped the influence of ice-rafted material.

In summary, there appear to be caveats associated with the interpretation of an ice-rafting influence based on lonestones. In addition, the approach does not account for the mudstone fraction, and it has long been known that till pellets can be incorporated into fine-grained rocks, providing more cryptic evidence of IRD. Till pellets are macroscopic, typically rounded, grains of clay or diamicton in modern and Quaternary deposits (Cowan *et al.*, 2012); they have long been thought to form from suspended sediment in interstices between melting ice crystals, developing in a range of supraglacial to subglacial environments (Ovenshine, 1970). The problem is that texturally identical structures are revealed as mudstone aggregates in fluvial settings (Gastaldo *et al.*, 2013) implying that they are not firmly diagnostic of ice-rafting.

Lateral and vertical facies association distributions

The studied sections preserve thick accumulations of thin bedded heterolithics, punctuated at irregular intervals by conglomeratic beds which are typically thicker towards the north-west and thin towards the south-east. The thickest conglomerate package (57 to 68 m Log 1, Fig. 2) can be walked out laterally where it thins to 2 m (4 to 6 m Log 2, Fig. 2). This relationship both demonstrates the extent of along-strike pinch out, and facilitates correlation between other beds.

Upsection, a succession of stacked normally graded conglomerates (88 to 102 m Log 1, Fig. 2) correlates down-dip with a much more heterogeneous package of thinner conglomerates and sandstones (32·5 to 59 m Log 2, Fig. 2), separated by lonestone-bearing and lonestone-free heterolithics. Similarly, three conglomeratic beds above (117 to 125 m Log 1, Fig. 2) thin over a distance of <100 m between logs 1 and 2, whereas siltstone and fine sandstone packages typically thicken to the south-east (Fig. 2). This is consistent with the regional trend of successions thickening to the south-east observed in the northern Kingston Range (Le Heron *et al.*, 2014) which, in tandem with the strongly preferred palaeoflow to the south-east (ripple foresets, Fig. 2), supports a regional south-east dipping palaeoslope. The pinch out relationships of the coarser facies are therefore interpreted to record proximal to distal thinning as sediment fallout proceeds downslope.

DISCUSSION

Palaeogeography

There is a strong motivation for integrating data from the southern Kingston Range with that from other outcrop belts across the Death Valley area into a regional context. Stratigraphic frameworks have been developed by many other workers, and a detailed facies model has been presented for the Panamint Range towards the west (Miller, 1985). To date, an integrated sedimentological framework for the eastern Death Valley area has not hitherto been proposed (Fig. 6). As a first step towards such a model, integrating data from the southern Kingston Range (present paper), the northern and central portions of the range (Le Heron *et al.*, 2014), Sperry Wash (Busfield & Le Heron, 2015; this volume) and the Silurian Hills (Kupfer, 1960; Basse, 1978) allows a gross depositional environment (palaeogeographic) map to be proposed for the south-eastern Death Valley region (Fig. 7). This map should be regarded as preliminary. When directional data from the south of the Kingston Range is integrated with the evidence for systematic and consistent thickening from the northern to the southern part of the range (Mrofka, 2010; MacDonald *et al.*, 2013; Le Heron *et al.*, 2014), strong evidence emerges of a regional south-east dipping slope (Fig. 7). From this map view, the olistostrome is interpreted to be restricted to a zone south of a north-east/south-west oriented growth fault system: this is proven in the northern Kingston Range (Prave, 1999; Le Heron *et al.*, 2014) yet speculative north of the Silurian Hills (Fig. 7): basement clasts and angular dolostone blocks are mapped in the Kingston Peak Formation in that area (Kupfer, 1960).

Owing to its palaeogeographic position, it is notable that strata in the southern Kingston Range exhibit much more evidence of IRD than

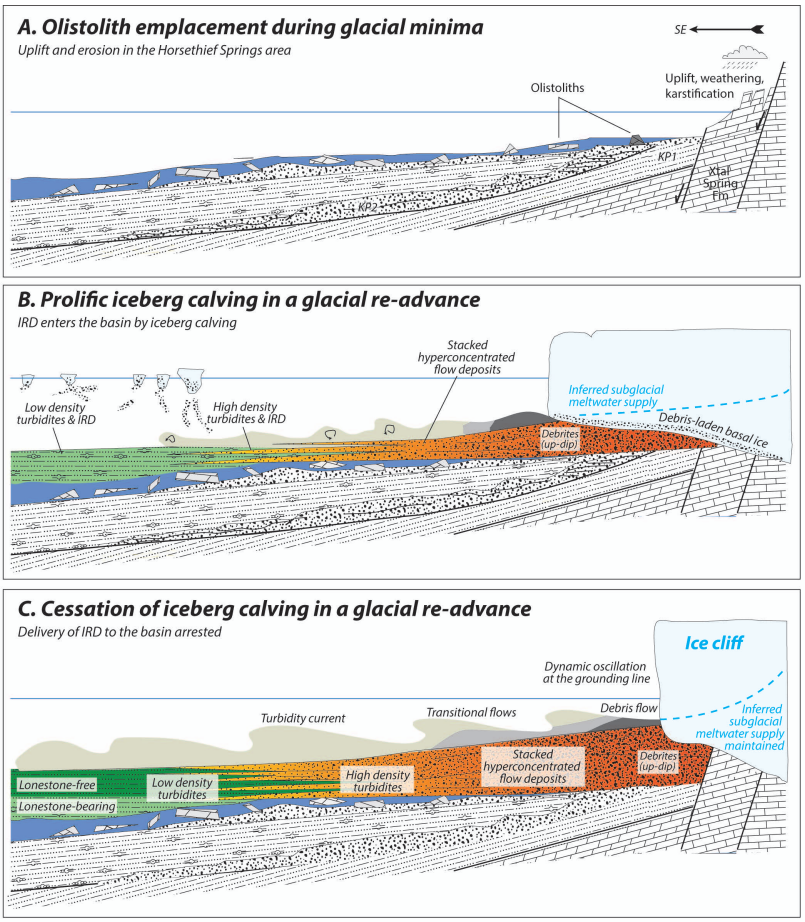

Fig. 6. Summary depositional model for the supra-olistostrome interval. Following a glacial minimum (A), when the olistostrome was emplaced, ice sheets repopulated highlands. Uplands were a source area for both the olistostrome and supra-olistostrome gravity flow deposits. During glacial re-advance (B), icebergs delivered debris-laden material to the ice front. A fairly constant meltwater supply was maintained to generate repetitively stacked gravity flow deposits, and icebergs shed ice-rafted debris (IRD). (C) Dynamic oscillation of the grounding line in the hinterland, in this case minor recession and cessation of iceberg calving, halted the delivery of IRD. Meanwhile, gravity flows continued to deliver sediment to the basin.

their northern counterparts. Towards the northern part of the range, IRD is restricted to strata immediately between the KP2 diamictite and the basal olistostrome strata where they occur over a *ca* 15 m interval (Le Heron *et al.*, 2014). This highlights the importance of palaeogeographic position in the recognition of IRD in Neoproterozoic strata, illustrating that in this case more proximal strata allow a less compelling case for a dropstone influence to be made. In terms of gross facies comparisons, sandy debrites are more commonplace in the northern Kingston Range (Le Heron *et al.*, 2014), whereas high density turbidites are the expression of the coarsest, thickest beds in the interbedded heterolithics in the southern part of the range. This implies that individual GDF lobes either terminate in an intermediate zone or pass distally into turbidites.

Some 50 km to the west of the southern Kingston Range, the Sperry Wash area is proposed to have periodically occupied an ice-grounding line position, and a generally more proximal position in the basin, during the deposition of unit KP3 (Fig. 7; Busfield & Le Heron, 2015, this volume). When integrated with the evidence for proximal–distal transition from debrites to turbidites in the Kingston Range, it is proposed that the belt dominated by debrite deposition is unlikely to have exceeded a width of more than about 10 km from proximal to distal at the ice maximum (Fig. 7). The Sperry Wash outcrop belt also exhibits evidence for a consistent south-east dipping palaeoslope, with almost identical palaeoflow orientations to the southern Kingston Range (Busfield & Le Heron, 2015, this volume). On the palaeogeographic map presented here, note that the east–west oriented ice margin is tentatively extended to the Saddle Peak Hills, where closely comparable graded beds, IRD-rich intervals and intrabed deformed zones to the Sperry Wash area can be observed.

Busfield & Le Heron (2015) suggest that the Sperry Wash area may have occupied a fjord setting, hence implying that this part of the basin was fed by a valley glacier draining an upland area to the north. Indeed, Wright *et al.* (1974)

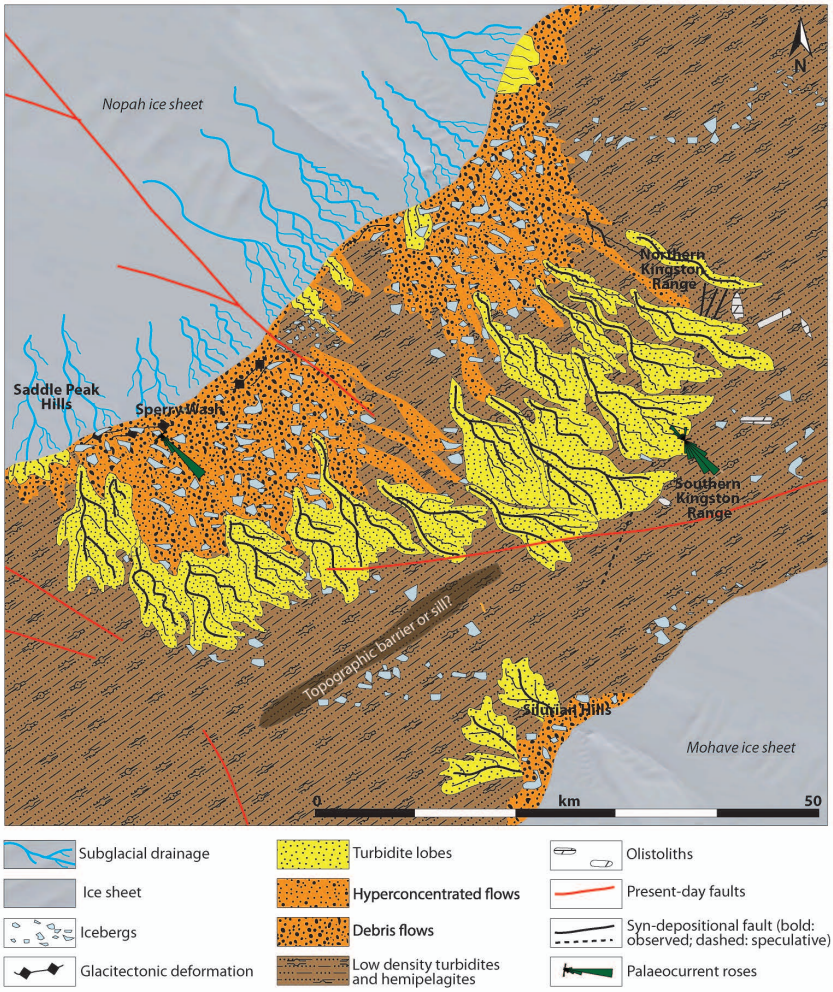

Fig. 7. Gross depositional environments (palaeogeographic) sketch map of the Death Valley area during Kingston Peak times, showing the posited location of the ice front over Sperry Wash (see Busfield & Le Heron, this volume), with the southern Kingston Range representing a comparatively ice-distal location. The southern Kingston Range received thick accumulations of turbidites and, less commonly, debrites ultimately derived from the ice margin located towards the north-west.

proposed that the area covered by the map in Fig. 7 was divided into two upland regions during deposition of the Pahrump Group: the Nopah Upland to the north of Sperry Wash and the Kingston Range, and the Mojave Upland range immediately south of the present day Silurian Hills. In addition to the palaeocurrent data herein and contained in Busfield & Le Heron (2015), further evidence for the presence of highlands include the direct contact of the Noonday Dolomite onto gneissose basement at the Gunsight Mine south of Tecopa (Mrofka, 2000).

In the model of Wright *et al.* (1974), regional slopes from the north and south fed down into an east–west oriented basin (the Armargosa Basin). This configuration is adopted in the preliminary palaeogeography herein, two ice masses are proposed which are termed the Mojave ice sheet and the Nopah ice sheet. The present authors also postulate the existence of a spur separating Sperry Wash and Silurian Hills (Fig. 7). The reason for this is that whilst lonestones in the Silurian Hills are almost exclusively gneiss, schist and granite (Basse, 1978), none of these lithologies have been observed in the Sperry Wash area, implying the presence of a physical barrier preventing the drift of icebergs towards the north. Conversely, the Sperry Wash area records no evidence for basement clasts akin to those recovered from the Silurian Hills (Busfield & Le Heron, 2015; this volume). Noting that lateral offset between these two areas also certainly occurred during the Cenozoic (Blakely *et al.*, 1999), two credible hypotheses emerge: (i) a silled basin; or (ii) a ridge of land to prevent the mixing of icebergs, and hence IRD, between them. No data are currently available that allow these hypotheses to be tested.

Further afield, a substantial dataset was collected in the Panamint Range at the western margin of Death Valley in the thesis work of Miller (1983). In the Panamints, the Kingston Peak Formation has historically been divided into a series of members, including the basal Limekiln Spring Member and overlying Surprise

Member (Miller, 1985; and references therein). These rocks, which are overlain by a carbonate unit (Sourdough Limestone Member), were argued to correspond to the first phase of rifting to affect the Death Valley region in the Cryogenian (Prave, 1999), stratigraphically equivalent to units KP2 and KP3 in the Kingston Range (MacDonald *et al.*, 2013) and hence to the Sturtian glacial event. A fence diagram and offlap relationships documented in Miller (1985) suggest a northward-dipping basin margin in that region during this glaciation, including during emplacement of basalts coeval with deposition of the Surprise Member.

Data from the Panamint Range, when considered alongside palaeocurrent data in Fig. 7, imply a complex regional basin configuration during deposition of the Sturtian-aged strata. In summary, the data suggest two opposing regional palaeoslopes: a northward slope in the Panamints (Miller, 1985) and in the Silurian Hills (Wright *et al.*, 1974); and a south-eastward slope in the Kingston Range/Sperry Wash area. Although regional rotation during Tertiary transtension cannot be ruled out, the regional data incorporating observations from the Panamints strengthens the interpretation of two ice masses flowing in opposing directions to the south (the Nopah ice sheet) and to the north (the Mohave ice sheet; Fig. 7).

Global implications

Careful investigation of the Southern Kingston Range succession, together with neighbouring outcrop belts in the Death Valley, illustrates that the strata exhibit strong evidence for glaciomarine sedimentation in a proglacial basin. The predominance of turbidite deposits, with well-expressed south-east directed palaeocurrents, are posited to have evolved from debrites further north in the Kingston Range. Documenting the lateral and vertical distribution of IRD in this region allows the present authors to emphasise that: (i) IRD has a complex lateral and vertical distribution on a local scale in proglacial strata but, in spite of this; (ii) the record of ice rafting is more clearly expressed at a distance of some tens of kilometres from the palaeo-ice margin than in more proximal settings. The palaeogeographic map (Fig. 7) based on these data is the first detailed attempt to do so in the eastern Death Valley area. Moreover, it allows a first order interpretation of the location and orientation of the ice grounding zone when integrated from data in Sperry Wash (Busfield & Le Heron, 2015, this volume). It is notable that grounding-line wedges have been documented from other Cryogenian sedimentary records (Domack & Hoffman, 2011), and their recognition is an important step in palaeogeographic reconstruction.

Cryogenian glacial deposits continue to be viewed as deposits of snowball Earth conditions (Hoffman *et al.*, 1998) by much of the geological community, rather than deposits of ice sheets exhibiting a near-identical sedimentary record to their Phanerozoic counterparts (e.g. Etienne *et al.*, 2007). Other interpretations such as a 'slushball Earth' compromise including the relative contributions of a high-tilt Earth and tectonic processes (see Fairchild & Kennedy, 2007; for a review) commonly are sidelined. Papers attempting to quantify, via numerical models, the magnitude of post-glacial sea-level rise (Creveling & Mitrovica, 2014), to simulate the climate of Cryogenian glaciations (Feulner & Kienert, 2014), or wishing to emphasize the significance of benthic macroscopic phototrophs (fossil finds) in associated strata (Ye *et al.*, 2015) all begin with the starting assumption of a snowball Earth with a global, or near global, ice cover. Predictions of the snowball Earth model stipulate equatorial temperatures of −20°C (Hoffman & Schrag, 2002). However, sedimentological evidence from the Marinoan glacial succession of South Australia reveals periglacial sand wedges demonstrating an active regolith layer at the palaeotropics, and therefore mean surface temperatures 'within a few degrees of freezing' (Ewing *et al.*, 2014).

In the Sturtian record, meanwhile, the Kingston Peak Formation does not support the interpretation of a continuous ice cover, with transitions from ice contact to proglacial basins envisaged. In concert with previous studies emphasising IRD abundance in Cryogenian strata (Condon *et al.*, 2002; Leather *et al.*, 2002), or wave generated structures implying ice-free areas (Allen & Etienne, 2008; Busfield & Le Heron, 2014), the present authors envisage highly dynamic, polythermal ice masses (Hambrey & Glasser, 2012). These ice masses exhibited multiple advance and retreat cycles, releasing prodigious volumes of meltwater to explain repeatedly stacked GDFs (in more proximal settings) and turbidites (in more distal settings) in tandem with IRD. These characteristics strongly negate the requirement for refugia or speculative polynyas to support 'survivalist' ecosystems (e.g. Ye *et al.*, 2015), particularly as glacial minima conditions

(Le Heron *et al.*, 2014) and possible interglacials are expected to yield open water conditions. In summary, the collection of basic sedimentological datasets, to facilitate the compilation of palaeogeographic maps, remains fundamental to the debate.

CONCLUSIONS

- In the southern part of the Kingston Range, a multi-kilometre thick succession of the Kingston Peak Formation includes an olistostrome succession and a supra-olistostrome succession in unit KP3. In the central Kingston Range, the olistostrome was interpreted as the deposits of a Sturtian glacial minimum, produced during an isostatic rebound event prior to glacial re-advance (Le Heron *et al.*, 2014). In the south of the range, exceptional exposure quality allows detailed documentation of the supra-olistostrome deposits via five high resolution sedimentary logs;
- The supra-olistostrome succession contains three facies associations. The pebble to boulder conglomerate facies association records deposition from hyperconcentrated flows to high density turbidity flows, ultimately debouched from the ice margin. The heterolithic facies association is the more distal part of this system, deposited by more dilute turbidity currents. The lonestone-bearing facies association, meanwhile, additionally records the accumulation of IRD in this underflow-dominated proglacial setting;
- Consideration of the lateral relationship between facies illustrates that although the thickest beds and intervals can be traced at outcrop over several hundreds of metres, significant bed thinning occurs over several tens of metres. Together with palaeocurrent data recovered from ripple cross-lamination, grooves and flutes casts, a pronounced south-east directed slope is identified;
- A preliminary palaeogeographic map of the eastern Death Valley area interprets a consistent south-east directed palaeoslope that included all parts of the Kingston Range and the Sperry Wash area. An ice mass grounded in the latter area released efflux as GDFs into the basin, forming a conglomerate-rich apron about 10 km in extent from proximal to distal. Beyond this zone, turbidite deposition was dominant, and IRD is well-preserved.

ACKNOWLEDGEMENTS

This work was part-supported by the Geological Society of London Fermor Fund. This paper is dedicated to Tony Prave to whom the authors are indebted for his general advice, and discussions in the field in an earlier field season which led to our 2014 paper from an earlier phase of work. We are grateful to the Chief Editor, Nigel Mountney, for his patience, to three anonymous reviewers, and to Julian Dowdeswell for his thoughts on the manuscript; this led to a much improved paper.

REFERENCES

Allen, J.R.L. (1984) *Sedimentary Structures: Their Character and Physical Basis*, Volumes I and II. Elsevier, Amsterdam.

Allen, P.A. and Etienne, J.L. (2008) Sedimentary challenge to snowball Earth. *Nat. Geosci.*, 1, 817 825.

Amy, L. and Talling, P.J. (2006) Anatomy of turbidite and debrite sandstones based on long distance (120 × 35 km) bed correlation, Marnoso arenacea Formation, Northern Apennines, Italy. *Sedimentology*, 53, 161 212.

Baas, J.H. (2000) Duration of deposition from decelerating high density turbidity currents. *Sed. Geol.*, 136, 71 88.

Baas, J.H., Best, J.L. and Peakall, J. (2011) Depositional processes, bedform development and hybrid flows in rapidly decelerated cohesive (mud sand) sediment flows. *Sedimentology*, 58, 1953 1987.

Basse, R.A. (1978) *Stratigraphy, Sedimentology and Depositional Setting of the Late Precambrian Pahrump Group, Silurian Hills, California*. MS Thesis, Stanford University, ?????, 86 pp.

Bennett, M.R., Doyle, P. and Mather, A.E. (1996) Dropstones: their origin and significance. *Palaeogeogr. Palaeoclimatol. Palaeoecol.*, 121, 331 339.

Blakely, R.J., Jachens, R.C., Calzia, J.P. and Langenheim, V.E. (1999) Cenozoic basins of the Death Valley extended terrane as reflected in regional scale gravity anomalies. In: *Cenozoic Basins of the Death Valley Region* (Eds L.A. Wright and B.W. Troxel), pp. ??? ???. Geological Society of America Special Paper 333, Boulder, Colorado.

Busfield, M.E. and Le Heron, D.P. (2014) Sequencing the Sturtian icehouse: dynamic ice behaviour in South Australia. *J. Geol. Soc. London*, 171, 443 456.

Busfield, M.E. and Le Heron, D.P. (2015, this volume) A Neoproterozoic ice advance sequence, Sperry Wash, California. *Sedimentology*, ???, ??? ???.

Condon, D.J., Prave, A.R. and Benn, D.I. (2002) Neoproterozoic glacial rainout intervals: observations and implications. *Geology*, 30, 35 38.

Cowan, E.A., Christofferson, P. and Powell, R.D. (2012) Sedimentological signature of a deformable bed preserved beneath an ice stream in a Late Pleistocene Glacial Sequence, Ross Sea, Antarctica. *J. Sed. Res.*, 82, 270 282.

Creveling, J.R. and Mitrovica, J.X. (2014) The sea level fingerprint of a Snowball Earth deglaciation. *Earth Planet. Sci. Lett.*, 399, 74 85.

Domack, E.W. and Hoffman, P.F. (2011) An ice grounding line wedge from the Ghaub glaciation (635 Ma) on the distal foreslope of the Otavi carbonate platform, Namibia, and its bearing on the snowball Earth hypothesis. *Geol. Soc. Am. Bull.*, 123, 1448 1477.

Escutia, C., Eittreim, S.L., Cooper, A.K. and Nelson, C.H. (2000) Morphology and acoustic character of the Antarctic Wilkes Land turbidite systems: icesheet sourced versus river sourced fans. *J. Sed. Res.*, 70, 84 93.

Etienne, J.L., Allen, P.A., Rieu, R. and Le Guerroue, E. (2007) Neoproterozoic glaciated basins: a critical review of the Snowball Earth hypothesis by comparison with Phanerozoic glaciations. In: *Glacial Processes and Products* (Eds M.J. Hambrey, P. Christoffersen, N.F. Glasser and B. Hubbard), *Int. Assoc. Sedimentol. Spec. Publ.*, ???, 436.

Evans, D.A.D. (2000) Stratigraphic, geochronological, and paleomagnetic constraints upon the Neoproterozoic climatic paradox. *Am. J. Sci.*, 300, 347 433.

Ewing, R.C., Eisenman, I., Lamb, M.P., Poppick, L., Maloof, A.C. and Fischer, W.W. (2014) New constraints on equatorial temperatures during a late Neoproterozoic snowball Earth glaciation. *Earth Planet. Sci. Lett.*, 406, 110 122.

Eyles, N. and Januszczak, N. (2004) 'Zipper rift': a tectonic model for Neoproterozoic glaciations during the breakup of Rodinia after 750 Ma. *Earth Sci. Rev.*, 65, 1 73.

Fairchild, I.J. and Kennedy, M.J. (2007) Neoproterozoic glaciation in the Earth System. *J. Geol. Soc. London*, 164, 895 921.

Feulner, G. and Kienert, H. (2014) Climate simulations of Neoproterozoic Snowball Earth events; similar critical carbon dioxide levels for the Sturtian and Marinoan glaciations. *Earth Planet. Sci. Lett.*, 404, 200 205.

Gastaldo, R.A., Pludow, B.A. and Neveling, J. (2013) Mud Aggregates from the Katberg Formation, South Africa: additional evidence for early Triassic Degradational Landscapes. *J. Sed. Res.*, 83, 531 540.

Hambrey, M.J. and Glasser, N.F. (2012) Discriminating glacier thermal and dynamic regimes in the sedimentary record. *Sed. Geol.*, 251, 1 33.

Hampton, M.A. (1972) The role of subaqueous debris flow in generating turbidity currents. *J. Sed. Petrol.*, 42, 775 793.

Hoffman, P.F. and Schrag, D.P. (2002) The snowball Earth hypothesis: testing the limits of global change. *Terra Nova*, 14, 129 155.

Hoffman, P.F., Kaufman, A.J., Halverson, G.P. and Schrag, D.P. (1998) A neoproterozoic snowball earth. *Science*, 281, 1342 1346.

Hyde, W.T., Crowley, T.J., Baum, S.K. and Peltier, R. (2000) Neoproterozoic 'snowball Earth' simulations with a coupled climate/ice sheet model. *Nature*, 405, 425 429.

Jobe, Z.R., Lowe, D.R. and Morris, W.R. (2012) Climbing ripple successions in turbidite systems: depositional environments, sedimentation rates and accumulation times. *Sedimentology*, 59, 867 898.

Kane, I.A. and Hodgson, D. (2010) Submarine channel levees: criteria for recognition of levee subenvironments: exhumed examples from The Rosario Fm (Baja, Mexico) and the Laingsburg Fm. (Karoo Basin). *Mar. Petrol. Geol.*, 28, 807 823.

Kneller, B.C. (1995) Beyond the turbidite paradigm: physical models for deposition of turbidites and their implications for reservoir potential. In: *Characterization of Deep Marine Systems* (Eds A.J. Hartley and D.J. Prosser), *Geol. Soc. Spec. Publ.*, 94, 31 49.

Kupfer, D.H. (1960) Thrust faulting and chaos structure, Silurian Hills, San Bernadino County, California. *GSA Bull.*, 71, 181 214.

Labotka, T.C., Albee, A.L., Lanphere, M.A. and McDowell, S.D. (1980) Stratigraphy, structure and metamorphism in the central Panamint Mountains (Telescope Peak quadrangle), Death Valley area, California. *Geol. Soc. Am. Bull.*, 91, 843 933.

Le Heron, D.P. (2015) The significance of ice rafted debris in Sturtian glacial successions. *Sed. Geol.*, 322, 19 33.

Le Heron, D.P., Busfield, M.E. and Prave, A.R. (2014) Neoproterozoic ice sheets and olistoliths: multiple glacial cycles in the Kingston Peak Formation, California. *J. Geol. Soc. London*. doi: 10.1144/jgs2013 130

Le Hir, G., Ramstein, G., Donnadieu, Y. and Pierrehumbert, R.T. (2007) Investigating plausible mechanisms to trigger a deglaciation from a hard Snowball Earth. *C. R. Geosci.*, 339, 274 287.

Leather, J., Allen, P.A., Brasier, M.D. and Cozzi, A. (2002) Neoproterozoic snowball Earth under scrutiny: evidence from the Fiq glaciation of Oman. *Geology*, 30, 891 894.

Link, P.K., Miller, J.M.G. and Christie-Blick, N. (1993) Glacial marine facies in a continental rift environment: Neoproterozoic rocks of the western United States Cordillera. In: *Earth's Glacial Record* (Eds M. Deynoux, J.M.G. Miller, E.W. Domack, N. Eyles, I.J. Fairchild and G.M. Young), pp. 29 46. Cambridge University Press, Cambridge.

Lowe, D.R. (1982) Sediment gravity flows: II. Depositional models with special reference to the deposits of high density turbidity currents. *J. Sed. Petrol.*, 52, 279 297.

MacDonald, F.A., Prave, A.R., Petterson, R., Smith, E.F., Pruss, S.B., Oates, K., Trotzuk, D. and Fallick, A.E. (2013) The Laurentian record of Neoproterozoic glaciation, tectonism, and eukaryotic evolution in Death Valley, California. *Geol. Soc. Am. Bull.*. doi:10.1130/B30789.1.

Mahon, R.C., Dehler, C.M., Link, P.K., Karlstrom, K.E. and Gehrels, G.E. (2014a) geochronologic and stratigraphic constraints on the Mesoproterozoic and Neoproterozoic Pahrump Group, Death Valley, California: a record of the assembly, stability, and breakup of Rodinia. *Geol. Soc. Am. Bull.*, 126, 652 664.

Mahon, R.C., Dehler, C.M., Link, P.K., Karlstrom, K.E. and Gehrels, G.E. (2014b) Detrital zircon provenance and paleogeography of the Pahrump Group and overlying strata, Death Valley, California. *Precambr. Res.*, 251, 102 117.

Miller, J.M.G. (1983) *Stratigraphy and Sedimentology of the Upper Proterozoic Kingston Peak Formation, Panamint Range, Eastern California*. PhD Thesis, University of California, Santa Barbara, California, 335 pp.

Miller, J.M.G. (1985) Glacial and syntectonic sedimentation: the upper Proterozoic Kingston Peak Formation, southern Panamint Range, eastern California. *Geol. Soc. Am. Bull.*, 96, 1537 1553.

Mrofka, D. (2010) *Competing Models for the Timing of Cryogenian Glaciation: Evidence from the Kingston Peak Formation, Southeastern California*. PhD dissertation, University of California, Riverside.

Mrofka, D. and Kennedy, M. (2011) The Kingston Peak Formation in the eastern Death Valley region. In: *The Geological Record of Neoproterozoic Glaciations* (Eds E.

Arnaud, G.P. Halverson and G. Shields Zhou), *Geol. Soc. London Mem.*, 36, 449 458.

Mulder, T. and Alexander, A. (2001) The physical character of subaqueous sedimentary density flows and their deposits. *Sedimentology*, 48, 269 299.

Mutti, E. (1992) *Turbidite Sandstones*. Istituto di Geologia Universita di Parma & AGIP, San Donato Milanese, 275 pp.

Mutti, E., Tinterri, R., Benevelli, G., diBase, D. and Cavanna, G. (2003) Deltaic, mixed and turbidite sedimentation of ancient foreland basins. *Mar. Petrol. Geol.*, 20, 733 755.

Ovenshine, A.T. (1970) Observations of iceberg rafting in Glacier Bay, Alaska, and the identification of ancient ice rafted deposits. *Geol. Soc. Am. Bull.*, 81, 891 894.

Petterson, R., Prave, A.R. and Wernicke, B.P. (2011) Glaciogenic and related strata of the Neoproterozoic Kingston Peak Formation in the Panamint Range, Death Valley region, California. In: *The Geological Record of Neoproterozoic Glaciations* (Eds E. Arnaud, G.P. Halverson and G. Shields Zhou), *Geol. Soc. London Mem.*, 36, 449 458.

Pierrehumbert, R.T. (2005) Climate dynamics of a hard snowball Earth. *J. Geophys. Res.*, 110 (D1), D01111. doi:10.1029/2004JD005162

Pierrehumbert, R.T., Abbot, D., Voight, A. and Koll, D. (2011) Neoproterozoic climate. *Annu. Rev. Earth Planet. Sci.*, 39, 417 460.

Prave, A.R. (1999) Two diamictites, two cap carbonates, two $\delta^{13}C$ excursions, two rifts: the Neoproterozoic Kingston Peak Formation, Death Valley, California. *Geology*, 27, 339 342.

Prélat, A. and Hodgson, D.M. (2013) The full range of turbidite bed thickness patterns in submarine lobes: controls and implications. *J. Geol. Soc.*, 170, 209 214.

Prélat, A., Covault, J.A., Hodgson, D.M., Fildani, A. and Flint, S.S. (2010) Intrinsic controls on the range of volumes, morphologies, and dimensions of submarine lobes. *Sed. Geol.*, 232, 66 76.

Rooney, A.D., MacDonald, F.A., Strauss, J.V., Dudás, F.O., Hallmann, C. and Selby, D. (2014) Re Os Geochronology and coupled Os Sr isotope constraints on the Sturtian snowball Earth. *Proc. Natl Acad. Sci. USA*, 111, 51 56.

Talling, P.J., Amy, L.A., Wynn, R.B., Blackbourn, G. and Gibson, O. (2007) Turbidity current evolution deduced from extensive thin turbidites: Marnoso Arenacea Formation (Miocene), Italian Apennines. *J. Sed. Res.*, 77, 172 196.

Talling, P.J., Masson, D.G., Sumner, E.J. and Malgesini, G. (2012) Subaqueous sediment density flows: depositional processes and deposit types. *Sedimentology*, 59, 1937 2003.

Taylor, J., Dowdeswell, J.A., Kenyon, N.H. and O'Cofaigh, C. (2002) Late Quaternary architecture of trough mouth fans: debris flows and suspended sediments on the Norwegian margin. In: *Glacier Influenced Sedimentation on High Latitude Continental Margins* (Eds J.A. Dowdeswell and C. O'Cofaigh), *Geol. Soc. London. Spec. Publ.*, 203, 55 71.

Tinterri, R., Drago, M., Consorni, A., Davoli, G. and Mutti, E. (2003) Modelling subaqeous bipartite sediment gravity flows on the basis of outcrop constraints: first results. *Mar. Pet. Geol.*, 20, 911 933.

Winsemann, J., Hornung, J.J., Meinsen, J., Bußmann, M. and Weber, C. (2009) Anatomy of a subaqueous ice contact fan and delta complex, Middle Pleistocene, North west Germany. *Sedimentology*, 56, 1041 1076.

Wright, L.A., Troxel, B.W., Williams, E.G., Roberts, M.T. and Diehl, P.E. (1974) Precambrian sedimentary environments of the Death Valley region, eastern California and Nevada. *Geological Society of America, Guidebook: Death Valley region, California and Nevada [Prepared for the 70th Annual Meeting of Cordilleran Section, Geological Society of America]* (Ed. ???. ?????), pp. 27 35. The Death Valley Publishing Company, Shoshone, CA.

Ye, Q., Tong, J., Xiao, S., Zhu, S., An, Z., Tian, L. and Hu, J. (2015) The survival of benthic macroscopic phototrophs on a Neoproterozoic snowball Earth. *Geology*, 43, 507 510.

Manuscript received 28 November 2014; revision accepted 5 August 2015

5.4. Progradational ice advance sequence, Sperry Wash

A Neoproterozoic ice advance sequence, Sperry Wash, California

Busfield, M.E. & Le Heron, D.P.

Sedimentology 2015-2016, *in press*
doi: 10.1111/sed.12210

Statement of contribution

- ***Data collection***
  - Busfield and Le Heron logged the studied section, and collected palaeocurrent and bedding data.
  - Busfield sampled the section for thin section analsysi, with particular emphasis on the strongly deformed units. Structural data, e.g. fold vergence, were also collected by Busfield.
  - Busfield described and interpreted the thin sections.
- ***Manuscript text***
  - Busfield decided to follow the facies association scheme of Le Heron et al. 2014b (Chapter 5.2) for consistency, and interpreted the facies and glacial history of the studied section. Busfield developed the depositional model of an advancing ice margin, and the evidence for ice-contact deformation.
  - Busfield authored the first draft of the manuscript, and all subsequent drafts following review and suggested edits from Le Heron.
- ***Figures***
  - Busfield illustrated all figures within the manuscript.
  - Busfield and Le Heron contributed photographs to the figures throughout.

Sedimentology (2015) doi: 10.1111/sed.12210

A Neoproterozoic ice advance sequence, Sperry Wash, California

MARIE E. BUSFIELD and DANIEL P. LE HERON
Department of Earth Sciences, Royal Holloway, University of London, Egham TW20 0EX, UK
(E-mail: marie.busfield.2011@live.rhul.ac.uk)

Associate Editor – Ian Fairchild

ABSTRACT

The Kingston Peak Formation is an archetypal Cryogenian succession that crops out across the Death Valley region of eastern California. Above pre-glacial strata (KP1), two distinct glacial phases have been recognized and are interpreted to be allied to the panglacial Sturtian (KP2 and KP3) and Marinoan (KP4) icehouse events. The thickest and most extensive unit, KP3, forms the entire exposed section at Sperry Wash. At this locality, ice-distal turbidites are succeeded in turn by ice-medial and ice-proximal facies, comprising a spectrum of ice-rafted debris-bearing turbidites, debrites and shales. These are overlain by ice-marginal grounding-line fan deposits interbedded with glacitectonically deformed heterolithics, supporting local advance to an ice-contact position. The succession records accumulation within a glacier-fed subaqueous shelf, wherein the clear progradational signature is driven by ice advance towards the south-east. Evolution of the subaqueous complex is five-fold, comprising: (i) ice-distal outwash; (ii) build-out of ice-medial depositional lobes; (iii) ice-proximal deposition and increased calving; (iv) resumed ice-margin advance; and (v) growth of ice-contact grounding-line fan. This sequence is unique in the Death Valley region for recording the first evidence of advance to ice-marginal and ice-contact settings, thereby enabling the location of the glacier terminus to be documented for the first time.

Keywords Cryogenian, Death Valley, grounding-line fan, ice advance, Kingston Peak Formation.

INTRODUCTION

The Cryogenian Period (*ca* 720 to 635 Ma) is characterized by two of the most extensive glaciations recorded in Earth history, broadly correlated with an older Sturtian (*ca* 717 to 662 Ma; Zhou *et al.*, 2004; Bowring *et al.*, 2007; Macdonald *et al.*, 2010) and younger terminating Marinoan (*ca* 635 Ma; Hoffmann *et al.*, 2004; Condon *et al.*, 2005) icehouse. Glacial deposits are recognized on almost all modern continents at various latitudes, described as a 'pan-glacial' state (Hoffman, 2009); their accumulation within low-latitude and low-altitude settings led to the development of the snowball Earth hypothesis (Hoffman *et al.*, 1998). Under a 'hard' snowball, pan-global ice sheets cover the Earth's surface, facilitating shutdown of the hydrological cycle. However, such conditions are inconsistent with widespread evidence for highly dynamic ice sheets and open water conditions (e.g. Le Heron *et al.*, 2011, 2013; Busfield & Le Heron, 2013, 2014; Fleming, 2014; Le Heron *et al.*, 2014a,b Arnaud, 2012). The data are more supportive of a 'soft' snowball state wherein mobile, wet-based ice sheets are subject to multiple advance–retreat cycles, and separated by expanses of ice-free open waters (e.g. Fairchild

& Kennedy, 2007). In order to improve understanding of the severity of Cryogenian glaciation, the glaciodynamics of Cryogenian ice masses need to be better constrained, and thus a detailed understanding of the extent and mobility of these ice sheets is required.

In eastern California, outstanding outcrops of the Pahrump Group preserve both the Sturtian and Marinoan glacial record within the Kingston Peak Formation (Prave, 1999; Macdonald *et al.*, 2013). These rocks are exposed in a broadly north-west/south-east trending outcrop belt spanning the Panamint Range and south-eastern Death Valley (Fig. 1; Noble, 1934; Hazzard, 1937; Hewett, 1940, 1956; Wright *et al.*, 1974; Macdonald *et al.*, 2013). In the former region, strata belonging to the Kingston Peak Formation have undergone up to amphibolite grade metamorphism (Petterson *et al.*, 2011b), whilst in the latter region the metamorphic overprint is minimal, resulting in the preservation of primary sedimentary structures. The type section, the Kingston Range, exposes 300 to 2400 m of heterolithic siliciclastics with evidence of a clear glacial influence on deposition, characterized by two periods of glacial advance, separated by significant ice meltback (Le Heron *et al.*, 2014b). These cycles record alternating ice-proximal to ice-distal conditions, within an exclusively proglacial setting. This study examines a spectacular exposure of the upper Kingston Peak Formation at Sperry Wash (Fig. 1), which demonstrates a clear ice advance signature from ice-distal to ice-marginal environments, with evidence of local advance to an ice-contact position. These deposits therefore represent the most ice-proximal settings recorded in the Death Valley region, and enable the position of the tidewater terminus to be constrained for the first time.

GEOLOGICAL SETTING

The Kingston Peak Formation is the topmost member of the tripartite Pahrump Group, comprising the mixed carbonate and siliciclastic Crystal Spring Formation at its base, overlain by microbial carbonates of the Beck Spring Dolomite and, in turn, the siliciclastic Kingston Peak. The lower Crystal Spring Formation is intruded by dolerite sills dated at 1087 ± 3 Myr and 1067 ± 3 Myr (U–Pb baddeleyite ages; Heaman & Grotzinger, 1992), whilst detrital zircon ages place the upper member of the Crystal Spring Formation at younger than 787 ± 11 Myr (recently re-allocated to the Horse Thief Springs Formation; Mahon *et al.*, 2014). The top of the Pahrump Group is truncated by an angular unconformity beneath the Ediacaran Noonday Dolomite (Prave, 1999; Petterson *et al.*, 2011a), which is therefore used to argue for a minimum depositional age of 635 Ma (Hoffmann *et al.*, 2004; Condon *et al.*, 2005; Macdonald *et al.*, 2013).

Deposition of the Pahrump Group spans both assembly and break-up of the Rodinian supercontinent along the south-western margin of Laurentia (e.g. Mahon *et al.*, 2014). The Kingston Peak Formation accumulated during the early stages of intracratonic rifting, with evidence of syn-depositional tectonism in the form of buried normal faults and significant along-strike thickness changes throughout the Death Valley region, as well as extension-related volcanism in the Panamint Range (Troxel, 1966; Labotka *et al.*, 1980; Hammond, 1983; Miller, 1985). Prave (1999) argues in favour of two discrete episodes of extension, broadly correlative with the older ('Sturtian') and younger ('Marinoan') glacial intervals, and cessation of rifting by the Ediacaran (i.e. deposition of the Noonday Dolomite).

In south-eastern Death Valley, a four-fold stratigraphic subdivision (KP1 to KP4) is commonly applied to the Kingston Peak Formation (Prave, 1999; Macdonald *et al.*, 2013; Le Heron *et al.*, 2014b). The basal KP1 is widely recognized as a pre-glacial succession (e.g. Prave, 1999), wherein its gradational basal contact supports inclusion in the previous (Beck Spring Dolomite) depositional cycle, and is argued to be genetically unrelated to the Kingston Peak Formation (Macdonald *et al.*, 2013). In places, this unit is unconformably overlain by the laterally discontinuous Virgin Spring Limestone, which is in turn truncated by the overlying KP2. Units KP2 and KP3 are volumetrically the most abundant strata in south-eastern Death Valley (Le Heron *et al.*, 2014b), succeeded in places by thin, laterally impersistent exposures of KP4 (Macdonald *et al.*, 2013). Based upon bounding unconformities, and correlation with strata in the Panamint Range, KP2 and KP3 are commonly attributed to the older Cryogenian ('Sturtian') glaciation, and unit KP4 is attributed to the younger Cryogenian ('Marinoan') glaciation (Petterson *et al.*, 2011b; Macdonald *et al.*, 2013), and likewise to the earlier and later extensional regimes of Prave (1999).

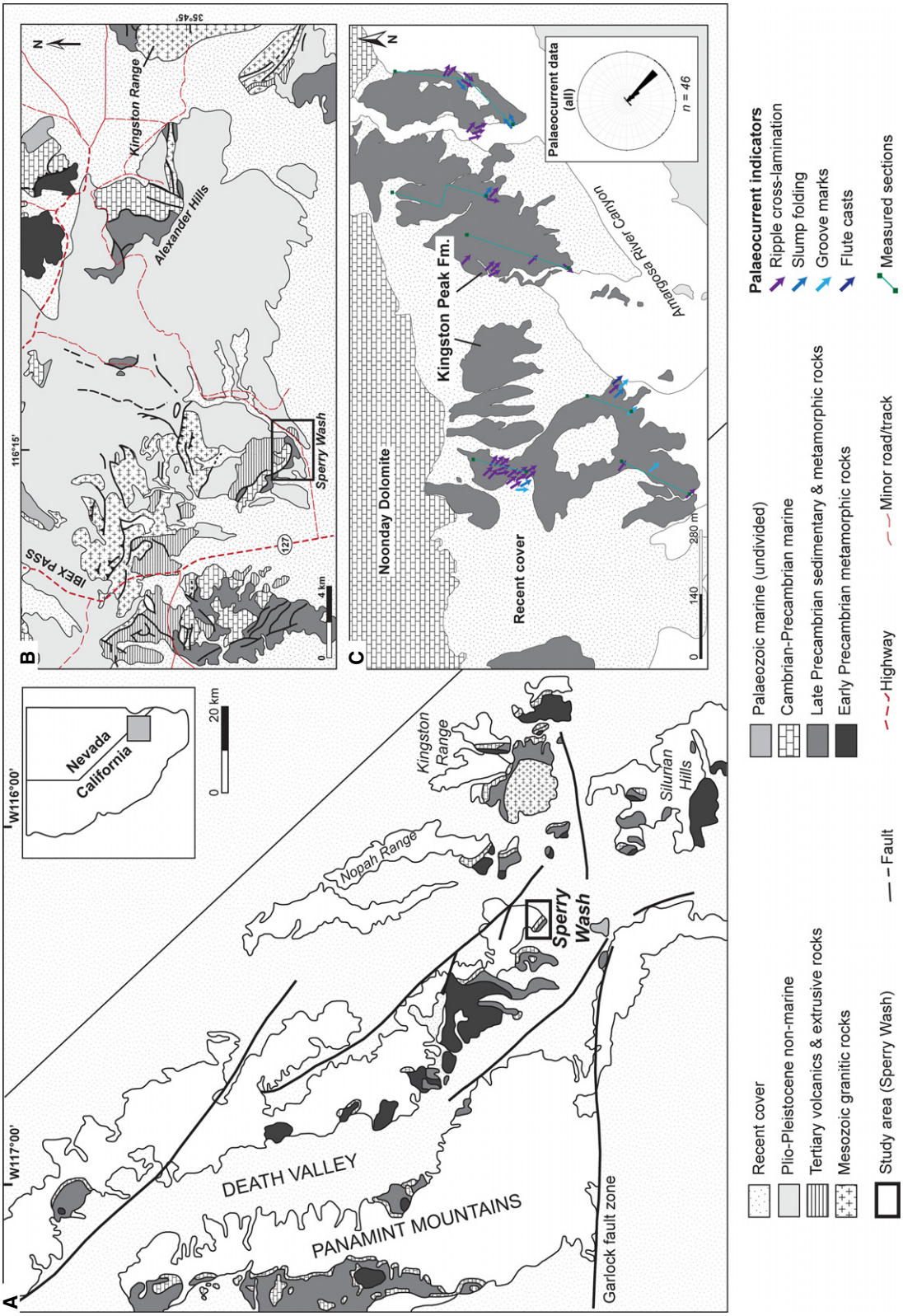

Fig. 1. (A) North-west/south-east trending outcrop belt which exposes Pahrump Group strata throughout the Panamint Range and eastern Death Valley, modified from Macdonald *et al.* (2013). (B) Geological map of south-eastern Death Valley region, including Sperry Wash study area, after Jennings *et al.* (1962). (C) Map of study section demonstrating dip-corrected palaeoflow azimuths. Overall, a clear south-eastward principal palaeoflow is recognized, with minor variability attributed to radial sediment distribution patterns and counter-flow slumping of unstable sediments (see text).

The present study focuses on an extremely well-exposed section at Sperry Wash, south-eastern Death Valley, which has not been subject to detailed sedimentological analysis in a generation (Troxel, 1966, 1982). The section is considered to correlate with member KP3 within the regional stratigraphic subdivision, although its stratigraphic thickness far exceeds correlative sections in the neighbouring Kingston Range (Le Heron *et al.*, 2014b; Le Heron & Busfield, this volume). The greater preserved thickness permits development of a high-resolution depositional history, which in tandem with the clear progradation from ice-distal to ice-contact settings offers insight into a considerably more diverse spectrum of glacial depositional environments than recorded elsewhere in the Death Valley region.

FACIES ANALYSIS

The Sperry Wash succession crops out at the northern margin of the Armagosa river canyon, *ca* 6 km from CA 127 (Death Valley Road; Fig. 1B and C). At 200 to 300 m above sea-level, the succession crops out in a hyper-arid basin and hence vegetation and soil-free outcrop conditions permit the collection of a high quality dataset. A 636 m thick succession (Fig. 2) was measured, supplemented by a substantive palaeocurrent dataset (Fig. 1C). The base of the section is not exposed, whilst the top is truncated by an angular unconformity with the Noonday Dolomite which oversteps unit KP3 to the north and east (Fig. 1C). Five facies associations are recognized and described below, including: (i) interbedded heterolithics; (ii) pebble to boulder conglomerate; (iii) diamictite; (iv) lonestone-bearing; and (v) tectonized.

Interbedded heterolithics facies association

Description

This facies association comprises a heterogeneous assortment of stratified siltstone, sandstone and pebbly sandstone, and volumetrically is the most abundant facies in the studied section (Fig. 2). Deposits most frequently fine upwards (Fig. 3A and B), from massive coarse-grained to pebbly sandstones into fine-grained sandstones, which locally preserve planar lamination. Both planar and irregular bed bases are recognized, whilst bed tops are planar throughout. Sandstone beds are separated by ungraded siltstones, which are predominantly parallel to ripple cross-laminated, although in some cases structureless. Thicker, uninterrupted siltstone intervals are more common towards the base of the studied section (Fig. 2). As the proportion of sandstone increases upsection, more common and thicker sandstone interbeds occur, accumulating in places as amalgamated bedsets. These bedsets often preserve progressively thicker and coarser normally graded deposits, stacked in coarsening-upward cycles (for example, *ca* 220 m, *ca* 240 m and *ca* 290 m, Fig. 2), and commonly overlain by deposits of the pebble to boulder conglomerate facies association (Fig. 3A and B). Amalgamated sandstone beds locally show evidence of channelization, characterized by erosive pebble-lined scours. An isolated erosively based sandstone wedge is recorded at 545 m (Figs 2 and 3C), downcutting into the underlying diamictite facies association, where it exhibits a feather-edge, pebble-lined contact. Towards the top of the studied section, ungraded sandstone interbeds dominate (above *ca* 340 m, Fig. 2). These deposits are associated with intrabed, bed-parallel pebble horizons or clusters, in contrast to the normally graded sediments where granule to pebble grade material is restricted to bed bases.

Within medium-grained to coarse-grained sandstones, irregularly folded and convoluted siltstone intraclasts are common (Fig. 3D), particularly in the first 400 m of the logged section (Fig. 2). The intraclasts tend to occur near the top of sandstone beds. In rare cases, sandstones also preserve recumbent and bed-parallel intrabed folds. Two examples of groove marks were observed at the sole of sandstone interbeds, trending 137° and 139° (*ca* 95 m and 146 m, Figs 2 and 3E). Current and climbing ripple cross-lamination within siltstones and fine-grained sandstones demonstrate foreset migration towards the south-east (Fig. 3F). Starved current ripple varieties (Fig. 3G) are typically associated with very finely laminated siltstone, delicately interbedded with fine sandstone on the centimetre-scale, giving a 'banded' appearance to the strata (Fig. 3H). These sediments are also associated with bed-parallel pebble horizons or clusters.

Interpretation

The predominant normally graded facies are interpreted as recording a spectrum of high to low-density T_{ABC} turbidites, supported by the presence of groove marks and flute casts on the soles of some sandstone beds. The abundant massive sandstone component indicates deposi-

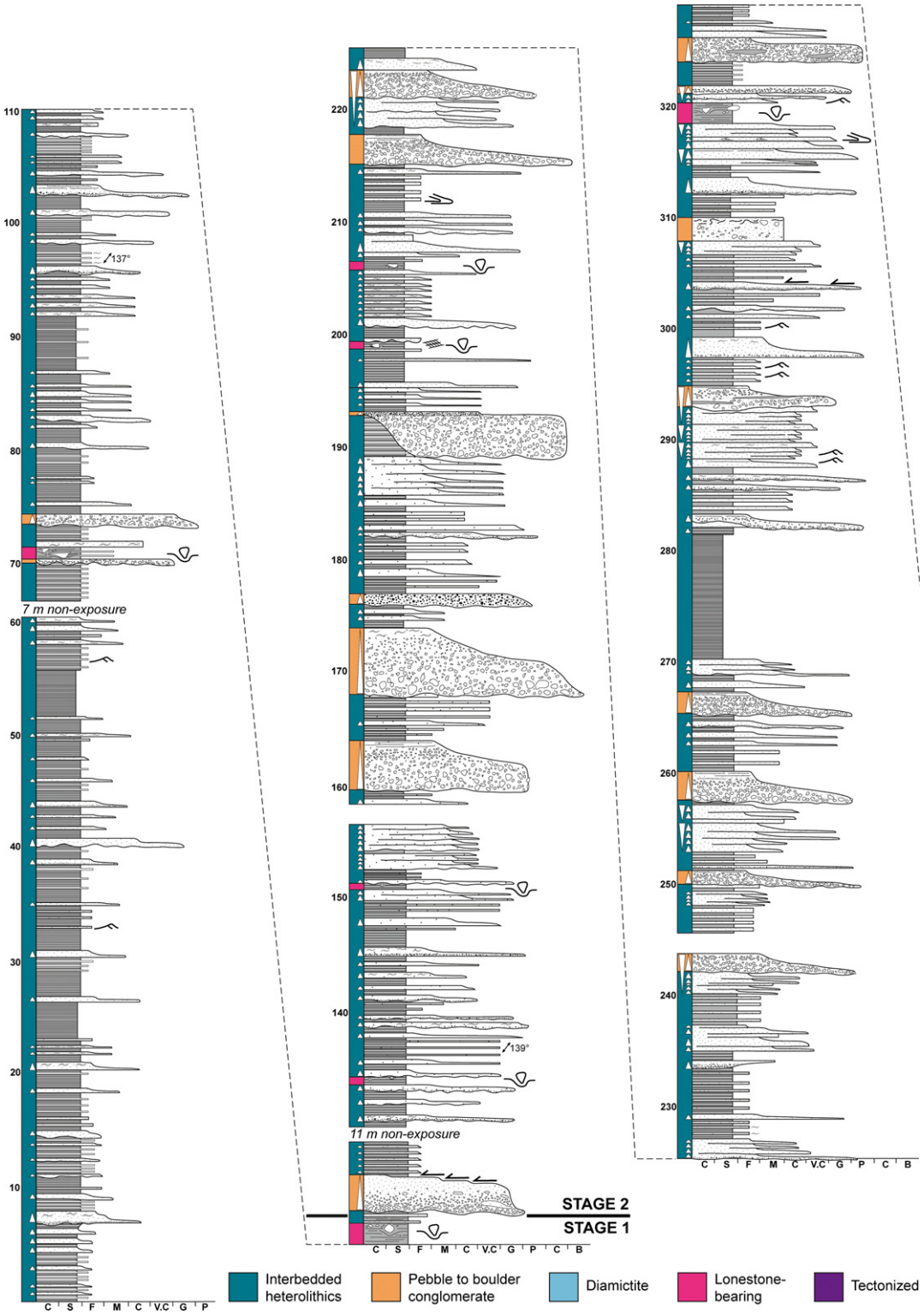

Fig. 2. A 636 m thick logged section of the Sperry Wash succession, divided into six segments for ease of display. Note the increased abundance of lonestone-bearing and diamictite facies associations up-section. Stages 1 to 5 refer to the multiphase depositional history discussed below (Fig. 8). Base of section: 35°42.038′N, 116°15.122′W. Top of section: 35°42.381′N, 116°14.515′W. Grain sizes, from left to right: C = clay; S = silt, F = fine sand; M = medium sand; C = coarse sand; V.C = very coarse sand; G = granule; P = pebble; C = cobble; B = boulder.

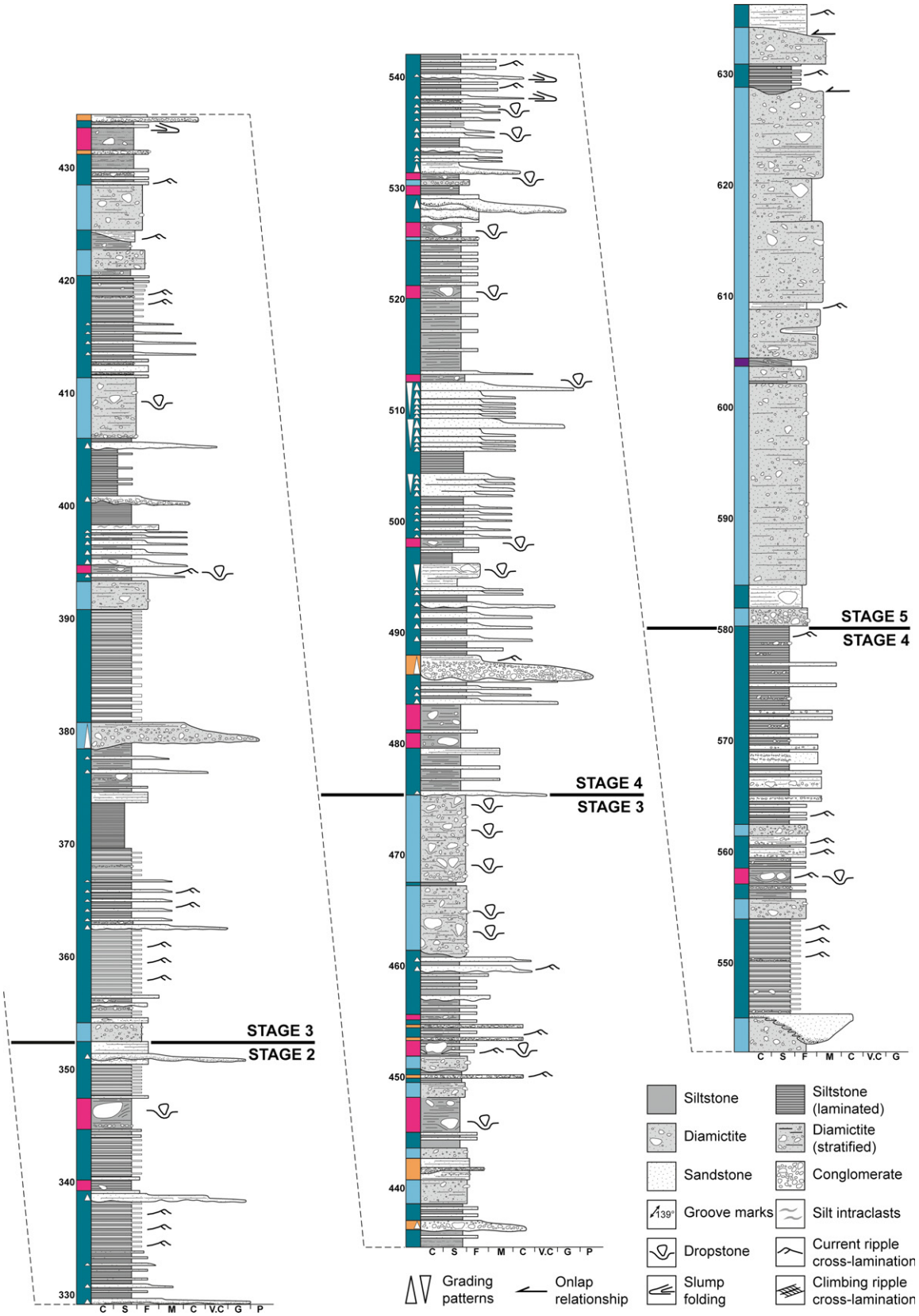

Fig. 2. continued

tion via high-density turbidity currents (T_A), where elevated near-bed sediment concentrations dampen turbulence and promote rapid deposition, and thus hinder bedform development (Kuenen, 1966; Middleton & Hampton, 1973; Talling *et al.*, 2012). Planar-laminated intervals reflect deposition from high-density traction carpets (T_{B2} or T_{B3}; Talling *et al.*, 2012), where sediment fallout rates drop sufficiently to enable lateral shearing near the base of the flow (Lowe, 1988; Leclair & Arnott, 2005; Sumner *et al.*, 2008). Such traction carpets are commonly found in association with high-density T_A facies (Talling *et al.*, 2012). Irregular, convoluted silt intraclasts in the sandstone beds are interpreted as rip-up clasts, incorporated through erosion and 'plucking' of semi-lithified interbedded siltstone facies. These intraclasts are likewise interpreted as reflecting lower sediment fallout rates, thereby minimizing their break-up during transport. Their organization along discrete horizons towards bed tops provides further credence to their transport within turbidity currents, as opposed to debris flows which would deposit chaotically distributed mud clasts (Talling *et al.*, 2012).

Distinct coarsening-upward packages composed of normally graded sandstone beds are interpreted as depositional lobe elements (Prélat *et al.*, 2009; Macdonald *et al.*, 2011). In the stratigraphic hierarchy of Prélat *et al.* (2009), lobe elements are built up from individual beds and bedsets, and stack to form lobes which, in turn, build up to form a lobe complex. The high sand to mud ratio and common bed amalgamation within these packages supports an axis to off-axis position within the lobe complex (Prélat *et al.*, 2009; Prélat & Hodgson, 2013). Such thickening and coarsening-upward trends are commonly recognized within depositional lobes (e.g. Hodgson *et al.*, 2006; Prélat *et al.*, 2009; Macdonald *et al.*, 2011, and references within). This behaviour demonstrates initiation and growth of the lobe/lobe elements towards a fixed point, which could be basinwards or across strike and therefore is not exclusively diagnostic of progradation (Prélat & Hodgson, 2013).

Ripple cross-laminated sandstone and siltstone units reflect fully turbulent near-bed conditions within low-density turbidity currents (T_C; Mulder & Alexander, 2001; Baas *et al.*, 2011; Talling *et al.*, 2012), where turbulence is no longer damped under much lower sediment fallout rates (e.g. Walker, 1967, 1978; Piper, 1978; Allen, 1982; Komar, 1985; Sylvester & Lowe, 2004). These ripples become 'starved' under elevated rates of tractional reworking (Talling *et al.*, 2007, 2012). Climbing ripple cross-lamination is also indicative of fully turbulent flow conditions, but under more rapid rates of sediment delivery (Kuenen & Humbert, 1969; Allen, 1991; Baas, 2000; Kane & Hodgson, 2010; Jobe *et al.*, 2012). Rare recumbent intrabed folds also support high rates of sediment delivery to induce instability and slumping (e.g. Maltman, 1994). Ripple cross-laminated intervals are commonly bounded by laminated and, less frequently, massive siltstone horizons, interpreted as densite mud deposited via a combination of low-density turbidity currents (T_D or $T_{E\text{-}1}$; Talling *et al.*, 2012) and hemipelagic fallout during waning flow (e.g. Allen *et al.*, 2004). Both T_D and $T_{E\text{-}1}$ intervals are characteristically very thin (e.g. Walker, 1967, 1978; Piper, 1978; Allen, 1982; Komar, 1985; Sylvester & Lowe, 2004; Talling *et al.*, 2012), and hence waning flow processes are favoured here. These sediments are thought to accumulate on the fringe and distal fringe of the lobe complex (Prélat *et al.*, 2009). Irregular basal contacts of sandstone interbeds record erosion and cannibalization during repeated emplacement of subaqueous flows. The isolated, erosively based sandstone wedge is interpreted as a channel fill, the origin of which will be discussed below. Planar, non-erosive basal contacts are interpreted as the product of hydroplaning at the head of the flow (e.g. Laberg & Vorren, 2000), and 'shear wetting' within the body of the flow (e.g. Ilstad *et al.*, 2004), both of which act to lubricate the base of the flow and protect underlying beds from cannibalization (Talling, 2013). As such,

Fig. 3. Interbedded heterolithics facies association. Person, *ca* 1·8 m; hammer, 26 cm; lens cap, 5 cm; coin, 1·9 cm; pen tip, 0·9 cm. Stratigraphic position refers to Fig. 2. (A) and (B) Thickening and coarsening-upward normally graded bedsets [(B): 240 m], capped by pebble to boulder conglomerate facies association in (A) (220 m). (C) White dashed line picks out pebble-lined channel feature (*ca* 543 m). (D) Irregular and convolute rip-up silt intraclast (224 m). (E) Groove marks on base of sandstone bed trending 139° (137 m). (F) Ripple cross-lamination, foreset migration towards the south-east (*ca* 252 m). (G) Starved ripple foresets (563 m), frequently associated with (H) centimetre-scale interbedded fine sandstone and siltstone, displaying striking 'banded' appearance (*ca* 575 m).

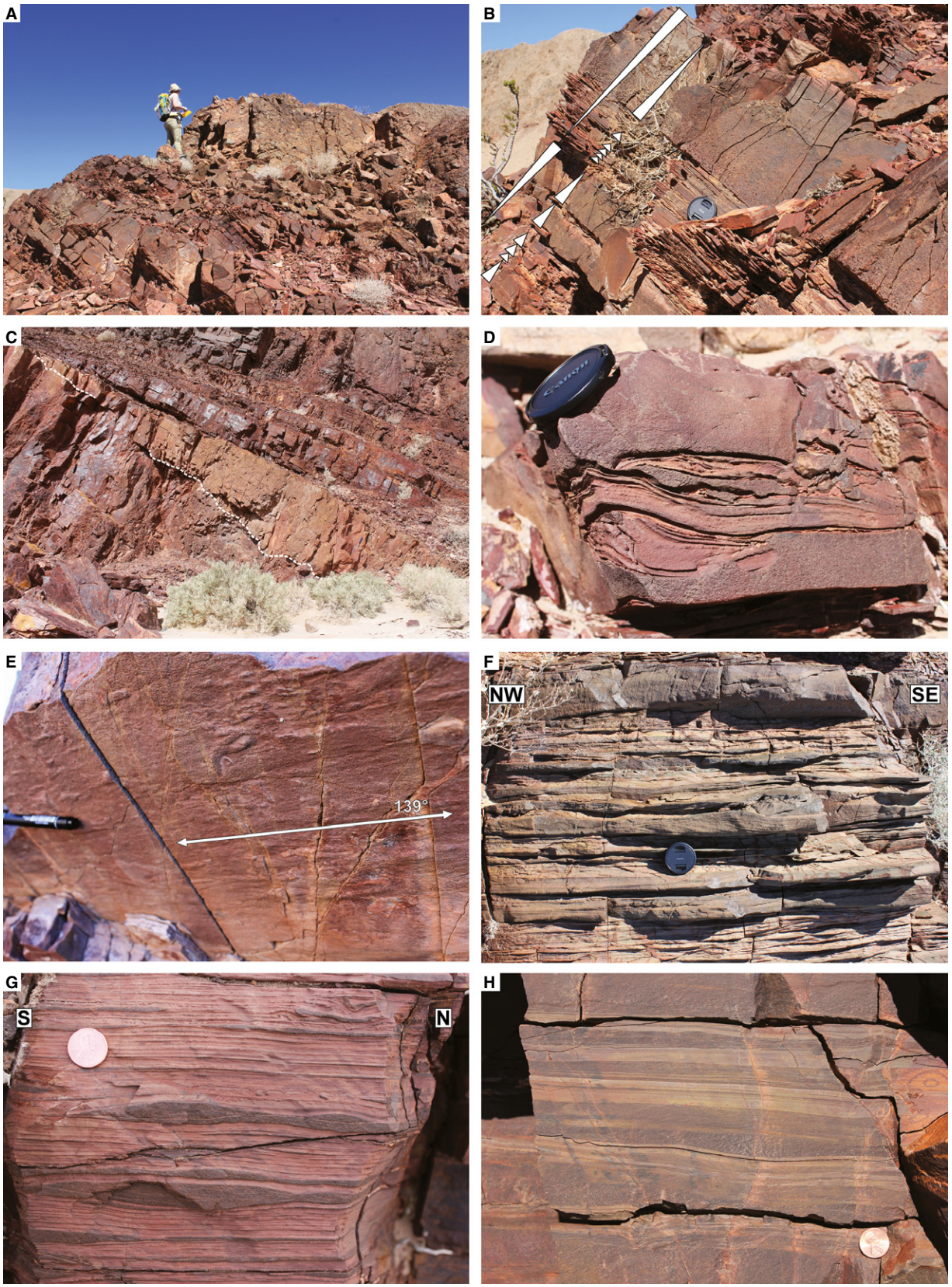

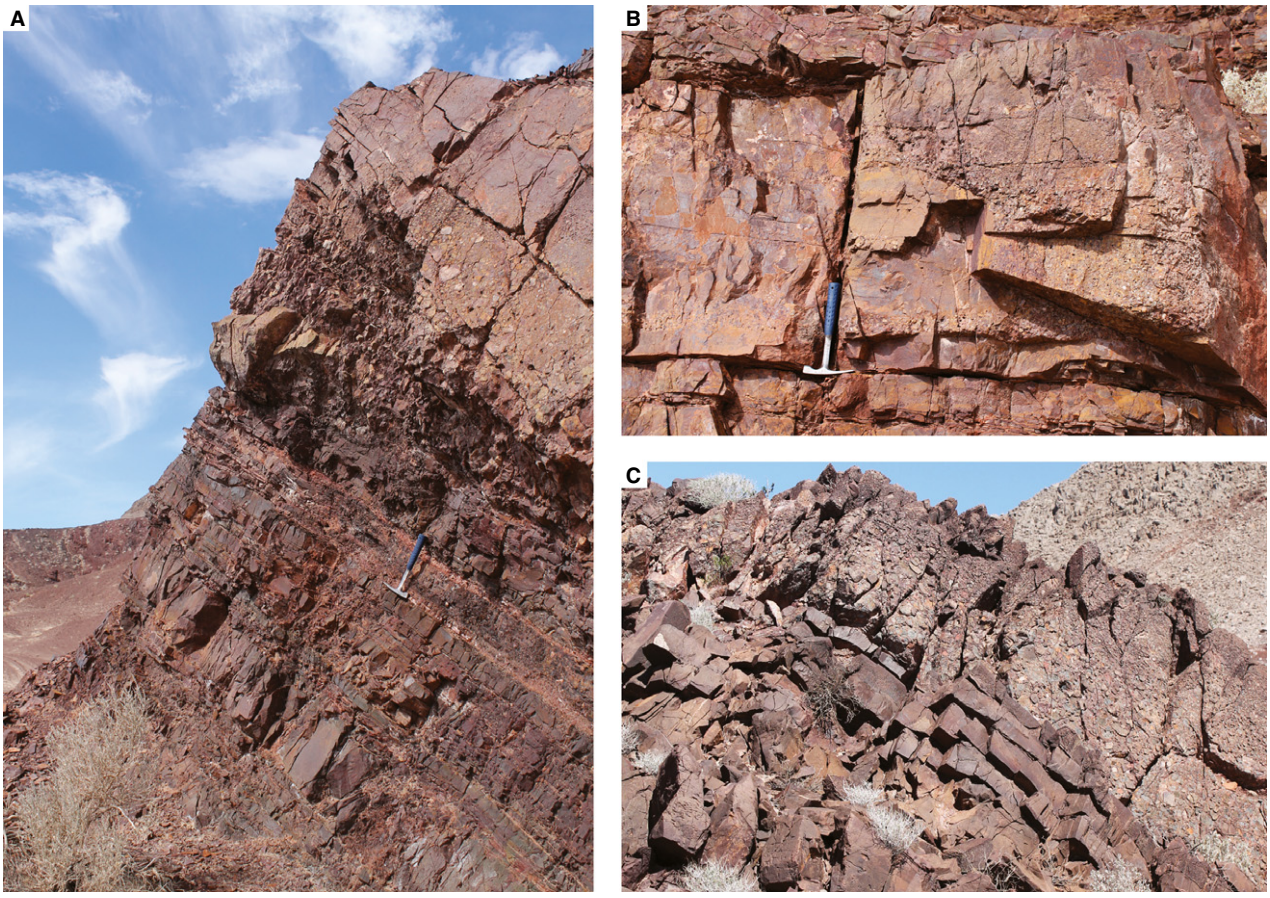

Fig. 4. Pebble to boulder conglomerate facies association. Hammer: 26 cm. Stratigraphic position refers to Fig. 2. (A) Erosively based normally graded conglomerate downcutting into the interbedded heterolithics facies association (487 m). (B) Internal channelization within normally graded conglomerate facies (528 m). (C) Conglomerate demarcates the top of coarsening and thickening-upwards bedsets (222 m).

this switch to non-erosive behaviour is probably driven by elevated water contents within more dilute flows, which would facilitate basal lubrication.

Pebble to boulder conglomerate facies association

Description

This facies association crops out intermittently throughout the basal two-thirds of the studied section, with the first recorded appearance at *ca* 70 m (Fig. 2). Deposits are predominantly massive, highly concentrated conglomerates with both clast-supported and matrix-supported textures. Basal contacts are irregular, downcutting into sediments of the interbedded heterolithics facies association (Fig. 4A), while upper contacts with these facies are sharp and planar. Channel-like geometries are frequently observed (Fig. 4B). The conglomerates commonly fine upwards from cobble–pebble grades, through coarse-grained to medium-grained sandstones (Fig. 4A and C). Crude stratification occurs in the sandier intervals. Other beds appear to be ungraded, fining upwards only at the very top. Clasts include karstified carbonate from the Beck Spring Dolomite and Crystal Spring Formation, and subordinate quartzite; they are predominantly sub-angular, although rounded clasts are also present. As seen in the interbedded heterolithics facies association, irregularly folded and convoluted siltstone intraclasts are preserved towards the top of fining-upward units, within the clast-poor sandier intervals. Isolated examples of sand-grade intraclasts are also recorded within one normally graded conglomerate unit (*ca* 115 m, Fig. 2).

Interpretation

Representing the product of hyperconcentrated sediment gravity flows (Lowe, 1982; Kneller,

1995; Mulder & Alexander, 2001; Winsemann *et al.*, 2007; Talling *et al.*, 2012), the pebble to boulder conglomerates are interpreted as high-density equivalents of the interbedded heterolithics facies association. Higher sediment concentrations are indicated by common erosive basal contacts and general absence of sedimentary structures. The latter is the result of hindered settling from high-density flows, typically characterized by rapid deposition and dampened turbulence (Talling *et al.*, 2012). Beds which are predominantly ungraded are interpreted as debris flows of moderate cohesive strength, containing too little mud to be fully cohesive and too much to be non-cohesive flow deposits (*sensu* Talling *et al.*, 2012). Such moderate cohesive strength flows are more susceptible to flow transformation, generating normally graded upper contacts where the flow mixes with the overlying water column. The predominant normally graded conglomerate beds are thus considered to reflect co-genetic high-density turbidites, derived through further dilution and mixing during downslope movement (Hampton, 1972; Talling *et al.*, 2012). The preservation of siltstone intraclasts towards the top of conglomerate beds must therefore reflect more dilute, low-density flow conditions, where lower sediment fallout rates inhibit disaggregation of the intraclasts.

The conglomerate beds commonly occur at the top of coarsening-upward packages of the interbedded heterolithics facies association, and thus represent the topmost lobe element within the lobe (*sensu* Prélat *et al.*, 2009). Their coarse calibre probably indicates a lobe axis position, and may correlate with the period of maximum lobe building prior to lobe switching or abandonment. This is supported by the consistent occurrence of fringe/distal fringe silt facies above the conglomerate beds.

Diamictite facies association

Description

These deposits are first recorded at 343 m, and become progressively more abundant upwards, accumulating as up to 20 m thick units at the top of the logged section (Fig. 2). They are readily differentiated from the pebble to boulder conglomerate facies association by their poor sorting, especially visible in the diverse spectrum of granule to large boulder-sized clasts within individual beds, and typically higher matrix content. The facies are predominantly ungraded, although an isolated normally graded bed is recorded at 380 m. Upper and lower bed contacts are commonly planar and conformable; erosive basal contacts, downcutting facies of the underlying interbedded heterolithics facies association, are rarely recorded. In places, the upper contacts of diamictite beds are highly irregular, where they are typically onlapped by siltstones and sandstones of the interbedded heterolithics facies association (Fig. 2).

Diamictite facies include both massive and stratified varieties, with crudely stratified units dominant. Clasts range from small pebbles to boulders, and consist of Beck Spring Dolomite and Crystal Spring Formation carbonates, with occasional quartzite clasts (Fig. 5A to F). In contrast to the pebble to boulder conglomerate facies association, clasts are predominantly rounded to well-rounded, with infrequent sub-angular morphologies. Isolated beds <5 m thick, are typical (Fig. 2). However, thicker beds occur between 460 m and 475 m, where they contain abundant cobble to boulder-sized clasts (Fig. 5A to F), some of which are striated (Fig. 5G), and the majority of which downwarp and puncture underlying laminae. Towards the top of the logged section (above 560 m, Fig. 2), downwarping relationships beneath the outsized clasts disappear.

Thick, almost continuous packages of diamictite (up to 20 m thick) return around 584 m, where they are locally interbedded with <1 m thick units of laminated siltstones and sandstones. These diamictite packages, whilst still matrix-supported, are notably clast-rich compared to underlying diamictite facies, with a higher proportion of coarser pebble, cobble and boulder-sized clasts. At 604 m the sequence is interrupted by a thin deposit of the of the tec-

Fig. 5. Diamictite facies association. Hammer, 26 cm; lens cap, 5 cm. Stratigraphic position refers to Fig. 2. (A) to (F) High concentration of outsized clasts with impact-related deformation structures within 15 m thick diamictite unit (460 to 475 m). (G) Striated clast associated with IRD-rich diamictite unit (460 to 475 m). (H) Fragmented carbonate clast, cavity infilled by surrounding diamictite. Jigsaw fit pattern of clast fragments supports *in situ* fracturing. Immediately above tectonized facies association (*ca* 604 m). (I) to (L) Bar width = 1 mm. Examples of arcuate grain alignments: smaller grains demonstrate circular arrangement around larger 'core stone'. Thin sections sampled immediately above tectonized heterolithics facies association.

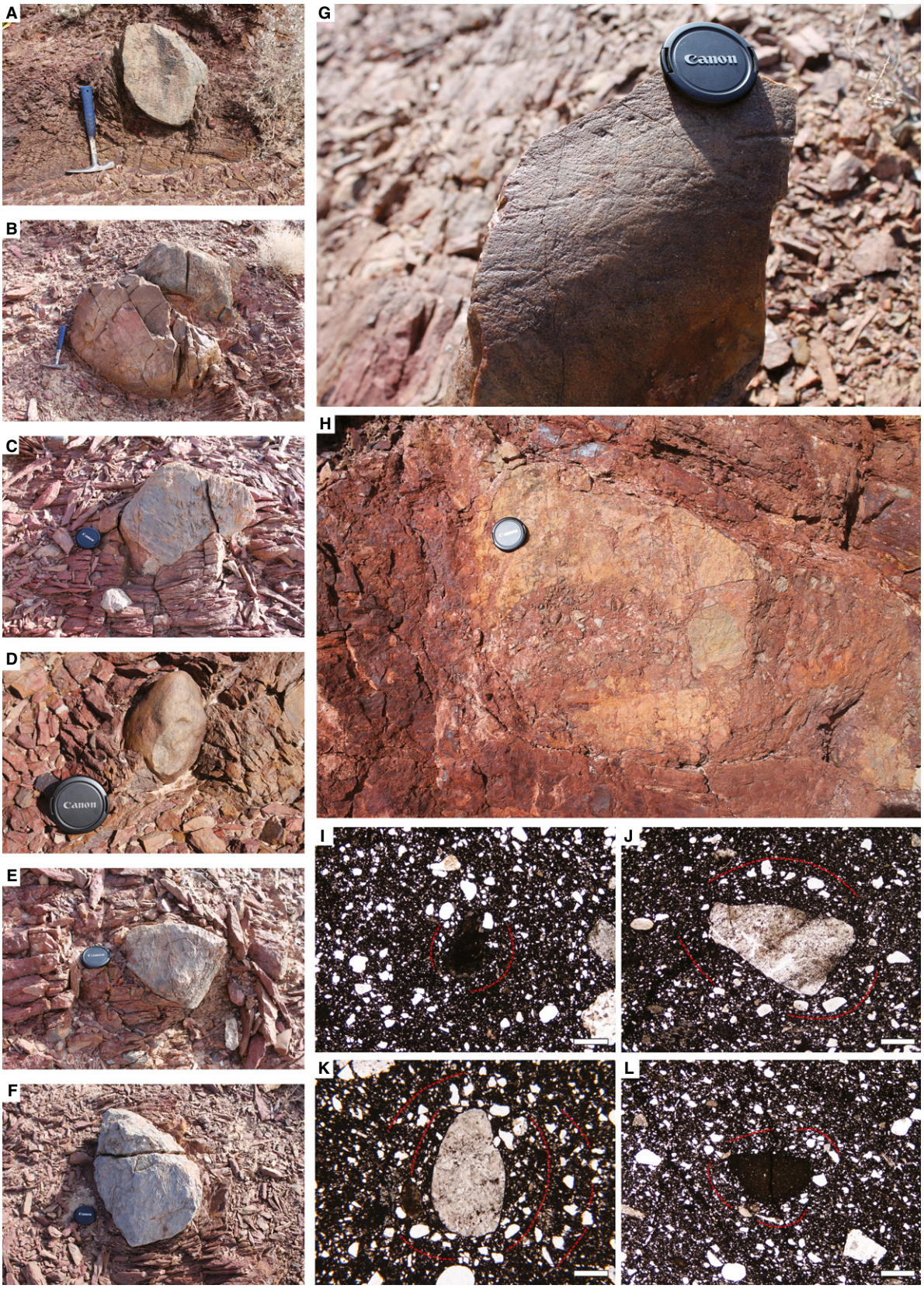

tonized facies association. Diamictite immediately overlying this interval exhibits small-scale folds verging south-east, in addition to a fragmented carbonate boulder, where the interstitial space is infilled with the matrix-rich diamictite of the host sediment (Fig. 5H). On the microscale, the surrounding diamictite exhibits arcuate grain alignments, wherein grains are arranged in a circular pattern around a core stone, or area of more rigid matrix (Fig. 5I to L).

Interpretation

With the exception of the thick diamictite packages, at 460 to 475 m and >584 m, this facies association consistently occurs as isolated, thin beds bounded by subaqueous density flow deposits of the interbedded heterolithics and lonestone-bearing facies associations. The absence of grading and pervasive crude stratification is typical of gravitationally reworked diamictites (e.g. Evans & Pudsey, 2002; Powell & Domack, 2002; Marenssi *et al.*, 2005; Henry *et al.*, 2012), commonly encountered within glacial regimes due to the rapid, dynamic and hydromorphic mode of sediment delivery and resultant instability of the sediment pile (Elverhøi *et al.*, 2002; Ó Cofaigh *et al.*, 2002; Powell & Domack, 2002). Their repeated stratigraphic association with the interbedded heterolithics and lonestone-bearing turbidite facies is used to support flow transformation, and generation of 'linked' turbidity currents. This process occurs through flow dilution during sediment reworking by mixing with the overlying water column, and is more effective on moderate cohesive strength debris flows, because higher cohesive strengths hinder mixing (Mulder & Alexander, 2001; Talling *et al.*, 2012). Flow transformation is further corroborated by the occurrence of a normally graded diamictite bed at 380 m, interpreted to reflect more dilute, turbulent flow conditions towards the top of the bed. Outsized clasts which downwarp and puncture underlying laminae are interpreted as ice-rafted debris (IRD). Their relative rarity within the isolated, thin diamictite beds characteristic of the lower succession is attributed to the combined influence of reworking during density flow remobilization, and less proximal position to the ice front, discussed below.

Within the first pronounced thickness of diamictite, at 460 to 475 m, a noteworthy increase in abundance of IRD is evident, alongside the first appearance of striated clasts in the logged section. The latter, indicative of subglacial debris entrainment (Boulton, 1978), were notably absent from the gravitationally reworked diamictite facies, where 'clast on clast' abrasion is anticipated to remove striations during remobilization (Le Heron *et al.*, 2013, 2014b). Their preservation, in tandem with abundant IRD is used to support deposition within an iceberg rain-out deposit, wherein striated clast varieties could be transported basinwards within icebergs without significant abrasion. The considerable increase in abundance of IRD is considered to reflect greater instability at the ice front, driving enhanced calving processes and iceberg distribution. Well-preserved impact structures beneath these dropstones are suggestive of minimal reworking, thus representing the product of highly concentrated, *in situ* rain-out. It is anticipated that icebergs would lose considerable debris during transport away from the ice front, particularly the coarser debris load, and therefore such an abundance of cobble to boulder grade IRD is more typical of ice-proximal settings. The introduction of subglacially striated boulders into the clast assemblage at this interval is also considered to corroborate a more proximal terminus position.

The second thick accumulation of this facies association (>584 m) records thicker, uninterrupted units of diamictite with an abundance of pebble, cobble and boulder-sized clasts, but a complete absence of impact-related deformation structures. This is interpreted to reflect more voluminous and rapid rates of sediment supply, promoting elevated and sustained ice-rafting processes into a thick and inherently unstable sediment pile, wherein delicate impact structures could be readily overprinted. This scenario is typical of debris-laden, ice-marginal settings where high volumes of coarse, poorly sorted debris flows commonly accumulate as grounding-line fans. In the ancient record, these systems are commonly devoid of impact-related deformation structures (e.g. Lønne, 1995), despite evidence supporting active ice-rafting within comparable modern ice front environments (Ovenshine, 1970; Dowdeswell, 1986, 1989). This may be due in part to: (i) the lithological and textural similarity between the rafted material and the 'host' fan deposits (cf. Lønne, 1995); (ii) sediment remobilization driven by periodically unstable fan-slope collapses; or (iii) current reworking through subglacial meltwater discharge. The latter process may also contribute to the development of crude stratification within the diamictite facies at this interval through minor reworking and removal of fines. It is pro-

posed these fine-grained sediments are remobilized as dilute, low-density turbidity currents and deposited in ephemeral channels on the grounding-line fan, thereby accumulating locally as interbedded siltstones and sandstones.

Both the small-scale folds verging towards the south-east and the fragmented carbonate clast are interpreted as syn-sedimentary deformation features. The recorded fold vergence parallels principal palaeoflow orientations recorded throughout the succession (Fig. 1C), while the 'jigsaw fit' pattern of the clast fragments, and infill of the interstitial space by the surrounding diamictite matrix, suggests *in situ* fracturing under soft sediment conditions. Within an ice-marginal fan system, these processes could be driven by either sediment remobilization or glacitectonic deformation, wherein both have the capacity to produce a similar suite of deformation structures. For example, the micro-scale arcuate grain alignments are a common feature of both subglacial environments and sediment density flows (Lachniet *et al.*, 2001; Menzies & Zaniewski, 2003; Phillips, 2006). In both scenarios, clast fracturing can be driven by pronounced pressure gradients within the deforming bed, varying from the highest strain conditions at the base of sediment gravity flows due to contact with the underlying substrate, or towards the top of glacitectonic sequences near the ice-bed interface. The significance of these features will be discussed in the context of the immediately underlying tectonized facies below.

Lonestone-bearing facies association

Description

This facies association occurs in thin (<5 m), comparatively rare horizons throughout the studied section, albeit with greater abundance above 430 m (Fig. 2). Well-stratified parallel-laminated siltstones, and rare interbedded sandstones, are characteristic. The siltstones locally show current and climbing ripple cross-lamination. Normal grading, a classic feature of the heterolithic facies association, is not recorded (Fig. 2). Moreover, outsized clasts do not occur as bed-parallel clast trains or clusters, but as isolated lonestones, frequently puncturing and downwarping underlying laminae and, in turn, are draped by overlying laminae (Fig. 6A to G). Outsized clasts range from pebble to large boulder (up to 1 m) in size, and consist predominantly of Beck Spring Dolomite, in tandem with the pebble to boulder conglomerate and diamictite facies associations.

Interpretation

These deposits are considered to accumulate via dilute, low-density turbidity currents and settling of hemipelagic fines during waning flow conditions. The facies are closely associated with normally graded turbidites of the interbedded heterolithics facies association, and gravitationally reworked debris flow deposits of the diamictite facies association, lending support to their co-genetic subaqueous density flow origin. Evidence of current and climbing ripple cross-lamination indicates fully turbulent conditions within low-density turbidity currents (T_C; Mulder & Alexander, 2001; Baas *et al.*, 2011; Talling *et al.*, 2012). The predominance of parallel lamination may be associated either with waning low-density turbidity currents (T_D or $T_{E\text{-}1}$; Talling *et al.*, 2012), or hemipelagic fallout during quiescent phases (e.g. Allen *et al.*, 2004). Abundant outsized clasts with impact structures within these finely laminated turbidites are interpreted as ice-rafted debris (IRD). The low-density subaqueous flows and preservation of delicate ripple structures preclude sediment flow rafting of the outsized clast fraction (e.g. Postma *et al.*, 1988).

Tectonized facies association

Description

This facies association is restricted to a single, *ca* 1 m thick horizon at 604 m (Fig. 2). It consists of finely interbedded fine-grained sandstones and siltstones that bear granule to small pebble-sized clasts. These well-stratified sediments are deformed into a series of south-east verging folds which ramp up relative to bedding (Fig. 7A). Stratified sediments within the fold limb also show small (<1 cm), local offsets. Note that folding is entirely confined to this facies association, neither affecting underlying nor overlying strata of the diamictite facies association.

On the micro-scale, sandstone horizons are normally graded, with clear load structures at their bases (Fig. 7B). Outsized clasts appear to 'sink' into their host siltstone or sandstone laminae, although evidence of clear downwarping or puncturing of laminae is absent. Laminae are locally displaced by minor fault offsets and deformed into open folds verging towards the south-east. In places, intraclasts of the finely interbedded siltstone and sandstone laminae occur as angular, randomly orientated fragments. The more clay-rich intervals display weak to moderate birefringence, either as linear zones of more

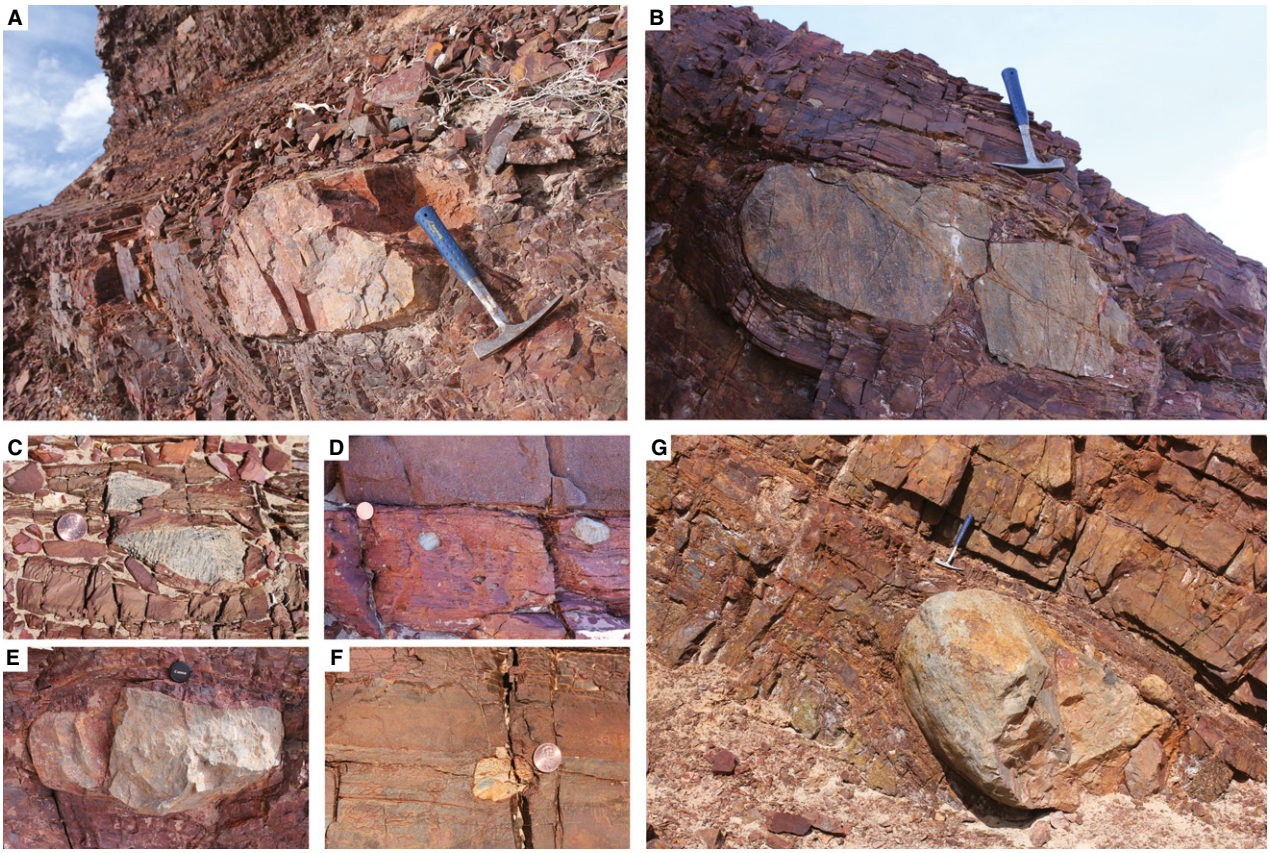

Fig. 6. Lonestone-bearing facies association. Hammer, 26 cm; lens cap, 5 cm; coin, 1·9 cm. Stratigraphic position refers to Fig. 2. (A) to (G) Small pebble to large boulder-sized lonestones with impact-related deformation structures, within both crudely and well-laminated siltstone and sandstone facies (at 496 m, 557 m, 71 m, 135 m, 480 m, 113 m and 526 m, respectively).

birefringent clay minerals, or as zones of elevated birefringence with no clear preferred orientation, characterized in micromorphological terms as unistrial and asepic plasmic fabrics, respectively (for definitions see Zaniewski & van der Meer, 2005).

Interpretation

As with the lonestone-bearing facies association, these sediments record deposition by low-density turbidity currents and background hemipelagic sedimentation. Their close stratigraphic relationship with the diamictite facies association suggests that these fine-grained sediments may have been winnowed and deposited in ephemeral channels on the grounding-line fan, in a similar manner to the interbedded siltstones and sandstones of the diamictite facies association discussed above. In contrast to these sediments, dilute turbidites within the tectonized facies association are then deformed into a series of south-east verging folds.

Within ancient successions, discriminating between sedimentary and tectonic origins for deformed strata is crucial. In this case, deformation is clearly restricted to one horizon, and does not affect underlying sediments, with only minimal deformation in the immediately overlying diamictite. Moreover, deformation is not facies-dependent, and thus equivalent facies elsewhere in the succession (low-density turbidites of the lonestone-bearing facies association and diamictite facies association) are also undeformed (e.g. Fleming, 2014). Finally, the succession as a whole demonstrates no pervasive deformation or cleavage development, in contrast to correlative sections in the Panamint Range (Petterson *et al.*, 2011b). The dominant ductile style of folding is therefore considered indicative of soft sediment deformation, potentially facilitated by elevated water contents as would be typical of dilute, low-density flows. Given the proximity of the ice margin, it is recognized that meltwater input could also contribute significantly to these higher pore-

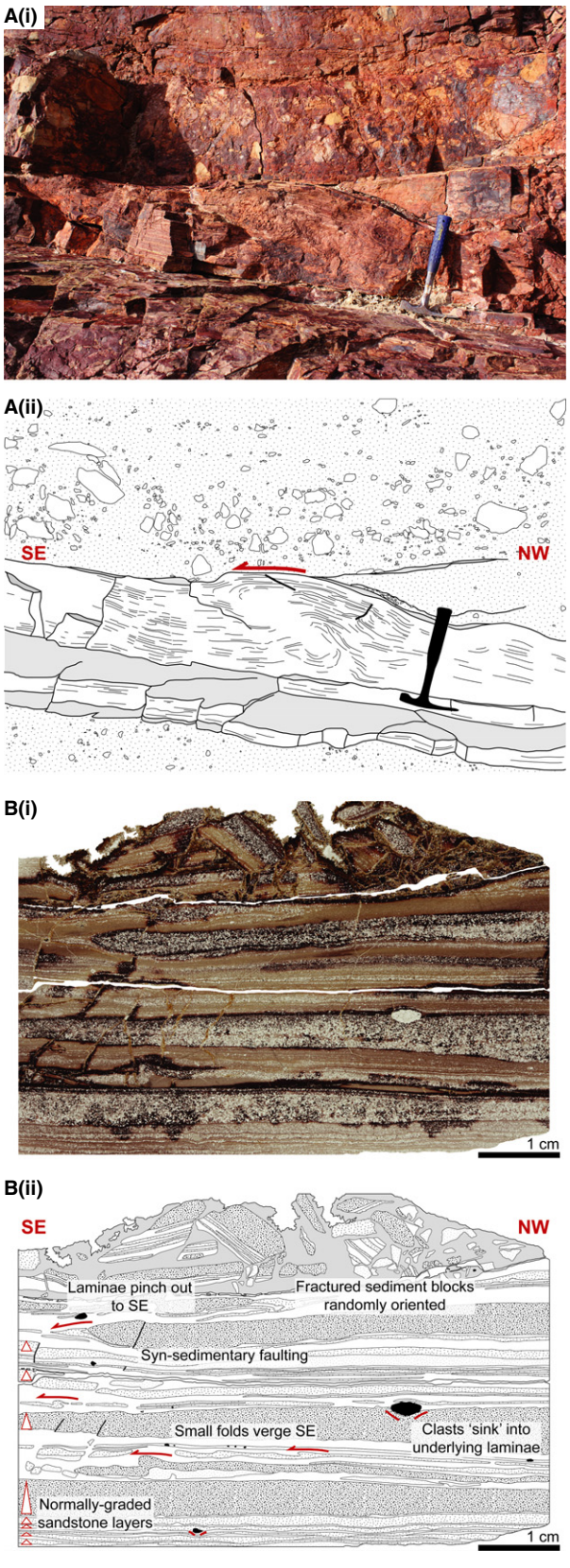

Fig. 7. Tectonized facies association. Hammer, 26 cm. [A (i) and (ii)] Macro-scale photograph and interpretive overlay of fold structures verging and ramping up towards the south-east (*ca* 604 m). Note the small fault offsets within limb of fold structure. [B (i) and (ii)] Micro-scale photograph and interpretive overlay show well-laminated normally graded sediments, in places deformed into south-east verging folds. Clasts appear to sink into underlying laminae, although unclear whether ice-rafted. Top of section shows randomly orientated fragments of laminated sediment, reflecting brittle deformation and re-organization.

water pressures. During deformation, elevated fluid contents can become overpressurized, promoting rapid water expulsion concomitant with a switch to more brittle styles of deformation (e.g. Denis *et al.*, 2010; Ravier *et al.*, 2014). This process is interpreted as accounting for the small fault offsets observed displacing the limbs of the fold structures, in addition to the fracturing and angular fragmentation of the sediments on the micro-scale.

In ice-marginal settings, soft sediment deformation could be the product of either sediment remobilization or glacitectonic deformation, wherein both proglacial and subglacial processes are plausible. Sediment instability and failure frequently occur due to rapid and high rates of sediment supply. Deposits of the tectonized facies association, accumulating within ephemeral channels on the grounding-line fan, could therefore have undergone either slump-related deformation driven by internal instability, or have subsequently been deformed beneath an overriding coarse debris flow during fan build-out. However, sediment gravity flow deformation observed throughout the remainder of the succession, particularly within the interbedded heterolithics facies association, generates consistently recumbent and bed-parallel folds. In contrast, within the tectonized facies association, fold structures ramp upwards, where folds essentially 'piggy-back' underlying fold structures towards the south-east (Fig. 7A). Arguably, the deposits could have been deformed through a bulldozing motion at the head of an advancing debris flow, but it is perhaps surprising that they were not then eroded and cannibalized within the significantly coarser and more competent flow, although it is recognized that such erosion could account for the limited preservation of this facies association. Overall, common features considered characteristic of sediment reworking in the tectonized facies association are curiously absent on both the

macro-scale (clasts with diamictite coatings, load structures and vertical water escape structures) and micro-scale (flow noses, tile structures and laminated grain coatings; see Busfield & Le Heron, 2013, and references within).

An alternative scenario, especially in light of the evidence favouring increasing proximity of the ice front throughout the succession (see discussion below), is that deformation occurs ahead of or beneath the advancing glacier terminus. In ice-contact settings, the elevated water contents argued to facilitate the dominantly ductile style of deformation would be further enhanced by input of both subglacial and englacial meltwater, as well as the high confining pressure of the overriding ice (Menzies, 2000; Phillips *et al.*, 2007; Lee & Phillips, 2008; Busfield & Le Heron, 2013). This is supported by the presence of unistrial plasmic fabrics, reflecting development of high strain planar shear fabrics within the deforming bed (e.g. Hiemstra & Rijsdijk, 2003; Busfield & Le Heron, 2013). In this scenario, the ramping-upward style of folding is considered to reflect ice-marginal deformation through glacitectonic thrusting (e.g. Ó Cofaigh *et al.*, 2011; Evans *et al.*, 2012), rather than the widespread isoclinal folding typical of shearing within the subglacial bed (e.g. Lee & Phillips, 2008; Busfield & Le Heron, 2013). Glacitectonic thrusting alongside a high sediment supply frequently results in the development of thick sediment piles in ice-marginal settings (e.g. Evans & Hiemstra, 2005; Ó Cofaigh *et al.*, 2011; Evans *et al.*, 2012) which could contribute to the notably thick accumulation of the diamictite facies association at the top of the logged section.

In light of: (i) the limited evidence of features diagnostic of sediment gravity flow deformation; (ii) the unique 'piggy-back' style of folding; (iii) the development of unistrial plasmic fabrics, typically associated with higher strain conditions than mass flow processes; and (iv) the clear evidence for an advancing ice margin throughout deposition of the Sperry Wash succession, proglacial glacitectonic deformation of the ice-marginal sediments is favoured here. However, it is contended that deformation of the tectonized facies association could plausibly have been driven by bulldozing at the head of a diamictic debris flow. In both situations, deformation is interpreted as occurring immediately adjacent to the ice margin, where the advancing glacier terminus delivered extremely high volumes of coarse, poorly sorted debris (diamictite facies association), most probably contributing to localized ice-contact deformation of the grounding-line fan.

PALAEOCURRENT INDICATORS

Numerous palaeocurrent indicators are recorded throughout the Sperry Wash succession, predominantly within the interbedded heterolithics and lonestone-bearing facies associations (Fig. 2). These features include ripple cross-lamination and soft sediment slump folding, as well as groove marks and flute casts on the base of turbidite beds. Dip corrected azimuths demonstrate principal palaeoflow towards the south-east at all stratigraphic levels (Fig. 1C); this is corroborated by the south-east verging glacitectonic fold structures within the tectonized facies association. These data therefore act to support south-eastwards palaeo-ice flow. Towards the top of the studied section, isolated examples of slump folds verging north-east (Fig. 1C) are interpreted as reflecting collapse of an unstable sediment pile as opposed to a change in sediment provenance; whilst limited evidence of palaeoflow towards the south/south-west probably reflects a degree of radial distribution within the subaqueous fan complex.

EVOLUTION OF A GLACIER-FED SUBAQUEOUS SYSTEM

The Sperry Wash section demonstrates a clear and pervasive glacial signature throughout, which significantly becomes more pronounced upsection. The predominance of subaqueous sediment gravity flow deposits is consistent with an active, periodically unstable glacier-fed slope, wherein the preserved facies associations and their stacking patterns are typical of ice-proximal subaqueous sediment complexes. Such complexes can accumulate within both freshwater and marine subaqueous settings, but the latter is favoured here due to the close stratigraphic association with thick carbonate successions both underlying and overlying the Kingston Peak Formation (Macdonald *et al.*, 2013), and occurring as kilometre-scale intraformational olistoliths in the neighbouring Kingston Range (Le Heron *et al.*, 2014b). Moreover, the vast preserved sediment thicknesses, >600 m in this study and >400 m in the Kingston Range (Le Heron *et al.*, 2014b), far exceed recorded examples from glacilacustrine systems (e.g. Johnsen &

Brennand, 2004, 2006; Etienne *et al.*, 2006; Winsemann *et al.*, 2007; Livingstone *et al.*, 2010; Perkins & Brennand, 2015).

The external geometry of the succession, i.e. whether it represents a radial (fan-shaped) or linear (apron) morphology, cannot be determined with certainty from the palaeocurrent data (Fig. 1C). It is recognized that a sufficiently expansive fan would also yield a very consistent palaeoflow (in this case to the south-east) over a small portion of its surface, and therefore these patterns are not necessarily indicative of a linear input. Moreover, at contemporary ice sheet margins, ice streams frequently focus sediment distribution to specific points along the ice front (Stokes & Clark, 2001; Bennett, 2003; Ó Cofaigh *et al.*, 2003), restricting broad, linear sediment routing systems. The absence of correlative sections immediately along-strike precludes investigation of the three-dimensional architecture of this subaqueous system, and thus the control on sediment distribution patterns remains subject to further investigation. Nonetheless, the almost 100% continuity within the studied section affords great vertical resolution. The evolution of this subaqueous system will be described in five key stages below, as illustrated in Fig. 8. Each of these stages corresponds to ascending stratigraphic levels on the measured sections.

Stage 1 – Ice-distal outwash (0 to 116 m)

The base of the section is composed almost exclusively of the interbedded heterolithics facies association, where sandstone interbeds are typically thinner, finer grained and less frequent than further upsection, separated by thicker laminated siltstone units (Fig. 2). The stacked, coarsening-upward lobe elements are not preserved. Evidence of glacial influence on sedimentation is restricted to two thin intervals of lonestone-bearing siltstone. The first occurs towards the middle of this stage (70 m) and is accompanied by two thin beds of erosively based pebble conglomerate. The second example occurs towards the top of this stage (*ca* 112 m), and is truncated by a prominent erosion surface beneath a thicker cobble to pebble conglomerate. Isolated lonestones are interpreted as recording iceberg rafting. Their close association with the infrequent conglomerate horizons is used to argue for contemporaneous pulses of sediment and iceberg distribution into the basin, possibly driven either by minor ice front oscillations, or as a product of debris destabilization and remobilization during calving processes at the terminus. The scarcity of these event beds, rare ice-rafting and overall fine-grained nature of the sediments indicates an ice-distal/ice-medial setting on the margins of the subaqueous fan complex (Fig. 8-1).

Stage 2 – Build-out of ice-medial depositional lobes (116 to 352 m)

The development of an onlap surface onto the thick pebble to boulder conglomerate, discussed above, is interpreted as recording local transgression, possibly driven by minor ice melt-back in the hinterland. Above this horizon, turbidites are coarser and volumetrically much more abundant than below (interbedded heterolithics facies association), and frequently occur as stacked lobe elements (Fig. 2). The lonestone-bearing and pebble to boulder conglomerate facies associations occur at thicker and more regular intervals, the latter commonly representing the peak of lobe build-out. Direct evidence of glaciation is again restricted to ice-rafted debris, albeit with more abundant and larger lonestones than the distal outwash setting below.

The initiation, growth and abandonment of depositional lobes on the glacier-fed shelf is interpreted as being driven by pulsed sediment delivery downslope from the ice front (e.g. Laberg & Vorren, 1995, 2000; Vorren *et al.*, 1998; Dimakis *et al.*, 2000; Benn & Evans, 2010), possibly triggered by a periodically unstable or oscillating ice front (Fig. 8-2). This setting promotes abundant and regular, although not necessarily sustained, sediment supply, enabling lobe build-out during periods of elevated sediment remobilization (grounding-line advance/oscillation), followed by lobe abandonment and increased hemipelagic sedimentation during periods of quiescence (grounding-line retreat).

Stage 3 – Ice-proximal deposition and increased calving (352 to 476 m)

The first appearance of diamictite (353 m, Fig. 2) records the onset of an ice-proximal regime. In more distal settings, debrites (diamictite facies association) become more diluted, undergoing flow transformation to deposit turbidites of the interbedded heterolithics and pebble to boulder conglomerate facies associations. In the ice-proximal zone, co-genetic turbidites are significantly less abundant, whereas diamictic debrites occur repeatedly throughout the succession. The predominance of debrites over co-genetic turbidites

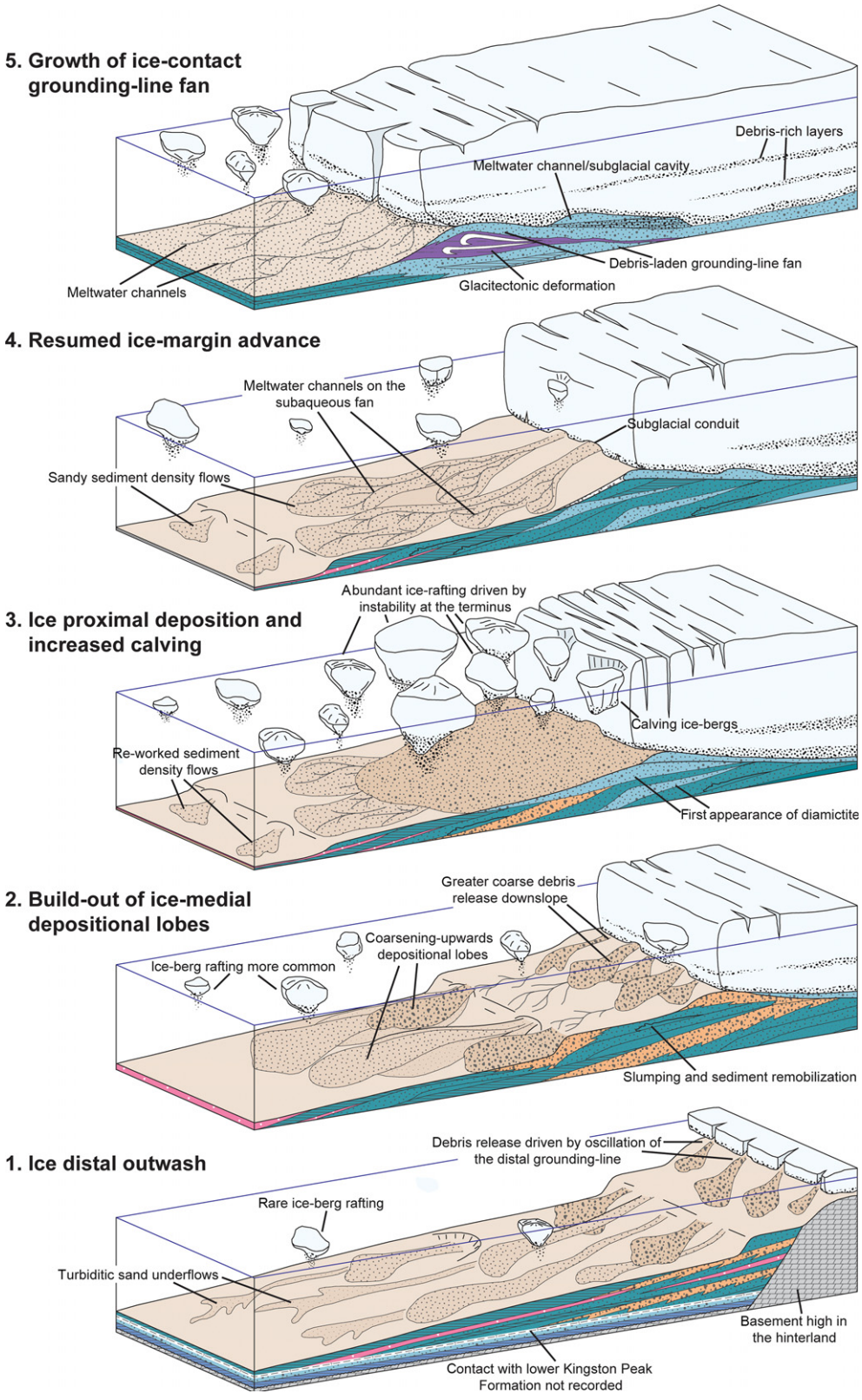

Fig. 8. Five stage depositional model demonstrating stepwise evolution of the glacier-fed subaqueous fan, see text for detailed description. Overall, a clear ice advance signature can be recognized, driving progradation of the subaqueous fan complex and an increase in glacial indicators up-section. This advance is subject to minor retreats and meltback phases, and thus supports dynamic ice sheet behaviour.

suggests limited flow transformation, attributed to a shorter transport distance and therefore less opportunity for mixing and dilution. This is used to support proximity to the ice margin (Fig. 8-3), further corroborated by the more regular recurrence of ice-rafted debris, and the preservation of subglacially striated clasts.

Diamictite is continuously more prevalent upsection, mirrored by an increase of IRD. Towards the top of this sequence a significant increase in calving processes at the ice front is recorded in a thick accumulation of iceberg rain-out diamictite (Fig. 8-3). This is considered to reflect increased instability at the ice front, triggering more widespread calving and greater iceberg distribution basinwards. These processes have the capacity to destabilize the ice margin (Benn *et al.*, 2007, and references within), potentially halting ice advance temporarily, or initiating a retreat phase. The latter is favoured here due to the resumed dominance of turbidites, more akin to the depositional characteristics of Stage 2 described above.

Stage 4 – Resumed ice-margin advance (476 to 580 m)

Above the iceberg rain-out deposit, the trend of more prevalent diamictite deposits upsection desists, replaced by renewed ice-medial turbidity currents of the interbedded heterolithics and pebble to boulder conglomerate facies associations. Initiation and growth of depositional lobes is again attributed to oscillation of the grounding-line, driving iceberg release and debris mass transport into the basin. At this stage, subglacial conduits feed meltwater channels on the glacier-fed shelf (e.g. Fleming, 2014), supporting more ice-proximal conditions (Fig. 8-4). This condition is accompanied by renewed accumulation of ice-proximal diamictites, which are now also channelized in places (543 m, Fig. 2), in contrast to lower in the sequence (Stage 3). These features, in tandem with the greater preservation of ripple cross-lamination, are suggestive of enhanced meltwater modification, consistent with increasing proximity of the glacier terminus. This also promotes elevated tractional reworking, leading to generation of the starved ripple and 'banded' facies described above. Channelization in this portion of the subaqueous fan system is considered to contribute to debris bypass downslope, thereby depositing a greater accumulation of interchannel siltstones towards the top of this portion of the sequence (*ca* 544 to 580 m, Fig. 2).

Stage 5 – Growth of ice-contact grounding-line fan (580 to 636 m)

At the top of the studied section a thick assemblage of glaciogenic debris flows (diamictite facies association) is interpreted as accumulating within an ice-marginal grounding-line fan (Fig. 8-5). Ice-marginal fans typically build-up steep slopes (Powell, 1990; Lønne, 1995; Lønne & Nemec, 2011a,b), promoting sediment gravity flow remobilization downslope on both the ice-proximal and ice-distal fan margins. This process is thought to account for the preservation of slump folds verging perpendicular to the principal palaeoflow orientation recorded throughout the remainder of the succession (Fig. 1C). Consistent with similar studies of ice-marginal subaqueous fan systems, impact-related deformation structures are not recognized (Lønne, 1995), although ice-rafting processes remain an important source of coarse debris.

Locally, the glacier terminus is considered to advance to an ice-contact position, leading to proglacial glacitectonic thrusting of the finer grained, and therefore less competent, facies (tectonized facies association). The dominantly ductile style of deformation supports elevated porewater pressures, attributed to a combination of dilute, water-rich sediment flows, the input of abundant meltwater and potentially overburden pressure of the advancing ice margin. The glacitectonic thrusting and high sediment supply may also contribute to thrust-stacking and thickening of the ice-marginal sediment pile. Onlap surfaces towards the top of the succession (at 628 m and 634 m, Fig. 2) are interpreted as recording local flooding of the grounding-line fan, driven by stillstand or early retreat of the ice front. At this stage, hemipelagic and sediment density flow sediments return. However, truncation of the top of the succession beneath the Noonday Dolomite obscures the full extent of retreat.

ICE SHEET DYNAMICS

Overall, a clear ice advance signature can be recognized within the Sperry Wash succession, where ice-distal environments are succeeded by medial, proximal and finally ice-marginal to ice-contact depositional settings. An advance sequence is recorded throughout the ice-distal

outwash (Stage 1), advancing through ice-medial settings (Stage 2) to an ice-proximal position (Stage 3). Throughout this sequence the ice margin is considered to become increasingly unstable, driving more widespread calving and increasingly greater iceberg distribution into the basin. This instability triggers a minor retreat phase, leading to resumed ice-medial conditions and a subsequent re-advance through ice-proximal (Stage 4) and finally ice-marginal settings (Stage 5), with evidence of local advance to an ice-contact position. Thus, basinward progradation of the subaqueous fan progresses throughout, subject to minor back-stepping, and is driven by dominant advance and minor retreat of the ice front (Fig. 8).

Regional mapping places the Sperry Wash sections in unit KP3 (e.g. Prave, 1999; Mrofka & Kennedy, 2011), permitting detailed comparison with other Death Valley outcrop belts. In the type area of the Kingston Range, unit KP3 is punctuated by an olistostrome succession at least 1·5 km thick (Macdonald *et al.*, 2013; Le Heron *et al.*, 2014b). This sequence has been interpreted as recording a significant ice meltback event, corresponding to glacial minimum conditions during the Sturtian glaciation (Le Heron *et al.*, 2014b). Following this event, widespread re-advance of the ice front is recorded in both the northern and southern Kingston Range (Le Heron *et al.*, 2014b; Le Heron & Busfield, this volume), depositing a succession of proglacial turbidites and glaciogenic debris flows (GDFs). In the northern sections boulder conglomerates and coarse sandstones dominate, whereas further south fine-grained siltstones and sandstones are notably abundant, interpreted to reflect proximal to distal facies trends.

The siltstone and sandstone dominated deposits of the southern Kingston Range compare closely to the Sperry Wash study interval, although thicker bedded conglomeratic intervals are more comparable to the northern Kingston Range sections (Le Heron *et al.*, 2014b; Le Heron & Busfield, this volume). Regular and stacked diamictite deposits within unit KP3, however, appear to be unique to the Sperry Wash succession. This represents an important distinction in the progress of ice advance across the three study intervals. In the Kingston Range, following the glacial minimum, ice sheets re-advanced to deposit ice-proximal sediments, within an exclusively proglacial position. At Sperry Wash, ice advance continues from ice-distal settings comparable to the southern Kingston Range (Le Heron & Busfield, this volume), through ice-proximal settings of the northern Kingston Range (Le Heron *et al.*, 2014b), to ice-marginal depositional environments. The top of each succession is truncated beneath the Noonday Dolomite, and therefore this disparity may simply reflect differential preservation. Alternatively, this change may be driven by basin configuration. Under this scenario, two configurations are plausible, although neither are mutually exclusive: (i) the northern and southern Kingston Range represent deeper and more distal 'slope' settings and Sperry Wash the shallower and more proximal 'shelf' (see Le Heron & Busfield, this volume); or (ii) the Sperry Wash succession was deposited in a narrower basin, leading to a more pronounced progradation signature. These tentative scenarios require further testing by comparison to other outcrop belts.

CONCLUSIONS

The Sperry Wash succession allows detailed insight into the dynamics of Sturtian ice sheets as recorded in a marine succession dominated by gravity flows. The succession belongs to the upper part of the Kingston Peak Formation in a stratigraphic unit previously defined as unit KP3 (Prave, 1999; Macdonald *et al.*, 2013). Sedimentological analysis of a 636 m measured section demonstrates that a clear, overall ice sheet advance signature can be recognized. Unique to this section, by comparison to other Death Valley outcrop belts, are ice-marginal and ice-contact deposits which are identifiable by a characteristic deformation zone near the top of the studied section. These features allow the authors to posit that grounding-line zones can be established in Neoproterozoic successions, with great capacity for mapping out the as yet unknown true scale of these globally distributed ice masses. Moreover, the style and influence of advance–retreat cycles is demonstrated to vary considerably over neighbouring outcrop belts, allowing an insight into the complexity of Sturtian glaciodynamics within only a small region of its arguably global extent.

ACKNOWLEDGEMENTS

Field data collection was supported by the Fermor Fund of the Geological Society of London. The authors thank Emrys Phillips and two anonymous reviewers for detailed comments which

greatly improved this manuscript, and likewise Associate Editor Ian Fairchild.

REFERENCES

Allen, J.R.L. (1982) *Sedimentary Structures. Their Character and Physical Basis*. Elsevier, Amsterdam, pp. 395–431.

Allen, J.R.L. (1991) The Bouma A division and the possible duration of turbidity currents. *J. Sediment. Petrol.*, **61**, 291–295.

Allen, P.A., **Leather, J.** and **Brasier, M.D.** (2004) The Neoproterozoic Fiq glaciation and its aftermath, Huqf supergroup of Oman. *Basin Res.*, **16**, 507–534.

Arnaud, E. (2012) The paleoclimatic significance of deformation structures in Neoproterozoic successions. *Sed. Geol.*, **243–244**, 33–56.

Baas, J.H. (2000) Duration of deposition from decelerating high-density turbidity currents. *Sed. Geol.*, **136**, 71–88.

Baas, J.H., **Best, J.L.** and **Peakall, J.** (2011) Depositional processes, bedform development and hybrid flows in rapidly decelerated cohesive (mud-sand) sediment flows. *Sedimentology*, **58**, 1953–1987.

Benn, D.I. and **Evans, D.J.A.** (2010) *Glaciers and Glaciation*. Hodder Education, London, 802 pp.

Benn, D.I., **Warren, C.R.** and **Mottram, R.H.** (2007) Calving processes and the dynamics of calving glaciers. *Earth Sci. Rev.*, **82**, 143–179.

Bennett, M.R. (2003) Ice streams as the arteries of an ice sheet: their mechanics, stability and significance. *Earth Sci. Rev.*, **61**, 309–339.

Boulton, G.S. (1978) Boulder shapes and grain-size distributions of debris as indicators of transport paths through a glacier and till genesis. *Sedimentology*, **25**, 773–799.

Bowring, S.A., **Grotzinger, J.P.**, **Condon, D.J.**, **Ramezani, J.** and **Newall, M.** (2007) Geochronologic constraints on the chronostratigraphic framework of the Neoproterozoic Huqf Supergroup, Sultanate of Oman. *Am. J. Sci.*, **307**, 1097–1145.

Busfield, M.E. and **Le Heron, D.P.** (2013) Glacitectonic deformation in the Chuos Formation of northern Namibia: implications for Neoproterozoic ice dynamics. *Proc. Geol. Assoc.*, **124**, 778–789.

Busfield, M.E. and **Le Heron, D.P.** (2014) Sequencing the Sturtian icehouse: dynamic ice behaviour in South Australia. *J. Geol. Soc. London*, **171**, 443–456.

Condon, D.J., **Zhu, M.**, **Bowring, S.A.**, **Wang, W.**, **Yang, A.** and **Jin, Y.** (2005) U-Pb ages from the Neoproterozoic Doushantuo Formation, China. *Science*, **308**, 95–98.

Denis, M., **Guiraud, M.**, **Konaté, M.** and **Buoncristiani, J.F.** (2010) Subglacial deformation and water-pressure cycles as a key for understanding ice stream dynamics: evidence from the Late Ordovician succession of the Djado Basin (Niger). *Int. J. Earth Sci.*, **99**, 1399–1425.

Dimakis, P., **Elverhøi, A.**, **Høeg, K.**, **Solheim, A.**, **Harbitz, C.**, **Laberg, J.S.** and **Marr, J.** (2000) Submarine slope stability on high-latitude glaciated Svalbard-Barents Sea margin. *Mar. Geol.*, **162**, 303–316.

Dowdeswell, J.A. (1986) The distribution and character of sediments in a tidewater glacier, southern Baffin Island, NWT, Canada. *Arct. Alp. Res.*, **18**, 45–56.

Dowdeswell, J.A. (1989) On the nature of Svalbard icebergs. *J. Glaciol.*, **35**, 224–234.

Elverhøi, A., **de Blasio, F.V.**, **Butt, F.A.**, **Issler, D.**, **Harbitz, C.**, **Engvik, L.** and **Marr, J.** (2002) Submarine mass-wasting on glacially-influenced continental slopes: processes and dynamics. *Geol. Soc. London Spec. Publ.*, **203**, 73–87.

Etienne, J.L., **Jansson, K.N.**, **Glasser, N.F.**, **Hambrey, M.J.**, **Davies, J.R.**, **Waters, R.A.**, **Maltman, A.J.** and **Wilby, P.R.** (2006) Palaeoenvironmental interpretation of an ice-contact glacial lake succession: an example from the late Devensian of southwest Wales, UK. *Quatern. Sci. Rev.*, **25**, 739–762.

Evans, D.J.A. and **Hiemstra, J.F.** (2005) Till deposition by glacier submarginal, incremental thickening. *Earth Surf. Proc. Land.*, **30**, 1633–1662.

Evans, J. and **Pudsey, C.J.** (2002) Sedimentation associated with Antarctic Peninsula ice shelves: implications for palaeoenvironmental reconstructions of glacimarine sediments. *J. Geol. Soc. London*, **159**, 233–237.

Evans, D.J.A., **Hiemstra, J.F.** and **Ó Cofaigh, C.** (2012) Stratigraphic architecture and sedimentology of a Late Pleistocene subaqueous moraine complex, southwest Ireland. *J. Quat. Sci.*, **27**, 51–63.

Fairchild, I.J. and **Kennedy, M.J.** (2007) Neoproterozoic glaciation in the Earth System. *J. Geol. Soc. London*, **164**, 895–921.

Fleming, E.J. (2014) Magnetic, structural and sedimentological analysis of glacial sediments: insights from modern, Quaternary and Neoproterozoic environments. PhD thesis, University of Birmingham, UK, 354 pp.

Hammond, J.G. (1983) Late Precambrian diabase intrusions in the southern Death Valley region, California: their petrology, geochemistry, and tectonic implications. PhD thesis, University of Southern California, 281 pp.

Hampton, M.A. (1972) The role of subaqueous debris flow in generating turbidity currents. *J. Sediment. Petrol.*, **42**, 775–793.

Hazzard, J.C. (1937) Paleozoic section in the Nopah and Resting Springs Mountains, Inyo County, California. *Calif. J. Min. Geol.*, **33**, 270–339.

Heaman, L.M. and **Grotzinger, J.P.** (1992) 1.08 Ga diabase sills in the Pahrump Group, California; implications for development of the Cordilleran miogeocline. *Geology*, **20**, 637–640.

Henry, L.C., **Isbell, J.F.**, **Fielding, C.R.**, **Domack, E.W.**, **Frank, T.D.** and **Fraiser, M.L.** (2012) Proglacial deposition and deformation in the Upper Carboniferous to Lower Permian Wynyard Formation, Tasmania: a process analysis. *Palaeogeogr. Palaeoclimatol. Palaeoecol.*, **315–316**, 142–157.

Hewett, D.F. (1940) New formation names to be used in the Kinsgton Range, Ivanpah Quadrangle, California. *J. Wash. Acad. Sci.*, **30**, 239–240.

Hewett, D.F. (1956) Geology and Mineral Resources of the Ivanpah Quadrangle, California and Nevada. US Geological Survey Professional Paper 275, 172 pp.

Hiemstra, J.F. and **Rijsdijk, K.F.** (2003) Observing artificially induced strain: implications for subglacial deformation. *J. Quat. Sci.*, **18**, 373–383.

Hodgson, D.M., **Flint, S.S.**, **Hidgetts, D.**, **Drinkwater, N.J.**, **Johannessen, E.P.** and **Luthi, S.** (2006) Stratigraphic evolution of fine-grained submarine fan systems, Tanqua depocentre, Karoo Basin, South Africa. *J. Sediment. Res.*, **76**, 20–40.

Hoffman, P.F. (2009) Pan-glacial – a third state in the climate system. *Geol. Today*, **25**, 100–107.

Hoffman, P.F., **Kaufman, A.J.**, **Halverson, G.P.** and **Schrag, D.P.** (1998) A Neoproterozoic Snowball Earth. *Science*, **281**, 1342–1346.

Hoffmann, K.-H., **Condon, D.J.**, **Bowring, S.A.** and **Crowley, J.L.** (2004) U-Pb zircon date from the Neoproterozoic Ghaub Formation, Namibia: constraints on Marinoan glaciation. *Geology*, **32**, 817–820.

Ilstad, T., **Elverhøi, A.**, **Issler, D.** and **Marr, J.G.** (2004) Subaqueous debris flow behaviour and its dependence on the sand/clay ratio: a laboratory study using particle tracking. *Mar. Geol.*, **213**, 415–438.

Jennings, C.W., **Burnett, J.L.** and **Troxel, B.W.** (1962) *Geologic Map of California – Trona Sheet*. Division of Mines and Geology, California.

Jobe, Z.R., **Lowe, D.R.** and **Morris, W.R.** (2012) Climbing-ripple successions in turbidite systems: depositional environments, sedimentation rates and accumulation times. *Sedimentology*, **59**, 867–898.

Johnsen, T.F. and **Brennand, T.A.** (2004) Late glacial lakes in the Thompson basin, British Columbia: palaeogeography and evolution. *Can. J. Earth Sci.*, **41**, 1367–1383.

Johnsen, T.F. and **Brennand, T.A.** (2006) The environment in and around ice-dammed lakes in the moderately high relief setting of the southern Canadian Cordillera. *Boreas*, **35**, 106–125.

Kane, I.A. and **Hodgson, D.** (2010) Submarine channel levees, criteria for recognition of subenvironments: exhumed examples from the Rosario Fm (Baja, Mexico) and the Laingsburg Fm (Karoo Basin). *Mar. Pet. Geol.*, **28**, 807–823.

Kneller, B. (1995) Beyond the turbidite paradigm: physical models for deposition of turbidites and their implications for reservoir prediction. *Geol. Soc. London Spec. Publ.*, **94**, 31–31.

Komar, P.D. (1985) The hydraulic interpretation of turbidites from their grain sizes and sedimentary structures. *Sedimentology*, **32**, 395–407.

Kuenen, P.H. (1966) Experimental turbidite lamination in a circular flume. *J. Geol.*, **74**, 523–545.

Kuenen, P.H. and **Humbert, F.L.** (1969) Grain size of turbidite ripples. *Sedimentology*, **13**, 253–261.

Laberg, J.S. and **Vorren, T.O.** (1995) Late Weichselian submarine debris flow deposits on the Bear Island Trough mouth fan. *Mar. Geol.*, **127**, 45–72.

Laberg, J.S. and **Vorren, T.O.** (2000) Flow behaviour of the submarine glacigenic debris flows on the Bear Island Trough Mouth Fan, western Barents Sea. *Sedimentology*, **47**, 1105–1117.

Labotka, T.C., **Albee, A.L.**, **Lanphere, M.A.** and **McDowell, S.C.** (1980) Stratigraphy, structure and metamorphism in the central Panamint Mountains (Telescope Peak quadrangle), Death Valley area, California. *Geol. Soc. Am. Bull.*, **91**, 843–933.

Lachniet, M.S., **Larson, G.J.**, **Lawson, D.E.**, **Evenson, E.B.** and **Alley, R.B.** (2001) Microstructures of sediment flow deposits and subglacial sediments: a comparison. *Boreas*, **30**, 254–264.

Le Heron, D.P. and **Busfield, M.E.** (this volume) Pulsed iceberg delivery driven by Sturtian ice sheet dynamics: an example from Death Valley, California. *Sedimentology*, (Accepted).

Le Heron, D.P., **Cox, G.**, **Trundley, A.** and **Collins, A.** (2011) Sea ice-free conditions during the Sturtian glaciation (early Cryogenian), South Australia. *Geology*, **39**, 31–34.

Le Heron, D.P., **Busfield, M.E.** and **Kamona, F.** (2013) An interglacial on snowball Earth? Dynamic ice behaviour revealed in the Chuos Formation, Namibia. *Sedimentology*, **60**, 411–427.

Le Heron, D.P., **Busfield, M.E.** and **Collins, A.S.** (2014a) Bolla Bollana boulder beds: a Neoproterozoic trough mouth fan in South Australia? *Sedimentology*, **61**, 978–995.

Le Heron, D.P., **Busfield, M.E.** and **Prave, A.R.** (2014b) Neoproterozoic ice sheets and olistoliths: multiple glacial cycles in the Kingston Peak Formation, California. *J. Geol. Soc. London*, **171**, 525–538.

Leclair, S.F. and **Arnott, R.W.C.** (2005) Parallel lamination formed by high-density turbidity currents. *J. Sediment. Res.*, **75**, 1–5.

Lee, J.R. and **Phillips, E.R.** (2008) Progressive soft sediment deformation within a subglacial shear zone—a hybrid mosaic–pervasive deformation model for Middle Pleistocene glaciotectonised sediments from eastern England. *Quatern. Sci. Rev.*, **27**, 1350–1362.

Livingstone, S.J., **Ó Cofaigh, C.** and **Evans, D.J.A.** (2010) A major ice drainage pathway of the last British-Irish Ice Sheet: the Tyne Gap, northern England. *J. Quat. Sci.*, **25**, 354–370.

Lønne, I. (1995) Sedimentary facies and depositional architecture of ice-contact glaciomarine systems. *Sed. Geol.*, **98**, 13–43.

Lønne, I. and **Nemec, W.** (2011a) Modes of sediment delivery to the grounding line of a fast-flowing tidewater glacier: implications for ice-margin conditions and glacier dynamics. *Geol. Soc. London Spec. Publ.*, **354**, 33–56.

Lønne, I. and **Nemec, W.** (2011b) The kinematics of ancient tidewater ice margins: criteria for recognition from grounding-line moraines. *Geol. Soc. London Spec. Publ.*, **354**, 57–75.

Lowe, D.R. (1982) Sediment gravity flows: II Depositional models with special reference to the deposits of high-density turbidity currents. *J. Sediment. Res.*, **52**, 279–297.

Lowe, D.R. (1988) Suspended-load fallout rate as an independent variable in the analysis of current structures. *Sedimentology*, **35**, 765–776.

Macdonald, F.A., **Schmitz, M.D.**, **Crowley, J.L.**, **Roots, C.F.**, **Jones, D.S.**, **Maloof, A.C.**, **Strauss, J.V.**, **Cohen, P.A.**, **Johnston, D.T.** and **Schrag, D.P.** (2010) Calibrating the Cryogenian. *Science*, **327**, 1241–1243.

Macdonald, H.A., **Peakall, J.**, **Wignall, P.B.** and **Best, J.** (2011) Sedimentation in deep-sea lobe-elements: implications for the origin of thickening-upward sequences. *J. Geol. Soc.*, **168**, 319–332.

Macdonald, F.A., **Prave, A.R.**, **Petterson, R.**, **Smith, E.F.**, **Pruss, S.B.**, **Oates, K.** and **Fallick, A.E.** (2013) The Laurentian record of Neoproterozoic glaciation, tectonism, and eukaryotic evolution in Death Valley, California. *Geol. Soc. Am. Bull.*, **125**, 1203–1223.

Mahon, R.C., **Dehler, C.M.**, **Link, P.K.**, **Karlstrom, K.E.** and **Gehrels, G.E.** (2014) Geochronologic and stratigraphic constraints on the Mesoproterozoic and Neoproterozoic Pahrump Group, Death Valley, California: a record of the assembly, stability, and breakup of Rodinia. *Geol. Soc. Am. Bull.*, **126**, 652–664.

Maltman, A. (1994) *The Geological Deformation of Sediments*. Chapman and Hall, Cambridge, 384 pp.

Marenssi, S.A., **Tripaldi, A.**, **Limarino, C.O.** and **Caselli, A.T.** (2005) Facies and architecture of a Carboniferous grounding-line system from the Guandacol Formation,

Paganzo Basin, northwestern Argentina. *Gondwana Res.*, **8**, 187–202.

Menzies, J. (2000) Micromorpholigcal analyses of microfabrics and microstructures indicative of deformation processes in glacial sediments. In: *Deformation of Glacial Materials* (Eds A.J. Maltman, B. Hubbard and M.J. Hambrey). *Geol. Soc. Spec. Publ. London*, **176**, 245–257.

Menzies, J. and **Zaniewski, K.** (2003) Microstructures within a modern debris flow deposit derived from Quaternary glacial diamicton—a comparative micromorphological study. *Sed. Geol.*, **157**, 31–48.

Middleton, G.V. and **Hampton, M.A.** (1973) Sediment gravity flows: mechanisms of flow and deposition. In: *Turbidites and Deep-water Sedimentation* (Eds G.V. Middleton and A.H. Bouma). *SEPM Pacific Section, Short Course Lecture Notes*, 1–38.

Miller, J.M.G. (1985) Glacial and syntectonic sedimentation: the Upper Proterozoic Kingston Peak Formation, southern Panamint Range, eastern California. *Geol. Soc. Am. Bull.*, **96**, 1537–1553.

Mrofka, D. and **Kennedy, M.** (2011) The Kingston Peak Formation in the eastern Death Valley region. In: *The Geological Record of Neoproterozoic Glaciations* (Eds E. Arnaud, G. Halverson and G. Shields-Zhou). *Geol. Soc. London Mem.*, **36**, 449–458.

Mulder, T. and **Alexander, A.** (2001) The physical character of subaqueous sedimentary density flows and their deposits. *Sedimentology*, **48**, 269–299.

Noble, L.F. (1934) Rock formations of Death Valley, CA. *Science*, **80**, 173–178.

Ó Cofaigh, C., **Taylor, J.**, **Dowdeswell, J.A.**, **Rosell-Melé, A.**, **Kenyon, N.H.**, **Evans, J.** and **Mienert, J.** (2002) Sediment reworking on high-latitude continental margins and its implications for palaeoceanographic studies: insights from the Norwegian-Greenland Sea. *Geol. Soc. London Spec. Publ.*, **203**, 325–348.

Ó Cofaigh, C., **Taylor, J.**, **Dowdeswell, J.A.** and **Pudsey, C.J.** (2003) Palaeo-ice streams, trough mouth fans and high-latitude continental slope sedimentation. *Boreas*, **32**, 37–55.

Ó Cofaigh, C., **Evans, D.J.A.** and **Hiemstra, J.F.** (2011) Formation of a stratified subglacial 'till' assemblage by ice-marginal thrusting and glacier overriding. *Boreas*, **40**, 1–14.

Ovenshine, A.T. (1970) Observations of iceberg rafting in Glacier Bay, Alaska, and the identification of ancient ice-rafted deposits. *Geol. Soc. Am. Bull.*, **81**, 891–894.

Perkins, A.J. and **Brennand, T.A.** (2015) Refining the pattern and style of Cordilleran Ice Sheet retreat: palaeogeography, evolution and implications of lateglacial ice-dammed lake systems on the southern Fraser Plateau, British Columbia, Canada. *Boreas*, **44**, 319–342.

Petterson, R., **Prave, A.R.**, **Wernicke, B.P.** and **Fallick, A.E.** (2011a) The Neoproterozoic Noonday Formation, Death Valley region, California. *Geol. Soc. Am. Bull.*, **123**, 1317–1336.

Petterson, R., **Prave, A.R.** and **Wernicke, B.P.** (2011b). Glaciogenic and related strata of the Neoproterozoic Kingston Peak Formation in the Panamint Range, Death Valley region, California. In: *The Geological Record of Neoproterozoic Glaciations* (Eds E. Arnaud, G.P. Halverson and G. Shields-Zhou). *Geol. Soc. London Mem.*, **36**, 449–458.

Phillips, E. (2006) Micromorphology of a debris flow deposit: evidence of basal shearing, hydrofracturing, liquefaction and rotational deformation during emplacement. *Quatern. Sci. Rev.*, **25**, 720–738.

Phillips, E., **Merritt, J.**, **Auton, C.** and **Golledge, N.** (2007) Microstructures in subglacial and proglacial sediments: understanding faults, folds and fabrics, and the influence of water on the style of deformation. *Quatern. Sci. Rev.*, **26**, 1499–1528.

Piper, D.J.W. (1978) Turbidite muds and silts on deep sea fans and abyssal plains. In: *Sedimentation in Submarine Canyons, Fans and Trenches*, pp. 163–176. (Eds D.J. Stanley and G. Kelling), Hutchinson and Ross, Pennsylvania.

Postma, G., **Nemec, W.** and **Kleinspehn, K.L.** (1988) Large floating clasts in turbidites – a mechanism for their emplacement. *Sed. Geol.*, **58**, 47–61.

Powell, R.D. (1990) Glacimarine processes at grounding-line fans and their growth into ice-contact deltas. In: *Glacimarine Environments: Processes and Sediments* (Eds J.A. Dowdeswell and J.D. Scourse). *Geol. Soc. London Spec. Publ.*, **53**, 53–73.

Powell, R.D. and **Domack, E.W.** (2002) Modern glacimarine environments. In: *Modern and Past Glacial Environments*, pp. 361–389. (Ed J. Menzies), Butterworth-Heinemann Ltd., Oxford.

Prave, A.R. (1999) Two diamictites, two cap carbonates, two $\delta^{13}C$ excursions, two rifts: the Neoproterozoic Kingston Peak Formation, Death Valley, California. *Geology*, **27**, 339–342.

Prélat, A. and **Hodgson, D.M.** (2013) The full range of turbidite bed thickness patterns in submarine lobes: controls and implications. *J. Geol. Soc.*, **170**, 209–214.

Prélat, A., **Hodgson, D.M.** and **Flint, S.** (2009) Evolution, architecture and hierarchy of distributary deep-water deposits: a high-resolution outcrop investigation from the Permian Karoo Basin, South Africa. *Sedimentology*, **56**, 2132–2154.

Ravier, E., **Buoncristiani, J.-F.**, **Clerc, S.**, **Guiraud, M.**, **Menzies, J.** and **Portier, E.** (2014) Sedimentological and deformational criteria for discriminating subglaciofluvial deposits from subaqueous ice-contact fan deposits: a Pleistocene example (Ireland). *Sedimentology*, **61**, 1382–1410.

Stokes, C.R. and **Clark, C.D.** (2001) Palaeo-ice streams. *Quatern. Sci. Rev.*, **20**, 1437–1457.

Sumner, E.J., **Amy, L.A.** and **Talling, P.J.** (2008) Deposit structure and processes of sand deposition from decelerating sediment suspensions. *J. Sediment. Res.*, **78**, 529–547.

Sylvester, Z. and **Lowe, D.R.** (2004) Textural trends in turbidites and slurry beds from the Oligocene flysch of the Carpathians, Romania. *Sedimentology*, **51**, 945–972.

Talling, P.J. (2013) Hybrid submarine flows comprising turbidity current and cohesive debris flow: deposits, theoretical and experimental analyses, and generalized models. *Geosphere*, **9**, 460–488.

Talling, P.J., **Amy, L.A.**, **Wynn, R.B.**, **Blackbourn, G.** and **Gibson, O.** (2007) Turbidity current evolution deduced from extensive thin turbidites: Marnosos-arenacea Formation (Miocene), Italian Appenines. *J. Sediment. Res.*, **77**, 172–196.

Talling, P.J., **Masson, D.G.**, **Sumner, E.J.** and **Malgesini, G.** (2012) Subaqueous sediment density flows: depositional processes and deposit types. *Sedimentology*, **59**, 1937–2003.

Troxel, B.W. (1966) Sedimentary features of the later Precambrian Kingston Peak Formation, Death Valley, California. *Geol. Soc. Am. Spec. Pap.* **101**, 341.

Troxel, B.W. (1982) Description of the uppermost part of the Kingston Peak Formation, Amargosa Rim Canyon, Death Valley region, California. In: *Geology of selected areas in the San Bernardino Mountains, western Mojave Desert, and southern Great Basin, California*, Geological Society of America Cordilleran Section Field Trip Guidebook and Volume, pp. 61–70. (Eds J.D. Cooper, B.W. Troxel and L.A. Wright), Death Valley Publishing Company, Shoshone, California.

Vorren, T.O., **Laberg, J.S.**, **Blaume, F.**, **Dowdeswell, J.A.**, **Kenyon, N.H.**, **Mienert, J.** and **Werner, F.** (1998) The Norwegian-Greenland Sea continental margins: morphology and late Quaternary sedimentary processes and environment. *Quatern. Sci. Rev.*, **17**, 273–302.

Walker, R.G. (1967) Turbidite sedimentary structures and their relationship to proximal and distal depositional environments. *J. Sediment. Petrol.*, **37**, 25–43.

Walker, R.G. (1978) Deep-water sandstone facies and ancient submarine fans – models for exploration and for stratigraphic traps. *AAPG Bull.*, **62**, 932–966.

Winsemann, J., **Asprion, U.**, **Meyer, T.** and **Schramm, C.** (2007) Facies characteristics of Middle Pleistocene (Saalian) ice-margin subaqueous fan and delta deposits, glacial Lake Leine, NW Germany. *Sed. Geol.*, **193**, 105–129.

Wright, L.A., **Troxel, B.W.**, **Williams, E.G.**, **Roberts, M.T.** and **Diehl, P.E.** (1974) Precambrian sedimentary environments of the Death Valley region, eastern California. In: *Guidebook: Death Valley Region, California and Nevada*, pp. 27–35. (Eds B.W. Troxel and L.A. Wright), Death Valley Publishing Company, Shoshone, CA.

Zaniewski, K. and **van der Meer, J.J.M.** (2005) Quantification of plasmic fabric through image analysis. *Catena*, **63**, 109–127.

Zhou, C., **Tucker, R.**, **Xiao, S.**, **Peng, Z.**, **Yuan, X.** and **Chen, Z.** (2004) New constraints on the ages of Neoproterozoic glaciations in South China. *Geology*, **32**, 437–440.

Manuscript received 15 August 2014; revision accepted 16 April 2015

6. Syntheses and conclusions

6. Syntheses and conclusions

The preceding chapters have demonstrated the diverse spectrum of subaqueous glacially-influenced sediments preserved within some of the classic Neoproterozoic successions of the Rodinian and Laurentian palaeocontinents. These study areas benefited from exceptional exposure, minimal metamorphic overprint, highly heterogeneous facies assemblages, and in places remarkable lateral continuity given their post-depositional tectonic history. Each paper presented acts as a stand-alone contribution with its own discussion regarding depositional environments and implications for the Neoproterozoic icehouse. This chapter will therefore serve to synthesise these results in the broader context of global Neoproterozoic glaciation, through reference to the constituent aims outlined in Chapter 1. Comparisons will be drawn throughout to younger icehouse intervals in order to discern whether the Cryogenian cryosphere was unique in its behaviour, a condition which might be anticipated to facilitate unusual low-latitude glaciation. Finally, the implications of this research in relation to existing conceptual and climatic models of Neoproterozoic glaciation will be discussed, alongside potential future research directions.

6.1. What glacial depositional environments are preserved in the Sturtian record?

The dataset presented herein, like much of the glacial depositional record, is biased towards glaciomarine successions. This is an inherent product of the greater accommodation space afforded by these environments, which is hugely advantageous in terms of preservation potential (Eyles, 1993; Bennett & Glasser, 2009; Benn & Evans, 2010), but at the price of a limited understanding of the terrestrial glacial landsystem. Nonetheless, the great thickness and heterogeneity of the studied successions provides a detailed insight into sedimentological processes active under the Sturtian icehouse (Chapters 3-5). This is fundamental for understanding glacier and ice sheet mass balance at this time, which has significant bearing on regional and global palaeoclimate, especially the hydrological cycle.

6.1.1. Glaciomarine vs. glaciolacustrine

Throughout this volume studied sections have consistently been described as glaciomarine, but it is pertinent to note that glaciogenic sediments deposited in marine and (large) lacustrine systems can share many facies characteristics. Both commonly preserve thick successions of laminated sediments, often subject to ice-rafting, and interrupted by coarser sediment underflows or mass movement deposits, whilst both may interdigitate with ice-contact grounding-line fans or subglacial diamictite assemblages in their ice-proximal regions (e.g.

Bennett & Glasser, 2009; Benn & Evans, 2010; Carrivick & Tweed, 2013 and refs within). However, it is widely recognised that marine-terminating glaciers typically deposit much thicker subglacial till sequences of several tens of metres (e.g. Busfield & Le Heron, 2013; Le Heron et al., 2013b), as opposed to a few metres thick beneath lake-terminating ice (Bennett & Glasser, 2009). The former are also often subject to more widespread calving (cf. Benn et al., 2007 and refs within), and hence more dominant rain-out processes (e.g. Busfield & Le Heron, in press; Le Heron & Busfield, accepted). Within the finer sediment fraction, rhythmically laminated facies are a characteristic component of glaciolacustrine sequences (e.g. Ashley, 1995; Carrivick & Tweed, 2013), frequently preserving thicker sand and thinner mud layers during the summer melt season, and vice versa during winter freeze (Ó Cofaigh & Dowdewell, 2001). These sedimentation patterns were not observed within the studied Sturtian sequences (Chapters 3-5). Moreover, glaciolacustrine systems are commonly dominated by suspension settling processes, with coarser grained input restricted to ice-contact settings and jökulhlaup outburst events (Benn & Evans, 2010; Carrivick & Tweed, 2013). This mode of coarse-grained sediment delivery is rejected owing to the absence of other facies characteristic of catastrophic outburst floods, e.g. metre-scale antidunes and megaripples (Duller et al., 2008; Le Heron et al., 2014b). In contrast, the majority of the studied sections are dominated by coarse, but commonly well-sorted, mass flow deposits with significantly more minor suspension settling activity (Chapters 3-5).

It is reasonable to expect that the vast thicknesses (>500 m) of dominantly coarse-grained sediment preserved in the studied sections accumulated within a glaciomarine setting (e.g. Busfield & Le Heron, 2014; Busfield & Le Heron, in press), given that these far exceed recorded examples from glaciolacustrine environments (e.g. Etienne et al., 2006; Johnsen & Brennand, 2004, 2006; Winsemann et al., 2007; Livingstone et al., 2010; Perkins & Brennand, 2014). Moreover, the common association of these glacially-influenced siliciclastic sediments with carbonate lithologies, occurring as intra-formational deposits (e.g. Busfield & Le Heron, 2013; Le Heron et al., 2014a), km-scale olistoliths plucked from the subglacial carbonate bedrock (e.g. Le Heron et al., 2014b) and post-glacial 'cap' carbonates (e.g. Le Heron et al., 2013a, b) provides strong support for marine-terminating ice sheets.

6.1.2. Sturtian glaciomarine environments

It is clear that comparable facies are recorded throughout the studied sections, although their thickness and stratigraphic recurrence within any individual logged section varies considerably (Chapters 3-5). This variation is largely driven by changing proximity of the ice margin (e.g. Le Heron et al., 2013b; Busfield & Le Heron, in press), in concert with irregular underlying palaeotopography (e.g. Busfield & Le Heron, 2014).

Despite some differences in nomenclature, the sedimentary assemblages are demonstrated to fall within eight facies associations (**Table 6.1**), recording a spectrum of ice-distal to subglacial depositional environments. These can be summarised as follows:

- **Ice-distal zone**

As might be anticipated, these sediments are most prevalent in the thickest studied sections (e.g. Busfield & Le Heron, 2014; Busfield & Le Heron, in press), and consist of dilute, well sorted silt to sand grade turbidites, interrupted by occasional conglomeratic event beds. Ice-rafting is rare, occurring as only sparse isolated lonestones. Unique assemblages in the central Flinders Ranges and northern Kingston Range are interpreted to record ice minimum conditions (**Table 6.1**), comprising hummocky cross-stratified sandstone and km-scale megaclasts, respectively (Busfield & Le Heron, 2014; Le Heron et al., 2014b). The extent of ice meltback during these intervals will be discussed below.

- **Ice-medial shelf**

This environment is again dominated by mass flow deposits, but these are often coarser, thicker and less well sorted than the distal shelf, and thus include intercalated turbidite and debrite deposits. Under elevated sediment supply stacked, coarsening-upward turbiditic lobes prograde across the shelf (e.g. Le Heron et al., 2014b; Busfield & Le Heron, in press). Closer proximity to the ice margin is manifest in more abundant IRD, although they remain as isolated lonestones (Le Heron et al., 2013b, 2014b; Busfield & Le Heron, in press).

- **Ice proximal zone**

The ice-proximal zone is characterised by much thicker units of coarse sandstone, conglomerate and diamictite, accumulating as high-density turbidites and debrites (e.g. Busfield & Le Heron, 2014; Le Heron et al., 2014b). In places, these mass flows build up to form thick trough mouth fan deposits (e.g. Le Heron et al., 2014a). Higher meltwater input is evident by channelisation of the subaqueous proglacial deposits (e.g. Le Heron et al., 2013b, 2014a; Busfield & Le Heron, in press), whilst ice-rafting processes are considerably more prevalent, occasionally occurring as debris-laden rain-out deposits representing more pronounced calving processes at the ice front (Busfield & Le Heron, in press).

	Northern Namibia			South Australia		Western USA			
Facies Associations	**3.2** *Le Heron et al. 2013a*	**3.3** *Le Heron et al. 2013b*	**3.4** *Busfield & Le Heron 2013*	**4.2** *Le Heron et al. 2014a*	**4.3** *Busfield & Le Heron 2014*	**5.2** *Le Heron et al. 2014b*	**5.3** *Busfield & Le Heron in press*	**5.4** *Le Heron & Busfield accepted*	**Depositional environment**
1. Pebble-boulder conglomerate					Diamictite & conglomerate	Pebble to boulder conglomerate			*Ice-proximal to ice-distal shelf and slope*
2. Diamictite	Diamictite	Massive & graded diamictite	Massive diamictite Stratified diamictite	Diamictite		Diamictite			*Ice-contact and ice-proximal shelf*
3. Interbedded heterolithics		Pebbly cross-stratified sandstone Clast-free shale		Channel belt Sheet heterolithics	Interbedded heterolithics				*Ice-proximal to ice-distal shelf and slope*
4. Lonestone-bearing		Lonestone-bearing shale			Lonestone bearing-siltstone	Lonestone-bearing			*Ice-proximal and ice-distal shelf and slope, iceberg rich waters*
5. Tectonised		Sheared diamictite	Sheared & laminated diamictite				Tectonised		*Ice-marginal and subglacial ice-contact settings*
6. HCS					Hummocky cross-stratified sandstone				*Ice free or ice minimum storm-agitated shelf*
7. Megaclast						Megaclast			
8. Ironstone	Ironstone				Ferruginous siltstone and sandstone				*Microbially colonised restricted basin*

Table 6.1: Summary table of lithofacies associations recorded throughout the studied sections. Aside from minor changes in nomenclature, eight facies associations are clearly picked out, the first four representing the most dominant lithologies within the Sturtian sequences.

- **Ice-marginal to ice-contact settings**

In this setting poorly sorted debris flows accumulate as grounding-line fans subject to widespread re-working and glaciotectonic deformation (Busfield & Le Heron, 2013; Busfield & Le Heron, in press). In subglacial settings, ice-bed decoupling and subsequent touchdown result in both ductile and brittle deformation of the sediment pile (e.g. Busfield & Le Heron, 2013; Le Heron et al., 2013b), and contribute to significant de-watering and hydrofracturing.

6.1.3. The sub ice-shelf problem

Identification of ice-contact conditions, or an 'ice-grounding zone', in both northern Namibia (Busfield & Le Heron, 2013; Le Heron et al., 2013b) and western USA (Busfield & Le Heron, in press) raises a question which is common to many glacial depositional models: is there evidence for a floating ice shelf? To generate a floating glacier or ice shelf, ice beyond the grounding-line must be below the pressure-melting point, where it may become buoyant. These conditions are associated with cold to polythermal glacier thermal regimes, e.g. Antarctica's Ross Ice Shelf, Amery Ice Shelf, Peninsula ice shelves (Domack et al., 1999; Evans & Pudsey, 2002; Hambrey & Glasser, 2012; Post et al., 2014). Deposition beneath such an ice shelf should have a unique sedimentary signature, but reliable depositional models are scarce. This is partly due to the difficulty of accessing sub ice-shelf settings at modern glaciers and ice sheets (e.g. Powell et al., 1996), and also driven by the commonly thin accumulations of sediment where they can be recovered (e.g. Domack & Harris, 1998; Evans & Pudsey, 2002; Hemer & Harris, 2003). Their recognition in ancient depositional systems is therefore hampered by a dearth of suitable modern analogues.

Many recorded examples of sub-ice shelf sedimentation preserve only a couple of metres of sediment, some even <0.5 m, making a detailed understanding of sedimentological processes extremely difficult. As such, 'diagnostic' facies are scarce, if at all recognised. Models developed beneath Antarctic ice shelves predict a 'null zone' between the grounding-line and open-marine settings where ice-rafting from the frozen ice shelf base is minimal, and deposition is dominated by mud to granulated mud grade sediment, alongside thin mud-rich diamictons (e.g. Domack & Harris, 1998; Domack et al., 1999). In places, these sediments preserve cross-lamination or cross-bedding, reflecting processes of tidal pumping or thermohaline flow within the sub-ice shelf cavity. Meltwater supply is widely considered to be limited beneath ice shelves, and thus meltwater-derived sediments are notably absent (Powell et al., 1996; Domack & Harris, 1998; Domack et al., 1999; Evans & Pudsey, 2002).

These features contrast with the majority of sedimentary rocks described throughout this thesis, which are not only dominated by coarse material (Chapters 3-5), at least occurring as coarse grained turbiditic interbeds where facies are generally finer (e.g. Busfield & Le Heron, 2014; Busfield & Le Heron, in press), but also contra to the evidence favouring sustained delivery of waterlain sediment from the grounding-line and hence significant meltwater supply (e.g. Le Heron et al., 2014b; Busfield & Le Heron, in press). As such, depositional models in which floating ice shelves are drawn herein should be treated with caution (e.g. Le Heron et al., 2014b), as the widespread evidence favouring meltwater-derived deposition, high debris load and recurrent iceberg rafting are more in line with polythermal ice sheets (e.g. Hambrey & Glasser, 2012 and refs within) where partially floating ice, if present, would be local and short-lived. This is corroborated by the rare, and where present extremely thin deposits associated with ice-lift off processes (e.g. Busfield & Le Heron, 2013).

In line with these observations, depositional models favour the development of a grounded, marine-terminating ice mass, wherein icebergs, proglacial meltwater streams and subglacial conduits deliver debris downslope, subject to widespread re-working by both laminar and turbulent sediment gravity flows (**Fig. 6.1**). These processes are consistent with sedimentary records from Pleistocene-Holocene temperate and polythermal regimes in Alaska (e.g. Cai et al., 1997; Powell & Cooper, 2002), Norway (e.g. Lysså et al., 2010; Lønne & Nemec 2011a, b) and the Greenland continental margin (e.g. Laberg & Vorren, 2000; Ó Cofaigh et al., 2013a, b). Although arguably, the limited evidence of glaciofluvial re-working, highly concentrated mass-flow deposits and ice-rafted debris, indicative of high basal debris load, and preservation of thick advance sequences are more typical of polythermal than temperate systems (e.g. Dowdeswell, 1986; Cai et al., 1997; Hambrey & Glasser, 2012). The implications of these analogues with reference to fjord versus continental shelf settings will be discussed below (see 6.1.3.2).

6.2. How do ironstones relate to Neoproterozoic glaciation?

The unusual re-appearance of ironstones in the stratigraphic record coincident with deposits supporting Neoproterozoic glaciation led many authors to invoke a genetic relationship between the two (Hoffman & Schrag, 2002 and refs within). Deposition of ironstones is reliant on elevated seawater anoxia in order to stabilise dissolved ferrous iron (Fe^{2+}) (Drever, 1974; Holland, 1973, 1984), and hence build up sufficient ions to precipitate an enriched deposit during oxidation. Early proponents of the Snowball Earth hypothesis argued in favour of anoxia beneath a globally widespread ice cover, followed by oxidation during ice meltback (Kirschvink, 1992; Klein & Beukes, 1993; Hoffman et al., 1998), leading to ironstone deposition at the close of

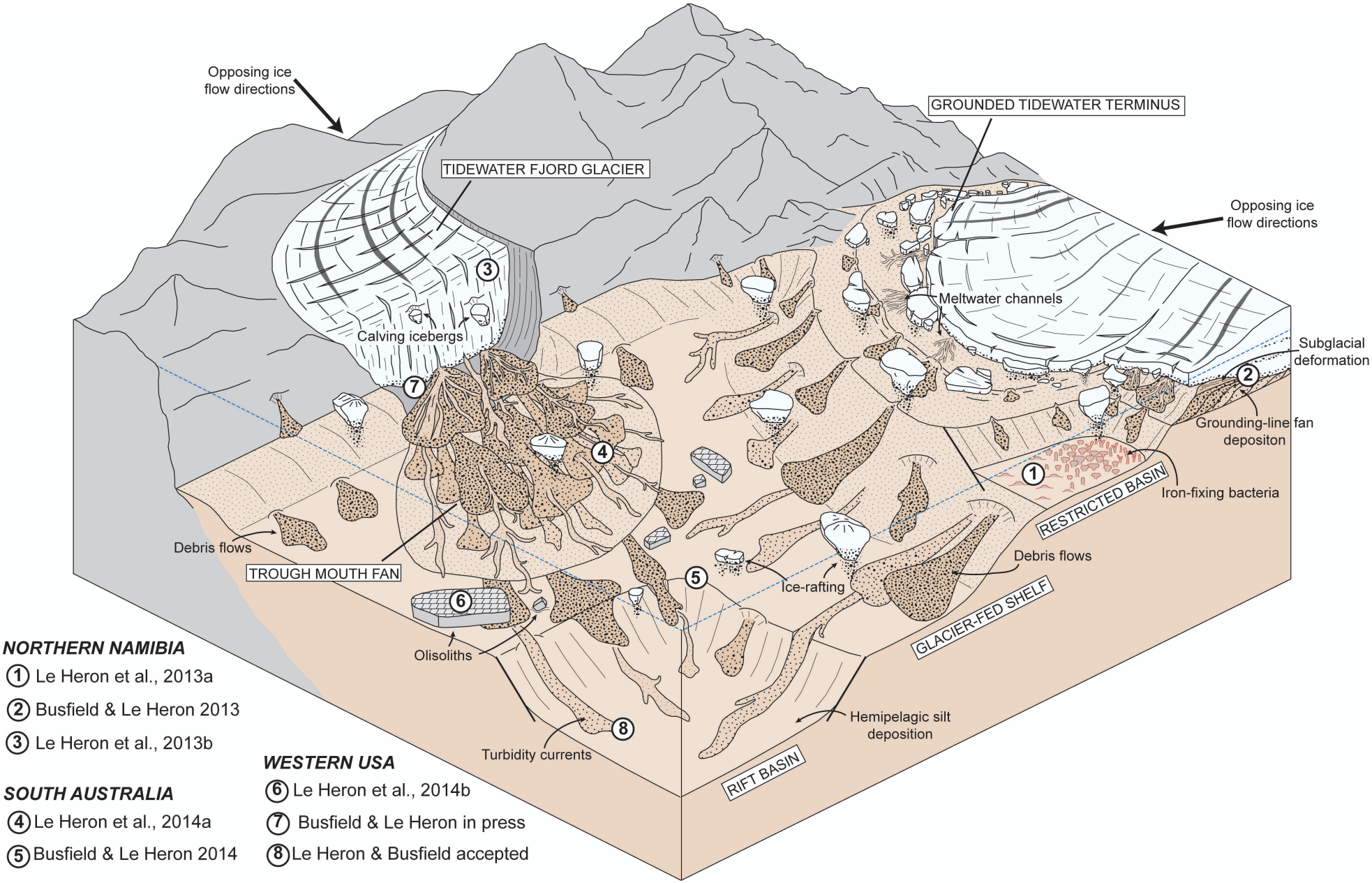

Fig. 6.1: Summary depositional model of glaciomarine sedimentary environments and processes recorded throughout the study areas (northern Namibia, South Australia and western USA). Overall, these settings are dominated by mass flow and ice-rafting processes, contributing to consistently high debris loads. These features, alongside evidence of meltwater re-working, warm-based subsole deformation and limited development of proglacial channel networks supports the presence of polythermal, grounded tidewater glaciers. Over-deepened basins may be suggestive of fjord to cross-shelf trough systems, see text for further discussion.

the glacial period. However, the stratigraphic position of ironstones both below and within Neoproterozoic glacial successions casts doubt on this model (e.g. Hoffman et al., 2011; Cox et al., 2013 and refs within), even when taking into account the preservational bias towards late glacial deposits in the geological record. Ironstone deposits are also notably more common in association with Sturtian glacial deposits (Kennedy et al., 1998), which has been used to suggest a purely rift-related origin for iron formations (Eyles & Januszczak, 2004).

6.2.1. Sedimentology and stratigraphy of iron formations

In the studied sections in northern Namibia and South Australia ironstones are exclusively associated with the base of the preserved glacial sequences, either immediately underlying them (e.g. Le Heron et al., 2013a) or closely interbedded with the basal succession (e.g. Busfield & Le Heron, 2014). In Namibia these occur as planar to cross-bedded ferruginous siltstones and sandstones colonised by microbial communities, which occur both underlying and interbedded with glacially-influenced diamictites (Le Heron et al., 2013a). Whilst in Australia, ferruginous facies comprise interbedded hemipelagic siltstones and turbiditic sandstones, bearing ice-rafted debris at the micro-scale (Busfield & Le Heron, 2014). Both studies provide strong support for the interaction of glaciers during ironstone deposition, consistent with several glacially-influenced Neoproterozoic ironstone successions globally (e.g. Yeo, 1981; Klein & Ladeira, 2004; Ilyin, 2009; Frimmel, 2011; Zhang et al., 2011). In light of the discussion above regarding sub ice-shelf sedimentation, the tentative earlier interpretation of Le Heron et al. (2013a) of deposition beneath an ice-shelf is rejected in favour of accumulation via proglacial sediment gravity flows, in line with comparable facies elsewhere in northern Namibia (Le Heron et al., 2013b), Australia (Busfield & Le Heron, 2014) and western USA (e.g. Le Heron et al., 2014b). Curiously, the absence of associated subglacial sediment or ice-grounding features, and close stratigraphic relationship with glaciogenic debris flow deposits (which would undergo flow transformation further from the ice front), suggests both studied iron formations are restricted to ice-proximal settings. This may simply reflect more prevalent erosion and re-working of ferruginous sediment within subglacial or ice-marginal settings, and similarly greater dilution and dissipation of ferric iron within more far-travelled sediments. Alternatively, the proximity of the ice front, and its influence on the supply of detrital material and oxygenated meltwaters (e.g. Urban et al., 1992; Halverson et al., 2011; Cox et al., 2013), may play a role in the accumulation of iron formations.

6.2.2. *Oxidative drivers*

Accumulation of ferrous iron in the water column requires anoxic conditions. Consequently a mechanism of oxidising Fe^{2+} is necessary to precipitate more stable Fe^{3+}(oxyhydr)oxides, and hence deposit ironstones. Various mechanisms have been proposed in the Neoproterozoic from ocean-wide oxidation during global ice meltback (Kirschvink, 1992), through subglacial oxygenated meltwater supply (Urban et al., 1992; Hoffman, 2005; Halverson et al., 2011) to expulsion of hydrothermal fluids into oxic basin waters (e.g. Volkert et al., 2010). In modern settings, biotic oxidative pathways are common, driven by both the aerobic and anaerobic behaviour of microbial communities (Cox et al., 2013). By analogy to modern Fe-oxidising bacteria, an additional oxidative pathway via anoxygenic photosynthesis is proposed for the Neoproterozoic, based upon the abundance of stromatolitic laminites in the Chuos Formation ironstone of northern Namibia (Le Heron et al., 2013a).

Iron-oxidising bacteria are a common feature of hydrothermal vent systems (e.g. Karl et al., 1988; Emerson & Moyer, 2002), mafic seafloor extrusions (e.g. Bach & Edwards, 2003) and acid mine drainage sites (e.g. Konhauser et al., 2011). In anoxic conditions, organisms can either scavenge available O_2 for aerobic oxidation (microaerophiles), or utilise anoxygenic photosynthesis to harbour sufficient photic energy to metabolise iron (Templeton, 2011; Konhauser et al., 2011). These photosynthetic organisms, in the absence of oxygen, utilise bicarbonate anions as terminal electron receptors for the iron cations (Fe^{2+}) (e.g. Widdel et al., 1993), in addition to requiring organic carbon to build biomass (Konhauser et al., 2002; Posth et al., 2014), and thus contribute to the drawdown of CO_2. This oxidative pathway is proposed in northern Namibia where microbial communities colonise siliciclastic bedforms, fixing ferrous iron within 'sticky' microbial mats between periods of bedform migration. Photosynthetic metabolism is an attractive pathway since it necessitates minimal ice cover, corroborated by the absence of direct glacial influence within the ironstones (Le Heron et al., 2013a), and offers an additional mechanism of CO_2 drawdown preceding glaciation, or at least re-advance of the ice mass in this region.

Similar mechanisms of microbial Fe^{2+} oxidation are also cited to account for thick accumulations of Archean-Palaeoproterozoic Banded Iron Formations (BIFs) (e.g. Cloud, 1965; Kappler et al., 2005; Planavsky et al., 2009; Bekker et al., 2010). This demonstrates its importance as an oxidative driver to promote ironstone deposition, but also highlights the fact that this process does not single-handedly account for the return of iron formations in the Neoproterozoic. The absence of microbial laminites in the studied iron formation in South Australia (Busfield & Le Heron, 2014), and elsewhere globally (e.g. Klein & Ladeira, 2004; Basta et al., 2011;

Halverson et al., 2011; Zhang et al., 2011), signifies its local as opposed to global role in iron-fixation, and by extension, any cooling associated with CO_2 drawdown would have had only local effect. This process is significant, however, in further discrediting models of ocean anoxia beneath a hard carapace of ice since this would have considerably restricted the amount of photic energy necessary to sustain a large microbial community in anoxic waters.

6.2.3. Models of ironstone deposition

The clear glacial influence on Neoproterozoic ironstones demonstrates that models invoking a purely rift-related origin are unsatisfactory. However, it is contended that rifting played a key role, both in terms of basin and slope configuration at the time of deposition (Le Heron et al., 2013a; Busfield & Le Heron, 2014), and as a potentially important source of ferrous iron. Several models predict hydrothermal iron input along basin-bounding faults (e.g. Breitkopf, 1988; Eyles & Januszczak, 2004; Volkert et al., 2010; Freitas et al., 2011), corroborated by major element (Fe, Si, Mn) and rare earth (Eu) element enrichment typical of hydrothermal fluids (Lottermoser & Ashley, 1999; ; Klein & Ladeira, 2004; Cox et al., 2013). The occurrence of many Neoproterozoic iron formations within rift-basins lends strong support to these models (e.g. Young, 1976; Hoffmann & Prave, 1996; Lottermoser & Ashley, 2000; Preiss, 2000), but if rifting was the sole driver the re-appearance of ironstones in the stratigraphic record should have occurred as much as 100 Ma earlier when extension began (Hoffman & Halverson, 2008; Preiss et al., 2011; Li et al., 2013; Evans, 2013).

Geochemical analyses of late Neoproterozoic marine sediment argue in favour of globally widespread anoxic and ferruginous subsurface waters from the late Neoproterozoic through to the mid-Ediacaran, i.e. the evolution of multicellular organisms (Canfield et al., 2007, 2008; Johnston et al., 2010; Hood & Wallace, 2014). These conditions are thought to be driven by increased input of dissolved iron, via hydrothermal sources, aided by reduced sulphate levels (Habicht et al., 2002; Kump & Seyfried, 2005; Johnston et al., 2010), possibly due to subduction of sedimentary sulphides (Canfield et al., 2008). Yet despite globally ferruginous oceans, iron formations are not ubiquitous at this time.

Thus far, at least one of two major events appears to be associated with all recorded Neoproterozoic iron formations: 1) glaciation and 2) mafic volcanism (Cox et al., 2013). In addition, all appear to be restricted to either rift-basins or restricted basins within Rodinia (Torsvik, 2003; Bekker et al., 2010; Li et al., 2013). An argument can be made, therefore, that background ocean chemistry sustaining anoxic and ferruginous conditions, in tandem with rift-related basin restriction and ferrous iron input generated environmentally

perturbed conditions. The onset of glaciation or eruption of basalts, or in places both, could have then tipped conditions in favour of ironstone deposition (Bekker et al., 2010; Cox et al., 2013). The significance of rift-basin configurations is that they enable local influences to exert additional control on iron precipitation e.g. photosynthetic microorganisms in northern Namibia (Le Heron et al., 2013a).

Therefore, many Neoproterozoic ironstones are glacially-influenced, but their deposition is dependent on several other external factors. The sedimentary evidence favouring ironstone deposition towards the base of preserved glacial successions (Busfield & Le Heron, 2014), biologically-mediated iron precipitation (Le Heron et al. 2013a), and dynamic, mobile ice masses (see below), alongside geochemical evidence supporting widespread anoxia prior to glaciation all contradict early models of late-glacial 'rusting of the seas' (Kirschvink, 1992).

6.3. What role did basin configuration play?

All three study areas occupy inter- and intracratonic rift-basins, developed during break-up of the supercontinent Rodinia. The timing of rifting in each region is subject to scrutiny, particularly the transition from rift to drift tectonism (e.g. Miller, 2008; Preiss et al., 2011; Yonkee et al., 2014). However, the configuration of rift basins will clearly have a strong influence on the deposition and especially preservation of Sturtian sequences. Within each study area, the effect of pre- to syn-depositional tectonic activity is highly variable, leading some authors to argue that it has a far greater control on depositional history than glaciation (Eyles & Januszczak, 2004). Studies within this thesis (Chapters 3-5), as well as others globally (e.g. Arnaud et al., 2011 and refs within) reinforce the view that the Sturtian sequences are subject to both a tectonic and glacial influence, and that the two signatures can be readily delineated.

6.3.1. Syn-depositional tectonic activity

Of the studied sequences, the Kingston Peak Formation preserves the most widespread evidence of an active tectonic regime during deposition (Le Heron et al., 2014b). Across the Death Valley region, significant thickness variations can be observed between studied sections, ranging from c. 200 m in the northern Kingston Range (Le Heron et al., 2014b) to >600 m at Sperry Wash (Busfield & Le Heron, in press). Some of these thickness variations are a product of differential preservation, where upper and basal contacts are commonly not recorded (e.g. Busfield & Le Heron, in press; Le Heron & Busfield, accepted), alongside the effects of truncation by an angular unconformity beneath the Noonday Dolomite (Prave, 1999; Petterson et al.,

2011). However, taking these effects into account, even the partially preserved record of unit KP3 at Sperry Wash is 100-400 m thicker than the cumulative thickness of successions of KP1, KP2 and KP3 in the northern Kingston Range (Le Heron et al., 2014b; Busfield & Le Heron, in press). Thus considerable changes in stratigraphic thickness are evident within (e.g. Le Heron et al., 2014b) and between neighbouring outcrop belts (Chapter 5). The presence of buried normal faults and MORB-type volcanism in the Kingston Range (Troxel, 1966; Hammond, 1983; Le Heron et al., 2014b), and equivalent strata in the Panamint Range (Lanphere et al., 1964; Labotka et al., 1980), provides strong support for syndepositional extensional tectonism (Miller, 1985; Prave, 1999). In places, these faults are sealed beneath the basal Noonday unconformity (Wright et al., 1976).

Perhaps the strongest evidence for a syn-depositional tectonic influence comes from the olistostrome succession within unit KP3 in the northern and southern Kingston Range (Le Heron et al., 2014b; Le Heron & Busfield, accepted). These up to km-scale blocks of carbonate bedrock have been attributed to unroofing of an elevated ridge north of the Kingston Range, and transportation as tabular slide blocks downslope (Macdonald et al., 2013). Their stratigraphic position within finely laminated shales subject to minor ice-rafting, both underlying and overlying coarse glacially-derived sediment gravity flows, suggests deposition during a period of ice meltback (Le Heron et al., 2014b). The retreat of ice from the elevated hinterland north of the Kingston Range is anticipated to have exposed the carbonate bedrock which supplied these olistoliths, and potentially contributed to the effects of tectonic break-up and remobilisation through isostatic rebound (Le Heron et al., 2014b). Similar processes of instability and downslope sliding have been triggered following Holocene glacier retreat and isostatic rebound in various Norwegian fjord systems (e.g. Lyså et al., 2008, 2010; Forwick & Vorren, 2012) The presence of granular conglomerate within the olistostrome succession, colloquially termed 'basement grit' (Mrofka & Kennedy, 2011; Macdonald et al., 2013), though not observed in the studied sections (Le Heron et al., 2014b; Le Heron & Busfield, accepted), has been used to argue in favour of a purely tectonic origin. However, preservation of ice-rafted debris between olistolith blocks demonstrates the persistence of a glacial influence, albeit reduced compared to the underlying KP2 and remaining KP3 successions (Le Heron et al., 2014b; Le Heron & Busfield, accepted). The olistostrome therefore supports strong evidence of a tectonic driver, mediated by glacial processes; it is considered improbable that preserved deposits would share facies characteristics of both processes if they operated completely independently.

In northern Namibia and South Australia, evidence of syn-depositional tectonic activity is largely restricted to locally enhanced thicknesses and changes in facies character recording transitions from shallow to deep basins. For example, the preservation of a thin succession of glaciotectonically deformed diamictite in

northern Namibia is interpreted to record ice-grounding on an elevated ridge or basement high (Busfield & Le Heron, 2013), particularly when compared to massive, undeformed debris flow deposits on the lower slope regions (Busfield & Le Heron, 2013; Le Heron et al., 2013a). Meanwhile, considerably thicker sediment accumulations at Omutirapo reflect preservation within an over-deepened basin, in this case a palaeovalley, the origin of which is attributed to the interaction of east-west trending growth faults and glacial incision (Le Heron et al., 2013b). In South Australia, similar trends can be observed where thinner, typically coarser successions are preserved on more proximal basement highs, whereas thicker and notably more heterogeneous facies are recorded in deeper and more distal basins (Busfield & Le Heron, 2014). This relationship has a significant control on the preservation of glacial cycles, discussed in more detail below, where the greater accommodation space afforded by deeper basins protects sediments from cannibalisation during later glacial advances, and thus records a more comprehensive glacial history (Busfield & Le Heron, 2014).

6.3.2. Glacially-modified basins

The evidence of interplay between glaciation and tectonic activity on depositional history also raises the question of their combined influence on basin configuration. The Omutirapo palaeovalley in northern Namibia is a classic example where both extensional faulting and glacial downcutting appear to have played a role in basin deepening (Le Heron et al., 2013b). A tunnel valley incision was tentatively proposed here, based upon comparable depth of incision and tunnel valley infill to sequences in the Late Ordovician record of Algeria (Lang et al., 2012). This is difficult to test at Omutirapo since the margins of the palaeovalley were not observed (Le Heron et al., 2013a), and therefore the characteristic abrupt beginning and termination of a tunnel valley cannot be recorded (e.g. van der Vegt, 2012). In addition, modes of glacial or post-glacial tunnel valley infill are highly variable (e.g. Ehlers & Linke, 1989; Huuse & Lykke-Andersen, 2000; Le Heron et al., 2004; Moreau & Huuse, 2014), and remain hotly debated (e.g. van der Vegt, 2012), making analogue predictions difficult to ascertain.

An alternative origin for the overdeepened basin at Omutirapo could be as a glacially-incised fjord to cross-shelf trough system (Le Heron et al., 2013b). The presence of E-W bounding growth faults (Hoffman & Halverson, 2008) may have topographically constrained ice flow, leading to enhanced glacial erosion of the rifted basin. Fjord systems are a common feature of polythermal and temperate glaciomarine systems in Alaska (e.g. Powell & Cooper, 2002), Greenland (e.g. Dowdeswell et al., 2014), Svalbard (e.g. Trusel et al., 2010) and Antarctica (e.g. Domack & Ishman, 1993). They are typically characterised by high sedimentation

rates, enabling preservation of high resolution sedimentary records (Lyså et al., 2008, 2010; Mugford & Dowdeswell, 2010). Sedimentation in these settings is dominated by meltwater-derived fines, glaciogenic debris flows and iceberg rafted debris, and commonly leads to build-up of ice-contact or grounding-line fan systems in their proximal regions (e.g. Powell & Cooper, 2002; Lyså et al., 2010; Mugford & Dowdeswell, 2010; Laberg et al., 2013; Dowdeswell et al., 2014). The preservation of numerous advance-retreat sequences, abundant evidence of iceberg rafting, jet-efflux deposits and ice-contact deformation features overlying a significant glacial erosion surface at Omutirapo (Le Heron et al., 2013b) is therefore consistent with glacier trough infill patterns.

A similar origin could be proposed for the Sperry Wash succession in the Death Valley region, western USA (Busfield & Le Heron, in press). This succession is also notably thicker than its counterparts in the northern and southern Kingston Range (Le Heron et al., 2014b; Le Heron & Busfield, accepted), and records a much more pronounced ice advance from ice-distal to ice-marginal depositional settings, as opposed to the exclusively ice-distal and ice-proximal environment of the Kingston Range. It is recognised that this may simply reflect either differential preservation beneath the sub-Noonday unconformity, or the more proximal position of Sperry Wash relative to the ice front (see Fig. 8, Le Heron & Busfield, accepted). However, under the latter scenario, the Sperry Wash succession might be anticipated to record consistently more proximal facies. Instead, a clear transition from ice-distal turbidites subject to ice-rafting, comparable to the more distal southern Kingston Range (Le Heron & Busfield, accepted), to an ice-contact grounding-line fan setting is recorded. These features are suggestive of either far greater accommodation to preserve the entire advance sequence, or a laterally-restricted basin forcing a more pronounced progradation signature (Busfield & Le Heron, in press). Both of these scenarios would be satisfied by deposition of the Sperry Wash succession in a deep, narrow glacial trough, delivering sediment to the unconfined shelf in the northern and southern Kingston Range (e.g. **Fig. 6.1**).

In South Australia, deposition of a trough-mouth fan in the northern Flinders Ranges (Le Heron et al., 2014a) is also consistent with accumulation at the unconfined shelf edge fed by a fjord or cross-shelf trough, comparable to the Uummannaq system in West Greenland (Ó Cofaigh et al., 2013b; Dowdewell et al., 2014). In this study area, the more proximal system feeding the Bolla Bollana trough-mouth fan is not recorded (Le Heron et al., 2014a). However, further south in the central Flinders Ranges, the highly irregular palaeotopography is attributed to the combined influence of rift activity and subglacial down-cutting (Busfield & Le Heron, 2014), corroborated by both local and basin-wide glacial erosion surfaces. This again contributes

to the deposition of a notably thicker succession at Holowilena Creek than elsewhere in the study region (Busfield & Le Heron 2014; Le Heron et al., 2014a).

The other important element of fjord or cross-shelf trough settings for the Sturtian sequences studied herein is the control on basin circulation. These settings are confined, and commonly protected from the wider ocean by a bedrock sill, often leading to restriction of iceberg distribution (e.g. Syvitski et al., 1996; Mugford & Dowdeswell, 2010; Howe et al., 2010). As such, sediments in these settings record a dominant influence from iceberg rafting, in line with the IRD-rich successions in northern Namibia (Le Heron et al., 2013b), South Australia (Busfield & Le Heron, 2014), and particularly western USA (Busfield & Le Heron, in press; Le Heron & Busfield, accepted). Restricted circulation is also a pre-requisite of ironstone deposition, and whilst rift-basin configuration is recognised to have a dominant control, the contribution of glacial modification to generating confined depositional basins should also be considered. This was beyond the scope of this study due to the limited vertical and especially lateral exposure of the studied ironstones, and thus their stratigraphic relationship to significant erosion surfaces or diagnostic sediment infill patterns associated with an over-deepened basin could not be explored.

6.4. How did Sturtian ice sheets behave?

The Neoproterozoic icehouse is widely cited as the most extreme glaciation recorded in Earth's history (see Fairchild & Kennedy, 2007 for review), yet evidence of 'extreme' palaeo-glaciological behaviour is not apparent in the sedimentary record. Close comparisons can be drawn between Neoproterozoic glacial successions and those deposited during later Phanerozoic icehouse periods (Etienne et al., 2007), casting doubt on the unique ice sheet behaviour thought to drive glaciation of low palaeolatitudes. The style of glaciation recorded during this interval requires rigorous testing in order to better characterise the Sturtian cryosphere, and thus generate models of Neoproterozoic glaciation which accord with the geological evidence. Arguments of globally widespread ice sheets and an inactive or diminished hydrological cycle (e.g. Hoffman et al., 1998) have proven difficult to substantiate with the geological record, as exemplified throughout this thesis (Chapters 3-5).

6.4.1. Ice mass mobility

Among the strongest evidence for mobile ice masses in the studied sections is the glaciotectonic deformation of sediments in northern Namibia (Busfield & Le Heron, 2013; Le Heron et al., 2013b) and western USA

(Busfield & Le Heron, in press), which had not previously been identified in either study area to the author's knowledge. In each of these sections, elevated porewater pressures beneath and in front of the ice promote ductile deformation, leading to folding, boudinage and high-strain shear of the sediment pile. These features act as excellent kinematic indicators for the direction of overriding ice flow, towards the north in the Otavi Mountainland (Busfield & Le Heron, 2013), to the south-west at Omutirapo (Le Heron et al., 2013b) and towards the south-east at Sperry Wash (Busfield & Le Heron, in press). This is particularly important in successions such as the Chuos Formation of northern Namibia where palaeocurrent indicators are few, and thus the source of glacially-derived debris is difficult to identify (Le Heron et al., 2013a, b; Busfield & Le Heron, 2013). Whilst in the Death Valley region, kinematic indicators mirror palaeoflow orientations towards the south-east, corroborating palaeocurrent data that indicate sediment delivery from an ice mass advancing from the north-west.

Evidence of ductile subglacial deformation under elevated porewater pressures provides strong support for temperate or polythermal glacier thermal regimes, since cold-based glaciers are characterised by minimal basal meltwater and periodically frozen bed bases (Hambrey & Glasser, 2012). Glacier and ice sheet movement commonly occurs through subsole deformation where they are warm-based (Evans et al., 2006; Hambrey & Glasser, 2012; Szuman et al., 2013), with elevated basal meltwater contributing to a weaker and more deformable substrate, and potentially velocity acceleration through sliding processes (e.g. Zwally et al., 2002). These deformation structures therefore provide evidence of not only mobile ice sheets, but also (at least ephemeral) warm-based polythermal to temperate basal conditions.

Further evidence of ice mass mobility comes in the form of the changing style and magnitude of glacial influence throughout successions. This is evident, to different degrees, in all studied sections within this thesis (Chapters 3-5). Analysis of sedimentary stacking patterns (i.e. grading/facies changes within and between bedsets), the nature of bed contacts and the presence or absence of glacial indicators enables periods of ice advance, retreat or stillstand to be identified. In the absence of reliable chronostratigraphic constraints, the significance of individual advance-retreat episodes beyond the local basin-scale cannot be inferred. However, it is hoped that the detailed sedimentological analysis conducted throughout these studies will permit regional and global correlation if and when more refined geochronology is available.

It is interesting to note that many of the studied sections preserve evidence of either one, or one more pronounced period of ice meltback (Le Heron et al., 2013b, 2014b; Busfield & Le Heron, 2014, in press). In South Australia, this retreat phase is associated with evidence of open water conditions, depositing hummocky

cross-stratified sandstone facies (Le Heron et al., 2011; Busfield & Le Heron, 2014), whereas in northern Namibia it records a marked hiatus in iceberg rafting and coarse sediment supply (Le Heron et al., 2013b). Ice meltback in the Death Valley region is inferred from the unusual accumulation of km-scale olistoliths, interpreted to have been plucked from the carbonate bedrock as it become exposed following retreat (Le Heron et al., 2014b). Across all three study areas, ice re-advance following these retreat phases is associated with a more pronounced progradation signature than underlying advance phase deposits (Le Heron et al., 2013b, 2014b; Busfield & Le Heron, 2014). This interval is associated with the build-out of a trough mouth fan in the northern Flinders Ranges (Le Heron et al., 2014a), and a striking progradation sequence at Sperry Wash (Busfield & Le Heron, in press), whilst evidence of ice-rafting processes in the distal southern Kingston Range sections demonstrate a dramatic increase (Le Heron & Busfield, accepted). These trends may reflect the greater preservation of presumably late-glacial advance sequences, with earlier advances subject to much more widespread erosion and re-working, or alternatively could be the product of a larger advance i.e. more extensive glacier or ice sheet growth. This is difficult to substantiate with the available dataset and therefore requires further testing.

With estimates of the duration of Sturtian glaciation currently at c. 55 Ma (Rooney et al., 2014), these meltback and re-advance phases could have easily occurred diachronously, and therefore no suggestion of global glacial-interglacial cycles is made here. What is clear, however, is that Sturtian ice masses in three globally discrete regions are subject to similarly dynamic accumulation and mass wasting processes.

6.4.2. Glacial sequence stratigraphy

In an attempt to try and characterise advance-retreat sequences, and aid in their correlation between sections, a glacial sequence stratigraphic scheme was developed in the central Flinders Ranges, South Australia (Busfield & Le Heron, 2014). The aim of the scheme was to define criteria which could be used to recognise advance and retreat trends, particularly where preserved successions are thin or incomplete. This was also viewed as potentially beneficial for integrating future geochronological and geochemical data with the sedimentological profile, as they become available.

In the central Flinders Ranges, four periods of glacial advance were recognised, separated by three intervals of ice meltback, attesting to much more dynamic mass balance changes than the advance-retreat-re-advance signature recorded at Holowilena Creek previously (Le Heron et al., 2011). Significantly, through correlation with neighbouring outcrop exposures, it could be demonstrated that the thicker, and more distal

Holowilena Creek preserved thick successions of alternating advance and retreat sequences, whereas the thinner, more proximal Oladdie Creek and Hillpara Creek sections were largely restricted to advance sequences separated by erosive sequence boundaries (Busfield & Le Heron, 2014). The sequence stratigraphic approach therefore produces a much higher resolution glacial history, and highlights the differential preservation of advance and especially retreat sequences on a local to regional scale, here interpreted as the product of available accommodation space between the deeper distal basin and the shallower proximal shelf (Busfield & Le Heron, 2014).

The disadvantage of the sequence stratigraphic scheme, as outlined in the Methods (Chapter 2), is that it is not yet sufficiently comprehensive to be used as a reliably reproducible technique. The example used in Chapter 2 was the appearance of ice-rafted debris as a glacial advance feature (sensu Powell & Cooper, 2002), although it could equally be a product of significant mass loss during glacial retreat (e.g. Benn et al., 2007). However, in the central Flinders Ranges, the re-appearance of IRD above deposits of open water conditions, within a coarsening upwards sequence and concomitant with IRD-bearing glaciogenic debris flows up-slope logically occurs within a glacial advance sequence (Busfield & Le Heron, 2014). Likewise, the preservation of hummocky cross-stratified sandstone typical of open water conditions, used to interpret glacial minimum systems tracts (GMiST, Busfield & Le Heron, 2014), is not a common feature of the studied glacially-related successions (Chapters 3-5), and therefore is arguably not a widely useful criterion. Individual 'diagnostic' features must be considered in the context of the host facies, and the succession as a whole, to understand their glacial sequence stratigraphic significance, whilst the most telling features in any one succession may not apply to another. Therefore, in order to develop robust glacial sequence stratigraphic schemes the model must be tested on several different successions, which accumulate under different glacier thermal regimes and within various basin configurations, including both proximity to the ice margin and tectonic setting. The proposed scheme in the central Flinders Ranges should therefore be viewed as a further test bed for models of Neoproterozoic glacial sequence stratigraphy, which requires expansion to become a reliable stratigraphic tool.

6.5. How extensive were Sturtian ice sheets?

One of the central tenets of the Snowball Earth hypothesis is the requirement of a global ice cover in order for glaciers to reach sub-tropical and equatorial palaeolatitudes, and thus an extremely restricted hydrological cycle (Kirschvink, 1992; Hoffman et al., 1998). The growing body of literature supporting mobile ice masses separated by regions of open water, and dynamic advance-retreat cyclicity, argues against this hypothesis (see

Chapters 3-5). However, mapping the lateral distribution of ice during this glacial period remains a problem. This is often hindered in pre-Pleistocene successions by a lack of robust palinspastic reconstructions. These successions commonly occur within tectonically dis-membered mountain belts (e.g. Miller, 2008; Preiss et al., 2011; Macdonald et al., 2013), and whilst preservation is often exceptional, and dip-corrected bedding and palaeoflow measurements are readily acquired, reliable accounts of any post-depositional offsets may be more limited. Nonetheless, cursory predictions of ice extent can be made utilising the distribution of sediments deposited within specific glacial depositional environments, and changing patterns of palaeoflow.

6.5.1. Recognition of the ice-grounding line

The abundance of meltwater derived facies and evidence of warm-based subsole deformation, discussed above, support deposition by temperate to polythermal glaciers and ice sheets. Under these thermal regimes, glacier termini will not develop floating ice shelves, and thus the 'grounding line' and 'calving line' converge at the tidewater terminus (Menzies, 2002). Therefore, recognition of the ice-grounding zone serves as a means of mapping the location of the ice front.

In northern Namibia and the Death Valley region, glaciotectonism is interpreted as the product of deformation beneath and in front of an oscillating ice-grounding line, respectively (Busfield & Le Heron, 2013, in press; Le Heron et al., 2013b). These structures compare closely with deformation features recorded within several Pleistocene subglacial and ice-marginal shear zones (e.g. van der Meer, 1993; Evans & Hiemstra, 2005; Evans et al., 2006; Phillips et al., 2007; Lee & Phillips, 2008; Ó Cofaigh et al., 2011; Evans et al., 2012). In glacial settings, deformation can also occur beneath the keels of periodically grounded icebergs, which would result in a markedly different palaeogeographical interpretation. Scouring beneath an iceberg produces a very similar suite of deformation structures, including sub-horizontal grain orientations and plasmic fabrics, folds, sheared intraclasts and water escape structures, making differentiation of iceberg scoured and subglacially deformed sediment difficult (e.g. Linch & van der Meer, 2014). However, it is recognised that turbate structures and kinking plasmic fabrics are scarce in deposits of interpreted iceberg scour origin (Linch et al., 2012; Linch & van der Meer, 2014), yet relatively abundant in the deformed strata studied herein (Busfield & Le Heron, 2013; Le Heron et al., 2013b). Meanwhile, evidence of multiple directions of shear might be more typical beneath an unconfined iceberg (Linch et al., 2012; Linch & van der Meer, 2014), in contrast to strong unidirectional fabrics within subglacially deformed sediments (e.g. Busfield & Le Heron, 2013; Le Heron et al., 2013b).

Within the studied sections, deformed sediments occur in association with deposits of subaqueous grounding-line fans (Busfield & Le Heron, 2013; Le Heron et al., 2013b), which in Sperry Wash represent the top of a strongly progradational sequence driven by ice advance (Busfield & Le Heron, in press). Therefore, the preservation of glaciotectonically-deformed sediments in northern Namibia and Death Valley are interpreted to record ice-grounding zone settings, and represent the maximum recorded extent of these ice masses during the studied interval. As such, the location of the ice front during the apparent maximum extent of these ice masses can be inferred.

6.5.2. Palaeo-ice flow indicators

Aside from pin-pointing the location of the ice front, the preserved deformation signatures in northern Namibia are also interesting for demonstrating two opposing ice flow directions. In the Otavi Mountainland, within the south-eastern region of the study area, kinematic indicators support ice overriding to the north/north-west (Busfield & Le Heron, 2013). By comparison, in the Omutirapo palaeovalley further north and west of the Otavi Mountainland, deformation signatures record a top to the south-west sense of shear (Le Heron et al., 2013b). In a similar manner, trough mouth fan deposits in the northern Flinders Ranges prograde to the south/south-west, evidenced in the deposition of proximal fan facies at Stubb's Waterhole and more distal fan facies at Weetootla Gorge (Le Heron et al., 2014a). Further south, in the central Flinders Ranges, palaeocurrent indicators record sediment delivery to the north/north-west, from the more proximal Hillpara Creek to more distal Holowilena Creek sections (Busfield & Le Heron, 2014). In both regions, the individual study sections are recognised to be deposited in separate sub-basins (Preiss, 2000; Hoffman & Halverson, 2008; Preiss et al., 2011), although the opposing palaeoflow orientations may also be used to argue in favour of separate ice masses. This is considered especially applicable in South Australia where ice-distal open water facies separate the more proximal glaciogenic debris flows delivered from the south-east and trough mouth fan deposits building out from the north (Busfield & Le Heron, 2014; Le Heron et al., 2014a).

In contrast, studied sections in the Death Valley region record remarkably consistent palaeoflow orientations to the south-east, supported by glaciotectonic folds verging in the same direction (Le Heron et al., 2014b; Busfield & Le Heron, in press; Le Heron & Busfield, accepted). The geographic distribution of studied sections in this region is significantly smaller than those in northern Namibia and South Australia (Chapters 3-4), which in tandem with the consistent palaeoflow orientations and proposed cross-shelf trough to open shelf trends, suggests deposition in the same basin, or connected sub-basins, fed by the same ice mass. Correlative strata in the Panamint Range, approximately 70 km west of the studied sections, record a glacier-

fed palaeoslope dipping to the north (Miller, 1985), and therefore opposing directions of ice flow are also plausible here. This hypothesis awaits testing.

6.6. Implications for models of Neoproterozoic glaciation

The Neoproterozoic icehouse continues to attract significant interest from both the geological and palaeoclimatological communities, but a concordant solution is yet to be reached. Evidence of marine-terminating ice sheets at low palaeolatitudes and the preservation of glacial deposits on almost every modern continent rationally led to models invoking globally widespread ice sheets, and more extreme glacial conditions than have been recorded on Earth since. The Snowball Earth hypothesis provided an excellent stimulus for further scientific research, which yields a complicated picture of palaeoclimate, palaeogeography and glaciation during this time period. Sedimentologically, the rationale behind the Snowball Earth hypothesis falters, since studies repeatedly demonstrate a much more dynamic, hydrologically active cryosphere than the model predicts. This thesis builds on pre-existing research following the early Snowball concepts, and adds detailed sedimentological analyses of exceptionally well-exposed but poorly understood Sturtian glacial sequences.

Glaciotectonic deformation structures have been identified for the first time to the author's knowledge in the Chuos Formation of northern Namibia (Busfield & Le Heron, 2013; Le Heron et al., 2013b) and the Kinsgton Peak Formation in the Death Valley region, western USA (Busfield & Le Heron, in press). These features are significant in recording a) the position of the ice front, b) mobile, warm-based Sturtian ice sheets, and c) readily differentiating tectonic, soft-sediment and subglacial deformation signatures. These structures clearly exemplify how the influence of tectonic activity and glacial activity can be picked apart, even within typically massive, genetically enigmatic diamictites (e.g. Eyles & Januszczak, 2004, 2007). Evidence of syn-glacial tectonic activity is widespread, and rift-basin architecture modifies both the deposition and preservation of Sturtian sediments, but the glacial influence on deposition is pervasive throughout all studied sections (Chapters 3-5). A strong tectonic control does not negate widespread, low-elevation glaciation, in contrast to the Zipper-Rift model (Eyles & Januszczak., 2004).

The glaciotectonic deformation features, alongside sedimentological evidence indicative of abundant meltwater input, widespread subaqueous sediment re-working, periodic open water conditions and multiple advance-retreat cycles throughout the preserved successions act to support dynamic, at least episodically warm-based temperate to polythermal glaciers or ice masses (Chapters 3-5), in contrast to the traditional

'hard' Snowball model (Hoffman et al., 1998). However, although evidenced in the geological record, regions of locally or seasonally ice-free ocean adjacent to marine-terminating equatorial glaciers remain a palaeoclimatological enigma. Often model experiments, and particularly those concerning Neoproterozoic climates, must make a series of assumptions with regards to boundary conditions. Important factors such as atmospheric CO_2 levels, palaeocontinental configuration, orography, surface albedo and cloud cover are still poorly understood (see reviews in Goddéris et al., 2011). Several model experiments begin with the view to modelling the 'Snowball Earth', assuming global ice cover, and especially sea ice cover, and the resultant effect this will have on planetary albedo (e.g. Micheels & Montenari, 2008; Tziperman et al., 2012; Abbot et al., 2013; Ashkenazy et al., 2013; Goodman & Strom, 2013). Of course these are complex simulations, which are difficult to ground-truth even within better understood climate conditions (e.g. Oglesby & Maasch, 2008; Crucifix, 2012), but the absence of representative reconstructions only serves to highlight the need for more detailed geological records. Without accurate boundary conditions, reliable models of descent into and escape from glaciation cannot be generated. On the basis of the geological evidence alone, the idea of a 'Slushball Earth' as a state of pan-global continental glaciation with regions of open water of as yet unknown extent seems reasonable. However, care should perhaps be taken to differentiate this idealised hypothesis from the model experiments which define a band of circum-equatorial open water separating hundreds of metre thick, globally widespread 'sea glaciers' (e.g. Warren et al., 2002; Goodman & Pierrehumbert, 2003; Abbot et al., 2013).

In terms of the glacial depositional record, the studies in this thesis agree with earlier comparisons drawn to Phanerozoic ice ages (e.g. Etienne et al., 2007). Aside from palaeomagnetic data which place marine-terminating glaciers at low palaeolatitudes, and the greater degree of lithification and local effects of metamorphism, the deposits themselves are strikingly similar to the Pleistocene record. Throughout this thesis, analogue sections have been drawn from numerous Pleistocene examples including the Bear Island Fan (e.g. Laberg & Vorren, 2000), offshore Newfoundland (e.g. Tripsansas & Piper, 2008), the British onshore (e.g. Lee & Phillips, 2008), Canada (e.g. Menzies & Zaniewski, 2003) and offshore Greenland (e.g. Ó Cofaigh et al., 2002, 2013b). The greater lateral distribution of Neoproterozoic glaciogenic sediments (Evans, 2000; Li et al., 2008), extremely thick deposits with a pervasive glacial influence (Chapters 3-5; Arnaud et al., 2011 and refs within), and arguments for the long duration of individual glaciations (e.g. Rooney et al., 2014) may support a more spatially and temporally extensive ice age than has been recorded on Earth since, but this in itself does not necessitate a global ice cover.

The evidence supporting mobile glaciers and ice sheets, regions of at least periodically open waters and glacier thermal regimes comparable to those established during later ice ages is overwhelming (e.g. Chapters 3-5; Condon et al., 2002; Leather et al., 2002; Allen et al., 2004; Corkeron, 2008; Etienne et al., 2011; Le Heron et al., 2011; Fleming, 2014). The results in this thesis which refute a Snowball Earth are not unique, and by no means the first studies to come to this conclusion, but they represent an important contribution to improving our understanding of how the Neoproterozoic cryosphere behaved. Through the application of detailed macro- and micro-scale sedimentology, new data have emerged which evidence more ice proximal conditions than had been previously recorded (e.g. Busfield & Le Heron, 2013; Busfield & Le Heron, in press), the first example to the author's knowledge of a trough mouth fan in the Neoproterozoic record (Le Heron et al., 2014a), the importance of combined tectonic and glaciological controls on both the preservation of glacial sequences (e.g. Le Heron et al., 2013b; Busfield & Le Heron, 2014) and the re-mobilisation of km-scale megaclasts (Le Heron et al., 2014b), the previously underappreciated role of biologically mediated iron-fixation (Le Heron et al., 2013a), and early inferences on topographically constrained ice masses feeding Sturtian tidewater termini (Busfield & Le Heron, in press; Le Heron & Busfield, accepted).

The true advantage of globally-widespread glaciogenic sediments is that they offer an extensive archive of glacier and ice mass behaviour during this interval; an archive which both requires and affords detailed sedimentological analysis. Through the recognition of ice-contact deposits, differentiation of ice-proximal to ice-distal regimes and the sequencing of advance-retreat phases this thesis aims to step closer to being able to 'map' Sturtian ice sheets. Identifying palaeo-ice flow indicators, the location of ice fronts and areas of ice minimum or open water conditions will aid in reconstructing the extent and distribution of these ice masses, leading to more reliable accounts of any 'pan-global' ice cover and potentially enable geologically reproducible palaeoclimate simulations. Moreover, as geochronological techniques continue to improve, the scope for understanding spatially and temporally constrained ice mass behaviour grows. Integrating these detailed sedimentological analyses worldwide, at both the macro- and micro-scale, is essential to underpinning these next steps in characterising the Cryogenian cryosphere.

6.7. Suggestions for future research

Studies within this thesis demonstrate the wealth of sedimentological data available in the Sturtian glacial depositional record, and its implications for understanding the extent, mobility and thermal characteristics of ice masses during this interval. Building on pre-existing research, this thesis highlights the dynamic behaviour

of Sturtian glaciers and ice sheets, and contributes to a growing body of research which casts doubt on concepts of a truly global ice-cover. In order to better resolve these issues, however, further study is needed.

The recognition of glaciotectonic deformation structures within the Sturtian successions of northern Namibia and western USA was integral in establishing the mobility of overriding ice sheets, and revealing multiple palaeo-ice flow directions. These studies were significantly aided by micromorphological analysis of deformed sequences: a technique which is widely used in Quaternary studies but still has minimal application in the ancient record. More micro-scale sedimentological and structural analyses would greatly benefit studies on Cryogenian sedimentary deposits, with wide ranging applications for determining depositional history, i.e. glacial or non-glacial, the availability of basal meltwater during ice-marginal or subglacial deformation, kinematic indicators for overriding ice flow and, of particular importance in the ancient record, differentiating syn-depositional and post-depositional (tectonic) deformation. Recent work has also demonstrated the value of applying Anisotropy of Magnetic Susceptibility to Neoproterozoic and younger glacial successions (Fleming, 2014), which would significantly enhance studies of macro- and micro-scale deformation.

Busfield and Le Heron (2014) developed a provisional glacial sequence stratigraphic scheme to analyse advance-retreat signatures of Sturtian ice masses in South Australia. The development of such schemes across other glacial depositional basins throughout the Neoproterozoic record would aid in establishing robust criteria for the recognition of advance, retreat and stillstand phases. With the advent of more refined geochrononology, these 'sequences' could offer the opportunity for regional and potentially even global correlation, and thus test the diachroneity of Cryogenian glaciation(s) worldwide. In order to become a reliable scheme, the technique requires testing in glaciated basins with variable configurations, i.e. rift basins, passive margins, foreland basins etc., under different glacial thermal regimes, and with changeable sedimentation rates. This would serve to test the reliability of 'diagnostic' features or trends across a broad spectrum of depositional settings.

The tentative proposition of a fjord to cross-shelf trough setting in the Death Valley region, and possibility of glacially over-deepened basins in Namibia and South Australia requires further testing. These configurations could aid in our understanding of the shape and extent of Sturtian ice masses, the nature of sedimentary basin infill and potentially play a role in ironstone deposition by generating restricted seaways. Further to constraining the distribution of glaciers and ice sheets, more comprehensive palaeocurrent datasets should be collected from Neoproterozoic glacial sequences, where possible. These data can aid in the

prediction of the location of the ice front (e.g. Le Heron & Busfield, in review), and in recognising palaeo-ice flow patterns.

6.8. Concluding remarks

- The studied Sturtian sequences in Namibia, Australia and western USA all represent the products of grounded, marine-terminating glaciers or ice sheets where mass flow remobilisation and iceberg rafting processes dominate the sedimentary infill patterns.
- The consistently high debris load, limited development of proglacial channel networks, evidence of widespread meltwater input and warm-based subglacial deformation support polythermal glacier thermal regimes.
- Clear progradational and retrogradational stacking patterns concomitant with increasing or decreasing glacial influence, respectively, evidence of open water conditions interrupting glacial sequences and the preservation of both subglacial and ice-marginal deformation driven by either advancing or overriding ice support mobile, dynamic ice masses subject to multiple episodes of advance and retreat, and argue against ideas of a globally frozen ocean.
- Glacial sequence stratigraphic schemes can prove a useful means of characterising these advance-retreat cycles, but require further development to become a widely applicable methodology.
- Variable and opposing ice flow directions in both the Namibian and Australian study sections may suggest separate glaciers or ice masses feeding the sedimentary basin(s).
- Ironstone deposits consistently occur at or towards the base of glacial successions, closely interbedded with glaciogenic deposits in places, and therefore do not represent post-glacial 'rusting of the seas'. In northern Namibia, prolific microbial communities are argued to drive the oxidation and precipitation of ferrous iron.
- The majority of studied sections record evidence of syn-depositional tectonic activity in the form of buried normal faults, along-strike thickness changes, olistolith remobilisation and irregular underlying palaeotopography. However, the pervasive glacial influence on deposition can be readily differentiated from the active tectonic regime throughout; these processes, and the evidence for these processes, are not mutually exclusive.
- Evidence favouring over-deepened basin infill and broader shelf successions may be indicative of fjord to cross-shelf trough systems, driving more pronounced ice advance signatures in the laterally-restricted

fjords (e.g. Omutirapo and Sperry Wash). This is also recognised as a potential contributor to the development of restricted basins, facilitating ironstone deposition, but awaits further testing.

- The preservation of subglacial and ice-marginal 'grounding zone' deformation structures is suggested as a useful tool in positioning the location of the ice front. Their recognition was significantly aided by micromorphological analytical techniques.
- The studied sections presented herein had either not been subject to recent re-examination (in light of our improved understanding of glacial sedimentary processes over the last few decades), or had been restricted to broad, stratigraphy based analysis. This thesis therefore presents new data which significantly improves the resolution of the sedimentary record, and offers a template for future geochronological and geochemical correlation.
- This thesis contributes to a growing body of sedimentological, geochemical, palaeoclimatological and modelling work which refutes early ideas of a 'hard' Snowball Earth. This work agrees with earlier comparisons drawn to Phanerozoic ice ages, and demonstrates that detailed sedimentological analysis provides an important insight into the extent, mobility and glaciological history of Cryogenian glaciers and ice sheets.

Bibliography

Aalto, K.R. 1981. The Late Precambrian Toby Formation of British Columbia, Idaho and Washington. In: Hambrey, M.J. & Harland, W.B. (eds.) *Earth's Pre-Pleistocene Glacial Record*. Cambridge University Press, Cambridge, 731-735.

Abbot, D.S., Voigt, A. & Koll, D. 2011. The Jormungand global climate state and its implications for Neoproterozoic glaciations. *Journal of Geophysical Research*, **116**, D18103.

Abbot, D.S., Voigt, A., Li, D., Le Hir, G., Pierrehumbert, R.T., Branson, M., Pollard, D. & Koll, D.B.D. 2013. Robust elements of a Snowball Earth atmospheric circulation and oases for life. Journal of Geophysical Research, **118**, 6017-6027.

Allaby, A. & Allaby, M. 2003. *Dictionary of Earth Sciences*. Oxford Paperback Reference, Oxford, 640 pp.

Allen, P.A. & Etienne, J.L. 2008. Sedimentary challenge to Snowball Earth. *Nature Geoscience*, **1**, 817-825.

Allen, P.A., Leather, J. & Brasier, M.D. 2004. The Neoproterozoic Fiq glaciation and its aftermath, Huqf Supergroup of Oman. *Basin Research*, **16**, 507-534.

Allen, P.A., Rieu, R., Etienne, J.L., Matter, A. & Cozzi, A. 2011. The Ayn Formation of the Mirbat Group, Dhofar, Oman. In: Arnaud, E., Halverson, G.P. & Shields-Zhou, G. (eds.) 2011. The Geological Record of Neoproterozoic Glaciations. *Geological Society of London Memoirs*, **36**, 239-249.

Allmendinger, R.W., Cardozo, N. & Fisher, D.M. 2012. *Structural Geology Algorithms: Vectors and Tensors*. Cambridge University Press, Cambridge, 302 pp.

Arnaud, E. 2008. Deformation in the Neoproterozoic Smalfjord Formation, northern Norway: an indicator of glacial depositional conditions? *Sedimentology*, **55**, 335-356.

Arnaud, E. 2012. The paleoclimatic significance of deformation structures in Neoproterozoic successions. *Sedimentary Geology*, **243**, 33-56.

Arnaud, E. & Fairchild, I.J. 2011. The Port Askaig Formation, Dalradian Supergroup, Scotland. Arnaud, E., Halverson, G.P. & Shields-Zhou, G. (eds.) 2011. The Geological Record of Neoproterozoic Glaciations. *Geological Society of London Memoirs*, **36**, 635-642.

Arnaud, E., Halverson, G.P. & Shields-Zhou, G. (eds.) 2011. The Geological Record of Neoproterozoic Glaciations. *Geological Society of London Memoirs*, **36**, 721 pp.

Ashkenazy, Y., Gildor, H., Losch, M., Macdonald, F., Schrag, D.P. & Tziperman, E. 2013. Dynamics of a Snowball Earth ocean. *Nature*, **495**, 90-95.

Ashley, G.M. 1995. Glaciolacustrine environments. In: Menzies, J. (ed.) *Modern Glacial Environments: Processes, Dynamics and Sediments*. Butterworth-Heinemann, Oxford, 417-444.

Bach, W & Edwards, K.J. 2003. Iron and sulfide oxidation within the basaltic ocean crust: implications for chemolithoautotrophic microbial biomass production. *Geochimica et Cosmochimica Acta*, **67**, 3871-3887.

Banerjee, I. 1966. Turbidites in a glacial sequence: a study from the Talchir Formation, Raniganj coalfield, India. *Journal of Geology*, **74**, 593-606.

Basta, F.F., Maurice, A.E., Fontbote, L. & Favarger, P.-Y. 2011. Petrology and geochemistry of the banded iron formation (BIF) of Wadi Karim and Um Anab, Eastern Desert, Egypt: implications for the origin of Neoproterozoic BIF. *Precambrian Research*, **187**, 277-292.

Bechstädt, T., Jager, H., Spence, G. & Werner, G. 2009. Late Cryogenian (Neoproterozoic) glacial and post-glacial successions at the southern margin of the Congo Craton, northern Namibia: facies, palaeogeography and hydrocarbon perspective. In: Craig, J., Thurow, J., Thusu, B., Whitham, A. & Abutarruma, Y. (eds.) *Global Neoproterozoic Petroleum Systems: The Emerging Potential in North Africa*. Geological Society, London, Special Publications, **326**, 255-287.

Beetz, W. 1929. Über das Wahrscheinlich altcambrische oder jungproterozoische Alter der Glazialschichten an der Basis des Kundelungu Systems in Katanga und am unteren Kongo. *Neues Jahrbuch für Mineralogie, Geologie und Paläontologie, Beilagebände, Abteiling B*, **61**, 61-82.

Bekker, A., Slack, J.F., Planavsky, N., Krapež, B., Hofmann, A., Konhauser, K.O. & Rouxel, O.J. 2010. Iron formation: the sedimentary product of a complex interplay among mantle, tectonic, oceanic and biospheric processes. *Economic Geology*, **105**, 467-508.

Benn, D.I. & Prave, A.R. 2006. Subglacial and proglacial glacitectonic deformation in the Neoproterozoic Port Askaifg Formation, Scotland. *Geomorphology*, **75**, 266-280.

Benn, D.I. & Evans, D.J.A. 2010. *Glaciers and Glaciation*. Hodder Education, London, 802 p.

Benn, D.I., Warren, C.R. & Mottram, R.H. 2007. Calving processes and the dynamics of calving glaciers. *Earth Science Reviews*, **82**, 143-179.

Bennett, M.R.. & Glasser, N.F. 2009. Glacial Geology. Ice Sheets and Landforms, 2nd ed. Wiley-Blackwell, 385 pp.

Bidgood, D.E.T. & Harland, W.B.1961. Palaeomagnetism in some East Greenland Sedimentary Rocks. *Nature*, **189**, 633-634.

Biju-Duval, B. & Gariel, O. 1969. Nouvelles observations sur les phénomènes glaciaires 'Éocambriens' de la bordure nord de la synéclise de Taoudeni, entre le Hank et la Tanezrouft, Sahara occidental. *Palaeogeography, Palaeoclimatology, Palaeoecology*, **6**, 283-315.

Bowring, S.A., Myrow, P., Landing, E., Ramezani, J. & Grotzinger, J.P. 2003. Geochronological constraints on terminal Neoproterozoic events and the rise of metazoans. European Geophysical Union Annual Meeting, Nice 2003. *Geophysical Research Abstracts*, **5**, p. 13219.

Breitkopf, J.H. 1988. Iron formations related to mafic volcanism and ensialic rifting in the southern margin of the Damara Orogen, Namibia. *Precambrian Research*, **38**, 111-130.

Brewer, R. 1976. *Fabric and Mineral Analysis of Soils*. Krieger, Huntington, 482 pp.

Briden, J.C. 1970. Palaeolatitude distribution of precipitated sediments. In: Runcorn, S.K. (ed.) *Palaeogeophysics*. Academic Press, London, 437-444.

Budyko, M.I. 1969. The effects of solar radiation variations on the climate of the Earth. *Tellus*, **XXI**, 611-619.

Busfield, M.E. & Le Heron, D.P. 2013. Glacitectonic deformation in the Chuos Formation of northern Namibia: implications for Neoproterozoic ice dynamics. *Proceedings of the Geologists' Association*, **124**, 778-789.

Busfield, M.E. & Le Heron, D.P. 2014. Sequencing the Sturtian icehouse: dynamic ice behaviour in South Australia. *Journal of the Geological Society*, **171**, 443-456.

Busfield, M.E. & Le Heron, D.P. in press. A Neoproterozoic ice advance sequence, Sperry Wash, California. *Sedimentology* Special Issue (2015-2016)

Cahen, L. & Lepersonne, J. 1981. Proterozoic diamictites of Lower Zaire. In: Hambrey, M.J. & Harland, W.B. (eds.) *Earth's Pre-Pleistocene Glacial Record*. Cambridge University Press, Cambridge, 153-161.

Cai, J., Powell, R.D., Cowan, E.A. & Carlson, P.R. 1997. Lithofacies and seismic reflection interpretations of temperate glacimarine sedimentation in Tarr Inlet, Glacier Bay, Alaska. *Marine Geology*, **145**, 5-37.

Caldeira, K. & Kasting, J.F. 1992. Susceptibility of the early Earth to irreversible glaciation caused by carbon dioxide clouds. *Nature*, **359**, 226-228.

Canfield, D.E., Poulton, S.W. & Narbonne, G.M. 2007. Late-Neoproterozoic deep-ocean oxygenation and the rise of animal life. *Science*, **315**, 92-95.

Canfield, D.E., Poulton, S.W., Knoll, A.H., Narbonne, G.M., Ross, G., Goldberg, T. & Strauss, H. 2008. Ferruginous conditions dominated later Neoproterozoic deep-water chemistry. *Science*, **321**, 949-952.

Carr, S.J., Holmes, R., van der Meer, J.J.M. & Rose, J. 2006. The Last Glacial Maximum in the North Sea Basin: micromorphological evidence of extensive glaciation. *Journal of Quaternary Science*, **21**, 131-153.

Carrivick, J.L. & Tweed, F.S. 2013. Proglacial lakes: character, behaviour and geological importance. *Quaternary Science Reviews*, **78**, 34-52.

Catuneanu, O. 2006. *Principles of Sequence Stratigraphy*. Elsevier, Oxford, 386 pp.

Chumakov, N.M. 1981. Upper Proterozoic glaciogenic rocks and their stratigraphic significance. *Precambrian Research*, **15**, 373-395.

Cloud, P.E. 1965. Significance of the Gunflint (Precambrian) microflora. *Science*, **148**, 27-35.

Coleman, A.P. 1916. Dry Land in Geology. *Geological Society of America Bulletin*, **27**, 175-192.

Coleman, A.P. 1926. *Ice Ages: Recent and Ancient*. MacMillan, New York, 705 pp.

Condon, D.J. & Bowring, S.A. 2011. A user's guide to Neoproterozoic geochronology. In: Arnaud, E., Halverson, G.P. & Shields-Zhou, G. (eds.) *The Geological Record of Neoproterozoic Glaciations*. Geological Society of London Memoirs, **36**, 135-149.

Condon, D.J., Prave, A.R. & Benn, D.I. 2002. Neoproterozoic glacial rain-outintervals: observations and implications. *Geology*, **20**, 35-38.

Cooper, B.J. 2010. 'Snowball Earth': the early contribution from South Australia. *Earth Sciences History*, **29**, 121-145.

Corkeron, M. 2008. Deposition and palaeogeography of a glacigenic Neoproterozoic succession in the east Kimberley, Australia. *Sedimentary Geology*, **204**, 61-82.

Cox, G.M., Halverson, G.P., Minarik, W.G., Le Heron, D.P., Macdonald, F.A., Bellefroid, E.J. & Strauss, J.V. 2013. Neoproterozoic iron formation: an evaluation of its temporal, environmental and tectonic significance. *Chemical Geology*, **362**, 232-249.

Crowell, J.C. 1957. Origin of pebbly mudstones. *Geological Society of America Bulletin*, **68**, 993-1010.

Crucifix, M. 2012. Traditional and novel approaches to palaeoclimate modelling. *Quaternary Science Reviews*, **57**, 1-16.

David, T.W.E. 1903. Note by T.W. Edgeworth David. *Report Australasian Association for the Advancement of Science*, **9**, 199-200.

David, T.W.E. 1932. Explanatory notes to accompany a new geological map of Australia: based on the maps already published by the geological surveys of the various states, etc. Australasian Medical Publishing Company.

Davies, K.A. 1940. The glacial series of Bunyoro, north Uganda. *17th International Geological Congress, Moscow, 1937*, **6**, 115-119.

Deynoux, M. & Trompette, R. 1981. Late Precambrian tillites of the Taoudeni Basin, West Africa. In: Hambrey, M.J. & Harland, W.B. (eds.) *Earth's Pre-Pleistocene Glacial Record*. Cambridge University Press, Cambridge, 123-131.

Domack, E.W. & Harris, P.T. 1998. A new depositional model for ice shelves, based upon sediment cores from the Ross Sea and the MacRobertson shelf, Antarctica. *Annals of Glaciology*, **27**, 281-284.

Domack, E.W. & Hoffman, P.F. 2011. An ice grounding-line wedge from the Ghaub glaciation (635 Ma) on the distal foreslope of the Otavi carbonate platform, Namibia, and its bearing on the snowball Earth hypothesis. *Geological Society of America Bulletin*, **123**, 1448-1477.

Domack, E.W. & Ishman, S. 1993. Oceanographic and physiographic controls on modern sedimentation within Antarctic fjords. *Geological Society of America Bulletin*, **105**, 1175-1189.

Domack, E.W., Jacobson, E.A., Shipp, S.S. and Anderson, J.B. 1999. Late Pleistocene-Holocene retreat of the West Antarctic Ice-Sheet system in the Ross Sea: Part 2 – sedimentologic and stratigraphic signature. *Geological Society of America Bulletin*, 111, 1517–1536.

Donnadieu, Y., Fluteau, F., Ramstein, G., Ritz, C. & Besse, J. 2003. Is there a conflict between the Neoproterozoic glacial deposits and the snowball Earth interpretation: an improved understanding with numerical modeling. *Earth and Planetary Science Letters*, **208**, 101-112.

Donnadieu, Y., Ramstein, G., Fluteau, F., Roche, D. & Ganopolski, A. 2004. The impact of atmospheric and oceanic heat transport on the sea ice-albedo instability during the Neoproterozoic. *Climate Dynamics*, **22**, 293-306.

Dow, D.B. 1965. Evidence of a Late Pre-Cambrian glaciation in the Kimberley Region of Western Australia. *Geological Magazine*, **102**, 407-419.

Dowdeswell, J.A. 1986. The distribution and character of sediments in a tidewater glacier, southern Baffin Island, N.W.T., Canada. *Arctic and Alpine Research*, **18**, 45-56.

Dowdeswell, J.A. & Ó Cofaigh, C. (eds.) 2002. *Glacier-Influenced Sedimentation on High-Latitude Continental Margins*. Geological Society, London, Special Publications, **203**, 378 pp.

Dowdeswell, J.A., Kenyon, N.H., Elverhøi, A., Laberg, J.S., Hollender, F.-J., Mienert, J. & Siegert, M.J. 1996. Large-scale sedimentation on the glacier-influenced Polar North Atlantic margins: long-range side-scan sonar evidence. *Geophysical Research Letters*, **23**, 3535-3538.

Dowdeswell, J.A., Hogan, K.A., O'Cofaigh, C., Fugelli, E.M.G., Evans, J. & Noormets, R. 2014. Late Quaternary ice flow in a West Greenland fjord and cross-shelf trough system: submarine landforms from Rink Isbrae to Uummannaq shelf and slope. *Quaternary Science Reviews*, **92**, 292-309.

Dreimanis, A. 1989. Tills: their genetic terminology and classification. In: Goldthwait, R.P. & Matsch, C.L. (eds.) *Genetic Classification of Glacigenic Deposits*. Balkema, Rotterdam, 17-84.

Drever, J.L. 1974. Geochemical model for the origin of Precambrian banded iron formations. Geological Society of America Bulletin, 85, 1099-1106.

Duller, R., Mountney, N.P., Russel, A.J. & Cassidy, N.C. 2008. Architectural analysis of a volcaniclastic jökulhlaup deposit, southern Iceland: sedimentary evidence for supercritical flow. *Sedimentology*, **55**, 939-964.

Dunn, P.R., Thomson, B.P. & Rankama, K. 1971. Late Pre-Cambrian glaciation in Australia as a stratigraphic boundary. *Nature*, **231**, 498-502.

Ehlers, J. & Linke, G. 1989. The origin of deep buried channels of Elsterian age in northwest Germany. *Journal of Quaternary Science*, **4**, 255-265.

Eisbacher, G.H. 1981. Late Precambrian tillites of the northern Yukon-Northwest Territories region, Canada. In: Hambrey, M.J. & Harland, W.B. (eds.) *Earth's Pre-Pleistocene Glacial Record*. Cambridge University Press, Cambridge, 724-727.

Elverhøi, A., de Blasio, F.V., Butt, F.A., Issler, D., Harbitz, C., Engvik, L., Solheim, A. & Marr, J. 2002. Submarine mass-wasting on glacially-influenced continental slopes: processes and dynamics. In: Dowdeswell, J.A. & O'Cofaigh, C.O. (eds.) *Glacier-Influenced Sedimentation on High-Latitude Continental Margins*. Geological Society, London, Special Publication, **203**, 73-87.

Embleton, B.J.J. & Williams, G.E. 1986. Low palaeolatitude of deposition for late Precambrian periglacial varvites in South Australia: implications for palaeoclimatology. *Earth and Planetary Science Letters*, **79**, 419-430.

Emerson, D. & Moyer, C.L. 2002. Neutrophilic Fe-oxidizing bacteria are abundant at the Loihi Seamount hydrothermal vents and play a major role in Fe oxide deposition. *Applied and Environmental Microbiology*, **68**, 3085-3093.

Emery, D. & Myers, K. (eds.). 2009. *Sequence Stratigraphy*. Wiley, Chichester, 304 pp.

Eriksson, E. 1968. Air-ocean-icecap interactions in relation to climatic fluctuations and glaciation cycles. *Meteorological Monographs*, **8**, 68-92.

Etienne, J.L., Jansson, K.N., Glasser, N.F., Hambrey, M.J., Davies, J.R., Waters, R.A., Maltman, A.J. & Wilby, P.R. 2006. Palaeoenvironmental interpretation of an ice-contact glacial lake succession: an example from the late Devensian of southwest Wales, UK. *Quaternary Science Reviews*, **25**, 739-762.

Etienne, J.L., Allen, P.A., Rieu, R. & Le Guerroué, E. 2007. Neoproterozoic glaciated basins: a critical review of the Snowball Earth hypothesis by comparison with Phanerozoic glaciations. In: Hambrey, M.J., Christoffersen, P., Glasser, N.F. & Hubbard, B. (eds.) *Glacial Sedimentary Processes and Products*. Blackwell Publishing Ltd., Oxford, p. 343-399.

Etienne, J.L., Allen, P.A., Le Guerroué, Heaman, L., Ghosh, S.K. & Islam, R. 2011. The Blaini Formation of the lesser Himalaya, NW India. In: Arnaud, E., Halverson, G.P. & Shields-Zhou, G. (eds.) *The Geological Record of Neoproterozoic Glaciations*. Geological Society of London Memoirs, **36**, 347-355.

Evans, D.A.D. 2000. Stratigraphic, geochronological, and palaeomagentic constraints upon the Neoproterozoic climatic paradox. *American Journal of Science*, **300**, 347-433.

Evans, D.A.D. 2013. Reconstructing pre-Pangean supercontinents. *Geological Society of America Bulletin*, **125**, 1735-1751.

Evans, D.A.D. & Raub, T.D. 2011. Neoproterozoic glacial palaeolatitudes: a global update. In: Arnaud, E., Halverson, G.P. & Shields-Zhou, G. (eds.) *The Geological Record of Neoproterozoic Glaciations*. Geological Society of London Memoirs, **36**, 93-112.

Evans, D.J.A. & Benn, D.I. 2004. *A Practical Guide to the Study of Glacial Sediments*. Arnold, London, 266 pp.

Evans, D.J.A. & Hiemstra, J.F. 2005. Till deposition by glacier submarginal, incremental thickening. *Earth Surface Processes and Landforms*, **30**, 1633–1662.

Evans, D.J.A., Phillips, E.R., Hiemstra, J.F. & Auton, C.A. 2006. Subglacial till: formation, sedimentary characteristics and classification. *Earth Science Reviews*, **78**, 115-176.

Evans, D.J.A., Hiemstra, J.F. & Ó'Cofaigh, C. 2012. Stratigraphic architecture and sedimentology of a Late Pleistocene subaqueous moraine complex, southwest Ireland. *Journal of Quaternary Science*, **27**, 51–63.

Evans, J. & Pudsey, C.J. 2002. Sedimentation associated with Antarctic Peninsula ice shelves: implications for palaeoenvironmental reconstructions of glacimarine sediments. *Journal of the Geological Society*, **159**, 233-237.

Eyles, N. 1993. Earth's glacial record and its tectonic setting. *Earth Science Reviews*, **35**, 1-248.

Eyles, N. & Januszczak, N. 2004. 'Zipper-rift': a tectonic model for Neoproterozoic glaciations during the breakup of Rodinia after 750 Ma. *Earth Science Reviews*, **65**, 1-73.

Eyles, N. & Januszczak, N. 2007. Syntectonic subaqueous mass flows of the Neoproterozoic Otavi Group, Namibia: where is the evidence of global glaciation? *Basin Research*, **19**, 179-198.

Eyles, N., Eyles, C.H. & Miall, A.D. 1983. Lithofacies types and vertical profile models: an alternative approach to the description and environmental interpretation of glacial diamict and diamictite sequences. *Sedimentology*, **30**, 393-410.

Fairchild, I.J. & Spiro, B. 1987. Petrological and isotopic implications of some contrasting Late Precambrian carbonates, NE Spitsbergen. *Sedimentology*, **34**, 973-989.

Fairchild, I. J. & Kennedy, M.J. 2007. Neoproterozoic glaciation in the Earth System. *Journal of the Geological Society, London*, **164**, 895-921.

Fairchild, I.J., Hambrey, M.J., Spiro, B. & Jefferson, T.H. 1989. Late Proterozoic glacial carbonates in northeast Spitsbergen: new insights into the carbonate-tillite association. *Geological Magazine*, **126**, 469-490.

Fleming, E.J. 2014. *Magnetic, structural and sedimentological analysis of glacial sediments: insights from modern, Quaternary and Neoproterozoic environments.* PhD thesis, University of Birmingham, 330 pp.

Flint, R.F., Sanders, J.E., Rodgers, J., 1960. Diamictite: a substitute term for symmictite. *Geological Society of America Bulletin,* **71**, 1809–1810.

Freitas, B.T., Warren, L.V., Boggiani, P.C., De Almeida, R.P. & Piacentini, T. 2011. Tectono-sedimentary evolution of the Neoproterozoic BIF-bearing Jacadigo Group, SW-Brazil. *Sedimentary Geology*, **238**, 48-70.

Forwick, M. & Vorren, T.O. 2012. Submarine mass wasting in Isfjorden, Spitsbergen. In: Yamada, Y., Kawamura, K., Ikehara, K., Ogawa, Y., Urgeles, R., Mosher, D., Chaytor, J. & Strasser, M. (eds.) *Submarine Mass Movement and Their Consequences.* Advances in Natural and Technological Hazards Research, **31**, 711-722.

Frimmel, H.E. 2011. The Kaigas and Numees formations, Port Nolloth Group in South Africa and Namibia. In: Arnaud, E., Halverson, G.P. & Shields-Zhou, G. (eds.) *The Geological Record of Neoproterozoic Glaciations.* Geological Society of London Memoirs, **36**, 223-232.

Garwood, E.J. & Gregory, J.W. 1898. Contribution to the glacial geology of Spitsbergen. *Quarterly Journal of the Geological Society, London*, **54**, 197-225.

Gevers, T.W. 1931. An ancient tillite in South-West Africa. *Transactions of the Geological Society of South Africa*, **34**, 1-17.

Gevers, T.W. & Beetz, W. 1940. Pre-Dwyka glacial periods in southern Africa. *17th International Geological Congress, Moscow, 1937*, **6**, 65-98.

Girdler, R.W. 1964. The palaeomagnetic latitudes of possible ancient glaciations. In: Nairn, A.E.M. (ed.) *Problems in Palaeoclimatology*. Interscience, London, 119-149.

Goddéris, Y., Le Hir, G. & Donnadieu, Y. 2011. Modelling the Snowball Earth. In: Arnaud, E., Halverson, G.P. & Shields-Zhou, G. (eds.) *The Geological Record of Neoproterozoic Glaciations*. Geological Society of London Memoirs, **36**, 151-161.

Goodman, J.C. 2006. Through thick and thin: marine and meteoric ice in a 'Snowball Earth' climate. *Geophysical Research Letters*, **33**, L16701.

Goodman, J.C. & Pierrehumbert, R.T. 2003. Glacial floating marine ice in 'Snowball Earth'. *Journal of Geophysical Research*, **108**, 3308.

Goodman, J.C. & Strom, D.C. 2013. Feedbacks in a coupled ice-atmosphere-dust model of the glacial Neoproterozoic 'Mudball Earth'. *Journal of Geophysical Research: Atmospheres*, **118**, 11,546-11,557.

Guimarães, J.T., Misi, A., Pedreira, A.J. & Dominguez, J.M.L. 2011. The Bebedouro Formation, Una Group, Bahia (Brazil). In: Arnaud, E., Halverson, G.P. & Shields-Zhou, G. (eds.) 2011. The Geological Record of Neoproterozoic Glaciations. *Geological Society of London Memoirs*, **36**, 503-508.

Habicht, K.S., Gade, M., Thamdrup, B., Berg, P. & Canfield, D.E. 2002. Calibration of sulphate levels in the Archean ocean. *Science*, **298**, 2372-2374.

Halverson, G.P., Poitrasson, F., Hoffman, P.F., Nédélec, A., Montel, J.-M. & Kirby, J. 2011. Fe isotope and trace element geochemistry of the Neoproterozoic syn-glacial Rapitan iron formation. *Earth and Planetary Science Letters*, **309**, 100-112.

Hambrey, M.J. 1994. *Glacial Environments*. UCL Press, London, 296 pp.

Hambrey, M.J. & Glasser, N.F. 2003. Glacial Sediments: Processes, Environments and Facies. In: Middleton, G.V. 2003. *Encyclopedia of Sediments and Sedimentary Rocks*. Kluwer Acdemic Publishers, Dordrecht, Netherlands, 316-331.

Hambrey, M.J. & Glasser, N.F. 2012. Discriminating glacier thermal and dynamic regimes in the sedimentary record. *Sedimentary Geology*, **251-252**, 1-33.

Hambrey, M.J. & Harland, W.B. 1981. *Earth's Pre-Pleistocene Glacial Record*. Cambridge University Press, Cambridge, 1004 pp.

Hambrey, M.J. & Harland, W.B. 1985. The Late Proterozoic glacial era. *Palaeogeography, Palaeoclimatology, Palaeoecology*, **51**, 255-272.

Hambrey, M.J., Harland, W.B. & Waddams, P. 1981. Late Precambrian tillites of Svalbard. In: Hambrey, M.J. & Harland, W.B. (eds.) *Earth's Pre-Pleistocene Glacial Record*. Cambridge University Press, Cambridge, 592-601.

Hambrey, M.J., Christoffersen, P., Glasser, N.F. & Hubbard, B. (eds.). 2007. *Glacial Sedimentary Processes and Products*. Blackwell Publishing Ltd., Oxford, 436 pp.

Hammond, J.G. 1983. *Late Precambrian diabase intrusions in the southern Death Valley region, California: their petrology, geochemistry and tectonic implications*. PhD thesis, University of Southern California, Los Angeles, 281p.

Harland, W.B. 1964a. Evidence of late Precambrian glaciation and its significance. In: Nairn, A.E.M. (ed.) *Problems in Palaeoclimatology*. Interscience, London, 119-149.

Harland, W.B. 1964b. Critical evidence for a great infra-Cambrian glaciation. *Geologische Rundschau*, **54**, 45-61.

Harland, W.B. & Bidgood, E.T. 1959. Palaeomagnetism in some Norwegian Sparagmites and the Late Pre-Cambrian ice age. *Nature*, **184**, 1860-1862.

Harland, W.B. & Wilson, C.B. 1956. The Hecla Hoek Succession in Ny Friesland, Spitsbergen. *Geological Magazine*, **93**, 2265-2286.

Harland, W.B., Herod, K.N. & Krinsley, D.H. 1966. The definition and identification of tills and tillites. *Earth Science Reviews*, **2**, 225-256.

Hazzard, J.C. 1939. Possibility of a pre-Cambric glaciation in southeastern California. *Pan-American Geologist*, **71**, 47–48.

Hedberg, R.M. 1979. *Stratigraphy of the Ovamboland Basin, South West Africa Bulletin*. Precambrian Research Unit, Cape Town, 325 pp.

Hemer, M.A. & Harris, P.T. 2003. Sediment core from beneath the Amery Ice Shelf, East Antarctica, suggests mid-Holocene ice-shelf retreat. *Geology*, **31**, 127-130.

Henry, G., Stanistreet, I.G., Maiden, K.J., 1986. Preliminary results of a sedimentological study of the Chuos Formation in the central zone of the Damara Orogen: evidence for mass flow processes and glacial activity. *Communications of the Geological Survey of South-West Africa/Namibia,* **2**, 75–92.

Hiemstra, J.F. & Rijsdijk, K.F. 2003. Observing artificially induced strain: implications for subglacial deformation. *Journal of Quaternary Science*, **18**, 373–383.

Hintze, F.F. 1913. A contribution to the geology of the Wasatch Mountains, Utah. *Annals of the New York Academy of Sciences*, **23**, 85-143.

Hoffman, P.F. 2005. 28th DeBeers Alex Du Toit Memorial lecture: on Cryogenian (Neoproterozoic) ice-sheet dynamics and the limitations of the glacial sedimentary record. *South African Journal of Geology*, **108**, 557-576.

Hoffman, P.F. 2009. Pan-glacial – a third state in the climate system. *Geology Today*, **25**, 100-107.

Hoffman, P.F. 2011. A history of Neoproterozoic glacial geology, 1871-1997. In: Arnaud, E., Halverson, G.P. & Shields-Zhou, G. (eds.) *The Geological Record of Neoproterozoic Glaciations*. Geological Society of London Memoirs, **36**, 17-37.

Hoffman, P.F. & Halverson, G.P. 2008. Otavi Group of the western Northern Platform, the Eastern Kaoko Zone and the western Northern Margin Zone. In: Miller, R. McG. (ed.) *The Geology of Namibia. Volume 2: Neoproterozoic to Lower Palaeozoic*. Ministry of Mines and Energy, Windhoek, 13-69-13-135.

Hoffman, P.F. & Li, Z-X. 2009. A palaeogeographic context for Neoproterozoic glaciation. *Palaeogeography, Palaeoclimatology, Palaeoecology*, **277**, 158-172.

Hoffman, P.F. & Schrag, D.P. 2002. The Snowball Earth hypothesis: testing the limits of global change. *Terra Nova*, **14**, 129-155.

Hoffman, P.F., Halverson, G.P., 2008. Otavi Group of the western Northern Platform, southern Damara Belt, SWA/Namibia. In: Miller, R.McG. (ed.) *The Geology of Namibia. Volume 2: Neoproterozoic to Lower Palaeozoic*. Ministry of Mines and Energy, Windhoek, pp. 13.69–13.136.

Hoffman, P.F. & Halverson, G.P. 2011. Neoproterozoic glacial record in the Mackenzie Mountains, northern Canadian Cordillera. In: Arnaud, E., Halverson, G.P. & Shields-Zhou, G. (eds.) 2011. The Geological Record of Neoproterozoic Glaciations. *Geological Society of London Memoirs*, **36**, 397-412.

Hoffman, P.F., Kaufman, A.J., Halverson, G.P. & Schrag, D.P. 1998. A Neoproterozoic Snowball Earth. *Science*, **281**, 1342-1346.

Hoffman, P.F., Macdonald, F.A. & Halverson, G.P. 2011. Chemical sediments associated with Neoproterozoic glaciation: iron formation, cap carbonate, barite and phosphorite. In: Arnaud, E., Halverson, G.P. & Shields-Zhou, G. (eds.) *The Geological Record of Neoproterozoic Glaciations*. Geological Society of London Memoirs, **36**, 67-80.

Hoffmann, K.-H. & Prave, A.R. 1996. A preliminary note on a revised subdivision and regional correlation of the Otavi Group based on glaciogenic diamictites and associated cap dolostones. *Communications of the Geological Survey of Namibia*, **11**, 77-82.

Holland, H.D. 1973. The oceans: a possible source of iron in iron-formations. *Economic Geology*, **68**, 1169-1172.

Holland, H.D. 1984. *The Chemical Evolution of the Atmosphere and Oceans*. Princeton University Press, New York, 582p.

Holland, T.H. 1908. On the occurrence of striated boulders in the Blaini Formation of Simla, with a discussion of the geological age of the beds. *Records of the Geological Survey of India*, **37**, 129-135.

Hood, A.V.S. & Wallace, M.W. 2014. Marine cements reveal the structure of an anoxic, ferruginous Neoproterozoic ocean. *Journal of the Geological Society, London*, **171**, 741-744.

Howchin, W. 1901. Preliminary note on the existence of glacial beds of Cambrian age in South Australia. *Transactions of the Royal Society of South Australia*, **21**, 74-86.

Howchin, W. 1903. Report on South Australian Glacial Investigation Committee. *Report of the Australasian Association for the Advancement of Science*, **9**, 194-200.

Howchin, W. 1920. Past glacial action in Australia. *Official Yearbook Australian Census and Statistics Bureau*, **13**, 1133-1146.

Howe, J.A., Austin, W.E.N., Forwick, M., Paetzel, M., Harland, R. & Cage, A.G. 2010. Fjord systems and archives: a review. In: Howe, J.A., Austin, W.E.N., Forwick, M. & Paetzel, M. (eds.) *Fjord Systems and Archives*. Geological Society of London Special Publication, **344**, 5-15.

Hubbard, B. & Glasser, N.F. 2005. Field Techniques in Glaciology and Glacial Geomorphology. Wiley, Chichester, 412 pp.

Hubert, J.F. 1966. Modification of the model for internal structures in graded beds to include a dune division. *Nature*, **211**, 614-615.

Huuse, M. & Lykke-Andersen, H. 2000. Overdeepened Quaternary valleys in the eastern Danish North Sea: morphology and origin. *Quaternary Science Reviews*, **19**, 1233-1253.

Hyde, W.T., Crowley, T.J., Baum, S.K. & Peltier, W.R. 2000. Neoproterozoic 'snowball Earth' simulations with a coupled climate/ice sheet model. *Nature*, **405**, 425-429.

Ilyin, A. 2009. Neoproterozoic banded iron formations. *Lithology and Mineral Resources*, **44**, 78-86.

Jack, R.L. 1913. The Mount Grainger goldfield. *Report of the Geological Survey of South Australia*, **2**, 1-24.

James, H.L. 1954, Sedimentary facies of iron-formation. *Economic Geology*, **49**, 235–293.

Johnsen, T.F. & Brennand, T.A. 2004. Late glacial lakes in the Thompson basin, British Columbia: palaeogeography and evolution. *Canadian Journal of Earth Sciences*, **41**, 1367-1383.

Johnsen, T.F. & Brennand, T.A. 2006. The environment in and around ice-dammed lakes in the moderately high relief setting of the southern Canadian Cordillera. *Boreas*, **35**, 106-125.

Johnston, D.T., Poulton, S.W., Dehler, C., Porter, S., Husson, J., Canfield, D.E. & Knoll, A.H. 2010. An emerging picture of Neoproterozoic ocean chemistry: insights from the Chuar Group, Grand Canyon, USA. *Earth and Planetary Science Letters*, **290**, 64-73.

Kappler, A., Pasquero, C., Konhauser, K.O., Newman, D.K. 2005. Deposition of banded iron formations by anoxygenic phototrophic Fe(II)-oxidizing bacteria. *Geology*, **33**, 865-868.

Karl, D.M., McMurty, G.M., Malahoff, A. & Garcia, M.O. 1988. Loihi Seamount, Hawaii: a mid plate volcano with a distinctive hydrothermal system. *Nature*, **335**, 532-535.

Katz, H.R. 1961. Late Precambrian to Cambrian stratigraphy in East Greenland. In: Raasch, G.O. (ed.) *Geology of the Arctic*, Vol. 1. University of Toronto Press, Toronto, 299-328.

Kirschvink, J.L. 1992. Late Proterozoic low-latitude glaciation. In: Schopf, J.W. (ed.) *The Proterozoic Biosphere*. Cambridge University Press, Cambridge, 51-52.

Kennedy, M.J. 1996. Stratigraphy, sedimentology, and isotopic geochemistry of Australian Neoproterozoic cap dolostones: deglaciation, $\delta^{13}C$ excursions, and carbonate precipitation. *Journal of Sedimentary Research*, **66**, 1050-1064.

Kennedy, M.J., Runnegar, B., Prave, A.R., Hoffmann, K.-H. & Arthur, M.A. 1998. Two or four Neoproterozoic glaciations? *Geology*, **26**, 1059-1063.

Kilburn, C., Pitcher, W.S. & Shackleton, R.M. 1965. The stratigraphy and origin of the Portaskaig Boulder Bed series (Dalradian). *Geological Journal*, **4**, 343-360.

Klein, C. 2005. Some Precambrian banded iron-formations (BIFs) from around the world: their age, geologic setting, mineralogy, metamorphism, geochemistry and origin. *American Mineralogist*, **90**, 1473-1499.

Klein, C. & Beukes, N.J. 1993. Sedimentology and geochemistry of the glaciogenic late Proterozoic Rapitan iron-formation in Canada. *Economic Geology*, **84**, 1733-1774.

Klein, C. & Ladeira, E.A. 2004. Geochemistry and mineralogy of Neoproterozoic banded-iron formations and some selected, siliceous manganese formations from the Urucum District, Mato Grosso Do Sul, Brazil. *Economic Geology*, **99**, 1233-1244.

Konhauser, K.O., Hamade, T., Raiswell, R., Morris, R.C., Ferris, F.G., Southam, G. & Canfield, D.E. 2002. Could bacteria have formed the Precambrian banded iron formations? *Geology*, **30**, 1079-1082.

Konhauser, K.O., Kappler, A. & Roden, E.E. 2011. Iron in microbial metabolisms. *Elements*, **7**, 89-93.

Knoll, A.H., Hayes, J.M., Kaufman, A.J., Swett, K. & Lambert, I.B. 1986. Secular variation in carbon isotope ratios from Upper Proterozoic successions of Svalbard and East Greenland. *Nature*, **321**, 832-838.

Knoll, A.H., Bambach, R.K., Canfield, D.E. & Grotzinger, J.P. 1996. Comparative Earth history and Late Permian mass extinction. *Science*, **273**, 452-457.

Kuenen, P.H. & Migliorini, C.I. 1950. Turbidity currents as a cause of graded bedding. *Journal of Geology*, **58**, 91-127.

Kulling, O. 1934. 'The Hecla Hoek Formation' round Hinlopenstredet. *Geografiska Annaler*, **16**, 161-253.

Kump, L.R. & Seyfried Jr, W.E. 2005. Hydrothermal Fe fluxes during the Precambrian: effect of low oceanic sulphate concentrations and low hydrostatic pressure on the composition of black smokers. *Earth and Planetary Science Letters*, **235**, 654-662.

Laberg, J.S. & Vorren, T.O. 2000. Flow behaviour of the submarine glacigenic debris flows on the Bear Island Trough Mouth Fan, western Barents Sea. *Sedimentology*, **47**, 1105-1117.

Laberg, J.S., Forwick, M., Husum, K. & Nielsen, T. 2013. A re-evaluation of the Pleistocene behaviour of the Scoresby Sund sector of the Greenland Ice Sheet. *Geology*, **12**, 1231-1234.

Labotka, T.C., Albee, A.L., Lanphere, M.A. & McDowell, S.C. 1980. Stratigraphy, structure and metamorphism in the central Panamint Mountains (Telescope Peak quadrangle), Death Valley area, California. *Geological Society of America Bulletin*, **91**, 843-933.

Lachniet, M.S., Strasser, J.C., Lawson, D.E., Evenson, E.B., Alley, R.D. 1999. Microstructures of glacigenic sediment-flow deposits, Matanuska Glacier, Alaska. In: Mickelson, D.M., Attig, J.W. (eds.) *Glacial Processes Past and Present*. Geological Society of America Special Paper 337, Boulder, Colorado, 45–57.

Lachniet, M.S., Larson, G.J., Lawson, D.E., Evenson, E.B. & Alley, R.B. 2001. Microstructures of sediment flow deposits and subglacial sediments: a comparison. *Boreas*, **30**, 254-264.

Lang, J., Dixon, R.J., Le Heron, D.P. & Winsemann, J. 2012. Depositional architecture and sequence stratigraphic correlation of Upper Ordovician glaciogenic deposits, Illizi Basin, Algeria. In: Huuse, M., Redfern, J., Le Heron, D.P., Dixon, R.J., Moscariello, A. & Craig, J. (eds.) *Glaciogenic Reservoirs and Hydrocarbon Systems*. Geological Society of London Special Publication, **368**, 293-317.

Lanphere, M.A., Wasserburg, G.J.F., Albee, A.L. & Tilton, G.R. 1964. Redistribution of strontium and rubidium isotopes during metamorphism, World Beater complex, Panamint Range, California. In: Craig, H. et al. (eds.) *Isotopic and cosmic chemistry*. North Holland Publishing, Amsterdam, 269-320.

Laskar, J., Joutel, F. & Boudin, F. 1993. Orbital, precessional, and insolation quantities for the Earth from -20Myr to +10Myr. *Astronomy and Astrophysics*, **270**, 522-533.

Lawson, D.E. 1981. *Sedimentological Characteristics and Classification of Depositional Processes and Deposits in the Glacial Environment*. Cold Regions Research and Engineering Laboratory, Report 81-27, Hanover, NH.

Le Heron, D.P. & Busfield, M.E. accepted. Re-advancing ice sheets in the aftermath of a Sturtian glacial minimum: perspectives from Death Valley, California. *Sedimentology* Special Issue (2015-2016)

Le Heron, D.P., Busfield, M.E., Le Ber, E., Kamona, A.F. 2013a. Neoproterozoic ironstones in northern Namibia: Biogenic precipitation and Cryogenian glaciation. *Palaeogeography, Palaeoclimatology, Palaeoecology*, **369**, 48-57.

Le Heron, D.P., Busfield, M.E., Kamona, A.F. 2013b. An interglacial on snowball Earth? Dynamic ice behaviour revealed in the Chuos Formation, Namibia. *Sedimentology*, **60**, 411-427.

Le Heron, D.P., Busfield, M.E., Collins, A.S. 2014a. Bolla Bollana boulder beds: A Neoproterozoic trough mouth fan in South Australia. Sedimentology, **61**, 978-995.

Le Heron, D.P., Busfield, M.E., Prave, A.R. 2014b. Neoproterozoic ice sheets and olistoliths: multiple glacial cycles in the Kingston Peak Formation, California. *Journal of the Geological Society*, 171, 525-538.

Le Heron, D.P., Sutcliffe, O., Bourgig, K., Craig, J., Visentin, C. & Whittington, R. 2004. Sedimentary architecture of Upper Ordovician tunnel valleys, Gargaf Arch, Libya: implications for the genesis of a hydrocarbon reservoir. *Geo Arabia*, **9**, 137-160.

Le Heron, D.P., Cox, G.M., Trundley, A. & Collins, A.S. 2011. Sea-ice free conditions during the Sturtian glaciation (early Cryogenian), South Australia. *Geology*, **39**, 31-34.

Le Roex, H.D. 1941. A tillite in the Otavi Mountains, S.W.A. *Transactions of the Geological Society of South Africa*, **44**, 207-218.

Lea, J.M. & Palmer, A. 2014. Quantification of turbate microstructures through a subglacial till: dimensions and characteristics. *Boreas*, **43**, 869-881.

Leather, J., Allen, P.A., Brasier, M.D. & Cozzi, A. 2002. Neoproterozoic snowball Earth under scrutiny: evidence from the Fiq glaciation of Oman. *Geology*, **30**, 891-894.

Lee, J.R. & Phillips, E.R., 2008. Progressive soft sediment deformation within a subglacial shear zone—a hybrid mosaic–pervasive deformation model for Middle Pleistocene glaciotectonised sediments from eastern England. *Quaternary Science Reviews*, **27**, 1350-1362.

Lee, J.S. & Lee, Y.Y. 1940. Sinian glaciation of China. *17th International Geological Congress, Moscow, 1937*, **6**, 33-41.

Leighton, I.D., Hiemstra, J.F. & Weidemann, C.T. 2013. Recognition of micro-scale deformation structures in glacial sediments – pattern perception, observer bias and the influence of experience. *Boreas*, **42**, 463-469.

Levrard, B. & Laskar, J. 2003. Climate friction and the Earth's obliquity. *Geophysical Journal International*, **154**, 970-990.

Lewis, J.P., Weaver, A.J. & Eby, M. 2007. Snowball versus slushball Earth: dynamic versus nondynamic sea ice? *Journal of Geophysical Research*, **112**, C11014.

Li, D. & Pierrehumbert, R.D. 2011. Sea glacier flow and dust transport on snowball Earth. *Geophysical Research Letters*, **38**, L17501.

Li, Z.-X., Bogdanova, S.V., Collins, A.S., Davidson, A., De Waele, B., Ernst, R.E., Fitzsimons, I.C.W., Fuck, R.A., Gladkochub, D.P., Jacobs, J., Karlstrom, K.E., Lu, S., Natapov, L.M., Pease, V., Pisarevsky, S.A., Thrane, K. & Vernikovsky, V. 2008. Assembly, configuration, and break-up history of Rodinia: a synthesis. *Precambrian Research*, **160**, 179-210.

Li, Z.-X., Evans, D.A.D. & Halverson, G.P. 2013. Neoproterozoic glaciations in a revised global palaeogeography from the breakup of Rodinia to the assembly of Gondwanaland. *Sedimentary Geology*, **294**, 219-232.

Linch, L.D., van der Meer, J.J.M. & Menzies, J. 2012. Micromorphology of iceberg scour in clays: Glacial Lake Agassiz, Manitoba, Canada. *Quaternary Science Reviews*, **55**, 125-144.

Linch, L.D. & van der Meer, J.J.M. 2014. Micromorphology of ice keel scour in pebbly sandy mud and fine-grained sand: Scarborough Bluffs, Ontario, Canada. Sedimentology, doi: 10.1111/sed.12142.

Link, P.K. & Christie-Blick, N. 2011. Neoproterozoic strata of southeastern Idaho and Utah: record of Cryogenian rifting and glaciation. In: Arnaud, E., Halverson, G.P. & Shields-Zhou, G. (eds.) 2011. The Geological Record of Neoproterozoic Glaciations. *Geological Society of London Memoirs*, **36**, 425-436.

Livingstone, S.J., Ó'Cofaigh, C. & Evans, D.J.A. 2010. A major ice drainage pathway of the last British-Irish Ice Sheet: the Tyne Gap, northern England. *Journal of Quaternary Science*, **25**, 354–370.

Lønne, I. & Nemec, W. 2011a. Modes of sediment delivery to the grounding-line of a fast-flowing tidewater glacier: implications for ice-margin conditions and glacier dynamics. In: Martini, I.P., French, H.M. & Pérez-Alberti, A. (eds.) *Ice-marginal and periglacial processes and sediments*. Geological Society, London, Special Publications, **354**, 33-56.

Lønne, I. & Nemec, W. 2011b. The kinematics of ancient tidewater ice margins: criteria for recognition from grounding-line moraines. In: Martini, I.P., French, H.M. & Pérez-Alberti, A. (eds.) *Ice-marginal and periglacial processes and sediments*. Geological Society, London, Special Publications, **354**, 57-75.

Lottermoser, B.G. & Ashley, P.M. 1999. Geochemistry, petrology and origin of Neoproterozoic ironstones in the eastern part of the Adelaide geosyncline, South Australia. *Precambrian Research*, **101**, 49-67.

Lottermoser, B.G. & Ashley, P.M. 2000. Geochemistry, petrology and origin of Neoproterozoic ironstones in the eastern part of the Adelaide Geosyncline, South Australia. *Precambrian Research*, **101**, 49–67.

Lund, K., Aleinikoff, J.N. & Evans, K.V. 2011. The Edwardsburg Formation and related rocks, Windermere Supergroup, central Idaho, USA. In: Arnaud, E., Halverson, G.P. & Shields-Zhou, G. (eds.) 2011. The Geological Record of Neoproterozoic Glaciations. *Geological Society of London Memoirs*, **36**, 437-448.

Lysså, A., Hansen, L., Christrensen, O., L'Heureux, J.-S., Longva, O., Olsen, H.A. & Sveian, H. 2008. Landscape evolution and slide processes in a glacioisostatic rebound area: a combined marine and terrestrial approach. *Marine Geology*, **248**, 53-73.

Lysså, A., Hjelstuen, B.O. & Larsen, E. 2010. Fjord infill in a high-relief area: rapid deposition influenced by deglaciation dynamics, glacio-isostatic rebound and gravitational activity. *Boreas*, **39**, 39-55.

Macdonald, F.A., Schmitz, M.D., Crowley, J.L., Roots, C.F., Jones, D.S., Maloof, A.C., Strauss, J.V., Cohen, P.A., Johnston, D.T. & Schrag, D.P. 2010. Calibrating the Cryogenian. *Science*, **327**, 1241-1243.

Macdonald, F.A., Prave, A.R., Petterson, R., Smith, E.F., Pruss, S.B., Oates, K., Waechter, F., Trotzuk, D. & Fallick, A.E. 2013. The Laurentian record of Neoproterozoic glaciation, tectonsim and eukaryotic evolution in Death Valley, California. *Geological Society of America Bulletin*, **125**, 652-664.

Manabe, S. & Broccoli, A.J. 1985. The influence of continental ice sheets on the climate of an ice age. *Journal of Geophysical Research*, **90**, 2167-2190.

Martin, H. 1965. The Precambrian Geology of South West Africa and Namaqualand. *Precambrian Research Unit Bulletin*, **1**, University of Cape Town, South Africa.

Martin, H., Porada, H., Walliser, O.H., 1985. Mixtite deposits of the Damara Sequence, Namibia, problems of interpretation. *Palaeogeography, Palaeoclimatology, Palaeoecology*, **51**, 159–196.

Master, S. & Wendorff, M. 2011. Neoproterozoic glaciogenic diamictites of the Katanga Supergroup, Central Africa. In: Arnaud, E., Halverson, G.P. & Shields-Zhou, G. (eds.) 2011. The Geological Record of Neoproterozoic Glaciations. *Geological Society of London Memoirs*, **36**, 173-184.

Mawson, D. 1941. Middle Proterozoic sediments in the neighbourhood of Copley. *Transactions of the Royal Society of South Australia*, **65**, 304-311.

Mawson, D. 1949. The Elatina glaciation: a third recurrence of glaciation evidenced in the Adelaide system. *Transactions of the Royal Society of South Australia*, **73**, 117-121.

McCabe, C. & Elmore, R.D. 1989. The occurrence and origin of late Paleozoic remagnetization in the sedimentary rocks of North America. *Reviews of Geophysics*, **27**, 471-494.

McCarroll, D. & Rijsdijk, K.F. 2003. Deformation styles as a key for interpreting glacial depositional environments. *Journal of Quaternary Science*, **18**, 473-489.

McKay, C. 2000. Thickness of tropical ice and photosynthesis on a snowball Earth. *Geophysical Research Letters*, **27**, 2153-2156.

Menzies, J. 2000a. Micromorphological analyses of microfabrics and microstructures indicative of deformation processes in glacial sediments. In: Maltman, A.J., Hubbard, B. & Hambrey, M.J. (eds.) *Deformation of Glacial Materials*. Geological Society, London, Special Publications, **176**, 245-257.

Menzies, J. 2000b. Microstructures in diamictites of the lower Gowganda Formation (Huronian), near Elliot Lake, Ontario: evidence for deforming-bed conditions at the grounding line? *Journal of Sedimentary Research*, **70**, 210-216.

Menzies, J. (ed.) 2002. *Modern and Past Glacial Environments*. Butterworth-Heinemann, Oxford, 543 pp.

Menzies, J. & Zaniewski, K. 2003. Microstructures within a modern debris flow deposit derived from Quaternary glacial diamicton – a comparative micromorphological study. *Sedimentary Geology*, **157**, 31-48.

Menzies, J., van der Meer, J.J.M. & Rose, J. Till – as a glacial 'tectomict', its internal architecture, and the development of a 'typing' method for till differentiation. *Geomorphology*, **75**, 172-200.

Micheels, A. & Montenari, M. 2008. A snowball Earth versus a slushball Earth: results from Neoproterozoic climate modelling sensitivity experiments. *Geosphere*, **4**, 401-410.

Middleton, G.V. 2003. *Encyclopedia of Sediments and Sedimentary Rocks*. Kluwer Acdemic Publishers, Dordrecht, Netherlands, 821 pp.

Miller, J.M.G. 1985. Glacial and syntectonic sedimentation: the Upper Proterozoic Kingston Peak Formation, southern Panamint Range, eastern California. *Geological Society of America Bulletin*, **96**, 1537-1553.

Miller, R.McG., 1983. Tectonic implications of the contrasting geochemistry of Damaran mafic volcanic rocks, South West Africa/Namibia. In: Miller, R.McG. (ed.) *Geodynamic Evolution of the Damara Orogen*. Geological Society of South Africa Special Publication **11**, Johannesburg, 115–138.

Miller, R. McG. (ed.) 2008. *The Geology of Namibia. Volume 2: Neoproterozoic to Lower Palaeozoic*. Ministry of Mines and Energy, Windhoek.

Moncrieff, A.C.M. 1989. Classification of poorly sorted sediments. *Sedimentary Geology*, **65**, 191-194.

Moraes Rego, L.F. DE. 1930. Glaciação eopaleozóica no centro do Brazil (Glaciation in the earliest Palaeozoic of central Brazil). *Anais Academia Brasileira de Ciências*, **2**, 109-112.

Moreau, J. & Huuse, M. 2014. Infill of tunnel valleys associated with landward-flowing ice sheets: the missing Middle Pleistocene record of the NW European rivers? *Geochemistry, Geophysics, Geosystems*, **15**, 1-9.

Mrofka, D. & Kennedy, M. 2011. The Kingston Peak Formation in the eastern Death Valley region. In: Arnaud, E., Halverson, G.P. & Shields-Zhou, G. (eds.) *The Geological Record of Neoproterozoic Glaciations*. Geological Society of London Memoirs, **36**, 449-458.

Mugford, R.I. & Dowdeswell, J.A. 2010. Modeling iceberg-rafted sedimentation in high-latitude fjord environments. *Journal of Geophysical Research*, **115**, F03024.

Narloch, W., Piotrowski, J.A., Wysota, W., Larsen, N.K. & Menzies, J. 2012. The signature of strain magnitude in tills associated with the Vistula Ice Stream of the Scandinavian Ice Sheet, central Poland. *Quaternary Science Reviews*, **57**, 105-120.

Néron de Surgy, O. & Laskar, J. 1997. On the long term evolution of the spin of the Earth. *Astronomy and Astrophysics*, **318**, 975-989.

Nichols, G. 2009. *Sedimentology and Stratigraphy* (2nd ed.). Wiley-Blackwell, Chichester, 419 pp.

Nikolaev, J. 1930. The glacial deposits (tillites) of Lower Cambrian age in the Yenissei Range. *Bulletin of the Geological and Prospecting Service of the U.S.S.R.*, **49**, 1-15.

Norin, E. 1937. Geology of the western Quruq Tagh, eastern Tien Shan. *Reports of the Sino-Swedish Expedition III. Geology*. Bokförlags Aktiebolaget Thule, Stockholm.

Ó Cofaigh, C. & Dowdeswell, J.A. 2001. Laminated sediments in glacimarine environments: diagnostic criteria for their interpretation. Quaternary Science Reviews, 20, 1411-1436.

Ó Cofaigh, C., Taylor, J., Dowdeswell, J.A., Rosell-Melé, A., Kenyon, N.H., Evans, J. & Mienert, J. 2002. Sediment reworking on high-latitude continental margins and its implications for palaeoceanographic studies: insights from the Norwegian-Greenland Sea. In: Dowdeswell, J.A. & Ó'Cofaigh, C. (eds.) *Glacier-Influenced Sedimentation on High-Latitude Continental Margins*. Geological Society, London, Special Publication, **203**, 325-348.

Ó Cofaigh, C., Taylor, J., Dowdeswell, J.A. & Pudsey, C.J. 2003. Palaeo-ice streams, trough mouth fans and high-latitude continental slope sedimentation. *Boreas*, **32**, 37-55.

Ó Cofaigh, C., Evans, D.J.A., Hiemstra, J.F., 2011. Formation of a stratified subglacial 'till' assemblage by ice-marginal thrusting and glacier overriding. *Boreas*, **40**, 1-14.

Ó Cofaigh, C., Dowdeswell, J.A., Jennings, A.E., Hogan, K.A., Kilfeather, A.A., Hiemstra, J.F., Noormets, R., Evans, J., McCarthy, D.J., Andrews, J.T., Lloyd, J.M. & Moros, M. 2013a. An extensive and dynamic ice sheet on the West Greenland shelf during the last glacial cycle. *Geology*, **41**, 219-222.

Ó Cofaigh, C., Andrews, J.T., Jennings, A.E., Dowdeswell, J.A., Hogan, K.A., Kilfeather, A.A. & Sheldon, C. 2013b. Glacimarine lithofacies, provenance and depositional processes on a West Greenland trough-mouth fan. *Journal of Quaternary Science*, **28**, 13-26.

Oglesby, R.J. & Maasch, K.A. 2009. Paleoclimate Modeling, Quaternary. In: Gornitz, V. (ed.) *Encyclopedia of Paleoclimatology and Ancient Environments*, pp 709-716.

Pais, M.A., Le Mouel, J.L., Lambeck, K. & Poirier, J.P. 1999. Late Precambrian paradoxical glaciation and obliquity of the Earth – a discussion of dynamical constraints. *Earth and Planetary Science Letters*, **174**, 155-171.

Palmer, A.P., Lee, J.A., Kemp, R.A. & Carr, S.J. 2008. *Revised laboratory procedures for the preparation of thin sections from unconsolidated material.* Unpublished Internal Report, Royal Holloway, University of London.

Pederson, S.A.S. 2012. Glaciodynamic sequence stratigraphy. In: Huuse, M., Redfern, J., Le Heron, D.P., Dixon, R.J., Moscariello, A. & Craig, J. (eds.) *Glaciogenic Reservoirs and Hydrocarbon Systems.* Geological Society, London, Special Publications, **368**, 29-51.

Perkins, A.J. & Brennand, T.A. *in press.* Refining the pattern and style of Cordilleran Ice Sheet retreat: palaeogeography, evolution and implications of lateglacial ice-dammed lake systems on the southern Fraser Plateau, British Columbia, Canada. *Boreas*, doi: 10.1111/bor.12100.

Perry, W.J. & Roberts, H.G. 1968. Late Precambrian glaciated pavements in the Kimberley region, Western Australia. *Journal of the Geological Society of Australia*, **15**, 51-56.

Petterson, R., Prave, A.R., Wernicke, B.P. & Fallick, A.E. 2011. The Neoproterozoic Noonday Formation, Death Valley region, California. *Geological Society of America Bulletin*, **123**, 1317-1336.

Pettijohn, F.J. 1957. *Sedimentary Rocks*, 2nd ed. Harper & Bros, New York, 718 pp.

Phillips, E., Merritt, J., Auton, C., Golledge, N., 2007. Microstructures in subglacial and proglacial sediments: understanding faults, folds and fabrics, and the influence of water on the style of deformation. *Quaternary Science Reviews*, **26**, 1499-1528.

Phillips, E., van der Meer, J.J.M. & Ferguson, A. A new 'microstructural mapping' methodology for the identification, analysis and interpretation of polyphase deformation within subglacial sediments. *Quaternary Science Reviews*, **30**, 2570-2596.

Pierrehumbert, R., Abbot, D., Voigt, A. & Koll, D. 2011. Climate of the Neoproterozoic. *Annual Review of Earth and Planetary Sciences*, **39**, 417-460.

Piotrowski, J.A., Larsen, N.K. & Junge, F.W. 2004. Reflections on soft subglacial beds as a mosaic of deforming and stable spots. *Quaternary Science Reviews*, **23**, 993-1000.

Planavsky, N., Rouxel, O., Bekker, A., Shapiro, R., Fralick, P. & Knudesen, A. 2009. Iron-oxidizing microbial ecosystems thrived in late Paleoproterozoic redox-stratified oceans. *Earth and Planetary Science Letters*, **286**, 230-242.

Plumb, K.A. 1991. New Precambrian time scale. *Episodes*, **14**, 139-140.

Pollard, D. & Kasting, J.K. 2001. Couple GCM-ice sheet simulations of Sturtian (750-720 Ma) glaciation: when in the snowball-Earth cycle can tropical glaciation occur? *Eos*, **82**, S8.

Pollard, D. & Kasting, J.K. 2005. A thin-ice solution with flowing sea glaciers. Journal *of Geophysical Research*, **110**, C07010.

Porada, H., 1983. Geodynamic model for the geosynclinal development of the Damara Orogen, Namibia, South West Africa. In: Martin, H., Eder, F.W. (eds.) *Intracontinental Fold Belts – Case Studies in the Variscan Belt of Europe and the Damara Belt in Namibia*. Springer, Heidelberg, 503–540.

Porada, H. & Wittig, R., 1983a. Turbidites in the Damara Orogen. In: Martin, H., Eder, F.W. (eds.) *Intracontinental Fold Belts – Case Studies in the Variscan Belt of Europe and the Damara Belt in Namibia*. Springer, Heidelberg, 543–576.

Porada, H. & Wittig, R., 1983b. Turbidites and their significance for the geosynclinals evolution of the Damara Orogen, South West Africa/Namibia. In: Miller, R.McG. (ed.) *Evolution of the Damara Orogen of South West Africa/Namibia*. Geological Society of South Africa Special Publication **11**, Johannesburg, 21–36.

Post, A.L., Galton-Fenzi, B.K., Riddle, M.J., Herraiz-Borreguero, L., O'Brien, P.E., Hemer, M.A., McMinn, A., Rasch, D. & Craven, M. 2014. Modern sedimentation, circulation and life beneath the Amery Ice Shelf, East Antarctica. *Continental Shelf Research*, **74**, 77-87.

Posth, N.R., Canfield, D.E. & Kappler, A. 2014. Biogenic Fe(III) minerals: from formation to diagenesis and preservation in the rock record. *Earth Science Reviews*, **135**, 103-121.

Poulsen, C.J. & Jacob, R.L. 2004. Factors that inhibit snowball Earth simulation. *Palaeoceanography*, **19**, PA4021.

Powell, R.D. & Cooper, J.M. 2002. A glacial sequence stratigraphic model for temperate, glaciated continental shelves. In: Dowdeswell, J.A. & Ó'Cofaigh, C. (eds.) *Glacier-Influenced Sedimentation on High-Latitude Continental Margins*. Geological Society, London, Special Publication, **203**, 215-244.

Powell, R.D., Dawber, M., McInnes, J.N. & Pyne, A.R. 1996. Observations of the grounding-line area at a floating glacier terminus. *Annals of Glaciology*, **22**, 217-223.

Prave, A.R. 1999. Two diamictites, two cap carbonates, two $\delta^{13}C$ excursions, two rifts: the Neoproterozoic Kingston Peak Formation, Death Valley, California. *Geology*, **27**, 339-342.

Prave, A.R., Hoffmann, K.-H., Hegenberger, W. & Fallick, A.E. 2011. The Witvlei Group of East-Central Namibia. In: Arnaud, E., Halverson, G.P. & Shields-Zhou, G. (eds.) 2011. The Geological Record of Neoproterozoic Glaciations. *Geological Society of London Memoirs*, **36**, 211-216.

Preiss, W.V. 2000. The Adelaide Geosyncline of South Australia and its significance in Neoproterozoic continental reconstruction. *Precambrian Research*, **100**, 21-63.

Preiss, W.V., Dyson, I.A., Reid, P.W. & Cowley, W.M. 1998. Revision of lithostratigraphic classification of the Umberatana Group. *MESA Journal*, **9**, 36–42

Preiss, W.V., Gostin, V.A., McKirdy, D.M., Ashley, P.M., Williams, G.E. & Schmidt, P.W. 2011. The glacial succession of Sturtian age in South Australia: the Yudnamutana Subgroup. In: Arnaud, E., Halverson, G.P. & Shields-Zhou, G. (eds.) *The Geological Record of Neoproterozoic Glaciations.* Geological Society of London Memoirs, **36**, 701-712.

Rankama, K. 1973. The Late Precambrian glaciation, with particular reference to the Southern Hemisphere. *Journal and Proceedings, Royal Society of New South Wales*, **106**, 89-97.

Ravier, E., Buoncristiani, J-F., Clerc, S., Guiraud, M., Menzies, J. & Portier, E. 2014. Sedimentological and deformational criteria for discriminating subglaciofluvial deposits from subaqueous ice-contact fan deposits: a Pleistocene example (Ireland). *Sedimentology*, **61**, 1382-1410.

Reading, H.G. & Walker, R.G. 1966. Sedimentation of Eocambrian tillites and associated sediments in Finnmark, northern Norway. *Palaeogeography, Palaeoclimatology, Palaeoecology*, **2**, 177-212.

Reusch, H. 1891. Skuringmærker og morængrus eftervist i Finnmarken fra en periode meget ældre end 'istiden' (Glacial striae and boulder-clay in Norwegian Lapponie from a period much older than the last ice age). *Norges Geologiske Undersøkelse*, **1**, 78-85 (English summary, 97-100).

Robert, M. 1940. La glaciation du Kundelungu au Katanga (Congo Belge). *17th International Geological Congress, Moscow*, **6**, 99-113.

Rocha-Campos, A.C. & Hasui, Y. 1981. The Precambrian Carandaí Formation of southeastern Minas Gerais, Brazil. In: Hambrey, M.J. & Harland, W.B. (eds.) *Earth's Pre-Pleistocene Glacial Record*. Cambridge University Press, Cambridge, 931-932.

Rocha-Campos, A.C. & Hasui, Y. 1981. Tillites of the Macaúbas Group (Proterozoic) in central Minas Gerais and southern Bahia, Brazil. In: Hambrey, M.J. & Harland, W.B. (eds.) *Earth's Pre-Pleistocene Glacial Record*. Cambridge University Press, Cambridge, 933-938.

Rocha-Campos, A.C., de Brito Neves, B.B., Babinksi, M., dos Santos, P.R., Oliveira, S.M.B. & Romano, A. Moema laminites: a newly recognized Neoproterozoic (?) glaciogenic unit, São Francisco Basin, Brazil.

In: Arnaud, E., Halverson, G.P. & Shields-Zhou, G. (eds.) 2011. The Geological Record of Neoproterozoic Glaciations. *Geological Society of London Memoirs*, **36**, 535-540.

Rodgers, J. 1957. The distribution of marine carbonate sediments: a review. In: Le Blanc, R.J. & Breeding, J.G. (eds.) *Regional Aspects of Carbonate Deposition.* Society of Economic Paleontologists and Mineralogists (SEPM) Special Publication No. 5, 2-14, Tulsa, Oklahoma.

Rogers, A.W. 1915. The geology of part of Namaqualand. *Transactions of the Geological Society of South Africa*, **18**, 72-101.

Rogers, A.W. 1927. Precambrian rocks of the union of South Africa. *Geological Society of America Bulletin*, **38**, 805-812.

Rooney, A.D., Macdonald, F.A., Strauss, J.V., Dudás, F.Ö., Hallmann, C. & Selby, D. 2014. Re-Os geochronology and coupled Os-Sr isotope constraints on the Sturtian snowball Earth. *PNAS*, **111**, 51-56.

Runnegar, B. 2000. Palaeoclimate: loophole for snowball Earth. *Nature*, **405**, 403-404.

Schermerhorn, L.J.G. 1974. Late Precambrian mixtites: Glacial and/or nonglacial? *American Journal of Science*, **274**, 673-824.

Schermerhorn, L.J.G. & Stanton, W.I. 1963. Tilloids in the West Congo geosynclines. *Quarterly Journal of the Geological Society of London*, **119**, 201-241.

Shields-Zhou, G.A., Deynoux, M. & Och, L. 2011. The record of Neoproterozoic glaciation in the Taoudéni Basin, NW Africa. In: Arnaud, E., Halverson, G.P. & Shields-Zhou, G. (eds.) 2011. The Geological Record of Neoproterozoic Glaciations. *Geological Society of London Memoirs*, **36**, 163-171.

Schmidt, P.W., Williams, G.E. & Embleton, B.J.J. 1991. Low palaeolatitude of Late Proterozoic glaciation: early timing of remanence in haematite of the Elatina Formation, South Australia. *Earth and Planetary Science Letters*, **105**, 355-367.

Schrag, D.P. & Hoffman, P.F. 2001. Life, geology and snowball Earth. *Nature*, **409**, 306.

Schrag, D.P., Berner, R.A. & Hoffman, P.F. 2002. On the initiation of a snowball Earth. *Geochemistry, Geophysics, Geosystems*, **3**, 1-21.

Schwarzbach, M. 1964. Criteria for the recognition of ancient glaciations. In: Nairn, A.E.M. (ed.) *Problems in Palaeoclimatology*. Interscience, London, 81-85.

Sellers, W. D. 1969. A global climatic model based on the energy balance of the Earth atmosphere system. *Journal of Applied Meteorology*, **8**, 392 – 400

Sohl, L.E., Christie-Blick, N. & Kent, D.V. 1999. Paleomagentic polarity reversals in Marinoan (ca. 600 Ma) glacial deposits of Australia: implications for the duration of low-latitude glaciations in Neoproterozoic time. *Geological Society of America Bulletin*, **111**, 1120-1139.

Spencer, A.M. 1971. Late Pre-Cambrian glaciation in Scotland. *Geological Society of London Memoir*, **6**, 99.

Spencer, A.M. 1981. The Late Precambrian Port Askaig Tillite in Scotland. In: Hambrey, M.J. & Harland, W.B. (eds.) *Earth's Pre-Pleistocene Glacial Record*. Cambridge University Press, Cambridge, 632-636.

Stouge, S., Christiansen, J.L., Harper, D.T., Houmark-Nielsen, M., Kristiansen, K., MacNiocaill, C. & Buchardt-Westergård, B. 2011. Neoproterozoic (Cryogenian-Ediacaran) deposits in East and North-East Greenland. In: Arnaud, E., Halverson, G.P. & Shields-Zhou, G. (eds.) 2011. The Geological Record of Neoproterozoic Glaciations. *Geological Society of London Memoirs*, **36**, 581-592.

Stow, D.A.V. 1981. Fine-grained sediments: terminology. *Quarterly Journal of Engineering Geology and Hydrogeology*, **14**, 243-244.

Sumner, D.Y., Kirschvink, J.L. & Runnegar, B.N. 1987. Soft-sediment paleomagnetic fold tests of late Precambrian glaciogenic sediments. *Eos*, **68**, 1251.

Syvitski, J.P.M., Andrews, J.T. & Dowdeswell, J.A. 1996. Sediment deposition in an iceberg-dominated glacimarine environment, East Greenland: basin fill implications. *Global and Planetary Change*, **12**, 251-270.

Szuman, I., Ewertowski, M. & Kasprzak, L. 2013. Thermo-mechanical facies representative of fast and slow flowing ice sheets: the Weichselian ice sheet, a central west Poland case study. *Proceedings of the Geologists' Association*, **124**, 818-833.

Templeton, A.S. Geomicrobiology of iron in extreme environments. *Elements*, **7**, 95-100.

Thompson, J. 1871. On the stratified rocks of Islay. *Report of the 41st Meeting of the British Association for the Advancement of Science, Edinburgh*. John Murray, London, 110-111.

Torsvik, T.H. 2003. The Rodinia jigsaw puzzle. *Science*, **300**, 1379-1381.

Tripsanas, E.K. & Piper, D.J.W. 2008. Glaciogenic debris-flow deposits of Orphan Basin, offshore eastern Canada: sedimentological and rheological properties, origin and relationship to meltwater discharge. *Journal of Sedimentary Research*, **78**, 724-744.

Trompette, R. 1982. Upper Proterozoic (1800-570 Ma) stratigraphy: a survey of lithostratigraphic, paleontological, radiochronological and magnetic correlations. *Precambrian Research*, **18**, 27-52.

Troxel, B.W. 1966. Sedimentary features of the later Precambrian Kingston Peak Formation, Death Valley, California. *Geological Society of America Special Paper*, **101**, 341p.

Troxel, B.W. 1982. Description of the uppermost part of the Kingston Peak Formation, Amargosa Rim canyon, Death Valley region, California. In: Cooper, J.D., Troxel, B.W. & Wright, L.A. (eds.) *Geology of Selected Areas in the San Bernadino Mountains, Western Mojave Desert, and Southern Great Basin, California*. Geological Society of America (Cordilleran Section) Volume and Guidebook. Death Valley Publishing Company, Shoshone, CA, 61–70.

Trusel, L.D., Powell, R.D., Cumpston, R.M. & Brigham-Grette, J. 2010. Modern glacimarine processes and potential future behaviour of Kronebreen and Kongsvegen polythermal tidewater glaciers, Kongsfjorden, Svalbard. In: Howe, J.A., Austin, W.E.N., Forwick, M. & Paetzel, M. (eds.) *Fjord Systems and Archives*. Geological Society of London Special Publication, **344**, 89-102.

Tucker, M.E. 1996. Sedimentary Rocks in the Field (2nd ed.). Wiley, Chichester, 153 pp.

Tucker, M.E. 2001. *Sedimentary Petrology: An Introduction to the Origin of Sedimentary Rocks* (3rd ed.). Wiley, Chichester, 272 pp.

Tucker, M.E. 2011. Sedimentary Rocks in the Field: a Practical Guide (4th ed.). Wiley, Chichester, 288 pp.

Tziperman, E., Abbot, D.S., Ashkenazy, Y., Gildor, H., Pollard, D., Schoof, C.G. & Schrag, D.P. 2012. Continental constriction and oceanic ice-cover thickness in a Snowball-Earth scenario. *Journal of Geophysical Research*, **117**, C05016.

Urban, H., Stribrny, B. & Lippolt, H.J. 1992. Iron and manganese deposits of the Urucum district Mato Grasso do Sul, Brazil. *Economic Geology*, **87**, 1375-1392.

van der Meer, J.J.M. 1993. Microscopic evidence of subglacial deformation. *Quaternary Science Reviews*, **12**, 553-587.

van der Meer, J.J.M. & Menzies, J. 2011. The micromorphology of unconsolidated sediments. *Sedimentary Geology*, **238**, 213-232.

van der Meer, J.J.M., Carr, S.J. & Palmer, A. 2012. Glossary of Terms. 8th International Workshop: Micromorphology of Glacial Sediments, Queen Mary, University of London.

van der Meer, J.J.M., Menzies, J. & Rose, J. 2003. Subglacial till: the deforming glacier bed. *Quaternary Science Reviews*, **22**, 1659-1685.

van der Vegt, P., Janszen, A. & Moscariello, A. 2012. Tunnel valleys: current knowledge and future perspective. In: Huuse, M., Redfern, J., Le Heron, D.P., Dixon, R.J., Moscariello, A. & Craig, J. (eds.) *Glaciogenic Reservoirs and Hydrocarbon Systems*. Geological Society of London Special Publication, **368**, 75-97.

van der Wateren, F.M. 2002. *Processes of glaciotectonism*. In: Menzies, J. (ed.) Modern & Past Glacial Environments. Butterworth & Heinemann, Oxford, 417–443.

Vanyo, J.P. & Awramik, S.M. 1982. Length of day and obliquity of the ecliptic 850 Ma ago – preliminary results of a stromatolite growth model. *Geophysics Research Letters*, **9**, 1125-1128.

Vaughan-Hirsch, D.P., Phillips, E., Lee, J.R. & Hart, J.K. 2013. Micromorphological analysis of poly-phase deformation associated with the transport and emplacement of glaciotectonic rafts at West Runton, north Norfolk, UK. *Boreas*, **42**, 376-394.

Visser, J.N.J. 1981. The Mid-Precambrian tillite in the Griqualand West and Transvaal Basins, South Africa. In: Hambrey, M.J. & Harland, W.B. (eds.) *Earth's Pre-Pleistocene Glacial Record*. Cambridge University Press, Cambridge, 180-184.

Volkert, R.A., Monteverde, D.H., Friehauf, K.C., Gates, A.E., Dalton, R.F. & Smith, R.C. 2010. Geochemistry and origin of Neoproterozoic ironstone deposits of the New Jersey Highlands and implications for the eastern Laurentian rifted margin in the north-central Appalachians, USA. *Geological Society of America Memoirs*, **206**, 283-306.

Walker, J.C.G., Hays, P.B. & Kasting, J.F. 1981. A negative feedback mechanism for the long-term stabilization of Earth's surface temperature. *Journal of Geophysical Research*, **86**, 9776-9782.

Warren, S.G., Brandt, R.E., Grenfell, T.C. & McKay, C.P. 2002. Snowball Earth: ice thickness on the tropical ocean. Journal of Geophyscial Research, 107, 3167.

Wentworth, C.K. 1922. A scale of grade and class terms for clastic sediments. *Journal of Geology*, **30**, 377-392.

Widdel, F., Schnell, S., Heising, S., Ehrenreich, A., Assmus, B. & Schink, B. 1993. Ferrous iron oxidation by anoxygenic phototrophic bacteria. *Nature*, **362**, 834-836.

Williams, G.E. 1972. Geological evidence relating to the origin and secular rotation of the solar system. *Modern Geology*, **3**, 165-181.

Williams, G.E. 1975. Late Precambrian glacial climate and the Earth's obliquity. *Geological Magazine*, **112**, 441-465.

Williams, G.E. 2000. Geological constraints on the Precambrian history of Earth's rotation and the Moon's orbit. *Reviews of Geophysics*, **38**, 37-59.

Williams, G.E. & Schmidt, P.W. 2004. Neoproterozoic glaciation: reconciling low palaeolatitudes and the geologic record. In: Jenkins, G.S., McMenamin, M., Sohl, L.E. & McKay, C.P. (eds.) *The Extreme Proterozoic: Geology, Geochemistry and Climate*. American Geophysical Union Monographs, **146**, 145-159.

Willis, B. 1904. Geological Research in eastern Asia. *Carnegie Institute of Washington, Yearbook* **3**, Washington, DC, 275-291.

Willis, B., Blackwelder, E. & Sargent, R.H. 1907. *Research in China, Vol. 1, Part 1.* The Carnegie Institution of Washington, Washington DC, 83-203.

Winsemann, J., Asprion, U., Meyer, T., & Schramm, C. 2007. Facies characteristics of Middle Pleistocene (Saalian) ice-margin subaqueous fan and delta deposits, glacial Lake Leine, NW Germany. *Sedimentary Geology*, **193**, 105-129.

Woodward, H.P. 1884. Report on the range of the east of Farina. *Parliamentary Papers for 1884.* Government of South Australia, **40**, 1-5.

Wright, L.A., Troxel, B.W., Williams, E.G., Roberts, M.T. & Diehl, P.E. 1976. Precambrian sedimentary environments of the Death Valley region, eastern California. *California Division of Mines and Geology Special Report*, **106**, 7-15.

Yang, J., Peltier, W. & Hu, Y. 2012. The initiation of modern "Soft Snowball" and "Hard Snowball" climates in CCSM3. Part I: the influences of solar luminosity, CO2 concentration, and the sea ice/snow albedo parameterization. *Journal of Climate*, **25**, 2711-2736.

Yeo, G.M. 1981. The Late Proterozoic Rapitan glaciation in the Northern Cordillera. In: Campbell, F. (ed.) *Proterozoic Basins of Canada.* Geological Survey of Canada Paper, **81-10**, 25-46.

Yokoyama, M. 1911. Climatic changes in Japan since the Pliocene Epoch. *The Journal of the Geological Society of Japan*, **18**, 1-18.

Yonkee, W.A., Dehler, C.D., Link, P.K., Balgord, E.A., Keeley, J.A., Hayes, D.S., Wells, M.L., Fanning, C.M. & Johnston, S.M. 2014. Tectono-stratigraphic framework of Neoproterozoic to Cambrian strata, west-central U.S.: protracted rifting, glaciation and evolution of the North American Cordilleran margin. *Earth Science Reviews*, **136**, 59-95.

Young, G.M. 1976. Iron-formation and glaciogenic rocks of the Rapitan Group, Northwest Territories, Canada. *Precambrian Research*, **3**, 137-158.

Young, G.M. & Gostin, V.A. 1988. Stratigraphy and sedimentology of Sturtian glaciogenic deposits in the western part of the North Flinders Basin, South Australia. *Precambrian Research*, **39**, 151–170.

Young, G.M. & Gostin, V.A. 1989. An exceptionally thick upper Proterozoic (Sturtian) glacial succession in the Mount Painter area, South Australia. *Geological Society of America Bulletin*, **101**, 834–845.

Young, G.M. & Gostin, V.A. 1990. Sturtian glacial deposition in the vicinity of the Yankaninna Anticline, North Flinders Basin, South Australia. *Australian Journal of Earth Sciences*, **37**, 447–458.

Young, G.M. & Gostin, V.A. 1991. Late Proterozoic (Sturtian) succession of the North Flinders Basin, South Australia; An example of temperate glaciation in an active rift setting. *In*: Anderson, J.R. & Ashley, G.M. (eds) *Glacial Marine Sedimentation: Palaeoclimatic Significance*. Geological Society of America, Special Papers, **261**, 207–222.

Zaniewski, K. van der Meer, J.J.M. 2005. Quantification of plasmic fabric through image analysis. *Catena*, **63**, 109–127.

Zhang, Q.-R., Chu, X.-L. & Feng, L.-J. 2011. Neoproterozoic glacial records in the Yangtze Region, China. In: Arnaud, E., Halverson, G.P. & Shields-Zhou, G. (eds.) *The Geological Record of Neoproterozoic Glaciations*. Geological Society of London Memoirs, **36**, 357-366.

Zwally, H.J., Abdalati, *W.*, Herring, T., Larson, K., Saba, J. & Steffen, K. 2002. Surface melt-induced acceleration of Greenland ice-sheet flow. *Science,* **297**, 218–222.